AR TARGET SHEET

The following document was too large to scan as one unit, therefore it has been broken down into sections.

DOCUMENT # SD-WM-EE-004

EDMC # 0035075

SECTION 2 OF 2

THIS PAGE INTENTIONALLY
LEFT BLANK

WHC-SD-WM-TI-528, Rev. 0

GROUT TREATMENT FACILITY

WASTE FEED PROJECTIONS

Prepared for
WESTINGHOUSE HANFORD COMPANY

by

D. W. Hendrickson
Westinghouse Hanford Company

J. M. Conner
Westinghouse Hanford Company

January 1993

THIS PAGE INTENTIONALLY LEFT BLANK

WHC-SD-WM-TI-528, Rev. 0

Grout Treatment Facility Waste Feed Projections

TABLE OF CONTENTS

Page

1.0 INTRODUCTION 1-1

2.0 WASTE DATA EVALUATION METHODS AND HISTORY 2-1
2.1 Wastes Described by Direct Sampling and Analysis 2-1
2.2 Wastes Described by Process and Transfer History 2-2
2.3 Wastes Described by Pretreatment Flowsheets 2-4

3.0 DATA HANDLING TECHNIQUES 3-1
3.1 Data Handling for Existent Waste Samples 3-3
3.1.1 Existent Dilute Waste Sample Data 3-4
3.1.2 Existent Concentrated Waste Sample Data 3-4
3.2 Data Handling for Process History Samples 3-5
3.2.1 Referenced Historical Process Analyses 3-5
3.2.2 Future Evaporator Product Estimation 3-5
3.2.3 Process Analyses for Previous Evaporator Products . . 3-6
3.3 Data Handling for Pretreatment Low-Level Streams 3-8
3.4 Data Summarization and Interpretation 3-9
3.4.1 Application of Uniform Decay Date 3-9
3.4.2 Evaluation of Dilute Waste Requirements 3-10
3.4.3 Use and Application of Limiting Values 3-11
3.4.4 Analytical Errors 3-12
3.4.5 Data Summary 3-13
3.5 Recommendations on Data Usage 3-14

4.0 SPECIAL ESTIMATES OF CRITICAL ISOTOPES 4-1
4.1 ^{135}Cesium Estimation 4-1
4.1.1 Back-Decay of ^{137}Cesium Data 4-3
4.1.2 ^{135}Cesium Production 4-3
4.1.3 ^{135}Cesium Estimate Usage 4-4
4.2 ^{237}Neptunium Estimation 4-4
4.2.1 Revision of ^{241}Americium Estimates 4-5
4.2.2 Revision of ^{237}Neptunium Estimates 4-8
4.3 ^{226}Radium Estimation 4-9
4.4 ^{129}Iodine Estimation 4-11
4.5 ^{126}Tin Estimation 4-12
4.6 ^{99}Technetium Estimation 4-12
4.7 ^{94}Niobium Estimation 4-13
4.8 ^{79}Selenium Estimation 4-13
4.9 ^{14}Carbon Estimation 4-13
4.10 ^{238}Uranium Estimation 4-14
4.11 Special Estimate Summary 4-15

5.0 REFERENCES 5-1

APPENDIX . . . . . A-i

LIST OF TABLES

TABLE		Page
1:	Grout Treatment Facility Waste Volume Expectations	2-2
2:	Tank 241-AN-104 Waste Source History	3-6
3:	Tank 241-AN-105 Waste Source History	3-7
4:	Grout Treatment Facility Waste Projection	3-17
5:	ORIGEN2 Yield Per Metric Ton of Fuel	4-2
6:	Waste ^{137}Cs Activity	4-4
7:	^{241}Americium Sources	4-6
8:	Special Estimates of Critical Isotopes	4-16

LIST OF FIGURES

		Page
Figure 1:	Waste Source Volume Distribution for Grout Disposal	2-3
Figure 2:	Grout Feed Material Data Flowsheet	3-2
Figure 3:	Profile of DSSF Family Wastes Relative to Sodium	3-3
Figure 4:	Distribution of Am-241 Sources to Grout (Assumes maximum allowable in 4AN/5AN)	4-7

9413222.1313

WHC-SD-WM-TI-528, Rev. 0

GROUT TREATMENT FACILITY WASTE FEED PROJECTIONS

1.0 INTRODUCTION

The *Final Environmental Impact Statement, Disposal of Hanford Defense High-Level, Transuranic and Tank Wastes, Hanford Site, Richland, Washington* [HDW-EIS] (DOE 1987) evaluated disposal alternatives for Double-Shell Tank (DST) wastes at the Hanford Site. The responsive Record of Decision [ROD] (DOE 1988) selected cementitious disposal via the Hanford Grout Disposal Program (HGDP) as the preferable alternative for the disposal of low-level radioactive liquid wastes contained in Hanford's DSTs.

Since the issuance of the HDW-EIS and ROD (DOE 1987, 1988) extensive review and analysis has been conducted to determine the specific nature and characteristics of DST wastes to be received and disposed under the HGDP.

The purpose of this document is to describe the current information available on the character of wastes identified as HGDP feed material. Grout feed material is to be composed of the low-level liquid pretreated residuals and supernatant fractions of all DSTs. Dilute waste materials contained within DSTs are, in large part, expected to be evaporated prior to HGDP processing in order to ease tank farm capacity constraints.

9413222.845

THIS PAGE INTENTIONALLY LEFT BLANK

2.0 WASTE DATA EVALUATION METHODS AND HISTORY

The DST wastes described in this document have been evaluated in four general manners. The first such manner is that of direct sampling and analysis for the purpose of characterization. The second is the use of historical process data surrounding material transfers and historical and expected Evaporator/Crystallizer campaign conduct. Thirdly, pretreatment flowsheet information is used to describe approximately one half of expected waste receipts to the HGPD. Finally, data resulting from the above evaluations are compared to relevant reactor history codes and Hanford Site documents. This last comparative evaluation is contained in §4.0.

A summary of expected wastes described in this document is contained in Table 1 and depicted in Figure 1. These wastes comprise the supernatant liquid fraction of current, future and pretreated DST contents expected to be received by the Hanford Grout Disposal Program. These wastes and their volumes are described by Hanlon (1992), and Lowe (1991), and are further developed within this document.

9413222.3346

2.1 Wastes Described by Direct Sampling and Analysis

The DST wastes described in this document for which information gathered was by direct sampling and analysis include concentrated waste tanks 241-AN-106, 241-AW-101, and 241-AN-103, and dilute waste tanks 241-AP-103, 241-AW-106, and 241-AW-102. Further discussion of the history of information accumulation on this waste category is provided below.

The first significant milestone in the evaluation of concentrated DST wastes was achieved in 1988 with the initial issuance of "Methods and Data for Use in Determining Source Terms for the Grout Disposal Program" (Hendrickson 1990). That document describes the analyses of the supernatant fractions of three DST waste tanks expected, at that time, to be representative of all wastes to be received at the HGDP. The three wastes discussed were those contained in tanks 241-AN-106, 241-AW-101, and 241-AN-103. These wastes are, respectively, concentrated phosphate wastes from N-Reactor, concentrated Facilities waste termed Double-Shell Slurry Feed (DSSF), and Double-Shell Slurry (DSS).

Additional milestones were achieved in the completion of detailed analyses of tanks 241-AN-106 and 241-AW-101 (Welsh 1991a and 1991b). These detailed analyses allowed significant analytical refinement and reduction in the estimation of waste variability (expressed as the standard deviation) for these wastes.

Characterization efforts in support of projected Evaporator/Crystallizer operation led to the sampling and analysis of dilute non-complexed wastes contained in tanks 241-AP-103, 241-AW-106, and 241-AW-102 between June and December 1991.

TABLE 1: Grout Treatment Facility Waste Volume Expectations

General Type	Description	Tanks	Volume (L x 10^6)
DSSF[1] Family	Concentrated Phosphate	241-AN-106	3.67
	Existent DSSF	241-AW-101 241-AP-105 241-AN-104 241-AN-105	3.83 3.15 3.02 4.27
	Future DSSF	Undefined	30.28
	DSS	241-AN-103	3.55
	Dilute Wastes	241-AP-106 and others	9.05
Pretreated Wastes (Low-Level Residual)	NCAW	241-AZ-101 241-AZ-102	3.60 3.61
	NCRW	241-AW-103 241-AW-105	12.87
	PFP	241-SY-102 and PFP	2.08
	Complexed Concentrate	241-SY-101 241-SY-103 241-AN-102 241-AN-107	39.0
Total			122.0

2.2 Wastes Described by Process and Transfer History

Wastes described in this document for which information gathered was by process and transfer history include concentrated waste tanks 241-AP-105, 241-AN-104, and 241-AN-105, and dilute waste tank 241-AP-106. Future evaporator products are estimated based on current dilute waste compositions and expected evaporative processing. Further discussion of the history of information accumulation on this waste category is provided below.

Detailed historical analysis of waste material transfers and Evaporator/Crystallizer operation allowed the development of waste composition estimates for dilute waste tank 241-AP-106 and DSSF tank 241-AP-105 (Hendrickson and Welsh 1992a, and 1992b). These material estimates were developed to support sampling and analysis of these tanks.

---

[1] Waste descriptions and acronyms are detailed in the following text and in Hanlon (1992).

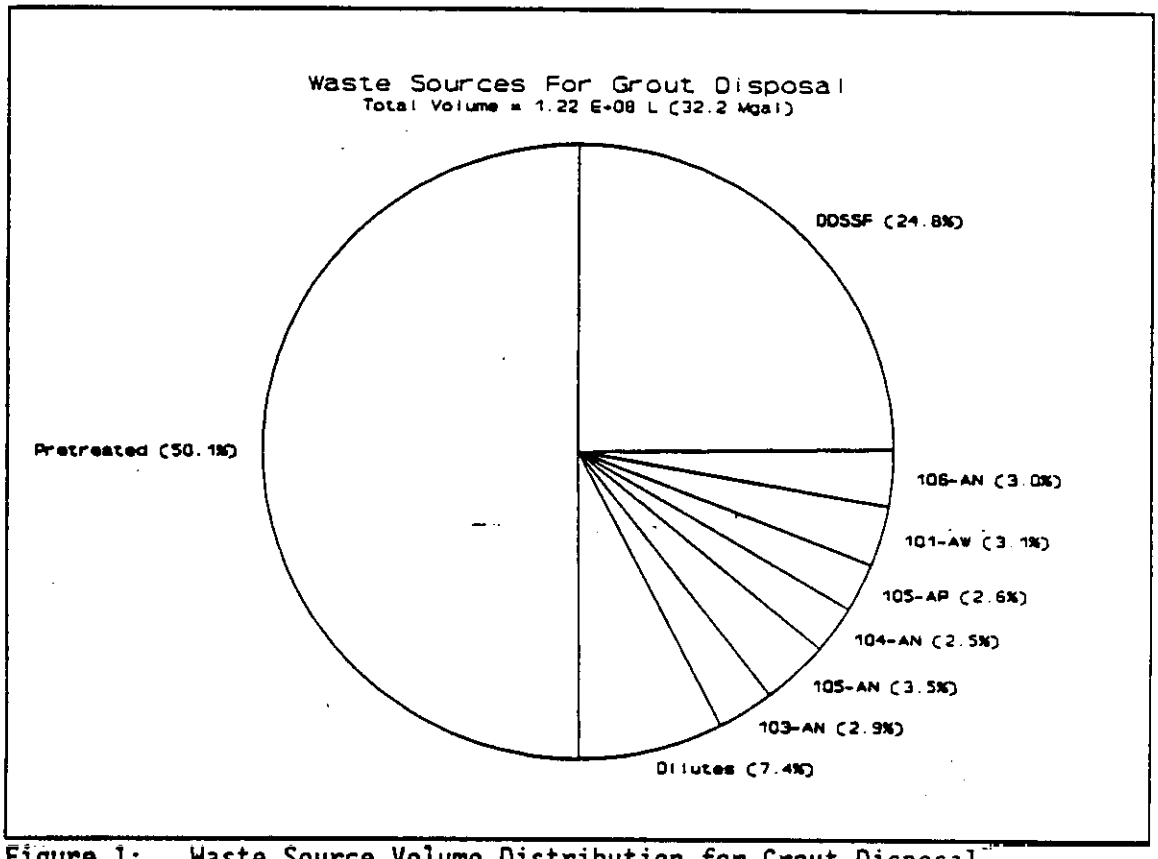

Figure 1: Waste Source Volume Distribution for Grout Disposal

Dilute wastes contained in tanks 241-AP-103, 241-AW-106, and 241-AW-102, as described in §2.1, were sampled and analyzed in support of Evaporator/ Crystallizer operation. These materials are intended to be evaporated in 242-A Evaporator/Crystallizer Campaign 93-1 (O'Rourke 1992). As these materials are miscellaneous facilities wastes, and as the source streams are expected to be the generation source for such future wastes, process evaluation of the evaporated [i.e. concentrated] product has been conducted to estimate the composition and concentration of future concentrated wastes. As described by O'Rourke, expectations are that the concentrated materials would not be as highly concentrated as current DSSF material and would be classified as dilute-DSSF wastes (DDSSF). Such concentrated product is, as depicted in Figure 1, expected to constitute approximately 25 percent of all HGDP feed material.

Concentrated waste materials (DSSF) contained within tanks 241-AN-104 and 241-AN-105 were produced in Evaporator/Crystallizer campaigns 84-3, 84-5, and 85-3. These campaigns, and sample data in support of evaporator operation, are documented in Certa (1985), Gratny (1985), and Pontious (1986). Waste volumes, and their analyses, distributed to these tanks were used to estimate the composition of these wastes.

2.3 Wastes Described by Pretreatment Flowsheets

Wastes described in this document for which information gathered was from pretreatment flowsheets include the low-level streams resulting from pretreatment of Neutralized Current Acid Waste (NCAW), Neutralized Cladding Removal Waste (NCRW), Plutonium Finishing Plant (PFP) waste, and Complexed Concentrate (CC) waste.

NCAW is currently stored in tanks 241-AZ-101 and 241-AZ-102. NCRW is currently stored in tanks 241-AW-103 and 241-AW-105. PFP waste is currently stored in 241-SY-102 and in the PFP. CC waste is currently stored in DST and SST tanks 241-SY-101 and -103, 241-AX-102 and -103, and 241-AN-102 and -107 (Hanlon 1992).

These wastes and the low-level streams resulting from their pretreatment are described in Lowe (1991). These flowsheets include globally the existence and pretreatment of CC waste within the single-shell tanks (SST) 241-AX-102 and 241-AX-103. Although this document is prepared to describe the disposal of DST wastes only, the differences in waste volume and contents due to the small volume of these SST contents (151 kgal) upon the Lowe (1991) flowsheets are conservatively neglected in this document.

3.0 DATA HANDLING TECHNIQUES

As described in §2.0, above, three general forms of data were available for compilation and interpretation. In reiteration, these forms of data were actual sample data of existent tank wastes, sample and process data for wastes placed (or to be placed) into tanks, and process flowsheet estimates for future pretreatment residuals. The handling of each of these types of data are described below. Each of the data handling operations described below is depicted in Figure 2.

Key to the handling of data within the first two categories (data based upon direct sampling or evaporative processing of current and future wastes which will not be pretreated) is the knowledge that the sources for these wastes are common. Each of these wastes are the combined product of the miscellaneous low-level liquid wastes of Hanford's 100, 200, 300, and 400 Areas. Because the waste sources are similar they constitute a family which is herein described as the "DSSF Family" of wastes. Within this "family" the concentration of nonvolatile constituents is inversely proportional to water content. This familial relationship, as illustrated in Figure 3, is not perfect but allows data gaps to be bridged and the mean concentration of an analyte to be reasonably estimated in the absence of some data. As an example, if potassium concentrations are described for four of six tanks in the family, the mean of all six tanks is represented as the mean of the four tanks for which data is provided.

As will be described in §3.3, the conduct of pretreatment operations and the data provided do not allow handling of data in the manner of the DSSF family. This data is recognized to be incomplete, as not all analytes were followed through the flowsheets and because the differing nature of the sources do not allow one to make generalizations based on similarity of waste sources. In addition, proposed treatment regimes differ for the various waste streams. Thus, in totalizing expected waste streams from these operations, the mean of all waste streams was calculated as the weighted average of all streams. If no data was provided for an analyte in a stream, the weight assigned was zero while the volume of that stream remained a part of the calculation. This may introduce some non-conservative estimates for some analytes; however, it is believed that most analytes of potential concern in large streams are reported and form the basis of this family's estimate.

Summary tables for the work described in §§3.1 through 3.4 are contained in Tables 1-1 through 1-4 of the Appendix. All data are converted to units of µCi/L for radionuclides, and molarity for other constituents unless specifically noted. All radionuclide data are decayed to October 1, 1993, unless specifically noted; further discussion of decay is provided in §3.4.

9413222.1551

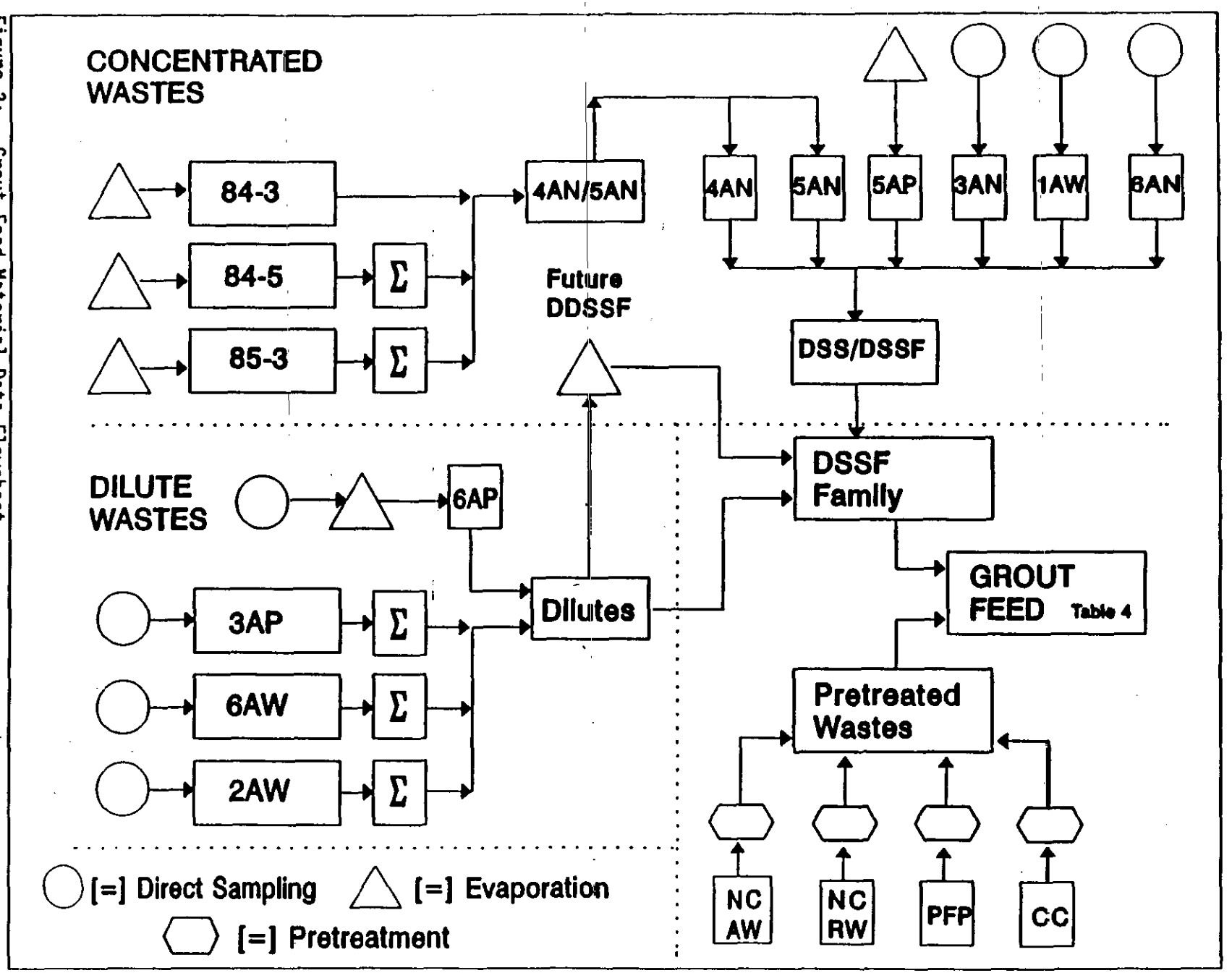

Figure 2: Grout Feed Material Data Flowsheet

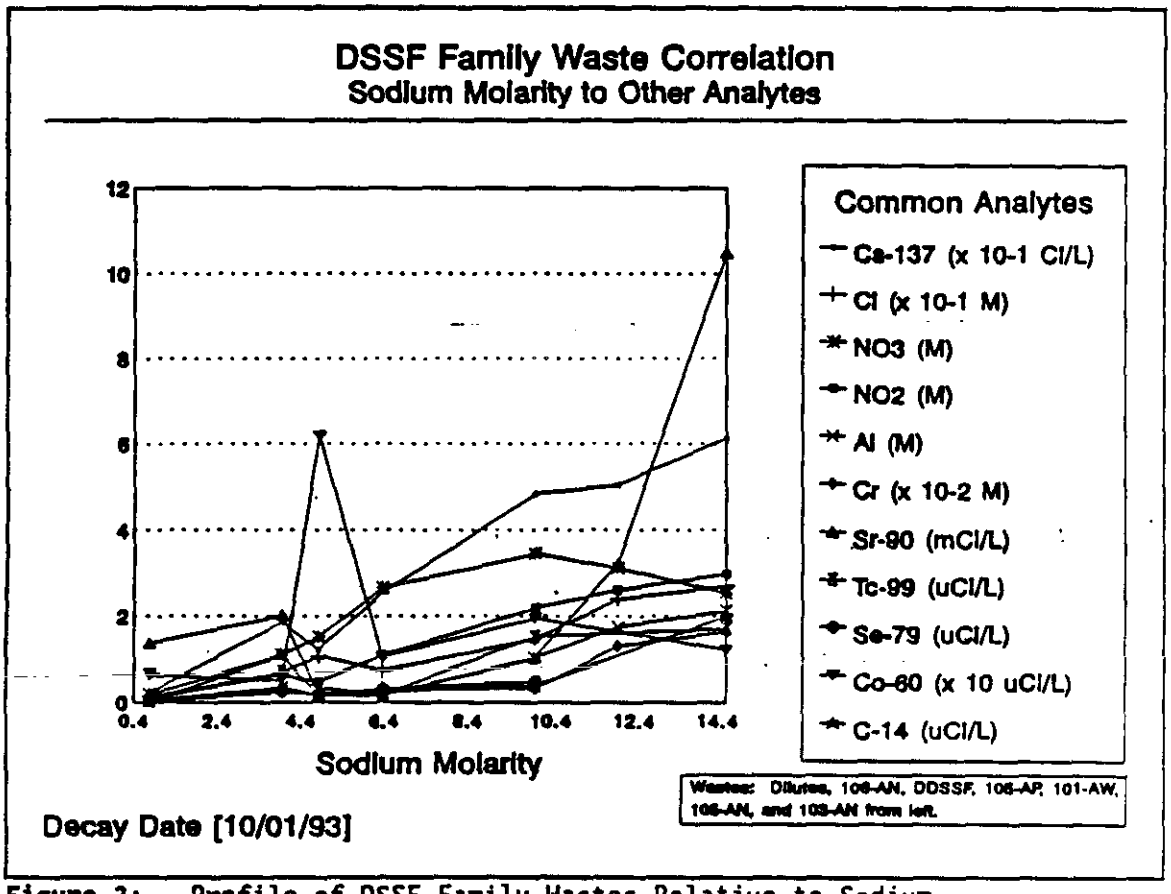

Figure 3: Profile of DSSF Family Wastes Relative to Sodium

3.1 Data Handling for Existent Waste Samples

Two types of existent waste have been directly sampled for the purpose of characterization. These wastes are dilute non-complexed wastes and concentrated wastes. In all, these data describe the contents of six DSTs. Data flows shown in Figure 2 for such direct sampling are initiated with the symbol of a circle (O).

3.1.1 Existent Dilute Waste Sample Data

Data described in this category includes sample data taken for dilute waste tanks 241-AP-103, 241-AW-106, and 241-AW-102. The sample constituent mean for these tanks was calculated as:

$$Mean_i = \frac{\sum_{j=1}^{n} [C_i]_j \times Volume_j}{\sum_{j=1}^{n} Volume_j} \qquad [Eq.\ 3.1]$$

Where: [C] = constituent concentration,
i = constituent identifier,
j = sample, tank, or stream identifier,
$Volume_j$ is assigned a value of zero when $[C_i]_j$ is unreported.

Tables 2-1, 2-2, and 2-3 of the Appendix contain the validated data for these dilute waste samples supporting O'Rourke (1992).

Tables 2-4, 2-5, and 2-6 of the Appendix contain the calculated summaries, by tank, of this analytical data. Appendix Table 1-1 contains a joint summary of these dilute wastes and includes an estimate of 241-AP-106 (Hendrickson and Welsh 1992a). These four tanks of dilute waste are used herein to describe future dilute waste receipts. Evaluation of expected evaporator operation for tanks 241-AP-103, 241-AW-106, and 241-AW-102 is calculated and displayed in Appendix Table 2-7 and included within Appendix Table 1-2; further discussion on this matter is provided in §3.2.2.

3.1.2 Existent Concentrated Waste Sample Data

Data described in this category includes sample mean data of concentrated waste tanks 241-AN-106 (Welsh 1991a), 241-AW-101 (Welsh 1991b), and 241-AN-103 (Hendrickson 1990). These data are incorporated in Appendix Tables 4-1 and 4-2. These tables do not embody any manipulation of the data other than unit conversion.

Particular aspects of the determination and use of the means for these tanks are embodied within the respective reference document, however, the following short summary is deemed appropriate.

Tank 241-AN-106 (Welsh 1991a) was sampled with the process knowledge that the tank was stratified into a high-phosphate concentration layer, a high-sulfate concentration layer, and at least one intermediate composition boundary layer. Twelve bottle-on-string samples of the waste were extracted and analyzed. Statistical analysis of the data indicated that the tank was indeed stratified and that the tank would be well represented by a stratified mean and sample deviation.

Tank 241-AW-101 (Welsh 1991b) was sampled with the expectation that the tank was relatively homogeneous. Twelve bottle-on-string samples were extracted and analyzed. Statistical analysis of the data indicated that the tank was homogeneous.

Tank 241-AN-103 (Hendrickson 1990) was sampled through core-drilling of the tank. The samples analyzed and reported were those of core composites.

3.2 Data Handling for Process History Samples

Both dilute and concentrated wastes are herein described by their evaporative process and analytical history. This category includes the dilute waste tank 241-AP-106, DSSF tanks 241-AP-105, 241-AN-104, and 241-AN-105, and future concentrated miscellaneous wastes. Data flows shown in Figure 2 for such evaporative process history and analysis are initiated with the symbol of a triangle (▲).

3.2.1 Referenced Historical Process Analyses

As described in §2.2, the contents, in terms of expected mean concentrations, of tanks 241-AP-106 and 241-AP-105 were estimated in Hendrickson and Welsh (1992a and 1992b). Appendix Table 1-1, containing a joint estimate of dilute wastes, incorporates 241-AP-106 estimates. Appendix Table 4-2 contains waste tank 241-AP-105 estimates. Each are, again, converted to the common units of μCi/L and molarity except where noted.

3.2.2 Future Evaporator Product Estimation

The composition of concentrated miscellaneous wastes, as introduced in §§2.2 and 3.1.2, has been estimated to be represented by the evaporative product of tanks 241-AP-103, 241-AW-106, and 241-AW-102. Table 2-7 of the Appendix details the expected composite of these tanks and their boil-down. Non-volatile constituent concentrations are calculated as:

$$Concentrated\ Mean_i = \frac{Non\text{-}Concentrated\ Mean_i}{(1 - WVR)} \qquad [Eq.\ 3.2]$$

Where: WVR = (1 - S/F) = Waste Volume Reduction factor (0.87),
S = Slurry Volume (concentrated product),
F = Feed Volume, and
Non-Concentrated $Mean_i$ is evaluated by Equation 3-1.

The 87% WVR used herein is that described by O'Rourke (1992) for expected Evaporator/Crystallizer operations. Thirty million liters (8×10^6 gallons) of this product, derived from Koreski and Strode (1992), are used in this estimate.

Volatile constituent concentrations (ammonia/ammonium and tritium) are calculated to be removed in the same ratio as water as:

$$Concentrated\ Mean_i = Non\text{-}Concentrated\ Mean_i \times \frac{\left(1 - \left(\frac{y_1}{z_1}\right) WVR\right)}{(1 - WVR)} \quad [Eq.\ 3.3]$$

Where: y_1 = molar density of pure water condensate (mol/L), and
z_1 = molar density of water in feed (mol/L).

3.2.3 Process Analyses for Previous Evaporator Products

The current volumes of DSSF material contained within tanks 241-AN-104 and 241-AN-105 were generated in Evaporator campaigns 84-3, 84-5, and 85-3 (Certa 1985; Gratny 1985; and Pontious 1986).

A brief synopsis of transfer history, derived from operating records, relating to the generation sources of these materials is contained in Tables 2 and 3. Each of these tanks contained a small heel of dilute non-complexed waste or concentrated waste prior to the introduction of current materials.

TABLE 2: Tank 241-AN-104 Waste Source History

Date	Activity	Volume (Kgal) Transferred	Tank Volume (Kgal) at Completion
Heel Present from Prior Activities			61
3/4/84	Evaporator Campaign 84-3 product to tank	290	351
4/84	Measured water loss	-3	348
9/84	Transfer to 3AN	-193	155*
10/5/84	Evaporator Campaign 84-5 product to tank	782	937
2/85	Measured water gain	3	940
4/6/85	Evaporator Campaign 85-3 product to tank	121	1,061

* Note: Shaded cells are those pertinent to calculations and analytical data.

TABLE 3: Tank 241-AN-105 Waste Source History

Date	Activity	Volume (Kgal) Transferred	Tank Volume (Kgal) at Completion
Heel Present from Prior Activities			11
12/82	Evaporator Campaign 83-2 product to tank	259	270
1/83	Evaporator Campaign 83-4 product to tank	369	639
3/84	Transfer	-30	609
3/84	Transfer from 4AN	499	1,108
2/85	Transfer to Evaporator	-954	154
3/85	Evaporator Campaign 85-3 product to tank	239*	393
4/85	Evaporator Campaign 85-3 product to tank	732	1,125

* Note: Shaded cells are those pertinent to calculations and analytical data.

For purposes of this estimation, the existent volumes were assumed to be the represented by the materials introduced. This is considered a reasonable approximation. Upon inspection of Table 2 one should observe that only 5% of the current contents of 241-AN-104 consist of materials present prior to the data applied. Similarly, approximately 14% of material present in 241-AN-105 was previously present; this material was dilute-DSSF.

Evaporator campaign 84-3, 84-5, and 85-3 data are presented in Appendix Tables 3-1, 3-2, and 3-3. Calculations upon this data are summarized on Appendix Tables 3-4 and 3-5, which include the decay of radioisotopes to the date of October 1, 1993. The method and selection basis for this decay date are described in §3.4, below.

The contents of tanks 241-AN-104 and 241-AN-105 are described in relation to analytical data supporting the above evaporator campaigns and the volumes received. Material transfers and minor discrepancies between transfer records and campaign post-run documentation result in the application of the following volumes (kgal) of materials i.. the estimation of material concentrations:

Evaporator Campaign	241-AN-104 Contribution	241-AN-105 Contribution
84-3	148.5	0
84-5	790	0
85-3	121	971

Thus, the analyses supporting the above volumes generated are weighted by volume to calculate the mean contents of these tanks in the manner of Equation 3-1. The resulting estimations for these tanks are contained in Appendix Table 4-3, decayed to the latest date of the above samples (April 1985).

9413222.1357

3.3 Data Handling for Pretreatment Low-Level Streams

At this time it is believed that Lowe (1991), provides the most complete and current estimate of material balances for pretreatment streams. Lowe's flowsheets are a function of what is currently known about NCAW, NCRW, CC, and PFP wastes and how they are currently planned to be pretreated. The pretreatment regimens are intended to separate a low volume of high level and transuranic material for deep geologic disposal from a large volume of low-level waste for near-surface disposal. The separation technology development and implementation is, admittedly, far from complete and subject to political, public perception, and funding variances. With this in mind, Lowe's flowsheets have been assigned an impact and quality assurance level consonant to no external review. As such, data used in this document are directly (some unit conversions) from this reference as no comparable data source exists. Should it become necessary to guide and require further pretreatment, the acceptance criteria for wastes embodied in Hendrickson (1991b) must be enforced prior to acceptance of wastes for disposal.

As described in §3.0, an assumption that the mean of all these waste streams would be represented by a mean of those reported is not considered appropriate. The reasons for this are that the original sources of the waste differ, and because the wastes would undergo differing treatment regimes. Table 1-4 of the Appendix details the data from Lowe (1991) and the evaluation of a mean as that described in Equation 3-1 with no volume weights assigned to zero.

In reiteration, this may introduce some non-conservative estimates for some analytes; however, it is believed that most analytes of potential concern in large streams are reported and form a valid basis of this family's estimate. The two lowest volume streams comprising 0.37% of the pretreated volumes to the HGDP are least well described by Lowe (1991); lack of explicit data on all aspects of these streams is considered insignificant.

3.4 Data Summarization and Interpretation

Data handling in §§3.1 through 3.3, above, resulted in the development of:

a) An estimate of the composition of dilute wastes to be received [Appendix Table 1-1],
b) An estimate of concentrated material to be produced in the future [Appendix Table 2-7],
c) Estimates of all currently available concentrated feed [Appendix Tables 4-1, 4-2, and 4-3], and
d) An estimate of all expected materials subject to pretreatment [Appendix Table 1-4].

In order to combine the above information and to determine an estimate of the overall inventory of materials to be received at the disposal facility, several aspects of process and data handling must be considered. These aspects include decay dates for radioactive materials, evaluation of requirements for dilute wastes, use and application of limiting values, and analytical errors. Each of these aspects and their impact on the estimate of overall inventory are described below.

3.4.1 Application of Uniform Decay Date

In order to combine analytical data on the radionuclide content of existent waste streams, a uniform decay date was selected. Unlike chemical constituents which will not significantly vary over time except through physical means, the radioactive components of the wastes continue to decrease in concentration through radioactive decay. The decay date chosen for this document has been that of October 1, 1993. This date has been chosen as it is the currently expected date of HGDP startup.

An example of the use and necessity of a uniform decay date in these calculations may be provided by describing the decay of ^{137}Cs in four existent concentrated waste tanks: 241-AN-103 and -106, 241-AW-101, and 241-AP-105. The analytical data is described within the Appendix tables as:

Tank	Sample Decay Date	^{137}Cs ($\mu Ci/L$)	Days before 10/01/93
241-AN-103	12/15/84	7.50 E+05	3,212
241-AP-105	01/30/89	2.85 E+05	1,705
241-AN-106	04/21/89	2.05 E+05	1,631
241-AW-101	07/17/90	5.20 E+05	1,172

The half-life of ^{137}Cs used within this document is 30.17 years (see Appendix Table 5-1 for other radionuclide data used). Conversion factors of 86,400 seconds per day and 31,556,736 seconds per sidereal year are used within decay

equations (Hendrickson 1991a) to determine the activity of remaining material at some given time as:

$$Activity(t) = Activity(t_0)\, e^{\left(\frac{-\lambda\, t}{t_{1/2}}\right)} \qquad [Eq.\ 3.4]$$

where: t = interval of decay, seconds
λ = decay constant [ln(2) = 0.693], and
$t_{1/2}$ = isotope half-life, s.

For 241-AN-103 data, the uniform date activity may be evaluated as:

$$Activity(t) = 7.5\ E{+}05\ e^{\left(\frac{-0.693 \cdot \left(3.212\ days \cdot \frac{86{,}400\ s}{day}\right)}{30.17\ year \cdot \left(\frac{31{,}556{,}736\ s}{year}\right)}\right)} \left(\frac{\mu Ci}{L}\right)$$

$$= 6.128E{+}05 \left(\frac{\mu Ci}{L}\right) \qquad [Eq.\ 3.5]$$

In this manner, the decayed activities of ^{137}Cs are calculated as:

Tank	^{137}Cs Activity (μCi/L)	
	Sample Data	Decayed Data to 10/01/93
241-AN-103	7.50 E+05	6.13 E+05
241-AP-105	2.85 E+05	2.56 E+05
241-AN-106	2.05 E+05	1.85 E+05
241-AW-101	5.20 E+05	4.83 E+05

In this fashion, and with the half-lives described in Appendix Table 5-1, all data which can be decayed are so calculated. Materials to be generated in the future are not decayed and are so marked.

3.4.2 Evaluation of Dilute Waste Requirements

Current waste acceptance criteria limit the radiolytic heat content of wastes to be disposed to the HGDP. Radiolytic heat loading is a calculation of the heat released to the waste through high energy decay. Limits on such heat loading have been established to adequately protect the disposal system and product grout from excessive temperature during and after operational activities.

The unit established for the evaluation of heat loading of grout waste feeds is the heat provided by the decay of one curie of ^{137}Cs and its metastable daughter ^{137}mBa [$^{137}CsmBa$]. Other high energy decay chains, of those expected

in the wastes, are prorated and summed as described in Hendrickson (1991a) to yield a decay heat evaluation in terms of ^{137}CsmBa heat equivalents. The limiting acceptance value for radiolytic heat loading has been established as 0.3718 Ci ^{137}CsmBa heat equivalents/L (Hendrickson 1991b) at the time of disposal.

Observation of radiolytic heat loading of existent wastes [Appendix Table 1-3] calculated in this fashion, following decay as described in §3.4.1, demonstrates that some wastes would exceed the heat loading limit if disposed in their current form and concentration. Specifically, wastes contained in DST waste tanks 241-AW-101, 241-AN-103, -104, and -105 are each anticipated to exceed the heat loading limit. As such, these wastes must be blended with dilute wastes to reduce the overall radiolytic heat load.

Appendix Table 1-3 calculations yield the volumetric feed fraction (%) at which these wastes may be blended with dilute wastes to yield a mixture at the heat loading limit. Direct calculations of required dilute waste volume and their summation result in the determination that approximately nine million liters (2.39 x 10^6 gallons) of dilute waste are required. The composition of these dilute wastes are discussed in §§2.1 and 2.2 and tabulated in Appendix Table 1-1. The volume and composition of these required dilute wastes are carried throughout subsequent calculations.

3.4.3 Use and Application of Limiting Values

All laboratory analyses have some limit of detection and quantitation. When the concentration of a constituent is below the limit of the method, the analytical value typically reported is the detection or quantitation limit value. Such data is tagged as a "less-than" value. Examples of such "less-than" results are contained within Appendix Tables 2-1 through 2-6 and 3-1 through 3-5. Where such "less-than" data are used within this document, they are acted upon and weighed with other analyses as if they were indeed real values.

This application of limiting values of detection and quantitation as real values is inherently conservative and has the unfortunate side effect of eliminating any estimate of analytical variability (e.g. see Welsh 1991a and 1991b). Thus, despite this shortfall in general statistical validity, it is considered the only reasonable way to handle this data directly while developing generalized inventory estimates.

In keeping with the application of "less-than" values as real values, summary tables (Table 4 and Appendix Tables 1-1, 1-2, 1-4 and 4-1 through 4-3) of this document no longer carry the "less-than" indicators. As is applied in §4.0, the existence and validity of the use of "less-than" values for a constituent may be investigated when the waste constituent is of significant importance.

3.4.4 Analytical Errors

Data used within this evaluation include a broad range of qualified and unqualified data. Errors inherent within any analytical report include those of sampling error as well as random and systematic measurement error.

Analytical summaries, such as those prepared for waste tanks 241-AN-106 and 241-AW-101 (Welsh 1991a and 1991b) have addressed the lack of significant effect of sampling error upon well characterized tanks when those tanks are considered homogenous. In this perspective, reported mean concentrations are considered adequate and often carry standard deviations of approximately 10% to 17%. The overall variance is composed of both sampling and measurement error.

For many data sources used within this document, it is not possible at this time to easily determine whether such analyses were conducted in duplicate, nor whether blanks, matrix spikes and other qualification methods were employed in data generation. Thus, the only available estimates of error on such reports are those of analytical measurement error.

The overall analytical measurement error is composed of two variance components. The first is known as the systematic error variance (S_s^2) and the second is the random error variance (S_r^2). The combined estimate of variance is:

$$S^2 = S_s^2 + \frac{S_r^2}{n} \qquad [Eq.3.6]$$

where n is the number of measurements used to estimate the concentration (the analytical measurement). The systematic error variance is usually estimated through the use of known standards. Examples of laboratory standard errors include percent standard deviations (one standard deviation) of 10.96% for ^{99}Tc at an activity near 2 μCi/L and 17.16% for ^{129}I at an activity near 1 μCi/L. For Westinghouse Hanford Company the laboratory standard results are reported and stored in the LMCS database. The random error variance is usually estimated from the duplicate sample results.

Estimates of these errors, in terms of standard deviation or relative standard deviation, have been computed based on analytical results from samples obtained from Tanks 241-SY-101, 241-AN-106, and 241-AW-101 (Herting et al. 1992; Welsh 1991a and 1992b). Standard deviation is the square root of the variance. The error estimates based on Tank 241-SY-101 sample data (Window E) are found in Tables 7.5, 7.6, and 7.10 in Herting et al. (1992). Although not directly specified, the magnitude of the random error component based on sample data from Tank 241-AN-106, can be obtained from the percent difference data (%Diff.) given in Appendix C of Welsh (1991a). The random error estimates based on Tank 241-AW-101 are found in Table 4 of Welsh (1991b).

For those analytes which are reported as "less than" values, the random analytical error can also be estimated from the analysis of laboratory standards.

The overall tank concentration error is a function of the analytical measurement error and the "degree" of homogeneity within the tank. If the tank is homogeneous, then the overall error is mainly comprised of the analytical error. The random variability within Tank 241-AW-101, which is estimated by the relative standard deviation [RSD] (standard deviation divided by the mean multiplied by 100), can be computed from Table 6 of Welsh (1991b). However, the random error (in terms of RSD) for the overall mean would be the RSD/$\sqrt{n}$. The random variability within Tank 241-AN-106, which is estimated by the relative standard deviation, can be computed from Table 6 of Welsh (1991a). The random error (in terms of RSD) for the overall mean would be the RSD/$\sqrt{n}$. Tank 241-AN-106 is known to be a stratified tank (not homogenous). Thus the within tank variability should be larger than the within tank variability of Tank 241-AW-101.

Overall analytical errors described above are expected to yield standard deviations about data in the region of 10% to 20%. Although sensitivity analyses may apply such error ranges about data in evaluating the environmental impact of waste constituents in the disposal action, the evaluation of a best estimate of overall inventory precludes direct application within this document.

3.4.5 Data Summary

The two basic groups of wastes, the "DSSF Family" and pretreatment family, remain substantially different in source and handling. Thus, the combination of these materials in this evaluation is conducted as the last action.

3.4.5.1 DSSF Family Waste Summary

The DSSF Family waste contribution to the HGDP waste feed projections is a combination of existent concentrated wastes, future concentrated wastes, and dilute wastes. The combination of these materials may be gathered and easily expressed.

Armed with the estimate of diluent waste volume required (§3.4.2), the DSSF family of wastes is collected on Appendix Table 1-2. This table shows the translation from the previous calculations of waste composition, such that each existent concentrated waste is decayed to the uniform decay date of October 1, 1993, by applying Equation 3.4. Dilute wastes and future concentrated wastes are not decayed. A summary of the DSSF family is calculated and presented on Appendix Table 1-2 in the manner of Equation 3.1. This summary is passed forward and presented as the first data column of Table 4.

9413222.1362

3.4.5.2 Grout Waste Feed Projection Summary

A final combination of DSSF family wastes and pretreated wastes is performed in the method of Equation 3.1. Just as the dilute and future concentrated wastes were not decayed to form Appendix Table 1-2, above, pretreated waste composition is not decayed. This is not considered a significant error in that the time of generation of these wastes is not yet known, and as the pretreatment regimes through which this material will pass are expected to remove the majority of intermediate-lived radionuclides (e.g. ^{137}Cesium) and may remove a majority of the long-lived transuranic material.

The resultant composition estimate is provided in Table 4. It must be noted that the third data column (Total Feed) of Table 4 is equivalent to that concentration for an analyte if that analyte is described in only one of the major streams. This is considered a conservative yet necessary assumption when no analysis for the analyte is available.

Certain radionuclides are considered sensitive enough, from a long-term release standpoint, that refinement or affirmation of an estimate contained in Table 4 is warranted. These "special estimates" are described in §4.0 and yield Table 8 which overrides some estimates described in Table 4.

3.5 Recommendations on Data Usage

It is recommended that the information provided herein, when used in summary form, be segmented by the two waste families described. As described in §3.3, fewer analytes are described for two low volume pretreatment streams, errors introduced from the lack of completeness of the preliminary pretreatment flowsheets is not expected to be significant with regard to these low volume streams.

It is recommended that more complete data be developed to accurately estimate the projected volume and concentration profile of future wastes, and that information provided herein as estimates be replaced with actual sample data when such becomes available. Of particular note, high ^{241}Americium data reported for Evaporator campaign 84-3, if representative, may prohibit (Hendrickson 1991b) the disposal of the DSSF wastes in tanks 241-AN-104 and 241-AN-105 without pretreatment.

Information acquisition on these, and other, tank wastes is often complicated by extensive safety precautions. Such precautions, and the development of documentation for such, may effectively prohibit significant information acquisition on these wastes in the near future.

Speciated organic chemical analysis has not been within the analytical compass of the majority of wastes described in this document, and as such, has been omitted herein. Although not described in this document, such analysis must be conducted to ensure that waste feeds remain acceptable for disposal (Hendrickson 1991b).

With the above considerations, the estimates provided within this document are considered to be the most current and complete estimate of waste feed materials to the Hanford Grout Disposal Program and may be used as a guide in regulatory compliance, general flowsheet, and performance assessment activities wherein an order of magnitude accuracy is required. This document, as it describes an average of the inherent differences between waste streams should not be construed to override single stream data for safety analyses or design especially when new data on each waste stream is acquired.

9413222.1364

9413222.1365

THIS PAGE INTENTIONALLY LEFT BLANK

TABLE 4: Grout Treatment Facility Waste Projection (Units: µCi/L for radionuclides, molarity for others unless noted)

Waste Component	DSSF Family	Pretreated Wastes	Total Feed
Ag	8.90 E-05	4.08 E-05	6.48 E-05
Al	4.92 E-01	4.05 E-01	4.48 E-01
As	2.00 E-04	1.97 E-04	1.99 E-04
B		3.37 E-03	3.37 E-03
Ba	4.66 E-05	1.18 E-04	8.22 E-05
Be	1.78 E-03		1.78 E-03
Bi	3.13 E-04		3.13 E-04
Ca	4.24 E-04	7.30 E-03	3.87 E-03
Cd	6.45 E-05	1.60 E-04	1.12 E-04
Ce		1.44 E-04	1.44 E-04
Cr	4.23 E-03	1.92 E-02	1.18 E-02
Cu	1.49 E-04	4.08 E-04	2.79 E-04
Fe	1.78 E-03	1.85 E-02	1.01 E-02
Hg	5.49 E-06		5.49 E-06
K	3.44 E-01	5.65 E-02	2.00 E-01
La		1.15 E-04	1.15 E-04
Li		6.81 E-05	6.81 E-05
Mg	1.61 E-03	4.05 E-03	2.83 E-03
Mn	2.62 E-04	7.03 E-03	3.66 E-03
Mo	4.24 E-04	8.54 E-04	6.40 E-04
Na	6.00 E+00	5.00 E+00	5.50 E+00

Decay Date = 10/01/93

9413222.1366

TABLE 4: Grout Treatment Facility Waste Projection (Units: µCi/L for radionuclides, molarity for others unless noted)

Waste Component	DSSF Family	Pretreated Wastes	Total Feed
Nd		1.20 E-04	1.20 E-04
Ni	6.22 E-04	1.89 E-03	1.26 E-03
P	4.98 E-02		4.98 E-02
Pb	5.37 E-04	1.19 E-04	3.27 E-04
Sb	1.31 E-03	6.13 E-05	6.86 E-04
Se	1.75 E-04	6.13 E-04	3.95 E-04
Si	3.38 E-03	8.77 E-03	6.08 E-03
Ta	1.36 E-05		1.36 E-05
Ti	9.14 E-05	9.95 E-05	9.55 E-05
U (g/L)	1.37 E-03	4.24 E-01	2.13 E-01
V	3.14 E-04		3.14 E-04
W	1.13 E-03		1.13 E-03
Zn	1.66 E-03	4.08 E-04	1.03 E-03
Zr	2.50 E-04	5.09 E-02	2.56 E-02
CN^-	4.01 E-04		4.01 E-04
NH_3	2.03 E-02	3.99 E-03	1.21 E-02
CO_3^{-2}	2.12 E-01	1.12 E-02	1.11 E-01
Cl^-	1.15 E-01	5.51 E-02	8.48 E-02
F^-	1.03 E+00	3.95 E-01	7.14 E-01
SO_4^{-2}	7.63 E-02	6.70 E-02	7.16 E-02
NO_3^-	1.72 E+00	3.76 E+00	2.74 E+00

Decay Date = 10/01/93

TABLE 4: Grout Treatment Facility Waste Projection (Units: µCi/L for radionuclides, molarity for others unless noted)

Waste Component	DSSF Family	Pretreated Wastes	Total Feed
NO_2^-	9.37 E-01	7.42 E-02	5.04 E-01
PO_4^{-3}	2.69 E-02	3.46 E-02	3.07 E-02
OH^-	2.15 E+00	1.55 E-01	1.15 E+00
TOC (g/L)	8.15 E+00	3.54 E-03	4.07 E+00
TIC (g/L)	5.19 E+00		5.19 E+00
SPG	1.29 E+00		
pH	1.35 E+01		
^{3}H	5.07 E+00		5.07 E+00
^{14}C	2.85 E-01	3.71 E+00	2.00 E+00
^{60}Co	3.91 E+01	1.56 E+01	2.73 E+01
^{63}Ni		1.19 E+02	1.19 E+02
^{79}Se	3.03 E+00		3.03 E+00
^{90}Sr	1.82 E+03	2.39 E+04	1.29 E+04
^{94}Nb	4.33 E+01		4.33 E+01
^{95}Nb	5.34 E+01	3.49 E+03	1.78 E+03
^{99}Tc	4.87 E+01	5.47 E+01	5.17 E+01
^{103}Ru	1.29 E+02		1.29 E+02
$^{106}RuRh$	1.62 E+03	2.07 E+03	1.84 E+03
^{113}Sn	1.78 E+02		1.78 E+02
^{129}I	2.18 E-01	2.61 E-02	1.22 E-01
^{134}Cs	5.77 E+02	6.21 E+01	3.19 E+02

Decay Date = 10/01/93

9413222.1368

TABLE 4: Grout Treatment Facility Waste Projection (Units: µCi/L for radionuclides, molarity for others unless noted)

Waste Component	DSSF Family	Pretreated Wastes	Total Feed
^{137}Cs	2.27 E+05	3.67 E+04	1.32 E+05
$^{144}CePr$	9.80 E+02	2.12 E+03	1.55 E+03
^{154}Eu	2.51 E+02	4.79 E+01	1.49 E+02
^{155}Eu	2.85 E+02	4.91 E+01	1.67 E+02
^{226}Ra	1.32 E+03		1.32 E+03
^{234}U	3.37 E-01		3.37 E-01
^{235}U	1.97 E-02		1.97 E-02
^{238}U	7.94 E-02		7.94 E-02
^{237}Np	8.81 E-01	2.90 E-04	4.39 E-01
^{238}Pu	2.23 E-01	9.41 E-02	1.59 E-01
$^{239/240}Pu$	2.09 E+00	3.08 E+00	2.59 E+00
^{241}Am	1.35 E+03	2.78 E+01	6.86 E+02
^{243}Cm	4.14 E-02		4.14 E-02
^{244}Cm	8.92 E-02	1.65 E-02	5.28 E-02
TB	1.56 E+04		1.56 E+04
AT	1.86 E+00		1.86 E+00
Volume (L)	6.08 E+07	6.12 E+07	1.220 E+08

Decay Date = 10/01/93

TABLE 4: Grout Treatment Facility Waste Projection (Units: µCi/L for radionuclides, molarity for others unless noted)			
Waste Component	DSSF Family	Pretreated Wastes	Total Feed
Additional analytes described for pretreated wastes			
^{95}Zr		1.73 E+03	1.73 E+03
^{125}Sb		5.41 E+02	5.41 E+02
^{152}Eu		4.08 E+00	4.08 E+00
^{241}Pu		8.90 E+00	8.90 E+00
^{242}Pu		1.57 E-05	1.57 E-05

Decay Date = 10/01/93

THIS PAGE INTENTIONALLY LEFT BLANK

4.0 SPECIAL ESTIMATES OF CRITICAL ISOTOPES

As described in §3.5, it is recommended that further analytical data be developed for the projection of grout waste estimates. Such additional data will not come rapidly nor inexpensively. In the meantime, however, waste material estimates derived above may either overestimate, underestimate or fail to address waste constituents critical to an assessment of the human and environmental protection afforded by the proposed disposal action (Performance Assessment).

In consideration of this, one may turn to methods other than direct waste analysis in order to evaluate whether such an assessment should consider application of constituent concentrations differing from those described in Table 4.

The purpose of this section is to consider, describe, and apply other methods of waste constituent estimation and to provide recommendations regarding waste constituents currently believed to be potentially critical in evaluation of the proposed disposal action. Sections 4.1 through 4.10 develop estimates and recommendations for waste constituents including ^{241}Am, ^{238}U, ^{237}Np, ^{230}Th, ^{226}Ra, ^{135}Cs, ^{129}I, ^{126}Sn, ^{99}Tc, ^{94}Nb, ^{79}Se, and ^{14}C. Section 4.11 summarizes and tabulates these estimates and recommendations.

Although it may be expected that ^{137}Cs and ^{90}Sr will play a major role in the assessment of disposal actions, estimates based on other than analytical data are not pursued in this section because these materials are routine waste analytes; as such, it is considered inappropriate to override analytical measurements with mathematical estimates.

4.1 ^{135}Cesium Estimation

Cesium-135 is not a routine analyte in waste analyses and is not represented in Table 4. The reasons for this are several and include incapability to chemically separate ^{135}Cs from ^{134}Cs and ^{137}Cs and a half-life five orders-of-magnitude [OM] greater than that of ^{137}Cs and six OM greater than that of ^{134}Cs.

The approach used herein to estimate ^{135}Cs content of wastes to be received at the HGDP is to apply data from the burnup of fuel with results in the form of ^{135}Cs and ^{137}Cs content from which a ratio of production may be made.

Hedengren (1985, 1986) and Hedengren and Goldberg (1987) have conducted calculations using the ORIGEN2 code to determine expectations of fission, actinide, cladding, and activation products from the irradiation of fuel under various conditions. Table 5 contains excerpts of data from these references as they apply to calculations within §4. of this document. The product data of Table 5 derive from ORIGEN2 runs assuming a 12% (^{240}Pu/total Pu) product using mixed Mark IV (80%) and Mark IA (20%) N Reactor fuel. Some benchmarking of ORIGEN2 for N reactor operations has been conducted but the code has not

9413222.372

completed verification and validation. Despite the unvalidated status of this code, it and its results are used within this document as they are expected to be approximately correct and because they provide the only reasonable nonclassified production estimate available at this time.

TABLE 5: ORIGEN2 Yield Per Metric Ton of Fuel (Ci) [For 12% Pu Mixed Mark IV and Mark IA Fuel Five Years After Discharge]

Isotope	Fuel Fission Product	Fuel Actinide Product	Cladding and Fuel Activation Product	Specific Activity (Ci/g)
^{14}C	1.024 E-05		2.023 E-02	4.46 E+00
^{79}Se	3.757 E-02			6.96 E-02
^{94}Nb	9.158 E-06		6.093 E-08	1.90 E-01
^{99}Tc	1.259 E+00		1.736 E-06	1.70 E-02
^{126}Sn	6.490 E-02			2.84 E-02
^{129}I	2.709 E-03			1.76 E-04
^{135}Cs	3.356 E-02			1.15 E-03
^{137}Cs	8.184 E+03			8.65 E+01
^{226}Ra (W)		6.150 E-10		9.89 E-01
^{230}Th		1.697 E-05		2.06 E-02
^{237}Np		2.213 E-02		7.05 E-04
^{238}U		2.656 E-01		3.36 E-07
^{241}Am		4.243 E+01		3.43 E+00
^{241}Pu		4.509 E+03		1.03 E+02

Note: Specific Activities derived from Walker et al. (1989). ^{226}Ra production in terms of watts (W).

As can be seen in Table 5, 0.03356 Ci of ^{135}Cs is produced for every 8,184 Ci of ^{137}Cs. Similar production ratios of other materials will be applied below.

4.1.1 Back-Decay of ^{137}Cesium Data

In order to apply the relative data given above, an estimate for ^{137}Cs is required. The estimate of cesium-137 production can be calculated from analysis at any date after production given the half-life of the material. Thus, where Table 1-2 of the Appendix contains ^{137}Cs data decayed to October 1, 1993, each of these analyses may be back-decayed to an estimated time of material separation.

For purposes of uniformity, the time of fuel discharge is assumed to be October 1, 1977, and fuel processed in PUREX on October 1, 1982. This period of five years between fuel discharge and processing (fuel "cooling" period) is assumed to be a slightly conservative and typical interval necessary in these and later calculations involving the ingrowth of radioisotopes. Fuel cooling periods of five years have been assumed in subsequent calculations to compensate for the ingrowth of radioactive isotopes; these may be significant when the parent radionuclide is present in high concentration in the irradiated fuel (e.g. ^{230}Th ingrowth from alpha decay of ^{234}U).

Although not all of the wastes described here were processed, sampled, or concentrated by the above dates, they provide a reasonable average fuel discharge date, and consequent initial generation and decay of cesium-137. Applying a half-life of 30.17 years and a decay time of -11 years to the ^{137}Cs data on Appendix Table 1-2 results in cesium activities, at that time, of 20.7 million curies. Details of this calculation are provided in Table 6, below.

It should be noted that close agreement between ^{137}Cs estimates may be found between that provided above and through the Integrated Data Base (DOE 1991 [Table 2-17]) (IDB). Back-decay of IDB data to October 1982 would yield ^{137}Cs activity in tanks to be 21.1 x 10^6 Ci.

4.1.2 ^{135}Cesium Production

The estimate of ^{135}Cs production may be made as the ORIGEN2 ratio of ^{135}Cs production to ^{137}Cs production times the analytical estimate of production five years after discharge of ^{137}Cs and computed as:

$$Cs\text{-}135\ (Ci) = \frac{0.03356\ Ci\ Cs\text{-}135}{8{,}184\ Ci\ Cs\text{-}137} * 20{,}663{,}000\ Ci\ Cs\text{-}137 \quad [Eq.\ 4.1]$$
$$= 84.73\ Ci\ Cs\text{-}135$$

For the purposes of the Performance Assessment, correction of this activity through decay to current values is insignificant (>99.9996% remaining in 1993) and thereby neglected.

TABLE 6: Waste ^{137}Cs Activity [Decay Date 10/1/1982]			
Tank	Cs-137 (Ci/L)	Volume (L)	Cs-137 (Ci)
106-AN	0.238	3,667,985	874,094
101-AW	0.622	3,826,969	2,378,645
105-AP	0.329	3,145,609	1,035,247
104-AN	0.973	3,024,479	2,941,880
105-AN	0.649	4,269,852	2,772,392
103-AN	0.789	3,546,854	2,798,393
Future DDSSF	0.156	30,282,640	4,713,889
Dilutes	0.02863	9,045,989	259,014
Pretreated	0.0472	61,164,750	2,889,253
Total		121,975,126	20,662,806

4.1.3 ^{135}Cesium Estimate Usage

The estimate of ^{135}Cs production given above as 84.7 Ci is greater than the reported current activity of 59.2 Ci within the IDB (DOE 1991 [Table 2-17]). Waste content of ^{135}Cs is not described within the HDW-EIS. At this time, no information has been identified which would suggest that ^{135}Cs has been preferentially separated from ^{137}Cs in any Site operations (chemically identical); thus reduction of either of these two estimates by any referencable factor is not reasonable.

In reference to the two estimates derived or given above, it is recommended that grouted waste inventory calculations use a base case not exceeding a maximum ^{135}Cs concentration applying the ORIGEN2 and analytically derived estimate of 0.695 μCi/L. Sensitivity analyses may be pursued of 0.485 μCi/L corresponding to IDB estimates of site inventory.

4.2 ^{237}Neptunium Estimation

An improved estimate of ^{237}Np is sought in this section due to the minimal data provided in reference information. Further complicating this estimate is the ingrowth of ^{237}Np from the alpha decay of ^{241}Am. This ingrowth is not explicitly incorporated in the transport and dose codes to be used in performance assessments, but the input may be manipulated to account for the ingrowth of the americium as its half-life is only 432.7 years compared to the neptunium half-life of 2.14 million years.

4.2.1 Revision of ^{241}Americium Estimates

The americium contained within the waste streams is the result of neutron bombardment of fuel and the ingrowth from beta-decay of ^{241}Pu. Under the conditions of burnup described in §4.1, Hedengren and Goldberg (1987, page I17), provide a five year post-discharge yield of 42.43 Ci ^{241}Am per metric ton of fuel. Using a calculation in the form of Equation 4.1, ^{241}Am content of wastes decayed to October 1993, would be 105,256 Ci. The IDB estimate of ^{241}Am in all Hanford Double-Shell wastes decayed to October 1993 is 52,253 Ci (DOE 1991).

The difficulty remains with estimation of realistic activities of the wastes. As can be seen in Appendix Tables 3-1 through 3-5, 4-3, and 1-2, the overall "DSSF Family" americium estimate of Table 4 is driven by one sample analysis from Evaporator Campaign 84-3 (Certa 1985). If this analytical value of 11,400 μCi/L accurately represents both tanks 241-AN-104 and 241-AN-105, the americium content of these tanks would be 83,155 Ci; clearly this activity, in excess of IDB estimates, is not reasonable. If the analytical value represented only that portion of 241-AN-104 which has above been attributed from Campaign 84-3, this portion of material would include 6,408 Ci of ^{241}Am. This is a possible, but not highly realistic value.

Omitting the analytical americium datum of Campaign 84-3, no data is available to consider for DSSF tanks 241-AN-104 and 241-AN-105. In the overall manner of this document, the preferred method of estimation should be that of bridging a data gap. Data may be bridged in this instance by choosing a maxima or by interpolation based upon other parameters, such as is depicted in Figure 3 of §3.0. Data does remain for other DSSF wastes, and may form a basis for revising the estimate.

4.2.1.1 TRU Limitation in DSSF Waste

Waste feeds to the HGDP are limited by regulatory requirements to a maximum of 100 nanocuries of transuranic (TRU) material per gram of waste (Hendrickson 1991b). Given the density of wastes contained within tanks 241-AN-104 and 241-AN-105, a maximum ^{241}Am concentration within these wastes is 153 μCi/L. Use of such a concentration is acceptable as a bounding value as these wastes would require pretreatment for TRU removal were they any higher. The use of this concentration is a factor of almost seventy-five below the analytically reported values (see §4.2.1 and Appendix Table 1-2) of other DSSF wastes.

A summary of the estimate of overall ^{241}Am to be received by the HGDP under the assumption that 241-AN-104 and -105 are at their TRU limits is contained in Table 7. These sources are ranked by expected contribution. It should be noted that the volumes described in Table 7 do not exactly equal those of Table 6 as no americium estimate for NCAW pretreatment streams 13 are provided in Lowe (1991); differences due to these small volume streams (0.37% of pretreatment volumes) are neglected in further calculations of this section.

TABLE 7: ^{241}Americium Sources [Decay Date 10/01/82]

Source	Am-241 (Ci/L)	Volume (L)	Am-241 (Ci)	Mean (Ci/L)
NCAW 2AZ	3.20 E-04	3.50 E+06	1,118.53	
DSSF (4AN/5AN Max.)	1.53 E-04	7.29 E+06	1,114.99	
PFP	1.76 E-04	2.08 E+06	366.29	
CC	3.05 E-06	3.90 E+07	119.08	
NCAW 1AZ	3.39 E-05	3.49 E+06	118.28	
DDSSF	8.96 E-07	3.03 E+07	27.14	
DSS/DSSF (not 4AN/5AN)	1.37 E-06	1.42 E+07	19.37	
NCRW 5AW	8.63 E-07	5.30 E+06	4.57	
Dilutes	1.04 E-07	9.05 E+06	0.94	
NCRW 3AW	9.96 E-08	7.57 E+06	0.75	
Total		1.22 E+08	2,889.94	2.374 E-05
Decayed to 10/01/93				2.33 E-05

Note: This assumes that tanks 241-AN-104 and -105 are bounded in ^{241}Am content at 100 nCi/g. NCAW 2AZ concentration believed to be erroneously high.

Relative contributions of ^{241}Am from projected waste feeds for this assumption are depicted in Figure 4. This image emphasizes the expectation that the vast majority (>98%) of ^{241}Am to be received in HGDP wastes is to be contained in pretreated waste streams and assumed maxima within DSSF tanks 241-AN-104 and 241-AN-105. Such an estimate, in conjunction with the impacts of near-surface disposal of this material, may be the basis for extended pretreatment to remove additional transuranic material.

4.2.1.2 Concentration Factor Evaluation in DSSF Waste

Although a conservative bound for ^{241}Am content may be found in §4.2.1.1, it is possible to use the observations depicted in Figure 3 to arrive at an estimate of ^{241}Am content in tanks 241-AN-104 and -105. Those concentrated waste tanks for which reasonable americium data are available include tanks 241-AN-106, 241-AW-101, 241-AN-103, and an estimate based on processing of 241-AP-105. The temporary exclusion of dilute, future concentrate, and pretreated wastes is necessary for this estimate as will be evident below.

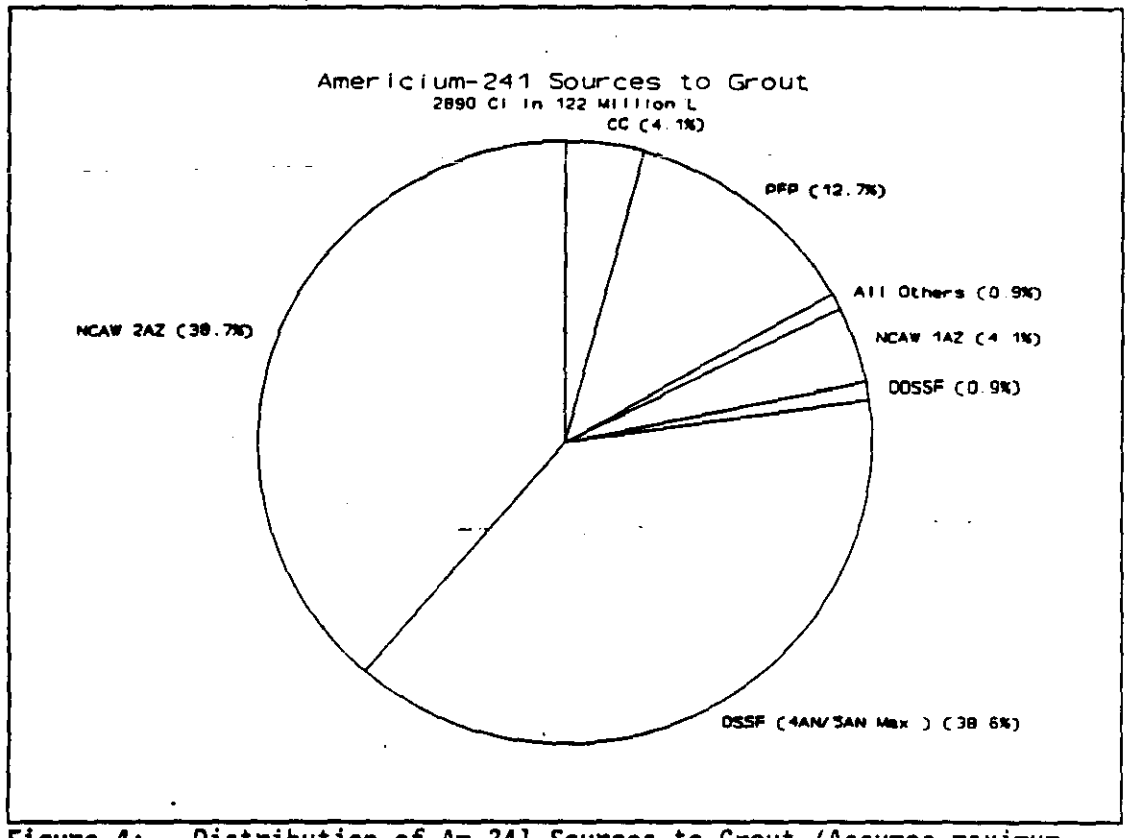

Figure 4: Distribution of Am-241 Sources to Grout (Assumes maximum allowable in 4AN/5AN)

Back-decay of ^{241}Am data for these four concentrated waste tanks to 1982 and comparing these data to waste sodium content, in the manner of Figure 3, provides a linear regression characterized by Equation 4.2 with a correlation coefficient of nearly 92%. This is considered a good fit and may allow global estimation of ^{241}Am content based upon sodium content. Applying waste volumes and sodium concentrations of the existent concentrated DSSF family wastes, one arrives at a weighted mean sodium molarity of 9.87 mol/L.

$$Am\text{-}241\ (\mu Ci/L) = 0.13867 * Na\ (M) + 0.16508 \quad [Eq.\ 4.2]$$

Applying this sodium concentration to Equation 4.2 yields a mean estimate of 1.533 µCi ^{241}Am/L for these 21.48 million liters (32.93 Ci). Continued calculation in the manner of Table 7 results in an overall estimated concentration of 14.4 µCi/L.

As described above, dilute and future concentrate wastes were not considered in the linear regression. The basis of this exclusion is that analytical data

on those wastes do not support the above regression; in fact, Equation 4.2 would predict approximately twice as much americium than has been analytically reported in the dilute wastes.

It is postulated that previous americium and cesium sources in the waste streams to the DSTs have slowly decreased in content of these materials with serial facility shutdowns. In this respect, the analytical estimates for dilute and future concentrates as described above will be conservative.

Pretreated waste streams should not follow Equation 4.2 as it is the express intent of such pretreatment to remove transuranic material. Thus, the flowsheets (Lowe 1991) continue to provide the appropriate estimation basis for these wastes.

4.2.1.3 Usage of ^{241}Americium Estimates

Revised estimates of americium content of HGDP waste feeds in §§4.2.1.1 have resulted in an expectation of a mean ^{241}Am content of 23.32 μCi/L [decay date 10/01/93] over all wastes. This estimate is recommended as a base case when applying such data. Three sensitivity case evaluations, each decayed to 10/01/93, of americium content beyond the base case are most well supported as:

Case I:	Linear regression of americium data relative to sodium content (Eq. 4-2) to describe existent concentrated DSSF Family wastes while using remainder of base case; 1,757.9 Ci (14.4 μCi/L), and
Case II:	IDB basis; 52,253 Ci (428.4 μCi/L).
Case III:	Production and decay, related to waste ^{137}Cs content [analogous to Eq. 4.1] for DSSF Family wastes plus pretreated waste estimate; 105,256 Ci (863 μCi/L).

A case for estimation based on IDB less that pretreated material to be shipped to the Hanford Waste Vitrification Project is untenable as the pretreatment flowsheet estimates (Lowe 1991) of material fed to pretreatment exceed ^{241}Am estimates of the IDB by greater than one OM. The HDW-EIS (DOE 1987 [Table 5.47]) anticipated 17,000 Ci of ^{241}Am in near-surface barriered disposal; this activity, in view of the span of the above cases, is sufficiently close to those cases that establishment of an another case for this estimate is not considered necessary.

4.2.2 Revision of ^{237}Neptunium Estimates

As described above, the neptunium contained within the waste streams is the result of bombardment of fuel ($^{235}U \xrightarrow{n} {}^{236}U \xrightarrow{n} {}^{237}U \xrightarrow{\beta} {}^{237}Np$) and the ingrowth from decay of ^{241}Pu and ^{241}Am. Under the conditions of burnup described in §4.1, Hedengren and Goldberg (1987 pages I15 and I17), provide yields of 4,509 Ci ^{241}Pu (43.78 g), 42.43 Ci ^{241}Am (12.38 g), and 0.02213 Ci ^{237}Np (31.40 g) per metric ton of fuel five years after discharge.

4.2.2.1 Production Estimation of ^{237}Neptunium

As described above, it is obvious that a calculation in the form of Equation 4.1 and subsequent decay would yield an inordinately large estimate of the neptunium and americium decay daughters of the plutonium. More simply, this type of relationship would not be appropriate as the plutonium has been extracted in fuel processing. Fractional retention of ^{241}Pu in the waste stream yields a negligible difference in the ^{237}Np content as a result of decay, thus an approximation of complete ^{241}Pu removal in fuel processing may be used. In the manner of Equation 4.1, a production estimate of ^{237}Np would be 55.87 Ci which, with additional decay from ^{241}Am (assuming 100% yield of ^{237}Np), would yield a 1993 estimate of 55.88 Ci ^{237}Np.

4.2.2.2 Usage of ^{237}Neptunium Estimates

A revised estimate, based on production, of neptunium content of HGDP waste feeds in §4.2.2.1, would result in the expectation of a mean ^{237}Np content of 0.458 μCi/L. The IDB estimate of 45.1 Ci, would yield a mean of 0.37 μCi ^{237}Np/L. As presented in Table 4, an analytically based estimate of content would be 53.6 Ci with a mean concentration of 0.439 μCi/L.

It is recommended that the base case of waste evaluation, when such is applied in long term dose assessments, remain that provided in Table 4. Two sensitivity cases, one of lower activity and one higher, may be supported with the IDB estimate and the expected production (§4.2.2.1) estimate, respectively. As each of these sensitivity cases is within a factor of two of the recommended base case, it is noted that inaccuracies or differences in transport modeling may obviate any long term dose sensitivity due to such a minor variance in waste activity.

4.3 ^{226}Radium Estimation

Radium-226 is produced within irradiated fuel and is a daughter of ^{230}thorium. Its radioactive daughters follow the decay chain of ^{226}Ra → ^{222}Rn → ^{218}Po → ^{214}Pb → ^{214}Bi → ^{214}Po → ^{210}Pb → ^{210}Bi → ^{210}Po → ^{206}Pb (stable), where the decays between, and following, radon and lead-210 are rapid. Lead-210 is unstable but has a much greater half-life than the intermediate daughters. A better estimate of the content of ^{226}Ra in the waste is required as significant quantities of ^{226}Ra may result in large dose consequences due to the decay of it and its daughters over the period of the Performance Assessment.

The estimate of ^{226}Ra given in Table 4 is derived from analyses of current dilute waste tanks (see §3.1.1). Data reported from these wastes are "less-than" values (see Appendix Tables 2-1 through 2-6) resulting in an extrapolated DSSF Family concentration of 1,325 μCi/L. Such an estimate would indicate expected disposal of 80,551 Ci of ^{226}Ra in DSSF Family wastes. This large estimate is not consistent with the absence of discussion of this isotope within the IDB and the HDW-EIS.

Lacking any other analytical data on this isotope, the waste content may again be approximated in the manner of §4.1.2, based upon production. Hedengren and Goldberg (1987) encompass the production of ^{226}Ra within fuel irradiation. However, due to the necessity to limit the publication of what was felt to be extraneous data (many zeros would be displayed and printed in the document if a limiter had not been applied) ^{226}Ra data is only displayed within tables of thermal power rather than directly in tables of mass or activity. Table I9 (Hedengren and Goldberg 1987, page I20) provides the thermal power of ^{226}Ra five years after discharge to be 6.15 x 10^{-10} watts. Browne et al. (1986) provide the delta of the alpha decay of ^{226}Ra to ^{222}Rn to be approximately 4.77 Mev/dis. Thus, the thermal power at that time may be calculated in terms of activity as:

$$Q\left(\frac{W}{Ci}\right) = \frac{4.77\ Mev}{dis} \times \frac{1.60219E\text{-}06\ erg}{Mev} \times \frac{1E\text{-}07\ Ws}{erg} \times \left(\frac{\frac{3.70E{+}10\ dis}{s}}{Ci}\right) \quad [Eq.\ 4.3]$$
$$= 2.8277E\text{-}02\ \left(\frac{W}{Ci}\right)$$

$$Ra\text{-}226\left(\frac{Ci}{tonne}\right) = \left(\frac{\frac{6.15E\text{-}10\ W}{tonne}}{\frac{2.828E\text{-}02\ W}{Ci}}\right) = 2.175\ E\text{-}08\ \left(\frac{Ci}{tonne}\right) \quad [Eq.\ 4.4]$$

$$Ra\text{-}226\ (Ci) = \frac{2.175E\text{-}08\ Ci\ Ra\text{-}226}{8{,}184\ Ci\ Cs\text{-}137} * 140{,}280{,}000\ Ci\ Cs\text{-}137 \quad [Eq.\ 4.5]$$
$$= 3.73\ E\text{-}04\ Ci\ Ra\text{-}226$$

Note that the ^{137}Cs value of Equation 4.5 is not that developed for and used in Equation 4.1. This higher ^{137}Cs number is derived from two sources in addition to that activity described in Table 6. The use of this higher value is in part due to the acknowledgement that lack of data on pretreatment flowsheets <u>does not</u> indicate the absence of a waste component. Explicitly, waste sources have or will have ^{137}Cs removed from the streams in processes which do not effect the removal of other analytes.

Pretreated waste streams may be corrected for ^{137}Cs content as an 11 year back-decayed ^{137}Cs estimate of material fed to pretreatment operations (Lowe 1991), thereby replacing the pretreated activity of 2.25 million curies of Table 6 with 46.41 million curies.

Both pretreated wastes and general DST contents may be corrected due to cesium scavenging in B Plant operations based upon cesium capsule content. This type

of correction recognizes that material separated from the product capsules was returned to single- and double-shell tanks. Current ^{137}Cs capsule content is described within the IDB (DOE 1991) as 59.2 million curies decayed to December 31, 1991. Back-decaying this activity to October 1, 1982 yields an activity of 73.21 million curies. Lacking determinate data on the destination of specific fractions of these byproduct liquids, it is herein assumed that the target analyte produced during the production of 73 million Ci of ^{137}Cs has been entirely transferred into materials destined for near-surface disposal.

Open literature discussion of pertinent aspects of chemistry and chemical separations of cladding and fuel are provided by Cotton (1989), Hodgson et al. (1985), Swanson (1988), and GE (1955).

Thus, use of a summation of 140.28 million Ci value assumes that the target isotope of this calculation is entirely deposited in grout waste.

This estimate of a total content of 3.73×10^{-4} Ci of ^{226}Ra is 9 OM lower than the estimate guided by the analytical values reported. One must note, however, that the analytical values reported were "less-than" values and were reported as the detection limit for this isotope. In the above regards, the recommended base case estimate for this isotope is 3.06×10^{-6} μCi/L, corresponding to the ORIGEN2 calculation as applied above. A calculated ^{230}Th parent concentration of 2.38×10^{-3} μCi/L should be included in the base case for further ingrowth of ^{226}Ra. With no further information available, no sensitivity cases are recommended.

Although caution may be advisable in the ORIGEN2 based estimate of ^{226}Ra, should ORIGEN2 errors result in actual activities several OM greater than described, it is expected that such activities will remain of little consequence in long term dose assessment.

4.4 ^{129}Iodine Estimation

Iodine-129 is a fission product within irradiated fuel. Its presence within the waste feed is of potential concern due to its greater than 15 million year half-life and expected mobility in soil systems.

Several estimates may be made of expectations of ^{129}I concentration within grout feed wastes. The IDB (DOE 1991 [Table 2-17]) estimates site inventory to be 0.265 Ci. Calculations resulting in iodine concentrations described in Table 4 would indicate that a total of 14.8 Ci ^{129}I would be disposed. Calculation in the form of Equation 4.5, using ORIGEN2 (Hedengren 1985 [Case I, page I34]), would indicate production of 46.4 Ci. The HDW-EIS (DOE 1987 [Table 5.47]) indicated an expectation of no more than 34 Ci to be placed in near-surface disposal.

Although it would obviously be beneficial to demonstrate that IDB estimates of site inventory limit ^{129}I disposition in grout wastes, the magnitude of investigation required to substantiate such is not within the scope of this

of correction recognizes that material separated from the product capsules was returned to single- and double-shell tanks. Current ^{137}Cs capsule content is described within the IDB (DOE 1991) as 59.2 million curies decayed to December 31, 1991. Back-decaying this activity to October 1, 1982 yields an activity of 73.21 million curies. Lacking determinate data on the destination of specific fractions of these byproduct liquids, it is herein assumed that the target analyte produced during the production of 73 million Ci of ^{137}Cs has been entirely transferred into materials destined for near-surface disposal.

Open literature discussion of pertinent aspects of chemistry and chemical separations of cladding and fuel are provided by Cotton (1989), Hodgson et al. (1985), Swanson (1988), and GE (1955).

Thus, use of a summation of 140.28 million Ci value assumes that the target isotope of this calculation is entirely deposited in grout waste.

This estimate of a total content of 3.73×10^{-4} Ci of ^{226}Ra is 9 OM lower than the estimate guided by the analytical values reported. One must note, however, that the analytical values reported were "less-than" values and were reported as the detection limit for this isotope. In the above regards, the recommended base case estimate for this isotope is 3.06×10^{-6} μCi/L, corresponding to the ORIGEN2 calculation as applied above. A calculated ^{230}Th parent concentration of 2.38×10^{-3} μCi/L should be included in the base case for further ingrowth of ^{226}Ra. With no further information available, no sensitivity cases are recommended.

Although caution may be advisable in the ORIGEN2 based estimate of ^{226}Ra, should ORIGEN2 errors result in actual activities several OM greater than described, it is expected that such activities will remain of little consequence in long term dose assessment.

4.4 ^{129}Iodine Estimation

Iodine-129 is a fission product within irradiated fuel. Its presence within the waste feed is of potential concern due to its greater than 15 million year half-life and expected mobility in soil systems.

Several estimates may be made of expectations of ^{129}I concentration within grout feed wastes. The IDB (DOE 1991 [Table 2-17]) estimates site inventory to be 0.265 Ci. Calculations resulting in iodine concentrations described in Table 4 would indicate that a total of 14.8 Ci ^{129}I would be disposed. Calculation in the form of Equation 4.5, using ORIGEN2 (Hedengren 1985 [Case I, page I34]), would indicate production of 46.4 Ci. The HDW-EIS (DOE 1987 [Table 5.47]) indicated an expectation of no more than 34 Ci to be placed in near-surface disposal.

Although it would obviously be beneficial to demonstrate that IDB estimates of site inventory limit ^{129}I disposition in grout wastes, the magnitude of investigation required to substantiate such is not within the scope of this

document. Further, as this case is one wherein the disposal inventory would be much smaller than the next lowest estimate, the application of any of the other expressed estimates would bound such an impact analysis.

It is recommended that the base case of waste evaluation be that provided in Table 4 of 0.122 µCi/L. Two sensitivity cases based upon ORIGEN2 and the HDW-EIS are supportable with estimates of 0.381 µCi/L and 0.279 µCi/L, respectively.

4.5 ^{126}Tin Estimation

Tin-126 is a fission product within irradiated fuel. Its presence within the waste feed is of potential concern due to its 100,000 year half-life and the very short half-life (12.4 days) of its radioactive daughter ^{126}Sb.

^{126}Sn is not a typical analyte and is not described within Table 4 or the HDW-EIS. The IDB (DOE 1991 [Table 2.17]) describes a tank inventory of 104 Ci. Calculation in the manner of Equation 4.5 yields an estimate of 1,112 Ci based upon ORIGEN2 data (Hedengren 1985 [Case I, page I33]).

The recommended base case in long term dose assessment is that of waste concentrations of 9.12 µCi/L based upon production. A sensitivity case is available as 0.853 µCi/L based upon IDB inventory but is not highly recommended.

4.6 ^{99}Technetium Estimation

Technetium-99 is primarily generated as a fission product in irradiated fuel and in activated cladding associated with irradiated fuel. In addition, it is generated from the decay of ^{99}Mo. For the purposes of this document and reality, complete molybdenum-99 decay occurs during fuel cooling. ^{99}Tc is again a concern in long term performance assessment due to its half-life of 213,000 years and potential mobility.

Table 4 estimates of ^{99}Tc disposal total to 6,311 Ci. The IDB (DOE 1991 [Table 2.17]) describes tank inventories of 13,300 Ci. The HDW-EIS (DOE 1987 [Table 5.47]) envisioned near-surface disposal of 19,000 Ci. Production estimates based upon Equation 4.5 yield 21,581 Ci. Technetium as an activation product has been neglected from the above calculations as the fission production outweighs activation by 6 OM (Hedengren 1985 and 1986).

In view of the proximity of Table 4 estimates (based upon waste analyses) to production and pretreatment estimates, the recommended base case for waste evaluation is that described in Table 4 of 51.74 µCi/L. Sensitivity cases for evaluation would be those of production at 176.9 µCi/L and of IDB inventory at 109 µCi/L.

4.7 ^{94}Niobium Estimation

Niobium-94 present within irradiated fuel, cladding, and resultant waste is primarily generated by neutron activation of ^{93}Nb (stable) and fission. ^{94}Nb retains a half-life of 20,000 years. A better estimate of waste content of this isotope is required due to its relatively long half-life, calculated concentrations (Table 4), and possible waste zone intrusion.

Table 4 DSSF Family estimates of ^{94}Nb are 43.3 µCi/L (2,634 Ci in that volume). Thorough research of ^{94}Nb data reported from these wastes indicates that these data are "less-than" values (see Appendix Tables 3-1 through 3-5 and 4-1 through 4-3 and their references). No information is provided in Lowe (1991) on niobium-94 concentrations, however, application of Equation 4.5 provides an ORIGEN2 fission and activation production of 0.158 Ci. This small estimate of ^{94}Nb may be the reason that this material is not described within either the IDB (DOE 1991) or the HDW-EIS (DOE 1987).

It is recommended that the base case of waste evaluation be that provided by production as a mean concentration of 1.30×10^{-3} µCi/L. This case considers analytical data (including "less-thans") and the relatively negligible production estimate described above. As no further information is available for consideration at this time, no sensitivity case is recommended in waste evaluation.

4.8 ^{79}Selenium Estimation

Selenium-79, with a half-life of 65,000 years, is generated by fission. A better estimate of waste content of this isotope is required due to its relative mobility and possible waste zone intrusion.

Table 4 DSSF Family estimates of ^{79}Se are 3.03 µCi/L (185 Ci in that volume). No information is provided in Lowe (1991) on selenium-79 concentrations, however, application in the form of Equation 4.5 provides an ORIGEN2 production (Hedengren 1985 [page I26]) estimate of 644 Ci. IDB (DOE 1991 [Table 2.17]) estimates of ^{79}Se in tanks total 65.8 Ci. The HDW-EIS (DOE 1987 [Table 5.47]) anticipated the placement of 260 Ci of ^{79}Se in near-surface disposal.

The recommended base case of waste evaluation is that described by Table 4 estimates of 3.03 µCi/L. This base case is greater than possible sensitivity cases of 0.54 µCi/L and 2.13 µCi/L based upon the IDB and HDW-EIS, respectively, and lower than a sensitivity case of 5.28 µCi/L based upon production.

4.9 ^{14}Carbon Estimation

Carbon-14 present within irradiated fuel, cladding, and resultant waste is primarily generated by neutron activation of natural carbon (^{12}C and ^{13}C) present in fuel and cladding as impurities. ^{14}C retains a half-life of 5,730

years. A better estimate of waste content of this isotope is required due to its expected concentrations (Table 4), and possible waste zone intrusion.

Table 4 estimates of ^{14}C including both analytical support for DSSF Family wastes and pretreatment projections yield waste expectations of 2.00 μCi/L (244 Ci in total volume). Applications of Equation 4.5 yield fission and activation product (Hedengren 1985 and 1986) expectations of 347 Ci of ^{14}C in the waste to be received. IDB (DOE 1991) estimates of ^{14}C in tanks total 569 Ci. The HDW-EIS (DOE 1987 [Table 5.47]) anticipated the placement of 2,300 Ci of ^{14}C in near-surface disposal.

Because of the analytical support provided for Table 4 estimates, the recommended base case for waste evaluation remains that of Table 4. Sensitivity cases available for evaluation are suggested based on production and the IDB at concentrations of 2.84 μCi/L and 4.66 μCi/L, respectively.

4.10 ^{238}Uranium Estimation

Uranium-238 is present within irradiated and non-irradiated fuel due to its abundance of approximately 99.1%. ^{238}U has a half-life of approximately 4.5 x 10^9 years and undergoes alpha and beta decay along the pathway $^{238}U \rightarrow {}^{234}Th \rightarrow {}^{234}Pa \rightarrow {}^{234}U \rightarrow {}^{230}Th$. Decay of ^{230}Th is described in §4.3, above. Due to the long-term impact of this decay chain of long-lived materials leading to a short-lived gaseous daughter, a better estimate of this material is sought.

Table 4 DSSF Family estimates of ^{238}U, based solely on analysis of tank 241-AN-103 and dilute evaporator feeds, result in expectations that 4.8 Ci would be disposed with these wastes. Lowe (1991) does not describe estimates of ^{238}U in feed materials to pretreatment operations. The IDB describes an estimate of 0.945 Ci (~2,800 kg) present in tank wastes. The HDW-EIS anticipated 20 Ci to be placed in near-surface disposal. Although a substantially larger amount of ^{238}U has been handled with the processing of irradiated fuel, IDB and HDW-EIS estimates are imbedded with an assumption of 99% extraction of uranium and plutonium from irradiated fuel (GE 1955). For this reason, production estimates may not be made in the manner of §4.1.2.

Although only limited analytical data supports ^{238}U estimates in the vicinity of that described by the IDB, the recommended base case for waste evaluation is that of the analytical concentrations in DSSF Family wastes (0.079 μCi/L). A suggested sensitivity case is that of the IDB at 7.75 x 10^{-3} μCi/L. At this time no sensitivity case is suggested which would entail the OM increase anticipated in the HDW-EIS.

4.11 Special Estimate Summary

Table 8, below, contains a summary of recommendations for base case and sensitivity case waste evaluations developed in §§4.2 through 4.10. As supported by the individual development of these special estimates, the constituent concentrations of these recommended base and sensitivity case estimates should replace or amend those displayed in Table 4 when such is used in the evaluation of the waste or proposed disposal action. Described above, the use of IDB and HDW-EIS estimates are not recommended within this document as they have not be subjected to a comprehensive review nor have their predictions been verified against actual sample data; as such, any such use may only be considered for sensitivity cases.

9413222.1307

TABLE 8: Special Estimates of Critical Isotopes

Isotope	Recommended Base Case Waste Concentration (μCi/L)	Recommendation Basis	Sensitivity Case Concentrations (μCi/L) and Bases	
^{241}Am	23.3	Waste Analysis/ Limited 4AN/5AN	14	Waste Analysis/Linear Regression 4AN/5AN
			440	IDB
			860	Production[2]
^{238}U	0.08	Waste Analysis	0.01	IDB
^{237}Np	0.44	Waste Analysis	0.37	IDB
			0.46	Production
^{230}Th	2.4 E-03	Production		None
^{226}Ra	3 E-06	Production		None
^{135}Cs	0.69	Production	0.49	IDB
^{129}I	0.12	Waste Analysis	0.38	Production
			0.28	HDW-EIS
^{126}Sn	9.1	Production	0.85	IDB
^{99}Tc	51.7	Waste Analysis	180	Production
			110	IDB
^{94}Nb	1.3 E-03	Production		None
^{79}Se	3.0	Waste Analysis	0.5	IDB
			2.1	HDW-EIS
			5.3	Production
^{14}C	2.0	Waste Analysis	2.8	Production
			4.7	IDB

[2] Production [=] Application of ORIGEN2 data to waste ^{137}Cs content.

9413222.1380

5.0 REFERENCES

Browne, E., R. B. Firestone and V. S. Shirley, Table of the Radioactive Isotopes, John Wiley & Sons, New York, NY, 1986.

Certa, P. J., 1985, "242-A Evaporator/Crystallizer FY 84 Campaign Run 84-3 Post Run Document," SD-WM-PE-018, April 30, 1985.

Cotton, F. Albert, and G. Wilkinson, 1989, *Advanced Inorganic Chemistry, Fifth Edition*, John Wiley & Sons, New York, NY, 1989.

DOE, 1987, *Final Environmental Impact Statement, Disposal of Hanford Defense High-Level, Transuranic and Tank Wastes, Hanford Site, Richland, Washington*, DOE/EIS-0113, U. S. Department of Energy, December 1987.

DOE, 1988, "Record of Decision," Federal Register, 53 FR 12449, April 14, 1988.

DOE, 1991, *Integrated Data Base for 1991: U. S. Spent Fuel and Radioactive Waste Inventories, Projections, and Characteristics*, DOE/RW-0006, Revision 7, October 1991, U. S. Department of Energy, Washington, D. C.

GE, 1955, *PUREX Technical Manual*, HW-31000DEL, General Electric Company, Richland, WA, March 25, 1955. Publicly released August 6, 1992.

Gratny, E. G., 1985, "242-A Evaporator/Crystallizer FY'84 Campaign 84-5 Post Run Document," SD-WM-PE-022, September 4, 1985.

Hanlon, B. M., 1992, "Tank Farm Surveillance and Waste Status Summary Report for February 1992," WHC-EP-0182-47, May 1992.

Hedengren, D. C., 1985, "ORIGEN2 Predictions of N Reactor Fuel Fission Product Composition," SD-CP-TI-077, Revision 0, March 14, 1985.

Hedengren, D. C., 1986, "ORIGEN2 Predictions of N Reactor Cladding and Fuel Activation Product Composition," SD-CP-TI-094, Revision 0, November 11, 1986.

Hedengren, D. C., and H. J. Goldberg, 1987, "ORIGEN2 Predictions of N Reactor Fuel Actinide Composition," SD-CP-TI-105, Revision 1, August 4, 1987.

Hendrickson, D. W., 1990, "Methods and Data for Use in Determining Source Terms for the Grout Disposal Program," SD-WM-TI-355, Revision 1, March 22, 1990.

Hendrickson, D. W., 1991a, "Radiolytic Heat Loading Calculation Methods for the Hanford Grout Disposal Facility," WHC-SD-WM-TI-455, Revision 0, January 2, 1991.

Hendrickson, D. W., 1991b, "Grout Treatment Facility Waste Feed Acceptance Criteria," WHC-SD-WM-RD-019, Revision 1, October 18, 1991.

Hendrickson, D. W. and T. L. Welsh, 1992a, "Tank 241-AP-106 Sampling and Characterization Plan," WHC-SD-WM-TP-117, Revision 0, January 30, 1992.

Hendrickson, D. W. and T. L. Welsh, 1992b, "Tank 241-AP-105 Sampling and Characterization Plan," WHC-SD-WM-TP-130, Revision 0, April 16, 1992.

Herting, D. L., D. B. Bechtold, B. E. Hey, B. D. Keele, L. Jensen, and T. L. Welsh, 1992, "Laboratory Characterization of Samples Taken in December 1991 (Window E) From Hanford Waste Tank 241-SY-101," WHC-SD-WM-DTR-026, Revision 0, August 20, 1992.

Hodgson, K. M., D. L. Herting, W. W. Schultz, L. A. Bray, and J. L. Swanson, 1985, "Content and Removal of TRU Elements from Aqueous Zirconium Cladding Waste," *Proceedings of the International Symposium on Actinide/Lanthanide Separations, Honolulu, Hawaii, USA, 16-22 December 1984*, World Scientific, 1985.

Koreski, G. M., and J. N. Strode, 1992, "Operational Waste Volume Projections," SD-WM-ER-029, Revision 16, October 28, 1992.

Lowe, S. S., 1991, "Preliminary Material Balances for Pretreatment of NCAW, NCRW, PFP and CC Wastes," WHC-SD-WM-TI-492, Revision 0, September 10, 1991.

O'Rourke, J. F., 1992, "Process Control Plan for 242-A Evaporator Campaign 93-1," WHC-SD-WM-PCP-008, Revision 0, November 24, 1992.

Pontious, N. L., 1986, "242-A Evaporator/Crystallizer FY 1985 Campaign 85-3 Post-Run Document," SD-WM-PE-023, Revision 0, February 24, 1986.

Swanson, J. L., 1988, *Recent Studies Related to Head-End Fuel Processing at the Hanford PUREX Plant*, PNL-6609, Battelle Pacific Northwest Laboratory, Richland, WA, August 1988.

Walker, F. W., J. R. Parrington, F. Feiner, 1989, *Nuclides and Isotopes*, 14th ed., General Electric Company, San Jose, CA, 1989.

Welsh, T. L., 1991a, "Tank 241-AN-106 Characterization Results," WHC-SD-CP-TP-065, Revision 0, March 8, 1991.

Welsh, T. L., 1991b, "Tank 241-AW-101 Characterization Results," WHC-SD-WM-TRP-055, Revision 0, December 19, 1991.

9413222.1391

APPENDIX

9413222.1392

THIS PAGE INTENTIONALLY LEFT BLANK

WHC-SD-WM-TI-528, Rev. 0

GROUT TREATMENT FACILITY WASTE FEED PROJECTIONS

Waste Analyses and Calculations

TABLE — Page

1-1: Dilute Waste Summary A-3
1-2: DSSF Family Waste Summary A-6
1-3: DSSF Family Radiolytic Heat Loading A-10
1-4: Pretreatment Waste Summary A-11

2-1: 241-AP-103 Validated Analysis Data A-14
2-2: 241-AW-106 Validated Analysis Data A-18
2-3: 241-AW-102 Validated Analysis Data A-22
2-3: 241-AW-102 Validated Analysis Data - cont. A-26
2-4: 241-AP-103 Analysis Summary A-30
2-5: 241-AW-106 Analysis Summary A-33
2-6: 241-AW-102 Analysis Summary A-36
2-7: Future Dilute DSSF Waste Summary A-39

3-1: Evaporator Campaign 84-3 Analysis Data A-43
3-2: Evaporator Campaign 84-5 Analysis Data A-46
3-3: Evaporator Campaign 85-3 Analysis Data A-49
3-4: Evaporator Campaign 84-5 Analysis Summary A-52
3-5: Evaporator Campaign 85-3 Analysis Summary A-55

4-1: Concentrated Waste Summary Data - 101AW, 103AN A-58
4-2: Concentrated Waste Summary Data - 105AP, 106AN A-61
4-3: Concentrated Waste Summary Data - 104AN, 105AN A-64

5-1: Radioisotope Decay Data A-67

FIGURE — Page

Figure A-1: Grout Feed Material Data Flowsheet. A-1

9413222.394

THIS PAGE INTENTIONALLY LEFT BLANK

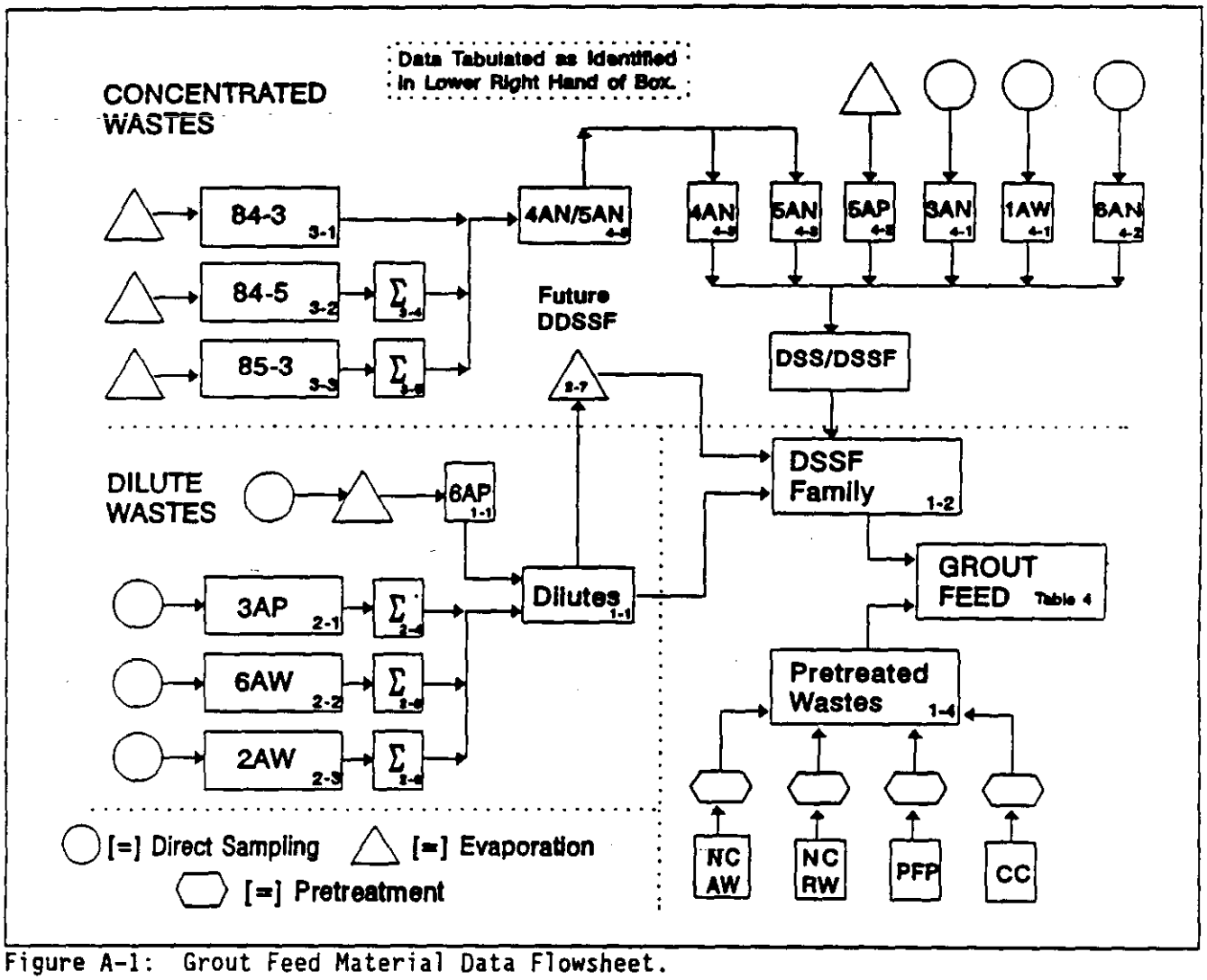

Figure A-1: Grout Feed Material Data Flowsheet.

Figure A-1, comparable to Figure 2 of this document, provides the schematic of data flow used in the calculation of inventory estimates of Sections 1.0 through 4.0. Table references provided in Figure A-1 are correlated with the index to this Appendix and will allow one to follow calculations where necessary.

Radiolytic decay dates are as noted on each table.

9413222.1396

THIS PAGE INTENTIONALLY LEFT BLANK

TABLE 1-1: Dilute Waste Summary

Dilute Waste Analyses and Estimates								
Units: Molarity; uCi/L for radionuclides; others as noted								
	Analytical Results			Estimate	Analytical		Overall Dilute	
Component	103AP	106AW	102AW	106AP	MEAN	S. Dev.	MEAN	S. Dev.
Ag	3.71e-07	4.46e-06	8.27e-06	3.15e-05	9.23e-06	2.36e-05	1.64e-05	2.05e-05
Al	9.12e-03	6.21e-02	1.81e-02	1.07e-01	1.95e-02	2.84e-02	4.76e-02	4.50e-02
As	6.44e-07	3.50e-05	2.01e-05	1.37e-06	1.30e-05	1.72e-05	8.85e-06	1.69e-05
B								
Ba	4.73e-07	1.26e-05	9.47e-06	6.98e-06	5.72e-06	6.28e-06	6.13e-06	5.14e-06
Be								
Bi				5.91e-05			5.91e-05	
Ca				6.48e-05			2.73e-05	
Cd	9.85e-07	2.64e-05	3.56e-06	1.10e-06	5.27e-06	1.40e-05	3.93e-06	1.23e-05
Ce								
Cr	7.10e-05	4.41e-04	2.05e-04	3.17e-04	1.73e-04	1.87e-04	2.19e-04	1.58e-04
Cu				3.89e-05			3.89e-05	
Fe	1.49e-05	1.34e-03	5.65e-04	8.12e-05	4.10e-04	6.63e-04	3.04e-04	6.09e-04
Hg	1.03e-08	5.21e-08	2.49e-08	8.22e-08	2.16e-08	2.12e-08	4.11e-08	3.17e-08
K				1.11e-01			1.11e-01	
La								
Li								
Mg	2.97e-05	4.36e-04	5.53e-04	2.20e-04	2.97e-04	2.75e-04	2.73e-04	2.32e-04
Mn	4.74e-07	1.22e-04	1.77e-05	4.87e-05	2.30e-05	6.60e-05	3.13e-05	5.39e-05
Mo				6.12e-05			6.12e-05	
Na	2.31e-01	1.73e+00	7.30e-01	1.08e+00	6.27e-01	7.63e-01	7.71e-01	6.29e-01
Nd								
Ni				1.75e-04			1.75e-04	
P				2.26e-03			2.26e-03	
Pb	1.93e-06	2.11e-04	3.86e-05	1.49e-04	4.35e-05	1.11e-04	7.75e-05	9.67e-05
Pd								
Sb								
Se	1.05e-07	1.04e-07	6.33e-08	4.30e-08	8.77e-08	2.38e-08	7.33e-08	3.08e-08
Si				4.40e-04			4.40e-04	
Sn								
Ta				1.88e-05			1.88e-05	
Ti				1.01e-05			1.01e-05	
U g/L			1.54e-08	2.27e-02	1.18e-08		7.29e-03	1.60e-02

WHC-SD-WM-TI-528, Rev. 0
TABLE 1-1 continued.

Dilute Waste Analyses and Estimates								
Units: Molarity; uCi/L for radionuclides; others as noted								
	Analytical Results			Estimate	Analytical		Overall Dilute	
Component	103AP	106AW	102AW	106AP	MEAN	S. Dev.	MEAN	S. Dev.
V								
W								
Zn	4.19e-06	1.59e-03	1.40e-04	6.04e-04	2.80e-04	8.77e-04	3.39e-04	7.17e-04
Zr				5.65e-05			5.65e-05	
CN-	2.29e-05	7.63e-05	4.93e-05	1.07e-04	4.06e-05	2.67e-05	6.19e-05	3.60e-05
S-2								
NH4+	2.75e-03	3.29e-03	1.03e-02	4.97e-04	5.95e-03	4.23e-03	4.20e-03	4.25e-03
NH3								
CO3-2				2.06e-02			2.06e-02	
Cl-	1.40e-03	1.51e-02	1.31e-02	1.51e-02	1.36e-02	7.41e-03	1.41e-02	6.59e-03
F-	6.81e-03	3.43e-01	2.12e-01	4.12e-04	2.29e-01	1.69e-01	1.56e-01	1.67e-01
SO4-2	3.65e-03	3.56e-02	2.43e-02	1.15e-03	1.62e-02	1.62e-02	1.14e-02	1.66e-02
NO3-	6.41e-02	5.79e-01	2.28e-01	1.55e-01	1.97e-01	2.63e-01	1.83e-01	2.25e-01
NO2-	2.82e-02	2.08e-01	5.59e-02	1.12e-01	6.24e-02	9.69e-02	7.83e-02	7.94e-02
PO4-3	1.45e-03	7.67e-03	1.84e-03	2.28e-03	2.40e-03	3.49e-03	2.36e-03	2.93e-03
OH-	8.99e-02	5.88e-01	1.70e-01	8.78e-01	1.86e-01	2.68e-01	4.09e-01	3.69e-01
TOC g/L	1.12e-01	1.05e+00	4.91e-01	5.10e-01	3.67e-01	4.70e-01	4.27e-01	3.84e-01
TIC g/L	5.14e-01	2.36e+00	8.42e-01	1.20e+00	8.83e-01	9.85e-01	9.85e-01	8.04e-01
SPG	1.00e+00	1.09e+00	1.03e+00	1.03e+00	1.02e+00	4.27e-02	1.03e+00	3.51e-02
TotSolids								
pH								
3H	5.24e+00	1.20e+01	5.68e+00	7.10e-01	6.28e+00	3.78e+00	4.49e+00	4.64e+00
14C	4.47e-03	7.47e-02		2.70e-02	1.96e-02	4.97e-02	2.20e-02	3.59e-02
54Mn								
59Mn								
60Co	1.06e+01	6.37e+00	5.64e+00	3.00e+00	8.02e+00	2.69e+00	6.40e+00	3.16e+00
63Ni								
79Se	1.12e-02	3.98e-02		4.80e-02	2.55e-02		3.27e-02	1.93e-02
90Sr	2.62e+00	2.95e+01	4.53e+01	4.20e+03	2.37e+01	2.16e+01	1.37e+03	2.09[illegible]
94Nb	9.31e+00	7.36e+00	5.51e+00	6.80e+00	7.49e+00	1.90e+00	7.27e+00	1.58e+00
95Nb	8.67e+00				8.67e+00		8.67e+00	
99Tc	1.08e+00	1.68e+01		1.50e+01	4.47e+00	1.11e+01	7.86e+00	8.60e+00
103Ru			2.10e+01		2.10e+01		2.10e+01	
106RuRh	2.66e+02	4.89e+02	3.98e+02	3.70e+02	3.49e+02	1.12e+02	3.56e+02	9.18e+01

TABLE 1-1 continued.

Dilute Waste Analyses and Estimates								
Units: Molarity; uCi/L for radionuclides; others as noted								
	Analytical Results			Estimate	Analytical		Overall Dilute	
Component	103AP	106AW	102AW	106AP	MEAN	S. Dev.	MEAN	S. Dev.
113Sn	2.38e+01	5.02e+01	2.80e+01		2.89e+01	1.42e+01	2.89e+01	1.42e+01
129I	3.19e-02	4.24e-02		3.00e-02	3.41e-02	7.46e-03	3.28e-02	6.69e-03
134Cs	1.05e+01	3.97e+02	1.75e+02	1.50e+02	1.27e+02	1.94e+02	1.35e+02	1.60e+02
137Cs	6.54e+03	5.07e+04	1.52e+04	3.60e+04	1.57e+04	2.34e+04	2.22e+04	2.00e+04
144CePr	1.33e+02	2.72e+02	1.54e+02		1.59e+02	7.47e+01	1.59e+02	7.47e+01
154Eu	2.80e+01	1.61e+01	2.17e+01		4.07e+01	5.97e+00	4.07e+01	5.97e+00
155Eu	4.37e+01	6.89e+01	4.23e+01		4.63e+01	1.50e+01	4.63e+01	1.50e+01
226Ra	1.44e+02	7.76e+01	3.37e+02		2.15e+02	1.35e+02	2.15e+02	1.35e+02
234U	6.52e-03	9.25e-03			4.17e-03	1.93e-03	4.17e-03	1.93e-03
235U	3.39e-04	9.21e-04			2.72e-04	4.11e-04	2.72e-04	4.11e-04
238U	1.26e-03	3.02e-03			9.59e-04	1.24e-03	9.59e-04	1.24e-03
237Np				3.10e-04			3.10e-04	
238Pu				1.00e-01			1.00e-01	
239/240Pu	6.97e-03	9.89e-02	3.61e-01	1.10e-01	1.65e-01	1.84e-01	1.44e-01	1.52e-01
241Am	1.14e-02	2.15e-02	2.57e-01	1.20e-01	1.14e-01	1.39e-01	1.03e-01	1.14e-01
242Cm								
243Cm								
244Cm				6.60e-03			6.60e-03	
TB			1.56e+04		1.56e+04		1.56e+04	
AT			1.86e+00		1.86e+00		1.86e+00	
Volume L	4.16e+06	1.15e+06	3.75e+06	4.29e+06	9.06e+06			

Notes: Where no values are displayed for an analyte in a tank, the mean for that analyte across the tanks is calculated as the weighted (volume) mean of those reported.
Less-than values calculated as real values.
Not decayed: Decay date assumed to be October 1, 1993.

9413222.1400

TABLE 1-2: DSSF Family Waste Summary

DSSF Family Wastes			Decayed to		10/01/93					
Units: Molarity; uCi/L for radionuclides; others as noted							| NOT Decayed |			
Waste	Tank	Tank	Tank	Tank	Tank	Tank	Future	Required	Total	ConcWaste
Component	106-AN	101-AW	105-AP	104-AN	105-AN	103-AN	DDSSF	Dilutes	Family	Std. Dev.
Ag	3.37e-05	3.09e-04	2.00e-04			1.48e-04	7.10e-05	1.64e-05	8.90e-05	1.14e-04
Al	3.44e-01	1.03e+00	1.60e-01	1.39e+00	1.74e+00	2.13e+00	1.50e-01	4.76e-02	4.92e-01	7.77e-01
As	9.61e-07	1.33e-07	8.58e-08			2.14e-03	1.00e-04	8.85e-06	2.00e-04	1.07e-03
B										
Ba	8.08e-05	6.80e-05	4.35e-05			1.17e-04	4.40e-05	6.13e-06	4.66e-05	3.04e-05
Be						1.78e-03			1.78e-03	
Bi	6.94e-04	5.79e-04	3.70e-04			2.30e-04		5.91e-05	3.13e-04	2.08e-04
Ca	2.25e-03	8.26e-04	1.08e-03			2.16e-03		2.73e-05	4.24e-04	7.30e-04
Cd	4.41e-04	1.08e-05	6.92e-06			1.42e-04	4.05e-05	3.93e-06	8.45e-05	2.04e-04
Ce										
Cr	1.08e-02	3.09e-03	3.32e-03	1.30e-02	1.30e-02	1.63e-02	1.33e-03	2.19e-04	4.23e-03	5.49e-03
Cu	5.90e-05	3.81e-04	2.42e-04			1.89e-04		3.89e-05	1.49e-04	1.33e-04
Fe	1.24e-04	7.86e-04	2.00e-04	2.00e-04	2.00e-04	1.26e-03	3.15e-03	3.04e-04	1.78e-03	4.61e-04
Hg	2.49e-07	7.82e-07	4.99e-07			7.98e-05	1.66e-07	4.11e-08	5.49e-06	3.96e-05
K	2.76e-02	1.07e+00	8.57e-01	1.83e-01	1.57e-01	3.89e-01		1.11e-01	3.44e-01	4.21e-01
La										
Li										
Mg	1.14e-04	2.16e-03	4.95e-04			1.18e-03	2.29e-03	2.73e-04	1.61e-03	8.96e-04
Mn	1.01e-03	4.76e-04	3.06e-04			5.24e-04	1.77e-04	3.13e-05	2.62e-04	3.04e-04
Mo	6.94e-04	6.00e-04	3.86e-04			9.17e-04		6.12e-05	4.24e-04	2.20e-04
Na	3.93e+00	1.00e+01	6.35e+00	1.20e+01	1.20e+01	1.46e+01	4.82e+00	7.71e-01	6.00e+00	3.98e+00
Nd										
Ni			2.15e-03			4.09e-04		1.75e-04	6.22e-04	1.23e-03

TABLE 1-2 continued.

DSSF Family Wastes			Decayed to		10/01/93					
Units: Molarity; uCi/L for radionuclides; others as noted							[NOT Decayed]			
Waste	Tank	Tank	Tank	Tank	Tank	Tank	Future	Required	Total	ConcWaste
Component	106-AN	101-AW	105-AP	104-AN	105-AN	103-AN	DDSSF	Dilutes	Family	Std. Dev.
P	1.97e-01		1.43e-02					2.26e-03	4.98e-02	1.29e-01
Pb	2.22e-03	1.46e-03	9.33e-04			3.47e-04	3.35e-04	7.75e-05	5.37e-04	7.96e-04
Pd										
Sb						1.31e-03			1.31e-03	
Se	1.70e-06	4.20e-07	2.73e-07			2.63e-03	6.74e-07	7.33e-08	1.75e-04	1.32e-03
Si		4.36e-03	3.53e-03			9.68e-03		4.40e-04	3.38e-03	3.34e-03
Sn										
Ta	7.18e-07							1.68e-05	1.36e-05	
Ti	7.33e-05	9.86e-05	6.38e-05			3.34e-04		1.01e-05	8.14e-05	1.29e-04
U g/L	1.68e-05	9.39e-04	6.06e-04			5.18e-04	9.08e-08	7.29e-03	1.37e-03	3.81e-04
V						3.14e-04			3.14e-04	
W						1.13e-03			1.13e-03	
Zn	1.44e-04	4.84e-03	1.16e-03			7.34e-04	2.00e-03	3.39e-04	1.66e-03	2.12e-03
Zr	3.05e-04	5.54e-04	3.59e-04			2.63e-04		5.65e-05	2.50e-04	1.29e-04
CN-	2.31e-04	1.03e-03	6.65e-04			1.29e-03	3.12e-04	6.19e-05	4.01e-04	4.61e-04
S-2										
NH4 +	7.22e-03	1.45e-02	2.34e-03				5.20e-03	4.20e-03		6.12e-03
NH3				6.99e-03	2.00e-02				2.03e-02	9.20e-03
CO3-2	3.27e-01	2.05e-01	2.53e-01	4.72e-01	3.63e-01	1.49e-01		2.06e-02	2.12e-01	1.17e-01
Cl-	6.94e-02	1.46e-01	7.28e-02	2.12e-01	2.40e-01	2.71e-01	1.05e-01	1.41e-02	1.15e-01	8.60e-02
F-	3.24e-03	4.02e-03	1.30e-01			3.87e-02	1.76e+00	1.56e-01	1.03e+00	5.96e-02
SO4-2	2.24e-02	1.07e-02	2.48e-02	6.82e-02	6.82e-02	1.67e-02	1.25e-01	1.14e-02	7.63e-02	2.60e-02
NO3-	1.09e+00	3.46e+00	2.66e+00	3.10e+00	3.12e+00	2.54e+00	1.51e+00	1.83e-01	1.72e+00	8.40e-01

9413222.1402

TABLE 1-2 continued.

DSSF Family Wastes			Decayed to		10/01/93					
Units: Molarity; uCi/L for radionuclides; others as noted								NOT Decayed		
Waste	Tank	Tank	Tank	Tank	Tank	Tank	Future	Required	Total	ConcWaste
Component	106-AN	101-AW	105-AP	104-AN	105-AN	103-AN	DDSSF	Dilutes	Family	Std. Dev.
NO2-	6.44e-01	2.19e+00	1.09e+00	1.92e+00	2.61e+00	2.99e+00	4.60e-01	7.83e-02	9.37e-01	8.96e-01
PO4-3	1.94e-01	2.22e-02	1.62e-02	2.94e-02	2.00e-02	9.77e-03	1.85e-02	2.36e-03	2.69e-02	7.14e-02
OH-	4.74e-01	5.07e+00	4.63e+00	4.09e+00	3.64e+00	5.74e+00	1.43e+00	4.09e-01	2.15e+00	1.85e+00
TOC g/L	3.26e+00	2.46e+00	3.92e+00	5.53e+01	4.66e+01	6.13e-01	2.98e+00	4.27e-01	6.15e+00	2.51e+01
TIC g/L		2.46e+00					6.79e+00	9.85e-01	5.191204	
SPG	1.23	1.56	1.347377	1.499809	1.503333	1.6	1.25e+00	1.03e+00	1.2905	1.40e-01
TotSolids										
pH				13.5	13.5				13.5	
3H	2.68e+00	5.90e+00	7.40e+00			2.44e+00	5.49e+00	4.49e+00	5.07e+00	2.44e+00
14C	3.35e-01	3.70e-01	2.36e-01			2.00e+00	1.51e-01	2.20e-02	2.85e-01	8.44e-01
54Mn										
59Mn										
60Co	5.10e+00	1.94e+01	1.04e+01			1.20e+01	6.17e+01	6.40e+00	3.91e+01	5.92e+00
63Ni										
79Se	2.40e-01	4.80e-01	3.06e-01			4.30e+01	1.96e-01	3.27e-02	3.03e+00	2.13e+01
90Sr	2.01e+03	1.01e+03	1.90e+02	9.84e+03	3.23e+03	1.05e+04	1.82e+02	1.37e+03	1.82e+03	4.55e+03
94Nb	2.30e+01	6.82e+01	4.35e+01			7.10e+00	5.76e+01	7.27e+00	4.33e+01	2.64e+01
95Nb							6.67e+01	8.67e+00	5.34e+01	
99Tc	6.92e+01	1.52e+02	1.79e+01			1.70e+02	3.44e+01	7.86e+00	4.67e+01	7.14e+01
103Ru							1.62e+02	2.10e+01	1.29e+02	
106RuRh	6.78e+01	4.18e+02	9.90e+01			1.73e-01	2.68e+03	3.56e+02	1.62e+03	1.86e+02
113Sn							2.22e+02	2.89e+01	1.78e+02	
129I	7.50e-02	3.03e-01	4.18e-02			5.20e-01	2.63e-01	3.28e-02	2.18e-01	2.23e-01

TABLE 1-2 continued.

DSSF Family Wastes			Decayed to		10/01/93					
Units: Molarity; uCi/L for radionuclides; others as noted							I NOT Decayed I			
Waste	Tank	Tank	Tank	Tank	Tank	Tank	Future	Required	Total	ConcWaste
Component	106-AN	101-AW	105-AP	104-AN	105-AN	103-AN	DDSSF	Dilutes	Family	Std. Dev.
134Cs	5.33e+00	5.20e+02	5.25e+02	7.20e+01	7.20e+01	5.75e+00	9.80e+02	1.35e+02	5.77e+02	2.52e+02
137Cs	1.85e+05	4.83e+05	2.56e+05	7.56e+05	5.04e+05	6.13e+05	1.21e+05	2.22e+04	2.27e+05	2.15e+05
144CePr							1.22e+03	1.59e+02	9.80e+02	
154Eu							3.13e+02	4.07e+01	2.51e+02	
155Eu							3.56e+02	4.63e+01	2.85e+02	
226Ra							1.66e+03	2.15e+02	1.32e+03	
234U						5.30e-02	3.21e-02	4.17e-03	3.37e-01	
235U						1.10e-03	2.10e-03	2.72e-04	1.97e-02	
238U						1.40e-02	7.38e-03	9.59e-04	7.94e-02	
237Np	2.11e+00	2.16e+00	1.39e+00			2.00e-02		3.10e-04	8.81e-01	9.98e-01
238Pu	1.93e-02		3.67e-02			9.14e-01		1.00e-01	2.23e-01	5.12e-01
239/240Pu	3.78e-02	1.14e+00	4.23e-02	1.04e+01	1.04e+01	1.90e+00	1.27e+00	1.44e-01	2.09e+00	5.03e+00
241Am	6.02e-01	1.20e+00	1.33e+00	1.12e+04	1.12e+04	2.27e+00	8.80e-01	1.03e-01	1.35e+03	5.80e+03
242Cm										
243Cm	4.23e-02	4.94e-02	3.07e-02						4.14e-02	9.42e-03
244Cm						3.00e-01		6.60e-03	8.92e-02	
TB								1.56e+04	1.56e+04	
AT								1.86e+00	1.86e+00	
Volume L	3667985	3826969	3145609	3024479	4269852	3546854	30282640	8045989	60810376	

Notes: Where no values are displayed for an analyte in a tank, the mean for that analyte across the tanks is calculated as the weighted (volume) mean of those reported.
Less-than values calculated as real values. NH_4^+ and NH_3 jointly summarized as NH_3 in overall summary.
Concentrate waste standard deviation is calculated using the first six tank data columns.

9413222.1404

TABLE 1-3: DSSF Family Radiolytic Heat Loading[1]

137CsmBa Heat Equivalents - calc by parent concentration										
	Heat equiv. (Ci 137CsmBa/Ci)	106-AN	101-AW	105-AP	104-AN	105-AN	103-AN	DDSSF	Dilutee	Total
60Co	3.1984	16.31067	62.17139	33.35944	0	0	38.24546	197.2573	20.48289	125.1419
90SrY	1.3967	2601.698	1403.93	265.7258	13739.06	4506.432	14726.26	254.4167	1906.786	2640.417
106RuRh	2.0004	135.5683	835.4356	197.9927	0	0	0.34575	5366.679	711.3283	3237.727
134Cs	2.1113	11.25261	1097.556	1109.116	152.0717	152.0717	12.13998	2068.492	284.2719	1218.438
137CsmBa	1	185096.5	482772.2	255627.1	755513.2	504323.6	612820.1	120907.5	22239.97	227020
144CePr	1.6624	0	0	0	0	0	0	2035.712	264.6428	1628.348
Total		188061.3	486171.3	257233.3	769404.3	508982.1	627697.1	130830	25429.48	235770.1
Heat Load Ratio										
%Volume (feed ratio)		100.0%	75.2%	100.0%	46.6%	71.6%	57.5%	100.0%		
Rqd Dilute for blending (L)		0	1263663	0	3471848	1691101	2619377	0		

Decay Date = 10/01/93.

1 Radiolytic heat loading is a calculation of the heat released to the waste through high energy radiolytic decay. A "^{137}CsmBa heat equivalent" is defined as the ratio of heat provided by one curie of the referenced decay chain relative to the heat released from the decay of one curie of ^{137}Cs and its high energy daughter ^{137}mBa. The basis for these calculations is provided in Hendrickson (1991a). These calculations result in evaluation of maximum feed fraction of each waste blended with dilute waste while complying with acceptance criteria for heat loading (Hendrickson, 1991b). A %Volume of 100% indicates that material may be fed without dilution.

TABLE 1-4: Pretreatment Waste Summary

Preliminary Pretreatment Material Balances (WHC-SD-WM-TI-492)									
Units: Molarity; uCi/L for radionuclides; others as noted									
					NCRW (no additional PUREX Ops)				Total
Waste	NCAW Str. 12		NCAW Str. 13		Stream 27		PFP Waste	CC Waste	Mean
Component	AZ 101	AZ 102	AZ 101	AZ 102	103-AW	105-AW		(Based on 5M Na)	
Ag							1.20e-03		4.08e-0
Al	4.38e-01	4.99e-01	3.00e-02	3.42e-02	4.20e-02	1.80e-02	5.50e-01	5.11e-01	4.05e-0
As							5.80e-03		1.97e-0
B					8.40e-03	9.70e-03	1.20e-02	1.69e-03	3.37e-0
Ba					2.80e-04	2.40e-04		9.75e-05	1.18e-0
Be									
Bi									
Ca					2.10e-03	3.00e-03	1.10e-01	4.77e-03	7.30e-0
Cd							4.70e-03		1.60e-0
Ce					2.10e-05	2.20e-05	4.10e-03		1.44e-0
Cr	1.05e-02	8.75e-03			7.60e-03	2.70e-03	2.70e-01	1.22e-02	1.92e-0
Cu							1.20e-02		4.08e-0
Fe	4.40e-05	1.51e-04			1.90e-03	5.80e-03	2.80e-01	1.28e-02	1.85e-0
Hg									
K	1.92e-01	1.44e-01	1.68e-01	1.26e-01	1.20e-01	8.00e-02	5.80e-02	2.04e-02	5.65e-0
La					4.70e-04	6.60e-04			1.15e-0
Li							2.00e-03		6.81e-0
Mg					1.10e-03	1.30e-03	4.90e-02	3.34e-03	4.05e-0
Mn					6.80e-05	3.00e-03	1.00e-01	5.27e-03	7.03e-0
Mo					3.20e-05	3.40e-06	5.80e-04	1.30e-03	8.54e-0
Na	5.00e+00	5.00e+00	5.00e+00	5.00e+00	5.01e+00	5.02e+00	5.00e+00	5.00e+00	5.00e+0
Nd					2.40e-04	3.40e-04	1.80e-03		1.20e-0
Ni					4.40e-04	6.30e-04	5.80e-03	2.49e-03	1.89e-0
P									
Pb							3.50e-03		1.19e-0
Pd									
Sb							1.80e-03		6.13e-0
Se							1.80e-02		6.13e-0
Si					3.70e-02	3.70e-02	2.90e-02		8.77e-0
Sn									
Ta									
Ti					1.90e-04	1.70e-04	1.80e-03		9.95e-0

WHC-SD-WM-TI-528, Rev. 0
TABLE 1-4 continued.

Preliminary Pretreatment Material Balances (WHC-SD-WM-TI-492)									
Units: Molarity; uCi/L for radionuclides; others as noted									
					NCRW (no additional PUREX Ops)				Total
Waste	NCAW Str. 12		NCAW Str. 13		Stream 27		PFP Waste	CC Waste	Mean
Component	AZ 101	AZ 102	AZ 101	AZ 102	103-AW	105-AW		(Based on 5M Na)	
U g/L					1.40e+00	2.19e+00	1.74e+00	1.59e-03	4.24e-0
V									
W									
Zn					9.70e-05	3.60e-05	4.10e-03	3.97e-04	4.08e-0
Zr	2.90e-05	1.28e-05			2.40e-01	2.40e-01	2.30e-03	4.97e-04	5.09e-0
CN-									
S-2									
NH4+									
NH3					1.40e-02	2.60e-02			3.99e-0
CO3-2							3.30e-01		1.12e-0
Cl-					6.60e-03	3.70e-03	1.10e-01	7.88e-02	5.51e-0
F-					1.69e+00	1.67e+00	2.20e-01	5.22e-02	3.95e-0
SO4-2	1.43e-01	2.19e-01			5.00e-04	3.70e-03	7.20e-02	6.81e-02	6.70e-0
NO3-	1.66e+00	1.80e+00	3.78e+00	4.09e+00	7.40e-01	7.70e-01	3.50e+00	5.13e+00	3.76e+0
NO2-	4.10e-01	4.48e-01	1.20e-02	1.31e-02	3.60e-02	2.20e-02	5.50e-01		7.42e-0
PO4-3	2.37e-02	3.21e-03					4.40e-01	2.83e-02	3.46e-0
OH-	1.29e+00		8.80e-01		2.60e-01	2.90e-01	6.50e-01		1.55e-0
TOC g/L	6.20e-02								3.54e-0
TIC g/L									
SPG					1.48	1.47	1.43		
TotSolids									
pH									
3H									
14C	1.70e+01	4.48e+01			5.90e-01	6.50e-01	1.50e+00		3.71e+0
54Mn									
59Mn									
60Co					[illegible]00e+01	6.10e+01	1.20e+02		1.56e+0
63Ni							3.50e+03		1.19e+0
79Se									
90Sr	1.53e+03	2.91e+03			2.20e+03	2.40e+03	5.80e+04	3.32e+04	2.39e+0
94Nb									
95Nb					2.40e+04	6.00e+03			3.49e+0
99Tc	2.24e+02	5.92e+02			4.30e+00	4.70e+00	2.10e+02		5.47e+0

TABLE 1-4 continued.

Preliminary Pretreatment Material Balances (WHC-SD-WM-TI-492)									
Units: Molarity; uCi/L for radionuclides; others as noted									
					NCRW (no additional PUREX Ops)				Total
Waste	NCAW Str. 12		NCAW Str. 13		Stream 27		PFP Waste	CC Waste	Mean
Component	AZ 101	AZ 102	AZ 101	AZ 102	103-AW	105-AW		(Based on 5M Na)	
103Ru									
106RuRh	1.26e+03	5.35e+03			9.40e+03	5.60e+03	1.20e+03		2.07e+0
113Sn									
129I	6.38e-02	1.78e-01			1.10e-02	1.20e-02	2.90e-01		2.61e-0
134Cs					3.00e+02	2.60e+02	7.30e+01		6.21e+0
137Cs	4.75e+04	1.36e+05	1.71e+06	4.89e+06	1.50e+04	1.10e+04	1.50e+05	9.72e+03	3.67e+0
144CePr					1.20e+04	6.90e+03	1.20e+03		2.12e+0
154Eu					9.30e+00	6.80e+01	1.20e+03		4.79e+0
155Eu					1.10e+01	8.00e+01	1.20e+03		4.91e+0
226Ra									
234U									
235U									
238U									
237Np							8.51e-03		2.90e-0
238Pu	2.71e-01	8.30e-01			9.15e-02	2.29e-01			9.41e-0
239/240Pu	1.87e+00	3.03e+00			1.18e+00	1.97e+00	4.90e+01	1.28e+00	3.08e+0
241Am	3.33e+01	3.14e+02			9.79e-02	8.48e-01	1.73e+02	3.00e+00	2.78e+0
242Cm									
243Cm									
244Cm							4.86e-01		1.65e-0
TB									
AT									
Volume L	3.49e+06	3.50e+06	1.12e+05	1.12e+05	7.57e+06	5.30e+06	2.08e+06	3.90e+07	6.12e+0
Additional analytes described for these wastes									
95Zr					1.20e+04	2.80e+03			1.73e+0
125Sb					2.50e+03	2.20e+03	1.20e+03		5.41e+0
152Eu							1.20e+02		4.08e+0
241Pu	1.69e+01	4.51e+01			1.47e+01	4.08e+01			8.90e+0
242Pu					2.28e-05	1.49e-04			1.57e-0

Note: Not Decayed. Decay date assumed as October 1, 1993.

TABLE 2-1: 241-AP-103 Validated Analysis Data

Tank 103AP Analyses				Sample										
17-Dec-91			<	933	934	935	936	937	941	942	943	944	945	949
Component	Units	MW												Comp
Ag	ppm	107.868	<	0.04	0.04	0.04	0.04	0.04	0.04	0.04	0.04	0.04	0.04	
Al	ppm	26.98154		102	76	307	103	230	269	560	104	171	550	
As	ppm	74.9216		0.052	0.035	0.055	0.0445	0.049	0.039	0.084	0.028	0.035	0.061	
B	ppm	10.81												
Ba	ppm	137.33	<	0.065	0.065	0.065	0.065	0.065	0.065	0.065	0.065	0.065	0.065	
Be	ppm	9.01218												
Bi	ppm	208.9804												
Ca	ppm	40.08												
Cd	ppm	112.41		0.0715	0.048	0.133	0.0645	0.124	0.126	0.183	0.081	0.097	0.18	
Ce	ppm	140.12												
Cr	ppm	51.996		3.535	2.05	4.87	3.38	4.48	4.86	6.8	0.353	0.416	6.4	
Cu	ppm	63.546												
Fe	ppm	55.847	<	0.435	0.481	0.98	0.435	0.435	1.355	2.67	0.63	0.435	0.435	
Hg	ppm	200.59	<	0.0017	0.0017	0.0017	0.0017	0.0017	0.002		0.005	0.002	0.002	
K	ppm	39.0983												
La	ppm	138.9055												
Li	ppm	6.941												
Mg	ppm	24.305	<	1.085	1.03	1.53	1.15	1.14	0.255	0.255	0.255	0.255	0.255	
Mn	ppm	54.938	<	0.015	0.015	0.0515	0.015	0.015	0.062	0.034	0.015	0.015	0.023	
Mo	ppm	95.94												
Na	ppm	22.98977		3665	2320	2460	3820	2050	6540	11700	3700	4870	12000	
Nd	ppm	144.24												
Ni	ppm	58.7												
P	ppm	30.97376												

TABLE 2-1 continued.

Tank 103AP Analyses				Sample										
17-Dec-91			<	933	934	935	936	937	941	942	943	944	945	949
Component	Units	MW												Comp
Pb	ppm	207.2	<	0.4	0.4	0.4	0.4	0.4	0.4	0.4	0.4	0.4	0.4	
Pd	ppm	106.4												
Sb	ppm	121.75												
Se	ppm	78.96	<	0.02	0.005	0.005	0.005	0.005	0.02	0.007	0.005	0.005	0.006	
Si	ppm	28.0855												
Sn	ppm	118.69												
Ta	ppm	180.9479												
Ti	ppm	47.9												
U	g/L	238.029												0.00369
V	ppm	50.9415												
W	ppm	183.85												
Zn	ppm	65.38	<	0.0335	0.02	1.21	0.55	0.221	0.046	0.309	0.02	0.02	0.309	
Zr	ppm	91.22												
CN-	ppm	26.0177	<	1	0.495	0.584	0.469	0.527	0.605	0.61	0.511	0.552	0.61	
S-2	ppm	32.06												
NH4 +	M	18.0383	<	0.0025	0.00125	0.0019	0.00125	0.00125	0.005	0.005	0.005	7e-04	0.004	
NH3	M	17.0304												
CO3-2	M	60.0092												
Cl-	ppm	35.453		36.55	34.5	49.8	31	17.8	51.1	92.9	38.3	39.8	103	
F-	ppm	18.9984		61.15	88.2	178	60.3	54.1	129.5	305	60.6	96.4	260	
SO4-2	ppm	96.0576		451.5	502	318	414	196	395.5	162	418	482	163	
NO3-	ppm	63.0049		1680	2060	3500	1720	3250	4480	9440	1620	2850	9790	
NO2-	ppm	46.0055		1135	983	1380	1130	1280	1255	1700	1120	1200	1810	
PO4-3	ppm	94.97136		127	147	151	121	135	137	149	112	134	168	

TABLE 2-1 continued.

Tank 103AP Analyses				Sample										
17-Dec-91			<	933	934	935	936	937	941	942	943	944	945	949
Component	Units	MW												Comp
OH-	M	17.0073		0.0321	0.05	0.111	0.0658	0.0882	0.089	0.207	8e-04	0.058	0.197	
TOC	g/L	12.011		0.1095	0.15	0.13	0.12	0.15	0.091	0.091	0.088	0.1	0.091	
TIC	g/L	12.011		0.544	0.498	0.522	0.43	0.46	0.449	0.65	0.53	0.544	0.512	
SPG	g/mL			0.9975	1.008	1.02	1.002	1.017	0.995	1.004	0.992	0.994	1.006	
TotSolids	wt%													
pH														
3H	uCi/L													5.24
14C	uCi/L													0.00447
54Mn	uCi/L													
59Mn	uCi/L													
60Co	uCi/L		<							10		12	11	9.46
63Ni	uCi/L													
79Se	uCi/L													0.01115
90Sr	uCi/L													2.62
94Nb	uCi/L		<							9.31				
95Nb	uCi/L		<							9.3				6.045
99Tc	uCi/L													1.08
103Ru	uCi/L													
106RuRh	uCi/L		<							340				192
113Sn	uCi/L		<							30				17.6
129I	uCi/L		<											0.03185
134Cs	uCi/L		<	18.3	10.4	9.69	9.94	8.32	10.32	9.43	9.17	8.62	11.3	9.51
137Cs	uCi/L			6700	7200	5800	7020	6590	6415	6500	6590	6930	4230	6010
144CePr	uCi/L		<							170				95.65

TABLE 2-1 continued.

Tank 103AP Analyses				Sample										
17-Dec-91			<	933	934	935	936	937	941	942	943	944	945	949
Component	Units	MW												Comp
154Eu	uCi/L		<							22		32	32	25.95
155Eu	uCi/L		<	83.6	52.1	48.3	50	50.2	26	22	47.4	32		25.35
226Ra	uCi/L		<							43				244
234U	uCi/L													0.00652
235U	uCi/L													0.00034
238U	uCi/L													0.00126
237Np	uCi/L													
238Pu	uCi/L													
239/240Pu	uCi/L		<											0.00697
241Am	uCi/L		<											0.01135
242Cm	uCi/L													
243Cm	uCi/L													
244Cm	uCi/L													
TB	uCi/L													
A.T	uCi/L													

TABLE 2-2: 241-AW-106 Validated Analysis Data

Tank 106AW Analyses				Sample										
20-Sep-91			<	318	319	320	321	322	326	327	328	329	330	348
Component	Units	MW												Comp
Ag	ppm	107.868	<R	2.28	7.44	4.8	4.8	4.8	4.8	4.8	4.8	4.8	4.8	
Al	ppm	26.98154	R	1450	1060	1350	1380	972	1395	4970	1400	1380	1400	
As	ppm	74.9216		2.455	2.33	2.37	2.59	2.62	2.48	4.14	2.49	2.35	2.41	
B	ppm	10.81												
Ba	ppm	137.33	<R	1.07	1.8	1.8	1.8	1.8	1.8	1.8	1.8	1.8	1.8	
Be	ppm	9.01218												
Bi	ppm	208.9804												
Ca	ppm	40.08												
Cd	ppm	112.41	<R	1.57	2.4	2.4	2.4	2.4	3.29	4.2	4.38	3.36	3.33	
Ce	ppm	140.12												
Cr	ppm	51.996	R	24.3	20.8	14.8	22.9	15.3	24.95	36.7	21.2	26.4	22.8	
Cu	ppm	63.546												
Fe	ppm	55.847	<R	126	52.2	52.2	52.2	52.2	52.2	52.2	52.2	202	52.2	
Hg	ppm	200.59	<R	0.0446	0.005	0.005	0.005	0.005	0.005	0.005	0.005	0.02	0.005	
K	ppm	39.0983												
La	ppm	138.9055												
Li	ppm	6.941												
Mg	ppm	24.305	<R	1.1	6.6	6.6	6.6	6.6	16.3	34.9	6.6	10.6	9.78	
Mn	ppm	54.938	R	24.6	5.58	5.22	4.08	5.46	3.245	7.62	3.36	4.56	3.51	
Mo	ppm	95.94												
Na	ppm	22.98977	R	37900	26400	36200	36000	26600	38100	85200	37100	37100	37100	
Nd	ppm	144.24												
Ni	ppm	58.7												
P	ppm	30.97376												

TABLE 2-2 continued.

Tank 106AW Analyses				Sample										
20-Sep-91			<	318	319	320	321	322	326	327	328	329	330	348
Component	Units	MW												Comp
Pb	ppm	207.2	<IR	11	46.6	46	40.8	46	46	46	46	46	46	
Pd	ppm	106.4												
Sb	ppm	121.75												
Se	ppm	78.96	<	0.01	0.01	0.001	0.01	0.001	0.01	0.01	0.01	0.01	0.01	
Si	ppm	28.0855												
Sn	ppm	118.69												
Ta	ppm	180.9479												
Ti	ppm	47.9												
U	g/L	238.029												0.00947
V	ppm	50.9415												
W	ppm	183.85												
Zn	ppm	65.38	R	81.6	138	121	78	128	77.5	184	41.4	105	73.2	
Zr	ppm	91.22												
CN-	ppm	26.0177		3.405	2.49	2.43	2.49	2.57	0.836	0.781	2.4	0.37	2.1	
S-2	ppm	32.06												
NH4+	M	18.0383	<	0.0033	0.00149	0.0015	0.00149	0.00139	0.002	0.018	0.001	0.002	0.001	
NH3	M	17.0304												
CO3-2	M	60.0092												
Cl-	ppm	35.453		557.5	431	447	470	489	432.5	1180	455	450	441	
F-	ppm	18.9984		8310	5900	6680	5840	5830						
SO4-2	ppm	96.0576		3885	2480	2560	2580	2490	2335	10600	2550	2350	2350	
NO3-	ppm	63.0049		33450	31600	36800	31400	32500	31100	75900	31900	30100	29800	
NO2-	ppm	46.0055		9050	8140	7350	7470	7450	8060	24000	8270	8060	7900	
PO4-3	ppm	94.97136		656.12	589	586	611	595	587.5	1820	605	584	653	

TABLE 2-2 continued.

Tank 106AW Analyses				Sample										
20-Sep-91			<	318	319	320	321	322	326	327	328	329	330	348
Component	Units	MW												Comp
OH-	M	17.0073		0.5646	0.518	0.511	0.53	0.588	0.467	1.3	0.556	0.531	0.318	
TOC	g/L	12.011		0.97	0.886	0.88	0.776	0.918	0.873	2.39	0.952	0.946	0.875	
TIC	g/L	12.011		2.08	2.47	2.27	2.16	2.3	1.895	3.97	2.17	2.15	2.03	
SPG	g/ml			1.0902	1.0077	1.0757	1.079	1.0795	1.084	1.188	1.079	1.075	1.102	
TotSolids	wt%													
pH														
3H	uCi/L													12
14C	uCi/L													0.0747
54Mn	uCi/L													
59Mn	uCi/L													
60Co	uCi/L		<											6.37
63Ni	uCi/L													
79Se	uCi/L													0.0398
90Sr	uCi/L													29.45
94Nb	uCi/L		<											7.38
95Nb	uCi/L													
99Tc	uCi/L													16.8
103Ru	uCi/L													
106RuRh	uCi/L		<											489
113Sn	uCi/L		<											50.15
129I	uCi/L		<R											0.0424
134Cs	uCi/L		<											397
137Cs	uCi/L													50650
144CePr	uCi/L		<											271.5

TABLE 2-2 continued.

Tank 106AW Analyses				Sample										
20-Sep-91			<	318	319	320	321	322	326	327	328	329	330	348
Component	Units	MW												Comp
154Eu	uCi/L		<											16.05
155Eu	uCi/L		<											68.85
226Ra	uCi/L		<											77.55
234U	uCi/L													0.00925
235U	uCi/L													0.00092
238U	uCi/L													0.00302
237Np	uCi/L													
238Pu	uCi/L													
239/240Pu	uCi/L		<											0.09885
241Am	uCi/L		<											0.02145
242Cm	uCi/L													
243Cm	uCi/L	nd												
244Cm	uCi/L	nd												
TB	uCi/L													
AT	uCi/L													

TABLE 2-3: 241-AW-102 Validated Analysis Data

Tank 102AW Analyses				Sample							
14-Jun-91			<	9394	9395	9396	9397	9401	9402	9403	9404
Component	Units	MW									
Ag	ppm	107.868	<	1.15	0.82	0.8	0.8				
Al	ppm	26.98154		476	482	491	501				
As	ppm	74.9216						1.45	1.56	1.405	1.61
B	ppm	10.81									
Ba	ppm	137.33	<	1.3	1.3	1.3	1.3				
Be	ppm	9.01218									
Bi	ppm	208.9804									
Ca	ppm	40.08									
Cd	ppm	112.41	<	0.4	0.4	0.4	0.4				
Ce	ppm	140.12									
Cr	ppm	51.996		10.75	10.4	10.9	10.6				
Cu	ppm	63.546									
Fe	ppm	55.847		45.65	50.6	23.9	6.17				
Hg	ppm	200.59	<					0.005	0.005	0.005	0.005
K	ppm	39.0983									
La	ppm	138.9055									
Li	ppm	6.941									
Mg	ppm	24.305		9.55	13.7	13.3	17.2				
Mn	ppm	54.938	<	0.3	0.3	3	0.3				
Mo	ppm	95.94									
Na	ppm	22.98977		16550	16600	17000	17000				
Nd	ppm	144.24									
Ni	ppm	58.7									
P	ppm	30.97376									

TABLE 2-3 continued.

Tank 102AW Analyses				Sample							
14-Jun-91			<	9394	9395	9396	9397	9401	9402	9403	9404
Component	Units	MW									
Pb	ppm	207.2	<	8	8	8	8				
Pd	ppm	106.4									
Sb	ppm	121.75									
Se	ppm	78.96	<					0.005	0.005	0.005	0.005
Si	ppm	28.0855									
Sn	ppm	118.69									
Ta	ppm	180.9479									
Ti	ppm	47.9									
U	g/L	238.029									
V	ppm	50.9415									
W	ppm	183.85									
Zn	ppm	65.38		3.245	7.3	5.1	20.9				
Zr	ppm	91.22									
CN-	ppm	26.0177									
S-2	ppm	32.06									
NH4+	M	18.0383	<								
NH3	M	17.0304									
CO3-2	M	60.0092									
Cl-	ppm	35.453									
F-	ppm	18.9984									
SO4-2	ppm	96.0576									
NO3-	ppm	63.0049									
NO2-	ppm	46.0055									
PO4-3	ppm	94.97136									

TABLE 2-3 continued.

Tank 102AW Analyses				Sample							
14-Jun-91			<	9394	9395	9396	9397	9401	9402	9403	9404
Component	Units	MW									
OH-	M	17.0073									
TOC	g/L	12.011									
TIC	g/L	12.011									
SPG	g/mL										
TotSolids	wt%										
pH											
3H	uCi/L										
14C	uCi/L										
54Mn	uCi/L										
59Mn	uCi/L										
60Co	uCi/L		<								
63Ni	uCi/L										
79Se	uCi/L										
90Sr	uCi/L		R								
94Nb	uCi/L		<								
95Nb	uCi/L										
99Tc	uCi/L										
103Ru	uCi/L		<								
106RuRh	uCi/L		<								
113Sn	uCi/L		<								
129I	uCi/L										
134Cs	uCi/L		<								
137Cs	uCi/L										
144CePr	uCi/L		<								

TABLE 2-3 continued.

Tank 102AW Analyses				Sample							
14-Jun-91			<	9394	9395	9396	9397	9401	9402	9403	9404
Component	Units	MW									
154Eu	uCi/L		<								
155Eu	uCi/L		<								
226Ra	uCi/L		<								
234U	uCi/L										
235U	uCi/L										
238U	uCi/L										
237Np	uCi/L										
238Pu	uCi/L										
239/240Pu	uCi/L										
241Am	uCi/L							0.0231	0.024	0.808	0.175
242Cm	uCi/L										
243Cm	uCi/L										
244Cm	uCi/L										
TB	uCi/L										
AT	uCi/L		<R								

9413222.1420

TABLE 2-3: 241-AW-102 Validated Analysis Data - cont.

Tank 102AW Analyses				Sample							
14-Jun-91			<	9408	9409	9410	9411	9415	9416	9417	9418
Component	Units	MW									
Ag	ppm	107.868	<								
Al	ppm	26.98154									
As	ppm	74.9216									
B	ppm	10.81									
Ba	ppm	137.33	<								
Be	ppm	9.01218									
Bi	ppm	208.9804									
Ca	ppm	40.08									
Cd	ppm	112.41	<								
Ce	ppm	140.12									
Cr	ppm	51.996									
Cu	ppm	63.546									
Fe	ppm	55.847									
Hg	ppm	200.59	<								
K	ppm	39.0983									
La	ppm	138.9055									
Li	ppm	6.941									
Mg	ppm	24.305									
Mn	ppm	54.938	<								
Mo	ppm	95.94									
Na	ppm	22.98977									
Nd	ppm	144.24									
Ni	ppm	58.7									
P	ppm	30.97376									

TABLE 2-3 continued.

Tank 102AW Analyses				Sample							
14-Jun-91			<	9408	9409	9410	9411	9415	9416	9417	9418
Component	Units	MW									
Pb	ppm	207.2	<								
Pd	ppm	106.4									
Sb	ppm	121.75									
Se	ppm	78.96	<								
Si	ppm	28.0855									
Sn	ppm	118.69									
Te	ppm	180.9479									
Tl	ppm	47.9									
U	g/L	238.029						0.0045	0.0019	0.004	0.004
V	ppm	50.9415									
W	ppm	183.85									
Zn	ppm	65.38									
Zr	ppm	91.22									
CN-	ppm	26.0177		1.22	1.32	1.21	1.38				
S-2	ppm	32.06									
NH4 +	M	18.0383	<	0.008	0.008	0.00347	0.023				
NH3	M	17.0304									
CO3-2	M	60.0092									
Cl-	ppm	35.453		623	175	582	481				
F-	ppm	18.9984		4280	3870	4090	3900				
SO4-2	ppm	96.0576		2190	2620	2550	1980				
NO3-	ppm	63.0049		14250	14400	14100	14600				
NO2-	ppm	46.0055		2520	2640	2540	2580				
PO4-3	ppm	94.97136		178	179	174	167				

9413222.1422

TABLE 2-3 continued.

Tank 102AW Analyses				Sample							
1[illegible]n-91			<	9408	9409	9410	9411	9415	9416	9417	9418
Component	Units	MW									
OH-	M	17.0073		0.177	0.154	0.179					
TOC	g/L	12.011		0.407	0.616	0.617	0.424				
TIC	g/L	12.011		0.684	0.856	1.07	0.758				
SPG	g/mL			1.024	1.024	1.027	1.026				
TotS[illegible]de	wt%										
pH											
3H	uCi/L							5.88	5.65	5.56	5.64
14C	uCi/L										
54Mn	uCi/L										
59Mn	uCi/L										
60Co	uCi/L		<					6.59	5.19	2.57	8.19
63Ni	uCi/L										
79Se	uCi/L										
90Sr	uCi/L		R					9.86	8.1	10.31	153
94Nb	uCi/L		<					5.49	6.02	2.97	7.55
95Nb	uCi/L										
99Tc	uCi/L										
103Ru	uCi/L		<					21.4	21.9	11.5	29.3
106RuRh	uCi/L		<					407.5	273	478	433
113Sn	uCi/L		<					27.3	28.7	16.5	39.5
129I	uCi/L										
134Cs	uCi/L		<					173.5	189	175	162
137Cs	uCi/L							14750	15000	16100	15100
144CePr	uCi/L		<					157	153	76.7	230

TABLE 2-3 continued.

Tank 102AW Analyses				Sample							
14-Jun-91			<	9408	9409	9410	9411	9415	9416	9417	9418
Component	Units	MW									
154Eu	uCi/L		<					20.05	21	6.85	36.9
155Eu	uCi/L		<					38.05	39	21	71
226Ra	uCi/L		<					314.5	315	307	412
234U	uCi/L										
235U	uCi/L										
238U	uCi/L										
237Np	uCi/L										
238Pu	uCi/L										
239/240Pu	uCi/L							0.0778	0.0368	1.29	0.04
241Am	uCi/L										
242Cm	uCi/L										
243Cm	uCi/L										
244Cm	uCi/L										
TB	uCi/L							14400	13200	14700	20200
AT	uCi/L		<R					1.44	1.68	2.16	2.16

TABLE 2-4: 241-AP-103 Analysis Summary

Tank 241-AP-103 Analyses							
17-Dec-91						Molarity	
Component	Units	n	<	Mean	S.Dev.	Mean	S.Dev.
Ag	ppm	10	<	0.04	4.74e-10	3.71e-07	4.40e-15
Al	ppm	10		246.2	179.8245	9.12e-03	6.66e-03
As	ppm	10		0.04825	0.016199	6.44e-07	2.16e-07
B	ppm						
Ba	ppm	10	<	0.065	0	4.73e-07	0.00
Be	ppm						
Bi	ppm						
Ca	ppm						
Cd	ppm	10		0.11075	0.046661	9.85e-07	4.15e-07
Ce	ppm						
Cr	ppm	10		3.6943	2.207772	7.10e-05	4.25e-05
Cu	ppm						
Fe	ppm	10	<	0.8301	0.717151	1.49e-05	1.28e-05
Hg	ppm	9	<	0.002067	0.0011	1.03e-08	5.48e-09
K	ppm						
La	ppm						
Li	ppm						
Mg	ppm	10	<	0.721	0.508575	2.97e-05	2.09e-05
Mn	ppm	10	<	0.02604	0.017424	4.74e-07	3.17e-07
Mo	ppm						
Na	ppm	10		5312.5	3689.37	2.31e-01	1.60e-01
Nd	ppm						
Ni	ppm						
P	ppm						
Pb	ppm	10	<	0.4	0	1.93e-06	0.00
Pd	ppm						
Sb	ppm						
Se	ppm	10	<	0.0083	0.006203	1.05e-07	7.86e-08
Si	ppm						

TABLE 2-4 continued.

Tank 241-AP-103 Analyses							
17-Dec-91						Molarity	
Component	Units	n	<	Mean	S.Dev.	Mean	S.Dev.
Sn	ppm						
Ta	ppm						
Ti	ppm						
U	g/L	1		0.00369			
V	ppm						
W	ppm						
Zn	ppm	10	<	0.27405	0.374165	4.19e-06	5.72e-06
Zr	ppm						
CN-	ppm	10	<	0.5963	0.150586	2.29e-05	5.79e-06
S-2	ppm						
NH4+	M	10	<	2.75e-03	1.74e-03	2.75e-03	1.74e-03
NH3	M						
CO3-2	M						
Cl-	ppm	10		49.475	27.30044	1.40e-03	7.70e-04
F-	ppm	10		129.325	89.98548	6.81e-03	4.74e-03
SO4-2	ppm	10		350.2	131.9398	3.65e-03	1.37e-03
NO3-	ppm	10		4039	3081.787	6.41e-02	4.89e-02
NO2-	ppm	10		1299.3	264.141	2.82e-02	5.74e-03
PO4-3	ppm	10		138.1	16.27165	1.45e-03	1.71e-04
OH-	M	10		0.089866	0.066742	8.99e-02	6.67e-02
TOC	g/L	10		0.11203	0.024337		
TIC	g/L	10		0.51385	0.062412		
SPG	g/mL	10		1.00366	0.009484		
TotSolids	wt%						
pH							
3H	uCi/L	1		5.24			
14C	uCi/L	1		0.00447			
54Mn	uCi/L						
59Mn	uCi/L						
60Co	uCi/L	4	<	10.615	1.122304		

WHC-SD-WM-TI-528, Rev. 0
TABLE 2-4 continued.

Tank 241-AP-103 Analyses							
17-Dec-91						Molarity	
Component	Units	n	<	Mean	S.Dev.	Mean	S.Dev.
63Ni	uCi/L						
79Se	uCi/L	1		0.01115			
90Sr	uCi/L	1		2.62			
94Nb	uCi/L	1		9.31			
95Nb	uCi/L	2	<	8.6725	0.887419		
99Tc	uCi/L	1		1.08			
103Ru	uCi/L						
106RuRh	uCi/L	2	<	266	104.6518		
113Sn	uCi/L	2	<	23.8	8.768124		
129I	uCi/L	1	<	0.03185			
134Cs	uCi/L	11	<	10.45455	2.732217		
137Cs	uCi/L	11		6544.091	1042.609		
144CePr	uCi/L	2	<	132.825	52.57339		
154Eu	uCi/L	4	<	27.9875	4.905843		
155Eu	uCi/L	10	<	43.695	18.37012		
226Ra	uCi/L	2	<	143.5	142.1285		
234U	uCi/L	1		0.00652			
235U	uCi/L	1		0.000339			
238U	uCi/L	1		0.001257			
237Np	uCi/L						
238Pu	uCi/L						
239/240Pu	uCi/L	1	<	0.00697			
241Am	uCi/L	1	<	0.01135			
242Cm	uCi/L						
243Cm	uCi/L						
244Cm	uCi/L						
TB	uCi/L						
AT	uCi/L						

9413222.1426

TABLE 2-5: 241-AW-106 Analysis Summary

Tank 241-AW-106 Analyses							
20-Sep-91						Molarity	
Component	Units	n	<	Mean	S.Dev.	Mean	S.Dev.
Ag	ppm	10	<R	4.812	1.216487	4.46e-05	1.13e-05
Al	ppm	10	R	1675.7	1168.542	6.21e-02	4.33e-02
As	ppm	10		2.6235	0.541449	3.50e-05	7.23e-06
B	ppm						
Ba	ppm	10	<R	1.727	0.230846	1.26e-05	1.68e-06
Be	ppm						
Bi	ppm						
Ca	ppm						
Cd	ppm	10	<R	2.973	0.89098	2.64e-05	7.93e-06
Ce	ppm						
Cr	ppm	10	R	22.915	6.087604	4.41e-04	1.17e-04
Cu	ppm						
Fe	ppm	10	<R	74.56	50.42793	1.34e-03	9.03e-04
Hg	ppm	10	<R	0.01046	0.012889	5.21e-08	6.43e-08
K	ppm						
La	ppm						
Li	ppm						
Mg	ppm	10	<R	10.588	9.392319	4.36e-04	3.86e-04
Mn	ppm	10	R	6.7235	6.419986	1.22e-04	1.17e-04
Mo	ppm						
Na	ppm	10	R	39770	16568.78	1.73e+00	7.21e-01
Nd	ppm						
Ni	ppm						
P	ppm						
Pb	ppm	10	<R	43.64	11.6957	2.11e-04	5.64e-05
Pd	ppm						
Sb	ppm						
Se	ppm	10	<	0.0082	0.003795	1.04e-07	4.81e-08
Si	ppm						

E.90

TABLE 2-5 continued.

Tank 241-AW-106 Analyses							
20-Sep-91						Molarity	
Component	Units	n	<	Mean	S.Dev.	Mean	S.Dev.
Sn	ppm						
Ta	ppm						
Ti	ppm						
U	g/L	1		0.00947			
V	ppm						
W	ppm						
Zn	ppm	10	R	103.77	43.29342	1.59e-03	6.62e-04
Zr	ppm						
CN-	ppm	10		1.98515	0.982056	7.63e-05	3.77e-05
S-2	ppm						
NH4+	M	10	<	3.29e-03	5.10e-03	3.29e-03	5.10e-03
NH3	M						
CO3-2	M						
Cl-	ppm	10		535.3	229.5887	1.51e-02	6.48e-03
F-	ppm	5		6512	1066.804	3.43e-01	5.62e-02
SO4-2	ppm	10		3418	2564.419	3.56e-02	2.67e-02
NO3-	ppm	10		36454.99	13999.66	5.79e-01	2.22e-01
NO2-	ppm	10		9575	5092.607	2.08e-01	1.11e-01
PO4-3	ppm	10		728.862	384.3368	7.67e-03	4.05e-03
OH-	M	10		0.58838	0.261077	5.88e-01	2.61e-01
TOC	g/L	10		1.0466	0.475226		
TIC	g/L	10		2.3595	0.582773		
SPG	g/mL	10		1.08595	0.04359		
TotSolids	wt%						
pH							
3H	uCi/L	1		12			
14C	uCi/L	1		0.0747			
54Mn	uCi/L						
59Mn	uCi/L						
60Co	uCi/L	1	<	6.37			

TABLE 2-5 continued.

Tank 241-AW-106 Analyses							
20-Sep-91						Molarity	
Component	Units	n	<	Mean	S.Dev.	Mean	S.Dev.
63Ni	uCi/L						
79Se	uCi/L	1		0.0398			
90Sr	uCi/L	1		29.45			
94Nb	uCi/L	1	<	7.38			
95Nb	uCi/L						
99Tc	uCi/L	1		16.8			
103Ru	uCi/L						
106RuRh	uCi/L	1	<	489			
113Sn	uCi/L	1	<	50.15			
129I	uCi/L	1	<R	0.0424			
134Cs	uCi/L	1	<	397			
137Cs	uCi/L	1		50650			
144CePr	uCi/L	1	<	271.5			
154Eu	uCi/L	1	<	16.05			
155Eu	uCi/L	1	<	68.85			
226Ra	uCi/L	1	<	77.55			
234U	uCi/L	1		0.009252			
235U	uCi/L	1		0.000921			
238U	uCi/L	1		0.003015			
237Np	uCi/L						
238Pu	uCi/L						
239/240Pu	uCi/L	1	<	0.09885			
241Am	uCi/L	1	<	0.02145			
242Cm	uCi/L						
243Cm	uCi/L						
244Cm	uCi/L						
TB	uCi/L						
AT	uCi/L						

E.92

TABLE 2-6: 241-AW-102 Analysis Summary

Tank 241-AW-102 Analyses							
14-Jun-91						Molarity	
Component	Units	n	<	Mean	S.Dev.	Mean	S.Dev.
Ag	ppm	4	<	0.8925	0.171925	8.27e-06	1.59e-06
Al	ppm	4		487.5	10.90871	1.81e-02	4.04e-04
As	ppm	4		1.50625	0.094989	2.01e-05	1.27e-06
B	ppm						
Ba	ppm	4	<	1.3	8.43e-09	9.47e-06	6.14e-14
Be	ppm						
Bi	ppm						
Ca	ppm						
Cd	ppm	4	<	0.4	4.21e-09	3.56e-06	3.75e-14
Ce	ppm						
Cr	ppm	4		10.6625	0.2136	2.05e-04	4.11e-06
Cu	ppm						
Fe	ppm	4		31.58	20.52946	5.65e-04	3.68e-04
Hg	ppm	4	<	0.005	1.45e-11	2.49e-08	7.22e-17
K	ppm						
La	ppm						
Li	ppm						
Mg	ppm	4		13.4375	3.128198	5.53e-04	1.29e-04
Mn	ppm	4	<	0.975	1.35	1.77e-05	2.46e-05
Mo	ppm						
Na	ppm	4		16787.5	246.2214	7.30e-01	1.07e-02
Nd	ppm						
Ni	ppm						
P	ppm						
Pb	ppm	4	<	8	0	3.86e-05	0.00
Pd	ppm						
Sb	ppm						
Se	ppm	4	<	0.005	1.45e-11	6.33e-08	1.83e-16
Si	ppm						

TABLE 2-6 continued.

Tank 241-AW-102 Analyses							
14-Jun-91						Molarity	
Component	Units	n	<	Mean	S.Dev.	Mean	S.Dev.
Sn	ppm						
Ta	ppm						
Ti	ppm						
U	g/L	4		3.67e-03	1.23e-03	1.54e-08	5.15e-09
V	ppm						
W	ppm						
Zn	ppm	4		9.13625	8.01573	1.40e-04	1.23e-04
Zr	ppm						
CN-	ppm	4		1.2825	0.081803	4.93e-05	3.14e-06
S-2	ppm						
NH4+	M	4	<	0.01033	0.008471	1.03e-02	8.47e-03
NH3	M						
CO3-2	M						
Cl-	ppm	4		465.25	202.4918	1.31e-02	5.71e-03
F-	ppm	4		4035	190.1754	2.12e-01	1.00e-02
SO4-2	ppm	4		2335	302.4897	2.43e-02	3.15e-03
NO3-	ppm	4		14337.5	213.6001	2.28e-01	3.39e-03
NO2-	ppm	4		2570	52.91503	5.59e-02	1.15e-03
PO4-3	ppm	4		174.5	5.446712	1.84e-03	5.74e-05
OH-	M	3		0.17	0.013892	1.70e-01	1.39e-02
TOC	g/L	4		0.491075	0.096256		
TIC	g/L	4		0.842	0.167531		
SPG	g/mL	4		1.025275	0.001578		
TotSolids	wt%						
pH							
3H	uCi/L	4		5.6825	0.137689		
14C	uCi/L						
54Mn	uCi/L						
59Mn	uCi/L						
60Co	uCi/L	4	<	5.635	2.382737		

E.94

WHC-SD-WM-TI-528, Rev. 0
TABLE 2-6 continued.

Tank 241-AW-102 Analyses							
14-Jun-91						Molarity	
Component	Units	n	<	Mean	S.Dev.	Mean	S.Dev.
63Ni	uCi/L						
79Se	uCi/L						
90Sr	uCi/L	4	R	45.3175	71.79467		
94Nb	uCi/L	4	<	5.5075	1.903827		
95Nb	uCi/L						
99Tc	uCi/L						
103Ru	uCi/L	4	<	21.025	7.30542		
106RuRh	uCi/L	4	<	397.875	88.20466		
113Sn	uCi/L	4	<	28	9.40709		
129I	uCi/L						
134Cs	uCi/L	4	<	174.875	11.06327		
137Cs	uCi/L	4		15237.5	593.5416		
144CePr	uCi/L	4	<	154.175	62.61301		
154Eu	uCi/L	4	<	21.7	11.53798		
155Eu	uCi/L	4	<	42.2625	20.86725		
226Ra	uCi/L	4	<	337.125	50.0506		
234U	uCi/L						
235U	uCi/L						
238U	uCi/L						
237Np	uCi/L						
238Pu	uCi/L						
239/240Pu	uCi/L	4		0.361225	0.619461		
241Am	uCi/L	4		0.25745	0.373926		
242Cm	uCi/L						
243Cm	uCi/L						
244Cm	uCi/L						
TB	uCi/L	4		15625	3118.092		
AT	uCi/L	4	<R	1.86	0.36		

9413222.1432

TABLE 2-7: Future Dilute DSSF Waste Summary[2]

Dilute Waste Analyses and Estimates		
Units: Molarity; uCi/L for radionuclides; others as noted		
2&6AW,3AP	Composite	Evap.
Component	MEAN	product
Ag	9.23e-06	7.10e-05
Al	1.95e-02	1.50e-01
As	1.30e-05	1.00e-04
B		
Ba	5.72e-06	4.40e-05
Be		
Bi		
Ca	0.00	0.00
Cd	5.27e-06	4.05e-05
Ce		
Cr	1.73e-04	1.33e-03
Cu		
Fe	4.10e-04	3.15e-03
Hg	2.16e-08	1.66e-07
K		
La		
Li		
Mg	2.97e-04	2.29e-03
Mn	2.30e-05	1.77e-04
Mo		
Na	6.27e-01	4.82e+00
Nd		
Ni		
P		

[2] 241-AP-106 concentration estimates developed in WHC-SD-WM-TP-117.

WHC-SD-WM-TI-528, Rev. 0
TABLE 2-7 continued.

Dilute Waste Analyses and Estimates		
Units: Molarity; uCi/L for radionuclides; others as noted		
2&6AW,3AP	Composite	Evap.
Component	MEAN	product
Pb	4.35e-05	3.35e-04
Pd		
Sb		
Se	8.77e-08	6.74e-07
Si		
Sn		
Ta		
Ti		
U g/L	1.18e-08	9.08e-08
V		
W		
Zn	2.60e-04	2.00e-03
Zr		
CN-	4.06e-05	3.12e-04
S-2		
NH4+	5.95e-03	5.20e-03
NH3		
CO3-2		
Cl-	1.36e-02	1.05e-01
F-	2.29e-01	1.76e+00
SO4-2	1.62e-02	1.25e-01
NO3-	1.97e-01	1.51e+00
NO2-	6.24e-02	4.[illegible]e-01
PO4-3	2.40e-03	1.85e-02
OH-	1.86e-01	1.43e+00
TOC g/L	3.87e-01	2.98e+00
TIC g/L	8.83e-01	6.79e+00

WHC-SD-WM-TI-528, Rev. 0
TABLE 2-7 continued.

Dilute Waste Analyses and Estimates		
Units: Molarity; uCi/L for radionuclides; others as noted		
2&6AW,3AP	Composite	Evap.
Component	MEAN	product
SPG	1.02e+00	~1.25
TotSolids		
pH		
3H	6.28e+00	5.49e+00
14C	1.96e-02	1.51e-01
54Mn		
59Mn		
60Co	8.02e+00	6.17e+01
63Ni		
79Se	2.55e-02	1.96e-01
90Sr	2.37e+01	1.82e+02
94Nb	7.49e+00	5.76e+01
95Nb	8.67e+00	6.67e+01
99Tc	4.47e+00	3.44e+01
103Ru	2.10e+01	1.62e+02
106RuRh	3.49e+02	2.68e+03
113Sn	2.89e+01	2.22e+02
129I	3.41e-02	2.63e-01
134Cs	1.27e+02	9.80e+02
137Cs	1.57e+04	1.21e+05
144CePr	1.59e+02	1.22e+03
154Eu	4.07e+01	3.13e+02
155Eu	4.63e+01	3.56e+02
226Ra	2.15e+02	1.66e+03
234U	4.17e-03	3.21e-02
235U	2.72e-04	2.10e-03
238U	9.59e-04	7.38e-03

TABLE 2-7 continued.

Dilute Waste Analyses and Estimates		
Units: Molarity; uCi/L for radionuclides; others as noted		
2&6AW,3AP	Composite	Evap.
Component	MEAN	product
237Np		
238Pu		
239/240Pu	1.65e-01	1.27e+00
241Am	1.14e-01	8.80e-01
242Cm		
243Cm		
244Cm		
TB		
AT		
Volume L	9.06e+06	1177332
WVR		87.00%

Note: Evaporator product calculated as 87% WVR.

9413222.1436

TABLE 3-1: Evaporator Campaign 84-3 Analysis Data[3]

Evap Camp. 84-3 Analyses				Sample	Decay to
07/03			<	R9991	Oct-93
Component	Units	MW			
Ag	ppm	107.868			
Al	M	26.9815		1.81	
As	ppm	74.9216			
B	ppm	10.81			
Ba	ppm	137.33			
Be	ppm	9.01218			
Bi	ppm	208.98			
Ca	ppm	40.08			
Cd	ppm	112.41			
Ce	ppm	140.12			
Cr	ppm	51.996		0.013	
Cu	ppm	63.546			
Fe	ppm	55.847		2e-04	
Hg	ppm	200.59			
K	ppm	39.0983			
La	ppm	138.906			
Li	ppm	6.941			
Mg	ppm	24.305			
Mn	ppm	54.938			
Mo	ppm	95.94			
Na	M	22.9898			
Nd	ppm	144.24			
Ni	ppm	58.7			
P	ppm	30.9738			
Pb	ppm	207.2			
Pd	ppm	106.4			
Sb	ppm	121.75			
Se	ppm	78.96			
Si	ppm	28.0855			
Sn	ppm	118.69			
Ta	ppm	180.948			
Ti	ppm	47.9			

3 Reference: SD-WM-PE-018

E.100

TABLE 3-1 continued.

Evap Camp. 84-3 Analyses				Sample	Decay to
07/03			<	R9991	Oct-93
Component	Units	MW			
U	g/L	238.029			
V	ppm	50.9415			
W	ppm	183.85			
Zn	ppm	65.38			
Zr	ppm	91.22			
CN-	ppm	26.0177			
S-2	ppm.	32.06			
NH4+	M	18.0383			
NH3	M	17.0304			
CO3-2	M	60.0092		0.28	
Cl-	M	35.453			
F-	M	18.9984			
SO4-2	M	96.0576		0.016	
NO3-	M	63.0049		2.72	
NO2-	M	46.0055		1.87	
PO4-3	M	94.9714		0.007	
OH-	M	17.0073		4.00	
TOC	M	12.011		0.3189	
TIC	g/L	12.011			
SPG	g/mL			1.464	
TotSolids	wt%				
pH					
3H	uCi/L				
14C	uCi/L				
54Mn	uCi/L				
59Mn	uCi/L				
60Co	uCi/L				
63Ni	uCi/L				
79Se	uCi/L				
90Sr	uCi/L			1270	1019
94Nb	uCi/L				
95Nb	uCi/L				
99Tc	uCi/L				
103Ru	uCi/L				
106RuRh	uCi/L				

TABLE 3-1 continued.

Evap Camp. 84-3 Analyses				Sample	Decay to
07/03			<	R9991	Oct-93
Component	Units	MW			
113Sn	uCi/L				
129I	uCi/L				
134Cs	uCi/L				
137Cs	uCi/L			624000	504603
144CePr	uCi/L				
154Eu	uCi/L				
155Eu	uCi/L				
226Ra	uCi/L				
234U	uCi/L				
235U	uCi/L				
238U	uCi/L				
237Np	uCi/L				
238Pu	uCi/L				
239/240Pu	uCi/L			10.422	
241Am	uCi/L			11400	
242Cm	uCi/L				
243Cm	uCi/L				
244Cm	uCi/L				
TB	uCi/L				
AT	uCi/L				
Note: Pu (total) assumed to be 239					

TABLE 3-2: Evaporator Campaign 84-5 Analysis Data[4]

Evap Camp. 84-5 Analyses				Sample				
15-Oct-84			<	R3303	R3305	R3307	R3413	R3415
Component	Units	MW						
Ag	ppm	107.868						
Al	M	26.98154		1.3	1.39	1.21	1.25	1.11
As	ppm	74.9216						
B	ppm	10.81						
Ba	ppm	137.33						
Be	ppm	9.01218						
Bi	ppm	208.9804						
Ca	ppm	40.08						
Cd	ppm	112.41						
Ce	ppm	140.12						
Cr	ppm	51.996						
Cu	ppm	63.546						
Fe	ppm	55.847						
Hg	ppm	200.59						
K	ppm	39.0983		0.154	0.178	0.408	0.085	0.11
La	ppm	138.9055						
Li	ppm	6.941						
Mg	ppm	24.305						
Mn	ppm	54.938						
Mo	ppm	95.94						
Na	M	22.98977		14.35		11.48	11.53	10.64
Nd	ppm	144.24						
Ni	ppm	58.7						
P	ppm	30.97376						
Pb	ppm	207.2						
Pd	ppm	106.4						
Sb	ppm	121.75						
Se	ppm	78.96						
Si	ppm	28.0855						
Sn	ppm	118.69						
Ta	ppm	180.9479						
Ti	ppm	47.9						

[4] Reference: SD-WM-PE-022

TABLE 3-2 continued.

Evap Camp. 84-5 Analyses				Sample				
15-Oct-84			<	R3303	R3305	R3307	R3413	R3415
Component	Units	MW						
U	g/L	238.029						
V	ppm	50.9415						
W	ppm	183.85						
Zn	ppm	65.38						
Zr	ppm	91.22						
CN-	ppm	26.0177						
S-2	ppm	32.06						
NH4+	M	18.0383						
NH3	M	17.0304	<	0.005				
CO3-2	M	60.0092		0.255	0.18	0.94	0.588	0.66
Cl-	M	35.453	<	0.215		0.2	0.23	0.167
F-	M	18.9984	<					
SO4-2	M	96.0576	<					0.078
NO3-	M	63.0049		2.88	2.31	4.09	3.14	3.4
NO2-	M	46.0055		1.97	2.16	1.31	2.05	1.64
PO4-3	M	94.97136		0.02	0.022	0.055	0.026	0.052
OH-	M	17.0073		4.6	4.72	3.84	4.35	3.37
TOC	M	12.011		6.6	5.95	4.31	6.01	4.72
TIC	g/L	12.011						
SPG	g/mL			1.49	1.54	1.52	1.51	1.47
TotSolids	wt%							
pH								
3H	uCi/L							
14C	uCi/L							
54Mn	uCi/L							
59Mn	uCi/L							
60Co	uCi/L							
63Ni	uCi/L							
79Se	uCi/L							
90Sr	uCi/L			17100	9710	21600	18000	11000
94Nb	uCi/L							
95Nb	uCi/L							
99Tc	uCi/L							
103Ru	uCi/L							
106RuRh	uCi/L							

TABLE 3-2 continued.

Evap Camp. 84-5 Analyses				Sample				
15-Oct-84			<	R3303	R3305	R3307	R3413	R3415
Component	Units	MW						
113Sn	uCi/L							
129I	uCi/L							
134Cs	uCi/L			1260				
137Cs	uCi/L			940000	1890000	783000	889000	665000
144CePr	uCi/L							
154Eu	uCi/L							
155Eu	uCi/L							
226Ra	uCi/L							
234U	uCi/L							
235U	uCi/L							
238U	uCi/L							
237Np	uCi/L							
238Pu	uCi/L							
239/240Pu	uCi/L							
241Am	uCi/L							
242Cm	uCi/L							
243Cm	uCi/L							
244Cm	uCi/L							
TB	uCi/L							
AT	uCi/L							

TABLE 3-3: Evaporator Campaign 85-3 Analysis Data[5]

Evap Camp. 85-3 Analyses				Sample				
03-Apr-85			<	R4680	R4681	R4683	R4684	R4687
Component	Units	MW						
Ag	ppm	107.868						
Al	M	26.98154		1.7		1.8		1.73
As	ppm	74.9216						
B	ppm	10.81						
Ba	ppm	137.33						
Be	ppm	9.01218						
Bi	ppm	208.9804						
Ca	ppm	40.08						
Cd	ppm	112.41						
Ce	ppm	140.12						
Cr	ppm	51.996						
Cu	ppm	63.546						
Fe	ppm	55.847						
Hg	ppm	200.59						
K	ppm	39.0983		0.14		0.18		0.15
La	ppm	138.9055						
Li	ppm	6.941						
Mg	ppm	24.305						
Mn	ppm	54.938						
Mo	ppm	95.94						
Na	M	22.98977		11.45		11.38		13.08
Nd	ppm	144.24						
Ni	ppm	58.7						
P	ppm	30.97376						
Pb	ppm	207.2						
Pd	ppm	106.4						
Sb	ppm	121.75						
Se	ppm	78.96						
Si	ppm	28.0855						
Sn	ppm	118.69						
Ta	ppm	180.9479						
Ti	ppm	47.9						

[5] Reference: SD-WM-PE-023

WHC-SD-WM-TI-528, Rev. 0
TABLE 3-3 continued.

Evap Camp. 85-3 Analyses				Sample				
03-Apr-85			<	R4680	R4681	R4683	R4684	R4687
Component	Units	MW						
U	g/L	238.029						
V	ppm	50.9415						
W	ppm	183.85						
Zn	ppm	65.38						
Zr	ppm	91.22						
CN-	ppm	26.0177						
S-2	ppm	32.06						
NH4+	M	18.0383						
NH3	M	17.0304	<			0.02		0.02
CO3-2	M	60.0092		0.7		0.14		0.25
Cl-	M	35.453		0.28		0.24		0.2
F-	M	18.9984	<					
SO4-2	M	96.0576	<					
NO3-	M	63.0049		4.18		2.13		3.05
NO2-	M	46.0055		2.42		2.28		3.13
PO4-3	M	94.97136		0.03		0.01		0.02
OH-	M	17.0073		3.05		4.48		3.38
TOC	M	12.011		4.1		5.3		2.23
TIC	g/L	12.011						
SPG	g/mL			1.53		1.5		1.48
TotSolids	wt%							
pH				13.5				
3H	uCi/L							
14C	uCi/L							
54Mn	uCi/L							
59Mn	uCi/L							
60Co	uCi/L							
63Ni	uCi/L							
79Se	uCi/L							
90Sr	uCi/L			3950				
94Nb	uCi/L							
95Nb	uCi/L							
99Tc	uCi/L							
103Ru	uCi/L							
106RuRh	uCi/L							

WHC-SD-WM-TI-528, Rev. 0
TABLE 3-3 continued.

Evap Camp. 85-3 Analyses				Sample				
03-Apr-85			<	R4680	R4681	R4683	R4684	R4687
Component	Units	MW						
113Sn	uCi/L							
129I	uCi/L							
134Cs	uCi/L							
137Cs	uCi/L			613000				
144CePr	uCi/L							
154Eu	uCi/L							
155Eu	uCi/L							
226Ra	uCi/L							
234U	uCi/L							
235U	uCi/L							
238U	uCi/L							
237Np	uCi/L							
238Pu	uCi/L							
239/240Pu	uCi/L							
241Am	uCi/L							
242Cm	uCi/L							
243Cm	uCi/L							
244Cm	uCi/L							
TB	uCi/L							
AT	uCi/L							

9413222.1445

TABLE 3-4: Evaporator Campaign 84-5 Analysis Summary

Evap Camp. 84-5 Analyses						
Oct-84						Oct-93
Component	Units	n	<	Mean	S.Dev.	
Ag	ppm	0				
Al	M	5		1.252	0.104019	
As	ppm	0				
B	ppm	0				
Ba	ppm	0				
Be	ppm	0				
Bi	ppm	0				
Ca	ppm	0				
Cd	ppm	0				
Ce	ppm	0				
Cr	ppm	0				
Cu	ppm	0				
Fe	ppm	0				
Hg	ppm	0				
K	ppm	5		0.187	0.128787	
La	ppm	0				
Li	ppm	0				
Mg	ppm	0				
Mn	ppm	0				
Mo	ppm	0				
Na	ppm	4		12	1.618991	
Nd	ppm	0				
Ni	ppm	0				
P	ppm	0				
Pb	ppm	0				
Pd	ppm	0				
Sb	ppm	0				
Se	ppm	0				
Si	ppm	0				
Sn	ppm	0				
Ta	ppm	0				
Ti	ppm	0				
U	g/L	0				
V	ppm	0				

TABLE 3-4 continued.

Evap Camp. 84-5 Analyses						
Oct-84						Oct-93
Component	Units	n	<	Mean	S.Dev.	
W	ppm	0				
Zn	ppm	0				
Zr	ppm	0				
CN-	ppm	0				
S-2	ppm	0				
NH4+	M	0				
NH3	M	1		0.006		
CO3-2	M	5		0.5246	0.310783	
Cl-	ppm	4		0.208	0.018601	
F-	ppm	0				
SO4-2	ppm	1		0.078		
NO3-	ppm	5		3.164	0.656453	
NO2-	ppm	5		1.826	0.347606	
PO4-3	ppm	5		0.035	0.017059	
OH-	M	5		4.176	0.563143	
TOC	g/L	5		5.518	0.961182	
TIC	g/L	0				
SPG	g/mL	5		1.506	0.027019	
TotSolids	wt%	0				
pH		0				
3H	uCi/L	0				
14C	uCi/L	0				
54Mn	uCi/L	0				
59Mn	uCi/L	0				
60Co	uCi/L	0				
63Ni	uCi/L	0				
79Se	uCi/L	0				
90Sr	uCi/L	5		15482	4994.809	12506.79
94Nb	uCi/L	0				
95Nb	uCi/L	0				
99Tc	uCi/L	0				
103Ru	uCi/L	0				
106RuRh	uCi/L	0				
113Sn	uCi/L	0				
129I	uCi/L	0				

TABLE 3-4 continued.

Evap Camp. 84-5 Analyses						
Oct-84						Oct-93
Component	Units	n	<	Mean	S.Dev.	
134Cs	uCi/L	1		1260		62.27367
137Cs	uCi/L	5		1033400	490346.1	841151.3
144CePr	uCi/L	0				
154Eu	uCi/L	0				
155Eu	uCi/L	0				
226Ra	uCi/L	0				
234U	uCi/L	0				
235U	uCi/L	0				
238U	uCi/L	0				
237Np	uCi/L	0				
238Pu	uCi/L	0				
239/240Pu	uCi/L	0				
241Am	uCi/L	0				
242Cm	uCi/L	0				
243Cm	uCi/L	0				
244Cm	uCi/L	0				
TB	uCi/L	0				
AT	uCi/L	0				

TABLE 3-5: Evaporator Campaign 85-3 Analysis Summary

Evap Camp. 85-3 Analyses						Decay to
Apr-85						Oct-93
Component	Units	n	<	Mean	S.Dev.	
Ag	ppm	0				
Al	M	3		1.743333	0.061316	
As	ppm	0				
B	ppm	0				
Ba	ppm	0				
Be	ppm	0				
Bi	ppm	0				
Ca	ppm	0				
Cd	ppm	0				
Ce	ppm	0				
Cr	ppm	0				
Cu	ppm	0				
Fe	ppm	0				
Hg	ppm	0				
K	ppm	3		0.156667	0.020817	
La	ppm	0				
Li	ppm	0				
Mg	ppm	0				
Mn	ppm	0				
Mo	ppm	0				
Na	M	3		11.97	0.961925	
Nd	ppm	0				
Ni	ppm	0				
P	ppm	0				
Pb	ppm	0				
Pd	ppm	0				
Sb	ppm	0				
Se	ppm	0				
Si	ppm	0				
Sn	ppm	0				
Ta	ppm	0				
Ti	ppm	0				
U	g/L	0				
V	ppm	0				

WHC-SD-WM-TI-528, Rev. 0
TABLE 3-5 continued.

Evap Camp. 85-3 Analyses						Decay to
Apr-85						Oct-93
Component	Units	n	<	Mean	S.Dev.	
W	ppm	0				
Zn	ppm	0				
Zr	ppm	0				
CN-	ppm	0				
S-2	ppm	0				
NH4+	M	0				
NH3	M	2		0.02	7.09e-11	
CO3-2	M	3		0.363333	0.296704	
Cl-	M	3		0.24	0.04	
F-	M	0				
SO4-2	M	0				
NO3-	M	3		3.12	1.026791	
NO2-	M	3		2.61	0.455741	
PO4-3	M	3		0.02	0.01	
OH-	M	3		3.636667	0.748755	
TOC	M	3		3.876667	1.547137	
TIC	g/L	0				
SPG	g/mL	3		1.503333	0.025166	
TotSolids	wt%	0				
pH		1		13.5		
3H	uCi/L	0				
14C	uCi/L	0				
54Mn	uCi/L	0				
59Mn	uCi/L	0				
60Co	uCi/L	0				
63Ni	uCi/L	0				
79Se	uCi/L	0				
90Sr	uCi/L	1		3950		3226.485
94Nb	uCi/L	0				
95Nb	uCi/L	0				
99Tc	uCi/L	0				
103Ru	uCi/L	0				
106RuRh	uCi/L	0				
113Sn	uCi/L	0				
129I	uCi/L	0				

TABLE 3-5 continued.

Evap Camp. 85-3 Analyses						Decay to
Apr-85						Oct-93
Component	Units	n	<	Mean	S.Dev.	
134Cs	uCi/L	0				
137Cs	uCi/L	1		613000		504323.6
144CePr	uCi/L	0				
154Eu	uCi/L	0				
155Eu	uCi/L	0				
226Ra	uCi/L	0				
234U	uCi/L	0				
235U	uCi/L	0				
238U	uCi/L	0				
237Np	uCi/L	0				
238Pu	uCi/L	0				
239/240Pu	uCi/L	0				
241Am	uCi/L	0				
242Cm	uCi/L	0				
243Cm	uCi/L	0				
244Cm	uCi/L	0				
TB	uCi/L	0				
AT	uCi/L	0				

TABLE 4-1: Concentrated Waste Summary Data - 101AW, 103AN[6]

Units: Molarity; uCi/L for radionuclides; others as noted						
	101-AW Analysis		Jul-90	103-AN Analysis		Dec-84
			Uniform			Uniform
Component	Units	MEAN	Unit mean	Units	MEAN	Unit mean
Ag	M	3.09e-04	3.09e-04	mg/g	1.00e-02	1.48e-04
Al	M	1.03e+00	1.03e+00	mg/g	3.60e+01	2.13e+00
As	M	1.33e-07	1.33e-07	mg/g	1.00e-01	2.14e-03
B	M			mg/g		
Ba	M	6.80e-05	6.80e-05	mg/g	1.00e-02	1.17e-04
Be	M			mg/g	1.00e-02	1.78e-03
Bi	M	5.79e-04	5.79e-04	mg/g	3.00e-02	2.30e-04
Ca	M	8.26e-04	8.26e-04	mg/g	5.40e-02	2.16e-03
Cd	M	1.08e-05	1.08e-05	mg/g	1.00e-02	1.42e-04
Ce	M			mg/g		
Cr	M	3.09e-03	3.09e-03	mg/g	5.30e-01	1.63e-02
Cu	M	3.81e-04	3.81e-04	mg/g	7.50e-03	1.89e-04
Fe	M	7.86e-04	7.86e-04	mg/g	4.40e-02	1.26e-03
Hg	mg/L	1.57e-01	7.82e-07	mg/g	1.00e-02	7.98e-05
K	M	1.07e+00	1.07e+00	mg/g	9.50e+00	3.89e-01
La	M			mg/g		
Li	M			mg/g		
Mg	M	2.16e-03	2.16e-03	mg/g	1.80e-02	1.18e-03
Mn	M	4.76e-04	4.76e-04	mg/g	1.80e-02	5.24e-04
Mo	M	6.00e-04	6.00e-04	mg/g	5.50e-02	9.17e-04
Na	M	1.00e+01	1.00e+01	mg/g	2.10e+02	1.46e+01
Nd	M			mg/g		
Ni	M			mg/g	1.50e-02	4.09e-04
P	M			mg/g		
Pb	M	1.46e-03	1.46e-03	mg/g	4.50e-02	3.47e-04
Pd	M			mg/g		
Sb	M			mg/g	1.00e-01	1.31e-03
Se	M	4.20e-07	4.20e-07	mg/g	1.30e-01	2.63e-03
Si	M	4.36e-03	4.36e-03	mg/g	1.70e-01	9.68e-03
Sn	M			mg/g		

6 References: WHC-SD-WM-TRP-055 and SD-WM-TI-355, Rev. 1. Less-thans calculated as real values.

WHC-SD-WM-TI-528, Rev. 0
TABLE 4-1 continued.

Units: Molarity; uCi/L for radionuclides; others as noted						
	101-AW Analysis		Jul-90	103-AN Analysis		Dec-84
			Uniform			Uniform
Component	Units	MEAN	Unit mean	Units	MEAN	Unit mean
Te	M			mg/g		
Tl	M	9.88e-05	9.88e-05	mg/g	1.00e-02	3.34e-04
U	M	9.39e-04	9.39e-04	mg/g	7.70e-02	5.18e-04
V	M			mg/g	1.00e-02	3.14e-04
W	M			mg/g	1.30e-01	1.13e-03
Zn	M	4.84e-03	4.84e-03	mg/g	3.00e-02	7.34e-04
Zr	M	5.54e-04	5.54e-04	mg/g	1.50e-02	2.63e-04
CN-	M	1.03e-03	1.03e-03	mg/g	2.10e-02	1.29e-03
S-2	M			mg/g		
NH4+	M	1.46e-02	1.46e-02	mg/g		
NH3	M			mg/g		
CO3-2	M	2.05e-01	2.05e-01	mg/g	5.60e+00	1.49e-01
Cl-	M	1.46e-01	1.46e-01	mg/g	6.00e+00	2.71e-01
F-	M	4.02e-03	4.02e-03	mg/g	4.60e-01	3.87e-02
SO4-2	M	1.07e-02	1.07e-02	mg/g	1.00e+00	1.67e-02
NO3-	M	3.46e+00	3.46e+00	mg/g	1.00e+02	2.54e+00
NO2-	M	2.19e+00	2.19e+00	mg/g	8.60e+01	2.99e+00
PO4-3	M	2.22e-02	2.22e-02	mg/g	5.60e-01	9.77e-03
OH-	M	5.07e+00	5.07e+00	mg/g	6.10e+01	5.74e+00
TOC g/L	g/L	2.46e+00	2.46e+00	mg/g	4.60e+00	6.13e-01
TIC g/L	g/L	2.46e+00	2.46e+00	mg/g		
SPG	g/cm3	1.56e+00	1.56e+00	g/cm3	1.60e+00	1.60e+00
TotSolids	wt%					
pH						
3H	uCi/L	7.07e+00	7.07e+00	Ci/L	4.00e-06	4.00e+00
14C	uCi/L	3.70e-01	3.70e-01	Ci/L	2.00e-06	2.00e+00
54Mn	uCi/L			Ci/L		
59Mn	uCi/L			Ci/L		
60Co	uCi/L	2.96e+01	2.96e+01	Ci/L	3.80e-05	3.80e+01
63Ni	uCi/L			Ci/L		
79Se	uCi/L	4.80e-01	4.80e-01	Ci/L	4.30e-05	4.30e+01
89/90Sr	uCi/L	1.09e+03	1.09e+03	Ci/L	1.30e-02	1.30e+04
94Nb	uCi/L	6.82e+01	6.82e+01	Ci/L	7.10e-06	7.10e+00
95Nb	uCi/L			Ci/L		

TABLE 4-1 continued.

Units: Molarity; uCi/L for radionuclides; others as noted						
	101-AW Analysis		Jul-90	103-AN Analysis		Dec-84
			Uniform			Uniform
Component	Units	MEAN	Unit mean	Units	MEAN	Unit mean
99Tc	uCi/L	1.52e+02	1.52e+02	Ci/L	1.70e-04	1.70e+02
103Ru	uCi/L			Ci/L		
106RuRh	uCi/L	3.70e+03	3.70e+03	Ci/L	6.80e-05	6.80e+01
113Sn	uCi/L			Ci/L		
129I	uCi/L	3.03e-01	3.03e-01	Ci/L	5.20e-07	5.20e-01
134Cs	uCi/L	1.53e+03	1.53e+03	Ci/L	1.10e-04	1.10e+02
137Cs	uCi/L	5.20e+05	5.20e+05	Ci/L	7.50e-01	7.50e+05
144CePr	uCi/L			Ci/L		
154Eu	uCi/L			Ci/L		
155Eu	uCi/L			Ci/L		
226Ra	uCi/L			Ci/L		
234U	uCi/L			Ci/L	5.30e-08	5.30e-02
235U	uCi/L			Ci/L	1.10e-09	1.10e-03
238U	uCi/L			Ci/L	1.40e-08	1.40e-02
237Np	g/L	3.06e-03	2.16e+00	Ci/L	2.00e-08	2.00e-02
238Pu	uCi/L			Ci/L	9.80e-07	9.80e-01
239/240Pu	uCi/L	1.15e+00	1.15e+00	Ci/L	1.90e-06	1.90e+00
241Am	uCi/L	1.20e+00	1.20e+00	Ci/L	2.30e-06	2.30e+00
242Cm	uCi/L			Ci/L		
243/4Cm	uCi/L	5.33e-02	5.33e-02	Ci/L		
244Cm	uCi/L			Ci/L	4.20e-07	4.20e-01
TB	uCi/L			Ci/L		
AT	uCi/L			Ci/L		
Volume	L		3.83e+06			3.49e+06

TABLE 4-2: Concentrated Waste Summary Data - 105AP, 106AN[7]

	Less-thans calculated as real values						
	105-AP Estimate			Jan-89	106-AN Analysis		Apr-89
		Top	Bottom	Uniform			Uniform
	Units	MEAN	MEAN	Unit mean	Units	MEAN	Unit mean
Ag	M	9.30e-05	2.80e-04	2.00e-04	mg/L	3.63e+00	3.37e-05
Al	M	2.80e-01	7.10e-02	1.60e-01	mg/L	9.28e+03	3.44e-01
As	M	4.00e-08	1.20e-07	8.58e-08	mg/L	7.20e-02	9.61e-07
B	M				mg/L		
Ba	M	2.00e-05	6.10e-05	4.36e-05	mg/L	1.11e+01	8.08e-05
Be	M				mg/L		
Bi	M	1.70e-04	5.20e-04	3.70e-04	mg/L	1.45e+02	6.94e-04
Ca	M	2.50e-04	1.70e-03	1.08e-03	mg/L	9.02e+01	2.25e-03
Cd	M	3.20e-06	9.70e-06	6.92e-06	mg/L	4.96e+01	4.41e-04
Ce	M				mg/L		
Cr	M	9.30e-04	5.10e-03	3.32e-03	mg/L	5.64e+02	1.08e-02
Cu	M	1.10e-04	3.40e-04	2.42e-04	mg/L	3.75e+00	5.90e-05
Fe	M	2.40e-04	1.70e-04	2.00e-04	mg/L	6.90e+00	1.24e-04
Hg	M	2.30e-07	7.00e-07	4.99e-07	mg/L	5.00e-02	2.49e-07
K	M	7,20e-01	9.60e-01	8.57e-01	mg/L	1.08e+03	2.76e-02
La	M				mg/L		
Li	M				mg/L		
Mg	M	6.50e-04	3.80e-04	4.95e-04	mg/L	2.78e+00	1.14e-04
Mn	M	1.40e-04	4.30e-04	3.06e-04	mg/L	5.57e+01	1.01e-03
Mo	M	1.80e-04	5.40e-04	3.86e-04	mg/L	6.66e+01	6.94e-04
Na	M	2.80e+00	9.00e+00	6.35e+00	mg/L	9.03e+04	3.93e+00
Nd	M				mg/L		
Ni	M	1.00e-03	3.00e-03	2.15e-03	mg/L		
P	M	6.70e-03	2.00e-02	1.43e-02	mg/L	6.11e+03	1.97e-01
Pb	M	4.40e-04	1.30e-03	9.33e-04	mg/L	4.60e+02	2.22e-03
Pd	M				mg/L		
Sb	M				mg/L		
Se	M	1.30e-07	3.80e-07	2.73e-07	mg/L	1.34e-01	1.70e-06
Si	M	1.30e-03	5.20e-03	3.53e-03	mg/L		
Sn	M				mg/L		

7 References: WHC-SD-WM-TP-130, WHC-SD-WM-TP-065, and SD-WM-TI-355, Rev. 1.

TABLE 4-2 continued.

	Less-thans calculated as real values						
	105-AP Estimate			Jan-89	106-AN Analysis		Apr-89
		Top	Bottom	Uniform			Uniform
	Units	MEAN	MEAN	Unit mean	Units	MEAN	Unit mean
Ta	M				mg/L	1.30e-01	7.18e-07
Tl	M	3.00e-05	8.90e-05	6.38e-05	mg/L	3.51e+00	7.33e-05
U	M	2.80e-04	8.50e-04	6.06e-04	g/L	4.00e-03	1.68e-05
V	M				mg/L		
W	M				mg/L		
Zn	M	1.50e-03	9.00e-04	1.16e-03	mg/L	9.44e+00	1.44e-04
Zr	M	1.70e-04	5.00e-04	3.59e-04	mg/L	2.78e+01	3.05e-04
CN-	M	3.10e-04	9.30e-04	6.65e-04	g/L	6.00e-03	2.31e-04
S-2	M				mg/L		
NH4+	M	5.30e-03	1.40e-04	2.34e-03	mg/L	1.30e+02	7.22e-03
NH3	M				mg/L		
CO3-2	M	2.70e-01	2.40e-01	2.53e-01	M	3.27e-01	3.27e-01
Cl-	M	3.90e-02	9.80e-02	7.28e-02	mg/L	2.46e+03	6.94e-02
F-	M	1.70e-01	1.00e-01	1.30e-01	mg/L	6.16e+01	3.24e-03
SO4-2	M	3.40e-02	1.80e-02	2.48e-02	mg/L	2.15e+03	2.24e-02
NO3-	M	1.80e+00	3.30e+00	2.66e+00	mg/L	6.85e+04	1.09e+00
NO2-	M	5.40e-01	1.50e+00	1.09e+00	M	6.44e-01	6.44e-01
PO4-3	M	2.50e-02	9.70e-03	1.62e-02	mg/L	1.84e+04	1.94e-01
OH-	M	3.20e+00	5.70e+00	4.63e+00	M	4.74e-01	4.74e-01
TOC g/L	g/L	2.20e+00	5.20e+00	3.92e+00	g/L	3.26e+00	3.26e+00
TIC g/L	g/L				g/L		
SPG	g/cm3	1.25e+00	1.42e+00	1.35e+00	g/cm3	1.23e+00	1.23e+00
TotSolids	wt%				wt%		
pH							
3H	uCi/L	1.10e+01	8.60e+00	9.63e+00	uCi/L	3.44e+00	3.44e+00
14C	uCi/L	1.10e-01	3.30e-01	2.36e-01	uCi/L	3.35e-01	3.35e-01
54Mn	uCi/L				uCi/L		
59Mn	uCi/L				uCi/L		
60Co	uCi/L	8.90e+00	2.70e+01	1.93e+01	uCi/L	9.15e+00	9.15e+00
63Ni	uCi/L				uCi/L		
79Se	uCi/L	1.40e-01	4.30e-01	3.06e-01	uCi/L	2.40e-01	2.40e-01
89/90Sr	uCi/L	3.10e+02	1.40e+02	2.13e+02	uCi/L	2.23e+03	2.23e+03
94Nb	uCi/L	2.00e+01	6.10e+01	4.35e+01	uCi/L	2.30e+01	2.30e+01
95Nb	uCi/L				uCi/L		

TABLE 4-2 continued.

	Less-thans calculated as real values						
	105-AP Estimate			Jan-89	106-AN Analysis		Apr-89
		Top	Bottom	Uniform			Uniform
	Units	MEAN	MEAN	Unit mean	Units	MEAN	Unit mean
99Tc	uCi/L	8.30e+00	2.50e+01	1.79e+01	uCi/L	6.92e+01	6.92e+01
103Ru	uCi/L				uCi/L		
106RuRh	uCi/L	1.10e+03	3.30e+03	2.36e+03	uCi/L	1.39e+03	1.39e+03
113Sn	uCi/L				uCi/L		
129I	uCi/L	2.00e-02	5.80e-02	4.18e-02	uCi/L	7.50e-02	7.50e-02
134Cs	uCi/L	1.60e+03	3.20e+03	2.52e+03	uCi/L	2.37e+01	2.37e+01
137Cs	uCi/L	1.70e+05	3.70e+05	2.85e+05	uCi/L	2.05e+05	2.05e+05
144CePr	uCi/L				uCi/L		
154Eu	uCi/L				uCi/L		
155Eu	uCi/L				uCi/L		
226Ra	uCi/L				uCi/L		
234U	uCi/L				uCi/L		
235U	uCi/L				uCi/L		
238U	uCi/L				uCi/L		
237Np	uCi/L	7.05e-01	1.90e+00	1.39e+00	g/L	3.00e-03	2.12e+00
238Pu	uCi/L	1.80e-02	5.30e-02	3.80e-02	uCi/L	2.00e-02	2.00e-02
239/240 Pu	uCi/L	2.00e-02	5.90e-02	4.23e-02	uCi/L	3.78e-02	3.78e-02
241Am	uCi/L	1.00e+00	1.60e+00	1.34e+00	uCi/L	6.06e-01	6.06e-01
242Cm	uCi/L				uCi/L		
243/4Cm	uCi/L	1.60e-02	4.80e-02	3.43e-02	uCi/L	4.70e-02	4.70e-02
244Cm	uCi/L				uCi/L		
TB	uCi/L				uCi/L		
AT	uCi/L				uCi/L		
Volume	L	1.34e+06	1.80e+06	3.15e+06			3.67e+06

TABLE 4-3: Concentrated Waste Summary Data - 104AN, 105AN

104AN and 105AN			85-3	84-5	84-3	Apr-85	Apr-85
Estimates			Apr-85	Oct-84	Jul-84	104-AN	105-AN
Component	Units	MW					
Ag	ppm	107.868					
Al	M	26.98154	1.74e+00	1.25e+00	1.81e+00	1.39e+00	1.74e+00
As	ppm	74.9216					
B	ppm	10.81					
Ba	ppm	137.33					
Be	ppm	9.01218					
Bi	ppm	208.9804					
Ca	ppm	40.08					
Cd	ppm	112.41					
Ce	ppm	140.12					
Cr	ppm	51.996			1.30e-02	1.30e-02	1.30e-02
Cu	ppm	63.546					
Fe	ppm	55.847			2.00e-04	2.00e-04	2.00e-04
Hg	ppm	200.59					
K	ppm	39.0983	1.57e-01	1.87e-01		1.83e-01	1.57e-01
La	ppm	138.9055					
Li	ppm	6.941					
Mg	ppm	24.305					
Mn	ppm	54.938					
Mo	ppm	95.94					
Na	M	22.98977	1.20e+01	1.20e+01		1.20e+01	1.20e+01
Nd	ppm	144.24					
Ni	ppm	58.7					
P	ppm	30.97376					
Pb	ppm	207.2					
Pd	ppm	106.4					
Sb	ppm	121.75					
Se	ppm	78.96					
Si	ppm	28.0855					
Sn	ppm	118.69					
Ta	ppm	180.9479					
Ti	ppm	47.9					
U	g/L	238.029					
V	ppm	50.9415					

WHC-SD-WM-TI-528, Rev. 0
Table 4-3 continued.

104AN and 105AN			85-3	84-5	84-3	Apr-85	Apr-85
Estimates			Apr-85	Oct-84	Jul-84	104-AN	105-AN
Component	Units	MW					
W	ppm	183.85					
Zn	ppm	65.38					
Zr	ppm	91.22					
CN-	ppm	26.0177					
S-2	ppm	32.06					
NH4+	M	18.0383					
NH3	M	17.0304	2.00e-02	5.00e-03		6.99e-03	2.00e-02
CO3-2	M	60.0092	3.63e-01	5.25e-01	2.80e-01	4.72e-01	3.63e-01
Cl-	M	35.453	2.40e-01	2.08e-01		2.12e-01	2.40e-01
F-	M	18.9984					
SO4-2	M	96.0576		7.80e-02	1.60e-02	6.82e-02	6.82e-02
NO3-	M	63.0049	3.12e+00	3.16e+00	2.72e+00	3.10e+00	3.12e+00
NO2-	M	46.0055	2.61e+00	1.83e+00	1.87e+00	1.92e+00	2.61e+00
PO4-3	M	94.97136	2.00e-02	3.50e-02	7.00e-03	2.94e-02	2.00e-02
OH-	M	17.0073	3.64e+00	4.18e+00	4.00e+00	4.09e+00	3.64e+00
TOC	g/L	12.011	4.66e+01	6.63e+01	3.83e+00	5.53e+01	4.66e+01
TIC	g/L	12.011					
SPG	g/mL		1.50e+00	1.51e+00	1.46e+00	1.50e+00	1.50e+00
TotSolids	wt%						
pH			1.35e+01			1.35e+01	1.35e+01
3H	uCi/L						
14C	uCi/L						
54Mn	uCi/L						
59Mn	uCi/L						
60Co	uCi/L						
63Ni	uCi/L						
79Se	uCi/L						
90Sr	uCi/L		3.95e+03	1.55e+04	1.27e+03	1.20e+04	3.95e+03
94Nb	uCi/L						
95Nb	uCi/L						
99Tc	uCi/L						
103Ru	uCi/L						
106RuRh	uCi/L						
113Sn	uCi/L						
129I	uCi/L						

WHC-SD-WM-TI-528, Rev. 0
Table 4-3 continued.

104AN and 105AN			85-3	84-5	84-3	Apr-85	Apr-85
Estimates			Apr-85	Oct-84	Jul-84	104-AN	105-AN
Component	Units	MW					
134Cs	uCi/L			1.26e+03		1.25e+03	1.25e+03
137Cs	uCi/L		6.13e+05	1.03e+06	6.24e+05	9.18e+05	6.13e+05
144CePr	uCi/L						
154Eu	uCi/L						
155Eu	uCi/L						
226Ra	uCi/L						
234U	uCi/L						
235U	uCi/L						
238U	uCi/L						
237Np	uCi/L						
238Pu	uCi/L						
239/240Pu	uCi/L				1.04e+01	1.04e+01	1.04e+01
241Am	uCi/L				1.14e+04	1.14e+04	1.14e+04
242Cm	uCi/L						
243Cm	uCi/L						
244Cm	uCi/L						
TB	uCi/L						
AT	uCi/L						
Volume	L		4.58e+05	2.99e+06	5.62e+05	4.01e+06	3.68e+06

TABLE 5-1: Radioisotope Decay Data[8]

Radionuclide		Half-life (term)		Half-life (seconds)	Specific Activity		Decay mode	Daughters (by decay mode)
					dpm/g	Ci/g		
3	H	1.23e+01	y	3.89e+08	2.15e+16	9.66e+03	Beta	3He
14	C	5.73e+03	y	1.81e+11	9.89e+12	4.46e+00	Beta	14N
32	P	1.43e+01	d	1233792	6.34e+17	2.86e+05	Beta	32S
35	S	8.72e+01	d	7534080	9.50e+16	4.28e+04	Beta	35Cl
51	Cr	2.77e+01	d	2393626	2.05e+17	9.24e+04	EC	51V
54	Mn	3.12e+02	d	26974080	1.72e+16	7.74e+03	EC	54Cr
55	Fe	2.73e+00	y	86149889	5.29e+15	2.38e+03	EC	55Mn
59	Fe	4.45e+01	d	3845664	1.10e+17	4.97e+04	Beta	59Co
58	Co	7.09e+01	d	6124032	7.05e+16	3.18e+04	EC	58Fe
60	Co	5.27e+00	y	1.66e+08	2.51e+15	1.13e+03	Beta	60Ni
60	mCo	1.05e+01	m	628.2	6.64e+20	2.99e+08	IT,Beta	60Co (99.75%), 60Ni (0.25%)
59	Ni	7.60e+04	y	2.40e+12	1.77e+11	7.97e-02	EC	59Co
63	Ni	1.00e+02	y	3.16e+09	1.26e+14	5.67e+01	Beta	63Cu
65	Zn	2.44e+02	d	21064320	1.83e+16	8.24e+03	EC	65Cu
67	Ga	3.26e+00	d	281750.4	1.33e+18	5.98e+05	EC	67Zn
75	Se	1.20e+02	d	10348992	3.23e+16	1.45e+04	EC	75As
79	Se	6.50e+04	y	2.05e+12	1.55e+11	6.96e-02	Beta	79Br
85	Kr	1.07e+01	y	3.39e+08	8.70e+14	3.92e+02	Beta	85Rb
86	Rb	1.87e+01	d	1611360	1.81e+17	8.14e+04	Beta	86Sr
89	Sr	5.05e+01	d	4364928	6.45e+16	2.90e+04	Beta	89Y
90	Sr	2.91e+01	y	9.18e+08	3.03e+14	1.36e+02	Beta	90Y
90	Y	2.67e+00	d	230774.4	1.21e+18	5.43e+05	Beta	90Zr
91	Y	5.85e+01	d	5055264	5.44e+16	2.45e+04	Beta	91Zr
93	Zr	1.50e+06	y	4.73e+13	5.69e+09	2.56e-03	Beta	93Nb
95	Zr	6.40e+01	d	5531328	4.77e+16	2.15e+04	Beta	95Nb
93	mNb	1.61e+01	y	5.08e+08	5.30e+14	2.39e+02	IT	93Nb
94	Nb	2.00e+04	y	6.31e+11	4.22e+11	1.90e-01	Beta	94Mo
95	Nb	3.50e+01	d	3021408	8.72e+16	3.93e+04	Beta	95Mo
99	Tc	2.13e+05	y	6.72e+12	3.76e+10	1.70e-02	Beta	99Ru

8 Reference: Walker et al., 1989

WHC-SD-WM-TI-528, Rev. 0
TABLE 5-1 continued.

Radionuclide		Half-life (term)		Half-life (seconds)	Specific Activity		Decay mode	Daughters (by decay mode)
					dpm/g	Ci/g		
99	mTc	6.01e+00	h	21621.6	1.17e+19	5.27e+06	IT	99Tc
103	Ru	3.93e+01	d	3392928	7.17e+16	3.23e+04	Beta	103Rh
106	Ru	1.02e+00	y	32187871	7.34e+15	3.31e+03	Beta	106Rh
103	mRh	5.61e+01	m	3367.2	7.22e+19	3.25e+07	IT	103Rh
106	Rh	2.18e+00	h	7848	3.01e+19	1.36e+07	Beta	106Pd
107	Pd	6.50e+06	y	2.05e+14	1.14e+08	5.14e-04	Beta	107Ag
110	Ag	2.46e+01	s	24.6	9.25e+21	4.17e+09	Beta,EC	110Cd (99.7%), 110Pd (0.3%)
110	mAg	2.50e+02	d	21582720	1.05e+16	4.75e+03	Beta,IT	110Cd (98.64%), 110Ag (1.36%)
113	mCd	1.41e+01	y	4.45e+08	4.98e+14	2.24e+02	Beta,IT	113In (99.9%), 113Cd (0.1%)
115	mCd	4.46e+01	d	3853440	5.65e+16	2.55e+04	Beta	115In
113	mIn	1.66e+00	h	5968.8	3.71e+19	1.67e+07	IT	113In
114	mIn	4.95e+01	d	4277664	5.14e+16	2.31e+04	IT,EC	114In (95.7%), 14Cd (4.3%)
113	Sn	1.15e+02	d	9944640	2.23e+16	1.00e+04	EC	113In
117	mSn	1.38e+01	d	1175904	1.82e+17	8.20e+04	IT	117Sn
119	mSn	2.93e+02	d	25315200	8.31e+15	3.74e+03	IT	119Sn
121	mSn	5.50e+01	y	1.74e+09	1.19e+14	5.37e+01	IT,Beta	121Sn (77.6%), 121Sb (22.4%)
123	Sn	1.29e+02	d	11162880	1.82e+16	8.22e+03	Beta	123Sb
125	Sn	9.63e+00	d	832032	2.41e+17	1.08e+05	Beta	125Sb
126	Sn	1.00e+05	y	3.16e+12	6.30e+10	2.84e-02	Beta	126Sb
124	Sb	6.02e+01	d	5201280	3.88e+16	1.75e+04	Beta	124Te
125	Sb	2.76e+00	y	87033478	2.30e+15	1.04e+03	Beta	125Te
126	Sb	1.24e+01	d	1071360	1.86e+17	8.36e+04	Beta	126Te
126	mSb	1.90e+01	m	1140	1.74e+20	7.85e+07	Beta,IT	126Te (86%), 126Se (14%)
123	mTe	1.20e+02	d	10342080	1.97e+16	8.87e+03	IT	123Te
125	mTe	5.80e+01	d	5011200	4.00e+16	1.80e+04	IT	125Te
127	Te	9.40e+00	h	33840	5.83e+18	2.62e+06	Beta	127I
127	mTe	1.09e+02	d	9417600	2.09e+16	9.43e+03	IT,Beta	127Te (97.6%), 127I (2.4%)
129	Te	1.16e+00	h	4176	4.65e+19	2.09e+07	Beta	129I
129	mTe	3.36e+01	d	290[illegible]40	6.69e+16	3.01e+04	IT,Beta	129Te (64%), 129I (36%)
125	I	6.01e+01	d	5196096	3.86e+16	[illegible].74e+04	EC	125Te
129	I	1.57e+07	y	4.95e+14	3.92e+08	1.76e-04	Beta	129Xe
131	I	8.04e+00	d	694656	2.75e+17	1.24e+05	Beta	130Xe

WHC-SD-WM-TI-528, Rev. 0
TABLE 5-1 continued.

Radionuclide		Half-life (term)		Half-life (seconds)	Specific Activity		Decay mode	Daughters (by decay mode)
					dpm/g	Ci/g		
133	Xe	5.24e+00	d	452995.2	4.16e+17	1.87e+05	Beta	133Cs
134	Cs	2.07e+00	y	65164660	2.87e+15	1.29e+03	Beta	134Ba
135	Cs	2.30e+06	y	7.26e+13	2.56e+09	1.15e-03	Beta	135Ba
137	Cs	3.02e+01	y	9.52e+08	1.92e+14	8.65e+01	Beta	137mBa, 137Ba
137	mBa	2.55e+00	m	153.12	1.19e+21	5.38e+06	IT	137Ba
141	Ce	3.25e+01	d	2808000	6.32e+16	2.85e+04	Beta	141Pr
144	Ce	2.85e+02	d	24589440	7.07e+15	3.19e+03	Beta	144Pr
143	Pr	1.36e+01	d	1172448	1.49e+17	6.73e+04	Beta	143Nd
144	Pr	1.73e+01	m	1036.8	1.68e+20	7.56e+07	Beta	144Nd
144	mPr	7.20e+00	m	432	4.03e+20	1.81e+08	IT,Beta	144Pr (99.96%), 144Nd (0.04%)
146	Pm	5.53e+00	y	1.75e+08	9.83e+14	4.43e+02	EC,Beta	146Nd (66.1%), 146Sm (33.9%)
147	Pm	2.62e+00	y	82785941	2.06e+15	9.27e+02	Beta	147Sm
148	Pm	5.37e+00	d	463968	3.65e+17	1.64e+05	Beta	148Sm
148	mPm	4.13e+01	d	3567456	4.74e+16	2.14e+04	Beta,IT	148Sm (95.4%), 148Pm (4.6%)
151	Sm	9.00e+01	y	2.84e+09	5.84e+13	2.63e+01	Beta	151Eu
152	Eu	1.35e+01	y	4.25e+08	3.87e+14	1.74e+02	EC,Beta	152Sm (72.08%), 152Gd (27.92%)
154	Eu	8.59e+00	y	2.71e+08	6.00e+14	2.70e+02	Beta	154Gd
155	Eu	4.71e+00	y	1.49e+08	1.09e+15	4.90e+02	Beta	155Gd
153	Gd	2.42e+02	d	20874240	7.84e+15	3.53e+03	EC	153Eu
160	Tb	7.23e+01	d	6246720	2.51e+16	1.13e+04	Beta	160Dy
192	Ir	7.38e+01	d	6378912	2.04e+16	9.21e+03	Beta,EC	192Pt (95.4%), 192Os (4.6%)
201	Tl	3.04e+00	d	262483.2	4.75e+17	2.14e+05	EC	201Hg
207	Tl	4.77e+00	m	286.2	4.23e+20	1.90e+08	Beta	207Pb
208	Tl	3.05e+00	m	183.18	6.57e+20	2.96e+08	Beta	208Pb
209	Pb	3.25e+00	h	11710.8	1.02e+19	4.61e+06	Beta	209Bi
211	Pb	3.61e+01	m	2166	5.48e+19	2.47e+07	Beta	211Bi
212	Pb	1.06e+01	h	38304	3.08e+18	1.39e+06	Beta	212Bi
211	Bi	2.14e+00	m	128.4	9.24e+20	4.16e+08	Alpha, Beta	207Tl (99.72%), 211Po (0.273%)
212	Bi	1.01e+00	h	3632.4	3.25e+19	1.46e+07	Alpha, Beta	208Tl (35.94%), 212Po (64.06%)
213	Bi	4.56e+01	m	2735.4	4.30e+19	1.94e+07	Alpha, Beta	209Tl (2.16%), 213Po (97.84%)
212	Po	2.98e-07	s	2.98e-07	3.96e+29	1.79e+17	Alpha	208Pb

WHC-SD-WM-TI-528, Rev. 0
TABLE 5-1 continued.

Radionuclide		Half-life (term)		Half-life (seconds)	Specific Activity		Decay mode	Daughters (by decay mode)
					dpm/g	Ci/g		
213	Po	4.00e-06	s	0.000004	2.94e+26	1.32e+16	Alpha	209Pb
215	Po	1.78e-03	s	0.00178	6.54e+25	2.95e+13	Alpha	211Pb
216	Po	1.45e-01	s	0.145	8.00e+23	3.60e+11	Alpha	212Pb
217	At	3.20e-02	s	0.032	3.61e+24	1.62e+12	Alpha	213Bi
219	Rn	3.96e+00	s	3.96	2.89e+22	1.30e+10	Alpha	215Po
220	Rn	5.56e+01	s	55.6	2.05e+21	9.22e+08	Alpha	216Po
222	Rn	3.82e+00	d	330350.4	3.41e+17	1.54e+05	Alpha	218Po
221	Fr	4.80e+00	m	288	3.93e+20	1.77e+08	Alpha	217At
223	Fr	2.18e+01	m	1308	8.59e+19	3.87e+07	Beta	223Ra
223	Ra	1.14e+01	d	987984	1.14e+17	5.12e+04	Alpha	219Rn
224	Ra	3.66e+00	d	316224	3.54e+17	1.59e+05	Alpha	220Rn
225	Ra	1.49e+01	d	1287360	8.65e+16	3.89e+04	Beta	225Ac
226	Ra	1.60e+03	y	5.05e+10	2.19e+12	9.89e-01	Alpha	222Rn
228	Ra	5.76e+00	y	1.82e+08	6.04e+14	2.72e+02	Beta	228Ac
225	Ac	1.00e+01	d	864000	1.29e+17	5.80e+04	Alpha	221Fr
227	Ac	2.18e+01	y	6.87e+08	1.61e+14	7.23e+01	Beta,Alpha	227Th (98.62%), 223Fr (1.38%)
228	Ac	6.15e+00	h	22140	4.96e+18	2.23e+06	Beta	228Th
227	Th	1.87e+01	d	1617408	6.82e+16	3.07e+04	Alpha	223Ra
228	Th	1.91e+00	y	60368036	1.82e+15	8.20e+02	Alpha	224Ra
229	Th	7.30e+03	y	2.30e+11	4.75e+11	2.14e-01	Alpha	225Ra
230	Th	7.54e+04	y	2.38e+12	4.58e+10	2.06e-02	Alpha	226Ra
231	Th	1.06e+00	d	91843.2	1.18e+18	5.32e+05	Beta	231Pa
232	Th	1.40e+10	y	4.42e+17	2.44e+05	1.10e-07	Alpha	228Ra
234	Th	2.41e+01	d	2082240	5.14e+16	2.32e+04	Beta	234Pa
231	Pa	3.28e+04	y	1.03e+12	1.05e+11	4.72e-02	Alpha	227Ac
233	Pa	2.70e+01	d	2332800	4.61e+16	2.08e+04	Beta	233U
234	mPa	1.17e+00	m	70.2	1.52e+21	6.87e+08	Beta,IT	234U (99.87%), 234Pa (0.13%)
232	U	7.00e+01	y	2.21e+09	4.89e+13	2.20e+01	Alpha	228Th
233	U	1.59e+05	y	5.02e+12	2.14e+10	9.64e-03	Alpha	229Th
234	U	2.46e+05	y	7.76e+12	1.38e+10	6.21e-03	Alpha	230Th
235	U	7.04e+08	y	2.22e+16	4.80e+06	2.16e-06	Alpha	231Th
236	U	2.34e+07	y	7.39e+14	1.44e+08	6.47e-05	Alpha	232Th

WHC-SD-WM-TI-528, Rev. 0
TABLE 5-1 continued.

Radionuclide		Half-life (term)		Half-life (seconds)	Specific Activity		Decay mode	Daughters (by decay mode)
					dpm/g	Ci/g		
238	U	4.47e+09	y	1.41e+17	7.46e+06	3.36e-07	Alpha	234Th
236	Np	1.55e+05	y	4.89e+12	2.17e+10	9.77e-03	EC,Beta,Alph	236U,236Pu,232Pa (91/8.9/0.2%)
237	Np	2.14e+06	y	6.75e+13	1.56e+09	7.06e-04	Alpha	233Pa
239	Np	2.36e+00	d	203472	5.15e+17	2.32e+05	Beta	239Pu
236	Pu	2.87e+00	y	90567832	1.17e+16	5.28e+02	Alpha	232U
238	Pu	8.77e+01	y	2.77e+09	3.60e+13	1.71e+01	Alpha	234U
239	Pu	2.41e+04	y	7.61e+11	1.38e+11	6.20e-02	Alpha	235U
240	Pu	6.56e+03	y	2.07e+11	5.04e+11	2.27e-01	Alpha	236U
241	Pu	1.44e+01	y	4.54e+08	2.29e+14	1.03e+02	Beta	241Am
242	Pu	3.75e+05	y	1.18e+13	8.74e+09	3.94e-03	Alpha	238U
244	Pu	8.00e+07	y	2.52e+15	4.07e+07	1.83e-05	Alpha,SPF	240U(99.85%),fiss.prod(0.125%)
241	Am	4.33e+02	y	1.37e+10	7.61e+12	3.43e+00	Alpha	237Np
242	Am	1.60e+01	h	57672	1.79e+18	8.08e+05	Beta,EC	242Cm (82.7%), 242Pu (17.3%)
242	mAm	1.41e+02	y	4.45e+09	2.33e+13	1.05e+01	IT,Alpha	242Am (99.55%), 238Np (0.45%)
243	Am	7.37e+03	y	2.33e+11	4.43e+11	2.00e-01	Alpha	239Np
242	Cm	1.63e+02	d	14065920	7.36e+15	3.31e+03	Alpha	238Pu
243	Cm	2.91e+01	y	9.18e+08	1.12e+14	5.05e+01	Alpha,EC	239Pu (99.76%), 243Am (0.24%)
244	Cm	1.81e+01	y	5.71e+08	1.80e+14	8.09e+01	Alpha	240Pu
245	Cm	8.50e+03	y	2.68e+11	3.81e+11	1.72e-01	Alpha	241Pu
246	Cm	4.76e+03	y	1.50e+11	6.78e+11	3.05e-01	Alpha	242Pu
247	Cm	1.56e+07	y	4.92e+14	2.06e+08	9.28e-05	Alpha	243Pu
248	Cm	3.48e+05	y	1.10e+13	8.19e+09	4.14e-03	Alpha,SPF	244Pu(91.74%),fiss.prod(8.26%)
252	Cf	2.64e+00	y	83246670	1.19e+16	5.38e+02	Alpha,SPF	248Cm(96.908%),fis.prd(3.092%)

Appendix F

Permanent Isolation Barrier and Warning Marker System

9413222.1466

This page intentionally left blank.

Appendix F

Permanent Isolation Barrier and Warning Marker System[a]

C. T. Kincaid, Pacific Northwest Laboratory

9413222.1468

F.1 Introduction

A multi-year program entitled the "Hanford Site Permanent Isolation Barrier Development Program (BDP)" has been organized to develop, test, and evaluate protective barrier and warning marker systems for use at Hanford. Initial work on barriers at the Hanford Site was begun in the early 1980s and focused primarily on constructability of surface covers (Phillips et al. 1985). Direction for the overall program was first formulated and published in a program plan by Adams and Wing (1986). That plan has been updated in Wing et al. (1992). Material for this appendix, which describes the isolation barrier and marker system, has been drawn from these program plan documents, a peer review report (Wing 1992), and the testing and monitoring plan for a prototype barrier (Gee et al. 1993).

The Operations and Engineering Contractor for the U.S. Department of Energy's (DOE) Hanford Site, Westinghouse Hanford Company (WHC), and DOE's Research and Development Contractor for the Hanford Site, Pacific Northwest Laboratory (PNL), are jointly developing and testing protective barrier and warning marker systems. Permanent isolation barrier and warning marker systems use engineered layers of natural materials to create an integrated structure with redundant protective features. The emphasis of this program has been on the development of barriers and markers for above-grade (mounded barrier) application to existing waste sites where the soil profile should not be disturbed. However, the barrier design described herein is also relevant and applicable to barriers at new waste disposal sites such as the Hanford Grouted Waste Facility. Drawings of conceptual permanent isolation barrier and warning marker systems are shown in Figures F.1 and F.2. The natural construction materials (e.g., fine soil, sand, gravel, rip-rap, clay, asphalt) have been selected to optimize barrier performance and

---

(a) In April 1993 a new prototype design for the permanent isolation barrier was issued. It differs from the design described in this appendix. Certainly, as data are gathered and the performance of the 1993 prototype is assessed, the design will be revised. Since one cannot assert that any design described here is final (i.e., because it will be constructed during site closure), it has been decided not to revise this text. The interested reader can obtain the new prototype design by acquiring the following report: WHC. 1993. *Prototype Surface Barrier at 200-BP-1 Operable Unit*, WHC-SD-EN-TI-142, Rev. 0, prepared by Kaiser Engineers Hanford for Westinghouse Hanford Company, Richland, Washington.

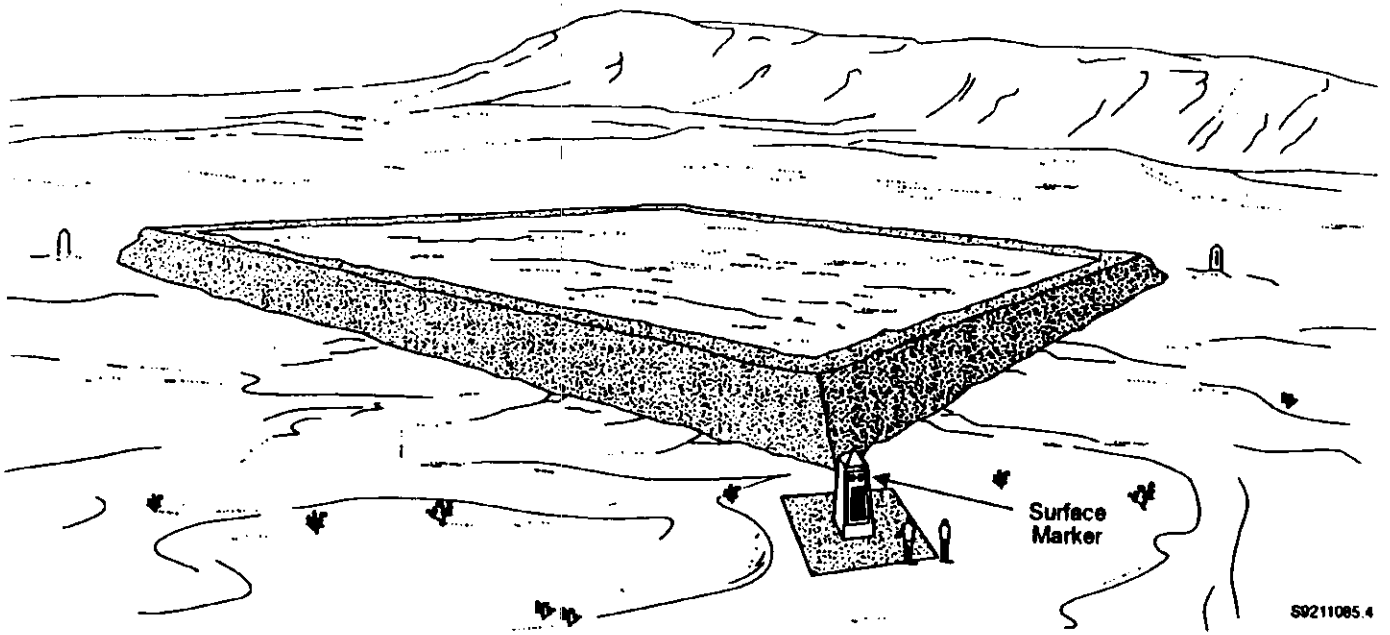

Figure F.1. Conceptual Permanent Isolation Surface Barrier and Warning Marker System for an Above Grade Application

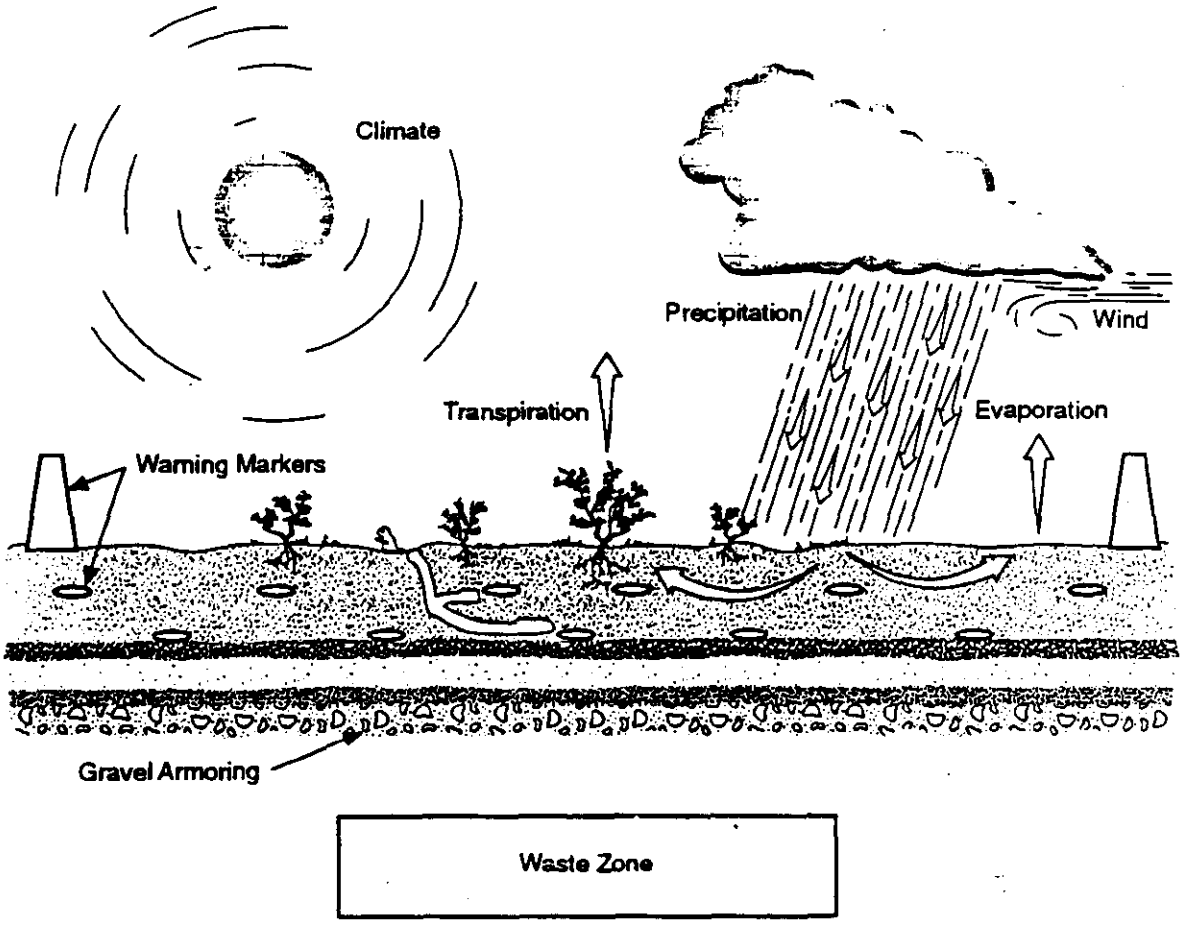

Figure F.2. Isolation Barrier and Warning Marker System

longevity. The objective of current designs is to use natural materials to develop a maintenance-free permanent isolation barrier and warning marker system that isolates wastes for a minimum of 1,000 years by limiting water drainage to near-zero amounts; reducing the likelihood of plant, animal, and human intrusion; controlling the exhalation of noxious gases; and minimizing erosion-related problems.

F.1.1 Short-Term versus Long-Term Barriers

Existing short-term barrier designs currently are available [U.S. Environmental Protection Agency (EPA) 1982, 1990]. In general, the design life of these covers is for relatively short periods, such as the 30-year post-closure period specified by the *Resource Conservation and Recovery Act* (RCRA) *of 1976*.

The performance of barriers during this relatively short period can be monitored, and maintenance activities can be performed to correct any problems that might be encountered. However, there exist waste management situations in which it is desirable to isolate wastes for much longer periods than the 30-year post-closure period (i.e., hundreds to a thousand years). For these waste management situations, the relatively short-term (RCRA) designs are not satisfactory. For example, many synthetic construction materials that might be effective for tens of years (e.g., geosynthetics) cannot be relied on to perform satisfactorily (or even exist) over 1,000 years. Consequently, a need arises for a long-term, permanent isolation barrier.

F.2 Performance Objectives

To direct the development of protective barrier and warning marker systems, performance objectives for the barriers and markers have been defined. The following list summarizes these performance objectives. The objectives are intended to be broad enough to encompass the various regulatory requirements for the types of wastes anticipated to be disposed of in shallow land deposits using barriers at the Hanford Site and other DOE sites in the arid and semiarid western United States.

- Functions in a semiarid to subhumid climate
- Limits the recharge of water through the waste to the water table to near-zero amounts; a long-term annual average of 0.05 cm (0.02 in.) of water per year [i.e., a drainage rate of approximately 2×10^{-9} cm/s]
- Remains maintenance free by minimizing the likelihood of plant, animal, or human intrusion, and minimizing the likelihood of wind and water erosion
- Lasts for a minimum of 1,000 years.

The BDP goal has been to provide defensible evidence that final barrier design(s) will control water infiltration; plant and animal intrusion; and wind and water erosion for a minimum of 1,000 years and will protect human health and the environment in accordance with applicable or relevant and appropriate requirements. In the event that institutional control is lost, warning marker systems will be provided to inform inadvertent human intruders (Adams and Kaplan 1986; Kaplan and Adams 1986).

The protective barrier is designed to prevent or minimize contaminant migration to the accessible environment through the following pathways (Figures F.3 and F.4):

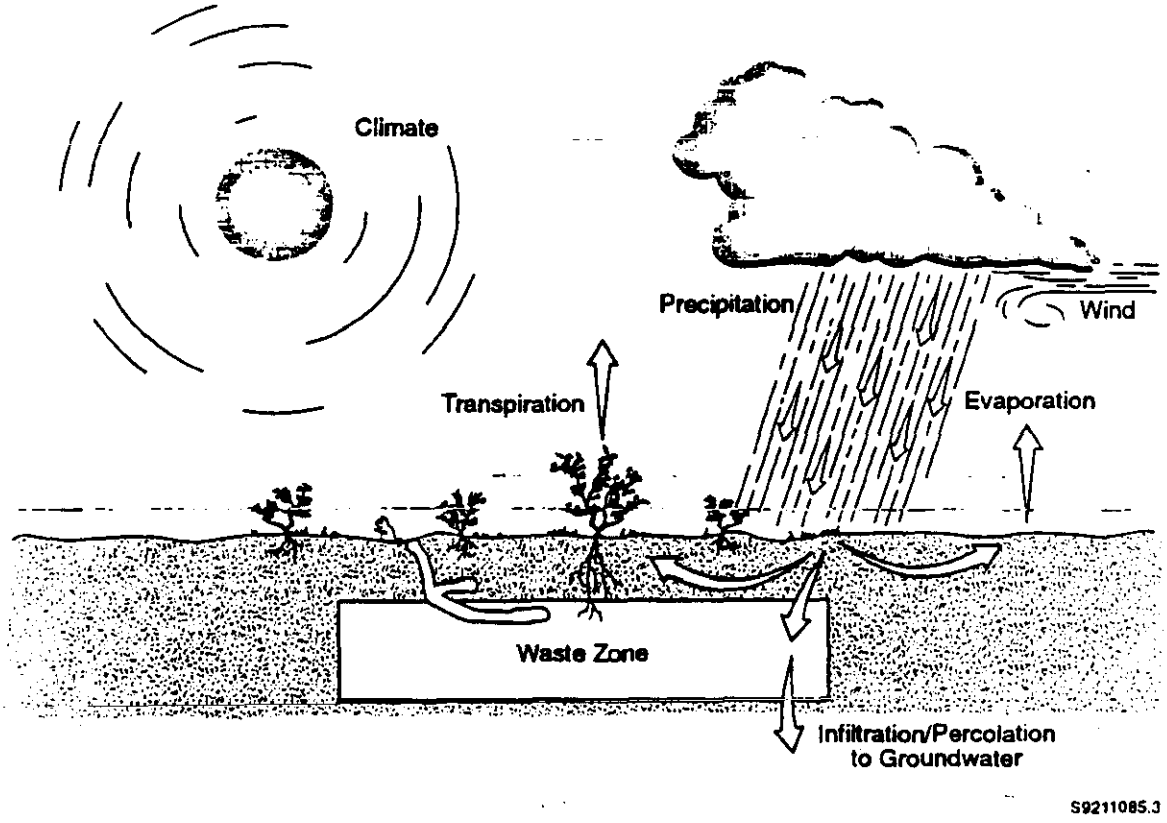

Figure F.3. Potential Problems of the Current Waste Management Situation

- Water infiltration--the infiltration and percolation of water through the waste zone leading to the leaching and subsequent transport of radionuclides and other contaminants to the water table.

- Biointrusion--the penetration of deep-rooting plants and burrowing animals into the waste zone below. The deep-rooting plants could draw radionuclides and other contaminants into its root system and subsequently translocate the contaminants to the above-ground portion of the plant. The contaminants in the above-grade portion of the plant could then be dispersed by wind or by animals that eat the plants. Animals burrowing directly into the waste zone could contact contaminants and subsequently bring them to the earth's surface as part of the soil castings. Erodible loose soil, cast to the surface by burrowing animals, could contribute

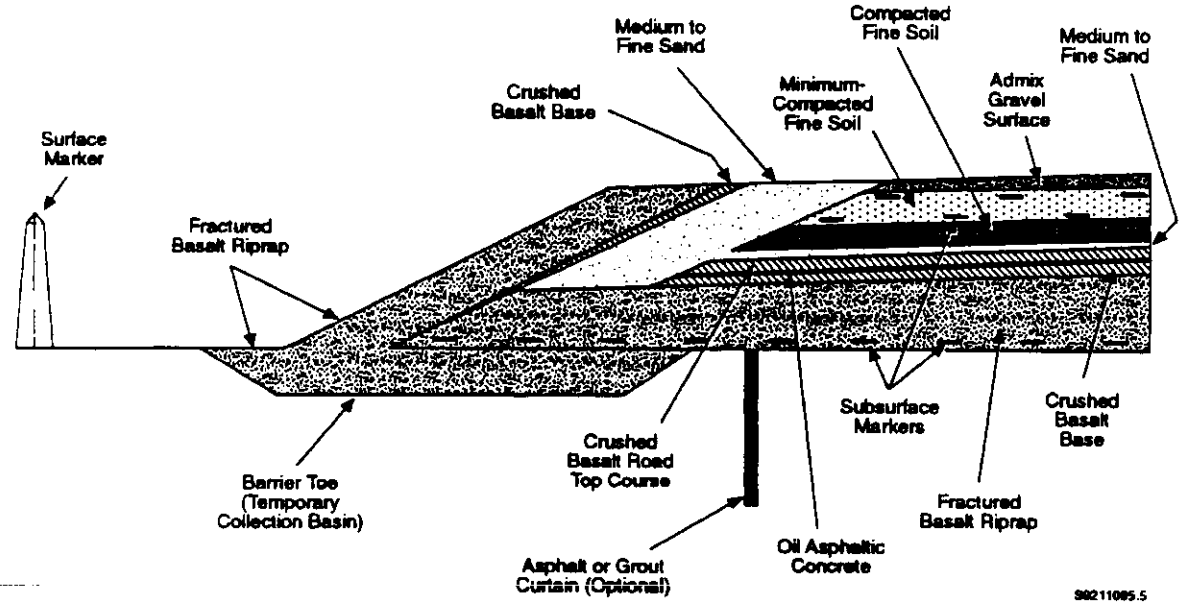

Figure F.4. Cross Section of a Conceptual Permanent Isolation Barrier and Warning Marker System

to accelerated erosion of the fine-soil surface layer. In addition, the presence of animal burrows may provide preferential pathways for infiltrating water to gain access to the waste zone.

- Wind and water erosion--the removal of the surface soils at a waste site from the effects of erosive forces. Erosion-related problems could provide a direct pathway for contaminant transport if the erosive forces are strong enough to remove the surface soils and expose the buried wastes to the accessible environment. A more probable scenario is for wind and water erosion to reduce the thickness of soils overlying a waste zone such that another transport pathway (i.e., water infiltration) becomes a more serious concern.

- Human interference--the inadvertent or intentional intrusion of humans into the waste sites (assuming institutional control is lost) and subsequent dispersion of contaminants.

- Gaseous release--the diffusion of noxious gases from the waste zone to the accessible environment.

F.3 Barrier Design

Engineered barrier and marker systems have been proposed to protect wastes disposed of in shallow land deposits from the transport pathways identified above. The protective barrier and warning marker systems consist of a variety of different materials (e.g., fine soil, sand, gravel, rip-rap, asphalt, clay, etc.) placed in layers to form an above-grade mound or at-grade profile directly over the waste zone. Surface markers are placed around the periphery of the waste sites to inform future generations of the nature and hazards of the buried wastes (see Figure F.1). In addition, throughout the protective barrier, subsurface markers are placed to warn any inadvertent human intruders of the dangers of the wastes below (Figure F.5).

The protective barrier design consists of a fine-soil layer overlying other layers of coarser materials including sand, gravel, or basalt rip-rap. Each of these layers shown in Table F.1 serves a distinct purpose. The fine-soil layer acts as a medium in which moisture is stored until the processes of evaporation and transpiration can recycle excess water back to the atmosphere. The fine-soil layer also provides the medium for establishing plants that are necessary for transpiration to take place. McGee Ranch silt loam

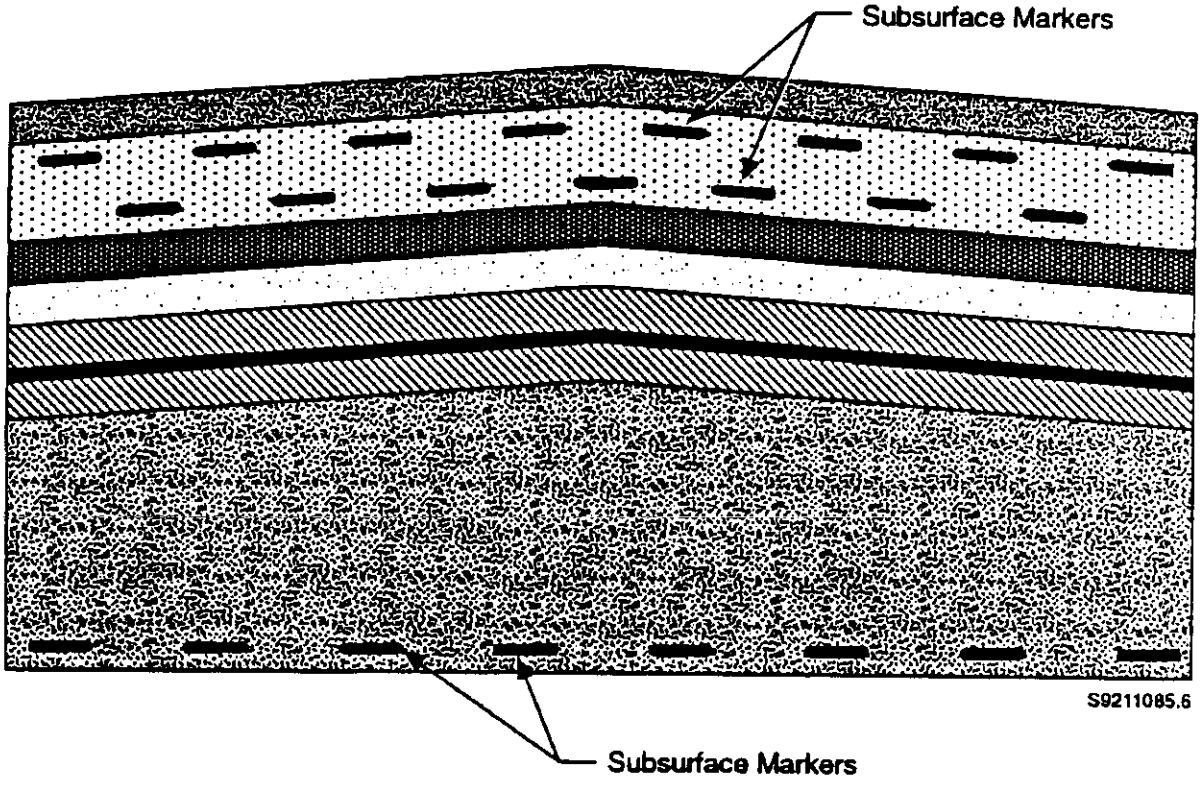

Figure F.5. Placement of Surface and Subsurface Markers

Table F.1. The Vertical Layering and Materials of the Protective Barrier

Layer Thickness	Description	Comment
2 m (6.6 ft)	McGee Ranch Silt Loam	The McGee Ranch silt loam will be placed in two lifts; 1.0 m (3.3 ft) of clean silt-loam soil will be placed immediately above the sand filter, then 1.0 m (3.3 ft) of silt mixed with pea gravel will be placed and shaped to the grade elevation of the site.
15 cm (5.9 in.)	Sand Filter	This sand will act as a hydraulic filter between the overlying silt and the underlying crushed rock gravel. A woven geotextile is to be installed between sand and silt layers.
30 cm (11.8 in.)	Gravel Filter	This crushed rock gravel filter will act as a hydraulic filter between the overlying fine sand filter and the underlying fractured basalt core of the barrier system.
50 cm (20 in.)	Basalt Rip-Rap	The fractured basalt rip-rap is the primary capillary break in the isolation barrier system. This media is to have a minimum of fines in its grain size distribution to ensure a considerable open porosity. The physics of unsaturated water flow require water to nearly reach saturation in the silts overlying the sand filter before water will enter the sand, and to nearly reach saturation in the sand overlying the gravel filter before water will enter the gravel.
30 cm (11.8 in.)	Gravel	This gravel layer acts as a cushion between the basalt rip-rap and the asphalt. It ensures against damage to the asphalt during placement of the basalt.
15 cm (5.9 in.)	Asphalt	Asphalt is placed in two lifts to provide added assurance that adequate compaction is achieved. In addition, this ensures that preferential flow does not occur through single joints or localized areas of lower integrity (e.g., lower compaction or higher conductivity) in a single layer.

is currently the fine-soil of choice because it will create a favorable environment for containing the biological cycles in the upper portion of the barrier, thereby reducing biointrusion into the lower layers. The coarser materials (i.e., successively coarser sand, gravel, and basalt rip-rap) that are placed directly below the fine-soil layer create a capillary break that inhibits the downward percolation of water through the barrier. The coarser materials will also help to deter inadvertent human intruders from digging deeper into the barrier profile. A low-permeability layer placed in the barrier profile below the capillary break is included in the protective barrier design. The purpose of the low-permeability layer is to divert any percolating water that gets through the capillary break away from the waste zone, and to limit the upward

movement of gases from the waste zone. The low-permeability material of choice is asphalt, which is hydrophobic (i.e., not wetted by water) and should be an excellent redundant barrier to recharge.

Because the barrier must perform for at least 1,000 years without maintenance, natural construction materials (e.g., fine soil, sand, gravel, cobble, crushed basalt rip-rap, asphalt, clay, etc.) have been selected to optimize barrier performance and longevity. Most of these natural materials are available in large quantities on the Hanford Site and are known to have existed in place for thousands of years or longer. In contrast to natural materials, the ability of man-made construction materials to survive and function properly for a thousand years is not known. Because of this uncertainty, man-made construction materials are not relied upon in this design.

The need for a maintenance-free barrier that lasts for a minimum of a thousand years necessitates the use of passive, as opposed to active, systems. Active systems are impractical because they require human involvement to operate, monitor, and maintain. For example, a leachate collection and removal system requires monitoring the collection of leachate and removing it from the collection system using a sump pump or similar device. The various components of the leachate collection and removal system will also need to be maintained periodically. This level of human activity over long periods of time is impractical.

The permanent isolation barrier is intended to remain functional throughout its design life without human intervention. Consequently, in designing a permanent isolation barrier, it has been important to understand the natural processes that are expected to act on the barrier during its design life. Knowledge of how natural processes affect barrier performance has resulted in a design that passively meets design and performance objectives.

F.4 Results of Barrier Development Program Research

During the period from 1986 through 1990, laboratory and field research efforts were undertaken by the BDP. The results of this research and findings to date are briefly summarized below.

F.4.1 Water Intrusion Control

At the Field Lysimeter Test Facility (FLTF) and the Small Tube Lysimeter Facility (STLF), studies are under way to quantify water balance under conditions that are currently found at Hanford waste sites and under conditions that may exist when surface isolation barriers are emplaced (Gee et al. 1989; Campbell et al. 1990; Campbell and Gee 1990; Sackschewsky et al. 1991; Waugh et al. 1991). These lysimeter studies are perhaps the most precise water balance studies conducted at an arid site to date.

F.4.1.1 Field Lysimeter Test Facility

Constructed in 1987, the FLTF consists of 14 large-diameter drainage-type lysimeters 3-m (9.8-ft) and 1.5-m (4.9-ft) deep, weighing lysimeters, and 6 additional clear plastic lysimeters (Gee et al. 1989; Campbell et al. 1990; Campbell and Gee 1990). Seven barrier treatment alternatives are being evaluated in this program. These alternatives all rely on a soil textural break to provide the infiltration barrier based on the outflow law for soil water proposed by Richards (1950). The outflow law limits the percolation of water from a fine-textured soil, which exhibits a high capillary pressure, to a coarse-grained, clean sand or gravel, which exhibits a very low capillary pressure; as a result, moisture will be retained in the overlying, fine-textured soil until the water content in the soil approaches saturation. The observations in the FLTF lysimeters demonstrate the need for at least a 1-m (3.3-ft) upper layer of fine soil with surface vegetation to enhance evapotranspiration. If vegetation is absent and a substantial sand or gravel layer is on the surface, precipitation has penetrated deeply and eventually drained through these lysimeters.

Through lysimeter experiments and modeling it has been shown that the silt-loam soil profile will recycle two and three times the normal precipitation from either vegetated or vegetation-free sites (Cadwell 1991; Waugh et al. 1991). Thus, for both natural fine soil (i.e., silt) profiles and a protective barrier using fine soils, virtually no net recharge would occur, and the currently used limit for recharge of 0.1 cm/yr (0.04 in.) or less could be applied indefinitely (Fayer et al. 1985; Fayer 1987; Fayer, Rockhold and Holford 1992).

F.4.1.2 Plant Transpiration/Evapotranspiration

In 1989 and 1990 the evaporation, evapotranspiration, and carbon dioxide exchange rates for the McGee silts were obtained with and without cheatgrass for use in water balance models. Once again, it was shown that vegetation significantly reduces water penetration and can be effective in preventing drainage (Link et al. 1990; Link et al. 1992a, 1992b).

F.4.1.3 Diversion Barrier Testing

Using the STLF, the effectiveness of asphalt and clay/grout barriers is being evaluated. To date, all of these barrier systems have prevented surface moisture from passing through the lysimeters (Freeman and Gee 1989a, 1989b; Relyea, Sackschewsky and Waugh 1989).

F.4.2 Biointrusion Control

One or more components of the prototype barrier should be an effective deterrent to animal burrowing and root intrusion. Evaluations of animal burrowing and root intrusion impacts on protective barriers are being conducted to determine parameters on the extent and nature of burrowing and intrusion that occur during the life of the barrier.

F.4.2.1 Small Mammal Intrusion Studies

An animal intrusion lysimeter facility (AILF) was constructed in 1988 to assess the effects of small mammal burrows on the infiltration of precipitation through soil layers such as may be used in the barrier. Data from lysimeter tests completed thus far indicate that no significant differences occurred in the water content at depth in soils with and without burrows. Additionally, the maximum depth of burrow penetration always exceeded 122 cm (4 ft) and typically reached the bottom of the lysimeters (Landeen 1990, 1991).

F.4.2.2 Large Mammal Intrusion Studies

Measurements obtained in 1989 and 1990 indicate that during natural rainfall, precipitation penetrates deeper beneath and adjacent to badger burrows. However, enhanced evapotranspiration in the proximity of the burrows leads to a rapid loss of this moisture (Cadwell, Eberhardt and Simmons 1989).

F.4.2.3 Root Intrusion Studies

Vegetation will function as an important component of the protective barrier, both to stabilize the soil surface and to extract soil moisture from the soil and recycle it to the atmosphere through evapotranspiration. For the prototype barrier design, in which fine soils overlie graded layers, the optimal root distribution for barrier function will be one in which roots fully exploit the fine-soil layer. However, the establishment and growth of deep-rooted plants on the barrier presents the possibility of intrusion of plant roots into the wastes and subsequent biotic transport of hazardous materials.

Based on limited small-diameter soil and root cores obtained in 1990, it was observed that grass roots dominate the upper 20 cm (8 in.) of the soil, while shrub roots dominate the soil below this level. The deepest penetrating roots (tumbleweeds) would extend to a depth of 100 cm (3.3 ft), which is well into the typical buried waste site, if an effective root barrier is not employed.

F.4.3 Erosion/Deposition Control

Erosive stresses on the 200 Area plateau of the Hanford Site will impact actual waste site barriers. The BDP is conducting research to 1) monitor the surface layer as it ages under exposure to natural conditions; 2) measure actual rates of surface deflation or inflation; 3) obtain micro-meteorological information about erosive, or shear, stresses that impact the barrier; 4) obtain information about abrasive sand particle scouring (saltation); 5) create a sand dune and monitor the impact on surface erosion, plant community viability, and soil reservoir water balance; and 6) study erosive impacts after an artificial wildfire removes all surface vegetat

F.4.3.1 Field Study of Gravel Admixture, Vegetation, and Soil

Six field plots were constructed in 1986 to evaluate the effect of varying surface treatments on plant growth and resistance to wind and water erosion. The data indicate that the gravel admixture does not limit vegetative growth or lead to an increase in the soil moisture beneath the admixture (Last et al. 1987; Waugh 1989; Waugh et al. 1990).

F.4.3.2 Small-Tube Lysimeter Tests

The small-tube lysimeter facility (STLF), containing 105 lysimeters, was constructed in 1988 to evaluate root penetration depth and infiltration from alternate erosion-resistant surfaces. Significant among the observations was the finding that a gravel surface with no vegetation will lead to significant infiltration of precipitation, regardless of the soil type underlying the gravel (Relyea, Sackschewsky and Waugh 1989; Sackschewsky et al. 1991).

F.4.3.3 Wind Erosion

Wind tunnel studies performed in 1990 indicated that the McGee silts are subject to significant deflation unless stabilized by vegetation or a gravel/soil cover. The addition of 15% to 30% pea gravel to the native surface silts halted wind erosion by providing a surface armor that simulates naturally occurring desert pavement (Ligotke 1988; Ligotke and Klopfer 1990).

F.4.3.4 Water Erosion

Small plots equipped with run-off flumes were tested at the McGee Ranch to demonstrate the effectiveness of the gravel admixtures in limiting erosion of the silts. Preliminary results indicate that the admixture reduces raindrop-splash induced erosion (Walters, Hoover and Cadwell 1990; Hoover, Cadwell and Walters 1990).

Erosion studies have shown that soil surfaces, once armored with rock, resist further erosion under the influence of arid or semi-arid climates. The surface soil of the Hanford Protective Barrier is designed to include a rock fraction, i.e., a pea-gravel admixture. Thus, if and when wind erosion removes the fine soils at the surface, a rock armoring will remain as a surface armoring to preclude further wind erosion. The nominal thickness of rock armoring required to defeat the wind erosion process is estimated to be 2 rock diameters or a maximum of 10 cm (3.9 in.). Conservatively, it is estimated that wind erosion may remove between 10 and 50 cm (3.9 and 19.7 in.) of fine soil during the creation of the armor surface. The creation of a desert pavement surface will leave at least 1.5 m (4.9 ft) of fine soil; an amount research has shown is ample to minimize infiltration into waste sites at arid sites such as Hanford.

F.4.4 Summary

These studies have aided in the selection of the cover materials and the quantification of water balance for a combination of selected soil-layer sequences. The deposit of silt-loam soil at the McGee Ranch location on the Hanford Site has been identified as the source of material for the fine soil. Sand and gravel filter layers have been identified as essential to prevent the migration of the fine soil into the pore space of the basalt rip-rap. An asphalt subsurface layer is currently proposed as a redundant water diversion that would prevent drainage of water below the multilayered soil barrier system for a thousand years or more.

F.5 Intrusion and Land Use Scenarios

F.5.1 Short-Term Human Intrusion Scenarios after Institutional Control

Markers will be placed in the protective barrier to warn those who would, for any reason, disturb the buried wastes (Adams and Kaplan 1986; Kaplan and Adams 1986). Absolute assurance can not be given that future generations would understand the warning or adhere to it. Thus, human intrusion scenarios may develop regarding the materials that comprise the protective barrier. Earthen materials in the barrier that have intrinsic value to society include the surface gravels (included in the surface soil to provide armoring), the silt-loam soil, and the underlying coarse rock. Possible scenarios include the following:

- *Gravels or Basalt Rock as a Commodity of Interest*: Consider the removal of surface gravel, wind erosion of the silt-loam, eventual exposure of the coarse gravels and basalt rip-rap, and removal of this coarse material. If this scenario is credible, it requires one of two approaches: 1) completely ignore the presence of the protective barrier and simply assume a backfill soil surface, or 2) develop a complex sequence of infiltration rates corresponding to the exposed surface material. Complete removal of surface and deeper gravel materials is believed to be highly unlikely; it is more likely that gravels and rock would be acquired from other abundant natural deposits on the Hanford Site.

  If the coarse material were removed, the redundant layer of asphalt placed at depth beneath the barrier provides an extra measure of protection. Until such time as the asphalt would biodegrade, assume a thousand years, this secondary infiltration barrier would act to divert direct infiltration. The study of asphalt layers for secondary protection in the barrier design is currently under way (Freeman, Gee and Relyea 1989; Freeman and Gee 1989b). This asphalt would be below the land surface and would not be exposed to daily or seasonal climate variations, thus the biodegradation rate is assumed to be the same as for the asphalt pavement surrounding the vault.

- *Silt-Loam Soils as a Commodity of Interest*: Consider the removal of the 2-m- (6.6-ft-) thick silt-loam surface deposit, and the exposure of underlying coarse gravels and basalt. If this

were to occur soon after the loss of institutional control, the waste underlying the disturbed portion of the barrier would be exposed to greatly enhanced recharge over its entire disposal period. A relatively thick layer of coarse gravel acts as a recharge basin; thus, infiltration through the gravel could result in drainage of a significant portion of the annual (~16-cm/yr; 6.3-in./yr) precipitation (Smoot et al. 1989). The underlying redundant asphalt layer(s) would then function as the primary barrier to high recharge rates. The study of asphalt degradation under the Hanford Grout Technology Program has led to assumed biodegradation of the asphalt-concrete diffusion barrier; therefore, asphalt within the isolation barrier is also assumed to biodegrade. Thus, direct leaching of the waste at high recharge rates could occur after approximately 1,000 years. Another key aspect to such a scenario would be the area or portion of the barrier surface assumed to be mined by the intruder.

- *Agricultural Use of the Barrier Surface*: consider the practice of agriculture on the silt-loam soils. The nature of future agricultural practice must be assumed (i.e., whether erosion would be controlled, likely crops, whether and how irrigation would be applied). All of this must be assumed before arriving at expected values for recharge. Under this scenario, the underlying asphalt would function as the primary barrier to net recharge past the waste form.

F.5.2 Long-Term Scenarios

Long-term scenarios range from a) pre-Hanford conditions with irrigated agriculture along the river and natural range land at and above the 200 Area plateau, to b) extensive irrigated agriculture throughout what is presently the Hanford Site. The role that water rights could play in the source and availability of water is unknown. The role that wildlife refuges may play is also unknown. Protection of the natural environment along the Hanford Reach of the Columbia River resulting from the declaration of a scenic river area is currently being debated.

The present agricultural development of lands surrounding the Hanford Site and the proximity of these lands to sources of water (e.g., the Columbia River and underlying basalt aquifers) contribute to a high likelihood of agricultural development of Hanford after the Site is returned to the public domain. Because very long-term institutional control cannot be assumed, one can assume that agricultural development will encroach upon the waste deposits in the 200 Area Plateau. One could even assume that the surface of the protective barrier would be farmed.

Regardless, the issue of long-term future land use seems to revolve around two options: 1) natural recharge of an environment even if precipitation triples, and 2) irrigated agriculture that would apply significantly greater amounts of water. It is uncertain that current irrigation practices could be sustained for

the indefinite future, i.e., thousands of years. However, irrigation practices will evolve and with the rotation of crops and evolution of agricultural practices, it is conceivable that some form of agriculture would be conducted over the long term at Hanford.

Findings of the barrier research program are that fine-soil profiles protect indefinitely against recharge even with up to twice the current precipitation rate. This is true for natural (e.g., layered) and disturbed silt profiles, and for cases with or without vegetation. Thus, if natural precipitation is used in a dry-land farming scenario, one can conclude minimal long-term recharge. If, however, irrigation is applied according to current practices, the surface soil and vegetation/crop capacity for storing and recycling water potentially could be overwhelmed, and significant amounts of recharge should be assumed. Future irrigation methods are unknown, however, the trend is toward localized irrigation (e.g., drip irrigation), and therefore, recharge through the silt-loam surface soil of the protective barrier could be assumed to be minimal for the long-term future. Salt build up in soils is prevented by applying sufficient irrigation to both supply the crop requirement and leach salts down into the soil profile and away from the root zone. Elsewhere on the Hanford Site, where silt soil profiles are not present at the land surface, greater amounts of recharge should be assumed to correspond to future irrigation scenarios.

9413272.1482

F.6 Estimates Of Recharge

Bauer and Vaccaro (1990) estimated groundwater recharge for the Hanford Site as part of their study of recharge affecting the Columbia Plateau regional aquifer. Using daily precipitation and temperature data for the period 1956 through 1977, and a water budget model, they estimated recharge for subareas of the Hanford Site ranging in size from 0.25 to 1.0 mi^2. Their model included the following physical processes: snow accumulation and melt, interception of precipitation, surface runoff, evaporation from foliar cover, evaporation from bare soil, and plant transpiration. It accounts for the influences of soil type, land use, plant growth, altitude, slope and aspect. The long-term (i.e., 21-year) average of annual recharge for the entire Hanford Site was estimated to be 0.97 cm/yr (0.38 in./yr). They estimated a long-term average recharge rate of 0.25 to 1.3 cm/yr (0.1 to 0.5 in./yr) at the location of the grout facility on the 200 Area plateau.

Routson and Johnson (1990) reviewed water infiltration data from a 13-year period of observation for a closed-bottom lysimeter located in the 200 East Area, and ^{137}Cs profile data from a solid waste burial ground trench in the 200 West Area. They concluded that for the natural soils and vegetation of the 200 Area plateau and for areas where natural near-surface conditions could be restored, there is very little potential for downward movement of contaminants in the upper vadose zone. The recharge rate of the closed-bottom lysimeter was estimated to be 0.0 ± 2 mm/yr based on the 13-year record. They recommended that management and cleanup efforts strive to maintain or recreate natural soil and vegetative cover conditions.

Gee et al. (1992) reviewed all published recharge studies for Hanford and described the reasons for highly variable observations of recharge. They describe the roles played by the three major factors of

climate, soil, and vegetation. Clearly, recharge is directly related to annual precipitation; where recharge is observed, more precipitation implies more recharge. Recharge has also been shown to depend on the seasonal distribution of precipitation, with maximum recharge events occurring after the wettest winter periods. Recharge is greatest for coarse-textured soils; least for fine-textured soils. It is greatest for surfaces that are maintained free of vegetation; least for surfaces supporting both shallow- and deep-rooted vegetation.

The lysimeter studies at Hanford show for present climate conditions [i.e., 160-mm (6.3-in.) annual average precipitation], as well as for accelerated precipitation [up to 320 mm/yr (12.6 in./yr) or more], that surface barriers consisting of more than 1 m (3.3 ft) of fine (i.e., silt or silt-loam) soil over coarse subsurface materials are capable of preventing water from draining into underlying soils or wastes. Gee et al. (1992) reported results obtained on the 200 Area plateau at the Hanford Site from lysimeters containing silt loam. Lysimeters that were exposed to two times (2x) normal precipitation from 1987 through 1990 produced no drainage regardless of the presence or absence of plants. Unpublished data from continued monitoring of these lysimeters, which have since been subjected to an excess of three times (3x) normal precipitation, reveal no drainage from vegetated lysimeters but drainage through lysimeters maintained free of vegetation. The studies have shown that deep-rooted sagebrush and tumbleweed plants are more efficient than shallow-rooted cheatgrass in removing soil water from a soil profile. All lysimeters with vegetation exhibit a greater ability to recycle water to the atmosphere than do bare-soil lysimeters. All of this suggests that a 1-m (3.3-ft) deposit of silt soil is ideally suited to limit water infiltration under the semiarid conditions of vegetation and climate at Hanford. It has also been shown that creating an armored desert pavement by adding a gravel mix to the surface deposit of silt protects the barrier from potential eolian erosive forces and does not degrade the water cycle performance of the barrier (Waugh et al. 1990).

The design of the protective barrier accounts for the potential of wind erosion by incorporating gravel admix in the upper silt layer. The potential for deposition of wind-blown soils is now being addressed by the barrier program. Dunes cover a significant portion of the Hanford Site, and are predominantly a fine sand. The majority of these dunes, which lie to the south and southeast of the Grout Disposal Facility, are vegetated to some extent, and recharge is expected to be low where vegetation is present (Gee et al. 1992) but recharge has not been measured directly on the dune areas. At present, the more active and least vegetated dunes lie to the southeast of the facility adjacent to the Columbia River. It is probable that shallow-rooted vegetation is better able than deep-rooted species to adapt to the dynamic active dune environment. As a result, infiltration and recharge at active dune locations could be a substantial fraction of the precipitation. However, the present location of dunes, being south and southeast and downwind of the Grout Disposal Facility, make it less probable that dune formation (deposition) events will dominate the future and more probable that wind erosion events will dominate.

The results of research reported by Gee et al. (1992) are more relevant to the surface barrier because it involves silt loam soils, vegetation, and climate specific to the barrier design and 200 Area plateau. Thus, the interpretation of field observations and supporting simulations of the near-surface environment, that there will be negligible or nonmeasurable recharge through an isolation barrier, is adopted.

The net infiltration design goal for the permanent isolation barrier is 0.05 cm/yr (0.02 in.) (i.e., a non-zero value), because the field measurement program could not achieve an absolute zero recharge goal. This value could have been adopted as the infiltration rate for the performance assessment analysis; however, it was doubled and the value 0.1 cm/yr (0.04 in./yr) was adopted to provide additional conservatism.

F.7 References

Adams, M. R. and M. F. Kaplan. 1986. "Marker Development for Hanford Waste Site Disposal." *In* R.G. Post (ed.), *Waste Management '86* (Vol. 1), pp. 425-431, University of Arizona, College of Engineering and Mines, Tucson, Arizona.

Adams, M. R., and N. R. Wing. 1986. *Protective Barrier and Warning Marker System Development Plan*. RHO-RE-PL-35 P, Rockwell Hanford Operations, Richland, Washington.

Bauer, H. H. and J. J. Vaccaro. 1990. *Estimates of Ground Water Recharge to the Columbia Plateau Regional Aquifer System; Washington, Oregon and Idaho for Predevelopment and Current Land Use Conditions*. WRIR 88-4108, U.S. Geological Survey, Tacoma, Washington.

Cadwell, L. L. (ed.). 1991. *Hanford Site Protective Barrier Development Program: Fiscal Year 1990 Highlights*. PNL-7831, Pacific Northwest Laboratory, Richland, Washington.

Cadwell, L. L., L. E. Eberhardt, and M. A. Simmons. 1989. *Animal Intrusion Studies for Protective Barriers: Status Report for FY 1988*. PNL-6869, Pacific Northwest Laboratory, Richland, Washington.

Campbell, M. D., G. W. Gee, M. J. Kanyid, and M. L. Rockhold. 1990. *Field Lysimeter Test Facility: Second Year (FY 1989) Test Results*. PNL-7209, Pacific Northwest Laboratory, Richland, Washington.

Campbell, M. D., and G. W. Gee. 1990. *Field Lysimeter Test Facility: Protective Barrier Test Results (FY 1990, the third year)*. PNL-7558, Pacific Northwest Laboratory, Richland, Washington.

Fayer, M. J. 1987. *Model Assessment of Protective Barrier Designs: Part II*. PNL-6297, Pacific Northwest Laboratory, Richland, Washington.

Fayer, M. J., W. Conbere, P. R. Heller, and G. W. Gee. 1985. *Model Assessment of Protective Barrier Designs*. PNL-5604, Pacific Northwest Laboratory, Richland, Washington.

Fayer, M. J., M. L. Rockhold, and D. J. Holford. 1992. *Model Assessment of Protective Barrier : Part III Status of FY 1990 Work*. PNL-7975, Pacific Northwest Laboratory, Richland, Washington.

Freeman, H. D., G. W. Gee, and J. F. Relyea. 1989. *Field Study Plan for Alternate Barrier*. PNL-6840, Pacific Northwest Laboratory, Richland, Washington.

Freeman, H. D., and G. W. Gee. 1989a. *Hanford Protective Barriers Program Asphalt Barrier Studies - FY 1988*. PNL-6874, Pacific Northwest Laboratory, Richland, Washington.

Freeman, H. D. and G. W. Gee. 1989b. *Hanford Protective Barriers Program: Status of Asphalt Barrier Study - FY 1989*. PNL-7513, Pacific Northwest Laboratory, Richland, Washington.

Gee, G. W., L. L. Cadwell, H. D. Freeman, M. W. Ligotke, S. O. Link, R. A. Romine, and W. H. Walters, Jr. 1993. *Testing and Monitoring Plan for the Permanent Isolation Surface Barrier Prototype*. PNL-8391, Pacific Northwest Laboratory, Richland, Washington.

Gee, G. W., M. J. Fayer, M. L. Rockhold, and M. D. Campbell. 1992. "Variations in recharge at the Hanford Site." *Northwest Science* 66(4):237-250.

Gee, G. W., R. R. Kirkham, J. L. Downs, and M. D. Campbell. 1989. *The Field Lysimeter Test Facility (FLTF) at the Hanford Site: Installation and Initial Tests*. PNL-6810, Pacific Northwest Laboratory, Richland, Washington.

Hoover, K. A., L. L. Cadwell, and W. H. Walters. 1990. *Hanford Protective Barriers Program: Water Erosion Studies - FY 1989*. PNL-7214, Pacific Northwest Laboratory, Richland, Washington.

Kaplan, M. F. and M. R. Adams. 1986. "Using the Past to Protect the Future: Marking Nuclear Waste Disposal Sites." *Archeology* 39(5):51-54.

Landeen, D. S. 1990. *Animal Intrusion Status Report for Fiscal Year 1989*. WHC-EP-0299, Westinghouse Hanford Company, Richland, Washington.

Landeen, D. S. 1991. *Animal Intrusion Status Report for Fiscal Year 1990*. WHC-EP-0398, Westinghouse Hanford Company, Richland, Washington.

Last, G. V., M. A. Glennon, M. A. Young, and G. W. Gee. 1987. *Protective Barrier Materials Analysis: Fine Soil Site Characterization*. PNL-6314, Pacific Northwest Laboratory, Richland, Washington.

Ligotke, M. W. 1988. *Soil Erosion Rates from Mixed Soil and Gravel Surfaces in a Wind Tunnel: A Preliminary Report*. PNL-6677, Pacific Northwest Laboratory, Richland, Washington.

Ligotke, M. W., and D. C. Klopfer. 1990. *Soil Erosion Rates from Mixed Soil and Gravel Surfaces in a Wind Tunnel*. PNL-7435, Pacific Northwest Laboratory, Richland, Washington.

Link, S. O., J. L. Downs, M. E. Thiede, D. J. Lettau, T. R. Twaddell, and R. A. Black. 1992a. *Evapotranspiration Studies for Protective Barriers: FY 1990 Status Report*. PNL-8032, Pacific Northwest Laboratory, Richland, Washington.

Link, S. O., M. E. Thiede, J. L. Downs, D. J. Lettau, and W. J. Waugh. 1992b. *Evapotranspiration Studies for Protective Barriers: FY 1989 Status Report.* PNL-8033, Pacific Northwest Laboratory, Richland, Washington.

Link, S. O., M. E. Thiede, R. D. Evans, J. L. Downs, and W. J. Waugh. 1990. *Evapotranspiration Studies for Protective Barriers: FY 1988 Status Report.* PNL-6985, Pacific Northwest Laboratory, Richland, Washington.

Phillips, S. J., M. R. Adams, T. W. Gilbert, C. C. Meinhardt, R. M. Mitchell, and W. J. Waugh. 1985. *Engineered Barrier Test Facility Status Report: 1984.* RHO-WM-SR-3P, Rockwell Hanford Operations, Richland, Washington.

Relyea, J. F., M. R. Sackschewsky, and W. J. Waugh. 1989. *Small-Tube Lysimeter Facility Status Report for Fiscal Year 1989.* WHC-EP-0297, Westinghouse Hanford Company, Richland, Washington.

Richards, L. A. 1950. "Laws of soil moisture." *Transactions American Geophyiscal Union* 31:750-756.

Routson, R. C., and V. G. Johnson. 1990. "Recharge estimates for the Hanford Site 200 Areas Plateau." *Northwest Science* 64(3):150-158.

Sackschewsky, M. R., C. J. Kemp, L. L. Cadwell, M. E. Thiede, and W. J. Waugh. 1991. *Status Report for the Small-Tube Lysimeter Facility Fiscal Year 1990.* WHC-EP-0381, Westinghouse Hanford Company, Richland, Washington.

Smoot, J. L., J. E. Szecsody, B. Sagar, G. W. Gee, and C. T. Kincaid. 1989. *Simulations of Infiltration of Meteoric Water and Contaminant Plume Movement in the Vadose Zone at Single-Shell Tank 241-T-106 at the Hanford Site.* WHC-EP-0332, Westinghouse Hanford Company, Richland, Washington.

U.S. Environmental Protection Agency (EPA). 1990. Seminars--*Design and Construction of RCRA/CERCLA Final Covers*, Center for Environmental Research Information 90-55, U.S. Environmental Protection Agency, Office of Research and Development, Washington, D.C.

U.S. EPA. 1982. *RCRA (Resource Conservation and Recovery Act) Guidance Document: Landfill Design. Liner Systems and Final Cover.* PB87-157657, National Technical Information Service, Springfield, Virginia.

Walters, W. H., K. A. Hoover, and L. L. Cadwell. 1990. *Project Test Plan for Runoff and Erosion on Fine-Soil Barrier Surfaces and Rock-Covered Side Slopes.* PNL-6791, Pacific Northwest Laboratory, Richland, Washington.

Waugh, W. J. 1989. *Gravel Admix, Vegetation and Soil Water Interactions in Protective Barriers: Experimental Design, Construction and Initial Conditions.* PNL-6616, Pacific Northwest Laboratory, Richland, Washington.

Waugh, W. J., M. E. Thiede, L. L. Cadwell, G. W. Gee, H. D. Freeman, M. R. Sackschewsky, and J. F. Relyea. 1991. *In* R. G. Allen (ed.), "Small lysimeters for documenting arid site water balance." *Proceedings of the International Symposium on Lysimetry*, Amer. Soc. Civil Engr., New York. pp. 151-159.

Waugh, W. J., M. E. Thiede, C. J. Kemp, L. L. Cadwell, and S. O. Link. 1990. *Field Study of Gravel Admix, Vegetation, and Soil Water Interactions: Protective Barrier Program Status Report - FY 1989.* PNL-7440, Pacific Northwest Laboratory, Richland, Washington.

Wing, N. R. September 1992. *A Peer Review of the Hanford Site Permanent Isolation Surface Barrier Development Program.* WHC-MR-0392. Westinghouse Hanford Company, Richland, Washington.

Wing, N. R., L. L. Cadwell, J. W. Cammann, J. C. Chatters, M. J. Fayer, H. D. Freeman, G. W. Gee, L. S. Hermann, M. W. Ligotke, D. R. Myers, K. L. Petersen, J. C. Sonnichsen, W. H. Walters, and M. Warn. August 1992. *Permanent Isolation Surface Barrier and Warning Marker System Development Plan.* WHC-AA-XXXX, Westinghouse Hanford Company, Richland, Washington.

Appendix G

Detailed Description of PORFLOW

9413222.1488

This page intentionally left blank.

Appendix G

Detailed Description of PORFLOW

M. G. Piepho and F. M. Mann, Westinghouse Hanford Company

G.1 Selection of PORFLOW

The criteria for selecting the PORFLOW code included consideration of the code's theoretical framework, implementation of the theory, documentation, quality control, acceptability by the technical community, and computation speed. The first criteria is that the theoretical framework be based on appropriate fundamental principles of chemistry and physics (e.g., continuity). The theoretical framework of PORFLOW is based on appropriate fundamental principles of chemistry and physics and well-established constitutive equations. The second criteria, which is related to the first, is that implementation of theory in the code be applicable to the problem being addressed. Overall, PORFLOW is applicable to problems of unsaturated flow in dry soils. Specific modifications were made to the code allowing simulation of degradation changes to engineered barriers to make a version (2.394gr) applicable for use in the grout performance assessment (Piepho et al. 1993). The primary code changes were to allow continuous time-dependent diffusion coefficients and the capability to model changes in hydraulic/transport properties (for example, saturated conductivities, moisture retention curves, partition coefficients) over time during one run.

The third and fourth criteria for selection were related to documentation of the code and quality assurance. Sufficient documentation must exist to describe the theoretical framework, computational techniques, and user interaction with the code (including examples). The framework and computational techniques for PORFLOW version 1.0 are documented in a WHC report (Sagar and Runchal 1990), while a user manual (Runchal and Sagar 1992) exists for version 2.40. (Version 2.40 is essentially the same as version 2.394gr.) The primary change in version 2.394gr was allowance of a time-dependent diffusion coefficient for asphalt, a feature that increases the diffusion coefficient of the asphalt-concrete barrier by six orders of magnitude (10^{-10} to 10^{-4} cm^2/s) over 90,000 years. Other changes include the ability to change hydraulic properties (saturated conductivity, porosity, moisture retention parameters, etc.) between SOLVE commands without having to restart.

To fulfill the requirements of quality assurance, the c[illegible] selected must have a verification report for the version used and be under configuration control. A number of verification and benchmarking efforts for version 2.394gr have been performed (Piepho et al. 1993). In addition, version 1.0 was

verified and benchmarked by Magnuson et al. (1990). Using the same procedures that were used for version 1.0, PORFLOW version 2.4 was verified and benchmarked as part of the performance assessment being prepared for the Savannah River Site Saltstone Disposal Facility.[a]

The fifth criteria is acceptance of the code by the technical community. The PORFLOW family of codes has been used extensively across the DOE complex. Version 1.0 of the PORFLO-3 code, an earlier version of the code, has been used at the Idaho National Engineering Laboratory to model a large organic vapor plume (Baca et al. 1988) and to model concrete barriers (Walton and Seitz 1991). In addition, as stated above, version 2.4 was used for the Savannah River performance assessment that is currently being prepared. At the Hanford Site, PORFLOW has been used many times, including applications for the Basalt Waste Isolation Project (U.S. DOE/RL 1982 and Baca et al. 1984), simulations of a single-shell tank leak (Smoot and Sagar 1990), evaluation of liquid effluent discharges from 200 Area cribs (WHC 1990), a preliminary single-shell tank performance assessment (Sonnichsen 1991), a study of effluent disposed to trenches in the 100-N Area (Connelly et al. 1991), and a comparison of three methods for solving flow equations (Piepho and Runchal 1991). PORFLOW was also selected to be one of three codes to be used for modeling performed under the Federal Facilities Agreement and Consent Order (i.e., the Tri-Party Agreement) between the U.S. Department of Energy, the U.S. Environmental Protection Agency, and the Washington Department of Ecology (U.S. DOE/RL 1991). Validation exercises have been performed with an older version of PORFLOW for simulation of flow and transport at an experimental trench in Las Cruces, New Mexico (Wittmeyer and Sagar 1992a,b and Rockhold and Wurstner 1991). The newer version (2.394gr) of PORFLOW has been able to repeat all test calculations that the older version has done, including the Las Cruces trench case (Piepho et al. 1993). All the cases used for grout are discussed and shown by Piepho (1993).

The sixth criteria is sufficient computational speed of the code to allow a simulation to be solved in a reasonable length of time. Because of the complexity of the simulations and the lengthy time scales being analyzed in this performance assessment (up to one million years), the PORFLOW code requires many hours of CRAY time. The codes TRACR3D (Travis 1984) and S301-2 (Farmer 1984), which were used in a previous evaluation of grout performance assessment, were slower and were used only for benchmarking in the current effort.

G.2 History of PORFLOW Version 2.394gr

The original version of PORFLOW (Kline et al. 1983 and Runchal et al. 1985), limited to saturated conditions in two-dimensional porous domains, was extensively verified and benchmarked by Eyler and

(a) McDowell-Boyer, L. Preliminary Predecisional Draft of Saltstone Disposal Facility Performance Assessment. Letter transmitting the SRS performance assessment to the Peer Review Panel. Oak Ridge National Laboratory, August 6, 1992.

Budden (1984) and also by Runchal et al. (1985). The code was extended to model variably saturated flow in three-dimensional geometry and was termed PORFLO-3, version 1.0 (Runchal and Sagar 1989, Sagar and Runchal 1990). A newer version able to treat multiphase problems (2.1) was developed for DOE and is the basis of the version used in this performance assessment. A commercially available version of PORFLOW version 2.41 (Runchal and Sagar 1992) was released in August 1992. Version 2.394 of PORFLOW was released in November 1991 and is the starting point for the special version 2.394gr tailored for use in this work (Piepho et al. 1993).

G.3 Theoretical Framework

G.3.1 Governing Equations and Assumptions

The equations solved in PORFLOW are based on the conservation principles of continuum mechanics. These equations describe fluid flow and mass transport processes in heterogeneous and anisotropic porous media. The equations are well accepted mathematical representations and are found in such standard texts as Bear and Bachmat (1990), Freeze and Cherry (1979), and Huyakorn and Pinder (1983). The specific partial differential equation solved in PORFLOW for isothermal fluid flow around and through the grout disposal facility is

$$S_e \frac{\partial P}{\partial t} = \frac{\partial}{\partial x_i}\left(K_{ij} \frac{\partial P}{\partial x_j} \right) + m_v$$

where S_e = fluid storage term (i.e., specific storage or moisture capacity term)

P = piezometric head (i.e., total hydraulic head)

K_{ij} = hydraulic conductivity tensor

mv = fluid volume source or sink term

t = time

x_i = distance in the ith direction.

The quantity P is defined by

$$P = h + z - z^*$$

where h = pressure head (capillary pressure head)

z = elevation head

z^* = reference value

and the quantity S_e is defined by

$$S_e = S(\alpha_s + \theta_e \alpha_f) + \theta_e \frac{\partial S}{\partial p}$$

where S = saturation level

αs = solid compressibility normalized by the specific weight of the fluid

α_f = fluid compressibility normalized by the specific weight of the fluid

θ_e = effective porosity.

Some of the basic assumptions made in the above mathematical formulations are

1. the fluid flow is laminar, slightly compressible, and single phase
2. the fluid flow obeys Darcy's law for porous flow
3. fluid viscosity is a function of temperature only
4. the hydraulic properties of the porous continuum are volume averages
5. osmotic effects (associated with the waste form) are negligible.

In general, these assumptions are satisfied in the hydrogeologic environment of the grout vaults except for assumption 5. The osmotic effects of grout are not modeled explicitly. Vapor return effects have been modeled by introducing a liquid water source, which represents the condensed vapor, at any exposed grout interfaces.

The specific partial differential equation solved in PORFLOW for contaminant transport from the grout vault is

$$R_f \phi_D \frac{\partial C}{\partial t} + \frac{\partial}{\partial x_i}(V_i C) = \frac{\partial}{\partial x_i}\left[\Gamma^C_{ij} \frac{\partial C}{\partial x_j}\right] - \phi_D R_f \lambda C + S_C + \Sigma_p \phi_D R_f^p \sigma^p \lambda^{mp} C$$

where C = contaminant concentration

V_i = Darcy velocity in i^{th} direction

R_f = retardation factor

Γ^C_{ij} = hydrodynamic dispersion tensor

λ = decay rate

S_c = mass source term

σ^p = fraction of decay of the parent mass species which generates the current species, and the superscript p refers to the parent mass species.

The last term in the above equation represents the ingrowth of mass species. The retardation factor R_f is defined by

$$R_f = \left[1 + (1-\theta_T)\frac{\rho_s R_d}{\theta_D}\right]$$

where ρ_s = solid (particle or grain) density

θ_T = total porosity

θ_D = total diffusive porosity

R_d = sorption (distribution) coefficient, (denoted by K_d in many other reports)

and Γ^C_{ij} is defined (Kemper and van Schaik 1966) by

$$\Gamma^C_{ij} = a\, D_M \exp(b\phi_D)$$

where ϕ_D = effective diffusive pore space saturated with water, (i.e., effective diffusive moisture content)

D_M = molecular diffusion coefficient

a,b = parameters (the "a" parameter can include tortuosity).

All other coefficients are as previously defined. The Kemper diffusion model is optional in PORFLOW and was the choice for the grout performance assessment.

Some of the key assumptions that limit the applicability of the above formulation are as follows:

1. contaminant concentrations are low enough that the fluid flow is independent of mass transport, i.e., concentrations do not affect the density or viscosity of the fluid

2. diffusion of the contaminants through the fluid obeys Frick's first law

3. adsorption (and desorption) of contaminants into the porous medium is an equilibrium process described by a linear isotherm.

The model formulation is applicable to both saturated and unsaturated flow conditions.

G.3.2 Initial and Boundary Conditions

The PORFLOW code accommodates the specification of standard mathematical boundary conditions. These include

1. Dirichlet (fixed head or concentration)

2. Neumann (specified flux)

3. Robin (mixed).

Detailed information on boundary conditions is given in Runchal and Sagar (1989 and 1992).

G.3.3 Numerical Techniques

In PORFLOW, the governing equations for flow and transport are solved using a method referred to as the Nodal Point Integration, a variation of the finite volume or integrated finite difference technique. In this method, the difference approximations to the governing equations are derived on a staggered grid system. The state variables are computed at the grid nodes whereas the fluid velocities and fluxes are computed at the cell faces (located midway between adjacent grid nodes). Three discretization schemes,

or basis functions to be integrated, are provided. The user may select which of the three schemes is to be used to maximize accuracy and stability.

The system of algebraic equations produced by the finite volume are solved using one of five techniques:

1. point successive overrelaxation
2. alternating direction implicit (ADI)
3. Cholesky decomposition
4. Gauss elimination
5. reduced system conjugate gradient method.

The nonlinearity of the governing equation for variably saturated flow is solved using a Picard iteration method. The ADI was the method used for all of the grout PA runs, since it has been very robust in previous work.

G.4 Code Inputs And Outputs

G.4.1 Input Data Structure

PORFLOW uses a free-form input which allows the user to document the input data deck. The input file uses a keyword approach to define primary input data groups. For typical flow and transport simulations, the input data groups consists of

1. title card and comments
2. finite difference grid specification, i.e. the number of grid nodes in each direction,
3. lists of grid node coordinates
4. zone definitions that specify the grid locations of distinct strata,
5. rock and hydraulic property specifications

   convergence and iteration parameters

7. initial pressures and concentrations

8. boundary values and/or fluxes

9. time step and output specifications.

Simulations of multidimensional flow and transport can be performed in either steady state or time-dependent mode.

G.4.2 Output Options

Results from PORFLOW consist of

1. total head

2. saturation

3. moisture content

4. contaminant concentration

5. Darcy velocities

for each grid block in the computational grid. The user can select to print out any or all of the output variables. Each of these variables can be post-processed to produced graphical output.

G.4.3 Documentation of User Instructions

PORFLOW, version 2.4, is documented in Runchal and Sagar (1992). This report describes the mathematical theory and numerical techniques, serves as a user's manual, and provides detailed information on the code organization, selection of computational grids and time steps, input structure, and keyword definitions.

G.5 References

Baca, R. G., R. C. Arnett, P. M. Clifton, and N. W. Kline. 1984. *Repository Horizon Identification Report*, Chapters I-VII, RHO-BW-ST-28P, Rockwell Hanford Operations, Richland, Washington.

Baca, R. G., J. C. Walton, and A. S. Rood. 1988. "Organic Contaminant Release from a Mixed Waste Disposal Site: Analysis of Vapor Transport through the Vadose Zone and Site Remediation," *Proceedings of the Tenth Annual DOE Low-Level Waste Management Conference*, Denver, Colorado.

Bear, J., and Y. Bachmat. 1990. *Introduction to Modelling of Transport Phenomena in Porous Media.* Kluwer Academic Publishers, Boston, Massachusetts.

Connelly, M. P., J. D. Davis, and P. D. Rittmann. 1991. *Numerical Simulation of ^{90}Sr Transport from the 100-N Area Liquid Waste Disposal Facilities*, WHC-SD-ER-TA-001, Westinghouse Hanford Company, Richland, Washington.

Eyler, L. L., and M. J. Budden. 1984. *Verification and Benchmarking PORFLO: An Equivalent Porous Continuum Code for Repository Scale Analysis*, PNL-5044, Pacific Northwest Laboratory, Richland, Washington.

Farmer, C. L. 1984. *A Moving Point Method for Numerical Calculation of Miscible Displacement*, AEEW-R 1895, Winfrith Atomic Energy Establishment, Winfrith, England, UK.

Freeze, R. A., and J. A. Cherry. 1979. *Groundwater*. Prentice-Hall, Inc., Englewood Cliffs, New Jersey.

Huyakorn, P. S., and G. F. Pinder. 1983. *Computational Methods in Subsurface Flow*. Academic Press, Inc., New York.

Kemper, W. O., and J. C. van Schaik. 1966. *Diffusion of Salts in Clay-Water Systems*. Soil Sc. Am. Proc. 30:534-540.

Kline, N. W., A. K. Runchal, and R. G. Baca. 1983. *PORFLO Computer Code: Users Guide*, RHO-BW-CR-138P, Rockwell Hanford Operations, Richland, Washington.

Magnuson, S. O., R. G. Baca, and A. J. Sondrup. 1990. *Independent Verification and Benchmark Testing of the PORFLO-3 Computer Code, Version 1.0*, EGG-BG-9175, EG&G Idaho, Inc., Idaho Falls, Idaho.

Piepho, M. G., and A. K. Runchal. 1991. *A Comparison of Three Methods for Solving Flow Equations of Two Immiscible Fluids in Variably-Saturated Media*, WHC-SA-1289-FP, Westinghouse Hanford Company, Richland, Washington.

Piepho, M. G., W. H. Sutherland, and P. D. Rittmann. 1993. *The Grout Performance Assessment Code System (GPACS) with Verification and Benchmarking*, WHC-SD-WM-UM-019, Draft, Westinghouse Hanford Company, Richland, Washington.

Piepho, M. G. 1993. *Grout Performance Assessment Results of Benchmark, Base, and Sensitivity Cases*. WHC-SD-WM-TI-561, Draft, Westinghouse Hanford Company, Richland, Washington.

Rockhold, M. L., and S. K. Wurstner. 1991. *Simulation of Unsaturated Flow and Solute Transport at the Las Cruces Trench Site Using the PORFLO-3 Computer Code*, PNL-7562, Pacific Northwest Laboratories, Richland, Washington.

Runchal, A. K., B. Sagar, R. G. Baca, and N.W. Kline. 1985. *PORFLO - A Continuum Model for Fluid Flow, Heat Transfer, Mass Transport in Porous Media*, RHO-BW-CR-150P, Rockwell Hanford Operations, Richland, Washington.

Runchal, A. K., and B. Sagar. 1989. *PORFLO-3: A Mathematical Model for Fluid Flow, Heat and Mass Transport in Variably Saturated Geologic Media.* Users' Manual, Ver 1.0, WHC-EP-0042, Westinghouse Hanford Company, Richland, Washington.

Runchal, A. K., and B. Sagar. 1992. *PORFLOW: A Mathematical Model for Fluid Flow, Heat and Mass Transport in Multifluid, Multiphase Fractured or Porous Media.* Users' Manual, Ver 12.4, ACRi/016/Rev G. Analytic and Computational Research Inc., Los Angeles, California.

Sagar, B., and A. K. Runchal. 1990. *PORFLO-3; A Mathematical Model for Fluid Flow, Heat, and Mass Transport in Variably Saturated Geologic Media, Theory and Numerical Methods, Version 1.0*, WHC-EP-0042, Westinghouse Hanford Company, Richland, Washington.

Smoot, J. L., and B. Sagar. 1990. *Three Dimensional Contaminant Plume Dynamics in the Vadose Zone: Simulation of the 241-T-106 Single-Shell Tank Leak at Hanford*, PNL-7221, Pacific Northwest Laboratory, Richland, Washington.

Sonnichsen, J. C. 1991. *Preliminary Performance Assessment Strategy for Single-Shell Tank Waste Disposal*, WHC-EP-0379, Westinghouse Hanford Company, Richland, Washington.

Travis, B. J. 1984. *TRACR3D: A Model of Flow and Transport in Porous/Fractured Media*, LA-9667-MS, Los Alamos National Laboratory, Los Alamos, New Mexico.

U.S. Department of Energy-Richland Operations Office (U.S. DOE/RL). 1982. *Site Characterization Report for the Basalt Waste Isolation Project*, DOE-RL 82-3, U.S. Department of Energy, Richland Operations Office, Richland, Washington.

U.S. DOE/RL. 1991. *Description of Codes and Models to be Used in Risk Assessment*, U.S. Department of Energy, Richland Operations Office, Richland, Washington.

Walton, J. C., and R. R. Seitz. 1991. *Performance of Intact and Partially Degraded Concrete Barriers in Limiting Fluid Flow*, NUREG/CR-5614, U.S. Nuclear Regulatory Commission, Washington, D.C. or EGG-2614, EG&G Idaho, Inc., Idaho Falls, Idaho.

Westinghouse Hanford Company (WHC). 1990. *Liquid Effluent Study Final Project Report*, WHC-EP-0367, Westinghouse Hanford Company, Richland, Washington.

Wittmeyer, G. W., and B. Sagar. 1992a. INTRAVAL Project: Las Cruces Trench Solute Transport Modeling Study, Plot 2, Experiments A and B. Report for Research Activities for Calendar Year 1991. W. C. Patrick, ed. CNWRA 91-01A. San Antonio, Texas.

Wittmeyer, G. W., and B. Sagar. 1992b. INTRAVAL Project: Las Cruces Trench Unsaturated Flow Modeling Study, Plot 2, Experiment B. NRC High-Level Radioactive Waste Research at CNWRA for Calendar January 1 through June 30, 1992. W. C. Patrick, ed. CNWRA 92-015. San Antonio, Texas.

9413222.1500

This page intentionally left blank.

Appendix H

Verification and Benchmark Testing of the Flow and Transport Codes Used for the Hanford Grout Performance Assessment

9413222.1502

This page intentionally left blank.

Appendix H

Verification and Benchmark Testing of the Flow and Transport Codes Used for the Hanford Grout Performance Assessment

M. L. Rockhold, Pacific Northwest Laboratory
W. H. Sutherland, Westinghouse Hanford Company
C. A. Oster and D. W. Langford, Boeing Computer Services

9413222.1504

H.1 Introduction

Computer codes were used to model unsaturated flow and contaminant transport for the performance assessment of grouted double-shell tank waste disposal at the Hanford Site. These computer codes were tested and evaluated to verify their capability of correctly simulating the type of problems related to the performance assessment. These computer codes include PORFLOW (Runchal and Sagar 1992), S301 (Wikramaratna and Farmer 1987), and TRACR3D (Travis and Birdsell 1991). This appendix describes the results of selected verification and benchmark test problems that were simulated with these codes.

Numerous methods exist for testing computer codes. These methods include 1) mass balance and consistency checks within a computer code during execution, 2) crosschecks between sequential runs of the same problem using finer spatial and temporal discretizations, 3) comparisons of numerical solutions with selected analytical solutions (a.k.a. verification), and 4) comparisons of numerical solutions from one code with solutions from another code for the same problem (a.k.a. benchmarking).

Computer codes can also be tested by comparing simulation results with observations from actual laboratory or field experiments. These comparisons test the conceptual model of the specific field site or experiment, the physics or mathematical representation of it, and the adequacy of the site or experimental characterization data. No single test method is sufficient to confirm that a computer code correctly calculates results. However, when used together the methods provide confidence that a code can reliably calculate correct results for the types of situations and conditions modeled.

The primary emphasis of this appendix is on the verification and benchmark testing of the PORFLOW, TRACR3D, and S301 computer codes. Additional verification and benchmark testing of the version of PORFLOW that was used for the performance assessment is described by Piepho et al. (1993). The results from independent verification and benchmark testing of an earlier version of the PORFLOW

code were reported by Magnusen, Baca, and Sondrup (1990). Benchmark comparisons between the PORFLOW and TRACR3D codes were also reported by Magnusen, Baca, and Sondrup (1990) and Thomas (1991).

This appendix is organized as follows. Governing equations used for unsaturated flow and contaminant transport modeling are discussed in Section H.2. Brief descriptions of the PORFLOW, TRACR3D, and S301 codes are presented in Section H.3. The performance indicators used to evaluate simulation results are described in Section H.4. Section H.5 contains a description of the verification and benchmark test problems and the results. The conclusions are given in Section H.6, and cited references are listed in Section H.7.

H.2 Governing Equations

Natural and engineered components of the proposed grout waste isolation system at the Hanford Site compose a geochemically complex, three-dimensional, multiphase, nonisothermal system. Here, the term multiphase refers to multiple fluid phases (i.e., aqueous and gas phases). This system was modeled as a two-dimensional, isothermal, single-phase (aqueous) system primarily for computational efficiency. The simplification to a two-dimensional system was justified because of the length-to-height ratio of the unsaturated zone and because of plans to construct the grout vaults in pairs. In addition, water flow in the unsaturated zone is predominantly vertical and moves into a horizontal, saturated flow system whose water table is essentially unaffected by the overlying grout facility. Nonisothermal effects associated with grout curing, asphalt cooling, and heat generation by the waste were assumed to be relatively insignificant.

The flow of a single fluid phase (water) and the transport of water-soluble contaminants under isothermal conditions are described using two governing mass conservation equations. The isothermal flow of water in a rigid, variably saturated porous medium is described using the Richards equation (Richards 1931). The two-dimensional form of the Richards equation is written as follows:

$$\frac{\partial \theta}{\partial t} = \frac{\partial}{\partial x}\left[K_{xx}\, k_r \frac{\partial h}{\partial x}\right] + \frac{\partial}{\partial z}\left[K_{zz}\, k_r \left(\frac{\partial h}{\partial z} + 1\right)\right] \tag{1}$$

where θ = volumetric water content (L^3/L^3)

t = time

K_{xx} = horizontal component of saturated hydraulic conductivity tensor (L/T)

K_{zz} = vertical component of saturated hydraulic conductivity tensor (L/T)

k_r = relative permeability (dimensionless)

h = pressure head (L)

x = horizontal coordinate (L)

z = vertical coordinate (L).

The primary dependent variable in Equation 1 is pressure head, h. Pressure head is linked to the secondary variables, θ, K, and k_r, by constitutive relations representative of the physical and hydraulic properties of the fluid and porous medium. Note that the principal directions of anisotropy are aligned with the cartesian coordinate system so that the cross-components of the saturated hydraulic conductivity tensor are 0.

The van Genuchten (1980) model, given by Equations (2) and (3), was used to describe the constitutive relations for relative permeability (k_r), effective saturation (S_e), and pressure head (h).

$$\theta = \begin{cases} \theta_s & h \geq 0 \\ \theta_r + (\theta_s - \theta_r)[1 + (-\alpha h)^n]^{-m} & h < 0 \end{cases} \tag{2}$$

$$k_r = S_e^{1/2}\left[1 - \left(1 - S_e^{1/m}\right)^m\right]^2 \tag{3}$$

where θ_s = saturated water content (L^3/L^3)

θ_r = residual water content (L^3/L^3)

α, n = curve-fitting parameters (L^{-1}, dimensionless)

m = $1 - 1/n$

S_e = $(\theta - \theta_r)/(\theta_s - \theta_r)$.

Transport of a conservative solute is described by the convective-dispersive mass transport equation, which is written as:

$$\frac{\partial}{\partial x}\left(D_{xx}\frac{\partial c}{\partial x}\right) + \frac{\partial}{\partial z}\left(D_{zz}\frac{\partial c}{\partial z}\right) + \frac{\partial}{\partial x}\left(D_{xz}\frac{\partial c}{\partial z}\right) + \frac{\partial}{\partial z}\left(D_{zx}\frac{\partial c}{\partial x}\right) - V_x\frac{\partial c}{\partial x} - V_z\frac{\partial c}{\partial z} - \lambda c = \frac{\partial c}{\partial t} \tag{4}$$

where $D_{xx}, D_{zz}, D_{xz}, D_{zx}$ = dispersion coefficients (L/T^2)

c = solute concentration (M/L^3)

V_x, V_z = x- and z-components of Darcy velocity vector (L/T)

λ = solute or species reaction rate (T^{-1}).

The dispersion coefficients incorporate the effects of hydrodynamic mixing and molecular diffusion. The common assumption that hydrodynamic dispersion is linearly proportional to the average pore water velocity (Bear 1972) leads to the following expressions for the dispersion coefficients (Scheidegger 1961):

$$D_{xx} = \alpha_L \frac{V_x^2}{|V|} + \alpha_T \frac{V_z^2}{|V|} + D_m \tag{5}$$

$$D_{zz} = \alpha_T \frac{V_x^2}{|V|} + \alpha_L \frac{V_z^2}{|V|} + D_m \tag{6}$$

$$D_{zx} = D_{xz} = (\alpha_L - \alpha_T)\frac{V_x V_z}{|V|} \tag{7}$$

where α_L, α_T = longitudinal and transverse dispersivities (L)

D_m = bulk solution coefficient of molecular diffusion (L^2/T).

A modified form of the dispersion coefficient used in the performance assessment simulations will be described later in this appendix for the second set of benchmark problems.

H.3 Code Descriptions

The PORFLOW, TRACR3D, and S301 codes are briefly described in this section. Complete descriptions of the numerical methods implemented in the different codes are given in the respective users' manuals or in theory documents cited below.

H.3.1 PORFLOW

PORFLOW Version 2.394gr was the primary numerical model used to support the performance assessment calculations. PORFLOW is a proprietary code that is copyrighted by Analytical and Computational Research, Inc., subject to limited government license (Runchal and Sagar 1992). Version 2.394gr is a fully three-dimensional, Eulerian (or fixed grid) finite difference code designed to simulate multiphase fluid flow, heat transfer, and multicomponent mass transport in variably saturated, heterogeneous, and anisotropic porous media.

The governing mass conservation equations and constitutive relations that were used by PORFLOW for the performance assessment simulations are essentially those shown in Equations (1-5). The governing equations were solved using an integrated finite difference method (Patankar 1980). Time derivatives were approximated using a first-order, implicit (backward difference) scheme. Several direct and iterative solution options were available to solve the resulting nonlinear algebraic equations. An alternating-direction-implicit scheme with Picard iteration (Huyakorn and Pinder 1983) was also used for the performance assessment simulations.

H.3.2 TRACR3D

The TRACR3D code is also a fully three-dimensional, Eulerian finite difference code that is designed to simulate multiphase fluid flow and multicomponent mass transport in variably saturated, heterogeneous, and anisotropic porous media (Travis and Birdsell 1991). TRACR3D does not account for heat transfer and, therefore, will only solve isothermal flow and transport problems. TRACR3D was used to model water flow for the benchmark and verification problems in this appendix. The code's solute transport simulation capabilities were not formally tested. The TRACR3D code is in the public domain and available from Los Alamos National Laboratory.

Like PORFLOW, TRACR3D also uses an integrated finite difference method. However, the resulting nonlinear finite difference equations are linearized and solved using an iterative Newton-Raphson technique (Huyakorn and Pinder 1983). Newton-Raphson implementations typically require more memory and more computational effort per iteration than Picard implementations, but they are quadratically convergent as opposed to linear. As a result, the Newton-Raphson method allows larger time steps and is more robust than the Picard method for highly nonlinear problems.

The PORFLOW and TRACR3D codes use cell-centered and node-centered finite difference schemes, respectively. In the cell-centered scheme, the node positions are specified, and the cell faces are

placed at the midpoints between nodes. In the node-centered finite difference scheme, the positions of the cell faces are specified, and the nodes are placed at the midpoints between the cell faces. The two schemes are identical for uniform grids, but can result in different node locations for nonuniform grids.

H.3.3 S301

The version of the S301 code used for these simulations is a two-dimensional, mixed Eulerian-Lagrangian code originally designed to simulate solute transport under steady, saturated flow conditions (Wikramaratna and Farmer 1987). The code was modified to use saturation and velocity fields generated by TRACR3D to perform transient transport simulations under unsaturated conditions. The S301 code was obtained through the purchase of a use agreement from the United Kingdom Atomic Energy Authority.

S301 code uses an explicit, 9-point finite difference approximation to generate solutions with minimal grid orientation effects (Wikramaratna and Farmer 1987). S301 uses the modified method of characteristics (Chiang, Wheeler, and Bedient 1989) to develop a first approximation of concentrations at new time levels. An adaptive moving point (particle tracking) technique is then used as an error recovery procedure in regions where numerical dispersion is significant (Farmer 1985). These regions are determined by calculating where grid Peclet numbers and concentration gradients exceed given threshold values (Wikramaratna and Farmer 1987). The S301 code was used to model solute transport for the verification and benchmark problems in this appendix.

H.4 Performance Indicators

Various performance indicators can be used to evaluate the accuracy of results generated by numerical models. Performance indicators should be selected to match the purpose of the simulations. For example, if a numerical model is used to forecast contaminant movement in groundwater, then the travel time of the contaminant from the source to some point of compliance, such as a water supply well, is a good performance indicator. Calculated fluxes crossing specified horizontal or vertical planes as a function of time, and contaminant arrival curves are also useful for evaluating the performance of numerical flow and transport codes for this type of application.

Other quantitative indicators of model performance include maximum absolute deviation, root-mean-squared error, and relative-root-mean-squared error. These are general indicators, but they can be useful for relative comparisons between the results generated by numerical models and analytical solutions.

Several performance indicators were used to evaluate the numerical models for this verification and benchmarking effort. For the verification problems, relative-root-mean-squared (RRMS) error calculations were used to provide a quantitative basis for comparing numerical and analytical solutions. The RRMS error was defined as:

$$\text{RRMS} = \sqrt{\sum_{i=1}^{k} \frac{[(a_i - n_i)/a_i]^2}{k}} \tag{8}$$

where a_i = analytical solution at point i

n_i = numerical solution at point i

k = number of comparison points.

Magnusen, Baca, and Sondrup (1990), who also used the RRMS error as a performance indicator, judged the accuracy of verification test results by defining four performance categories. These categories were 1) Excellent - RRMS ≤ 0.01, 2) Good - RRMS ≤ 0.05, 3) Acceptable - RRMS ≤ 0.10, and 4) Unacceptable - RRMS > 0.10. The ranges for these categories were arbitrarily selected and, thus, are meaningless with respect to quantifying contaminant fluxes or arrival times. Therefore, in this appendix, RRMS values are only used to provide a quantitative basis for relative comparisons.

For the benchmark problems, instantaneous fluxes crossing specified vertical and horizontal planes, and outflow arrival distribution curves were used to compare the results generated by the different numerical models. Contour plots of water content or normalized concentrations were also generated for qualitative comparisons.

H.5 Descriptions of Test Problems and Simulation Results

Two verification problems were selected to test the PORFLOW, TRACR3D, and S301 codes. The first verification problem tested the ability of the PORFLOW and TRACR3D codes to simulate two-dimensional water infiltration into homogeneous, unsaturated soil. The second verification problem tested the ability of the PORFLOW and S301 codes to simulate two-dimensional solute transport in a homogeneous medium, with different grid Peclet numbers. These verification problems also constituted benchmarks for the respective codes. Two additional sets of benchmark simulations were conducted to compare the results generated by the different codes for more realistic flow and transport problems similar to the type required for the performance assessment.

H.5.1 Verification Test Problem 1

The first verification test problem was designed to test the ability of the PORFLOW and TRACR3D codes to simulate the advance of a moisture front into homogeneous soil from a surface infiltration source. The analytical and numerical solution problem domains, and the boundary and initial conditions for this problem are illustrated in Figure H.1. The analytical solution problem domain is the semi-infinite plane below the z = 0 line shown in Figure H.1. The boundary conditions along the top of the domain are Neumann, with the flux = 0 for x < -5 cm and x > 5 cm, and an infiltration flux (expressed as a rate per unit width and length) for the strip source of 400 $cm^3/cm^2/d$. No boundary conditions were imposed along the other boundaries for the analytical solution problem domain, because they extend to infinity.

Warrick and Lomen (1976) developed an analytical solution for this problem using a Kirchoff integral transformation (Carslaw and Jaeger 1959) and defining a matric flux potential, ϕ, after Gardner (1958) as:

$$\phi = \int_{h_{min}}^{h} K(h)\,dh \tag{9}$$

with

$$K(h) = K_0 \exp(\alpha h) \tag{10}$$

where h_{min} = initial pressure head (L)

h = pressure head (L)

K = hydraulic conductivity (L/T)

K_0 = saturated hydraulic conductivity (L/T)

α = empirical constant (L^{-1}).

The pressure head, h, is then equal to:

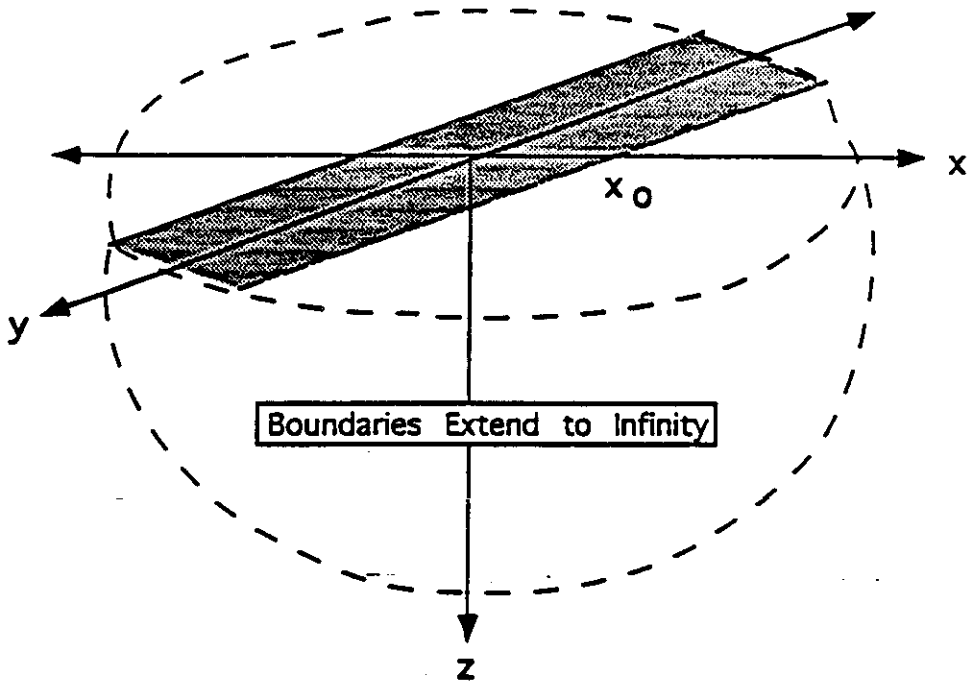

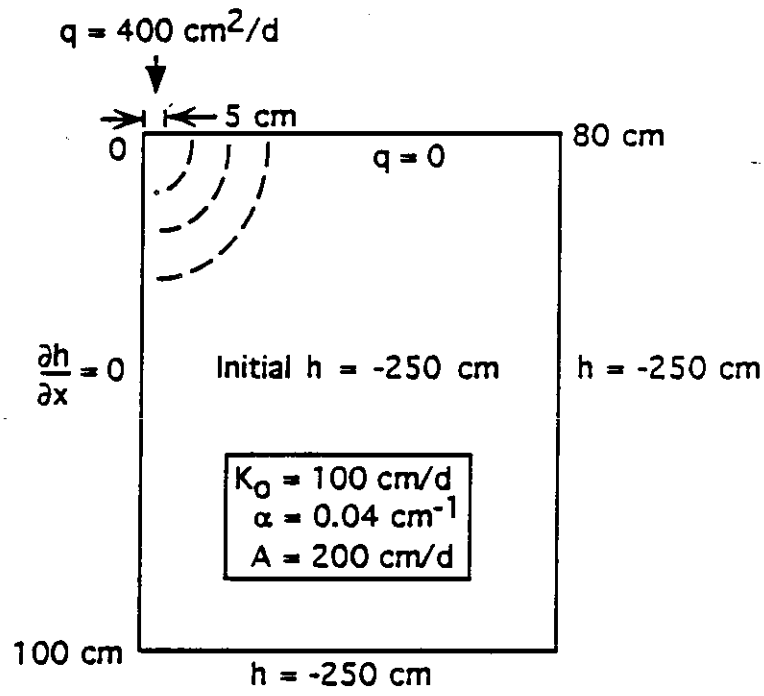

Figure H.1. Analytical and Numerical Solution Problem Domains and Boundary and Initial Conditions for Verification Test Problem 1

$$h(x,z,t) = 1/\alpha \ln(\alpha/K_0 \phi) \tag{11}$$

where

$$\phi(X,Z,T) = (q_0/2\pi)\ \Phi(X,Z,T) \tag{12}$$

and

$$\begin{aligned}\Phi(X,Z,T) = \frac{\sqrt{\pi}\ \exp Z}{2X_0}\int_0^T \Big[& \tau^{-1/2} \exp(-\tau - Z^2/4\tau) \\ & - \sqrt{\pi}\ \exp Z\ \mathrm{erfc}\ (Z/2\sqrt{\tau} + \sqrt{\tau})\Big] \\ & \cdot \Big[\mathrm{erf}\left\{(X + X_0)/2\sqrt{\tau}\right\} - \mathrm{erf}\left\{(X - X_0)/2\sqrt{\tau}\right\}\Big] d\tau\end{aligned} \tag{13}$$

The dimensionless variables $X = \alpha x/2$, $Z = \alpha z/2$, and $T = \alpha kt/4$ were introduced to facilitate obtaining the analytical solution. The parameters x and z are the true (unscaled) horizontal and vertical distances, respectively, measured from the center of the surface strip source, and t is the actual (unscaled) time. The terms erf and erfc are the standard definitions of the error function and the complementary error function, respectively (Abramowitz and Stegun 1964). The integral in Equation (13) was evaluated numerically using the IMSL subroutine DQDAGS (IMSL 1987).

Celia, Ahuja, and Pinder (1987) and Bouloutas (1989) compared numerical solutions with the analytical solution by Warrick and Lomen (1976) for infiltration from a surface strip source using parameters reported by Warrick (1974) for the Panoche loam soil. Volumetric water content was expressed as a function of pressure head as:

$$\theta(h) = (K_o/A) \exp(\alpha h) \tag{14}$$

with the values of K_o, α, and A taken to be 100 cm/d (0.0694 cm/min), 0.04 m^{-1}, and 200 cm/d (0.1388 cm/min), respectively. The half-width of the strip source was taken to be 5 cm. The surface boundary flux, q, was set equal to 400 cm^2/d (0.277 cm^2/min), and the initial pressure head was set equal to -250 cm. Warrick and Lomen (1976) used a value of $h_{min} = -\infty$ as initial and boundary conditions, but their solution is applicable for other initial and boundary conditions, provided that the boundaries are

located a sufficient distance from the source. For the numerical simulations of this problem, the bottom and right-hand side boundaries were maintained at an initial pressure head of -250 cm.

The problem described above was simulated using the PORFLOW and TRACR3D codes. A non-uniform grid with 29 nodes in the x-direction and 31 nodes in the z-direction was used to discretize the 80-cm-wide by 100-cm-deep model domain. The numerical solution problem domain and boundary and initial conditions are also shown in Figure H.1. The numerical model domain represents the right-hand side of the analytical solution problem domain, assuming an axis of symmetry along the center line of the surface strip source.

For the computational grid used by TRACR3D, the coordinates of the nodes in the x-direction are 0.5, 1.5, 2.5, 3.5, 4.5, 5.5, 6.75, 8.5, 10.5, 12.5, 14.5, 16.5, 18.5, 20.5, 22.5, 24.5, 26.5, 28.5, 31.0, 34.5, 38.5, 42.5, 46.5, 50.5, 54.5, 58.5, 63.0, 69.0, and 76.25 cm. The z-coordinates of the nodes used by TRACR3D are 0.5, 1.5, 2.5, 3.5, 4.5, 5.5, 6.75, 8.5, 10.5, 12.5, 14.5, 16.5, 18.5, 20.5, 22.5, 24.5, 26.5, 28.5, 31.0, 34.5, 38.5, 42.5, 46.5, 50.5, 54.5, 58.5, 63.5, 70.5, 78.5, 86.5, and 95.25 cm. The analytical solution was evaluated at these same node coordinates.

The x-coordinates of the nodes used for PORFLOW simulations were the same as those used for the TRACR3D simulations, except for nodes at 6.5, 30.5, 62.5, 68.5, and 76.5 cm. Similarly, the z-coordinates of the nodes used for PORFLOW simulations differed from TRACR3D by nodes at 6.5, 30.5, 62.5, and 94.5 cm. The above listed node coordinates were used in the PORFLOW simulations in place of the closest respective node coordinates listed for TRACR3D. As noted previously, the differences in the node locations were a result of the node-centered versus cell-centered finite difference schemes used by TRACR3D and PORFLOW, respectively.

The numerical solutions for this verification test problem are shown with the analytical solution results for time equal to 72 minutes in Figure H.2. The RRMS errors for the PORFLOW and TRACR3D solutions are 0.042 and 0.011, respectively. The RRMS error calculations were only made at node coordinates that were common to both the analytical and numerical solution grids. In addition, comparisons were only made for values of pressure head ≥ -200 cm.

The numerical solutions from both TRACR3D and PORFLOW appeared to match the analytical solution relatively well. No grid convergence tests were conducted for this problem, but the RRMS errors would presumably be even smaller if finer spatial discretizations were used for the numerical model grids.

H.5.2 Verification Test Problem 2

The second verification test problem was designed to test the ability of the PORFLOW and S301 codes to simulate two-dimensional solute transport in a saturated, homogeneous porous medium. Numerical solutions were obtained using PORFLOW and S301 with different grid Peclet numbers to test the accuracy and stability of the different transport schemes.

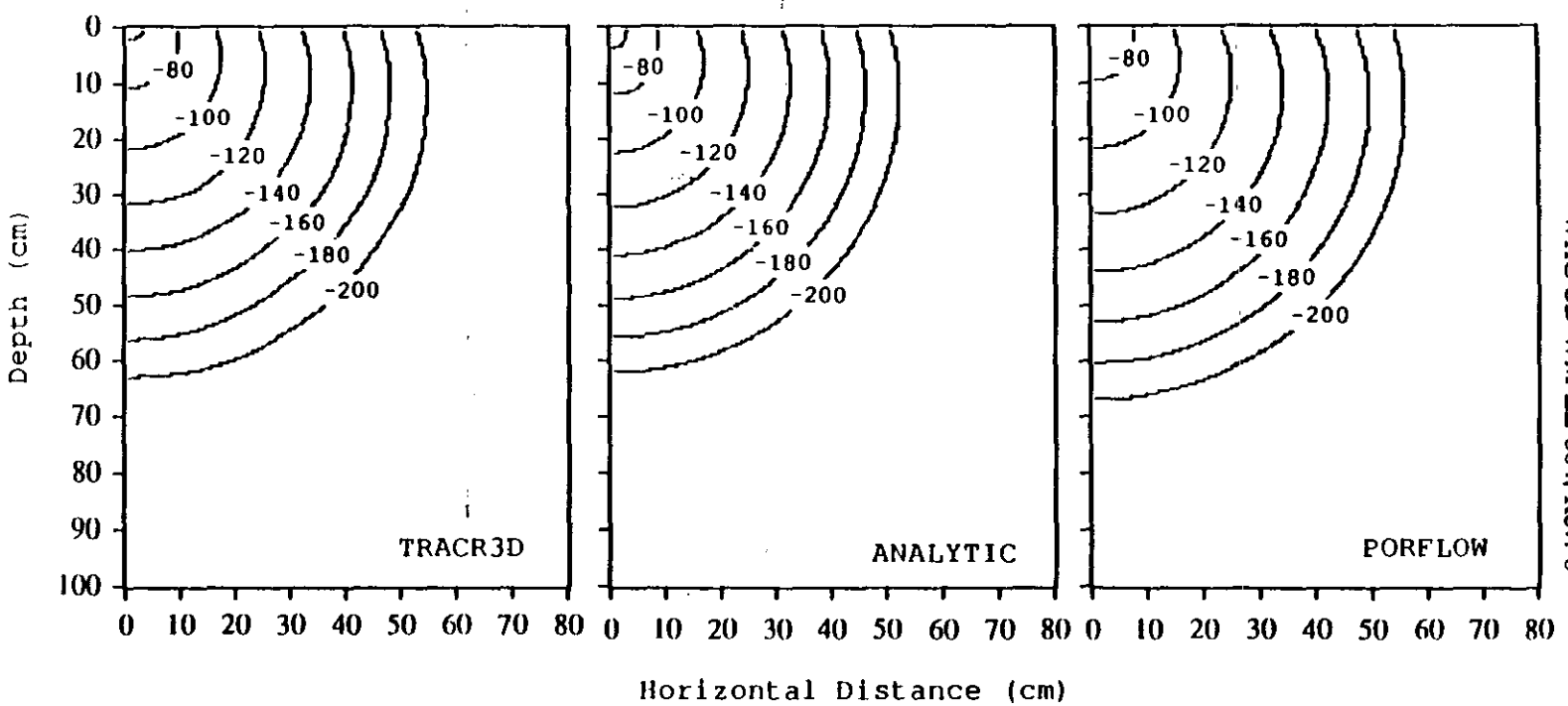

Figure H.2. Pressure Head at t = 72 Minutes for Verification Test Problem 1

For a one-dimensional system, the grid Peclet number, Pe, is defined as:

$$Pe = V\ dx/D \tag{15}$$

where V = Darcy velocity (L/T)

dx = grid block size (L)

D = dispersion coefficient (L^2/T).

The grid Peclet number is a measure of the relative strengths of diffusion and advection, with a Peclet number of 0 corresponding to a pure diffusion problem. The grid Peclet number can be used along with the Courant number to identify potential inaccuracies in numerical solutions to the transport equation. The Courant number, Cn, is defined as:

$$Cn = V\ dt/dx \tag{16}$$

where dt is the time step size, and all other symbols have been previously defined. "Rules-of-thumb," that Pe ≤2, and Cn ≤1, are frequently followed to ensure the accuracy and stability of numerical solutions to the convective-dispersive mass transport equation for many standard finite difference approximations. Maintaining Cn at a value ≤1 prevents solute particles from traveling more than one grid block per time step.

The spatial and temporal discretizations required to satisfy the Pe and Cn conditions are not always practical for large problem domains. If the grid Peclet or Courant numbers violate the above criteria, then the process of differencing the advective terms in the transport equation may introduce a diffusive error effect, which behaves as though the fluid possesses an artificial diffusivity of magnitude ε_a (Trent 1975). This diffusive error effect can result in shorter-than-actual arrival times and lower predicted peak concentrations. The magnitude of this error (a.k.a. numerical dispersion) can be approximated by:

Upwind:

$$\varepsilon_a = 1/2\ V\ dx\ (1-Cn) \tag{17}$$

Central-Space:

$$\varepsilon_a = 1/2\ V^2\ dt \tag{18}$$

for upwind weighting and central-space differencing schemes (Trent 1975). Note that for the upwind differencing scheme, the diffusive error effect goes to 0 for Cn = 1. However, this situation is realistically obtainable only for one-dimensional flow (Trent 1975). Failure to satisfy the Pe number criteria also results in a diffusive error effect.

Note, also, that upwind differencing suffers from considerably more numerical dispersion for small values of the Courant number, which suggests it should be replaced by central-space differencing for small values of Cn (Trent 1975). However, the central-space differencing scheme may become unstable if the grid Pe number exceeds a critical value of 2 (Patankar 1980). The PORFLOW code uses a hybrid scheme to combat this difficulty. This scheme uses central-space differencing when the local grid Pe number is <2, and upwind weighting when the Pe number >2 (Runchal and Sagar 1992). However, no checks are made within PORFLOW to ensure that the Courant condition is satisfied. Therefore, it is the user's responsibility to ensure this condition is satisfied.

The effective artificial dispersivity, α_a, that can be generated by standard finite difference approximations to the convective-dispersive mass transport equation can be calculated by:

$$\alpha_a = \varepsilon_a / V \tag{19}$$

The analytical solution domain that was selected to test the transport algorithms consists of a two-dimensional area with a line source of finite length at the inlet boundary. The edges of the inlet boundary were assumed to be an infinite distance away from the line source. The outlet boundary was assumed to be located an infinite distance from, and perpendicular to the inlet boundary. The analytical and numerical solution model domains for this problem are depicted in Figure H.3.

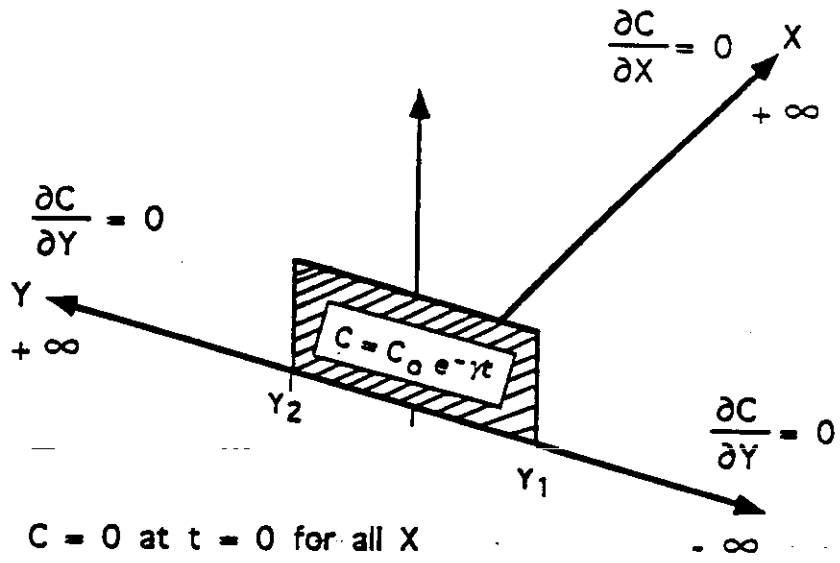

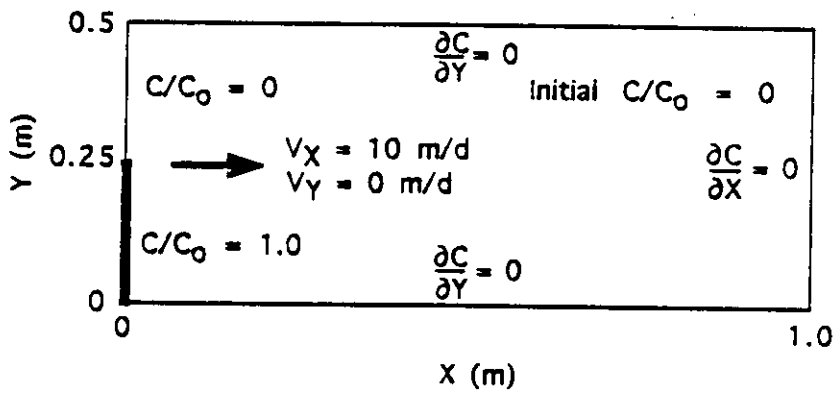

Figure H.3. Analytical and Numerical Solution Problem Domains and Boundary and Initial Conditions for Verification Test Problem 2

The analytical solution is given by Cleary and Ungs (1978) in Equation 20,

$$C(X,Y,t) = \frac{C_o X}{4\sqrt{\pi D_x}} \exp\left\{\frac{V_x X}{2D_x} - \gamma t\right\}$$

$$\cdot \int_{\tau=0}^{t} \frac{\exp\left\{-\left(K - \gamma + \frac{V_x^2}{4D_x}\right)\tau - \frac{X^2}{4D_x\tau}\right\}}{\tau^{3/2}} \tag{20}$$

$$\cdot \left[-\operatorname{erfc}\left\{\frac{(Y_2 - Y)}{2\sqrt{D_y\tau}} + \frac{V_y}{2}\sqrt{\frac{\tau}{D_y}}\right\}\right.$$

$$\left. + \operatorname{erfc}\left\{\frac{(Y_1 - Y)}{2\sqrt{D_y\tau}} + \frac{V_y}{2}\sqrt{\frac{\tau}{D_y}}\right\}\right] d\tau$$

where all symbols have been defined previously. The integral in Equation 20 was evaluated numerically using the IMSL subroutine DQDAGS (IMSL 1987).

The transport verification problem described above was simulated for several grid Peclet numbers to test the accuracy and stability of the numerical schemes used by the PORFLOW and S301 codes. A 1-m-long by 0.5-m-wide model domain was discretized using uniform 0.025-m node spacing in both the x- and y-directions. This discretization resulted in 40 nodes in the x-direction and 20 nodes in the y-direction, totaling 800 nodes in the active computational domains. A line source was specified along the left boundary of the model domains, extending from y = 0 m to y = 0.25 m. A dimensionless concentration of 1.0 was specified for the source strength. A constant Darcy velocity of 10 m/d was specified for the longitudinal or x-direction, with a constant Darcy velocity of 0 m/d in the transverse or y-direction. The numerical model domain and boundary and initial conditions for this problem are shown in Figure H.3.

The computational grids and velocities were held constant for all simulation cases. The time steps were allowed to vary from a minimum of 1.25E-3 days to a maximum of approximately 2.5E-3 to satisfy the Cn condition. The S301 code automatically checked the Cn condition and adjusted the time steps as needed to satisfy the condition Cn ≤ 1.

The diffusion coefficients were varied to generate grid Peclet numbers of 2.222, 80, and 2222. The grid Peclet number 2.222 resulted in a diffusion dominated transport problem. The grid Peclet numbers 80 and 2222 resulted in advection dominated problems. Figure H.4 shows the results from the analytical solution and the numerical solutions obtained using PORFLOW and S301, for t = 0.08 days, with a grid Peclet number of 2.222. The relative concentration contours for all three solutions are quite similar.

The results from the analytical and numerical solutions for Peclet numbers 80 and 2222 are shown in Figures H.5 and H.6, respectively. The numerical solutions for the high Peclet number cases are not as close to the analytical solution as the results for the diffusion dominated case. However, the results obtained using the particle tracking feature in S301 (S301-P) are much closer to the analytical solution than the results obtained using the fully Eulerian methods.

The RRMS errors that were calculated for the PORFLOW and S301 solutions for the 3 Peclet numbers are shown in Table H.1 for time = 0.08 days. No boundary nodes, and only concentrations ≥0.001 and ≤0.999 were used in the RRMS calculations. A lower limit was imposed on the concentrations used in the RRMS calculations to avoid comparing very small numbers, which can result in large RRMS errors. RRMS error values computed for other times were similar to the values for t = 0.08 days, with no obvious increases or decreases as a function of time.

The contour plots of relative concentration for this problem indicate the numerical solutions matched the analytical solution fairly well for the case with a grid Peclet number of 2.222. However, the other cases with larger grid Peclet numbers demonstrate the effects of excessive numerical dispersion.

The S301 code required approximately 7 times more computational effort (CPU time) for this 800-node verification problem when the particle tracking option was invoked (S301-P), relative to the solution obtained using only the modified method of characteristics without particle tracking (S301). The run times required for the PORFLOW and S301 solutions, without particle tracking, were comparable. As shown by the RRMS values and contour plots, the solutions obtained using the particle tracking feature in S301 were more accurate. However, the particle tracking feature was found to be much more computationally expensive and impractical to use for the larger performance assessment simulations.

The inability to control numerical dispersion is inherent in many numerical transport codes. In theory, the grid Peclet and Courant numbers can be reduced to eliminate or reduce inaccuracies in solutions of the transport equation by decreasing the node spacing and reducing the size of the time steps. However, in practice, grid refinements and time steps that are small enough to eliminate numerical dispersion using standard finite difference or finite element solution methods often result in excessive simulation time that is impractical for simulating large-scale, transient unsaturated flow and transport problems. The excessive CPU time needed by the S301 code with particle tracking for problems the size of those required for the performance assessment was the primary motivation for using the PORFLOW code instead of TRACR3D and S301.

Although contaminant arrival curves and mass fluxes as a function of time were not compared for these verification problems, such comparisons were made previously by Magnusen, Baca, and Sondrup (1990). These comparisons showed good agreement between the results generated by PORFLOW and analytical or quasi-analytical solutions for two- and three-dimensional flow and transport problems.

H.5.3 Issues Regarding Internodal Conductance Averaging

In general, the results generated by PORFLOW and TRACR3D have compared favorably with each other and with analytical solutions for simple two-dimensional, unsaturated flow and transport problems with homogeneous porous media when the grid Peclet and Courant conditions were satisfied. However, the results generated by PORFLOW and TRACR3D have been quite different when the simulated problems involved heterogeneous media with highly contrasting material properties (Magnusen, Baca, and Sondrup 1990; Thomas 1991). These differences have been attributed primarily to the different methods used to calculate internodal hydraulic conductivities and velocity components.

TRACR3D computes internodal conductances using the product of the harmonic mean values of intrinsic permeabilities and upwind (or upstream) weighted relative permeabilities. PORFLOW computes internodal conductances using simple arithmetic, geometric, or harmonic averaging of the hydraulic conductivities in adjacent grid blocks.

Under fully water-saturated conditions, the harmonic mean is physically correct and is typically used for saturated flow modeling. However, for unsaturated conditions, hydraulic conductivity is a non-linear function of capillary pressure or water content, and there is no consensus regarding a general finite difference internodal conductivity averaging scheme that is practical and accurate under all conditions.

Table H.1. RRMS Values for Verification Problem 2

	RRMS[a]		
Peclet Number	PORFLOW	S301	S301-P
2.222	0.2750	0.1779	0.1897
80.0	10.6131	19.4604	1.4913
2222.0	111.2601	186.4761	0.8389

(a) RRMS values calculated for $0.001 \leq C/C_o \leq 0.999$.

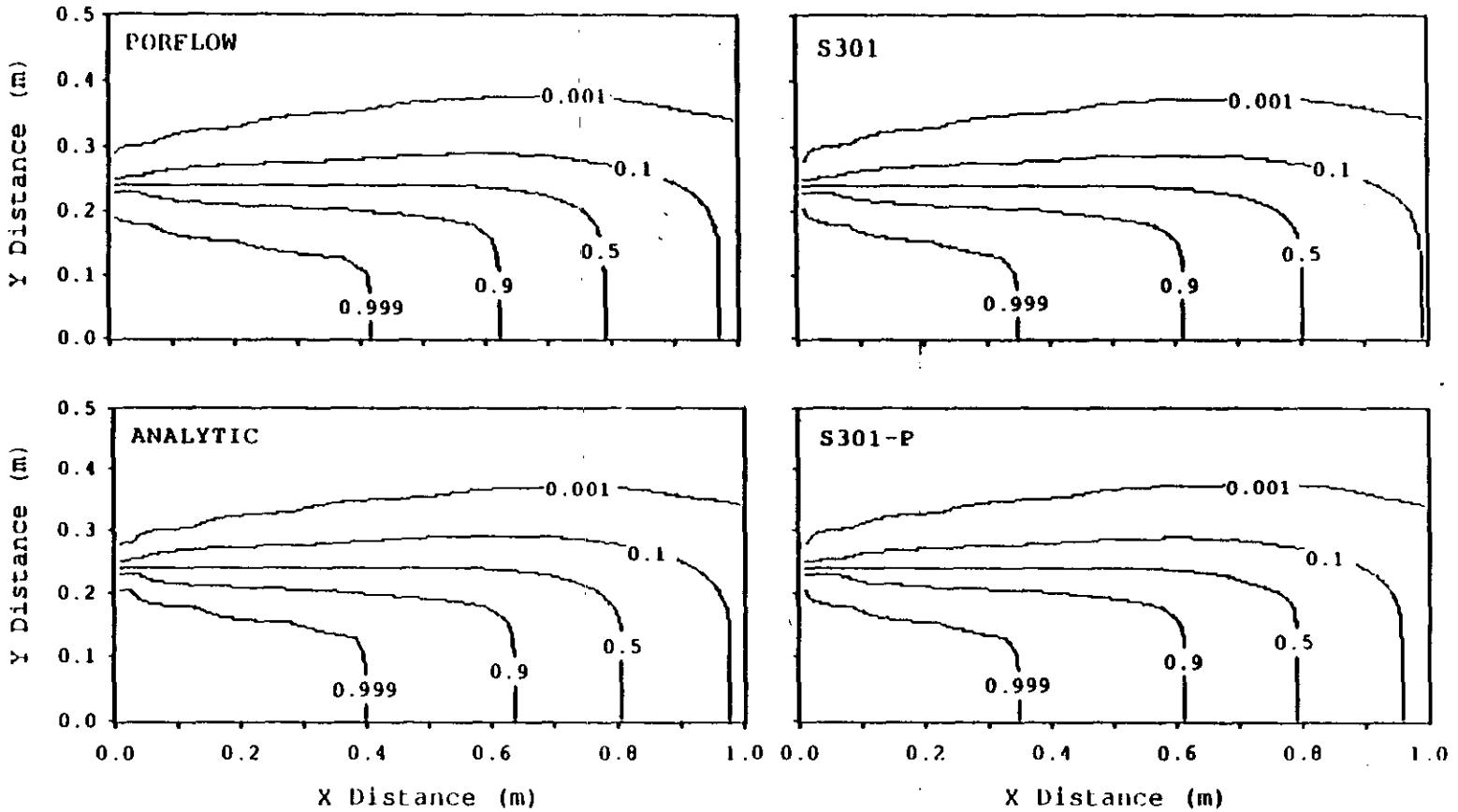

Figure H.4. Relative Concentrations at t = 0.08 Hours for Verification Test Problem 2 with Grid Peclet Number = 2.222

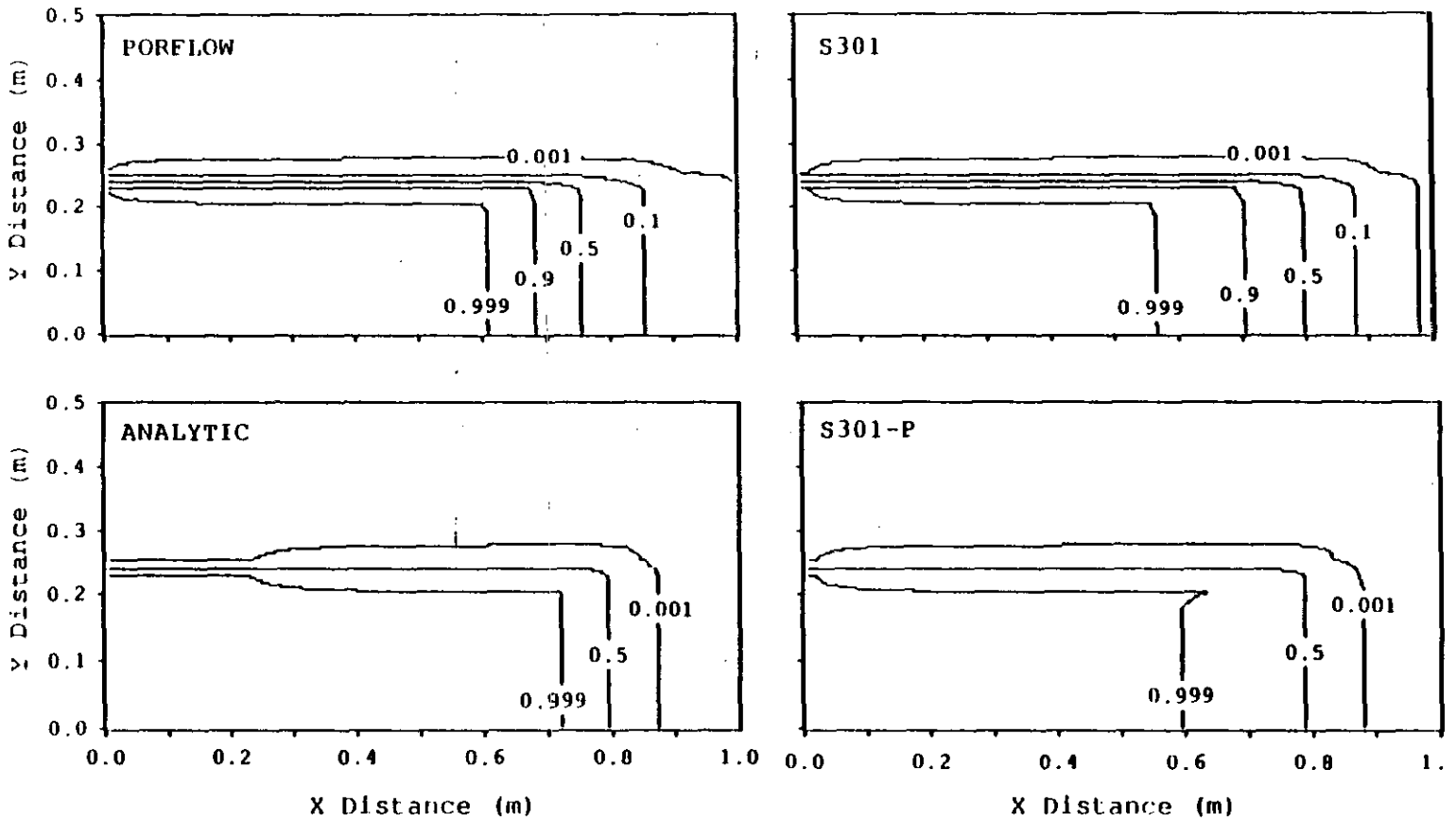

Figure H.5. Relative Concentrations at t = 0.08 Hours for Verification Test Problem 2 with Grid Peclet Number = 80.0

9413222.1524

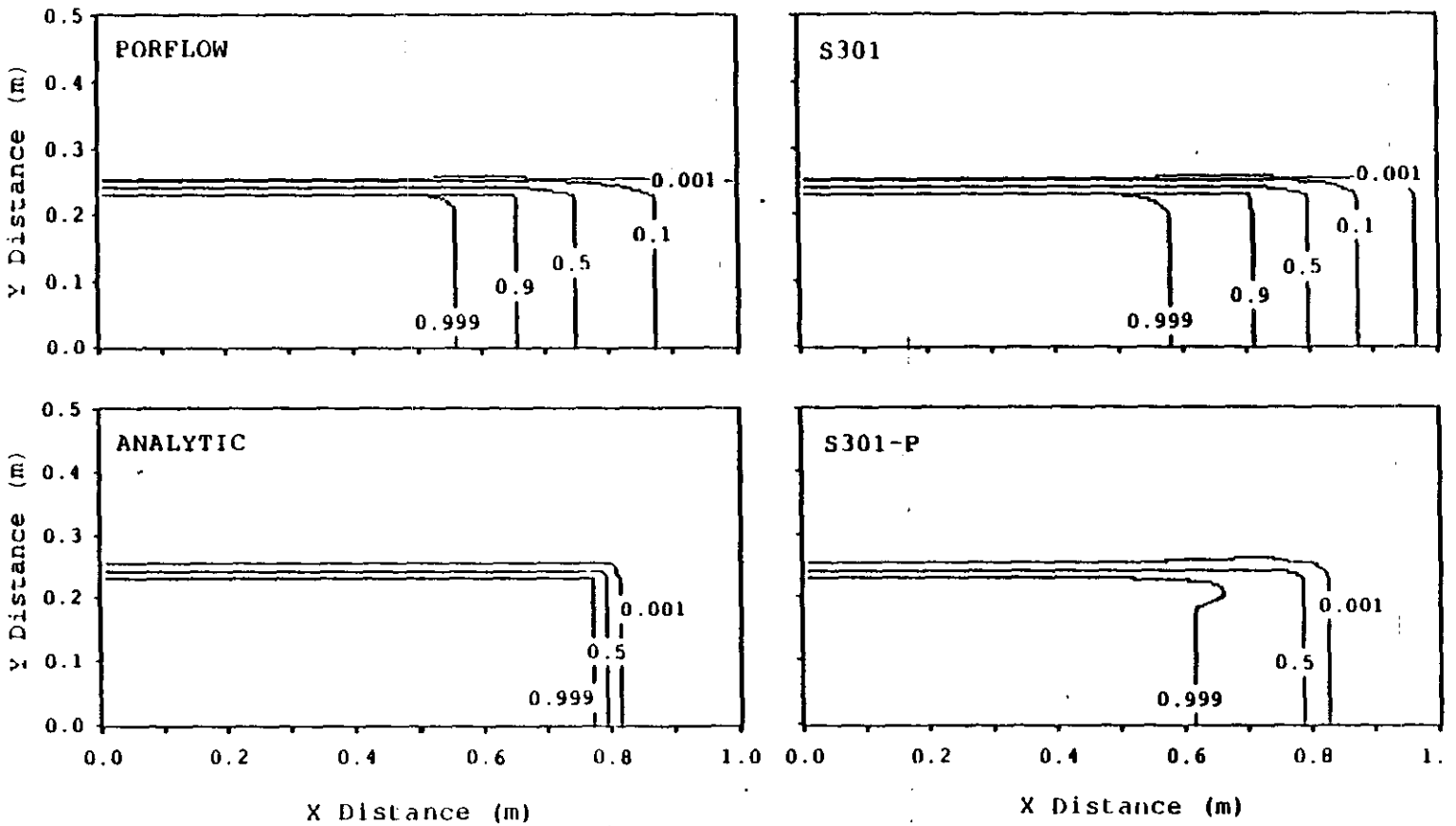

Figure H.6. Relative Concentrations at t = 0.08 Hours for Verification Test Problem 2 with Grid Peclet Number = 2222.22

Numerous researchers have investigated the effects of various internodal conductance averaging schemes. Brutsaert (1971) suggested that full upstream weighting of hydraulic conductivities is the most appropriate averaging scheme for problems in which saturations vary rapidly with time (e.g., infiltration fronts, cone of depression near a well bore). Havercamp and Vauclin (1979) found the geometric mean to be the most preferable weighting option in terms of flexibility, accuracy, and feasibility for simulating one-dimensional transient water flow in partially saturated soil. Schnabel and Ritchie (1984) conducted one-dimensional simulations of infiltration in partially saturated soil and suggested that when possible the hydraulic conductivity-capillary pressure function should be integrated to determine internodal conductances. The geometric mean was suggested as a second choice for the soils in their study. The harmonic mean was found to yield unrealistic results for all unsaturated flow simulations, particularly when simulating infiltration into soils with very dry initial conditions.

Schnabel and Ritchie (1984) determined that the time required to attain steady-state decreased in order from harmonic to geometric to arithmetic to upstream weighted conductance, while the calculated flux increased in the same order, from the harmonic through the upstream weighted conductance. Thus, the rate at which a simulated front moves or a pulse dissipates should occur in the inverse order, with the rate being greatest for the upstream weighted and least for the harmonic mean conductance.

Zaidel and Russo (1992) and Warrick (1991) showed that an averaging scheme based on the Kirchoff integral transformation (as described previously for verification test problem 1) is the most accurate internodal hydraulic conductivity averaging scheme for homogeneous media. This transformation is based on the integration of the hydraulic conductivity-capillary pressure function and linearizes the capillary component of the Darcy velocity giving an exact value of fluid flux between grid blocks. However, when the constitutive relations between capillary pressure, saturation, and relative permeability are spatially dependent (i.e., in heterogeneous porous media systems) or are not analytically integrable, the use of the Kirchoff transformation in a numerical procedure requires excessive computational effort (Zaidel and Russo 1992). Therefore, the procedure is generally not considered to be practical.

Zaidel and Russo (1992) stated that ". . . we may conclude that there is no universal weighting scheme capable of following successfully sharp fronts for a relatively coarse grid. Of course, the errors introduced by all the weighting schemes diminish if Δx is reduced, but this may require a huge computational effort, especially when simulation of multidimensional flow in relatively large domains is concerned." Zaidel and Russo (1992) suggested that local adaptive grid refinement techniques may be effective in reducing the errors associated with internodal hydraulic conductivity averaging for unsaturated flow modeling.

Judging from these references, the original permeability averaging scheme employed in the TRACR3D code appears to be well suited for simulating problems with sharp fronts in which saturations vary rapidly with time. The scheme used in TRACR3D also reduces to simple harmonic averaging when the porous medium is fully water saturated, which is physically correct under such conditions. This scheme also facilitates the numerical implementation of zero-flux default boundary conditions. However,

as will be shown, the original internodal conductance averaging scheme that is used in TRACR3D can generate results quite different from those generated using simple arithmetic or harmonic averaging.

Modifications to TRACR3D were necessary to obtain results comparable with PORFLOW for simulations with heterogeneous porous media. Options were added for using harmonic, geometric, arithmetic, and weighted conductance averaging schemes. PORFLOW was not modified.

H.5.4 Benchmark Test Problem 1

A small-scale benchmark problem was developed based on literature pertaining to the effects of various internodal conductance averaging schemes. The problem was designed to test whether the averaging options added to TRACR3D were implemented correctly and to determine if the different internodal conductance averaging schemes were the primary cause for the differences observed in larger scale benchmark simulation results from TRACR3D and PORFLOW. Benchmark problem 1 simulated two-dimensional water flow in a vertical cross section consisting of a sloping clay layer embedded within coarse sandy material. This problem was analogous to water flow through and around the clay cap that is part of the final cover required by the Resource and Conservation Recovery Act (RCRA) for hazardous waste landfills in Title 40 of the *Code of Federal Regulations* (40 CFR).

A schematic of the modeled two-dimensional cross section for benchmark problem 1 is shown in Figure H.7. The modeled domain represented a 36-m-wide by 6-m-deep cross section, with uniform 0.4-m node spacing in the horizontal direction and uniform 0.3-m node spacing in the vertical direction. This spatial discretization resulted in 90 nodes in the horizontal direction and 20 nodes in the vertical direction, for a total of 1800 nodes in the active computational domain.

A sloping, 28-m-wide by 0.6-m-thick clay cap was embedded within the modeled domain. Because of constraints imposed by the cartesian grid system, the 7.5% slope of the clay cap was represented using a series of 7 "stair steps" extending downward from the left edge of the modeled domain. This problem was similar in dimension to the upper part of the modeled domain used for the performance assessment simulations. The thickness of the clay cap was represented by 2 nodes for this benchmark problem.

The U.S. Environmental Protection Agency's (EPA) technical guidance document for final covers on hazardous waste landfills and surface impoundments (EPA/530-SW-89-047) requires a minimum thickness of 0.6 m for the low-permeability layer in the final cover (i.e., the clay cap), with a slope ≥3%. The slope and thickness of the clay cap were approximately 10% and 0.6 m, respectively, as discretized in the base case for the revised performance assessment. A minimum of 3 nodes was used to represent the thickness of the clay cap in the finite difference grid for the performance assessment simulations.

Two internal flux planes were specified for benchmark problem 1. The instantaneous and cumulative fluxes crossing these planes were calculated as a function of time. To quantify the flux of water passing through the clay cap, a horizontal flux plane was specified, extending from the left edge of the model domain to the right edge of the clay cap at a depth of 3.6 m below the surface. To quantify the flux of

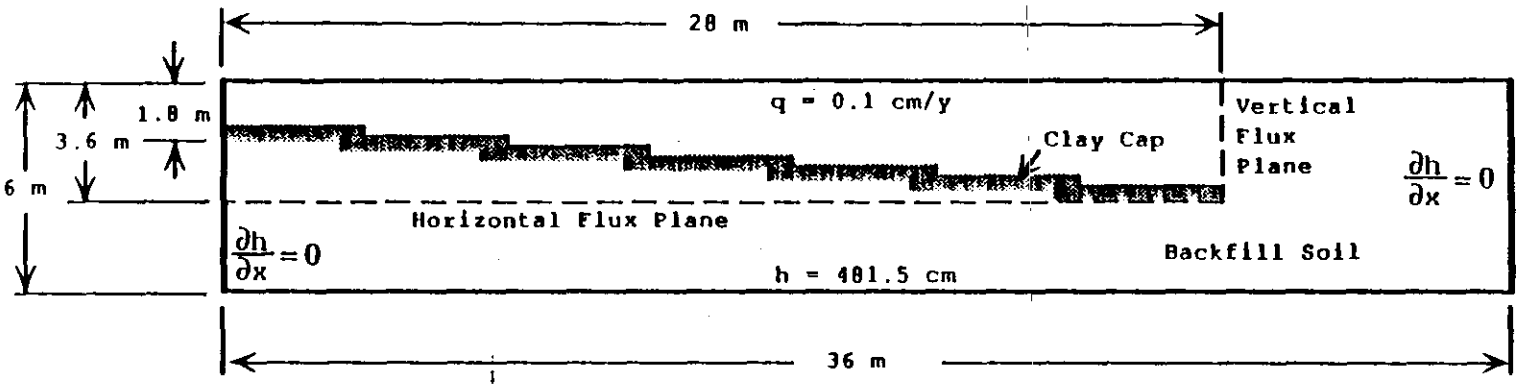

Figure H.7. Schematic View of Modeled Two-Dimensional Cross Section and Boundary Conditions for Benchmark Problem 1

water diverted laterally around the clay cap, a vertical flux plane was specified, extending from the surface to a depth of 3.6 m at the right edge of the clay cap. These flux planes are also depicted in Figure H.7.

A uniform flux, corresponding to a recharge rate of 0.1 cm/yr, was specified for the upper boundary condition of the model domain. The lower boundary was held at a pressure head of approximately -481.5 cm, which corresponded to a volumetric water content of 0.04058 for the backfill soil. This water content and pressure head were consistent with a 0.1 cm/yr recharge rate and a unit hydraulic gradient. A unit hydraulic gradient boundary condition would have been more appropriate for this problem, but this option was not available in the PORFLOW code. Lateral boundaries were specified as zero-flux or no-flow boundaries. The initial conditions were specified as uniform liquid saturations of 0.265958 and 0.9241 for the backfill soil and clay cap, respectively. The water retention and saturated hydraulic conductivity parameters that represented the backfill soil and clay cap for this benchmark problem are listed in Table H.2.

Benchmark problem 1 was simulated with PORFLOW by using arithmetic and harmonic averaging of the internodal hydraulic conductivities for a 500-year simulation period. This problem was also simulated with TRACR3D by using arithmetic, geometric, and harmonic averaging, in addition to the code's original averaging scheme, which uses the product of the harmonic mean of intrinsic permeabilities and fully upstream weighted relative permeabilities.

Table H.2. Water Retention and Hydraulic Conductivity Parameters for Benchmark Problem 1

Material Type	Ks(cm/s)	θ_s	θ_r	$\alpha(cm^{-1})$	n
Backfill Soil	3.0×10^{-2}	0.376	0.018	0.086	1.742
RCRA Clay Cap	9.4×10^{-9}	0.448	0.000	5.4×10^{-4}	1.324

In Figure H.8, instantaneous fluxes passing through the horizontal and vertical flux planes for three different internodal conductance averaging schemes are plotted as a function of time. The geometric mean option is not shown because this option was not used in the PORFLOW simulations, and the results obtained using this option with TRACR3D were intermediate between the results obtained using arithmetic and harmonic averaging.

The original averaging scheme used by TRACR3D resulted in a horizontal-to-vertical flux ratio of approximately 100:1 for this problem. In other words, when the original TRACR3D internodal hydraulic conductivity averaging scheme was used, the flux of water that was laterally diverted around the clay cap was approximately 100 times greater than the flux of water allowed to pass through the clay cap. When arithmetic or harmonic averaging was used, this horizontal-to-vertical flux ratio was reversed.

Steady-state flow fields were obtained within 75 to 100 years of simulation time with both PORFLOW and TRACR3D when arithmetic or harmonic averaging was used. However, a steady-state flow field had still not been achieved after 500 years of simulation time using the original TRACR3D averaging scheme.

Efforts were made to ensure consistency between the parameters that were input to PORFLOW and TRACR3D for this benchmark problem. However, the codes were allowed to adjust time step sizes as needed. Therefore, the differences in the instantaneous fluxes calculated by the codes using the arithmetic or harmonic averaging schemes may be due in part to differences in time step sizes. Both codes require different units for initial and boundary conditions, fluid properties, etc. Therefore, some of the differences between the simulation results might also be attributed to the number of significant figures that were carried through the unit conversions. However, the differences between the results generated by the codes using the same averaging schemes were relatively small and probably negligible compared to the differences that resulted from arithmetic or harmonic averaging versus the original TRACR3D averaging scheme.

Volumetric water content values generated by the different averaging schemes were also compared. The absolute value 1.369×10^{-4} at t = 500 years for the maximum difference between the volumetric water content values generated by TRACR3D and PORFLOW using the arithmetic mean of internodal hydraulic conductivities. In contrast, the absolute value was 5.646×10^{-2} at t = 500 years for the maximum difference between volumetric water content values generated using TRACR3D with its original averaging scheme and PORFLOW with arithmetic averaging.

Volumetric water content values generated by TRACR3D with its original and arithmetic averaging schemes and PORFLOW with arithmetic averaging are shown in cross section for the modeled domain in Figure H.9. Only the 0.05 and 0.4 cm^3/cm^3 contours are plotted to provide clarity for these comparisons. For the arithmetic averaging case, only the outline of the clay cap is evident from the results generated by both PORFLOW and TRACR3D. However, for the case using the original TRACR3D averaging scheme, a distinct "spill-over" lobe is shown by the 0.05 contour, which illustrates the lateral diversion of water over the clay cap.

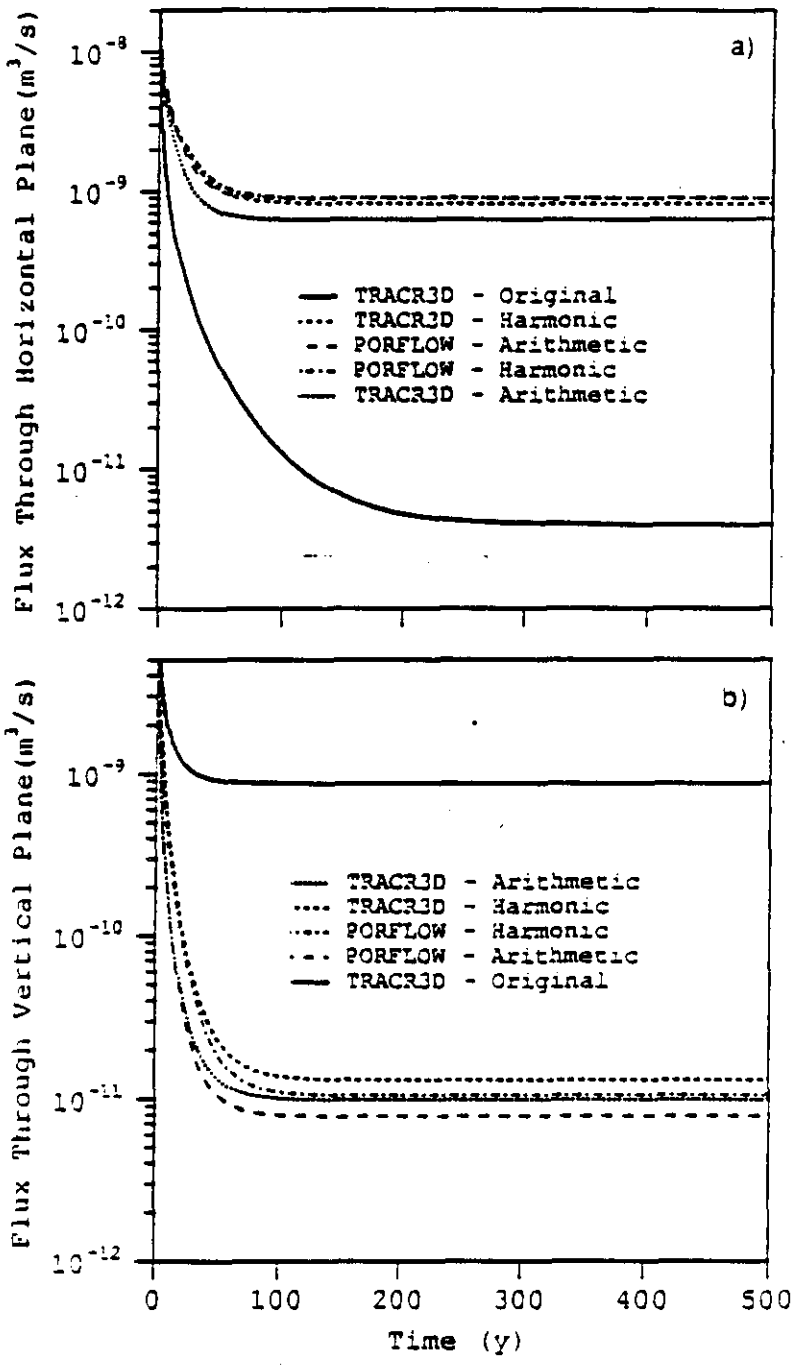

Figure H.8. Instantaneous Fluxes Passing Through a) Horizontal and b) Vertical Flux Planes as a Function of Time for 3 Intermodal Hydraulic Conductivity Averaging Schemes for Benchmark Problem 1

9413222.1531

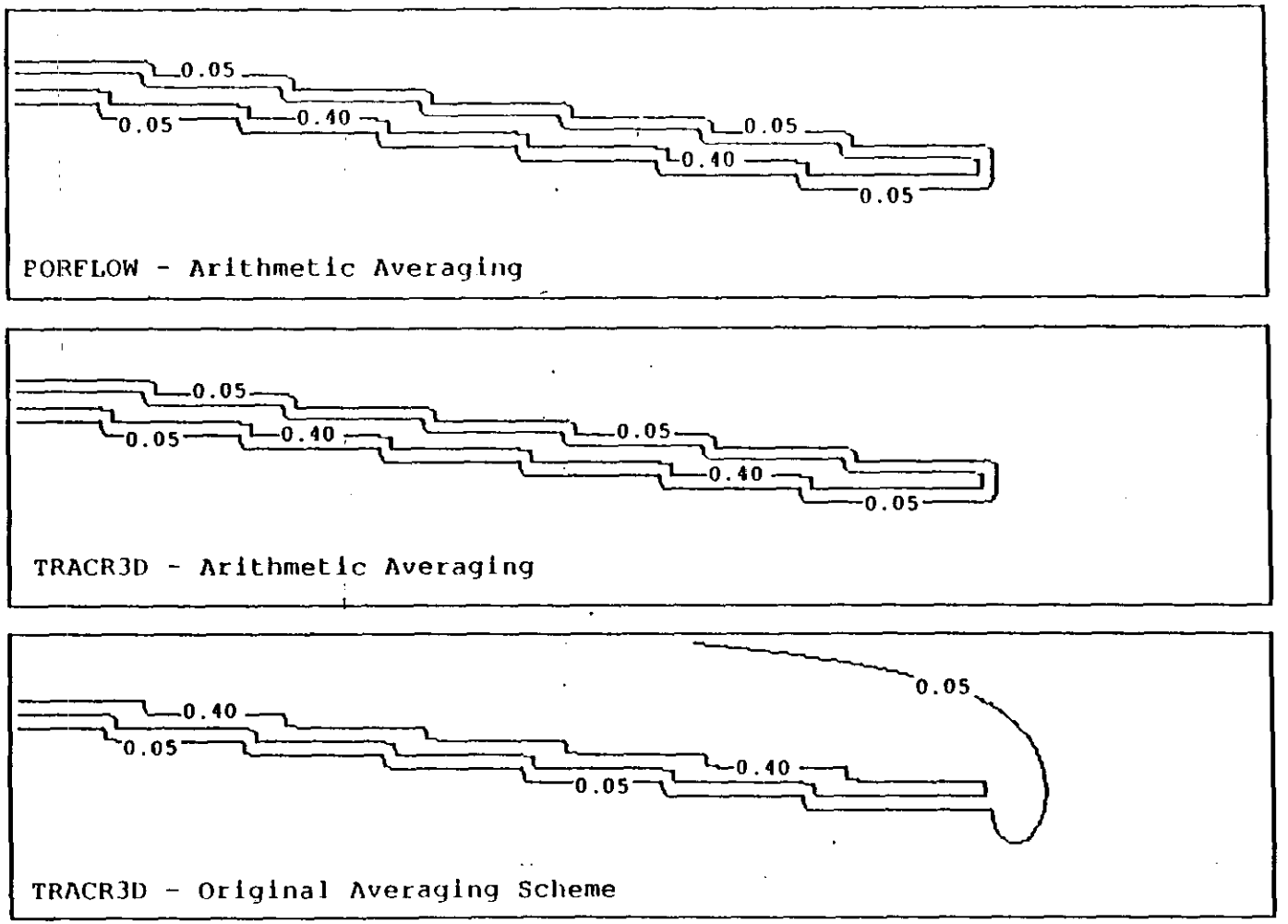

Figure H.9. Volumetric Water Content at t = 500 Years for Benchmark Problem 1

The results of this benchmark problem confirmed the hypothesis that differences in the results generated by TRACR3D and PORFLOW for simulations with heterogeneous material properties can be attributed primarily to different internodal conductance averaging schemes. With respect to transport simulations for the performance assessment, higher water fluxes passing directly through the clay cap, obtained using arithmetic averaging, translated into a potential for greater simulated releases of contaminants from the underlying grout waste form.

Results of a literature review indicated that none of the commonly used averaging schemes for unsaturated flow modeling are necessarily accurate with relatively coarse grids for all conditions. The differences between results generated using the different averaging schemes become less pronounced with finer discretization, although at additional computational expense. To obtain comparable simulation results with the TRACR3D and PORFLOW codes, and to minimize computer CPU time, the arithmetic averaging option was adopted for use in the performance assessment simulations.

9413222.1532

H.5.5 Benchmark Test Problem 2

Benchmark problem 2 represented a full-sized performance assessment flow and transport problem. The modeled domain represented a 34.9-m-wide by 85.35-m-high cross section, extending from the assumed postclosure position of the water table to the ground surface at the Grout Treatment Facility. This cross section is depicted in Figure H.10.

The finite difference grid used by TRACR3D for benchmark problem 2 is shown in Figure H.11. This grid consists of 77 nodes in the horizontal direction and 162 nodes in the vertical direction, for a total of 12,474 nodes in the active computational domain. As noted previously, the TRACR3D and PORFLOW codes use block-centered and node-centered discretization schemes, respectively. Therefore, the finite difference grid used for the PORFLOW simulations was slightly different than the grid shown in Figure H.11. However, both grids were designed with same-size "hot grout" areas (Figure H.10) so that both codes would start with identical initial volumes of contaminant. Minimum and maximum node spacings of approximately 0.1 and 1.0 m were used for both grids, and a minimum of 3 nodes was used to represent the thickness of any given material. The finite difference grids were also designed to prevent the distance between adjacent nodes from increasing or decreasing by more than a factor of approximately 2.

A flux of water corresponding to a recharge rate of 0.1 cm/yr was specified for the upper surface of the modeled domain. A fixed concentration equal to 0.0 was also specified for the upper boundary. The lower boundary was held at a pressure head equal to 0, corresponding to a water table at atmospheric pressure. A zero-concentration-gradient boundary condition was also specified for the lower boundary. The side boundaries were specified as no-flow and zero-concentration-gradient boundaries, based on symmetry considerations.

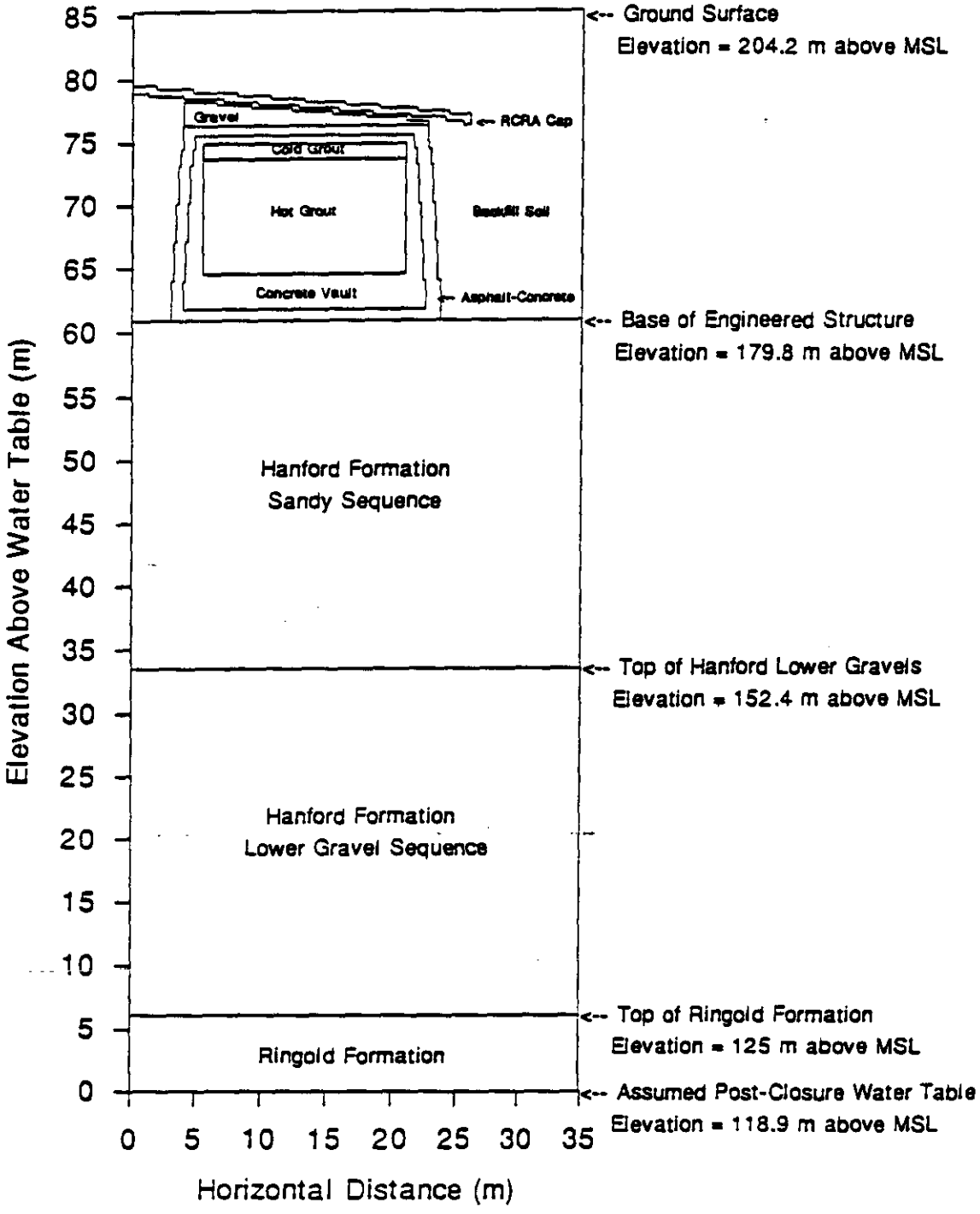

Figure H.10. Modeled Cross Section for Benchmark Problem 2

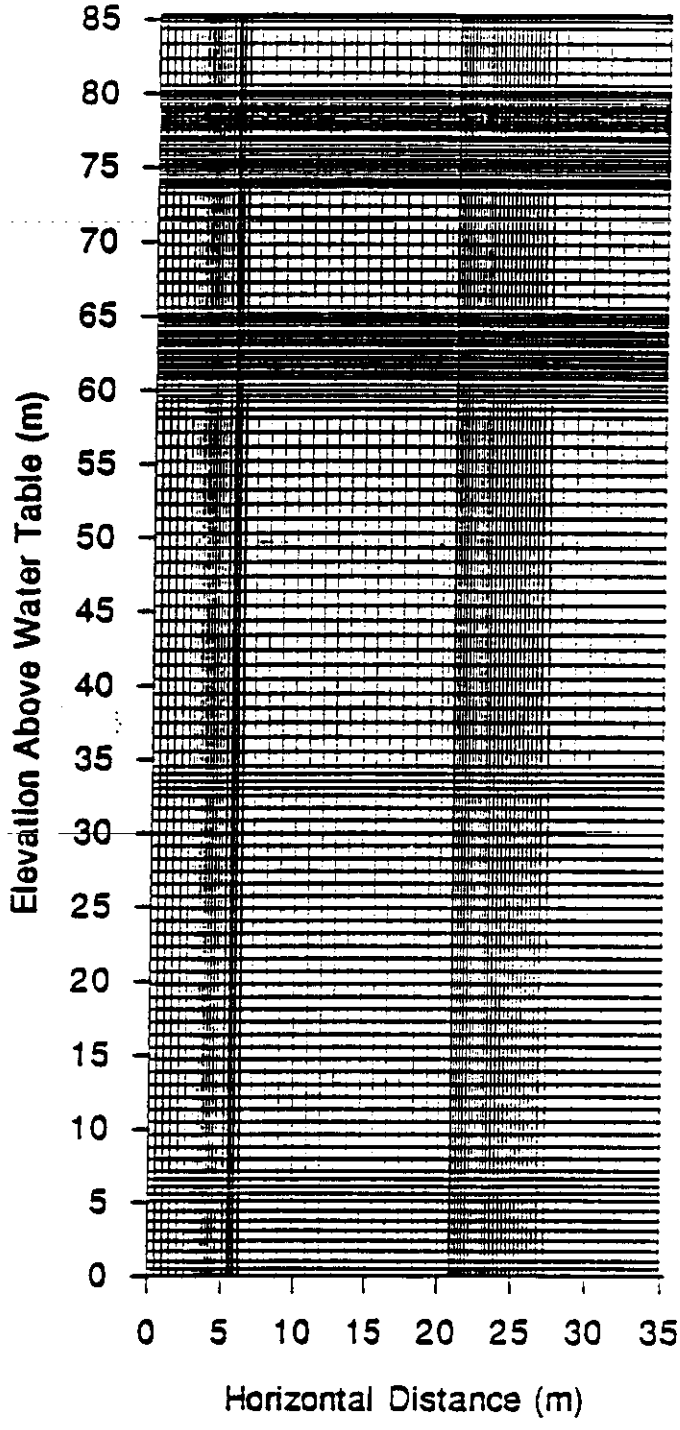

Figure H.11. Finite Difference Grid for Benchmark Problem 2

An initial pressure head of approximately -74.9 cm was specified for all the engineered materials and backfill soil. This pressure head corresponded to an assumed volumetric water content of 10% for the backfill soil. The initial pressure heads in the soils underlying the engineered materials and backfill soil were assigned values corresponding to a recharge flux of 0.1 cm/yr under a unit hydraulic gradient.

The initial normalized concentrations for the transport simulations were specified as 0 everywhere, except for the domain region labeled "hot grout" in Figure H.10. An initial normalized concentration of 1.0 was specified for this region.

The material properties used for benchmark problem 2 were similar to those used for the performance assessment simulations, with the exception of the gravel overlying the grout vault, and other modifications to approximate asphalt cracking, and degradation. The material properties assigned to the region labeled "gravel" in Figure H.10 were assigned the values of the backfill soil properties. The saturated hydraulic conductivities, van Genuchten model water retention parameters, and bulk densities for these materials are listed in Table H.3. The hydraulic and transport properties assigned to cold grout and hot grout are identical.

The change from gravel to backfill soil properties in the region of the model domain overlying the grout vault was necessary because the gravel properties create a capillary break, which laterally diverts water over the gravel. This lateral diversion of water creates very high velocities in this region of the domain. The S301 code automatically checks Courant numbers. This code also forces the time

Table H.3. Hydraulic Parameters for Benchmark Problem 2

Material	K_s(cm/s)	θ_s	θ_r	α(cm^{-1})	n	ρ_b(g/cc)
Hanford Formation						
Sandy sequence	1.55×10^{-3}	0.4203	0.0234	0.1943	1.868	1.68
Gravel sequence	2.73×10^{-4}	0.3584	0.0213	0.0290	1.613	1.73
Ringold Formation	2.42×10^{-6}	0.4982	0.0283	0.0176	1.338	1.45
Backfill Soil	3.00×10^{-2}	0.3710	0.0450	0.0683	2.080	1.65
RCRA Clay Cap	1.00×10^{-7}	0.4480	0.0000	5.39×10^{-4}	1.324	1.45
DSSF Grout	1.47×10^{-8}	0.5781	0.0000	1.08×10^{-5}	1.650	1.10
Concrete	3.75×10^{-10}	0.2258	0.0000	7.61×10^{-6}	1.393	1.98
Asphalt[a] 1	1.00×10^{-20}	0.162	0.0000	1.00×10^{-7}	2.000	1.75
Asphalt 2	3.00×10^{-2}	0.202	0.0450	0.0683	2.080	1.38

(a) Asphalt 1 and 2 refer to the hydraulic parameters assigned to the asphalt at $t \leq 90{,}000$ yr and $t > 90{,}000$ yr, respectively.

steps to be small enough to satisfy the Courant condition ($Cn \leq 1$) over the entire modeled domain, ensuring stability of the explicit solution scheme. The high velocities in the gravel overlying the grout vault forced the time steps used by the S301 code to be too small to allow conduct of simulations within a reasonable amount of time. Therefore, for the purposes of these benchmark comparisons, the hydraulic properties in the region of model domain representing gravel were simply changed to the properties of the backfill soil, which allowed for much larger time steps. For the performance assessment simulations, the contaminants are located in the grout itself, below the gravel. Therefore, large Courant or Peclet numbers in the gravel overlying the grout vault were considered to be relatively insignificant.

To simulate contaminant transport, the adsorption behavior of various radioactive species in the different materials was represented using distribution coefficients, R_d, which are defined as:

$$R_d = \frac{\text{amount of radionuclide adsorbed on solid per g solid}}{\text{amount of radionuclide in solution per mL of solution}} \tag{21}$$

The distribution coefficient is related to the retardation factor, R_f, as:

$$R_f = 1 + (\rho_b/e)R_d \tag{22}$$

where ρ_b is the dry bulk density (M/L^3), and e is the porosity. The porosity was assumed equivalent to the saturated water content, θ_s.

The retardation factor represents the ratio of the mean water velocity to the mean contaminant velocity in the porous medium. The porosity or saturated water content was used for calculating retardation factors to conservatively estimate solute mobilities, even though most of the materials in the performance assessment simulations are unsaturated.

Three different cases or "bins" were simulated. These bins represented groupings of radioactive species having similar retardation behavior, without directly accounting for specie half-lives. The parameters for Bin 1A conservatively represented species such as ^{129}I and ^{106}Ru. The parameters for Bins 2A and 2B conservatively represented species such as ^{99}Tc and ^{94}Nb, respectively. Transport parameters for the different material types and bin numbers selected for this benchmark problem are shown in Table H.4.

It was assumed that no contaminants are attenuated in the concrete vault or in the asphalt diffusion barrier. Therefore, the distribution coefficients and retardation factors for all contaminants in these materials were assigned values of $R_d = 0.0$ and $R_f = 1.0$, respectively.

Table H.4. Retardation Factors and Distribution Coefficients for Benchmark Problem 2

Bin	$\theta T D_m$ [(a)]	Grout R_f	Soil R_d	Species
1A	5.781×10^{-7}	1.0	0.0	^{129}I, ^{106}Ru
2A	5.781×10^{-7}	4.8	0.0	^{99}Tc
2B	5.781×10^{-7}	4.8	0.67	^{94}Nb

(a) θ = 0.5781 (volume fraction pore water in grout)
T = 0.04 (tortuosity factor)
D_m = 2.5E-5 cm^2/s (coefficient of molecular diffusion).

Dispersivities were set equal to 0 for all material types in this benchmark problem and in the performance assessment simulations. Effective diffusion coefficients for the different material types were assumed to be a function of volumetric water content, θ, following the empirical relationship of Kemper and van Schaik (1966):

$$D_e(\theta) = D_m \cdot a \cdot \exp(b\theta) \tag{23}$$

where a and b are empirical constants.

Data from Olsen, Kemper, and van Schaik (1965) and Porter et al. (1960) for soils using NaCL as the diffusing species fit the exponential equation fairly well, with "b" = 10 and "a" as a function of soil surface area. Olsen and Kemper (1965) cite values of "a" ranging from 0.005 to 0.001 for soils ranging in texture from sandy loam to clay. For this benchmark problem and the performance assessment simulations, the values of "a" and "b" were selected as 0.005 and 10, respectively. The diffusion coefficient parameters used for the different material types are shown in Table H.5. Note that for grout, concrete, and asphalt (prior to 90,000 years), the values of "a" and "b" listed in Table H.5 are 1 and 0, respectively. Hence, the effective diffusion coefficients are modeled as independent of volumetric water content for these materials.

Table H.5. Effective Diffusion Coefficients Used for Benchmark Problem 2 and Performance Assessment Simulations

Material	D_m (cm^2/s)	a	b
Hanford Fm, Sands	2.5×10^{-5}	0.005	10
Hanford Fm, Gravels	2.5×10^{-5}	0.005	10
Ringold Fm	2.5×10^{-5}	0.005	10
Backfill Soil	2.5×10^{-5}	0.005	10
Grout	1.0×10^{-10}	1.000	0
Concrete	5.0×10^{-8}	1.000	0
RCRA Clay Cap	2.5×10^{-5}	0.005	10
Asphalt[a] 1	1.0×10^{-10}	1.000	0
Asphalt 2	2.5×10^{-5}	0.005	10

(a) Asphalt 1 and 2 refer to parameters for $t \leq 90{,}000$ yr, and $t > 90{,}000$ yr, respectively. (See note below regarding time-dependent effective diffusion coefficients.)

9413222.1536

The effective diffusion coefficients representing the asphalt diffusion barrier were modified as a function of time to approximate the expected degradation of the asphalt. The time-dependent, effective diffusion coefficient, D_t, was assumed to change according to the following equation:

$$D_t = D_e/[1-(1-1 \times 10^{-6})\ (t/90000)] \qquad t \leq 90{,}000 \text{ yr}$$
$$D_t = D_e \qquad t > 90{,}000 \text{ yr} \tag{24}$$

where t is time in years and all other parameters have already been defined. The rates of degradation and change to a constant effective diffusion coefficient after 90,000 years were arbitrarily selected for this benchmark problem. Some of the mechanisms expected to contribute to this degradation include oxidation, volatilization, polymerization, and biodegradation. Measurements of biodegradation rates in asphalt were made after this benchmark problem was simulated and are described in the main performance assessment document.

It was also assumed that the concrete vault and asphalt diffusion barrier will eventually develop cracks or stress fractures from seismic events or overburden pressure, for example. The exact sizes and locations of these cracks or fractures are unknown. However, the concrete vault was designed so that primary cracks likely to develop will be located in the corners of the vault.

A simplified representation of cracks in the concrete vault and asphalt-concrete diffusion barrier was developed. A horizontal row of grid blocks in each of the lower corners of the vault was assigned the same flow and transport parameters as the backfill soil to represent hypothetical cracks in the lower corners of the vault and diffusion barrier. Each row extended outward from the "hot grout" through the concrete vault and asphalt diffusion barrier to the backfill soil. A vertical column and horizontal row of grid blocks in each of the upper corners, extending outward from the "cold grout" through the concrete vault and asphalt diffusion barrier, were also assigned the properties of the backfill soil to represent hypothetical cracks in the upper corners of the vault and diffusion barrier. The grid blocks for these cracks were 10 cm wide. The hypothetical cracks and hydraulic properties assigned to them were considered to be conservative. However, the equivalent hydraulic properties of the materials in the vicinity of these cracks are highly uncertain and likely to change with time.

Three different transport cases were simulated to represent the different bins. The time domain for the simulations was extended until the outflow concentrations at the lower boundary of the model domain had reached their peak values. Contour plots of average relative concentrations at the water table are shown in Figures H.12, and H.13 for the Bin 1A simulations at times of 1000 and 10,000 years, respectively. These figures show excellent agreement between the results generated by the PORFLOW and TRACR3D/S301 codes. The effects of the hypothetical cracks are clearly evident and show that the waste inventory is depleted the fastest near the corners of the vault.

Contour plots of relative concentration are shown in Figures H.14 and H.15 for the Bin 2A simulations at times of 1000, and 10,000 years, respectively. Again, the results generated from PORFLOW and TRACR3D/S301 are very similar.

The results generated from the Bin 2B simulations at times of 1000, and 10,000 years are shown in Figures H.16 and H.17, respectively. Considering the complexity of this benchmark problem and the differences in numerical solution techniques, the agreement between the PORFLOW and TRACR3D/S301 results is considered excellent.

Log-transformed grid Peclet numbers generated from the S301 code using the saturation and velocity fields from TRACR3D at a time of 5000 years are shown in Figure H.18 for the upper 25.34 m of the modeled domain. The top half of Figure H.18 shows the approximate range of grid Peclet numbers generated from this simulation. The locations of the hypothetical cracks through the reinforced concrete and asphalt-concrete are evident. In the lower half of Figure H.18, only the grid Peclet numbers >2 are shown (Ln 2 = 0.693).

The finite difference grid for this problem was designed so that the grid Peclet numbers would be <2 over the entire modeled domain, before the cracking effects were considered. The Peclet number maps shown in Figure H.18 suggest the cracks that were embedded within the model domain are inducing high velocities and creating large grid Peclet numbers within the domain area representing the

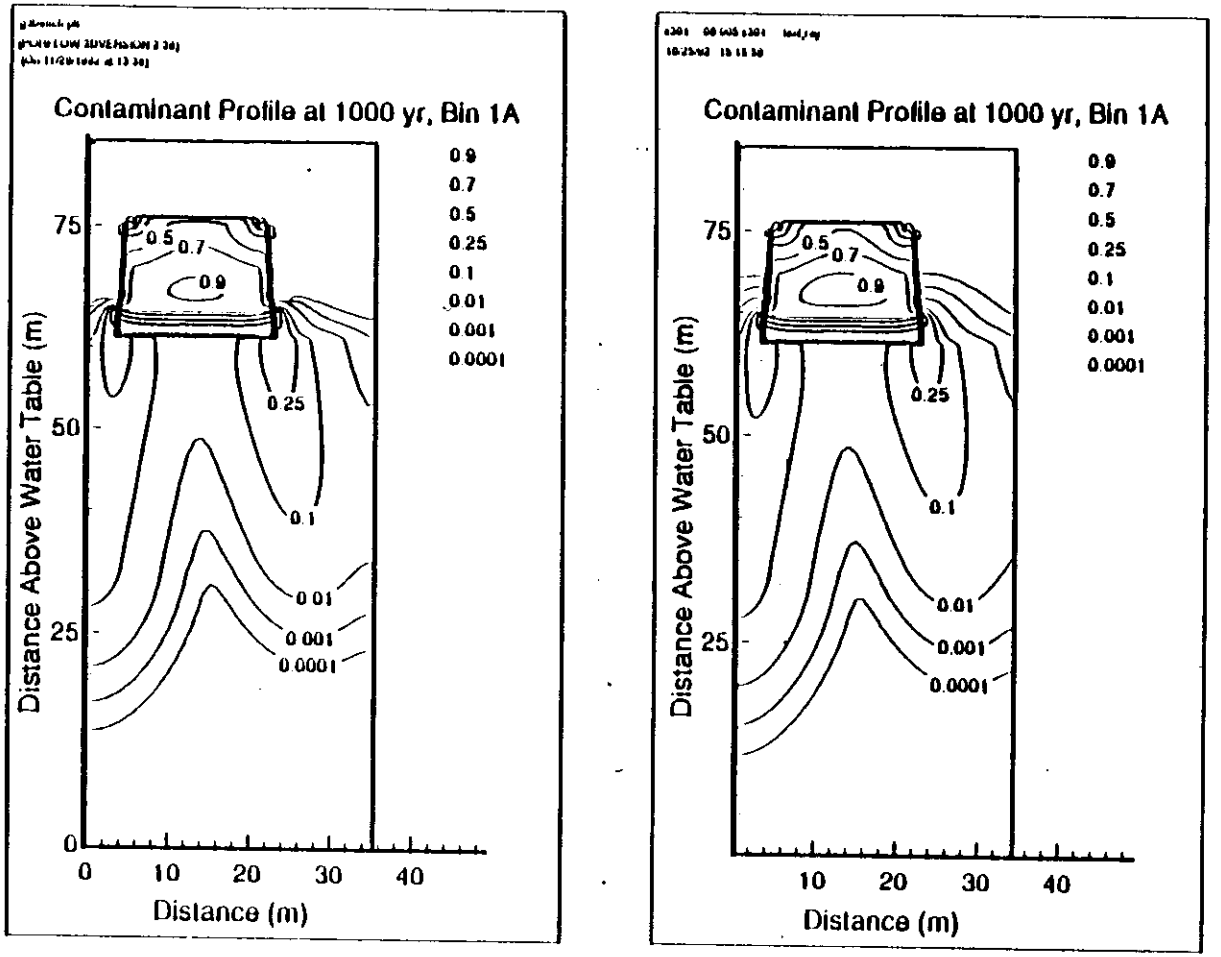

Figure H.12. Normalized Concentration Profiles from PORFLOW and TRACR3D/S301 for Bin 1A at t = 1000 Years

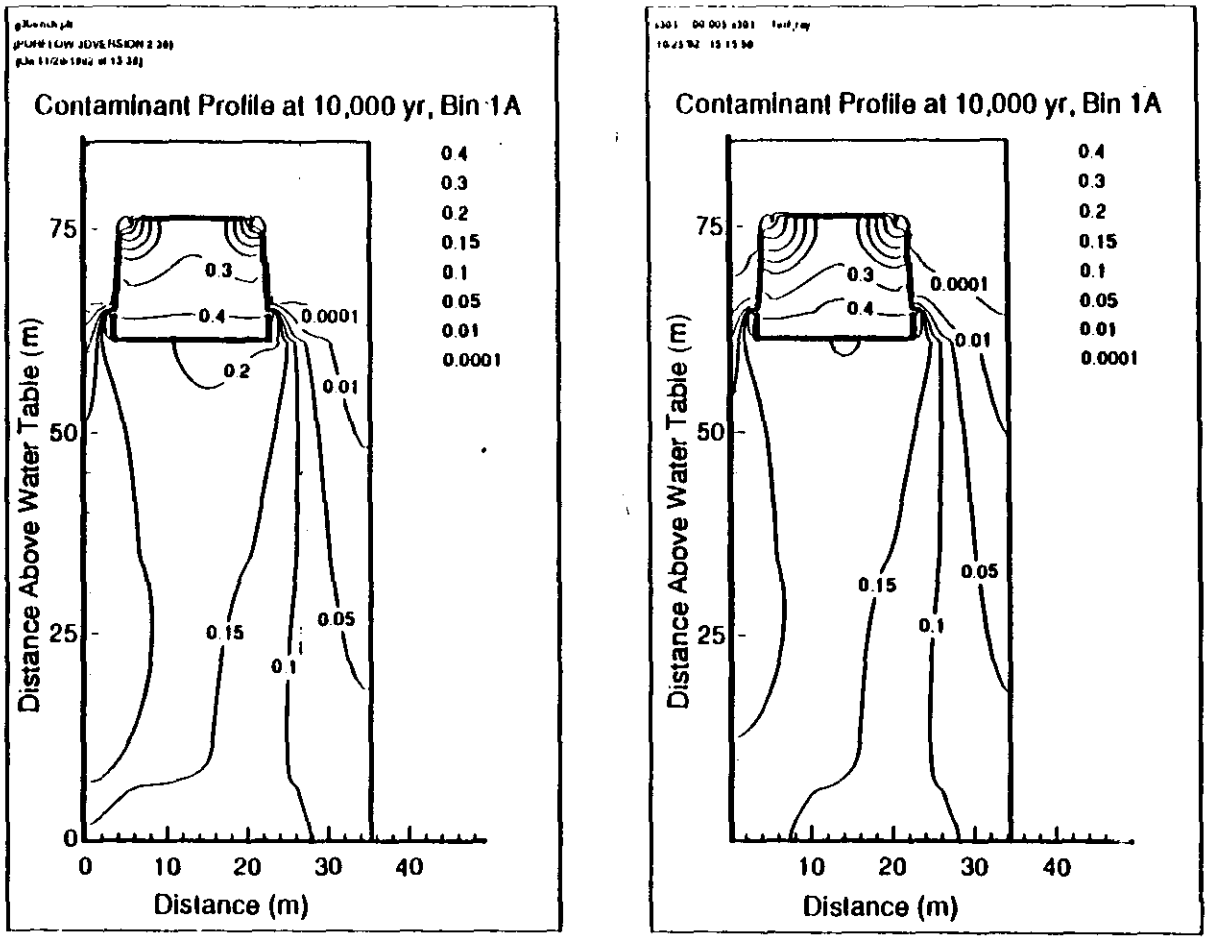

Figure H.13. Normalized Concentration Profiles from PORFLOW and TRACR3D/S301 for Bin 1A at t = 10,000 Years

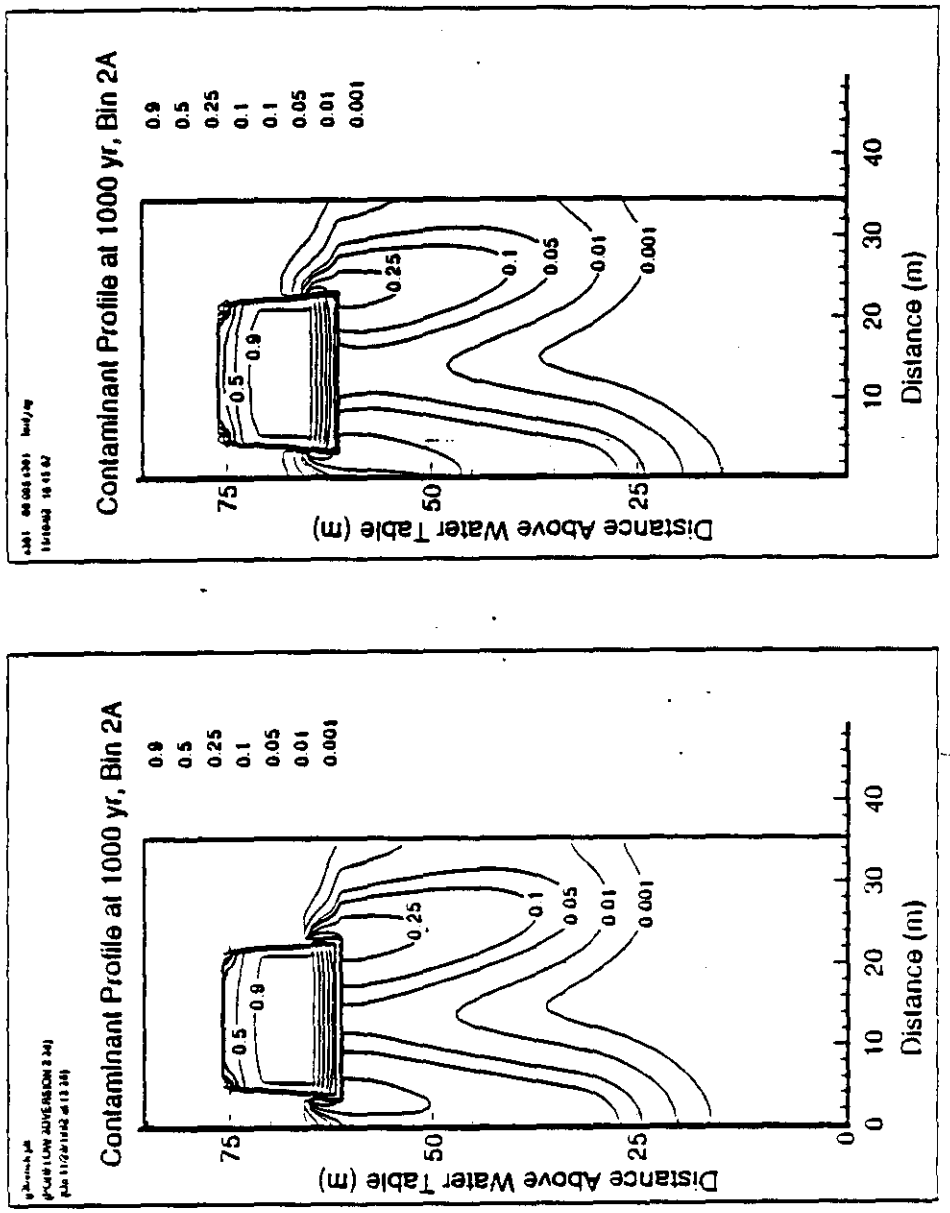

Figure H.14. Normalized Concentration Profiles from PORFLOW and TRACR3D/S301 for Bin 2A at t = 1000 Years

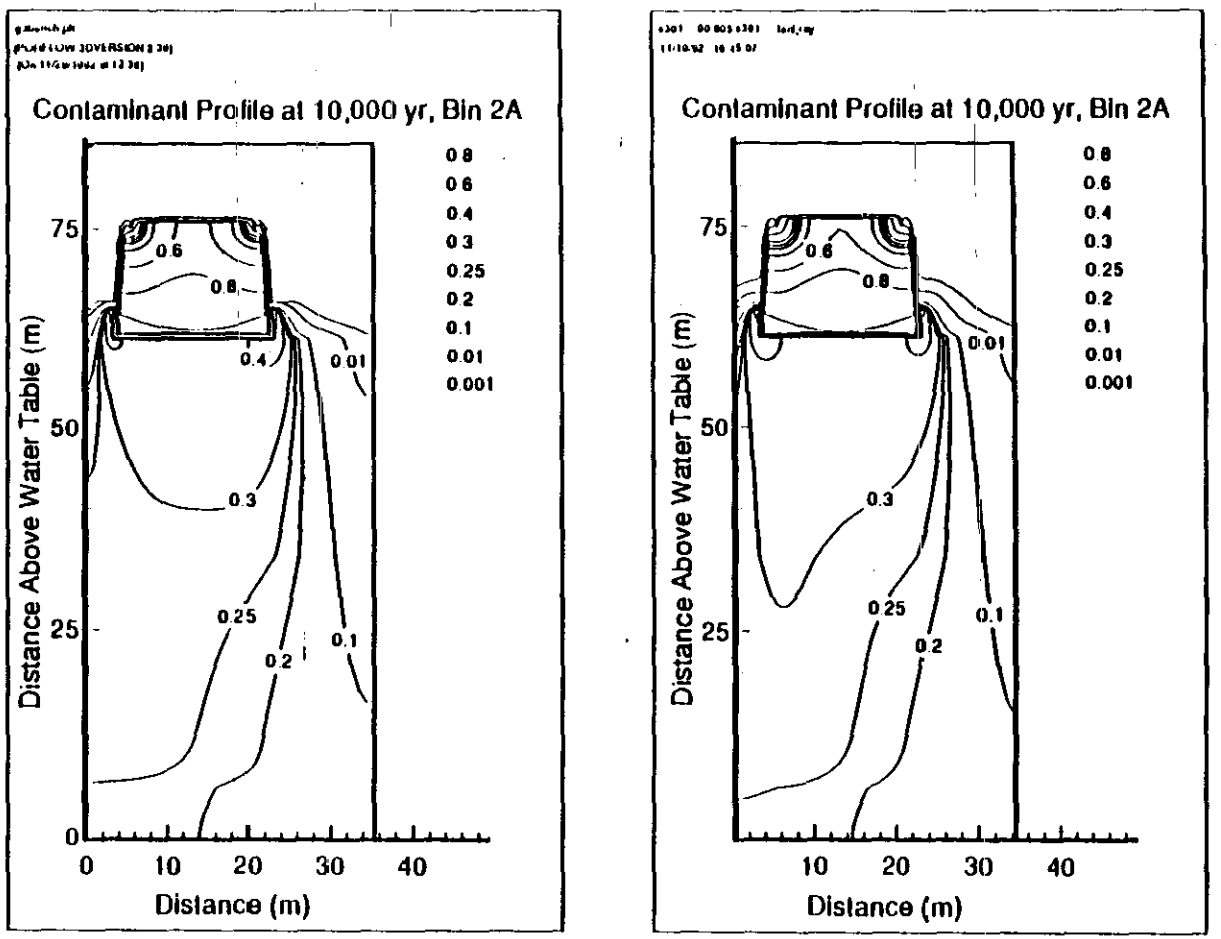

Figure H.15. Normalized Concentration Profiles from PORFLOW and TRACR3D/S301 for Bin 2A at t = 10,000 Years

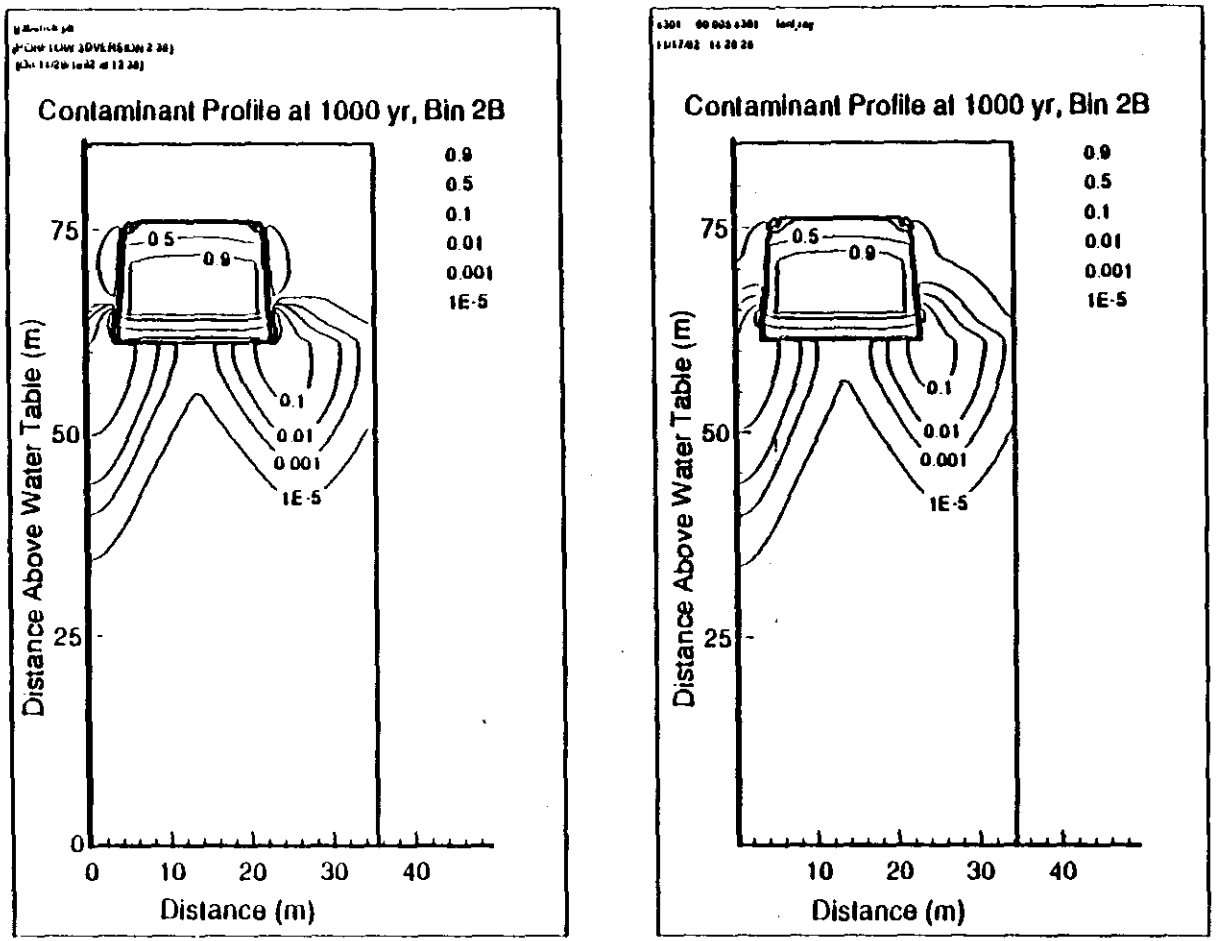

Figure H.16. Normalized Concentration Profiles from PORFLOW and TRACR3D/S301 for Bin 2B at t = 1000 Years

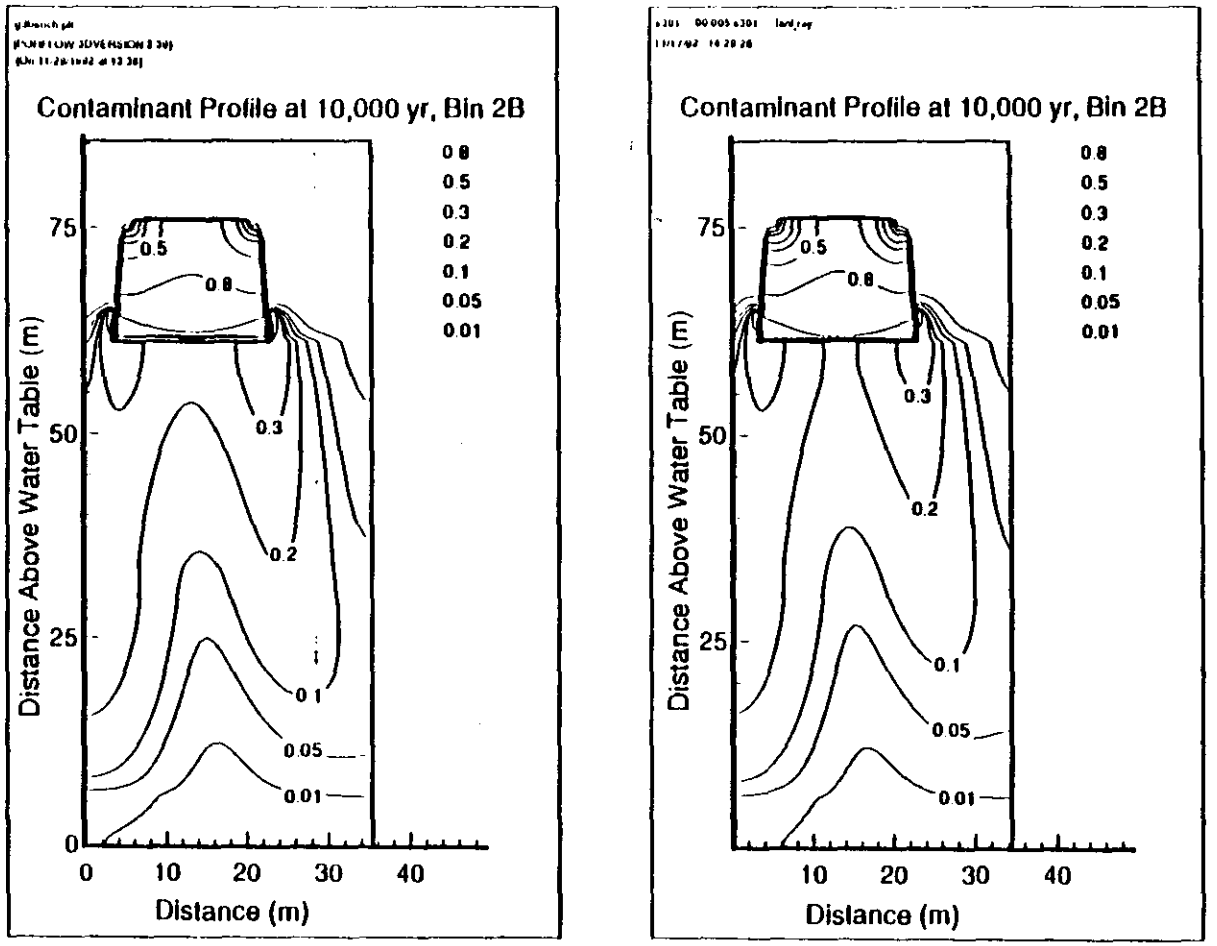

Figure H.17. Normalized Concentration Profiles from PORFLOW and TRACR3D/S301 for Bin 2B at t = 10,000 Years

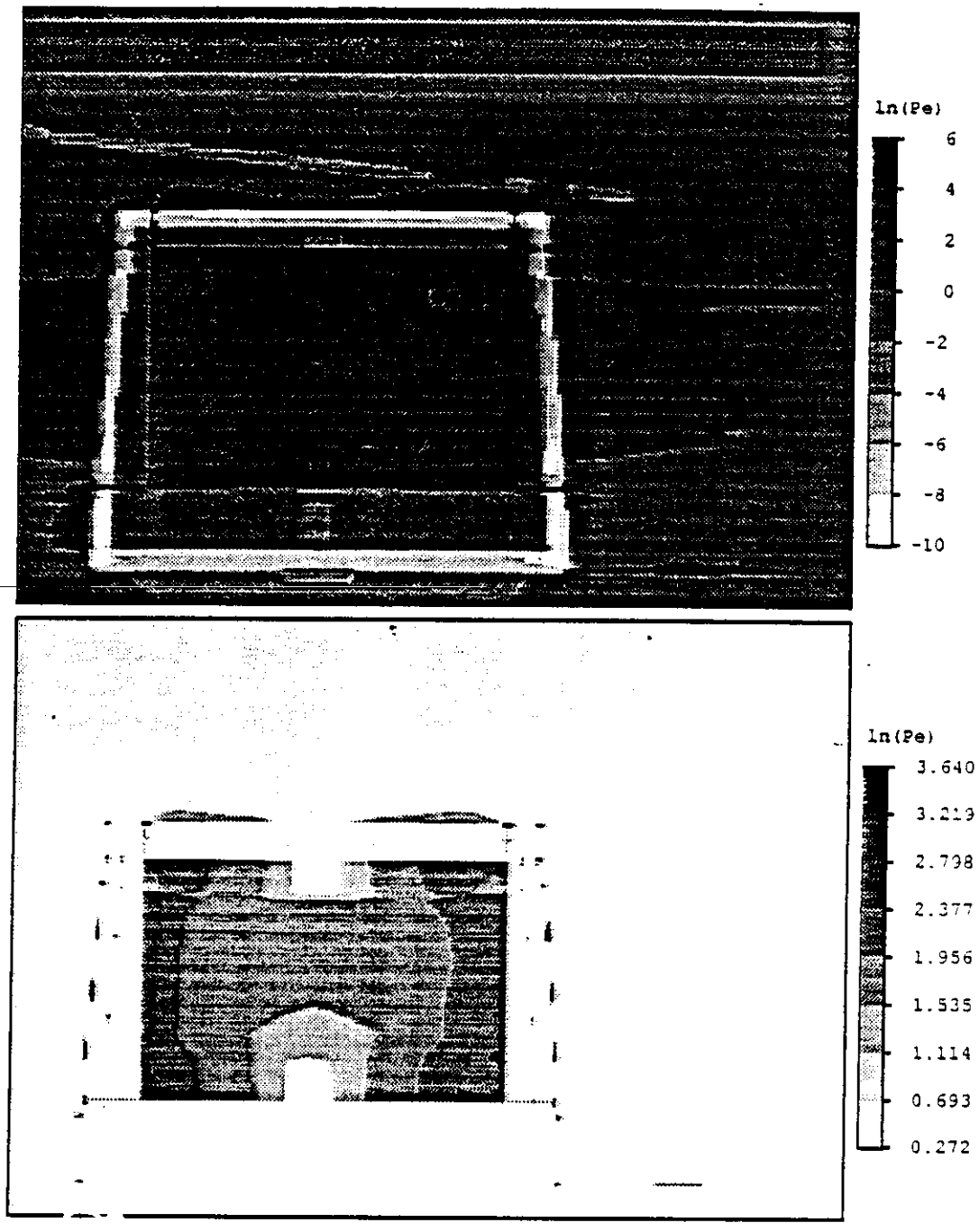

Figure H.18. Log-Transformed Grid Peclet Numbers from TRACR3D/S301 for Benchmark Problem 2 at t = 5000 Years

grouted waste form. This suggests that further grid refinement in the region of the domain representing the grouted waste form may be required (depending on the specific hydraulic properties that are assigned to the cracks) to reduce possible inaccuracies in peak arrival times and concentrations resulting from numerical diffusion.

As stated previously, the cracks appeared to be the primary feature controlling simulated contaminant releases from the grout vault for this case. Therefore, an accurate representation of these cracks was essential.

Average relative concentrations as a function of time at the water table are shown in Figure H.19 for the Bin 1A, 2A, and 2B simulations. These outflow concentrations also show excellent agreement between the PORFLOW and TRACR3D/S301 codes. Note that the TRACR3D/S301 results only show partial simulations (i.e., they were not run out as far in time as the PORFLOW simulations). The second peaks in the bimodal arrival distribution curves for Bins 2A and 2B reflect the assumed complete degradation of the asphalt-diffusion barrier at a time of 90,000 years.

H.6 Conclusions

Selected verification and benchmark problems were simulated using the PORFLOW, TRACR3D, and S301 computer codes to test the ability of the codes to accurately solve unsaturated flow and transport problems of the type required for the performance assessment.

Simulation results of a simple, two-dimensional flow verification problem using both the PORFLOW and TRACR3D codes showed good to excellent accuracy based on RRMS error calculations. Simulation results generated using both the PORFLOW and S301 codes for a simple, two-dimensional solute transport verification problem were judged to be of acceptable accuracy when the grid Peclet number was close to 2 (2.222). The transport results from both codes showed unacceptable accuracy for larger grid Peclet numbers (80 and 2222), based on RRMS error calculations. This unacceptable accuracy was attributed to excessive numerical dispersion.

Although the results of these verification problems generally agreed with the selected analytical solutions, difficulties were encountered in trying to obtain comparable benchmark results from PORFLOW and TRACR3D for more complex problems with heterogeneous materials. These differences made it necessary to modify the original intermodal conductance averaging scheme in the TRACR3D code. Options were added to TRACR3D for calculating intermodal hydraulic conductivities using arithmetic, harmonic, or geometric averaging, or a weighted conductance averaging scheme. The implementations of these averaging schemes were then tested using a simple, two-dimensional flow benchmark problem.

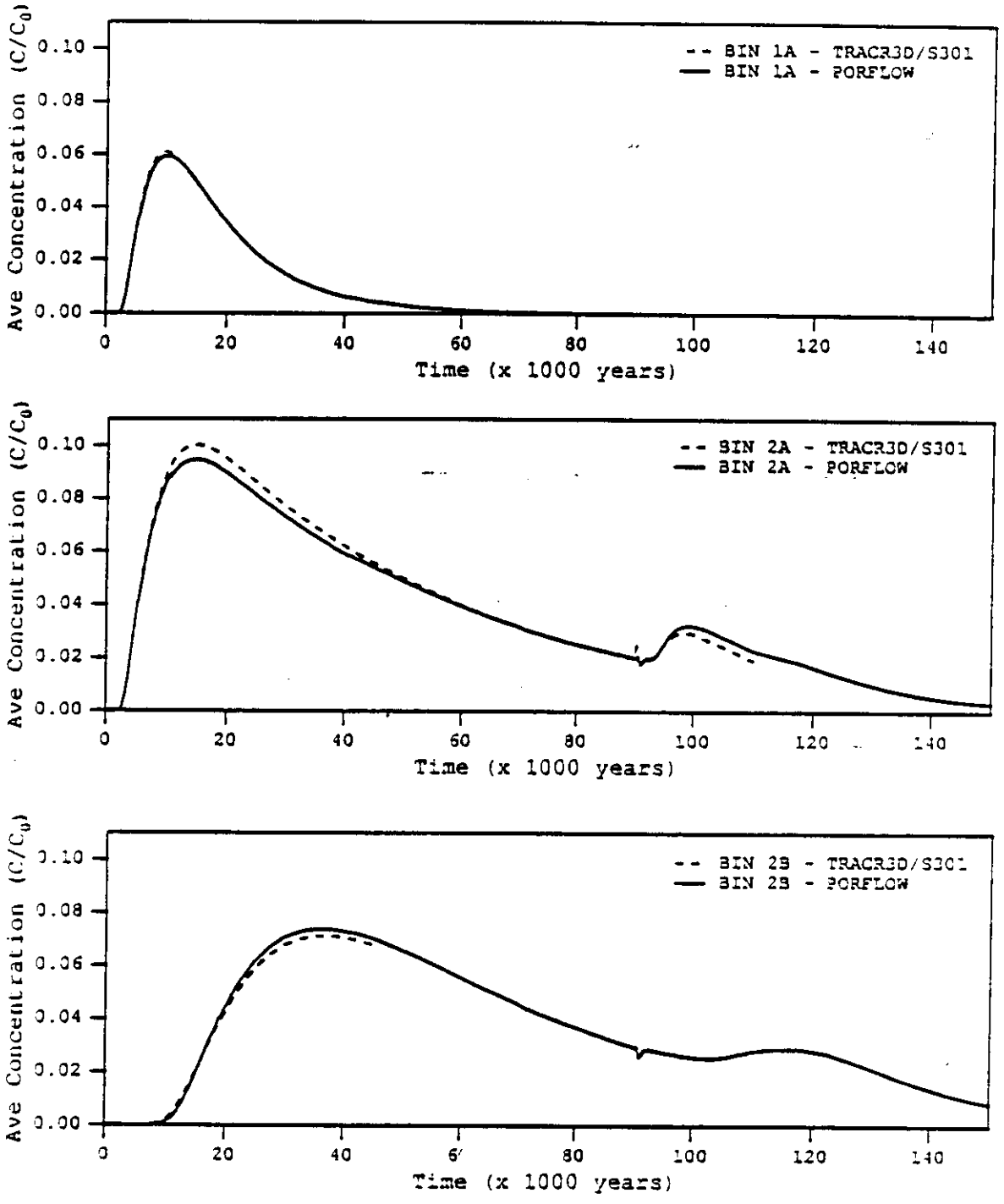

Figure H.19. Average Relative Outflow Concentrations at the Water Table as a Function of Time for Benchmark Problem 2

Nearly identical flow solutions were obtained with PORFLOW and TRACR3D using the same internodal conductance averaging schemes. However, there appears to be no consensus in the literature regarding a general, finite difference, internodal conductance averaging scheme for unsaturated flow modeling that is practical and accurate under all conditions. Therefore, the arithmetic mean was selected for the verification and benchmark problems in this appendix and for all the performance assessment simulations.

After modifying the internodal conductance averaging schemes in TRACR3D, nearly identical results were also obtained using PORFLOW and TRACR3D/S301 for a complex, large-scale, two-dimensional flow and transport benchmark problem. This benchmark problem used the same computational grid and most of the hydraulic and transport parameters that were used for the performance assessment simulations. The hydraulic properties of hypothetical cracks embedded within the model domain appeared to be the primary (most sensitive) parameters controlling the simulated release of contaminants from the waste form. Therefore, an accurate representation of these cracks is essential. Considering the complexity of this benchmark problem and the differences in the numerical approximations used by the different codes, the similarity of the results obtained for benchmark problem 2 was considered excellent.

Extensive grid convergence tests were not conducted for the benchmark problems because of the excessive CPU time already required for the large-scale simulations. Therefore, the effects of possible solution inaccuracies resulting from inadequate spatial discretization have not been quantified. However, the grid Peclet numbers for the benchmark problem 2 and for the low recharge cases (0.1 cm/yr) in the performance assessment simulations are <2 over most of the modeled domain. Therefore, these results are assumed to be reasonably close to the "true" numerical solutions.

Because of the difficulties in accurately solving large-scale, advection-dominated transport problems using standard finite difference and finite element methods, mixed Eulerian-Lagrangian solution methods have been developed, such as that incorporated in the S301 code. The particle-tracking feature of the S301 code was specifically designed to correct for artificial numerical dispersion in high grid Peclet number problems, but was found to be impractical for the large-scale performance assessment simulations because it required excessive computational time. Other numerical approaches, such as flux corrected transport schemes (Zalesek 1978), should be investigated as possible alternatives. Recent advances in computer hardware, such as high-speed, massively parallel computers, should also allow large-scale, transient unsaturated flow and transport problems to be simulated efficiently and accurately, with much higher resolution than is currently practical with conventional computational platforms (Dougherty 1991). The higher resolution and speed attained using parallel processing will help eliminate some of the difficulties associated with using standard finite difference and finite element methods to simulate large-scale, transient, unsaturated flow and transport problems.

H.7 References

Abramowitz, M., and I. A. Stegun. 1964. *Handbook of Mathematical Functions*, Vol. 55. Nat. Bur. Stand., Appl. Math. Ser. U.S. Government Printing Office, Washington, D.C.

Bear, J. 1972. *Dynamics of Fluids in Porous Media*. Elsevier, New York.

Brutsaert, W. F. 1971. "A Functional Iteration Technique for Solving the Richards Equation Applied to Two-Dimensional Infiltration Problems." *Water Resour. Res.* 7:1583-1596.

Bouloutas, E. T. 1989. "Improved Numerical Methods for Modeling Flow and Transport Processes in Partially-Saturated Porous Media." Ph.D. Dissertation. Massachusetts Institute of Technology, Boston, Massachusetts.

Carslaw, H. S., and J. C. Jaeger. 1959. *Conduction of Heat in Solids*. Oxford University Press, New York.

Celia, M. A., L. R. Ahuja, and G. F. Pinder. 1987. "Orthogonal Collocation and Alternating-Direction Procedures for Unsaturated Flow Problems." *Adv. Water Resour.* 10:178-187.

Chiang, C. Y., M. F. Wheeler, and P. B. Bedient. 1989. "A Modified Method of Characteristics Technique and Mixed Finite Element Method for Simulation of Groundwater Solute Transport." *Water Resour. Res.* 25:1541-1549.

Cleary, R. W., and M. J. Ungs. 1978. *Analytical Models for Groundwater Pollution and Hydrology*. Report 78-WR-15. Water Resources Program, Department of Civil Engineering, Princeton University, Princeton, New Jersey.

Dougherty, D. E. 1991. "Hydrologic Applications of the Connection Machine CM-2." *Water Resour. Res.* 27:2137-3147.

Farmer, C. L. 1985. "A Moving Point Method for Arbitrary Peclet Number Multi-Dimensional Convection-Diffusion Equations." *IMA Journal of Numerical Analysis* 5:465-480.

Gardner, W. H. 1958. "Some Steady State Solutions to the Unsaturated Moisture Flow Equation with Application to Evaporation from a Water Table." *Soil Sci.* 85:228-232.

Havercamp, R., and M. Vauclin. 1979. "A Note on Estimating Finite Differenc Interblock Hydraulic Conductivity Values for Transient Unsaturated Flow Problems." *Water Resour. Res.* 15:181-187.

Huyakorn, P. S., and G. F. Pinder. 1983. *Computational Methods in Subsurface Flow*. Academic Press, Orlando, Florida.

International Math Subroutine Library (IMSL). 1987. *IMSL User's Manual, Version 1.0*, Math/Library FORTRAN Subroutines for Mathematical Applications. Houston, Texas.

Kemper, W. D., and J. C. van Schaik. 1966. "Diffusion of Salts in Clay Water Systems." *Soil Sci. Soc. Am. Proc.* 30:534-540.

Magnusen, S. W., R. G. Baca, and A. J. Sondrup. 1990. *Independent Verification and Benchmark Testing of the PORFLO-3 Computer Code, Version 1.0*. EGG-BG-9175, Idaho National Engineering Laboratory, Idaho Falls, Idaho.

Olsen, S. R., and W. D. Kemper. 1965. "Movement of Nutrients to Plant Roots." *Adv. Agron.* 30:91-151.

Olsen, S. R., W. D. Kemper, and J. C. van Schaik. 1965. "Self-Diffusion Coefficients of Phosphorus in Soil Measured by Transient and Steady-State Methods." *Soil Sc. Am. Proc. 29:154-158.*

Patankar, S. V. 1980. *Numerical Heat Transfer and Fluid Flow*. McGraw-Hill, New York.

Piepho, M. G., W. H. Sutherland, P. D. Rittman, and F. M. Mann. 1993. *The Grout Performance Assessment Code System (GPACS) with Verification and Benchmarking*. WHC-SD-WM-UM-019 (Draft), Westinghouse Hanford Company, Richland, Washington.

Porter, L. K., W. D. Kemper, R. D. Jackson, and B. C. Stewart. 1960. "Chloride Diffusion in Soils as Influenced by Moisture Content." *Soil Sc. Soc. Am. Proc.* 24:460-463.

Richards, L. A. 1931. "Capillary Conduction of Liquids in Porous Mediums." *Physics* 1, 318-333.

Runchal, A. K., and B. Sagar. 1992. *PORFLOW: A Model for Fluid Flow, Heat, and Mass Transport in Multifluid, Multiphase, Fractured or Porous Media - Users Manual, Version 2.4*. ACRi/016/REV.G, Analytical and Computational Research, Inc., Los Angeles, California.

Scheidegger, A. E. 1961. "General Theory of Dispersion in Porous Media." *J. Geophys. Res.* 66:3273-3278.

Schnabel, R. R., and E. B. Ritchie. 1984. "Calculation of Internodal Conductances for Unsaturated Flow Simulations: A Comparison." *Soil Sci. Soc. Am. J.* 48:1006-1010.

Thomas, T. R. 1991. *Solute Transport Benchmark Studies for TRACR3D Code Verification*. WINCO-1083, Idaho National Engineering Laboratory, Idaho Falls, Idaho.

Travis, B. J., and K. H. Birdsell. 1991. *TRACR3D: A Model of Flow and Transport in Porous Media.* LA-11798-M, Los Alamos National Laboratory, Los Alamos, New Mexico.

Trent, D. S. 1975. *Mathematical Modeling of Transport Processes in Aquatic Systems.* BNWL-SA-5379, Pacific Northwest Laboratory, Richland, Washington.

van Genuchten. 1980. "A Closed Form Equation for Predicting the Hydraulic Conductivity of Unsaturated Soils." *Soil Sc. Soc. of Am. J.* 44:892-898.

Warrick, A. W. 1974. "Time-Dependent Linearized Infiltration. I. Point Sources." *Soil Sci. Soc. Am. Proc.* 38:383-386.

Warrick, A. W. 1991. "Numerical Approximations of Darcian Flow Through Unsaturated Soil." *Water Resour. Res.* 27:1215-1222.

Warrick, A. W., and D. O. Lomen. 1976. "Time-Dependent Linearized Infiltration: III. Strip and Disc Sources." *Soil Science Soc. Amer. Proc.* 40:639-643.

Wikramaratna, R. S., and C. L. Farmer. 1987. *The S301 High Resolution Miscible Displacement Simulator, 2-D Version with User-Specified Velocities.* Technical Report S301-2/1. Oil Recovery Projects Division, Winfrith Atomic Energy Establishment, Dorset, United Kingdom.

Zaidel, J., and D. Russo. 1992. "Estimation of Finite Difference Interblock Conductivities for Simulation of Infiltration Into Initially Dry Soils." *Water Resour. Res.* 28:2285-2295.

Zalesak, S. T. 1978. "Fully Multidimensional Flux-Corrected Transport Algorithms for Fluids." *J. Comp. Phys.* 31:335-362.

9413222.1553

This page intentionally left blank.

Appendix I

GENII Computer Code

9413222.1554

This page intentionally left blank.

Appendix I

GENII Computer Code: Description Of The GENII and GENII-S Computer Codes

K. Rhoads and S. F. Snyder, Pacific Northwest Laboratory

The GENII computer code version 1.485 (Napier et al. 1988) was used to perform the environmental accumulation and dose assessment calculations for all exposure scenarios except the drinking water dose assessment. GENII (GENeration II), the second generation of Hanford environmental dosimetry computer codes, was originally developed for environmental pathway analyses at Hanford. It has been used for several years to perform dose calculations for the Hanford Site Annual Environmental Report as well as for other routine assessments of Hanford facilities. Because GENII was developed specifically for environmental accumulation and dose estimate calculations for the Hanford region, use of this code is most appropriate for the performance assessment.

The GENII computer code was developed at Pacific Northwest Laboratory (PNL)[a] to incorporate the internal dosimetry models recommended by the International Commission on Radiological Protection (ICRP 1977, 1979-1988, 1986) into updated versions of existing environmental pathway analysis models. The GENII system was developed to provide a state-of-the-art, technically peer-reviewed, documented set of programs for calculating radiation doses from radionuclides released to the environment. Although the codes were developed for use at Hanford, they were designed with the flexibility to accommodate input parameters for a wide variety of generic sites.

The system includes the capabilities for calculating radiation doses for acute releases, with options for annual dose, committed dose, and cumulative dose; for calculating the same types of doses from chronic releases; for evaluating exposure pathways including direct exposure via water (swimming, boating, and fishing), soil (surface and buried sources), air (semi-infinite cloud and finite cloud geometries), inhalation, and ingestion pathways. The release scenarios include acute releases to air from ground level or elevated sources, or to water; and initial contamination of soil or surfaces. Source term variations include decay of radionuclides to the start of the exposure scenario, input of total radioactivity or specified fractions, and input of measured concentrations in specified environmental media. Interfaces are provided for external calculations of atmospheric dispersion,

(a) Pacific Northwest Laboratory is operated by Battelle Memorial Institute for the U.S. Department of Energy under Contract DE-AC06-76RLO 1830.

geohydrology, biotic transport, and surface water transport. Target populations are identified by distance and direction for individuals, populations, and for intruders into contained sources. To accommodate the initial requirements on the design of the codes, the Hanford Environmental Dosimetry System was written to determine radiation doses to individuals or populations from a wide variety of potential exposure scenarios. The core system may be used to calculate annual doses, dose commitments, or accumulated doses from acute or chronic releases of radioactive materials to air or water.

The Hanford Environmental Dosimetry System (GENII) is composed of seven linked computer codes and their associated data libraries. These codes and their linkages are illustrated in Figure I.1. The computer programs are of three types: user interfaces (i.e., interactive, menu-driven programs to assist the user with scenario generation and data input), internal and external dose factor generators, and the environmental dosimetry programs. For maximum flexibility, the portion of the code used for an analysis of short-term scenarios (as opposed to 10,000-year migration analyses) has been divided into three interrelated but separate exposure and dose calculations, respectively.

GENII is described in three volumes of documentation (Napier et al. 1988). Volume 1 describes the theoretical considerations of the system, including conceptual diagrams, mathematical representation of the solutions, and descriptions of solution techniques, where appropriate. The second volume is a Users' Manual, providing code structure, users' instructions, required system configurations, and topics related to quality assurance (QA). The third volume is a Code Maintenance Manual for the user who requires knowledge of code detail, including code logic diagrams, global dictionary, worksheets, example hand calculations, and listings of the code and its associated data libraries.

I.1 Quality Assurance Requirements for the GENII Computer Code

The GENII software package was developed under a QA framework that implemented the requirements of ANSI/ASME NQA-1 (ASME 1986). NQA-1 specifies that the following items be addressed for hardware design control:

- design input
- design process, including design analysis
- design verification
- change control
- interface control
- documentation and records.

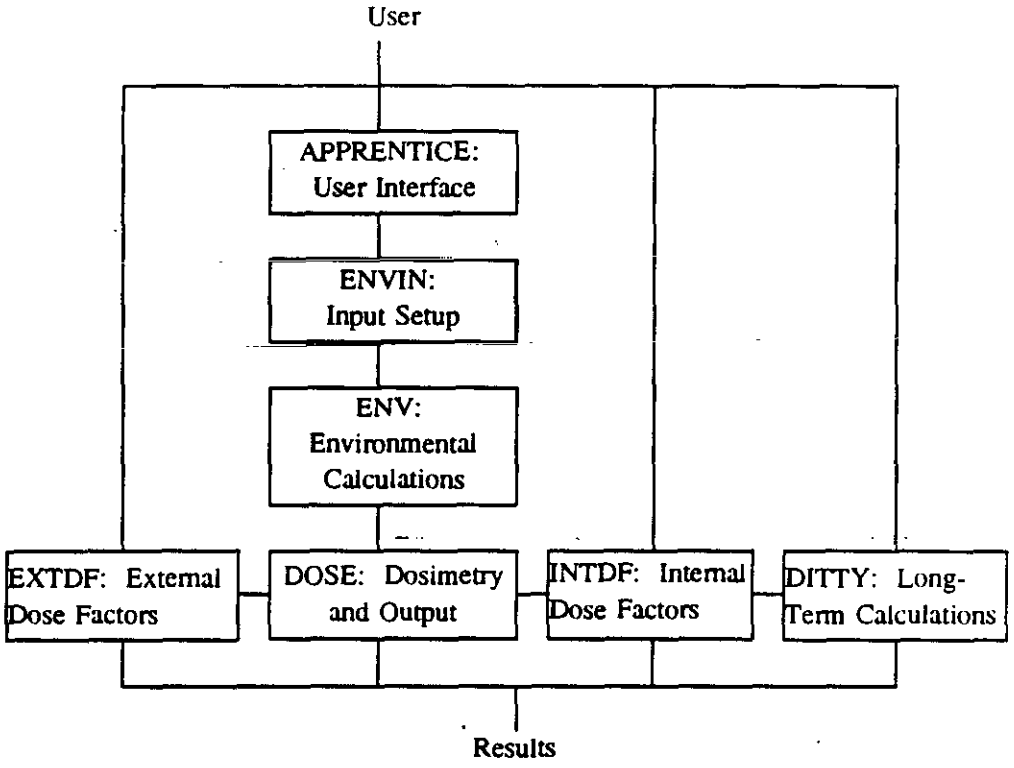

Figure I.1. Component Programs of the GENII Software Package

The QA procedures applied during development of the GENII code were an interpretation of the NQA-1 hardware requirements for software. The software design process consisted of developing and internally testing software in accordance with the design input. The GENII package has been extensively tested and verified by hand calculations and benchmarked against similar Hanford environmental dosimetry programs. Also, the models implemented by the code have undergone technical review by an external panel of experts.

I.2 Performance Assessment Use of GENII

GENII was used in this performance assessment to produce estimates of

- external exposure doses from radionuclides in groundwater, surface water, surface soil, and buried waste
- inhalation doses from resuspended material

- ingestion doses from intakes of contaminated water, food crops, animal products (e.g., meat, eggs), and inadvertently consumed soil.

All pathway dose estimates are essentially the product of radionuclide concentration in the medium of interest (i.e., air, water, or food); the intake rate via ingestion and inhalation or exposure time for external exposure; and the appropriate dose conversion factor (DCF). The appropriate combination of pathway algorithms (external exposure, inhalation, or ingestion) was activated for each scenario. A brief description of how each pathway is modeled in GENII is provided in Section I.1.

Values for many input parameters needed to produce GENII dose estimates are specified by the user as part of the scenario definition process. Default values for a number of other parameters are incorporated directly into the GENII code or into data files that are generally not modified by the user (e.g., the GENIINDEFAULT.IN file). Parameters that are common to several scenarios are discussed in Section I.5; parameters specific to each scenario are tabulated in the individual scenario discussions (see Appendix J).

Rather than using the GENII code to produce final dose estimates, the code was used to generate "scenario dose factors" (scenario DFs) based on unit radionuclide concentrations in grout, groundwater, or surface water. This approach was used because development of the waste inventory and groundwater transport modeling were done concurrently with scenario development. Scenario DFs were used to calculate dose to the receptor by multiplying the final concentration in waste or environmental media by the radionuclide-specific DF.

To derive a scenario DF, it was assumed that a unit activity of a given radionuclide was contained in grout, soil, or the downgradient water supply. External exposure, inhalation, and ingestion dose estimates for unit concentrations of each relevant radionuclide were then calculated using GENII. The scenario DFs also include the dose contributions from buildup of radioactive progeny following decay of parent nuclides in the media of interest.

I.3 The GENII-S Computer Code

In addition to the GENII code, GENII-S (Leigh et al. 1992) was used to determine the sensitivity of dosimetry results to the exposure pathway and dosimetry parameters used for this PA. GENII-S is a modified version of the GENII code that maintains the original software algorithms incorporated into a sensitivity and uncertainty analysis software (SUNS) shell. Implementation of the SUNS shell gives the user the capability to perform sensitivity analyses in a single operation, thereby eliminating the need for manual interfaces between the results of multiple GENII calculations and an independent sensitivity analysis software package.

GENII-S allows the user to specify ranges for variable parameters along with their associated probability density functions (PDFs). Permissible types of PDFs within the code include uniform, log-

uniform, triangular, normal, and lognormal. The code selects random values for each variable using a Latin hypercube sampling technique based on the user-specified parameter ranges and distributions. The GENII software is then run for a predetermined number of trials using a different set of randomly selected variables for each run. The results of the trials are complied into a cumulative distribution function, and other statistical analyses are also available to determine the interdependence of various parameters in the calculation. A discussion of PDF selection can be found in Snyder et al. 1992. Ranges for the variable parameters and their associated PDFs used in this analysis are listed in Appendix Q.

I.4 GENII Exposure Pathways

Following shallow-land burial, several pathways may account for an individual's exposure to radioactive materials, including external exposure, inhalation, and ingestion. All of the internal dose estimates reported in this analysis represent a 50-year committed dose resulting from intake during a single year. A summary of the GENII exposure pathway models are presented in the following sections. A more detailed description of the GENII modelling approach can be found in the code documentation (Napier et al. 1988).

I.4.1 GENII External Exposure Dose Models

External exposure in this performance assessment is the result of exposure to penetrating radiation from radionuclides in contaminated surface soil and the grout vaults themselves. External doses from surface soil are the result of either exhumation of a portion of the grout during well drilling or contamination that results from irrigation water applications. The dose from surface soil exposure considers uniform distribution of radionuclides in the upper 15 cm of soil, depletion of the initial radionuclide concentration by radioactive decay, and depletion by leaching of radionuclides in the plow layer to deeper soil layers over the growing season.

Dose estimates for penetrating radiation from the buried grout are modelled to account for attenuation by the 5-m layer of soil above the grout vaults. No external doses were calculated from resuspended soil because they are negligible compared to other pathways. Two components of the external exposure dose calculation - finite area corrections and indoor and outdoor exposures - require more detailed discussion in the following sections.

I.4.1.1 Finite Area Contamination

An external exposure correction factor is included in the calculations for external doses from small areas of contaminated ground. Areas larger than 1250 m^2 are considered to be an "infinite plane" source, whereas smaller areas require use of a dose rate reduction factor. The code data library contains surface contamination DFs for an infinite plane source, and they must be adjusted by the reduction factor if the contaminated area is sufficiently small. A dose rate reduction factor was used

only in the driller scenario because contamination was assumed to be limited to an area 100 m^2. The external ground surface dose factors used for this analysis were also based on the assumption that contamination was uniformly mixed in the top 15 cm of soil.

I.4.1.2 Indoor and Outdoor Exposure

The exposure time to soil contamination used for external exposure dose calculations in the post-drilling, irrigated farm, and Columbia River scenarios warrants clarification. Radionuclides in the upper soil layers present a pathway for external exposure. If an individual is outdoors at all times, the dose calculation is relatively straightforward. However, individuals located indoors have a reduced exposure to penetrating radiation from radionuclides in the soil because of increased distance and shielding by building materials. For the purposes of this PA, individuals are assumed to spend a portion of their time indoors.

External exposure dose estimates can be calculated by considering the indoor and outdoor exposure periods separately, or alternatively as done for this PA, as an "effective outdoor exposure time." The calculation of the effective outdoor exposure time is shown in Equation 1.

$$t_{out,eff} = t_{out} + (t_{in} \cdot S) \tag{1}$$

where $t_{out,eff}$ = effective outdoor exposure time

t_{out} = time spent outdoors, h/yr

t_{in} = time spent indoors, h/yr

S = shielding factor, dimensionless

Each parameter in the above equation is subject to substantial uncertainty. The amount of time spent outdoors depends on weather, demographic characteristics, and personal preferences. The shielding factor depends on the radioisotope content of the upper soil layer and building construction (both design and materials). The assumptions used for this PA are based on an effective outdoor exposure time of 0.5, which would be equivalent to the following assumptions:

t_{out} = 789 h

t_{in} = 7977 h

S = 0.45

I.4.1.3 Scenario External Exposure Doses

Sources of external exposure to radionuclides include both the buried grout and the radionuclides transported to the upper soil layer. The following lists the external dose contributors used for each scenario:

Scenario	External dose from
Driller	Buried grout, upper soil layer
Post-driller	Buried grout, upper soil layer (effective outdoor exposure)
Irrigated farm	Upper soil layer (effective outdoor exposure)
Columbia River	Upper soil layer (effective outdoor exposure)
Drinking water	No external dose

No external doses were calculated for resuspended soil, because screening calculations indicated that external doses from resuspended materials were 5 orders of magnitude lower than those from the upper soil layer. Therefore, neglect of this pathway does not affect the external doses estimated for the PA.

I.4.2 GENII Inhalation Dose Model

Internal doses may result from inhalation of radionuclides resuspended from the soil surface by wind or other mechanical disturbance. A mass loading model was used to approximate the radionuclide concentrations in airborne particulates by assuming the particulate concentrations were equivalent to the radionuclide concentrations in soil. Instantaneous equilibrium between the activity in soil and airborne particulates was assumed. Individuals were assumed to inhale contaminated air at the rate of 8520 m^3/yr, a value consistent with inhalation rates for the reference man (ICRP 1975). All scenarios except the drinking water scenario evaluate the inhalation dose from soil resuspension.

I.4.3 GENII Ingestion Dose Models

Internal doses can also result from the intake via ingestion of contaminated water, food crops, animal products, and soil. The radionuclide concentrations in food products are calculated by the GENII code from their concentrations in soil or in water (surface- or groundwater) used for irrigation or direct consumption.

Ingestion of radioactive materials via food crops may result from root uptake, irrigation with contaminated water, and soil resuspension with subsequent deposition onto leaves. Radionuclide concentrations in food crops following root uptake are calculated using concentration ratios (CRs), which are empirically determined estimates of radionuclide concentrations in plants based on the radionuclide

concentration in soil. External contamination of the food crop via deposition of resuspended soil or irrigation water is determined using an interception fraction, which is related to the above-ground biomass for each type of crop.

Radioactive materials ingested by animals via contaminated water and feed subsequently become incorporated into edible products (meat, milk, eggs) consumed by humans. Radionuclide concentrations in animal products are calculated from the rates of intake by animals multiplied by a transfer factor. The transfer factor is an empirical quantity that relates the animal's radionuclide intake rate to the concentration ultimately found in edible products. Again, instantaneous equilibrium is assumed between the radionuclide concentrations in animal feed and water and that in the edible food products.

9413222.563

I.5 Databases used by GENII

This section describes and lists parameters used in the GENII code. Radionuclide-dependent (e.g., dose conversion factor) and element-dependent (e.g., concentration ratio) data are distributed with the code in the form of text or binary data libraries. Some of the values for parameters in the default databases distributed with the GENII code were replaced with alternate values for use with this analysis. The alternative databases were developed either to incorporate updated parameter values or to substitute values that better represent scenario-specific pathways and conditions.

I.5.1 Dose Conversion Factors

Dose conversion factors (DCFs) are radionuclide-specific parameters that represent the dose resulting from a unit intake or exposure to a unit-concentration source of a given radionuclide. Five different types of radionuclide DCFs are used to calculate the final scenario DFs for this analysis. Inhalation and ingestion DCFs represent the internal dose following intake of a unit quantity of radionuclides via each pathway. External DCFs include the external dose from radionuclides per unit concentration in surface soil, buried waste, or immersion in water. The dose from external sources depends on the radionuclide concentration in the source medium, its geometry with respect to the receptor, the type and quantity of shielding material (if any), and the time over which the individual is exposed to the source. Listings of both external and internal dose conversion factors have been published by the U.S. Department of Energy (1988a, 1988b).

I.5.1.1 Internal DCFs

Internal DCFs for the inhalation and ingestion pathways are calculated by the GENII code for a particular exposure and dose commitment period based on models recommended by the International Commission on Radiological Protection in Publications 26, 30, and 48 (ICRP 1977, 1979-1988, and 1986). The GENII libraries for inhalation and ingestion DCFs are provided as incremental dose factors in a binary format to permit calculations for a variable dose commitment period. To display the internal DCFs calculated by the GENII code for a 1-year exposure with a 50-year dose

commitment period, a test scenario was performed to generate a listing of the inhalation and ingestion DCFs for pertinent radionuclides (See Exhibit I.1).

Inhalation and ingestion DCFs depend, in part, on the chemical form of the radionuclide at the time of intake. The chemical forms associated with the maximum DCF values for each radionuclide were used for this analysis because the chemical forms of the radionuclides are either unknown or are subject to change after release from the waste site. For comparison purposes only, the maximum GENII and maximum DOE (1988b) internal DCF values are listed in Exhibit I.1 for all grout inventory radionuclides and their progeny evaluated in this PA. Differences between the maximum GENII and maximum DOE DCFs are the result of minor differences in the derivation method and metabolic model assumptions. Exhibit I.1 shows that the GENII and DOE ingestion and inhalation DCFs generally agree within ± 10%.

I.5.1.2 External DCFs

External DCFs were used in this PA to determine the dose from exposure to contaminated soil or grout and from immersion in contaminated water. GENII soil surface DCFs represent the dose from a unit concentration of radionuclide uniformly dispersed in the upper 15-cm soil layer, whereas DOE soil-surface DCFs indicate the dose from a unit concentration of radionuclide on the ground surface. The GENII values are somewhat lower than the DOE values because of the added shielding effect of having the radionuclides dispersed through the soil surface layer. Because the PA scenarios involving contaminated soil result from excavation of buried grout or irrigation deposition on cultivated ground (as opposed to air deposition of radionuclides on the soil surface), the GENII soil surface DCFs are more appropriate for this analysis and are used in preference to the DOE soil-surface DCFs.

The water immersion DCFs were used in the Columbia River Scenario for exposure during swimming only. The default water immersion DCFs distributed with the GENII code were calculated by a simplified adaptation of the method used to determine the DOE values (DOE 1988a). For this analysis, a library containing the DOE values for radionuclides evaluated in the Columbia River scenario was substituted for the GENII default library because the DOE DCFs were calculated in a more rigorous manner. These values are shown in Exhibit I.2.

I.5.2 Concentration Ratios and Transfer Factors

Concentration ratios (CRs) are used to estimate the radionuclide concentrations in vegetation from root uptake of radionuclides in soil. Transfer factors (TFs) are used to calculate the animal product contamination levels resulting from animal ingestion of radionuclides via feed and drinking water. The values for CRs and TFs are element dependent rather than radionuclide dependent. For this analysis, the default CR and TF libraries distributed with the GENII code were replaced with a library containing values from Kennedy and Strenge (1992), which are based on a more recent comprehensive literature review (IUR 1989). Most TFs for poultry and eggs in the revised library were identical to

the GENII default values because little new information was available in this area. The Kennedy and Strenge CRs and TFs are listed in Exhibit I.3. As in the original GENII library, CR and TF values are not provided for noble gases because they are not concentrated in plant or animal tissues.

Parameters similar to the animal product TFs are used in the Columbia River Scenario to estimate the radionuclide concentrations in fish that inhabit contaminated water. This parameter, the bioaccumulation factor, relates the concentrations of radionuclides in aquatic animals and plants to the concentrations in surrounding water. The GENII default values, listed in Exhibit I.4, were used for freshwater fish, and no other aquatic foods were considered in this analysis. The only element evaluated in the Columbia River Scenario for which a bioaccumulation factor was not available was francium, which results from decay of plutonium-239. However, this radionuclide is not present in large enough quantities to contribute substantially to the dose.

I.5.3 Miscellaneous Default Parameters

A number of input parameters are used to describe regional and demographic conditions (e.g., irrigation rate, food consumption rates, etc.). In the GENII code these parameters are incorporated into the dose calculation via both the "scenario input file" (i.e., the scenario.IN file) and a "default parameter file" (i.e., the DEFAULT.IN file in the distribution version of GENII). Scenario input files are used to provide values for variables that would be expected to change from case to case (see Appendix J), whereas the DEFAULT.IN file contains parameters specific to a particular region, but which remain relatively constant for all types of scenarios.

The default parameter values used for this PA are shown in Exhibit I.5 (driller scenario) and I.6 (post driller, irrigated farm, and Columbia River scenarios). Both default parameter files are equivalent to the original GENII distribution version except for the soil ingestion rates. Although the soil ingestion rates shown in Exhibits I.5 and I.6 differ, the soil ingestion rates used in both scenarios were equivalent to 100 mg/d. Because the exposure period was limited to 5 days in the driller scenario, the total soil ingestion for the driller was equivalent to 100 mg/d for five days. The GENII code models soil ingestion over a 1-year period, therefore an effective soil ingestion rate over the entire year was calculated (as 100 mg/d * 5 d/yr * 1 yr/365.25 d = 1.37 mg/d) for use in the driller scenario DEFAULT.IN file.

Exhibit I.1. Maximum GENII and DOE Inhalation and Ingestion DCFs for Radionuclides Considered in the Dose Assessment

Inhalation				Ingestion			
Radionuclide	GENII	DOE	G/D[a]	Radionuclide	GENII	DOE	G/D
H 3	9.0E - 05	6.3E - 05	1.4	H 3	6.1E - 05	6.3E - 05	1.0
C 14	2.1E - 03	2.1E - 03	1.0	C 14	2.1E - 03	2.1E - 03	1.0
CO 60	2.0E - 01	1.5E - 01	1.3	CO 60	2.6E - 02	2.6E - 02	1.0
NI 63	3.0E - 03	3.0E - 03	1.0	NI 63	5.5E - 04	5.4E - 04	1.0
SE 79	9.5E - 03	8.9E - 03	1.1	SE 79	8.3E - 03	8.3E - 03	1.0
SR 90	2.0E - 01	2.3E - 01	0.9	SR 90	1.2E - 01	1.3E - 01	0.9
Y 90	8.7E - 03	8.2E - 03	1.1	Y 90	1.1E - 02	1.0E - 02	1.1
ZR 95	2.3E - 02	1.9E - 02	1.2	ZR 95	3.7E - 03	3.4E - 03	1.1
NB 95M	2.5E - 03	2.2E - 03	1.1	NB 95M	2.3E - 03	2.0E - 03	1.2
NB 95	5.7E - 03	4.5E - 03	1.3	NB 95	2.5E - 03	2.2E - 03	1.1
NB 94	3.8E - 01	3.3E - 01	1.2	NB 94	7.2E - 03	5.1E - 03	1.4
TC 99	8.6E - 03	7.5E - 03	1.1	TC 99	2.2E - 03	1.3E - 03	1.7
RU 103	9.0E - 03	7.8E - 03	1.2	RU 103	3.0E - 03	2.7E - 03	1.1
PD 103	1.6E - 03	1.4E - 03	1.1	PD 103	7.8E - 04	6.9E - 04	1.1
RH 103M	4.9E - 06	4.6E - 06	1.1	RH 103M	1.2E - 05	1.1E - 05	1.1
RU 106	4.7E - 01	4.4E - 01	1.1	RU 106	2.7E - 02	2.1E - 02	1.3
SN 113	1.1E - 02	8.9E - 03	1.2	SN 113	3.1E - 03	2.7E - 03	1.1
IN 113M	4.2E - 05	3.4E - 05	1.2	IN 113M	1.1E - 04	1.0E - 04	1.1
SB 125	1.2E - 02	9.8E - 03	1.2	SB 125	2.8E - 03	2.6E - 03	1.1
TE 125M	7.2E - 03	6.7E - 03	1.1	TE 125M	3.7E - 03	3.4E - 03	1.1
SN 126	9.8E - 02	8.6E - 02	1.1	SN 126	1.9E - 02	1.7E - 02	1.1
SB 126M	2.9E - 05	2.8E - 05	1.0	SB 126M	9.1E - 05	7.3E - 05	1.2
SB 126	1.2E - 02	1.0E - 02	1.2	SB 126	1.0E - 02	9.6E - 03	1.0
I 129	1.5E - 01	1.8E - 01	0.8	I 129	2.5E - 01	2.8E - 01	0.9
CS 134	4.3E - 02	4.7E - 02	0.9	CS 134	6.8E - 02	7.4E - 02	0.9
CS 135	4.5E - 03	4.5E - 03	1.0	CS 135	6.8E - 03	7.1E - 03	1.0
CS 137	3.0E - 02	3.2E - 02	0.9	CS 137	4.7E - 02	5.0E - 02	0.9
CE 144	3.7E - 01	3.5E - 01	1.1	CE 144	2.1E - 02	2.0E - 02	1.1
PR 144M	1.9E - 05	0.0E + 00	–	PR 144M	4.8E - 05	0.0E + 00	–
PR 144	4.5E - 05	4.2E - 05	1.1	PR 144	1.2E - 04	1.1E - 04	1.1
EU 152	2.1E - 01	2.2E - 01	1.0	EU 152	6.3E - 03	6.0E - 03	1.1
EU 154	2.7E - 01	2.6E - 01	1.0	EU 154	9.2E - 03	9.1E - 03	1.0
EU 155	4.0E - 02	3.9E - 02	1.0	EU 155	1.5E - 03	1.3E - 03	1.2
TH 230	3.2E + 02	3.2E + 02	1.0	TH 230	5.4E - 01	5.3E - 01	1.0
RA 226	8.1E + 00	7.9E + 00	1.0	RA 226	9.5E - 01	1.1E + 00	0.9
RN 222	0.0E + 00	0.0E + 00	–	RN 222	0.0E + 00	0.0E + 00	–
PB 210	1.4E + 01	1.3 + 01	1.1	PB 210	5.3E + 00	5.1E + 00	1.0
BI 210	2.0E - 01	1.9E - 01	1.1	BI 210	6.3E - 03	5.9E - 03	1.1

Exhibit I.1. (contd)

Inhalation				Ingestion			
Radionuclide	GENII	DOE	G/D[a]	Radionuclide	GENII	DOE	G/D
H 3	9.0E - 05	6.3E - 05	1.4	H 3	6.1E - 05	6.3E - 05	1.0
PO 210	9.7E + 00	8.1E + 00	1.2	PO 210	1.9E + 00	1.6E + 00	1.2
U 234	1.3E + 02	1.3E + 02	1.0	U 234	2.8E - 01	2.6E - 01	1.1
U 235	1.2E + 02	1.2E + 02	1.0	U 235	2.6E - 01	2.5E - 01	1.0
TH 231	8.3E - 04	8.1E - 04	1.0	TH 231	1.3E - 03	1.3E - 03	1.0
PA 231	1.3E + 03	1.3E + 03	1.0	PA 231	1.1E + 01	1.1E + 01	1.0
AC 227	6.7E + 03	6.7E + 03	1.0	AC 227	1.4E + 01	1.4E + 01	1.0
TH 227	1.6E + 01	1.6E + 01	1.0	TH 227	3.8E - 02	3.6E - 02	1.1
FR 223	7.8E - 03	6.1E - 03	1.3	FR 223	1.1E - 02	8.6E - 03	1.3
RA 223	7.7E + 00	7.5E + 00	1.0	RA 223	2.7E - 01	5.5E - 01	0.5
NP 237	6.4E + 02	4.9E + 02	1.3	NP 237	5.2E + 00	3.9E + 00	1.3
PA 233	9.5E - 03	8.6E - 03	1.1	PA 233	3.6E - 03	3.3E - 03	1.1
U 238	1.2E + 02	1.2E + 02	1.0	U 238	2.6E - 01	2.3E - 01	1.1
TH 234	3.5E - 02	3.3E - 02	1.1	TH 234	1.3E - 02	1.3E - 02	1.0
PA 234	8.5E - 04	7.4E - 04	1.1	PA 234	2.2E - 03	2.1E - 03	1.0
PU 242	4.0E + 02	4.8E + 02	0.8	PU 242	3.3E + 00	4.1E + 00	0.8
NP 238	4.3E - 02	3.1E - 02	1.4	NP 238	4.0E - 03	3.4E - 03	1.2
PU 238	3.9E + 02	4.6E + 02	0.8	PU 238	3.2E + 00	3.8E + 00	0.8
CM 244	2.5E + 02	2.7E + 02	0.9	CM 244	2.0E + 00	2.3E + 00	0.9
PU 244	4.0E + 02	4.8E + 02	0.8	PU 244	3.3E + 00	4.0E + 00	0.8
U 240	2.3E - 03	2.1E - 03	1.1	U 240	4.6E - 03	4.1E - 03	1.1
PU 240	4.3E + 02	5.1E + 02	0.8	PU 240	3.6E + 00	4.3E + 00	0.8
PU 241	8.2E + 00	1.0E + 01	0.8	PU 241	6.8E - 02	8.6E - 02	0.8
AM 241	4.4E + 02	5.2E + 02	0.8	AM 241	3.6E + 00	4.5E + 00	0.8
CM 243	3.1E + 02	3.5E + 02	0.9	CM 243	2.5E + 00	2.9E + 00	0.9
PU 243	1.5E - 04	1.5E - 04	1.0	PU 243	3.2E - 04	3.3E - 04	1.0
AM 243	4.4E + 02	5.2E + 02	0.8	AM 243	3.6E + 00	4.5E + 00	0.8
NP 239	2.5E - 03	2.2E - 03	1.1	NP 239	3.3E - 03	2.9E - 03	1.1
PU 239	4.3E + 02	5.1E + 02	0.8	PU 239	3.6E + 00	4.3E + 00	0.8

(a) The G/D value indicates the ratio of the GENII value to the DOE value.

Exhibit I.2. External Dose Factors for Surface Soil Contamination and Water Immersion

Soil Surface (GENII)		Water Immersion (DOE)	
Radionuclide	mrem/yr per $\mu Ci/m^3$	Radionuclide	mrem/yr per $\mu Ci/m^3$
H 3	2.57E - 10	C 14	0.00E + 00
CO60	5.80E + 01	SE79	0.00E + 00
NI63	1.40E - 06	NB94	1.77E + 01
SE79	3.93E - 05	TC99	6.18E - 06
SR90	2.62E - 03	I 129	1.07E - 01
Y 90	1.46E - 01	U 234	1.86E - 03
ZR95	1.79E + 01	U 235	1.72E + 00
NB95M	1.21E + 00	TH231	1.37E - 01
NB95	1.94E + 01	PA231	3.34E - 01
NB94	3.58E + 01	AC227	1.44E - 03
TC99	3.71E - 04	FR223	5.33E - 01
RU103	1.25E + 01	RA223	1.51E + 00
PD103	2.31E - 02	NP237	2.68E - 01
RH103M	2.45E - 03	PA233	2.37E + 00
RU106	5.61E + 00	U 238	1.29E - 03
SN113	1.14E - 01	TH234	9.13E - 02
IN113M	5.66E + 00	PA234	2.21E + 01
SB125	1.14E + 01	AM241	2.33E - 01
C 14	5.51E - 05		
TE125M	6.47E - 02		
SN126	3.83E - 01		
SB126M	4.03E + 01		
SB126	6.79E + 01		
I 129	4.08E - 02		
CS134	4.00E + 01		
CS135	1.07E - 04		
CS137	1.39E + 01		
CE144	2.28E - 01		
PR144M	3.93E - 02		
PR144	1.03E + 00		
EU152	2.77E + 01		
EU154	2.87E + 01		
EU155	6.62E - 01		
TH230	3.01E - 03		
RA226	6.72E - 02		

Exhibit I.2. (contd)

Soil Surface (GENII)		Water Immersion (DOE)	
Radionuclide	mrem/yr per $\mu Ci/m^3$	Radionuclide	mrem/yr per $\mu Ci/m^3$
RN222	4.32E + 01		
PB210	7.66E - 03		
BI210	2.10E - 02		
PO210	2.05E - 04		
U 234	1.39E - 03		
U 235	1.76E + 00		
TH231	1.08E - 01		
PA231	6.87E - 01		
AC227	1.89E - 03		
TH227	2.02E + 00		
FR223	7.19E - 01		
RA223	6.13E + 00		
NP237	2.16E - 01		
PA233	5.19E + 00		
U 238	6.32E - 04		
TH234	4.79E - 01		
PA234	4.67E + 01		
PU242	3.83E - 04		
NP238	1.36E + 01		
PU238	4.62E - 04		
CM244	3.73E - 04		
PU244	2.72E - 04		
U 240	8.94E + 00		
PU240	4.59E - 04		
PU241	8.55E - 10		
AM241	1.05E - 01		
CM243	2.16E + 00		
PU243	2.43E - 01		
AM243	3.85E - 01		
NP239	2.96E + 00		
PU239	1.02E - 03		

Exhibit I.3. Concentration Ratios[a] and Transfer Factors[b] used in this PA

Element	Number	Leafy Vegetable	Other Vegetable	Fruit –	Grain –	Beef day/kg	Poultry day/kg	Milk day/L	Egg day/kg
H	1	–	–	–	–	–	–	–	–
BE	4	1.0E - 2	1.5E - 3	1.5E - 3	1.5E - 3	1.0E - 3	4.0E - 1	9.0E - 7	2.0E - 2
C	6	–	0.7	0.7	0.7	–	–	–	–
N	7	3.0E + 1	3.0E + 1	3.0E + 1	3.0E + 1	7.5E - 2	1.0E - 1	2.5E - 2	8.0E - 1
F	9	6.0E - 2	6.0E - 3	6.0E - 3	6.0E - 3	1.5E - 1	1.0E - 2	1.0E - 3	2.0E + 0
NA	11	7.5E - 2	5.5E - 2	5.5E - 2	5.5E - 2	5.5E - 2	1.0E - 2	3.5E - 2	2.0E - 1
MG	12	1.0E + 0	5.5E - 1	5.5E - 1	5.5E - 1	5.0E - 3	3.0E - 2	4.0E - 3	1.6E + 0
SI	14	3.5E - 1	7.0E - 2	7.0E - 2	7.0E - 2	4.0E - 5	2.0E - 1	2.0E - 5	8.0E - 1
P	15	3.5E + 0	3.5E + 0	3.5E + 0	3.5E + 0	5.5E - 2	1.9E - 1	1.5E - 2	1.0E + 1
S	16	1.5E + 0	1.5E + 0	1.5E + 0	1.5E + 0	1.0E - 1	9.E - 1	1.5E - 2	7.0E + 0
CL	17	7.0E + 1	7.0E + 1	7.0E + 1	7.0E + 1	8.0E - 2	3.0E - 2	1.5E - 2	2.0E + 0
AR	18	–	–	–	–	–	–	–	–
K	19	1.0E + 0	5.5E - 1	5.5E - 1	5.5E - 1	2.0E - 2	4.0E - 1	7.0E - 3	7.0E - 1
CA	20	3.5E + 0	3.5E - 1	3.5E - 1	3.5E - 1	7.0E - 4	4.4E - 2	1.0E - 2	4.4E - 1
SC	21	6.0E - 3	1.0E - 3	1.0E - 3	1.0E - 3	1.5E - 2	4.0E - 3	5.0E - 6	3.0E - 3
CR	24	7.5E - 3	4.5E - 3	4.5E - 3	4.5E - 3	5.5E - 3	2.0E - 1	1.5E - 3	8.0E - 1
MN	25	5.6E - 1	1.5E - 1	5.0E - 2	2.9E - 1	4.0E - 4	5.0E - 2	3.5E - 4	6.5E - 2
FE	26	4.0E - 3	1.0E - 3	1.0E - 3	1.0E - 3	2.0E - 2	1.5E + 0	2.5E - 4	1.3E + 0
CO	27	8.1E - 2	4.0E - 2	7.0E - 3	3.7E - 3	2.0E - 2	5.0E - 1	2.0E - 3	1.0E - 1
NI	28	2.8E - 1	6.0E - 2	6.0E - 2	3.0E - 2	6.0E - 3	1.0E - 3	1.0E - 3	1.0E - 1
CU	29	4.0E - 1	2.5E - 1	2.5E - 1	2.5E - 1	1.0E - 2	5.1E - 1	1.5E - 3	4.9E - 1
ZN	30	1.4E + 0	5.9E - 1	9.0E - 1	1.3E + 0	1.0E - 1	6.5E + 0	1.0E - 2	2.6E + 0
GA	31	4.0E - 3	4.0E - 4	4.0E - 4	4.0E - 4	5.0E - 4	3.0E - 1	5.0E - 5	8.0E - 1
AS	33	4.0E - 2	6.0E - 3	6.0E - 3	6.0E - 3	2.0E - 3	8.3E - 1	6.0E - 5	8.0E - 1
SE	34	2.5E - 2	2.5E - 2	2.5E - 2	2.5E - 2	1.5E - 2	8.5E + 0	4.0E - 3	9.3E + 0
BR	35	1.5E + 0	1.5E + 0	1.5E + 0	1.5E + 0	2.5E - 2	4.0E - 3	2.0E - 2	1.6E + 0
KR	36	–	–	–	–	–	–	–	–
RB	37	1.5E - 1	7.0E - 2	7.0E - 2	7.0E - 2	1.5E - 2	2.0E + 0	1.0E - 2	3.0E + 0
SR	38	1.6E + 0	8.1E - 1	1.7E - 1	1.3E - 1	3.0E - 4	3.5E - 2	1.5E - 3	3.0E - 1
Y	39	1.5E - 2	6.0E - 3	6.0E - 3	6.0E - 3	3.0E - 4	1.0E - 2	2.0E - 5	2.0E - 3
ZR	40	2.0E - 3	5.0E - 4	5.0E - 4	5.0E - 4	5.5E - 3	6.4E - 5	3.0E - 5	1.9E - 4
NB	41	2.0E - 2	5.0E - 3	5.0E - 3	5.0E - 3	2.5E - 1	3.1E - 4	2.0E - 2	1.3E - 3
MO	42	2.5E - 1	6.0E - 2	6.0E - 2	6.0E - 2	6.0E - 3	1.9E - 1	1.5E - 3	7.8E - 1
TC	43	4.4E + 1	1.1E + 0	1.5E + 0	7.3E - 1	8.5E - 3	3.0E - 2	1.0E - 2	3.0E + 0
RU	44	5.2E - 1	2.0E - 2	2.0E - 2	5.0E - 3	2.0E - 3	7.0E - 3	6.0E - 7	6.0E - 3
RH	45	1.5E - 1	4.0E -2	4.0E - 2	4.0E - 2	2.0E - 3	5.0E - 1	1.0E - 2	1.0E - 1
PD	46	1.5E - 1	4.0E - 2	4.0E - 2	4.0E - 2	4.0E - 3	3.0E - 4	1.0E - 2	4.0E - 3
AG	47	2.7E - 4	1.3E - 3	8.0E - 4	1.0E - 1	3.0E - 3	5.0E - 1	2.0E - 2	5.0E - 1
CD	48	5.5E - 1	1.5E - 1	1.5E - 1	1.5E - 1	5.5E - 4	8.4E - 1	1.0E - 3	1.0E - 1
IN	49	4.0E - 3	4.0E - 4	4.0E - 4	4.0E - 4	8.0E - 3	3.0E - 1	1.0E - 4	8.0E - 1

Exhibit I.3. (contd)

Element	Number	Leafy Vegetable	Other Vegetable	Fruit –	Grain –	Beef day/kg	Poultry day/kg	Milk day/L	Egg day/kg
SN	50	3.0E - 2	6.0E - 3	6.0E - 3	6.0E - 3	8.0E - 2	2.0E - 1	1.0E - 3	8.0E - 1
SB	51	1.3E - 4	5.6E - 4	8.0E - 5	3.0E - 2	1.0E - 3	6.0E - 3	1.0E - 4	7.0E - 2
TE	52	2.5E - 2	4.0E - 3	4.0E - 3	4.0E - 3	1.5E - 2	8.5E - 2	2.0E - 4	5.2E + 0
I	53	3.4E - 3	5.0E - 2	5.0E - 2	5.0E - 2	7.0E - 3	1.8E - 2	1.0E - 2	2.8E + 0
XE	54	–	–	–	–	–	–	–	–
CS	55	1.3E - 1	4.9E - 2	2.2E - 1	2.6E - 2	2.0E - 2	4.4E + 0	7.0E - 3	4.9E - 1
BA	56	1.5E - 1	1.5E - 2	1.5E - 2	1.5E - 2	1.5E - 4	8.1E - 4	3.5E - 4	1.5E + 0
LA	57	5.7E - 4	6.4E - 4	4.0E - 3	4.0E - 3	3.0E - 4	1.0E - 1	2.0E - 5	9.0E - 3
CE	58	1.0E - 2	4.0E - 3	4.0E - 3	4.0E - 3	7.5E - 4	1.0E - 2	2.0E - 5	5.0E - 3
PR	59	1.0E - 2	4.0E - 3	4.0E - 3	4.0E - 3	3.0E - 4	3.0E - 2	2.0E - 5	5.0E - 3
ND	60	1.0E - 2	4.0E - 3	4.0E - 3	4.0E - 3	3.0E - 4	4.0E - 3	2.0E - 5	2.0E - 4
PM	61	1.0E - 2	4.0E - 3	4.0E - 3	4.0E - 3	5.0E - 3	2.0E - 3	2.0E - 5	2.0E - 2
SM	62	1.0E - 2	4.0E - 3	4.0E - 3	4.0E - 3	5.0E - 3	4.0E - 3	2.0E - 5	7.0E - 3
EU	63	1.0E - 2	4.0E - 3	4.0E - 3	4.0E - 3	5.0E - 3	4.0E - 3	2.0E - 5	7.0E - 3
GD	64	1.0E - 2	4.0E - 3	4.0E - 3	4.0E - 3	3.5E - 3	4.0E - 3	2.0E - 5	7.0E - 3
TB	65	1.0E - 2	4.0E - 3	4.0E - 3	4.0E - 3	4.5E - 3	4.0E - 3	2.0E - 5	7.0E - 3
DY	66	1.0E - 2	4.0E - 3	4.0E - 3	4.0E - 3	5.5E - 3	4.0E - 3	2.0E - 5	7.0E - 3
HO	67	1.0E - 2	4.0E -3	4.0E - 3	4.0E - 3	4.5E - 3	4.0E - 3	2.0E - 5	7.0E - 3
ER	68	1.0E - 2	4.0E - 3	4.0E - 3	4.0E - 3	4.0E - 3	4.0E - 3	2.0E - 5	7.0E - 3
HF	72	3.5E - 3	8.5E - 4	8.5E - 4	8.5E - 4	1.0E - 3	6.0E - 5	5.0E - 6	2.0E - 4
TA	73	1.0E - 2	2.5E - 3	2.5E - 3	2.5E - 3	6.0E - 4	3.0E - 4	3.0E - 6	1.0E - 3
W	74	4.5E - 2	1.0E - 2	1.0E - 2	1.0E - 2	4.5E - 2	2.0E - 1	3.0E - 4	8.0E - 1
RE	75	1.5E + 0	3.5E - 1	3.5E - 1	3.5E - 1	8.0E - 3	4.0E - 2	1.5E - 3	4.0E - 1
OS	76	1.5E - 2	3.5E - 3	3.5E - 3	3.5E - 3	4.0E - 1	1.0E - 1	5.0E - 3	9.0E - 2
IR	77	5.5E - 2	1.5E - 2	1.5E - 2	1.5E - 2	1.5E - 3	5.0E - 1	2.0E - 6	1.0E - 1
AU	79	4.0E - 1	1.0E - 1	1.0E - 1	1.0E - 1	8.0E - 3	5.0E - 1	5.5E - 6	5.0E - 1
HG	80	9.0E - 1	2.0E - 1	2.0E - 1	2.0E - 1	2.5E - 1	1.1E - 2	4.5E - 4	2.0E - 1
TL	81	4.0E - 3	4.0E - 4	4.0E - 4	4.0E - 4	4.0E - 2	3.0E - 1	2.0E - 3	8.0E - 1
PB	82	5.8E - 3	3.2E - 3	9.0E - 3	4.7E - 3	3.0E - 4	2.0E - 1	2.5E - 4	8.0E - 1
BI	83	3.5E - 2	5.0E - 3	5.0E - 3	5.0E - 3	4.0E - 4	1.0E - 1	5.0E - 4	8.0E - 1
PO	84	2.5E - 3	9.0E - 3	4.0E - 4	4.0E - 4	3.0E - 4	9.0E - 1	3.5E - 4	7.0E + 0
RN	86	–	–	–	–	–	–	–	–
RA	88	7.5E - 2	3.2E - 3	6.1E - 3	1.2E - 3	2.5E - 4	3.0E - 2	4.5E - 4	2.0E - 5
AC	89	3.5E - 3	3.5E - 4	3.5E - 4	3.5E - 4	2.5E - 5	4.0E - 3	2.0E - 5	2.0E - 3
TH	90	6.6E - 3	1.2E - 4	8.5E - 5	3.4E - 5	6.0E - 6	4.0E - 3	5.0E - 6	2.0E - 3
PA	91	2.5E - 3	2.5E - 4	2.5E - 4	2.5E - 4	1.0E - 5	4.0E - 3	5.0E - 6	2.0E - 3
U	92	1.7E - 2	1.4E - 2	4.0E - 3	1.3E - 3	2.0E - 4	1.2E + 0	6.0E - 4	9.9E - 1
NP	93	1.3E - 2	9.4E - 3	1.0E - 2	2.7E - 3	5.5E - 5	4.0E - 3	5.0E - 6	2.0E - 3

Exhibit I.3. (contd)

Element	Number	Leafy Vegetable	Other Vegetable	Fruit –	Grain –	Beef day/kg	Poultry day/kg	Milk day/L	Egg day/kg
PU	94	3.9E - 4	2.0E - 4	4.5E - 5	2.6E - 5	5.0E - 7	1.5E - 4	1.0E - 7	8.0E - 3
AM	95	5.8E - 4	4.1E - 4	2.5E - 4	5.9E - 5	3.5E - 6	2.0E - 4	4.0E - 7	9.0E - 3
CM	96	3.0E - 4	2.4E - 4	1.5E - 5	2.1E - 5	3.5E - 6	4.0E - 3	2.0E - 5	2.0E - 3
CF	98	1.0E - 2	1.0E - 2	1.0E - 2	1.0E - 2	5.0E - 3	4.0E - 3	7.5E - 7	2.0E - 3

(a) Concentration ratios for terrestrial foods are pCi/g (dry weight) of edible portions of plants per Pci/g (dry weight) of soil.
(b) Transfer factors for animal products are Ci/kg of edible flesh and eggs or Ci/L milk per Ci/day intake.

9417277.572

Exhibit I.4. Freshwater Fish Bioaccumulation Factors used with the GENII Code

Element	pCi/kg Fish per pCi/L Water
AC	330.0
AM	100.0
C	9000.0
I	50.0
NP	2500.0
NB	100.0
PA	30.0
RA	50.0
SE	1000.0
TH	100.0
TC	15.0
U	50.0

9413222.1573

Exhibit I.5. Default Parameters for the Driller Scenario

GR_PA/GENII Default Parameters (9/92-sfs) Driller

Inventory Parameters		
0.037, 3.7E4, 3.7E7, 3.7E10, 1.0	NVU	Source input conversion
10, 0.15, 224.0	SVU	Soil source conversion
Environmental Parameters		
0.008	ABSHUM	Absolute humidity (kg/m^3)
2	PRCNTI	Air dispersion conserv. flag
0.001	DPVRES	Deposition vel./resuspension
1.0E-9	LEAFRS	Leaf resuspension factor
2.0, 2.0, 3.0, 0.8, 0.8, 0.8, 1.0, 0.8, 1.0, 1.5	BIOMAS,	BIOMA2, Biomass (kg/m^2)
0.25	DEPFR2	Interception frac./irrigate
15.0	SURCM	Depth of surface soil (cm)
224.0	SLDN	Surface soil density (kg/m^2)
1.5E3	SSLDN	Soil density (kg/m^3)
True	HARVST	Harvest removal considered?
1.37	SOLING	Soil ingested (mg/da) *
14.0	WTIM	Weathering time (da)
1.0, 0.1, 0.1, 0.1	TRANS	Translocation, plants
0.1, 0.1, 0.1, 0.1, 1.0, 1.0	TRANSA	Translocation, animal food
68.0, 0.12, 55.0, 0.12, 68.0, 55.0	CONSUM	Animal Consumption (kg/da)
50.0, 0.3, 60., 0.3	DWATER	Animal drinking water (L/da)
0.0, 0.8, 1.0, 0.8	FRACUT	Acute fresh forage by season
0.2, 0.3, 0.5, 1.0	SHORWI	Shore width factors
0.02	INGWAT	Swim water ingested (L/hr)
25295.0	TCWS	H2O/sed. transfer ($L/m^2/yr$)
0.4, 5.0, 4.0	YELDBT	BIOT: Veg. prod. ($kg/m^2/yr$)
9.41E-4, 2*7.48E-4	TOTEXC	BIOT: Excavation (m^2/m^3-yr)
1.0, 0.81, 0.19, 0.02, 0.008, 0.002, 1.0, 0.9, 0.096, 0.006, 0.0005, 0.0005, 1.0, 0.9, 0.096, 0.006, 0.0005, 0.0005	EXCAV	BIOT: Frac. soil brought to the surface from within the waste by animal excavation

Exhibit I.5. (contd)

GR_PA/GENII Default Parameters (9/92-sfs) Driller

270.0	RINH	Chronic breathing (cm^3/sec)
330.0	RINHA	Acute breathing (cm^3/sec)
10	NDIST	Number of distances
805.0, 2414.0, 4023.0, 5632.0, 7241.0, 12068.0, 24135.0, 40255.0, 56315.0, 72405.0	X	JF/chi/Q/pop grid dist. (m)
0.1, 0.25, 6*0.18, 2*0.2	DRYFAC, DRYFA2	dry/wet ratio
Metabolic Parameters		
0.5, 50.0, 500.0	XDIV	
0.5, 0.5, 0.95, 0.05, 0.8, 0.0, 0.0, 0.2, 0.0, 0.1, 0.9, 0.5, 0.5, 0.15, 0.4, 0.4, 0.05, 0.0, 0.01, 0.99, 0.01, 0.99, 0.05, 0.4, 0.4, 0.135, 0.015	ADJ	
Dose Parameters		
0.25, 0.15, 0.12, 0.12, 0.03, 0.03, 5*0.06	WT	Weighting factors
2.0	SI2I	Semi-infinite/inf

Exhibit I.6. Default Parameters for the Post-Driller, Irrigated Farm, and River Scenarios

GR_PA/GENII Default Parameter Values (10/92-sfs) PD,IF,RV

Inventory Parameters		
0.037, 3.7E4, 3.7E7, 3.7E10, 1.0	NVU	Source input conversion
1.0, 0.15, 224.0	SVU	Soil source conversion
Environmental Parameters		
0.008	ABSHUM	Absolute humidity (kg/m^3)
2	PRCNTI	Air dispersion conserv. flag
0.001	DPVRES	Deposition vel./resuspension
1.0E-9	LEAFRS	Leaf resuspension factor
2.0, 2.0, 3.0, 0.8, 0.8, 0.8, 1.0, 0.8, 1.0, 1.5	BIOMAS	BIOMA2 Biomass (kg/m^2)
0.25	DEPFR2	Interception frac./irrigate
15.0	SURCM	Depth of surface soil (cm)
224.0	SLDN	Surface soil density (kg/m^2)
1.5E3	SSLDN	Soil density (kg/m^3)
True	HARVST	Harvest removal considered?
100.0	SOLING	Soil ingested (mg/da) *
14.0	WTIM	Weathering time (da)
1.0, 0.1, 0.1, 0.1	TRANS	Translocation, plants
0.1, 0.1, 0.1, 0.1, 1.0, 1.0	TRANSA	Translocation, animal food
68.0, 0.12, 55.0, 0.12, 68.0, 55.0	CONSUM	Animal Consumption (kg/da)
50.0, 0.3, 60., 0.3	DWATER	Animal drinking water (L/da)
0.0, 0.8, 1.0, 0.8	FRACUT	Acute fresh forage by season
0.2, 0.3, 0.5, 1.0	SHORWI	Shore width factors
0.02	INGWAT	Swim water ingested (L/hr)
25295.0	TCWS	H2O/sed. transfer (L/m^2/yr)
0.4, 5.0, 4.0	YELDBT	BIOT: Veg. prod. (kg/m^2/yr)
9.41E-4, 2*7.48E-4	TOTEXC	BIOT: Excavation (m^2/m^3-yr)
1.0, 0.81, 0.19, 0.02, 0.008, 0.002,1.0, 0.9, 0.096, 0.006, 0.0005, 0.0005,1.0, 0.9, 0.096, 0.006, 0.0005, 0.0005	EXCAV	BIOT: Frac. soil brought to surface from within the waste by animal excavation
270.0	RINH	Chronic breathing (cm^3/sec)

Exhibit I.6. (contd)

GR_PA/GENII Default Parameter Values (10/92-sfs) PD,IF,RV

330.0	RINHA	Acute breathing (cm^3/sec)
10	NDIST	Number of distances
805.0, 2414.0, 4023.0, 5632.0, 7241.0, 12068.0, 24135.0, 40255.0, 56315.0, 72405.0	X	JF/chi/Q/pop grid dist. (m)
0.1, 0.25, 6*0.18, 2*0.2	DRYFAC, DRYFA2	dry/wet ratio
Metabolic Parameters		
0.5, 50.0, 500.0	XDIV	
0.5, 0.5, 0.95, 0.05, 0.8, 0.0, 0.0, 0.2, 0.0, 0.1, 0.9, 0.5, 0.5, 0.15, 0.4, 0.4, 0.05, 0.0, 0.01, 0.99, 0.01, 0.99, 0.05, 0.4, 0.4, 0.135, 0.015	ADJ	
Dose Parameters		
0.25, 0.15, 0.12, 0.12, 0.03, 0.03, 5*0.06	WT	Weighting factors
2.0	SI2I	Semi-infinite/inf

References

American Society of Mechanical Engineers (ASME). 1986. *Quality Assurance Program Requirements for Nuclear Facilities*. ANSI/ASME NQA-1, ASME, New York, New York.

International Commission on Radiological Protection (ICRP). 1975. *Report on the Task Group on Reference Man*. ICRP Publication 23, Pergamon Press, New York.

International Commission on Radiological Protection (ICRP). 1977. *Recommendations of the International Commission on Radiological Protection*. ICRP Publication 26, Pergamon Press, New York.

International Commission on Radiological Protection (ICRP). 1979-1988. *Limits for Intakes of Radionuclides by Workers*. ICRP Publication 30, Parts 1-4 (and supplements), Vol. 2 (No. 3/4), Vol.4 (No. 3/4), Vol. 6 No. 2/3), Vol. 8 (No. 4), and Vol. 19 (No.4), Pergamon Press, Elmsford, New York.

International Commission on Radiological Protection (ICRP). 1986. *The Metabolism of Plutonium and Related Elements*. ICRP Publication 48, Vol. 16 (No. 2/3), Pergamon Press, New York.

International Union of Radioecologists (IUR). 1989. *Sixth Report of the Working Group on Soil-to-Plant Transfer Factors*. RIVM, Bilthoven, The Netherlands.

Kennedy, W. E., Jr. and D. L. Strenge. 1992. *Residual Radioactive Contamination from Decommissioning: Volume 1, Technical Basis for Translating Contamination Levels to Annual Effective Dose Equivalent*. NUREG/CR-5512, Pacific Northwest Laboratory, Richland, Washington.

Leigh, C. D., B. M. Thompson, J. E. Campbell, D. E. Longsine, R. A. Kennedy, and B. A. Napier. 1992. *User's Guide for GENII-S: A Code for Statistical and Deterministic Simulations of Radiation Doses to Humans from Radionuclides in the Environment*. SAND91-0561A, Sandia National Laboratories, Albuquerque, New Mexico.

Napier, B. A., R. A. Peloquin, D. L. Strenge, J. V. Ramsdell. 1988. *GENII - The Hanford Environmental Radiation Dosimetry Software System*. Vols. 1, 2, and 3. Pacific Northwest Laboratory, Richland, Washington.

Snyder, S. F., W. T. Farris, B. A. Napier, T. A. Ikenberry, J. C. Simpson. 1992. *Parameters Used in the Environmental Pathways (DESCARTES) and Radiological Dose (CIDER) Modules of the Hanford Environmental Dose Reconstruction Code (HEDRIC) for the Air Pathway*. PNWD-2023 HEDR, Battelle Pacific Northwest Laboratories, Richland, Washington.

U.S. Department of Energy (DOE). 1988a. *External Dose-Rate Conversion Factors for Calculation of Dose to the Public*. DOE/EH-0070, U.S. DOE, Assistant Secretary for Environment, Safety and Health, Washington, D.C.

U.S. Department of Energy (DOE). 1988b. *Internal Dose Conversion Factors for Calculation of Dose to the Public*. DOE/EH-0071, U.S. DOE, Assistant Secretary for Environment, Safety and Health, Washington, D.C.

Appendix J

Physical and Hydraulic Properties of Sediments and Engineered Materials Associated with Grouted Double-Shell Tank Waste Disposal at Hanford[a]

(a) This appendix is a reproduction of PNL-8813 (M. L. Rockhold, M. J. Fayer, and P. R. Heller. 1993. *Physical and Hydraulic Properties of Sediments and Engineered Materials Associated with Grouted Double-Shell Tank Waste Disposal at Hanford.* PNL-8813, Pacific Northwest Laboratory, Richland, Washington.

This page intentionally left blank.

WHC-SD-WM-EE-004. Rev. 0

PNL-8813
UC-510

9413222.1582

PHYSICAL AND HYDRAULIC PROPERTIES OF SEDIMENTS AND ENGINEERED MATERIALS ASSOCIATED WITH GROUTED DOUBLE-SHELL TANK WASTE DISPOSAL AT HANFORD

M. L. Rockhold
M. J. Fayer
P. R. Heller

September 1993

Prepared for
the U.S. Department of Energy
under Contract DE-AC06-76RLO 1830

Pacific Northwest Laboratory
Richland, Washington 99352

SUMMARY

Numerical models are used to predict the fate of contaminants in the environment for durations of 10,000 years and more. At the Hanford Site, these models are being used to evaluate the potential health effects and environmental impacts associated with the disposal of double-shell tank waste in grouted vaults. These models require information on the properties of the earthen and manufactured materials that compose the vault system and its surroundings. This report documents the physical and hydraulic properties of the materials associated with burial of grouted double-shell tank waste at the Hanford Site.

A conceptual model of the grout site and engineered structures was used to identify those materials that are, in a first-order sense, dominant controllers of the flow and transport regime. These materials are the Hanford formation sandy sequence, Hanford formation lower gravels, Ringold Formation, backfill soil, gravel, asphalt, concrete, clay cap, and the grouted waste form itself. The published physical and hydraulic data for these materials were identified. If unpublished but available, the data were included in this report. If data were non-existent, estimates were provided along with the rationale for the estimates.

In numerical flow and transport models, the hydraulic properties of porous media are represented by mathematical functions. For the grout performanee assessment, the chosen functions were the van Genuchten water retention function and the Mualem hydraulic conductivity function. The parameters in these functions were fitted to the data provided in the Appendix or taken from other publications. For each material in the conceptual model, parameter values were assigned for use in the performance assessment models. For some materials, the number of samples allowed for calculation of means and variances of the parameters. For other materials, the parameters were determined from only one sample. Recommendations are provided for future data collection and parameter estimation. What is needed most is a program dedicated to identifying the important materials, identifying the conditions to which those materials will be subjected, and measuring the properties under

those conditions. Creating a research program now would ensure that the appropriate hydraulic models are identified and parameters for simulations are obtained in a timely fashion.

9413222.1981

ACKNOWLEDGMENTS

This work was conducted by the Pacific Northwest Laboratory (PNL) in collaboration with Westinghouse Hanford Company (WHC) for the U. S. Department of Energy. We would like to thank Andy Felmy for estimating water activities for grout and concrete using the GMIN computer code and Charley Kincaid and Gary Streile for providing technical review comments.

9413222.1585

CONTENTS

SUMMARY iii

ACKNOWLEDGMENTS v

1.0 INTRODUCTION 1.1

2.0 MATERIAL IDENTIFICATION 2.1

2.1 STRATIGRAPHIC SECTION 2.1

2.2 CONCEPTUAL MODEL 2.1

2.2.1 Hanford Formation Sandy Sequence 2.1

2.2.2 Hanford Formation Lower Gravels 2.4

2.2.3 Ringold Formation 2.5

2.2.4 Backfill Soil 2.5

2.2.5 Gravel 2.5

2.2.6 Clay 2.6

2.2.7 Asphalt 2.6

2.2.8 Concrete 2.6

2.2.9 Grout 2.7

3.0 MEASUREMENTS AND ESTIMATES OF PROPERTIES 3.1

3.1 METHODS 3.1

3.1.1 Particle Size Distribution 3.1

3.1.2 Particle Density 3.2

3.1.3 Bulk Density 3.2

3.1.4 Total Porosity 3.2

3.1.5 Water Retention 3.2

3.1.6 Saturated Hydraulic Conductivity 3.9

3.2 RESULTS 3.11

3.2.1 Hanford Formation Sandy Sequence 3.11

3.2.2 Hanford Formation Lower Gravels 3.12

3.2.3 Ringold Formation 3.12

3.2.4 Backfill Soil 3.12

3.2.5 Gravel 3.13

3.2.6 Clay 3.13

3.2.7 Asphalt 3.14

3.2.8 Concrete 3.15

3.2.9 Grout 3.15

4.0 HYDRAULIC PARAMETERS 4.1

4.1 HYDRAULIC FUNCTIONS 4.1

4.2 PARAMETER ESTIMATION PROCEDURE 4.2

4.3 CORRECTIONS FOR GRAVEL CONTENT 4.3

4.4 PARAMETER SUMMARY 4.4

5.0 DISCUSSION 5.1

5.1 METHODS 5.1

5.2 BULK DENSITY 5.3

5.3 HYDRAULIC CONDUCTIVITY 5.3

5.4 GRAVEL CONTENT 5.4

5.5 SPATIAL VARIABILITY 5.5

5.6 HYSTERESIS 5.6

5.7 ANISOTROPY 5.6

5.8 TEMPERATURE AND SOLUTE EFFECTS 5.7

5.9 GEOCHEMISTRY 5.9

5.10 DEGRADATION 5.10

6.0 REFERENCES 6.1

APPENDIX - PHYSICAL AND HYDRAULIC PROPERTY DATA A.1

9413222.1588

FIGURES

2.1 Relative Locations of the Grout Treatment Facility and Characterization Wells Around the 200 East Area 2.2

2.2 Sediment Stratigraphy in the Vicinity of the Grout Site 2.3

2.3 Conceptual Model of Vertical Cross Section Through a Grout Vault and Underlying Sediment Stratigraphy 2.4

3.1 Schematic of Apparatus Used to Measure Water Retention by the Hanging Water Column Method 3.5

3.2 Schematic of Apparatus Used to Measure Water Retention by the Pressure-Plate Method 3.6

3.3 Schematic of Apparatus Used to Measure Saturated Hydraulic Conductivity by the Falling-Head Method 3.10

4.1 Average Water Retention and Hydraulic Conductivity Curves 4.6

A.1 Water Retention and Hydraulic Conductivity Data and Curves for Samples 5A, 5B, 19A, and 19B from Well No. 299-E25-234 . . . . . A.16

A.2 Water Retention and Hydraulic Conductivity Data and Curves for Samples 25A, 25B, 25C, and 25D from Well No. 299-E25-234 . . . . . A.17

A.3 Water Retention and Hydraulic Conductivity Data and Curves for Samples 29A, 29B, 37A, and 37B from Well No. 299-E25-234 . . . . . A.18

A.4 Water Retention and Hydraulic Conductivity Data and Curves for Samples 46A, 46B, 54A, and 54B from Well No. 299-E25-234 . . . . . A.19

A.5 Water Retention and Hydraulic Conductivity Data and Curves for Samples 69A, 69B, 83A, and 83B from Well No. 299-E25-234 . . . . . A.20

A.6 Water Retention and Hydraulic Conductivity Data and Curves for Samples 99A, 99B, 110A, and 110B from Well No. 299-E25-234 . . . . . A.21

A.7 Water Retention and Hydraulic Conductivity Data and Curves for Samples 117A, 117B, 126A, and 126B from Well No. 299-E25-234 ..... A.22

A.8 Water Retention and Hydraulic Conductivity Data and Curves for Samples 133A and 133B from Well No. 299-E25-234 ..... A.23

A.9 Water Retention and Hydraulic Conductivity Data and Curves for Backfill Soil A.24

A.10 Water Retention and Hydraulic Conductivity Data and Curves for Gravel A.24

A.11 Water Retention and Hydraulic Conductivity Data and Curves for RCRA Clay Cap A.25

A.12 Water Retention and Hydraulic Conductivity Data and Curves for Concrete Samples CL-40A, CL-40B, CL-40C, and CL-40D A.26

A.13 Water Retention and Hydraulic Conductivity Data and Curves for Concrete Samples CL-40E and CL-40F A.27

A.14 Water Retention and Hydraulic Conductivity Data and Curves for DSSF Grout Samples A26, A38, A73, and B06 ..... A.28

A.15 Water Retention and Hydraulic Conductivity Data and Curves for DSSF Grout Samples B33, B52, C16, and C48 ..... A.29

A.16 Water Retention and Hydraulic Conductivity Data and Curves for DSSF Grout Sample C82 ..... A.30

9413222.1590

TABLES

4.1 Average Water Retention Parameters and Vertical Saturated Hydraulic Conductivity Values Used for Grout Vadose Zone Flow and Transport Modeling 4.5

A.1 Particle-Size Distribution Data for Sediment Samples from Well No. 299-E25-234 ..... A.1

A.2 Bulk and Particle Density Data for Samples from Well No. 299-E25-234 ..... A.5

A.3 Particle Size Distribution and Water Retention Data for Backfill Soil A.6

A.4 Water Retention Data for Gravel A.6

A.5 Water Retention Data for Clay A.7

A.6 Bulk and Particle Density and Saturated Hydraulic Conductivity Data for Concrete A.7

A.7 Water Retention Data for Concrete A.8

A.8 Bulk and Particle Density and Saturated Hydraulic Conductivity Data for DSSF Grout Samples from the 14 November 1988 Adiabatic Pilot-Scale Test A.9

A.9 Water Retention Data for DSSF Grout A.10

A.10 Water Retention Parameters and Saturated Hydraulic Conductivity Data for the Sandy Sequence of the Hanford Formation A.12

A.11 Water Retention Parameters and Saturated Hydraulic Conductivity Data for the Upper and Lower Gravel Units of the Hanford Formation A.14

A.12 Water Retention Parameters and Saturated Hydraulic Conductivity Data for the Ringold Formation A.14

A.13 Water Retention Parameters and Saturated Hydraulic Conductivity Data for Concrete A.15

A.14 Water Retention Parameters and Saturated Hydraulic Conductivity Data for DSSF Grout A.15

9413222.592

1.0 INTRODUCTION

At the Hanford Site in south-central Washington State, numerical models are being used in a performance assessment to evaluate the potential health effects and environmental impacts associated with the disposal of double-shell tank waste in grouted vaults. These models require information on the properties of the earthen and manufactured materials that compose the vault system and its surroundings. The data and parameter estimates contained in this report support the unsaturated flow and contaminant transport modeling studies and sensitivity analyses for the Hanford Grout Technology Program (HGTP) Performance Assessment (PA) Task. This work was conducted for the U.S. Department of Energy by Pacific Northwest Laboratory (PNL)[a] in collaboration with Westinghouse Hanford Company (WHC).

9413222.1593

The two purposes of this report are to identify the significant materials and sediments that govern the movement of water and contaminants in and around the proposed Grout Treatment Facility (GTF) and to estimate the parameters that describe the hydraulic properties of those materials. The data supporting the parameter estimate came from three sources: published reports, laboratory record books, or estimates. The published data and parameters are referenced in this report. All unpublished data and estimated parameters are included in this report as an appendix.

This report is organized as follows. Section 2 describes the grout site and sediment sample locations at Hanford, the general sediment stratigraphy at the grout site, and the operative conceptual model of a buried grout vault. Section 3 describes the methods used to determine physical and hydraulic properties and identifies the data sources (if the data are not reported here). Section 4 describes the parameter estimation procedures and identifies the average hydraulic parameters to be used in the grout PA simulations. Section 5 discusses the data and assumptions to be used for

(a) Operated for the U.S. Department of Energy by Battelle Memorial Institute under contract DE–AC06–76RLO 1830.

unsaturated flow modeling. The Appendix contains the physical and hydraulic property data that have not been reported elsewhere, as well as the hydraulic parameters for all samples used to describe the average hydraulic properties of each material.

9413222.1594

2.0 MATERIAL IDENTIFICATION

The purpose of this section is to identify the sediments and engineered materials composing the grout disposal system that are important to the system's performance regarding the release of contaminants. Figure 2.1 shows the position of the GTF within the 200 East Area of the Hanford Site. The hydrogeology of the 200 East Area is summarized by Cushing (1992).

2.1 STRATIGRAPHIC SECTION

The available well logs and sediment sample analyses were reviewed to identify the dominant sediment features at the GTF. Figure 2.1 shows the locations of these wells and sediment samples relative to the GTF. Figure 2.2 shows the stratigraphy at the GTF. Based on that information, a general stratigraphy of the GTF was developed. Underlying the Ringold Formation (Figure 2.2) is the Elephant Mountain Member. The permeability of this basalt member is much lower than that for the overlying sediments and the member was therefore considered to be impermeable. For that reason, the Elephant Mountain Member was not considered part of the hydrologic system at the GTF and was not evaluated for this report.

2.2 CONCEPTUAL MODEL

Figure 2.3 shows the current conceptual model of a grout vault at the GTF. Each material type is briefly described below.

2.2.1 Hanford Formation Sandy Sequence

The sandy sequence of the Hanford formation is a coarse-to-fine-grained sand unit that averages 60-m thick in the 200 East Area. Information representing the sandy sequence was derived from 28 samples collected from well No. 299-E25-234, 5 samples from the 241 AP Tank Farm Facility, 21 samples from the U.S. Ecology site, 3 samples from the 200-BP-1 site, and 3 measurements at the bottom of the existing grout pit (Dames and Moore 1988).

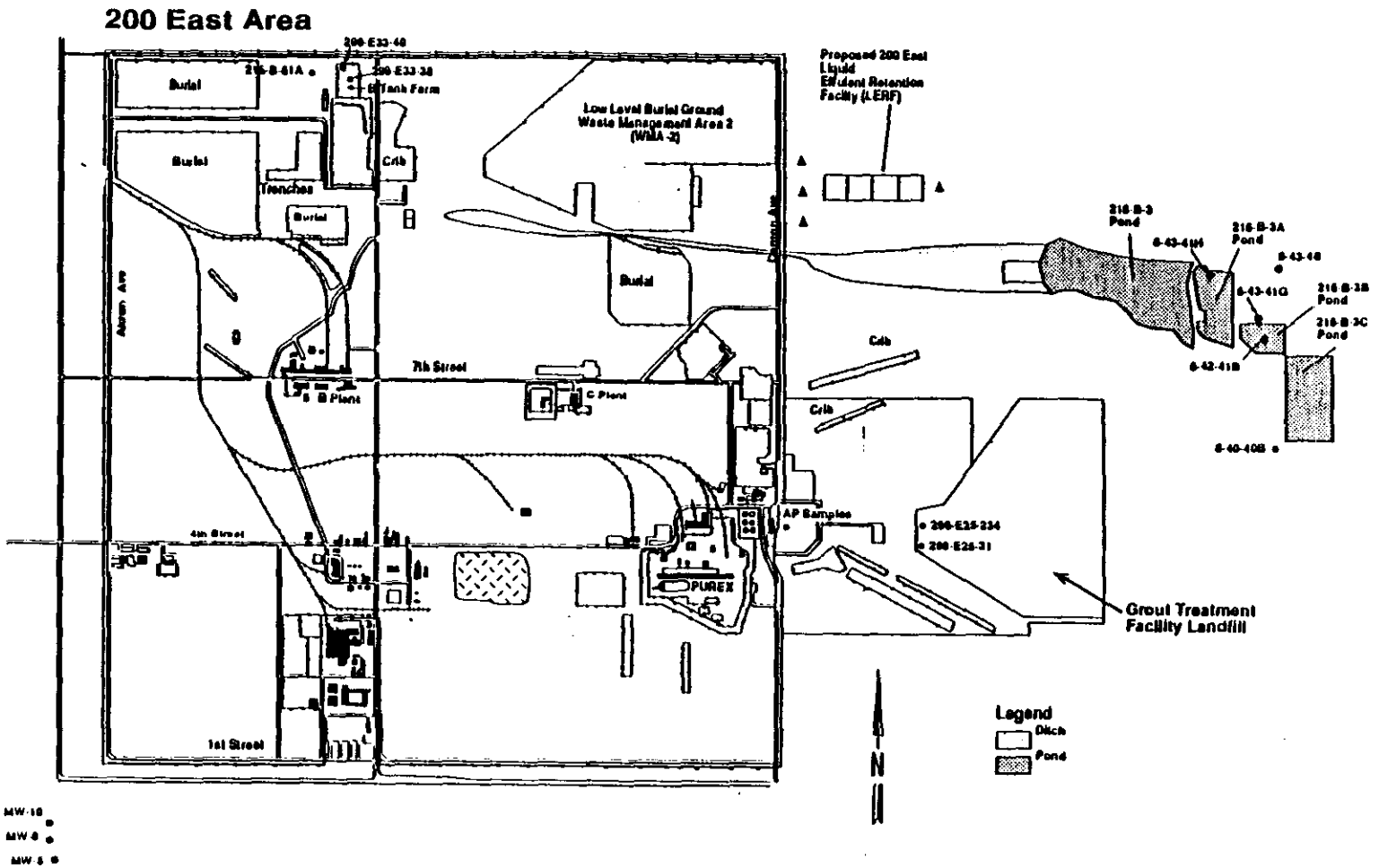

FIGURE 2.1. Relative Locations of the Grout Treatment Facility and Characterization Wells Around the 200 East Area (some sample locations were identified from Connelly et al. 1992b). Sample locations are identified by closed-circle symbols.

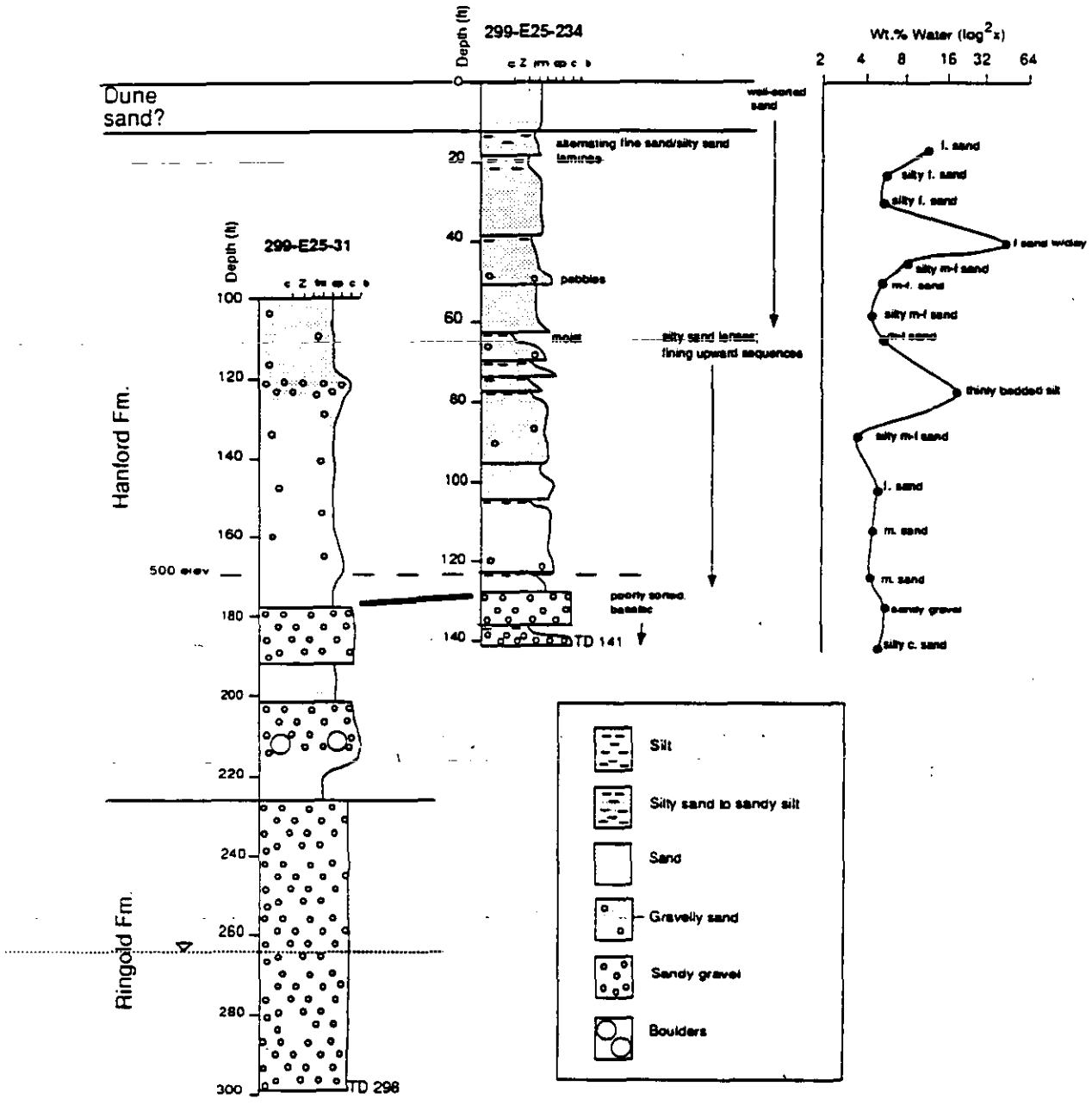

FIGURE 2.2. Sediment Stratigraphy in the Vicinity of the Grout Site

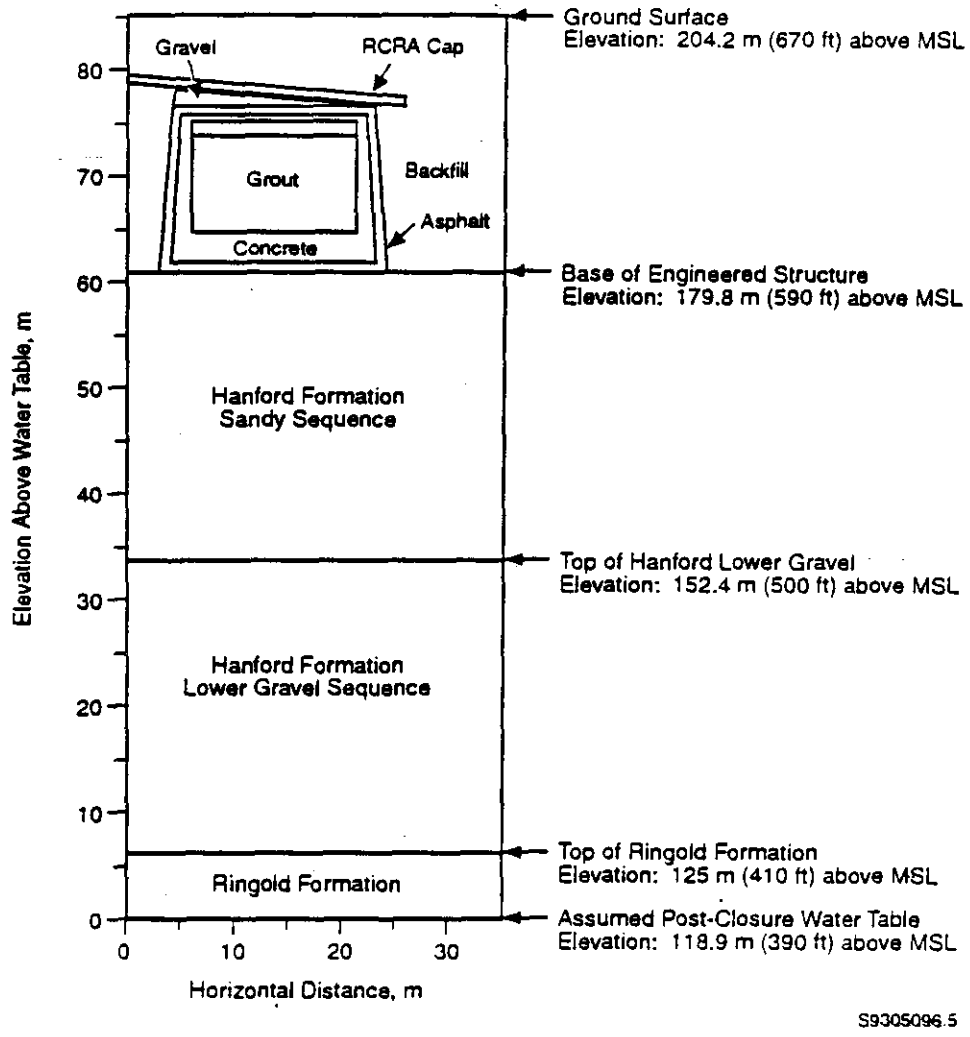

FIGURE 2.3. Conceptual Model of Vertical Cross Section Through a Grout Vault and Underlying Sediment Stratigraphy (MSL = Mean Sea Level)

2.2.2 Hanford Formation Lower Gravels

This material is a pebbly, very coarse sand-to-sandy gravel, about 10 m thick, that overlies the Ringold Formation. Inform ate' representing the lower gravels was derived from two samples that were obtained from well No. 299-E25-234, eight samples from the 200-BP-1 site, two samples from B Pond, and two samples from the U.S. Ecology site. Some of the samples were from the upper

gravel sequence of the Hanford formation, which is absent in the vicinity of the GTF. The upper and lower gravel sequences of the Hanford formation are texturally similar and more or less indistinguishable from each other except for stratigraphic position (Connelly et al. 1992a, 1992b).

2.2.3 Ringold Formation

The Ringold Formation averages 30 m thick and consists of well-rounded pebble- to cobble-size gravel with a matrix of sand, silt, and some clay. The Ringold Formation is variably indurated and consolidated, ranging from well-cemented conglomerate to open-work uncemented gravel. Information representing the Ringold Formation was obtained from four samples from B Pond and one sample from the U.S. Ecology site. No samples of the Ringold Formation beneath the GTF were available.

2.2.4 Backfill Soil

During construction, the Hanford formation sandy sequence will be excavated to depths of 20 m. This material will be stockpiled and then used to backfill around the vaults when the vaults are completed. Because the sediments will be somewhat mixed, retaining none of the in situ layering, and because it will be compacted to specifications, the backfill material was considered to be a unique and important material.

The material used to represent the backfill soil was obtained from a stockpile of sand that was excavated during construction of the grout pit. The material was sieved so that only the <2-mm size fraction was used to determine hydraulic properties. The resulting particle size distribution was 91% sand, 3% silt, and 6% clay.

2.2.5 Gravel

Gravel will serve as the drainage layer (not shown in Figure 2.3) in the collection basin beneath the grout. Gravel will also be formed into a sloped capillary barrier above the vault, serving to

redirect downward-flowing water to the region beyond the sides of the vault where it can drain freely without impacting the vault contents. Several gravel sizes will be used as filters and drains. No samples of the actual gravel that will be used were available. As a surrogate for whatever gravel is used, a gravel sample was prepared from 0.5-in.- (1.3-cm-) diameter chipped gravel that was wet sieved through an 8-mm sieve and retained on a 3.962-mm sieve. This procedure left a clean gravel material (i.e., clean in that it was free of fine materials like sands, silts, and clays).

2.2.6 Clay

A compacted clay layer will be used to satisfy the Resource Conservation and Recovery Act (RCRA) requirement for a compacted clay cap over the disposal site. The clay layer will be sloped to divert percolating water away from the vault. The material that was used to represent the RCRA clay cap was a 1:3 mixture of bentonite and Warden silt loam. This silt loam was obtained from the McGee Ranch, which is located on the west side of the Hanford Site, adjacent to the Yakima barricade.

2.2.7 Asphalt

Asphalt will surround the grout vault and, being nearly impermeable, will serve as a barrier to water flow and contaminant diffusion. No samples of asphalt were available for testing.

2.2.8 Concrete

Concrete will be used to create a structure, or vault, into which the contaminant-grout mixture can be poured, cured, and stored. A sample of concrete was obtained by PNL in 1984 from Sandia National Laboratories, who had obtained the concrete from the U.S. Army Waterways Experiment Station. The sample was a cylinder that was 15 cm long and 7.5 cm in diameter. Six subsamples were cut from the original sample and analyzed for hydraulic properties. Because these data were readily available, they were used to represent the hydraulic properties of the concrete used at the GTF.

2.2.9 Grout

Grout is a stabilizing agent used to improve the structural properties or reduce the permeability of earthen materials. For the current grout PA, wastes from the double-shell tanks will be processed into a grout; the resulting mixture is called double-shell slurry feed (DSSF) grout.

On 14 November 1988 a pilot-scale test was conducted to determine physical and chemical characteristics of a single formulation of DSSF grout. That formulation was a blend of (by weight) 47% blast furnace slag, 47% fly ash, and 6% type I/II Portland cement (Lokken et al. 1992a). Core samples were obtained and tested to obtain physical and hydraulic data. Simulated wastes with the same formulation used for the pilot-scale test were generated for durability studies (Lokken et al. 1992b). Information from the durability studies was used to supplement data from the core samples.

3.0 MEASUREMENTS AND ESTIMATES OF PROPERTIES

Measurements of physical and hydraulic properties are needed to determine the hydraulic property parameters for the materials that comprise the conceptual model in Figure 2.3. In lieu of measurements, reasonable estimates of the properties are required. This section summarizes the methods and results.

3.1 METHODS

The methods described below were used to measure or estimate the physical and hydraulic properties reported in the Appendix and by Smoot et al. (1989).

3.1.1 Particle Size Distribution

The distribution of particle sizes is one of the basic (and commonly the only) measures of the physical properties of the sediment. Generally, the sample is sieved to remove those particles greater than 2 mm in diameter before further testing is conducted. The particles removed are categorized as gravel. The percentage of the total sample that is gravel is rarely reported although, for the sediments at the Hanford Site, the percentages can be quite high.

Ideally, the distribution of particle sizes below 2 mm in diameter is not used directly to calculate hydraulic parameters. Rather, the distribution is used to qualitatively classify sediments into categories known as textures, such as clay or sand. If other data are lacking, however, these classifications can be used to infer hydraulic properties based on the hydraulic properties of sediments with similar texture.

The two procedures used to determine particle size distribution were those of the American Society for Testing and Materials (ASTM) (1985) and Gee and Bauder (1986). Approximately 50 g

of material that passed a 2-mm sieve was used with the hydrometer method and wet sieving to measure the distribution over the full range of sizes below 2 mm.

3.1.2 Particle Density

The density of particles (ρ_s) was determined using the pycnometer method (Blake and Hartge 1986a). About 10 g of the material less than 2 mm in diameter was used. Although significant gravel percentages were measured in some sediment samples, the density of the gravel was not determined.

3.1.3 Bulk Density

The dry bulk density (ρ_b) of a porous medium is the ratio of its oven-dried mass to its total volume. The bulk densities of the materials described in this report were determined using the method outlined by Blake and Hartge (1986b).

3.1.4 Total Porosity

The total porosity (ϕ_t) of a porous material is a measure of the relative volume of pores capable of filling with water and/or air. Total porosity can be calculated from particle and bulk densities according to the equation (Hillel 1982):

$$\phi_t = 1 - \rho_b/\rho_s \tag{3.1}$$

The total porosity of all the engineered materials described in this report was determined using Equation (3.1).

3.1.5 Water Retention

Four different methods were used to determine water retention data over the full range of matric potentials from fully saturated to residual (irreducible) saturation. In all cases, the

measurements were conducted on drained or draining samples. No measurements were made as the samples were wetted, which would have documented the extent of hysteresis.

The methods used were 1) the hanging water column method (Klute 1986), 2) a column method, 3) the pressure-plate extraction method (Klute 1986), and 4) the vapor equilibrium (or thermocouple psychrometer) method (Rawlins and Campbell 1986). When possible, undisturbed samples that retained the in situ structure were obtained. Most of the samples, however, were disturbed (i.e., did not retain their in situ structure); to conduct the tests, these samples were packed to known densities. Water retention varies more between disturbed and undisturbed samples when matric potentials are near zero.

Water retention is the relationship between the water content and the matric potential of a porous medium. The total potential (h_t) of the water in a sample is commonly expressed as the sum of the individual water-potential components as follows (Hillel 1982) :

$$h_t = h_{os} + h + h_g + h_p \tag{3.2}$$

where h_{os} = osmotic potential,

h = matric potential,

h_g = gravitational potential,

h_p = pressure potential.

The osmotic potential represents the attractive forces of water to locations of higher solute concentration. The matric potential represents the capillary and adsorptive forces that attract and bind water to the soil matrix. The gravitational potential is the energy associated with the location of water in the earth's gravitational field, measured with respect to some reference level such as the soil surface or the water table. The pressure potential represents external pressure forces, such as the weight of ponded water.

The application of this total potential concept to soil water equilibrium and transport is not exact because the osmotic potential applies only to the water, and the other components apply to the soil solution (Corey and Klute 1985; Sposito 1986). It is commonly assumed, however, that the osmotic component of the total water potential has only a negligible effect on the transport of water in soil, especially considering the absence of a differentially permeable membrane in the water flow path (Taylor and Ashcroft 1972; Hillel 1982). Exceptions to the assumption of negligible osmotic potentials for grout and concrete are noted later in this report.

9413222.1605

3.1.5.1 Hanging Water Column

Water retention was measured in the 0- to -150-cm range of matric potential using the hanging water column method. Figure 3.1 shows a typical hanging water column apparatus. The soil sample was placed on the porous plate, saturated, then allowed to drain until hydraulic equilibrium was established between the soil water and the water in the reference system. The reference elevation was the soil-plate interface. With that reference, the matric potential of the soil water at the bottom of the sample was equivalent to the negative of the distance (Z_1) between the outflow point and the plate.

Decreasing matric potentials were obtained by increasing the distance Z_1. After equilibrium was established following a decrease in potential, outflow volumes were measured. After equilibrium was achieved following the final decrease in potential, the final volumetric water content was measured and used to calculate the water contents at the intermediate potentials. If the sample was undisturbed (i.e., not packed), the bulk density was also determined.

3.1.5.2 Column Method

A column method was used to measure retention in the matric potential range from 0 to -100 cm (or more, depending on column length) for the backfill material and the gravel. Two Plexiglass columns, composed of short lengths and taped together, were filled with one of the materials. The columns were saturated and then allowed to drain. Following the cessation of drainage, the

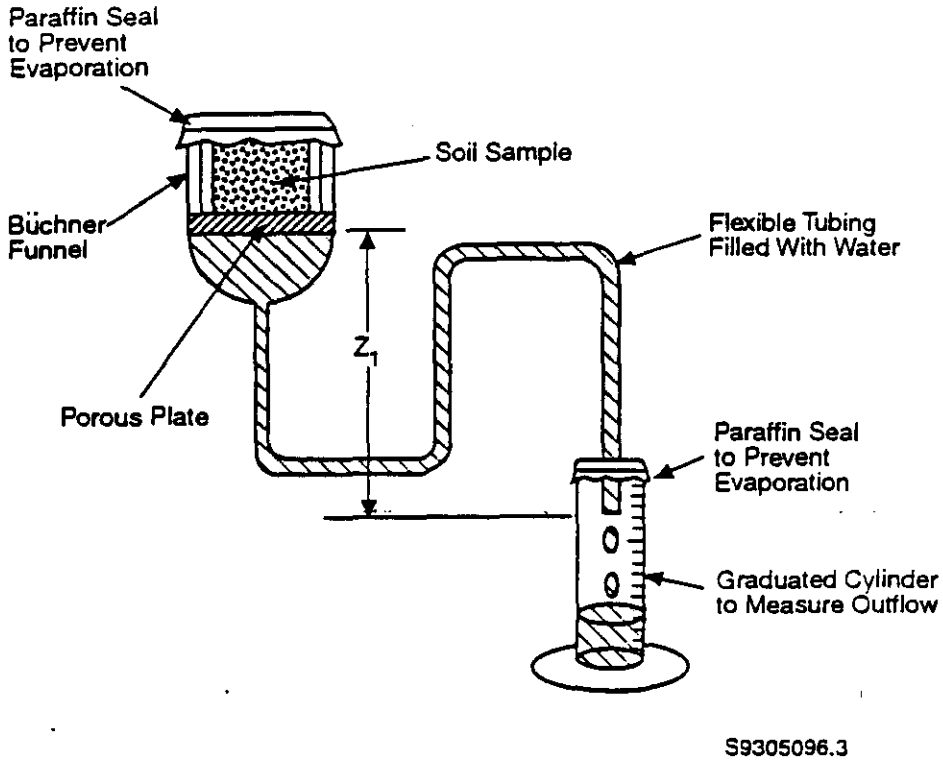

FIGURE 3.1. Schematic of Apparatus Used to Measure Water Retention by the Hanging Water Column Method

columns were sectioned to determine water contents along their length. The matric potentials in each section were ascribed to the negative of the distance from the section midpoint to the drain, assuming the column was in equilibrium with the drain.

3.1.5.3 Pressure-Plate Extraction Method

Water retention was measured in the -310- to -15,300-cm range of matric potential using two variations of the pressure-plate extraction method. Figure 3.2 shows the typical extraction method in which multiple samples are simultaneously subjected to the same pressure force, one pressure increment at a time. The samples and porous plate were saturated, the pressure vessel sealed, the internal pressure raised to a predetermined level, and the samples allowed to equilibrate at the new pressure.

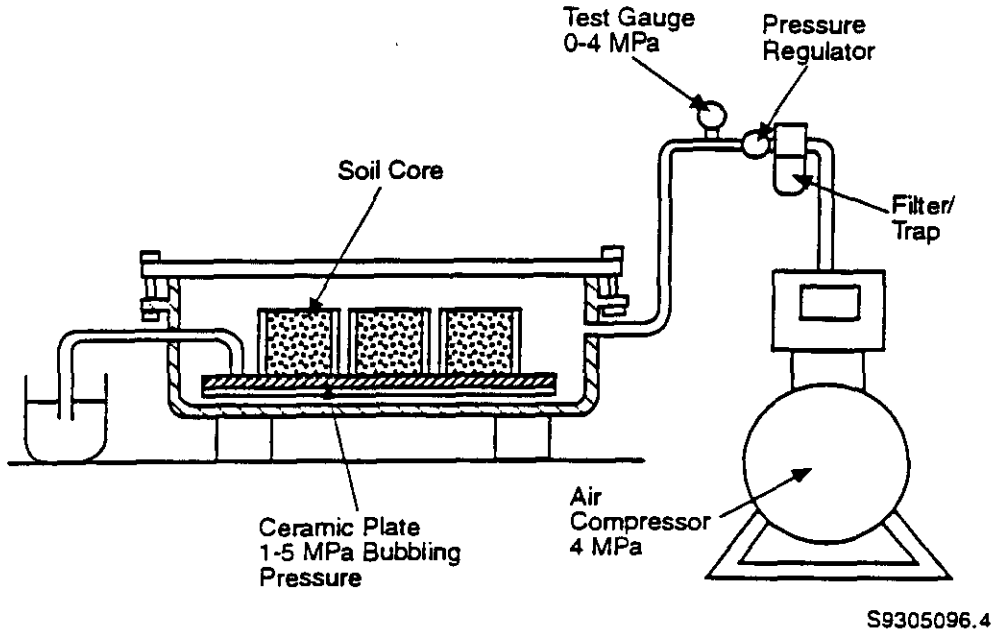

FIGURE 3.2. Schematic of Apparatus Used to Measure Water Retention by the Pressure-Plate Method

After the samples equilibrated, the pressure vessel was opened and the samples were weighed to determine gravimetric water contents. These water contents were converted to volumetric values by multiplying by the bulk density of the material.

A variation of the pressure-plate extraction method, the Tempe cell, was used and allowed an individual sample to be subjected to multiple pressures before the vessel was opened. The change in weight between each step increase in pressure determined the water content after the final water content was measured.

3.1.5.4 Vapor Equilibrium Method

Water retention was measured at all matric potentials less than -15,300 cm using the vapor equilibrium method. Water retention was also measured with this method at potentials up to

-1,000 cm, although the sensitivity of this method in that potential range is not as great (e.g., relative humidity varies from approximately 1.0 at -1,000 cm to 0.989 at -15,300 cm). The matric potential of water in a porous material can be calculated from measurements of the vapor phase in equilibrium with the liquid in the pores. When the vapor phase is represented by the relative humidity (p/p^*), the total potential (assuming h_p and h_g are zero) is:

$$h_t = (RT / M) \ln (p/p^*) \tag{3.3}$$

where M = molecular weight of water (0.01802 kg mol^{-1}),

R = ideal gas constant (8.3143 x 10^{-3} kg MPa mol^{-1} K^{-1}),

T = Kelvin temperature of the liquid phase (°C + 273.16),

p = water vapor pressure in equilibrium with the liquid phase,

p^* = saturated water vapor pressure at temperature T.

If the osmotic potential is negligible, the matric potential is equivalent to the total potential in Equation (3.3). When the osmotic potential is significant, the matric potential is calculated as the difference between the total and osmotic potentials. The osmotic potential of a solution (outside the porous medium) is calculated by determining the water activity (A_w) based on the total ionic concentration of the solution, and then applying an equation similar to Equation (3.3), where p/p^* and h_t are replaced with A_w and h_{os}, respectively.

The vapor equilibrium tests were conducted using a commercially available instrument (either the SC-10 or CX-1 Water Activity Meter, Decagon Devices, Inc., Pullman, WA 99163) or several saturated salt solutions with known vapor pressures. Because vapor adsorption is relatively independent of bulk density, no attempt was made to pack the samples to a specific density.

The SC-10 uses a thermocouple psychrometer to measure the wet-bulb depression in a closed chamber containing a soil sample. The CX-1 uses a cooled mirror to measure the dewpoint

temperature. The saturated salt solutions used were LiCl, $MgCl_2$, and $Mg(NO_3)_2$. These solutions yielded relative humidities (and corresponding matric potentials in MPa) of 11.3% (-300), 32.8% (-153), and 52.9% (-87.6), respectively, at a temperature of 25°C (Greenspan 1977).

The salt content of the pore water solutions of the sediments in the vicinity of the grout test facility were unknown. Murphy et al. (1991) reported ionic concentrations for six of the major surface soils at the Hanford Site. The low concentrations (e.g., for K^+, 100 μg/g soil for two different sands) suggested that osmotic potential would not significantly affect the measurement of total potential using the vapor equilibrium method. Therefore, the matric potentials for the sediment samples were assumed to be equal to the measured total potentials.

Total pore solution concentrations of 12 ions in six samples of simulated DSSF grout ranged from 315 to 410 g/L and the solution pH values were greater than 13 (Lokken et al. 1992b). These high salt concentrations suggested that the osmotic potential of this grout was significant. Likewise, data for the aqueous phase of concrete suggested that this material could also have a significant osmotic potential (Bailey and Hampsen 1982; Angus and Glasser 1985; Reardon 1990).

Osmotic potentials for the grout and concrete were calculated from solution chemistry data using the GMIN chemical equilibrium model (Felmy 1990), and Equation (3.3). The GMIN model was used to estimate the activity of water with multiple solutes in the pore waters of the materials. The mathematical algorithm in GMIN is based on a constrained minimization of the Gibbs free energy. The excess free energy in the aqueous phase (as indicated by the activity coefficient) is represented using the equations developed by Pitzer (1973; 1979), and parameters from Harvie et al. (1984) that are valid for solutions with high ionic strengths.

3.1.6 Saturated Hydraulic Conductivity

Laboratory measurements of the saturated hydraulic conductivity (K_s) of a porous medium are based on the application of the Darcy flow equation to a sample of uniform cross-sectional area. Two different methods were used to determine K_s for the materials in this study. For the majority of materials, the falling-head method was used. For the high-permeability materials such as the coarse sands and gravels, a constant head method was used. For the low-permeability materials such as the grout and concrete, a modified constant-head method was used.

3.1.6.1 Falling-Head Method

Figure 3.3 is a schematic representation of the apparatus used for measuring K_s by the falling-head method (Klute and Dirksen 1986). The calculation of K_s is as follows:

$$K_s = (aL/At)\ln(H_1/H_2) \tag{3.4}$$

where a = cross-sectional area of the standpipe,

L = length of the sample,

A = cross-sectional area of the sample,

t = time required for the head difference to decrease from H_1 to H_2,

H_1, H_2 = initial and final hydraulic head differences, respectively.

3.1.6.2 Constant Head Method

In the constant head method, the apparatus is similar to that in Figure 3.3. The difference is that the head at the inflow port is held constant at H_2 and the volume of outflow is measured. The calculation of K_s is as follows:

$$K_s = VL / (A\ t\ H_2) \tag{3.5}$$

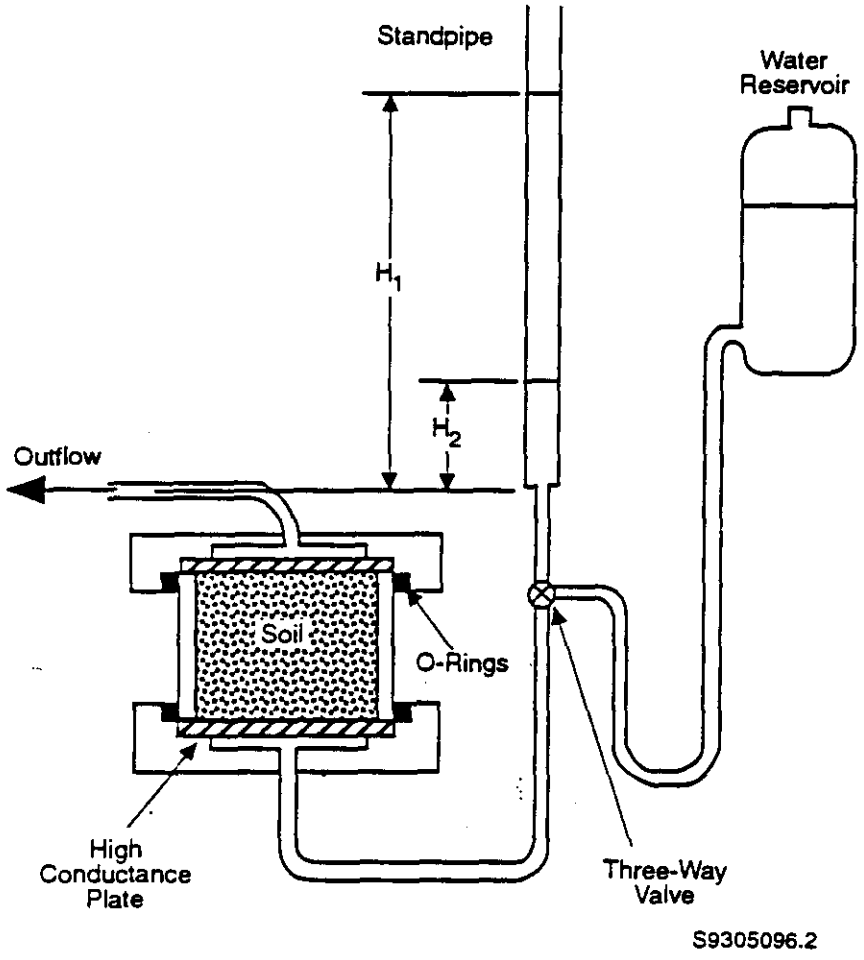

FIGURE 3.3. Schematic of Apparatus Used to Measure Saturated Hydraulic Conductivity by the Falling-Head Method

where V = volume of water flowing through the sample,

L = length of sample,

A = cross-sectional area of sample,

t = time,

H_2 = constant hydraulic head difference.

For the clay, concrete, and grout samples, the K_s values were determined using the Ruska permeameter (Model No. 1013-801-00, Ruska Instrument Corp., Houston, Texas). The Ruska permeameter is a constant head device that confines small samples under relatively high pressures. The K_s value of a sample is calculated using Equation (3.5), where the hydraulic head difference (H_2) equals the difference between the applied pressure and atmospheric pressure (Klute and Dirksen 1986).

3.2 RESULTS

This section summarizes the measured and estimated hydraulic properties. If data were reported elsewhere, the reference(s) was cited.

3.2.1 Hanford Formation Sandy Sequence

The water retention and saturated hydraulic conductivity data describing the Hanford sandy sequence were reported by Smoot et al. (1989; 33 samples) and Connelly et al. (1992b; 27 samples). While most of the characterization data for well No. 299-E25-234 at the GTF were reported by Smoot et al. (1989), the particle size distributions were not included. For completeness, those data are included in this report in Table A.1 of the Appendix. All particles greater than 2 mm in diameter were included in the gravel percentage for each sample.

Smoot et al. (1989) reported bulk density values for the samples from well E25-234. Those data are included in Table A.2 of the Appendix to show how bulk density varied as a function of depth and sample size. Also contained in Table A.2 are the average particle density values determined on the less than 2-mm-diameter size fraction. These data were not reported by Smoot et al. (1989).

3.2.2 Hanford Formation Lower Gravels

The water retention and saturated hydraulic conductivity data describing the Hanford gravels were reported by Smoot et al. (1989; two samples) and Connelly et al. (1992b; 12 samples). Of the 14 samples, gravel contents were reported for 10. The gravel contents ranged from 0% to 79%, with an average of approximately 50%. Table A.1 contains the average particle size distribution and Table A.2 the bulk and particle density data for samples from well No. 299-E25-234 (Smoot et al. 1989). Connelly et al. (1992b) reported dry sieve data for 8 of the 12 samples, but did not report bulk or particle density values.

3.2.3 Ringold Formation

The water retention and saturated hydraulic conductivity data describing the Ringold Formation were reported in Connelly et al. (1992b; 5 samples). Particle size distribution and bulk and particle densities were not estimated because the hydraulic parameters were already provided.

3.2.4 Backfill Soil

The water retention properties of backfill were determined between 0 and -100 cm of matric potential using the column method with two Plexiglass columns packed to a bulk density of 1.65 g cm^{-3}. This density represented 90% of the maximum dry density (Dames and Moore 1988). The retention data from the column method were combined with pressure plate and vapor adsorption data to describe the full range of water retention. Particle size distribution and water retention data are contained in Table A.3 of the Appendix. Particle density was assumed to be 2.8 g cm^{-3}.

The saturated hydraulic conductivity was determined with the constant head method using two 30-cm-long columns with an area of 17.65 cm^2. A 2-cm head was maintained on the surface, resulting in a head gradient of 1.067 across the columns. Four 10-s repetitions of the test on each column yielded average saturated conductivity values of 0.024 and 0.036 cm s^{-1}, for an overall

average K_s of 0.030 cm s^{-1}. The source of the retention and conductivity data for the backfill soil was PNL laboratory record book BNW 53071.

3.2.5 Gravel

The water retention properties of gravel were determined between 0 and -10 cm of matric potential using the column method with two Plexiglass columns packed to a bulk density of 1.38 g cm^{-3}. Those data were combined with a vapor adsorption datum and linear interpolation to estimate the full range of water retention. Particle density was assumed to be 2.8 g cm^{-3}. The water retention data are contained in Table A.4 of the Appendix. The only information on particle size distribution is that all particles are between 3.692 mm and 8 mm in diameter.

The saturated hydraulic conductivity was determined with the constant head method using a 10-cm-long column with an area of 17.65 cm^2. A head gradient of 2.5 cm was maintained across the column. Five 10-second repetitions yielded a range of values from 1.77 to 1.97 cm s^{-1} and an average value of 1.85 cm s^{-1}. The K_s value (1.85 cm s^{-1}) and the experimental design may have resulted in a Reynolds number in excess of 80, which would indicate turbulence, decreased flow through the sample, and deviation from Darcy's law. Assuming that the effect of the turbulence would be to reduce flow relative to flow under laminar conditions, the actual conductivity value was probably somewhat higher than that reported. In the absence of any other data, however, these hydraulic conductivity estimates were assumed to be reasonable first approximations. The source of the retention and conductivity data for the gravel was PNL laboratory record book BNW 53071.

3.2.6 Clay

The water retention properties of the clay were determined using the pressure plate method (samples were packed to a density of 1.45 g cm^{-3}, which represented roughly 90% of the maximum

dry density as extrapolated from data in Dames and Moore [1988]) and the vapor adsorption method. Particle density was assumed to be 2.6 g cm^{-3}. The water retention data are contained in Table A.5 of the Appendix.

The saturated hydraulic conductivity was determined in triplicate using the constant head method and the Ruska permeameter. The applied pressure difference was 510 cm across a 6.45-cm-long sample with an area of 18.1 cm^2. The tests were run for about 54 hours and outflow volumes were 8 to 10 cm^3. The three conductivity values were 1.23×10^{-9}, 7.75×10^{-9}, and 8.26×10^{-9} cm s^{-1}, for an average value of 9.4×10^{-9} cm s^{-1}. After the tests, the conductivity samples remained in the sample cells for 42 days and swelled. The increase in sample length was roughly 30%. The conductivity test was performed again with a pressure difference of 1,020 cm. After about 0.4 hours, the outflow was about 2 cm^3. The average calculated K_s value was 1.8×10^{-7} cm s^{-1}, or approximately 20 times the original value. The source of the retention and conductivity data was PNL laboratory record book BNW 53071.

3.2.7 Asphalt

No data were initially available. Asphalt was assumed to be impermeable to liquid water; hence, hydraulic properties were assigned to satisfy that assumption yet remain compatible with properties of adjacent materials. The assigned values of saturated and residual water contents were 0.162 and 0.0 cm^3 cm^{-3}, respectively. The assigned value of saturated conductivity was 10^{-20} cm s^{-1}. After this report was drafted, asphalt data became available. Clemmer et al. (1992) estimated that the total porosity of three samples was 3% to 4%, which was about 1/4 the assumed value of 16.2%. Based on the permeability to N_2, the asphalt permeability to water was estimated to be 2×10^{-13} cm s^{-1}.

3.2.8 Concrete

Bulk density, particle density, and hydraulic conductivity data are contained in Table A.6 of the Appendix. Saturated hydraulic conductivity was determined using the constant head method and the Ruska permeameter with a pressure difference of 2,068 cm across the samples. The average value, 3.88 x 10^{-10} cm s^{-1}, was within the range of values reported by Whiting (1988) for seven types of concrete.

Water retention by concrete was determined using only the vapor equilibrium technique because the pressures required to remove water from this material were much greater than those that could be obtained with the other techniques. Water retention data for the concrete are reported in Table A.7 of the Appendix.

Bailey and Hampsen (1982) listed ion concentrations for the aqueous phase of Portland cement before and after complex ion formation. They cited a "typical" molarity for calcium sulfate in the aqueous phase of Portland cement of 0.0258 mol L^{-1}. Using concentrations of sodium, calcium, sulfate, and hydroxide of 15, 57, 58, and 35 mmol L^{-1}, respectively, as reported by Bailey and Hampsen (1982), the GMIN model predicted the activity of water to be 0.99978. Substituting this water activity into Equation (3.3) yielded an estimate of the osmotic potential for cement of approximately -0.03 MPa (i.e., -306 cm). This value of osmotic potential was considered to be relatively small. Therefore, the total potentials inferred from the thermocouple psychrometer measurements for the Sandia concrete were related directly to matric potential (for calculating retention parameters) without any corrections for osmotic potential. The source of the retention and conductivity data for the concrete was PNL laboratory record books BNW 4042 and BNW 50881.

3.2.9 Grout

Bulk density, particle density, and hydraulic conductivity data are contained in Table A.8 of the Appendix. Saturated hydraulic conductivity was determined using the constant head method and

the Ruska permeameter with a pressure difference of 510 cm across the samples. Water retention by grout was determined using only the vapor equilibrium technique because the pressures required to remove water from this material were much greater than those that could be obtained with the other techniques. Water retention data for the DSSF grout are tabulated in Table A.9 in the Appendix.

The data reported by Lokken et al. (1992b) indicated that the molarity of the grout pore water solution was in excess of 4.0 mol L^{-1}. Because of the high molarity, the osmotic potential was calculated to correct the vapor adsorption data. The average concentrations of 6 of the 12 measured constituents (i.e., Na, K, NO_3, NO_2, SO_4, and Cl) from Table 3.1 in Lokken et al. (1992b) were used as input to the GMIN chemical equilibrium model (Felmy 1990) to estimate the activity of water in the DSSF grout pore solutions. The activity of water estimated by the GMIN code was 0.8448. Substituting this water activity into Equation (3.3) yielded an osmotic potential of approximately -23.2 MPa (-232 bar). This value of osmotic potential was subtracted from all total water potential data for the DSSF grouts to estimate the matric potentials reported in Table A.9. Implicit in this osmotic potential correction is the assumption that the osmotic potential of the grout will remain more or less constant and will not change as a function of saturation. The source of the retention and conductivity data for the DSSF grout was PNL laboratory record book BNW 53294.

4.0 HYDRAULIC PARAMETERS

Flow and transport through an unsaturated porous medium is governed by the relationships among water content, matric potential, and hydraulic conductivity. Within numerical models, these relationships can be represented by mathematical functions containing one or more fitted parameters. This section specifies the hydraulic functions used, the parameter fitting procedure, and the corrections for gravel content, and summarizes the average parameters to be used to describe the hydraulic properties of the materials in the conceptual model in Figure 2.3.

4.1 HYDRAULIC FUNCTIONS

The water retention function that was used was proposed by van Genuchten (1980) as follows:

$$\theta(h) = \theta_r + (\theta_s - \theta_r)[1+(\alpha h)^n]^{-m} \tag{4.1}$$

where $\theta(h)$ = volumetric water content (dimensionless) as a function of h, the matric potential

θ_s = saturated water content (dimensionless)

θ_r = residual water content (dimensionless)

α = reciprocal of air-entry matric potential (cm^{-1})

h = matric potential (cm)

n, m = curve-fitting parameters (dimensionless), with m=1-1/n.

Describing water retention with the van Genuchten function enabled calculation of unsaturated hydraulic conductivity, K(h), as follows (van Genuchten 1980):

$$K(h) = K_s \frac{\{1 - (\alpha h)^{n-1}[1 + (\alpha h)^n]^{-m}\}^2}{[1+(\alpha h)^n]^{m/2}} \tag{4.2}$$

using the predictive hydraulic conductivity model of Mualem (1976). In Equation (4.2), the pore interaction term was fixed at a value of 0.5.

4.2 PARAMETER ESTIMATION PROCEDURE

The retention parameters θ_s, θ_r, α, and n from Equation (4.1) were fit to water retention data using the nonlinear, least-squares, curve-fitting program known as RETC (Yates et al. 1992). Generally, the water retention data from the various measurement methods were combined and used to fit the parameters in the van Genuchten water retention function. When data from the pressure plate and hanging water column methods overlapped, the overlapping pressure plate data were omitted during the curve fitting because they were considered less reliable. Smoot et al. (1989) reported fitted parameters for samples from well No. 299-E25-234 in which the retention data from duplicate samples were combined before fitting. For this report, the water retention data from each duplicate subsample were refit individually to obtain fitted parameters. Therefore, the parameter estimates in the Appendix for samples from well No. 299-E25-234 vary somewhat from those reported in Smoot et al. (1989) and Connelly et al. (1992b).

The sandy sequence of the Hanford formation was represented by combining 28 sets of parameters from well No. 299-E25-234, 5 sets of parameters from the 241 AP Tank Farm Facility, 21 sets of parameters from the U.S. Ecology site, 3 sets of parameters from the 200-BP-1 site, and 3 values of in situ saturated hydraulic conductivity determined using a borehole permeameter at the bottom of the existing grout pit (Dames and Moore 1988).

The lower gravel sequence of the Hanford formation was represented by combining two sets of parameters from well No. 299-E25-234, eight sets of parameters from the 200-BP-1 site, two sets of parameters from B Pond, and two sets of parameters from the U.S. Ecology site. Some of the parameter sets were from samples of the upper gravel sequence of the Hanford formation, which is absent in the vicinity of the GTF. However, the upper and lower gravel sequences of the Hanford

formation are texturally similar and more or less indistinguishable from each other except for stratigraphic position (Connelly et al. 1992a, 1992b).

The Ringold Formation was represented by combining four sets of parameters from the Ringold Formation near B Pond and one set of parameters from the U.S. Ecology site. No data or sets of parameters were available for the Ringold Formation beneath the GTF.

Parameters for the backfill soil, clay, gravel, concrete, and grout were fitted to the data reported in the Appendix. Given the lack of data on asphalt properties, parameters for the asphalt were estimated. Parameter sets for all of the materials having more than one parameter set are reported in Tables A.10 to A.14 of the Appendix, along with the estimated means and variances.

4.3 CORRECTIONS FOR GRAVEL CONTENT

In a summary of the hydrogeology of the 200 East Area, Cushing (1992) mentioned the presence of gravel throughout portions of the vadose zone. Except for samples collected above the 126-ft (38.4-m) depth from well No. 299-E25-234, all water retention and hydraulic conductivity data used for this report were generated using the less than 2-mm-diameter particle-size fraction.

Bouwer and Rice (1983) proposed a technique for calculating the bulk hydraulic properties of a mixture containing sand and gravel from the hydraulic properties of the sand fraction alone and the volume fraction of the gravel. The water retention of the sand-gravel mixture was determined as follows:

$$\theta_b = (1-V_f)\,\theta_s \tag{4.3}$$

where θ_b = volumetric water content of the sand-gravel mixture

θ_s = volumetric water content of the sand fraction

V_r = volume fraction of the gravel.

The bulk saturated hydraulic conductivity, K_b, of the sand-gravel mixture was calculated as

$$K_b = K_s\,(e_b / e_s) = K_s\,(\theta_b/\theta_s)\,(1-\theta_s) / (1-\theta_b) \tag{4.4}$$

where K_s = saturated hydraulic conductivity of the sand (less than 2-mm-diameter size fraction)

e_b = void ratio of sand-gravel mixture

e_s = void ratio of sand

and the void ratio is simply the volume of voids divided by the volume of solids. In Equation (4.4), θ_b and θ_s are the saturated values. Bouwer and Rice (1983) suggested that, in practice, the above procedure could be made more accurate if the saturated water content of the sand-gravel mixture was determined in situ. This value could then be used as a matching point when fitting parameters to describe the relationship between K and θ.

Equations (4.3) and (4.4) were used to scale the hydraulic properties of samples 1 and 4 from the 241-AP Tank Farm (Smoot et al. 1989). The scaled hydraulic properties were referenced as sample 1G and 4G, where the "G" indicated that the properties were scaled to account for the gravel fraction. Samples 1G and 4G contained 38% and 10% gravel, respectively. Thus, utilizing Equation (4.3), their effective θ_s values were reduced by 38% and 10%, respectively. Utilizing Equation (4.4), the K_s values were reduced by 51% and 17%, respectively, for samples 1G and 4G. For these calculations, the particle density of the gravel was assumed to equal that of the sediments. Similar corrections for gravel content were not performed for the samples representing the Hanford formation lower gravels.

4.4 PARAMETER SUMMARY

The average parameters for sediments from the Hanford and Ringold Formations and for the other materials comprising the grout waste isolation system are listed in Table 4.1. These parameters

TABLE 4.1. Average Water Retention Parameters and Vertical Saturated Hydraulic Conductivity Values Used for Grout Vadose Zone Flow and Transport Modeling

	Water Retention					Unsaturated Hydraulic Conductivity	
Material Type	No. of Samples	θ_s	θ_r	α cm^{-1}	n	No. of Samples	K_s cm s^{-1}
Hanford Formation[a]							
Sandy Sequence	57	0.4203	0.0234	0.1943	1.868	45	1.55×10^{-3}
Lower Gravels	14	0.3584	0.0213	0.0290	1.613	13	2.73×10^{-4}
Ringold Formation[a] (undifferentiated)	5	0.4982	0.0283	0.0176	1.338	5	2.42×10^{-6}
Backfill Soil [b]	2	0.3710	0.0450	0.0683	2.080	2	3.00×10^{-2}
Gravel [b]	2	0.5180	0.0140	3.5366	2.661	1	1.85
Clay[b]	3	0.4480	0.0000	5.39×10^{-4}	1.324	3	9.40×10^{-9}
Asphalt [c]	0	0.162	0.0	1.00×10^{-7}	2.0	0	1.0×10^{-20}
Concrete[d]	6	0.2258	0.0000	7.61×10^{-6}	1.393	6	3.75×10^{-10}
DSSF Grout [e]	9	0.5781	0.0000	1.08×10^{-5}	1.650	3	1.47×10^{-8}

[a] Original data for well No. 299-E25-234 contained in laboratory record book BNW 52457; other data sources were Smoot et al. (1989), Connelly et al. (1992b), and Dames and Moore (1988).
[b] Original data contained in laboratory record book BNW 53071.
[c] Estimated parameters; no available data.
[d] Original data contained in laboratory record books BNW 4042 and BNW 50881.
[e] Original data contained in laboratory record book BNW 53294.

were used for the base-case flow and transport simulations for the grout PA. The parameters in Table 4.1 are arithmetic mean values with the exception of the K_s values, which are geometric mean values. Geometric mean values of the saturated hydraulic conductivities were used because saturated hydraulic conductivity has often been shown to be lognormally distributed (Hills and Wierenga 1991; Sudicky 1986).

Figures A.1 through A.16 show the retention and conductivity data along with the fitted functions for the samples from well No. 299-E25-234, the backfill soil, gravel, clay, concrete, and grout. Smoot et al. (1989) reported the data and a parameter set for each depth in Well E25-234, but they had lumped the data from individual samples to calculate the parameters. As noted previously in this report, each sample was fitted separately. Connelly et al. (1992b) reported plots of the remaining functions in Tables A.10 to A.12.

The water retention and hydraulic conductivity curves corresponding to the average parameters from Table 4.1 are shown in Figure 4.1. The saturated hydraulic conductivities of the different

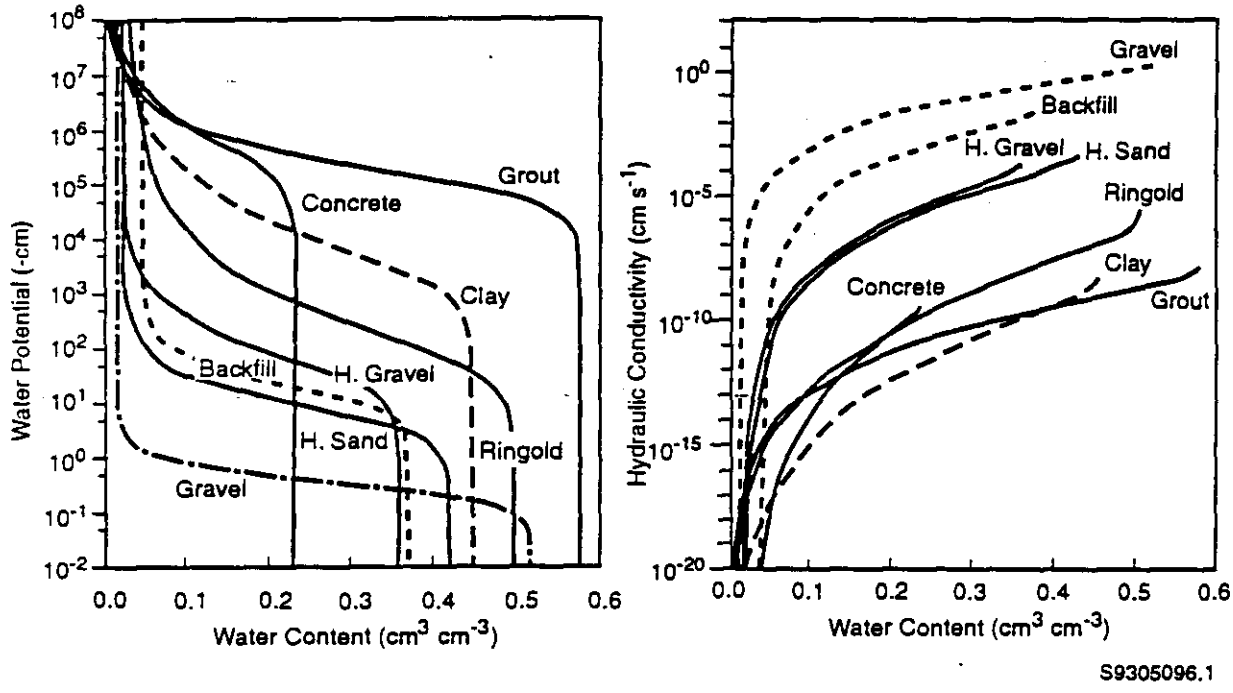

FIGURE 4.1. Average Water Retention (a) and Hydraulic Conductivity (b) Curves. The parameters used to generate the curves are listed in Table 4.1.

materials depicted in Figure 4.1 range over 9 to 10 orders of magnitude. Similarly, the air-entry potentials (reciprocal of α) of these materials range over 6 to 7 orders of magnitude. Insufficient data were available to reliably determine representative probability distributions of the parameters for the sediments beneath the GTF. However, means, variances, and minimum and maximum values of the parameters were calculated for this limited number of samples to show the potential ranges of parameter variability.

9413272.1624

5.0 DISCUSSION

The parameters in Table 4.1 were used in single-phase isothermal flow and transport simulations reported in the grout PA. Summarized here are the assumptions and observations that underlie the generation of those parameters and suggestions for improving the methods used to collect the data and generate new parameters. What is needed most is a program dedicated to identifying the important materials, identifying the conditions to which those materials will be subjected, and measuring the properties under those conditions. Burial of grouted and other defense wastes may eventually require simulations of two-phase nonisothermal flow with reactive transport. The effects of osmotic potential on the flow of water vapor may need to be coupled directly with either isothermal or nonisothermal liquid water flow. Creating a research program now would ensure that the appropriate hydraulic models are identified and parameters for simulations are obtained in a timely fashion.

5.1 METHODS

Overall, the data quality was not consistent. Some sources documented the sample location and reported a range of replicated tests that were well described and referenced; other sources provided only a number. Because the analysis methods have some leeway for interpretation and application, the precise methods used should be documented, along with the sample sizes. Ideally, undisturbed samples should be obtained and analyzed for particle size, particle size distribution (including gravel distribution and clay content), particle density, bulk density, water retention over the entire range of matric potentials, and saturated hydraulic conductivity (and at least one unsaturated conductivity value, if possible). Although not performed on the samples used in this report, chemical tests would reveal useful information such as $CaCO_3$ content and osmotic potential. All tests should be run in duplicate if not triplicate.

The backfill soil, clay, and asphalt warrant further testing because they are such prominent components of the near-field region of the vaults. The backfill soil was analyzed in duplicate compared

to the more than 50 samples used to represent the Hanford sandy sequence. The method used to measure retention in the backfill (i.e., a column method) remains to be verified by established procedures. The data for the backfill appear to vary significantly from the data for other similar materials; thus, more analyses are needed. For example, the saturated conductivity of the backfill was 10- to 100-fold higher than the values measured for intact cores from the Hanford formation that had almost identical particle size distributions and similar bulk density values. The value was also 100-fold higher than the K_s value for stockpile samples reported by Dames and Moore (1988).

The clay was actually a bentonite/silt mix with the propensity to swell considerably (as demonstrated in the lab). As noted in Section 3.2.6, the K_s of the swelled clay (about 2×10^{-7} cm s^{-1}) was 20 times higher than originally measured. The properties of the clay must be evaluated under the expected conditions, i.e., under a load, under a large temperature cycle as the grout temperature rises and subsides, and under drying. Some test results were reported by Dames and Moore (1988), but the methods and testing ranges must be examined. For the grout PA, the properties used to simulate water behavior in the asphalt barrier were assumed. The properties of the asphalt in its original and degraded states should also be measured and reported.

The properties of the concrete were determined on a sample from Sandia National Laboratories. Some measurements of the properties of the concrete to be used at the GTF must be made to verify the similarity to the Sandia sample. If the properties are not similar, the GTF concrete properties should be evaluated fully.

The properties for DSSF grout were determined for a special formulation. For reasons related to the need to optimize parameters such as leachability and strength, the formulation is subject to revision. Lokken and Mason (1992) discussed DSSF grout formulations in which the ratios of blast furnace slag, cement, fly ash, and limestone flour, and two dilutions of the tank waste, were tested for their effects on properties. As the grout formulation is varied, the resulting grout should be evaluated

for the need to conduct physical and hydraulic tests specific to that formulation, as much as two separate soil samples are treated separately or together depending on their similarities.

Measurements of the physical and hydraulic properties of DSSF grout could be affected by changes in the pore solution and grout structure as the samples are dried (e.g., precipitation near surfaces) or water is passed through (e.g., K_s test). The measurement techniques need to be evaluated to determine whether or not such changes have a significant effect on the measurement of properties. During the design life of the GTF, the grout material will experience similar changes or degradation; the results from the evaluation of measurement techniques will be transferable to the evaluation of degradation.

5.2 BULK DENSITY

Table A.2 shows how bulk density varied with depth within the same formation (Smoot et al. 1989). Most of the data used to fit parameter values were derived from samples that were not packed to the in situ bulk densities, which were unknown, the packed samples certainly did not have the structure of the in situ sediment material.

Sample size may have affected the observations of bulk densities. The conductivity cores in Table A.2 were roughly 40 times larger in volume than the water retention cores. Table A.2 shows that the mean bulk density value of the conductivity cores was 0.15 g/cm^3 (i.e., 10%) greater than that of the water retention cores. The difference in bulk density was either the result of the subsampling technique or the indirect method used to calculate the bulk density of the conductivity core.

5.3 HYDRAULIC CONDUCTIVITY

For each material, the predicted hydraulic conductivities reported in the Appendix range from over 3 to 4 orders of magnitude near saturation and more than 10 orders of magnitude near the residual or irreducible water content. However, it should be noted that the unsaturated hydraulic

conductivity curves were generated using the saturated hydraulic conductivity as a single matching point. Therefore, there is much more uncertainty in the predicted unsaturated hydraulic conductivity values at lower water contents.

Yates et al. (1992) compared measurements of unsaturated hydraulic conductivity for 23 different soils with predicted values generated using water retention and saturated hydraulic conductivity data with the RETC code and the Mualem model. In general, the predicted unsaturated hydraulic conductivity values were in reasonable agreement with the actual hydraulic conductivity data. Rockhold et al. (1988) compared measured and predicted unsaturated hydraulic conductivities for a sandy soil on the Hanford Site using field and laboratory data. The comparisons indicated differences of up to one order of magnitude between unsaturated hydraulic conductivities predicted using only water retention data and saturated hydraulic conductivity with the Mualem model and the RETC code, and actual unsaturated hydraulic conductivity data generated using the steady-state flux control method in laboratory column experiments (Klute and Dirksen 1986). The lack of unsaturated hydraulic conductivity data for the materials in the grout PA precluded direct comparisons of measured and predicted unsaturated hydraulic conductivities.

5.4 GRAVEL CONTENT

Gravel is a constituent of much of the vadose zone. The percentages of gravel should always be reported. The higher the percentage of gravel, the more important it is to measure the particle density of the gravel fraction. Scaling the hydraulic properties of two samples with high percentages of gravel significantly reduced the values of effective porosity and saturated hydraulic conductivity relative to the values determined using the less than 2-mm particle-size fraction. The accuracy of this method for scaling the hydraulic properties to account for the gravel-size fraction should be verified for the materials in the grout PA. This method or an analogous procedure should, however, be consistently applied to correct the hydraulic properties of all samples containing a measurable gravel content.

5.5 SPATIAL VARIABILITY

The intact sediment cores from well No. 299-E25-234 were lined and did not permit visual examination. Thus, lenses and stratifications noted in the driller's log were not observed in the cores, even though those features may have been present. Two subsamples, one from each end of each core, were used to represent the entire core. Of 13 intact cores, nine cores yielded retention data for two subsamples that were consistent for each end of the core. In contrast, four cores yielded subsamples with a large degree of variability. For one of those cores (Sample 25), a second set of hanging water column tests was conducted to see if the first set was an anomaly. The results from those tests indicated that, indeed, a significant variation in properties indeed existed within Sample 25 over a distance of 4 cm (Smoot et al. 1989).

Based on the laboratory results, heterogeneity on the scale of the individual conductivity cores (15 cm diameter, 15 cm long) evidently existed. The question of what is the correct scale of measurement necessary to quantify the spatial variability and determine effective flow parameters remains a research topic. However, it may be possible to correlate data obtained from geophysical logging techniques and granulometric (i.e., particle size) data to more clearly delineate lenses and stratifications that control the flow and transport processes.

Insufficient data were available to reliably estimate spatial correlation lengths for the hydraulic properties of the sediments beneath the GTF. If such data were available, conditional simulations could potentially be used to forecast the transport of contaminants from the grout vaults (Journel and Huijbregts 1978; Clifton and Neuman 1982). Conditional simulation allows spatially correlated random hydraulic property fields to be generated with the proper spatial and statistical structures and preserves the values of the field observations at their measurement locations. This type of simulation can be carried out using the Monte Carlo method to generate probabilistic assessments of contaminant migration and fate. Various other techniques for incorporating data and parameter uncertainties into performance assessment models are described by Zimmerman et al. (1990).

5.6 HYSTERESIS

Hysteresis effects were shown to be significant during transient unsaturated flow (Kaluarachchi and Parker 1987; Lenhard and Parker 1987). However, none of the numerical models used for the grout PA simulations accounted for hysteresis in the constitutive relationships describing water retention or conductivity and no data were collected to support such modeling. Given the burial depth, however, the extent of wetting and drying cycles (when hysteresis is manifested) should be minimal. One or more simulations could be conducted to verify the veracity of this assumption. The analysis is not straightforward, however, because the current simulations do not address the movement of water vapor in response to the temperature pulse and osmotic effects, which are likely to be the two major drivers of water content changes.

9413222.1630

5.7 ANISOTROPY

In the groundwater hydrology literature it is common to see references to regional anisotropy, with saturated hydraulic conductivities in the horizontal direction that are 10 or more times greater than those in the vertical direction (Freeze and Cherry 1979). Apparent anisotropy results from the preferred orientation of mineral grains in the horizontal direction and from material heterogeneities (Freeze and Cherry 1979; Marcus and Evenson 1961). Laboratory measurements of saturated hydraulic conductivity generally represent the vertical direction because of the vertical orientation of the samples. Hydraulic conductivities calculated from aquifer test data are more representative of the horizontal direction, and integrate much larger sample volumes. Such tests, however, apply only to the saturated zone of the aquifer and not to the vadose zone.

Graham et al. (1981) reported conductivities in the 200 Area of 0.7 to 3.5 cm s^{-1} in the Hanford formation, 0.003 to 0.08 in the middle Ringold Formation, and 0.001 to 0.004 in the lower Ringold Formation. They determined an anisotropy ratio in one well that ranged between 16 and 13. Analyses of aquifer test data from the 200 East Area indicated that saturated hydraulic conductivities in the lower gravel sequence of the Hanford formation and the Ringold Formation (gravel unit A)

ranged from approximately 0.7 to 6.8 cm s^{-1} (Newcomer et al. 1992). These values were 4 to 8 orders of magnitude greater than the range of values determined using laboratory methods. This discrepancy was attributed to anisotropy, heterogeneity, and scale differences resulting from different sampling volumes. Also, when collecting split spoon samples, sediments may be compacted during drilling, producing lower saturated hydraulic conductivities. Neither laboratory nor field measurements of horizontal conductivity values in the vadose zone of the GTF were available. Without supporting field data, the selection of anisotropy ratios for the vadose zone would be arbitrary. Therefore, hydraulic conductivities were assumed to be isotropic for the vadose zone flow and transport simulations that were conducted for this grout PA. To support the use of anisotropy ratios in the vadose zone, measurements of conductivity are needed in both the horizontal and vertical directions on the same undisturbed samples without observable sediment layering or preferred channels. In lieu of measurements, transient flow data are needed that can be used to calibrate flow and transport models with the anistropy ratio as a calibration parameter.

5.8 TEMPERATURE AND SOLUTE EFFECTS

The testing and analyses reported here did not account for the effects of temperature changes and solutes on the physical and hydraulic properties of the grout and other materials at the GTF. Temperatures in the grout were expected to reach 90°C and above. The solute content of the pore water in DSSF grout was shown to exceed 400 g L^{-1} (Lokken et al. 1992b). Such high temperatures and solute contents will affect the conductivity of water, the retention of water, the water vapor pressure, and the volume of clays.

The conductivity of water in a porous medium is a function of density and viscosity, which in turn are functions of temperature. Density changes over temperature ranging from 0°C to 100°C are no more than 4% and likely exert a minor effect on predictions of flow and transport. Viscosity changes over the same range, however, are roughly ± 75% relative to the viscosity at 20°C. The effect of temperature on viscosity might be accounted for by varying saturated conductivity ± 75%,

although such an analysis would ignore all of the associated effects caused by temperature changes (e.g., vapor pressure changes, solubility changes). Whether the temperature dependence of viscosity explains all of the temperature dependence of unsaturated conductivity is an unresolved issue (Constantz 1982; Hopmans and Dane 1986).

At a constant temperature, the conductivity of water is inversely related to the kinematic viscosity. For a $NaNO_3$ concentration of 367 g L^{-1}, comparable to those seen by Lokken et al. (1992b), the relative kinematic viscosity would be 1.3, meaning a 23% reduction in conductivity. This reduction appears to be less significant than the changes in viscosity caused by temperature, and certainly smaller than the natural variability of conductivity. For these reasons, viscosity changes were not considered in the grout PA.

Temperature also affects water retention through its dependence on surface tension (between 0°C and 100°C, surface tension varies ± 12% from the value at 50°C). The measured effect, however, is much greater; Constantz (1982) reported that retention was reduced 3- to 4-fold more than predicted from surface tension alone as the temperature was increased from 2°C to 25°C to 45°C. Giakoumakis and Tsakiris (1991) saw a similar response in retention between 3°C and 20°C for both drying and wetting experiments.

Vapor flow is affected by osmotic potentials and temperature gradients, both of which will be highest in and around the vaults. Vapor flow resulting from the osmotic potential gradient was estimated and considered in the grout PA. A conservative analysis showed the impact to be much lower than the impact of liquid flow. Vapor flow resulting from a temperature gradient is most likely to be highest during the early years of the GTF and then decrease in importance as the GTF cools. To understand the effect of temperature on vapor flow, consider that the vapor pressure of water approximately doubles as the temperature is raised from 0°C to 10°C, then doubles again at the following temperatures: 21°C, 33°C, 45°C, 60°C, 75°C, and 93°C. Nasser et al. (1992) reported the results of

experiments and modeling dealing with the combined effects of heat, water, and solutes in porous media. They looked at temperatures between 9°C and 27°C. Their model performed best at matching the experimental results when the initial water contents were high (0.134 to 0.166 $cm^3\ cm^{-3}$) and the initial solute concentration was low (< 0.1 mol). When the water contents were low, or when the solute concentration was high (i.e., 0.5 mol), the model either underestimated or overestimated water flow. Their results indicate an incomplete understanding of the physics and chemistry of their system. By implication, their results are likely applicable to the GTF, which could see temperatures near 90°C and solute concentrations above 4.0 mol. An analysis should be conducted to determine whether the experiment-model discrepancies, when scaled to the conditions of the GTF, would have a significant impact on the grout PA.

Clay-size particles have the greatest likelihood for volume changes from flocculation or dispersion caused by the presence of solutes. The volume changes induced in the surrounding sediments by contact with the grout solution is unknown. The clay contents seen in most of the sediment samples were small; for the samples reported in the Appendix, the clay contents were 6% or less. Laboratory tests should be conducted in which the materials (i.e., the concrete, asphalt, and sediments) are subjected to grout pore water and observed for geochemical changes, physical changes, and hydraulic changes.

5.9 GEOCHEMISTRY

The testing and analyses reported here did not account for the effects of geochemical changes in the GTF, particularly within, and in the vicinity of, the grout vaults. These changes will be brought on by precipitation/dissolution reactions as the high-concentration grout pore water interacts with the low-concentration sediment pore water and by the temperature and water content variations experienced by the materials of the GTF over their lifetime. The precipitation/dissolution reactions will cause volume changes that can lead to cracks or the plugging of cracks and pores (e.g., see Lowell et al. [1993] for an example of permeability affected by precipitation). In either case, the physical

and hydraulic properties will be changed. Criscenti and Serne (1988) studied the geochemistry of a grouted commercial waste form in contact with soil, but they did not explore the associated physical and hydraulic changes. A literature review and laboratory tests of the actual grout formulations and wastes of the GTF should be conducted to determine the geochemical effects on physical and hydraulic properties.

5.10 DEGRADATION

The testing and analyses reported here did not account for the effects of material degradation, which is defined as any change from the original properties. During the course of compiling the PA, many mechanisms for degradation were proposed that could only be addressed with gross approximations or estimates. Examples include 1) fines infiltrating the gravel and negating the capillary break, 2) concrete spalling and cracking that creates flow pathways within the vault and through the concrete wall, 3) loss of the asphalt to vaporization and biodegradation, leaving only the aggregate mix, and 4) cracking of the asphalt after it becomes brittle from the heat. All proposed degradation mechanisms should be evaluated for validity and impact; those mechanisms that are valid and could significantly affect the PA must be the subject of further tests. An accurate assessment, based on testing, should be made of the rates of degradation and the associated changes in the physical and hydraulic properties.

6.0 REFERENCES

Angus, M. J. and F. P. Glasser. 1985. "The Chemical Environment in Cement Matrices." Mat. Res. Soc. Symp. Proc. 50:547-556.

American Society for Testing and Materials. 1985. "Standard Test Method for Particle-size Analysis of Soils. D 422-63 (1972)." 1985 Annual Book of ASTM Standards 04.08:117-127. American Society for Testing and Materials, Philadelphia.

Bailey, J. E. and C. J. Hampsen. 1982. "The Chemistry of the Aqueous Phase of Portland Cement." Cement and Concrete Res. 12:227-236.

Blake, G. R. and K. H. Hartge. 1986a. "Particle Density." In Methods of Soil Analysis, Part 1, ed. A. Klute, pp. 377-382. American Society of Agronomy, Madison, Wisconsin.

Blake, G. R. and K. H. Hartge. 1986b. "Bulk Density." In Methods of Soil Analysis, Part 1, ed. A. Klute, pp. 363-375. American Society of Agronomy, Madison, Wisconsin.

Bouwer, H. and R. C. Rice. 1983. "Effect of Stones on Hydraulic Properties of Vadose Zones." In Proceedings of the Characterization and Monitoring of the Vadose (Unsaturated) Zone. National Water Well Association, Worthington, Ohio.

Clemmer, R. G., R. P. Allen, and L. K. Fetrow. 1992. Hydrogen Permeation of Asphalt Test Results - FY-1992, Hanford Grout Technology Program. HGTP392-0605-02, Pacific Northwest Laboratory, Richland, Washington.

Clifton, P. M. and S. P. Neuman. 1982. "Effects of Kriging and Inverse Modeling on Conditional Simulation of the Arva Valley Aquifer." Water Resour. Res. 18:1215-1234.

Connelly, M. P., B. H. Ford, and J. V. Borghese. 1992a. Hydrogeologic Model for the 200 West Groundwater Aggregate Area. WHC-SD-EN-TI-014, Westinghouse Hanford Company, Richland, Washington.

Connelly, M. P., B. H. Ford, J. V. Borghese, S. Trent, and J. Lindberg. 1992b. Hydrogeologic Model for the 200 East Groundwater Aggregate Area. WHC-SD-EN-TI-019, Westinghouse Hanford Company, Richland, Washington.

Constantz, J. 1982. "Temperature Dependence of Unsaturated Conductivity of Two Soils." Soil Sci. Soc. Am. J. 46:466-470.

Corey, A. T. and A. Klute. 1985. "Application of the Potential Concept to Soil Water Equilibrium and Transport." Soil Sci. Soc. Am. J. 49:3-11.

Criscenti, L .J. and R. J. Serne. 1988. Geochemical Analysis of Leachates from Cement/Low-Level Radioactive Waste/Soil Systems. PNL-6544, Pacific Northwest Laboratory, Richland, Washington.

Cushing, C. E. 1992. Hanford Site National Environmental Policy Act (NEPA) Characterization. PNL-6415, Rev. 5, Pacific Northwest Laboratory, Richland, Washington.

Dames and Moore. 1988. "Geotechnical and Corrosion Investigation, Grout Vaults, Hanford, Washington." October 10, 1988. Report for Kaiser Engineers, Inc, by Dames and Moore, Seattle, Washington. Contract No. 10805-282-016.

Felmy, A. R. 1990. GMIN: A Computerized Chemical Equilibrium Model Using a Constrained Minimization of the Gibbs Free Energy. PNL-7281, Pacific Northwest Laboratory, Richland, Washington.

Freeze, R. A. and J. A. Cherry. 1979. Groundwater. Prentice-Hall, Inc., Englewood Cliffs, New Jersey.

Gee, G. W. and J. W. Bauder. 1986. "Particle-Size Analysis." In Methods of Soil Analysis, Part 1, ed. A. Klute, pp. 383-409. American Society of Agronomy, Madison, Wisconsin.

Giakoumakis, S. G. and G. P. Tsakiris. 1991. "Eliminating the Effect of Temperature from Unsaturated Soil Hydraulic Functions." J. Hydrol. 129:109-125.

Graham, M. J., M. D. Hall, S. R. Strait, and W. R.Brown. 1981. Hydrology of the Separations Area. RHO-ST-42, Rockwell Hanford Operations, Richland, Washington.

Greenspan, L. 1977. "Humidity Fixed Points of Binary Saturated Aqueous Solutions." J. Res. Natl. Bur. Stand. Sect. A. 81:201-203.

Harvie, C. E., N. Møller, and J. H. Weare. 1984. "The Prediction of Mineral Solubilities in Natural Waters: The Na-K-Mg-Ca-H-Cl-SO_4-OH-HCO_3-CO_3-H_2O System in High Ionic Strengths at 25°C." Geochim. Cosmochim. Acta 48:723-751.

Hillel, D. 1982. Introduction to Soil Physics. Academic Press, Inc., Orlando, Florida.

Hills, R. G. and P. J. Wierenga. 1991. Model Validation at the Las Cruces Trench Site. NUREG/CR-5716, U. S. Nuclear Regulatory Commission, Washington, D. C.

Hopmans, J. W., and J. H. Dane. 1986. "Temperature Dependence of Soil Hydraulic Properties." Soil Sci. Soc. Am. J. 50:4-9.

Journel, A. G. and Ch. J. Huijbregts. 1978. Mining Geostatistics. Academic Press, Inc., London.

Kaluarachchi, J. J. and J. C. Parker. 1987. "Effects of Hysteresis with Air Entrapment on Water Flow in the Unsaturated Zone." Water Resour. Res. 23:1967-1976.

Klute, A. 1986. "Water Retention: Laboratory Methods." In Methods of Soil Analysis, Part 1, ed. A. Klute, pp. 635-660. American Society of Agronomy, Madison, Wisconsin.

Klute, A. and C. Dirksen. 1986. "Hydraulic Conductivity and Diffusivity: Laboratory Methods." In Methods of Soil Analysis, Part 1, ed. A. Klute, pp. 687-732. American Society of Agronomy, Madison, Wisconsin.

Lenhard, R. J. and J. C. Parker. 1987. "A Model for Hysteretic Constitutive Relations Governing Multiphase Flow: 2. Permeability-Saturation Relations." Water Resour. Res. 3:2197-2206.

Lokken, R. O. and P. F. C. Martin. 1992. Durability of Double-Shell Slurry Feed Grouts: FY-90 Results. PNL-7838, Pacific Northwest Laboratory, Richland, Washington.

Lokken, R. O., P. F. C. Martin, and J. W. Shade. 1992a. Characterization of Double-Shell Slurry Feed Grout Produced in a Pilot-Scale Test. PNL-7979, Pacific Northwest Laboratory, Richland, Washington.

Lokken, R. O., P. F. C. Martin, and J. W. Shade. 1992b. Durability of Double-Shell Tank Waste Grouts. PNL-7835, Pacific Northwest Laboratory, Richland, Washington.

Lowell, R. P., P. van Cappellen, and L. N. Germanovich. 1993. "Silica Precipitation in Fractures and the Evolution of Permeability in Hydrothermal Upflow Zones." Science 260:192-194.

Marcus, H. and D. E. Evenson. 1961. Directional Permeability in Anisotropic Porous Media. Water Resour. Center, Contrib. No. 31, Univ. of California, Berkeley, California.

Mualem, Y. 1976. "A New Model for Predicting the Hydraulic Conductivity of Unsaturated Porous Media." Water Resour. Res. 12:513-522.

Murphy, E. M., J. E. Szecsody, and S. J. Phillips. 1991. A Study Plan for Determining Recharge Rates at the Hanford Site Using Environmental Tracers. PNL-7626, Pacific Northwest Laboratory, Richland, Washington.

Nasser, I. N., R. Horton, and A. M. Globus. 1992. "Simultaneous Transfer of Heat, Water, and Solute in Porous Media: II. Experiment and Analysis." Soil Sci. Soc. Am. J. 56:1357-1365.

Newcomer, D. R., M. A. Chamness, D. L. McAlister, R. J. Brockman, A. W. Pearson, and S. T. Teel. 1992. Unconfined Aquifer Hydrologic Test Data Package for the 200 East Area. WHC-SD-EN-TI-030, Westinghouse Hanford Company, Richland, Washington.

Pitzer, K. S. 1973. "Thermodynamics of Electrolytes I: Theoretical Basis and General Equations." J. Phys. Chem. 77:268-277.

Pitzer, K. S. 1979. Activity Coefficients in Electrolyte Solutions. CRC Press, Boca Raton, Florida.

Rawlins, S. L. and G. S. Campbell. 1986. "Water Potential: Thermocouple Psychrometry." In Methods of Soil Analysis, Part 1, ed. A. Klute, pp. 597-617. American Society of Agronomy, Madison, Wisconsin.

Reardon, E. J. 1990. "Anion Interaction Model for the Determination of Chemical Equilibria in Cement/Water Systems." Cement and Concrete Res. 20:175-192.

Rockhold, M. L., M. J. Fayer, and G. W. Gee. 1988. Characterization of Unsaturated Hydraulic Conductivity at the Hanford Site. PNL-6488, Pacific Northwest Laboratory, Richland, Washington.

Smoot, J. L., J. E. Szecsody, B. Sagar, G. W. Gee, and C. T. Kincaid. 1989. Simulations of Infiltration of Meteoric Water and Contaminant Plume Movement in the Vadose Zone at Single-Shell Tank 241-T-106 at the Hanford Site. WHC-EP-0332, Westinghouse Hanford Company, Richland, Washington.

Sposito, G. 1986. "The Physics of Soil Water Physics." Water Resour. Res. 22:83S-88S.

Sudicky, E. A. 1986. "A Natural Gradient Experiment on Solute Transport in a Sand Aquifer: Spatial Variability and its Role in the Dispersion Process." Water Resour. Res. 22:2069-2082.

Taylor, S. A. and G. L. Ashcroft. 1972. Physical Edaphology: The Physics of Irrigated and Non-irrigated Soils. W. H. Freeman and Company, San Francisco.

van Genuchten, M. Th. 1980. "A Closed-Form Equation for Predicting the Hydraulic Conductivity of Unsaturated Soils." Soil Sci. Soc. Am. J. 44:892-898.

Whiting, D. 1988. "Permeability of Selected Concretes." In Permeability of Concretes, ed. D. Whiting and A. Walitt, pp. 195-222. SP-108, American Concrete Institute, Detroit, Michigan.

Yates, S. R., M. Th. van Genuchten, A. W. Warrick, and F. J. Leij. 1992. "Analysis of Measured, Predicted, and Estimated Hydraulic Conductivity Using the RETC Computer Program." Soil Sci. Soc. Am. J. 56:347-354.

Zimmerman, D. A., K. K. Wahl, A. L. Gutjahr, and P. A. Davis. 1990. A Review of Techniques for Propagating Data and Parameter Uncertainties in High-Level Radioactive Waste Repository Performance Assessment Models. NUREG/CR-5393, SAND89-1432, Sandia National Laboratories, Albuquerque, New Mexico.

9413272.1639

APPENDIX

PHYSICAL AND HYDRAULIC PROPERTY DATA

9413222.1640

APPENDIX

PHYSICAL AND HYDRAULIC PROPERTY DATA

TABLE A.1. Particle-Size Distribution Data for Sediment Samples from Well No. 299-E25-234. For two samples with gravel contents >10%, 1-kg samples were wet sieved to determine gravel size distribution.

Sample	Particle Size µm	% Less Than	Sample	Particle Size µm	% Less Than
5	2000.00	98.93	19	2000.00	98.23
1% Gravel	1000.00	91.18	2% Gravel	1000.00	95.57
88% Sand	500.00	56.55	62% Sand	500.00	88.01
7% Silt	250.00	25.88	31% Silt	250.00	69.84
4% Clay	106.00	15.15	5% Clay	106.00	47.35
	75.00	12.55		75.00	41.19
	53.00	10.67		53.00	36.33
	48.72	10.13		48.20	21.13
	28.21	8.75		28.11	16.63
	15.48	7.75		15.51	13.25
	8.93	6.88		8.99	9.88
	6.32	5.00		6.36	7.63
	5.15	4.25		5.22	5.25
	4.47	3.63		4.52	5.50
	1.31	3.62		1.32	5.25
25	2000.00	99.74	29	2000.00	99.84
86% Sand	1000.00	97.07	95% Sand	1000.00	98.16
9% Silt	500.00	85.07	2% Silt	500.00	77.67
5% Clay	250.00	51.27	3% Clay	250.00	40.23
	106.00	21.97		106.00	11.83
	75.00	16.98		75.00	7.74
	53.00	13.83		53.00	4.75
	49.19	19.00		49.96	13.38
	28.66	14.88		29.07	9.50
	15.84	10.75		15.97	8.00
	9.19	8.13		9.22	6.75
	6.48	6.00		6.54	2.88
	5.28	6.00		5.33	3.25
	4.58	5.00		4.62	2.63
	1.34	4.63		1.35	2.75

TABLE A.1. (contd)

Sample	Particle Size µm	% Less Than	Sample	Particle Size µm	% Less Than
37	2000.00	98.63	46	2000.00	99.56
1% Gravel	1000.00	92.71	04% Sand	1000.00	97.57
77% Sand	500.00	81.34	4% Silt	500.00	73.37
17% silt	250.00	55.50	3% Clay	250.00	27.39
5% Clay	106.00	32.19		106.00	12.06
	75.00	26.92		75.00	9.78
	53.00	23.24		53.00	8.43
	50.18	21.25		51.33	6.50
	29.21	17.25		29.69	5.38
	16.07	15.38		16.26	4.75
	9.36	10.5		9.38	4.50
	6.62	8.75		6.61	4.25
	5.41	7.00		5.39	3.63
	4.68	6.63		4.66	2.50
	1.37	5.00		1.39	2.75
54	2000.00	99.47	69	2000.00	96.98
1% Gravel	1000.00	96.62	3% Gravel	1000.00	85.03
82% Sand	500.00	81.48	90% Sand	500.00	49.98
11% Silt	250.00	48.28	5% Silt	250.00	26.30
6% Clay	106.22	31.02	2% Clay	106.00	15.97
	75.00	26.75		75.00	13.55
	53.00	23.63		53.00	11.80
	50.11	17.75		50.29	7.00
	29.12	15.75		29.05	6.75
	16.05	12.00		15.92	5.25
	9.30	8.88		9.22	3.25
	6.59	7.88		6.53	2.50
	5.37	7.00		5.33	2.75
	4.65	7.38		4.62	2.00
	1.34	6.00		1.34	2.00

9413272.1642

TABLE A.1. (contd)

Sample	Particle Size µm	% Less Than	Sample	Particle Size µm	% Less Than
83	2000.00	95.92	99	2000.00	99.51
4% Gravel	1000.00	79.70	58% Sand	1000.00	97.07
85% Sand	500.00	47.85	40% Silt	500.00	86.13
9% Silt	250.00	26.15	2% Clay	250.00	66.46
2% Clay	106.22	15.36		106.00	49.42
	75.00	12.74		75.00	44.97
	53.00	11.00		53.00	42.31
	49.93	7.13		49.84	8.49
	28.86	6.75		28.98	6.28
	15.85	5.63		15.93	4.76
	9.19	4.00		9.25	2.97
	6.51	3.00		6.55	2.63
	5.32	2.00		5.36	1.87
	4.61	2.00		4.65	1.70
	1.33	2.25		1.34	2.72
110	2000.00	93.82	117	2000.00	96.54
6% Gravel	1000.00	71.65	3% Gravel	1000.00	93.32
81% Sand	500.00	45.45	86% Sand	500.00	59.69
11% Silt	250.00	29.70	8% Silt	250.00	35.33
2% Clay	106.00	16.81	3% Clay	106.00	19.87
	75.00	15.32		75.00	15.98
	53.00	13.32		53.00	13.24
	49.91	8.75		50.49	10.13
	28.89	7.38		29.20	9.00
	15.88	5.88		16.06	6.25
	9.20	4.63		9.27	6.75
	6.52	3.00		6.56	4.50
	5.33	2.00		5.35	4.50
	4.62	1.75		4.64	3.75
	1.34	2.75		1.34	2.63

TABLE A.1. (contd)

Sample	Particle Size µm	% Less Than	Sample	Particle Size µm	% Less Than
126	2.00 (in)	100.00	133	2.00 (in)	100.00
51% Gravel	1.00 (in)	84.19	30% Gravel	1.00 (in)	100.00
39% Sand	0.75 (in)	71.72	48% Sand	0.75 (in)	98.50
9% Silt	0.50 (in)	66.80	19% Silt	0.50 (in)	89.38
1% Clay	4.75 (mm)	58.31	3% Clay	4.75 (mm)	80.70
	2000.00	48.78		2000.00	69.88
	1000.00	36.60		1000.00	57.57
	500.00	22.56		500.00	45.30
	250.00	16.07		250.00	36.77
	106.22	11.84		106.22	28.21
	75.00	10.78		75.00	25.00
	53.00	10.06		53.00	22.24
	50.24	2.13		47.41	15.82
	29.03	2.01		27.68	12.41
	15.90	2.01		15.31	9.79
	9.21	1.22		8.94	5.86
	6.51	1.16		6.35	4.20
	5.33	0.98		5.20	3.41
	4.62	0.55		4.51	3.15
	1.34	0.49		1.30	3.32

9413222.1641

TABLE A.2. Bulk and Particle Density Data for Samples from Well No. 299-E25-234. Sample volumes were 68 cm^3 for the retention cores and 2600 cm^3 for the conductivity cores. Particle density values are the average of three replicates, except for samples 19 and 117, which are averages of two replicates.

Sample	Bulk Density ($g\ cm^{-3}$) Water Retention Cores	Conductivity Cores	Particle Density ($g\ cm^{-3}$)
5	1.62, 1.75	1.79	2.82
19	1.45, 1.36	1.61	2.77
25	1.36, 1.31, 1.34, 1.31	1.43	2.72
29	1.53, 1.50	1.83	2.71
37	1.27, 1.29	1.38	2.64
46	1.44, 1.61	1.72	2.68
54	1.47, 1.42	1.66	2.68
69	1.70, 1.62	1.82	2.72
83	1.65, 1.68	1.80	2.73
99	1.71, 1.69	1.84	2.70
110	1.55, 1.58	1.89	2.72
117	1.47, 1.59	1.44	2.71
126	1.80, 1.76	1.82	2.79
133	1.97, 1.96	2.03	2.73
Mean Values[a]	= 1.53	1.68	2.72

(a) Water retention cores for samples 126 and 133 were packed in the laboratory. Therefore, bulk densities at these two depths were not included in the calculation of mean bulk density.

TABLE A.3. Particle Size Distribution and Water Retention Data for Backfill Soil. Bulk density was 1.65 g cm^{-3}. Particle density was assumed to be 2.8 g cm^{-3}.

Particle Size Distribution Diameter	% Less Than	Matric Potential, -cm	Water Content, cm^3 cm^{-3}	Method
2000	99.47	0	0.36	Estimated
1000	94.0	5	0.358	Column; mean of 2 reps
500	55.52	15	0.304	"
250	24.0	25	0.181	"
106	15.32	35	0.133	"
75	13.33	45	0.127	"
53	11.73	55	0.116	"
50.1	12.0	65	0.115	"
28.95	12.25	75	0.119	"
15.92	10.0	85	0.113	"
9.213	8.25	95	0.108	"
6.529	7.25	102	0.071	Pressure Plate; mean of 3 reps
5.324	7.25	306	0.068	"
4.611	7.25	1020	0.066	"
1.339	5.5	3060	0.055	"
		31180	0.056	?
		103200	0.05	?
		812600	0.031	?
		1511000	0.023	?
		2483000	0.018	?

TABLE A.4. Water Retention Data for Gravel. Bulk density was 1.38 g cm^{-3}. Particle density was assumed to be 2.8 g cm^{-3}.

Matric Potential, -cm	Water Content cm^3 cm^{-3}	Method
0	0.51	Estimated from bulk and particle densities
0.5	0.14	Column; mean of 2 reps
1	0.1	Interpolated from column data at 0.5 and 1.5 cm
1.5	0.075	Column; mean of 2 reps
2.5	0.044	"
5	0.017	Interpolated from column data at 4.5 and 5.5 cm (not shown)
10	0.01	Extrapolated from column data at 8.5 cm (not shown)
100	0.0095	Interpolated between values at 10 and 3.0E6 cm
1000	0.009	"
10000	0.0088	"
100000	0.0083	"
1000000	0.007	"
3000000	0.004	Vapor adsorption

TABLE A.5. Water Retention Data for Clay (i.e., a 1:3 Bentonite/Silt Loam Mix). The bulk density was 1.45 g cm^{-3}. The particle density was assumed to be 2.6 g cm^{-3}.

Matric Potential, -cm	Water Content, $cm^3\ cm^{-3}$	Method
0	0.442	Estimated from bulk and particle densities
10	0.442	Assumed value
102	0.442	Pressure plate value of 0.66 exceeded porosity; reset to porosity
306	0.442	Pressure plate value of 0.61 exceeded porosity; reset to porosity
1020	0.44	Pressure plate
3060	0.31	"
12400	0.258	Vapor adsorption
23600	0.188	"
291000	0.101	" (average of two samples at different potentials)
1920000	0.028	"

TABLE A.6. Bulk and Particle Density and Saturated Hydraulic Conductivity Data for Concrete. Sample diameters ranged from 1.400 to 1.408 cm. Particle densities estimated from bulk densities and calculated values of saturated water content (Table A.7). Conductivity values for samples D, E, and F were determined in the opposite direction used for samples A, B, and C.

Sample	Sample Length, cm	Sample Volume, cm^3	Bulk Density, g cm^{-3}	Estimated Particle Density, g cm^{-3}	Saturated Conductivity: Total Flow, cm^{-3}	Saturated Conductivity: Total Time of all Tests, h	Saturated Conductivity: Average Test Value, cm s^{-1}
CL-40A	1.155	1.78	2.08	2.57	0.25	72	3.55E-10
CL-40B	1.146	1.78	2.02	2.59	0.25	115	2.19E-10
CL-40C	1.153	1.79	1.93	2.61	0.25	54	4.69E-10
CL-40D	1.155	1.79	1.99	2.61	0.50	102	4.97E-10
CL-40E	1.150	1.79	2.02	2.59	0.50	114	4.43E-10
CL-40F	1.135	1.77	1.90	2.55	0.50	144	3.46E-10
Average			1.99	2.59			3.88E-10

TABLE A.7. Water Retention Data for Concrete. Values at zero matric potential were calculated using weights of supposedly saturated samples.

CL-40A		CL-40B		CL-40C	
Water Potential, -cm	Water Content, $cm^3\ cm^{-3}$	Water Potential, -cm	Water Content, $cm^3\ cm^{-3}$	Water Potential, -cm	Water Content, $cm^3\ cm^{-3}$
0	0.186	0	0.219	0	0.26
2400	0.186	1900	0.219	4100	0.26
10300	0.175	6000	0.213	55000	0.249
30400	0.175	14800	0.207	63100	0.247
43600	0.172	22700	0.204	89700	0.245
55700	0.17	35100	0.198	105500	0.24
61600	0.167	45100	0.196	112700	0.239
86900	0.156	64800	0.194	132600	0.237
90700	0.15	84900	0.188	153000	0.232
105000	0.15	117400	0.182	165300	0.229
128400	0.141	161400	0.173	176200	0.225
166400	0.122	167300	0.154	275700	0.213
205600	0.12	239100	0.143	885100	0.152
885100	0.09	885100	0.112	1164700	0.111
1164700	0.068	1164700	0.087	1468500	0.115
1468500	0.063	1468500	0.081	3077300	0.098
3077300	0.052	3077300	0.068		

CL-40D		CL-40E		CL-40F	
Water Potential, -cm	Water Content, $cm^3\ cm^{-3}$	Water Potential, -cm	Water Content, $cm^3\ cm^{-3}$	Water Potential, -cm	Water Content, $cm^3\ cm^{-3}$
0	0.238	0	0.221	0	0.254
3100	0.238	2700	0.221	3100	0.254
20000	0.227	19700	0.205	44700	0.242
42500	0.222	35100	0.197	65900	0.236
74600	0.217	49100	0.189	71500	0.227
92000	0.214	60700	0.187	94100	0.223
102300	0.211	77600	0.182	102700	0.22
117800	0.209	92200	0.18	117500	0.218
125100	0.207	102500	0.177	132800	0.216
135700	0.206	128300	0.175	202600	0.211
152900	0.198	144100	0.173	277700	0.207
183200	0.192	161900	0.163	885100	0.142
295200	0.188	168100	0.159	1164700	0.112
885100	0.121	211000	0.155	1[illegible]0	0.105
1164700	0.098	885100	0.109	3077300	0.08
1468500	0.089	1164700	0.079		
3077300	0.072	1468500	0.079		
		3077300	0.067		

TABLE A.8. Bulk and Particle Density and Saturated Hydraulic Conductivity Data for DSSF Grout Samples from the 14 November 1988 Adiabatic Pilot-Scale Test. Bulk density samples were 10 to 12 cm^3. Diameter of conductivity samples was 1.34 cm.

Sample	Maximum Temperature During Curing, °C	Bulk Density, $g\ cm^{-3}$	Particle Density, $g\ cm^{-3}$	Saturated Conductivity: Sample Length, cm	Total Flow, cm^{-3}	Total Time of all Tests, h	Average Value, $cm\ s^{-1}$
A26	85	1.07	-	-	-	-	-
A38	87	1.09	-	-	-	-	-
A73	78	1.06	2.58	-	-	-	-
B06	80	1.15	-	-	-	-	-
B33	94	-	-	-	-	-	-
B52	91	1.09	2.62	-	-	-	-
C16	93	1.12	-	-	-	-	-
C48	99	1.11	-	-	-	-	-
C82	75	1.10	2.63	-	-	-	-
A	-	-	-	2.92	2.1	289	5.52E-9
B	-	-	-	2.95	1.1	257	1.10E-8
C	-	-	-	1.64	6.6	78	5.22E-8
Average		1.10	2.61				2.29E-8

TABLE A.9. Water Retention Data for DSSF Grout (1 bar = 0.1 MPa = 1020 cm).

Sample A26		Sample A38		Sample A73	
Water Potential, -bars	Water Content, 100 (g g^{-1})	Water Potential, -bars	Water Content, 100 (g g^{-1})	Water Potential, -bars	Water Content, 100 (g g^{-1})
249.41	44.18	229.93	45.69	274.53	45.55
275.36	43.18	273.49	45.01	301.05	44.89
290.83	41.16	280.69	43.34	280.69	43.34
293.02	39.62	292.92	41.91	322.57	41.86
316.83	38.75	317.26	41.06	347.49	41.15
333.50	37.56	335.59	40.01	371.48	40.16
344.91	35.47	344.91	38.40	381.33	38.74
375.01	34.50	380.69	37.40	412.00	37.80
393.46	33.14	390.84	36.26	438.08	36.72
393.97	32.32	399.48	35.54	427.92	36.03
455.56	30.63	455.10	33.94	497.97	34.60
459.16	28.84	455.76	32.35	513.48	32.88
472.16	25.81	418.97	29.79	479.95	26.46
504.09	23.16	453.03	27.50	470.85	28.02
709.95	17.89	634.14	22.01	725.06	22.16
749.84	14.43	679.64	17.27	684.39	18.31
758.30	13.30	709.39	15.20	726.31	16.63
882.43	12.31	779.07	14.36	760.60	15.76
1050.27	10.22	985.74	11.40	960.59	12.75
1249.67	8.20	1251.84	8.99	1151.95	10.10
Sample B06		Sample B33		Sample B52	
301.96	42.47	249.16	41.97	247.68	44.37
283.90	41.59	251.90	41.27	264.76	43.65
309.93	39.94	389.24	38.93	299.34	41.88
330.52	38.60	290.74	37.21	299.14	40.54
333.16	37.89	313.59	36.12	318.67	39.77
363.78	36.87	362.71	34.79	333.72	38.70
370.61	35.35	350.69	32.73	343.61	37.05
408.29	34.36	388.09	31.17	386.27	36.01
432.55	33.21	411.11	29.56	394.10	34.87
439.25	32.46	416.41	28.66	399.75	34.08
498.47	30.86	496.32	26.46	464.73	32.47
513.48	29.13	515.67	24.56	463.18	30.73
479.95	26.46	507.39	21.88	416.69	28.31
515.21	24.39	596.40	19.25	472.18	25.53
749.09	19.12	839.59	14.26	679.18	19.62
758.88	15.59	908.04	11.44	749.34	15.37
755.07	13.79	842.92	10.97	754.05	14.05
846.92	13.01	926.72	10.47	877.21	12.64

TABLE A.9. (contd)

Sample B06		Sample B33		Sample B52	
Water Potential, -bars	Water Content, 100 (g g^{-1})	Water Potential, -bars	Water Content, 100 (g g^{-1})	Water Potential, -bars	Water Content, 100 (g g^{-1})
1024.26	11.25	1081.36	9.59	1027.32	11.01
1203.06	9.10	1309.42	7.92	1270.74	8.59

Sample C16		Sample C48		Sample C82	
296.41	40.24	234.90	42.00	256.01	44.86
273.77	39.57	240.36	41.11	258.10	44.32
287.74	37.79	284.45	39.18	289.14	42.76
284.16	36.25	285.95	37.55	299.24	41.52
317.15	35.42	294.73	36.67	327.36	40.74
337.46	34.27	329.01	35.48	347.84	39.70
350.93	32.54	333.27	33.55	341.73	38.12
377.20	31.36	372.16	32.34	388.22	37.05
378.34	30.08	387.44	31.34	394.37	35.87
394.23	29.28	375.90	30.16	412.55	35.14
459.71	27.40	442.62	28.14	484.18	33.37
458.45	25.74	463.97	26.13	481.52	31.72
474.58	22.98	458.48	23.12	458.79	29.44
559.41	20.65	550.41	20.42	501.60	26.73
731.20	15.44	746.47	15.36	700.11	21.25
848.06	11.69	856.03	11.81	686.89	17.83
839.57	10.71	840.99	11.04	733.57	16.08
938.70	10.24	920.41	10.44	791.77	14.89
1095.82	9.03	1087.05	9.06	934.32	12.91
1264.66	7.64	1288.62	7.52	1077.55	10.05

TABLE A.10. Water Retention Parameters and Saturated Hydraulic Conductivity Data for the Sandy Sequence of the Hanford Formation. Parameters for location 241-AP are from Smoot et al. (1989). Data for location 88-1 are from Dames and Moore (1988). Parameters for locations 299-E33-38 and MW are from Connelly et al. (1992b).

Well # or Location	Sample	Depth m	θ_s $cm^3\ cm^{-3}$	θ_r $cm^3\ cm^{-3}$	α 1/cm	n	K_s $cm\ s^{-1}$
299-E25-234	5A	1.5	0.4131	0.0188	0.1479	1.3090	5.73E-4
299-E25-234	5B	1.5	0.3367	0.0336	0.0211	1.5364	-
299-E25-234	19A	5.8	0.4700	0.0426	0.1165	1.4816	8.88E-4
299-E25-234	19B	5.8	0.5026	0.0364	0.2728	1.5327	-
299-E25-234	25A	7.6	0.4406	0.0540	0.0473	2.0595	1.80E-3
299-E25-234	25B	7.6	0.5228	0.0345	0.0519	1.3424	-
299-E25-234	25C	7.6	0.5074	0.0282	0.0292	1.3517	-
299-E25-234	25D	7.6	0.5193	0.0000	0.1944	1.3494	-
299-E25-234	29A	8.8	0.4341	0.0000	0.2722	1.1927	2.41E-5
299-E25-234	29B	8.8	0.4387	0.0000	0.1034	1.2240	-
299-E25-234	37A	11.3	0.5114	0.0706	0.0774	1.2924	5.77E-4
299-E25-234	37B	11.3	0.5304	0.0851	0.0894	1.3353	-
299-E25-234	46A	14.0	0.4581	0.0000	0.2923	1.3658	2.99E-4
299-E25-234	46B	14.0	0.3708	0.0000	0.0613	1.4343	-
299-E25-234	54A	16.5	0.4434	0.0278	0.1205	1.4776	1.38E-5
299-E25-234	54B	16.5	0.4543	0.0217	0.1450	1.4421	-
299-E25-234	69A	21.0	0.3722	0.0000	0.3359	1.2658	1.21E-3
299-E25-234	69B	21.0	0.4087	0.0000	0.3553	1.4411	-
299-E25-234	83A	25.3	0.3925	0.0000	0.3198	1.3117	1.78E-4
299-E25-234	83B	25.3	0.3712	0.0011	0.1230	1.3815	-
299-E25-234	99A	30.2	0.3692	0.0000	0.7424	1.2557	2.24E-4
299-E25-234	99B	30.2	0.3774	0.0000	0.4371	1.2961	-
299-E25-234	110A	33.5	0.4293	0.0325	0.1964	1.8193	2.82E-4
299-E25-234	110B	33.5	0.4201	0.0327	0.1991	1.8015	-
299-E25-234	117A	35.7	0.4538	0.0260	0.1114	1.6538	3.63E-3
299-E25-234	117B	35.7	0.3831	0.0012	0.0230	1.5239	-
299-E25-234	126A	38.4	0.3637	0.0000	1.9541	1.2634	1.98E-3
299-E25-234	126B	38.4	0.3747	0.0000	0.8990	1.3152	-
241-AP	1G	-	0.2585	0.0200	0.1008	2.9224	1.24E-3
241-AP	2	-	0.5210	0.0958	0.0309	3.1071	5.97E-4
241-AP	3	-	0.4360	0.0552	0.0494	3.2863	8.10E-4
241-AP	4G	-	0.4086	0.0377	0.0666	2.6751	1.87E-3
241-AP	5	-	0.4280	0.0133	0.0118	1.3945	4.94E-5
88-1	TEST #1	4.8	-	-	-	-	3.01E-2
88-1	TEST #2	9.1	-	-	-	-	5.97E-3
88-1	TEST #3	18.3	-	-	-	-	5.20E-3
299-[illegible]38	-	15.1	0.2390	0.0000	1.4263	1.2658	5.70E-5
299-E33-38	-	51.0	0.2459	0.0000	0.4612	1.2507	5.00E-4
299-E33-38	-	57.1	0.3714	0.0018	0.0513	1.5057	7.10E-5
MW-10	-	13.7	0.4200	0.0223	0.0640	1.6950	5.31E-3
MW-10	-	26.2	0.4600	0.0253	0.0462	1.9281	1.97E-2

TABLE A.10. (contd)

Well # or Location	Sample	Depth m	θ_s $cm^3\ cm^{-3}$	θ_r $cm^3\ cm^{-3}$	α 1/cm	n	K_s $cm\ s^{-1}$
MW-10	-	32.0	0.3900	0.0271	0.0460	1.6380	1.73E-3
MW-10	-	38.1	0.4400	0.0214	0.0441	1.7647	4.39E-3
MW-10	-	50.3	0.4600	0.0308	0.0351	2.3036	6.63E-3
MW-10	-	59.4	0.3300	0.0487	0.0267	2.3731	2.65E-3
MW-10	-	62.5	0.3600	0.0214	0.0760	1.6255	6.63E-3
MW-10	-	74.7	0.4400	0.0179	0.0630	1.7787	7.39E-3
MW-10	-	80.8	0.4200	0.0169	0.0386	2.1470	2.65E-3
MW-10	-	86.9	0.4700	0.0168	0.0512	2.0848	3.54E-3
MW-5	-	15.2	0.4400	0.0293	0.0810	1.9709	3.53E-2
MW-5	-	21.3	0.4400	0.0485	0.0144	5.4201	1.57E-3
MW-5	-	27.4	0.4400	0.0218	0.0605	2.4414	2.16E-3
MW-5	-	39.6	0.4700	0.0311	0.0184	3.3059	4.42E-2
MW-5	-	51.8	0.4400	0.0281	0.0278	2.7143	3.81E-3
MW-5	-	57.9	0.4300	0.0242	0.0427	3.0699	5.78E-3
MW-5	-	64.0	0.4300	0.0302	0.1533	2.0330	5.42E-3
MW-5	-	70.1	0.4400	0.0243	0.0427	3.1603	5.31E-3
MW-5	-	82.3	0.4400	0.0000	0.1109	1.3428	5.54E-4
MW-8	-	44.2	0.4200	0.0335	0.0186	2.1503	8.86E-4
MW-8	-	56.5	0.4000	0.0367	0.0764	2.0668	7.19E-3
Number of Samples			57	57	57	57	45
Minimum			0.2390	0.0000	0.0118	1.1927	1.38E-5
Maximum			0.5304	0.0960	1.9541	5.4201	4.42E-2
Mean			0.4203	0.0234	0.1943	1.8680	5.48E-3
Variance			3.86E-3	4.63E-4	0.1142	0.5866	8.90E-5
Geom. Mean			0.4152	-	0.0918	1.7562	1.55E-3

TABLE A.11. Water Retention Parameters and Saturated Hydraulic Conductivity Data for the Upper and Lower Gravel Units of the Hanford Formation. All parameters, except those for Well No. 299-E25-234, are from Connelly et al. (1992b).

Well # or Location	Sample ID	Depth m	θ_s $cm^3\ cm^{-3}$	θ_r $cm^3\ cm^{-3}$	α 1/cm	n	K_s cm s
299-E25-234	133A	40.5	0.2732	0.0000	0.0182	1.3095	2.76E-5
299-E25-234	133B	40.5	0.2669	0.0000	0.0321	1.2590	-
299-E33-38	-	1.9	0.5256	0.0000	0.0081	1.7389	2.00E-5
299-E33-38	-	57.9	0.4187	0.0000	0.0027	1.5688	2.10E-6
299-E33-38	-	62.3	0.2905	0.0000	0.0101	1.3652	4.20E-3
299-E33-40	-	14.0	0.3021	0.0000	0.1028	1.2734	6.00E-4
216-B-61A	-	4.1	0.3465	0.0352	0.0061	1.5248	1.80E-3
216-B-61A	-	5.8	0.3253	0.0488	0.0060	1.5120	2.80E-3
216-B-61A	-	7.0	0.3430	0.0000	0.0134	1.2816	4.00E-4
216-B-61A	-	8.8	0.2801	0.0201	0.0609	1.2811	1.80E-5
6-43-41H	-	16.6	0.4510	0.1041	0.0165	1.7894	1.10E-5
6-42-41B	-	25.8	0.3550	0.0301	0.0426	1.3900	5.40E-3
MW-8	-	4.6	0.4400	0.0390	0.0440	3.0387	1.70E-3
MW-10	-	93.0	0.4000	0.0205	0.0427	2.2500	4.42E-3
Number of Samples			14	14	14	14	13
Minimum			0.2669	0.0000	0.0027	1.2590	2.10E-6
Maximum			0.5256	0.1041	0.1028	3.0390	5.40E-3
Mean			0.3584	0.0213	0.0290	1.6130	1.65E-3
Variance			6.12E-3	8.75E-4	7.79E-4	0.2348	3.80E-6
Geom. Mean			0.3509	-	0.0184	1.5600	2.73E-4

TABLE A.12. Water Retention Parameters and Saturated Hydraulic Conductivity Data for the Ringold Formation (undifferentiated). Parameters are from Connelly et al. (1992b).

Well # or Location	Sample ID	Depth m	θ_s $cm^3\ cm^{-3}$	θ_r $cm^3\ cm^{-3}$	α 1/cm	n	K_s cm s
6-42-41B	-	36.1	0.5730	0.0083	0.0132	1.2586	3.00E-8
699-40-40B	-	38.3	0.5680	0.0000	0.0051	1.1732	1.00E-8
699-43-41G	-	50.8	0.5710	0.0941	0.0150	1.4173	1.90E-6
699-43-40	-	39.9	0.3790	0.0387	0.0089	1.4739	1.90E-4
MW-5	-	91.4	0.4000	0.0000	0.0456	1.3661	7.66E-4
Number of Samples			5	5	5	5	5
Minimum			0.3790	0.0000	0.0051	1.1732	1.00E-8
Maximum			0.5730	0.0940	0.0456	1.4739	7.66E-4
Mean			0.4982	0.0283	0.0176	1.3378	1.92E-4
Variance			9.90E-3	1.61E-3	2.61E-4	1.48E-2	1.10E-7
Geom. Mean			0.4897	-	0.0133	1.3333	2.42E-6

TABLE A.13. Water Retention Parameters and Saturated Hydraulic Conductivity Data for Concrete

Sample ID	θ_s $cm^3\ cm^{-3}$	θ_r $cm^3\ cm^{-3}$	α 1/cm	n	K_s cm/s
CL-40A	0.1857	0.0000	1.220E-5	1.3567	3.55E-10
CL-40B	0.2146	0.0000	9.862E-6	1.3409	2.19E-10
CL-40C	0.2593	0.0000	3.826E-6	1.4412	4.69E-10
CL-40D	0.2322	0.0000	4.365E-5	1.4726	4.97E-10
CL-40E	0.2150	0.0000	1.074E-5	1.3396	4.43E-10
CL-40F	0.2480	0.0000	4.669E-6	1.4054	3.46E-10
Number of Samples	6	6	6	6	6
Minimum	0.1857	-	3.826E-6	1.3396	2.19E-10
Maximum	0.2593	-	1.220E-5	1.4726	4.97E-10
Mean	0.2258	-	7.610E-6	1.3927	3.88E-10
Variance	7.012E-4	-	1.389E-11	3.14E-11	1.06E-20
Geom. Mean	0.2245	-	6.822E-6	1.3918	3.75E-10

TABLE A.14. Water Retention Parameters and Saturated Hydraulic Conductivity Data for DSSF Grout

Sample ID	θ_s $cm^3\ cm^{-3}$	θ_r $cm^3\ cm^{-3}$	α 1/cm	n	K_s cm/s
GRT_A26	0.5853	0.0000	1.503E-5	1.5679	5.52E-9
GRT_A38	0.5775	0.0000	9.165E-6	1.6957	-
GRT_A73	0.5891	0.0000	8.804E-6	1.6690	-
GRT_B06	0.5611	0.0000	6.959E-6	1.7719	1.10E-8
GRT_B33	0.5725	0.0000	1.190E-5	1.6304	-
GRT_B52	0.5840	0.0000	1.141E-5	1.6227	-
GRT_C16	0.5741	0.0000	1.574E-5	1.5740	5.22E-8
GRT_C48	0.5779	0.0000	8.946E-6	1.6585	-
GRT_C82	0.5817	0.0000	8.970E-6	1.6565	-
Number of Samples	9	9	9	9	3
Minimum	0.5611	-	6.959E-6	1.5679	5.52E-9
Maximum	0.5891	-	1.574E-5	1.7719	5.22E-8
Mean	0.5781	-	1.077E-5	1.6496	2.29E-8
Variance	6.96E-5	-	9.008E-12	3.884E-3	6.61E-16
Geom. Mean	0.5781	-	1.042E-5	1.6486	1.47E-8

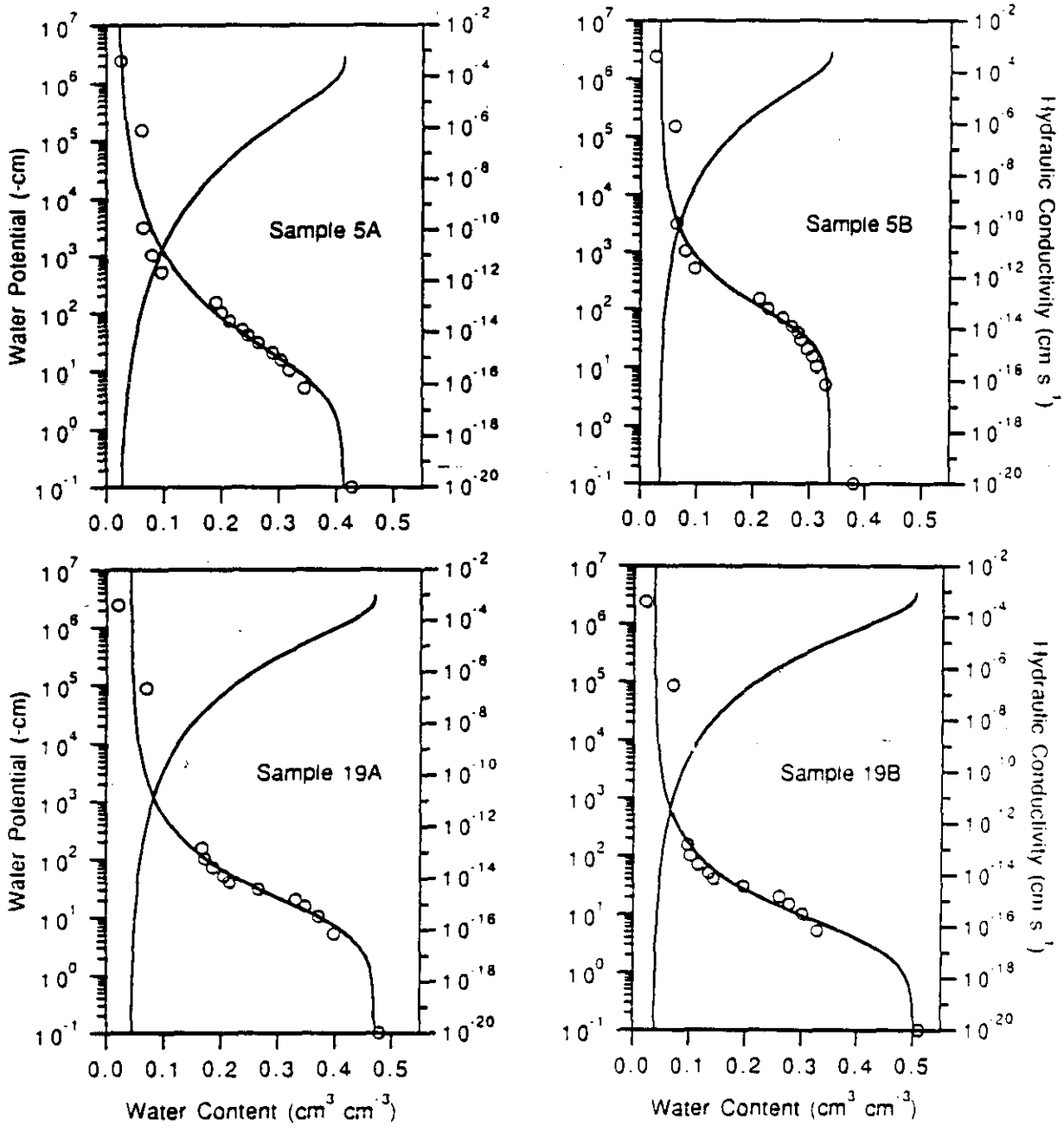

FIGURE A.1. Water Retention and Hydraulic Conductivity Data and Curves for Samples 5A, 5B, 19A, and 19B from Well No. 299-E25-234

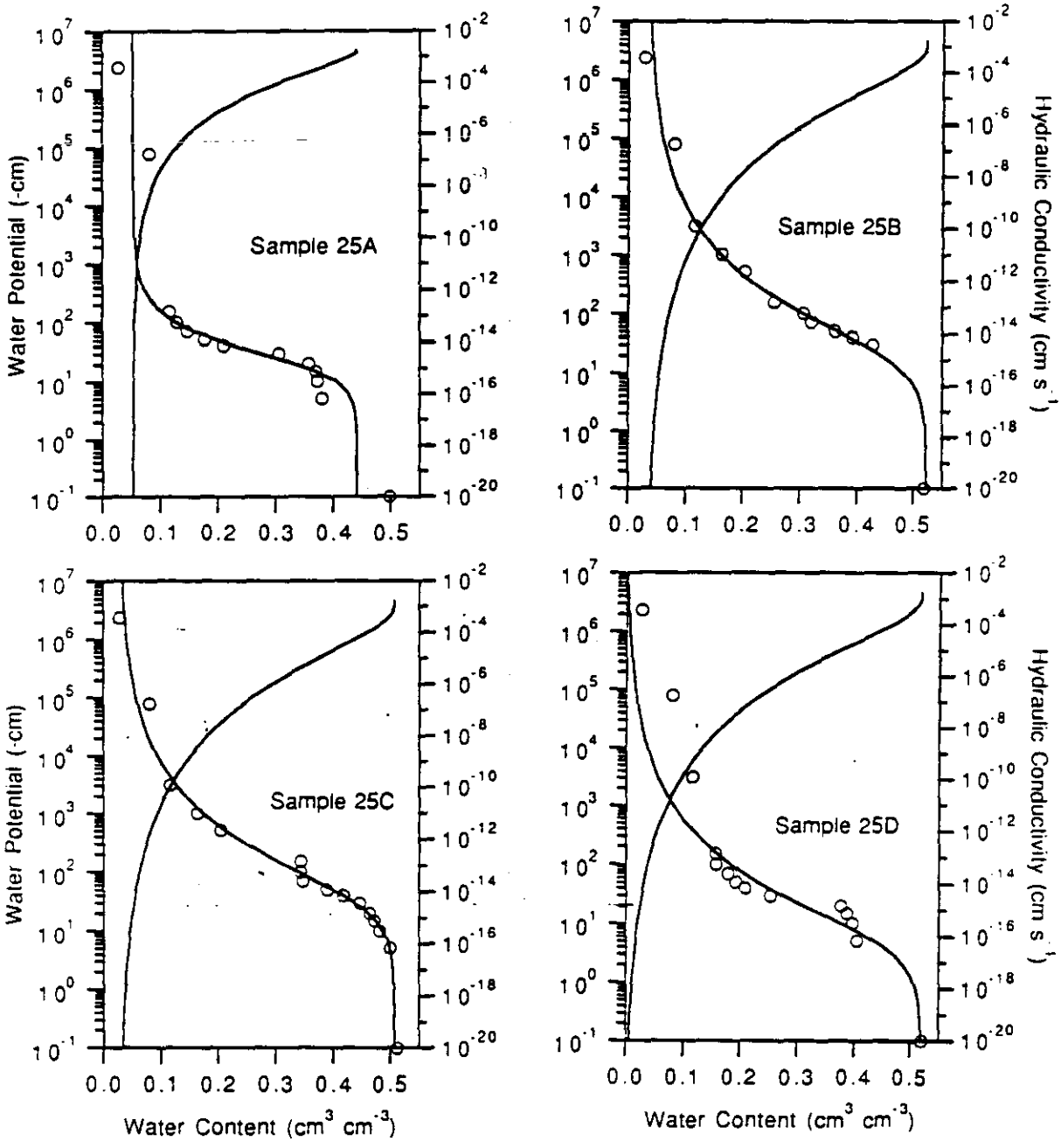

FIGURE A.2. Water Retention and Hydraulic Conductivity Data and Curves for Samples 25A, 25B, 25C, and 25D from Well No. 299-E25-234

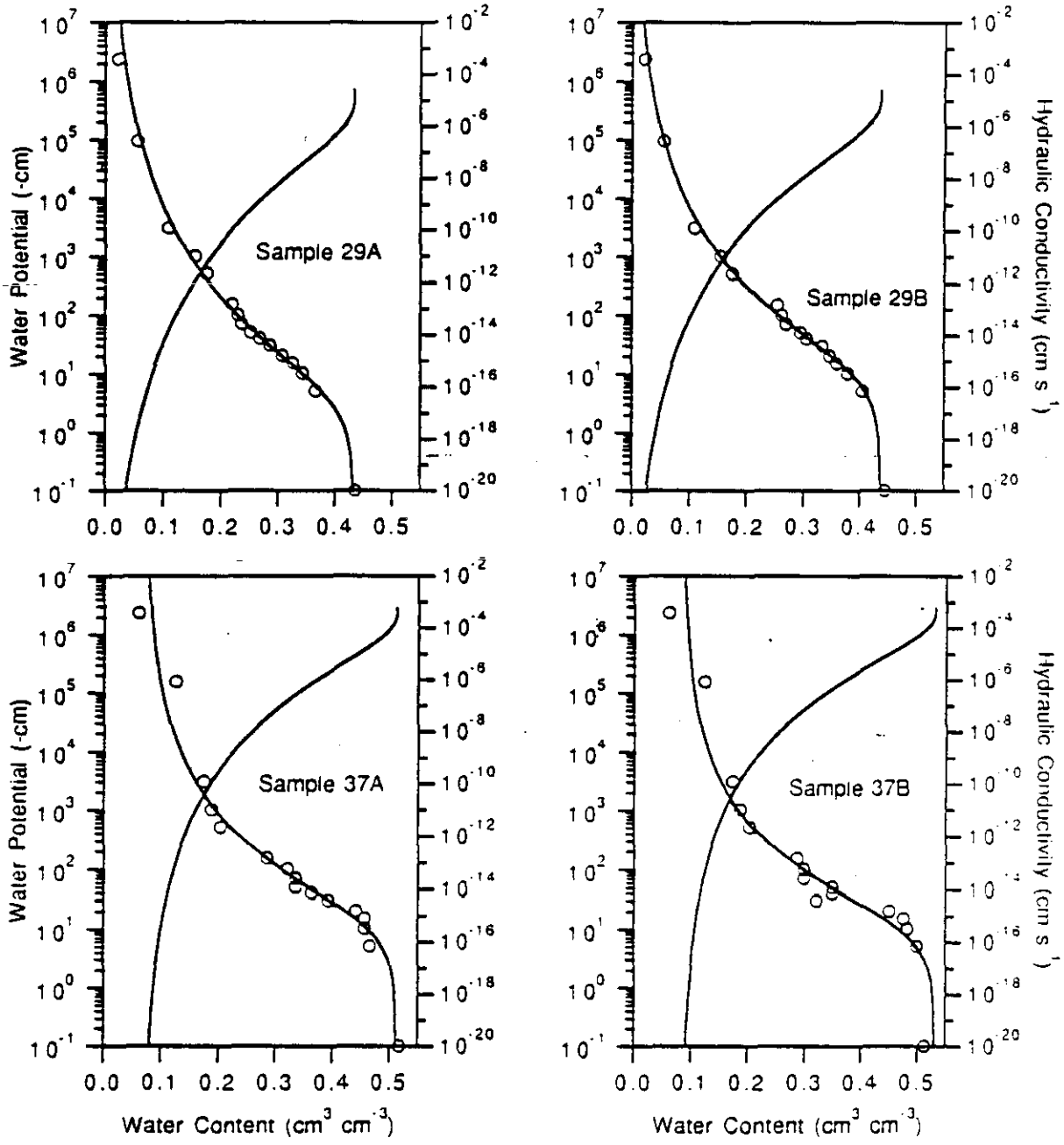

FIGURE A.3. Water Retention and Hydraulic Conductivity Data and Curves for Samples 29A, 29B 37A, and 37B from Well No. 299-E25-234

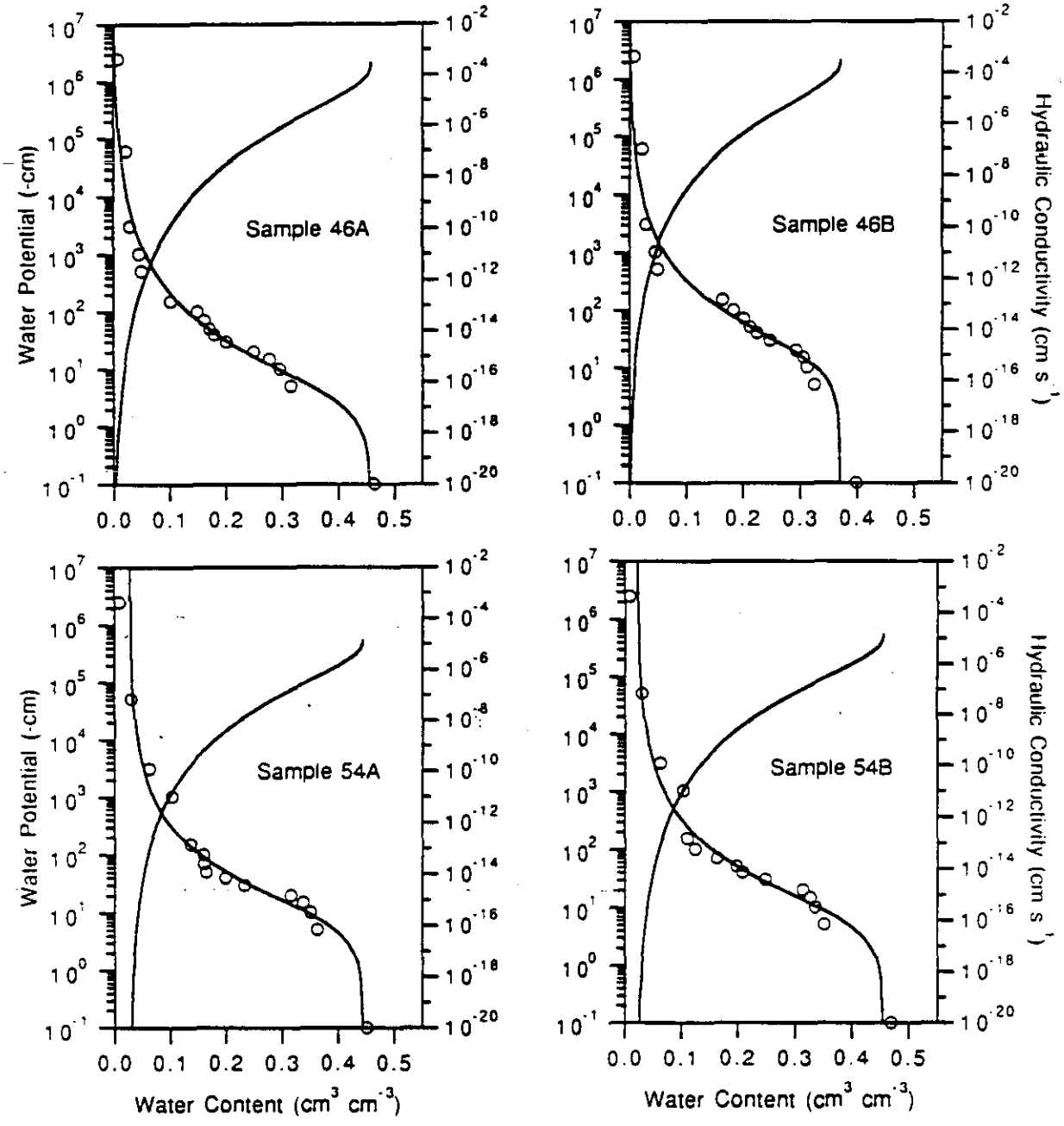

FIGURE A.4. Water Retention and Hydraulic Conductivity Data and Curves for Samples 46A, 46B, 54A, and 54B from Well No. 299-E25-234

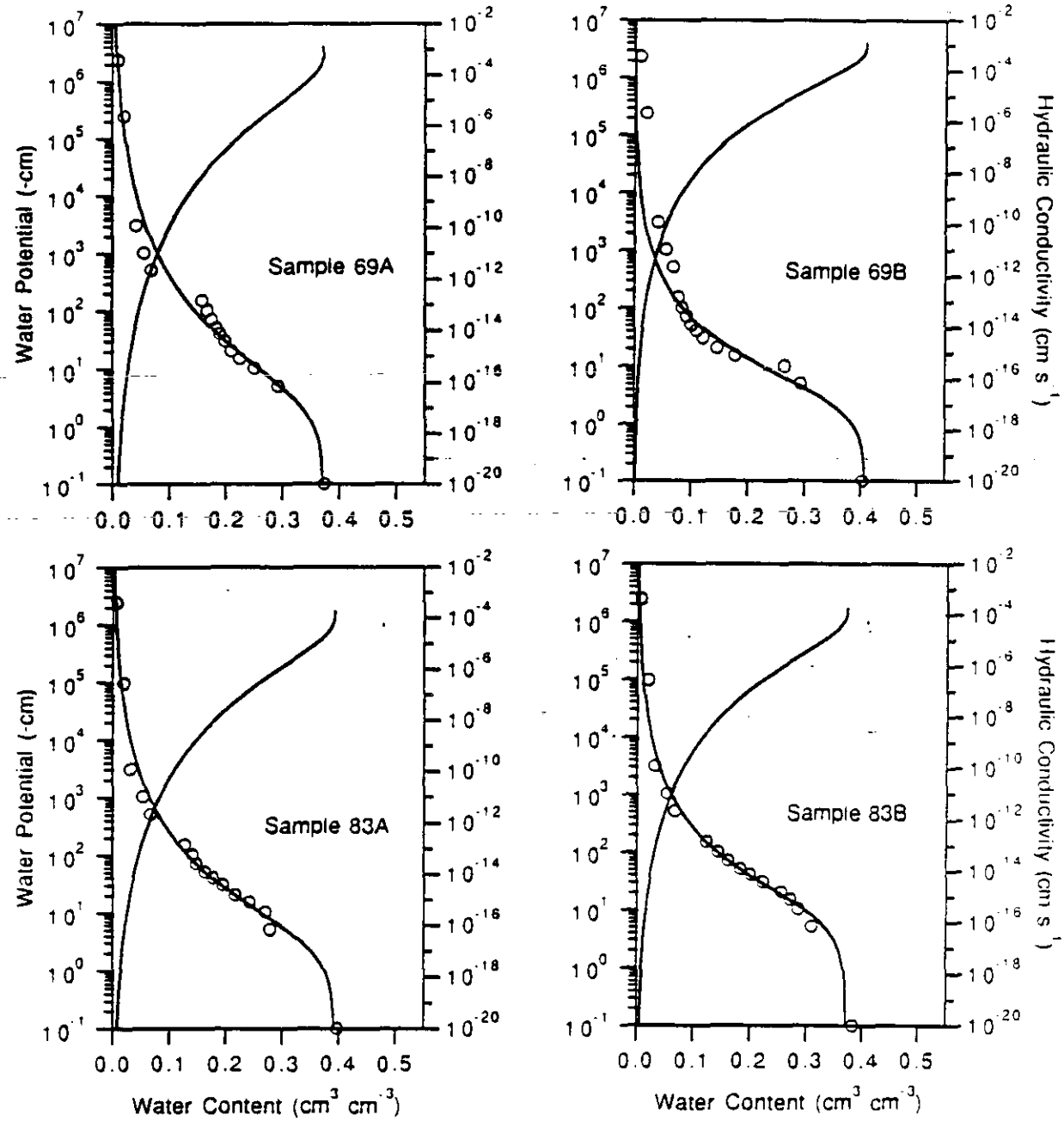

FIGURE A.5. Water Retention and Hydraulic Conductivity Data and Curves for Samples 69A, 69B, 83A, and 83B from Well No. 299-E25-234

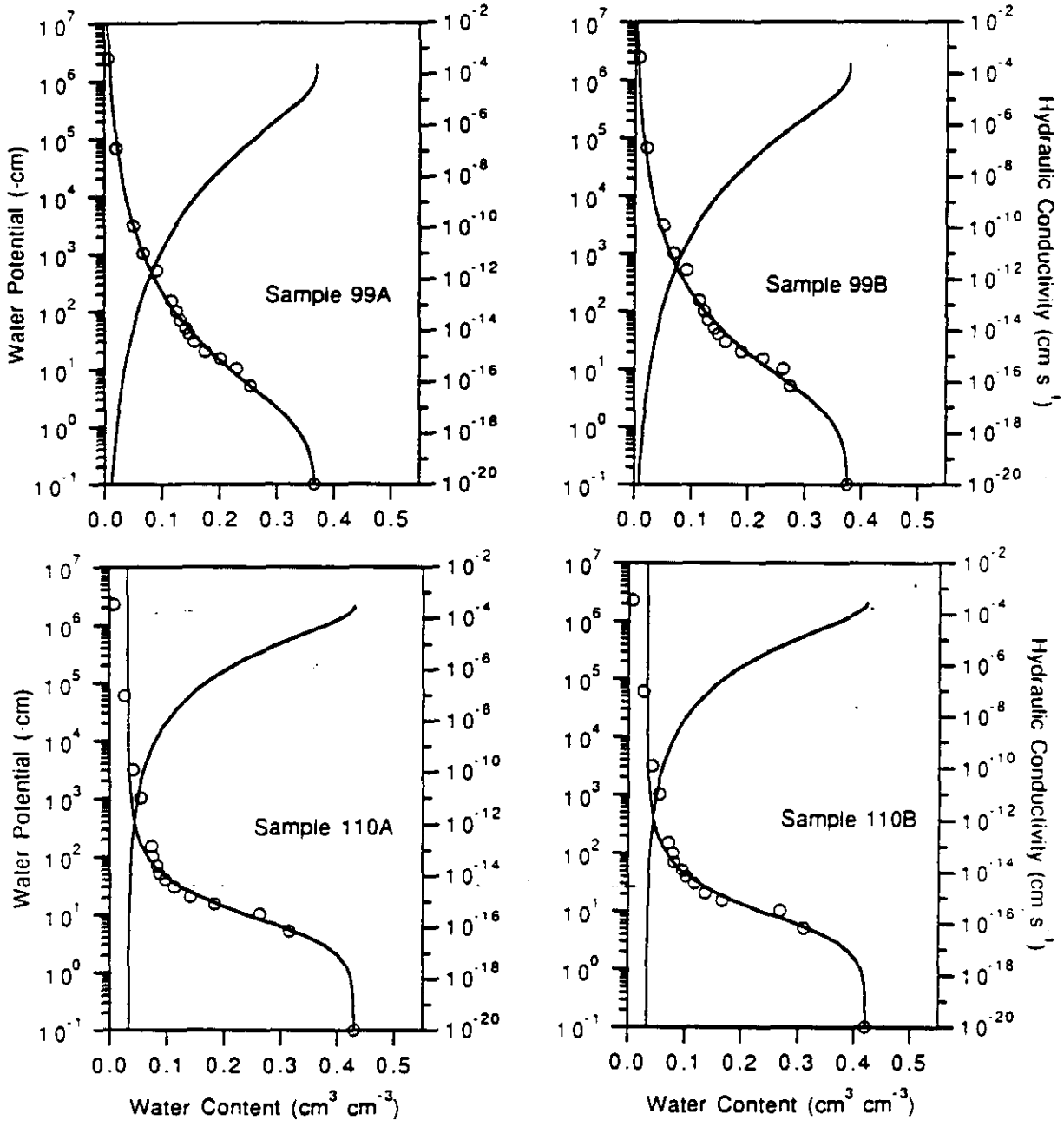

FIGURE A.6. Water Retention and Hydraulic Conductivity Data and Curves for Samples 99A, 99B, 110A, and 110B from Well No. 299-E25-234

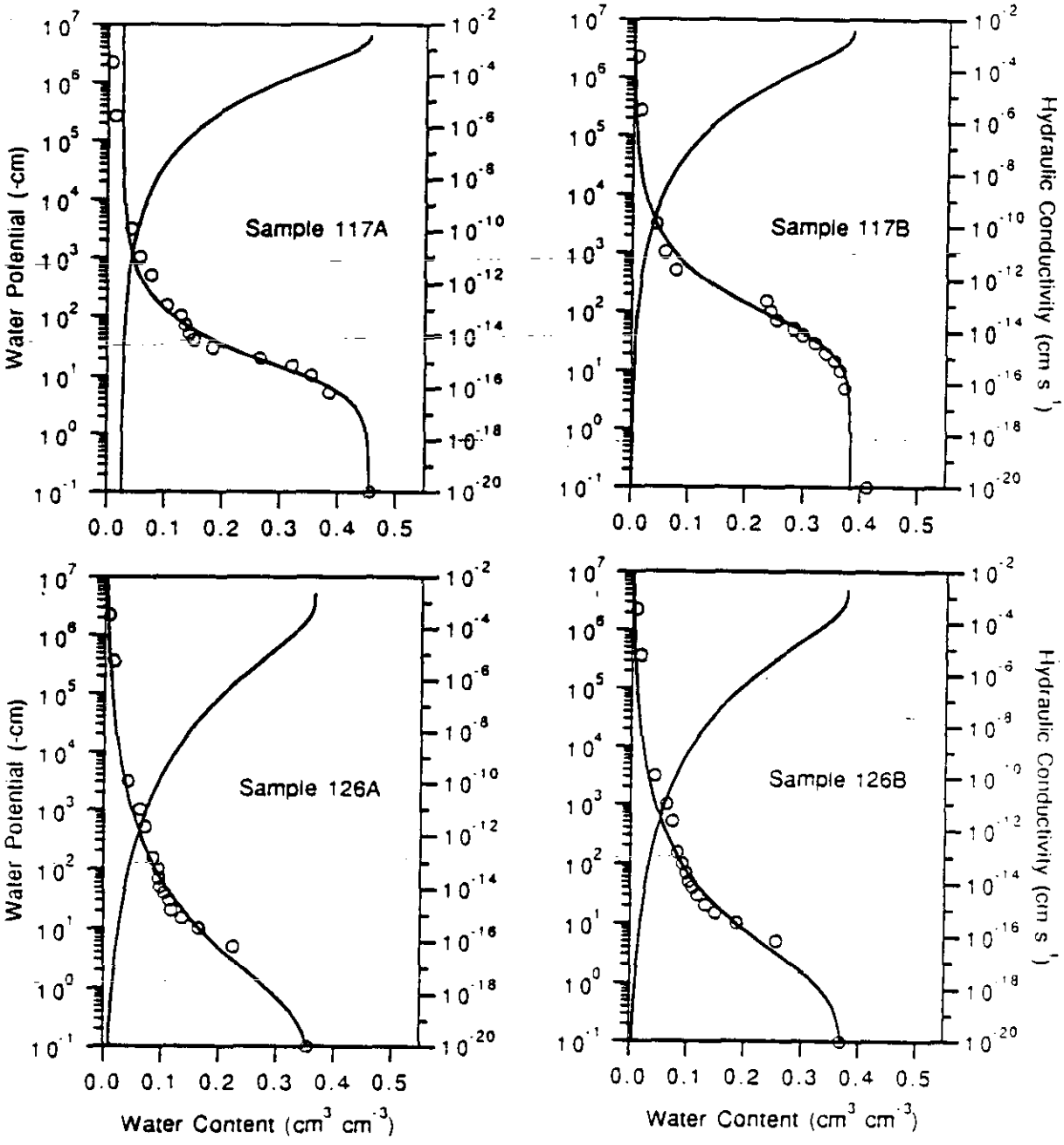

FIGURE A.: Water Retention and Hydraulic Conductivity Data and Curves for Samples 117A, 117B, 126A, and 126B from Well No. 299-E25-234

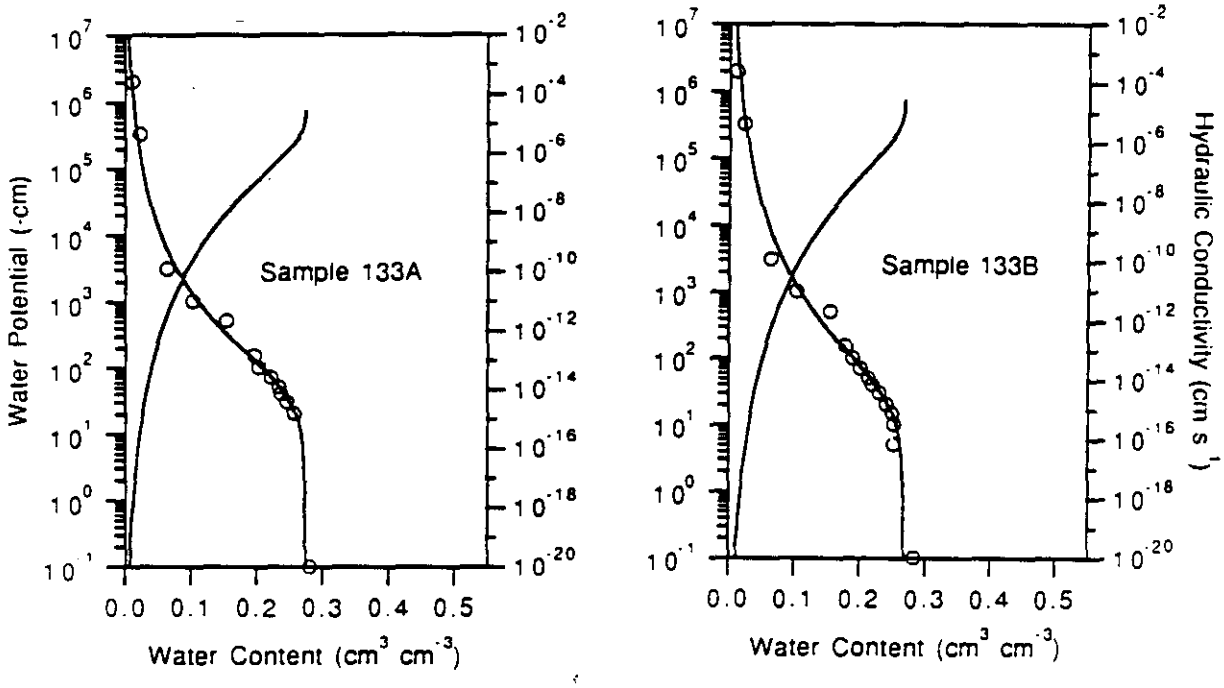

FIGURE A.8. Water Retention and Hydraulic Conductivity Data and Curves for Samples 133A and 133B from Well No. 299-E25-234

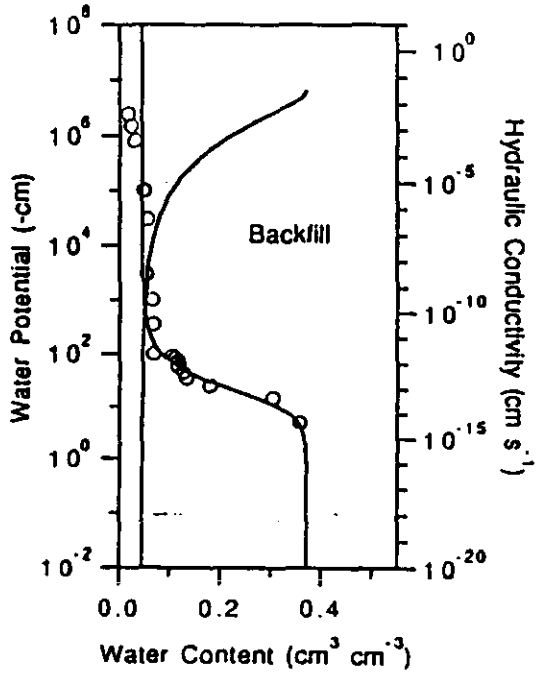

FIGURE A.9. Water Retention and Hydraulic Conductivity Data and Curves for Backfill Soil

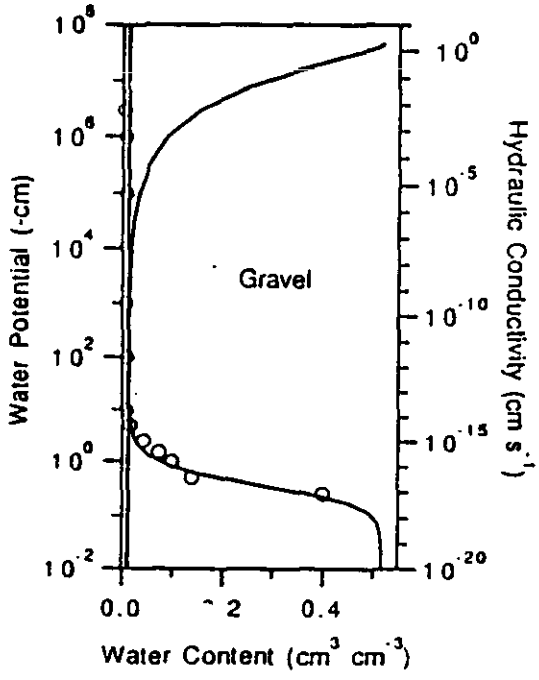

FIGURE A.10. Water Retention and Hydraulic Conductivity Data and Curves for Gravel

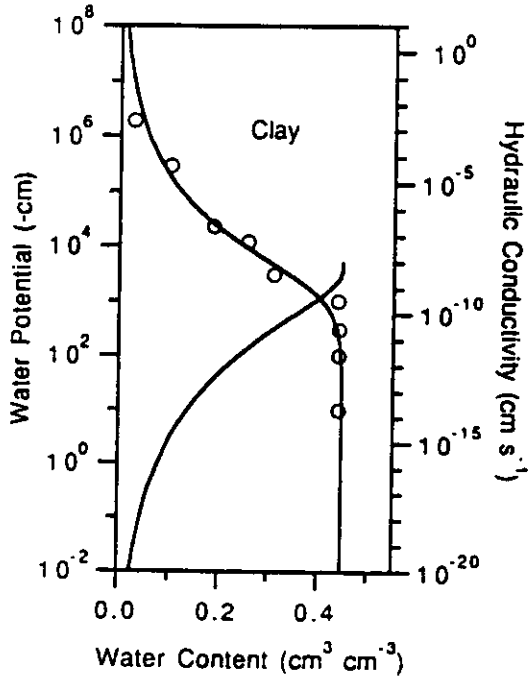

FIGURE A.11. Water Retention and Hydraulic Conductivity Data and Curves for RCRA Clay Cap

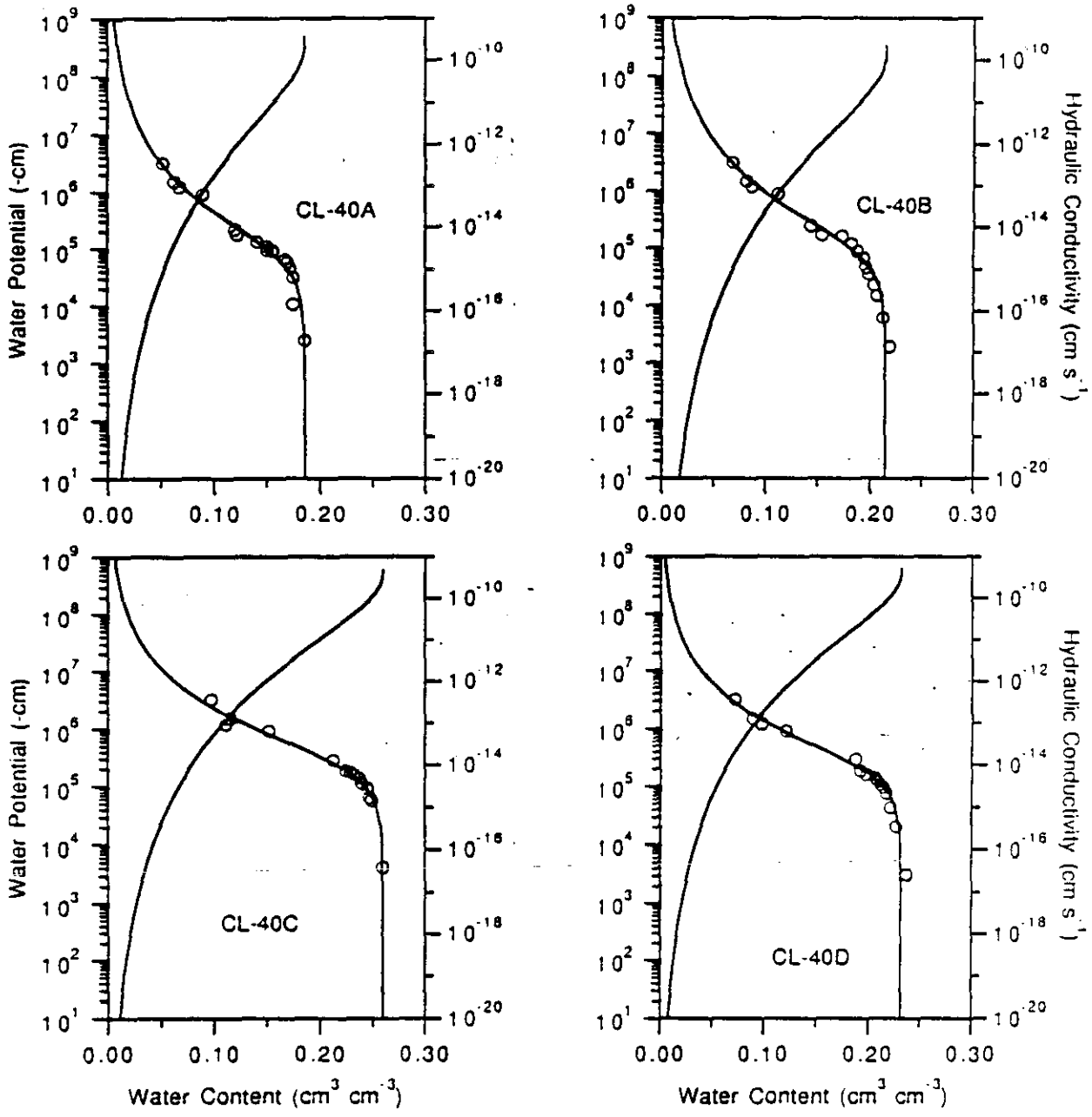

FIGURE A.12. Water Retention and Hydraulic Conductivity Data and Curves for Concrete Samples CL-40A, CL-40B, CL-40C, and CL-40D

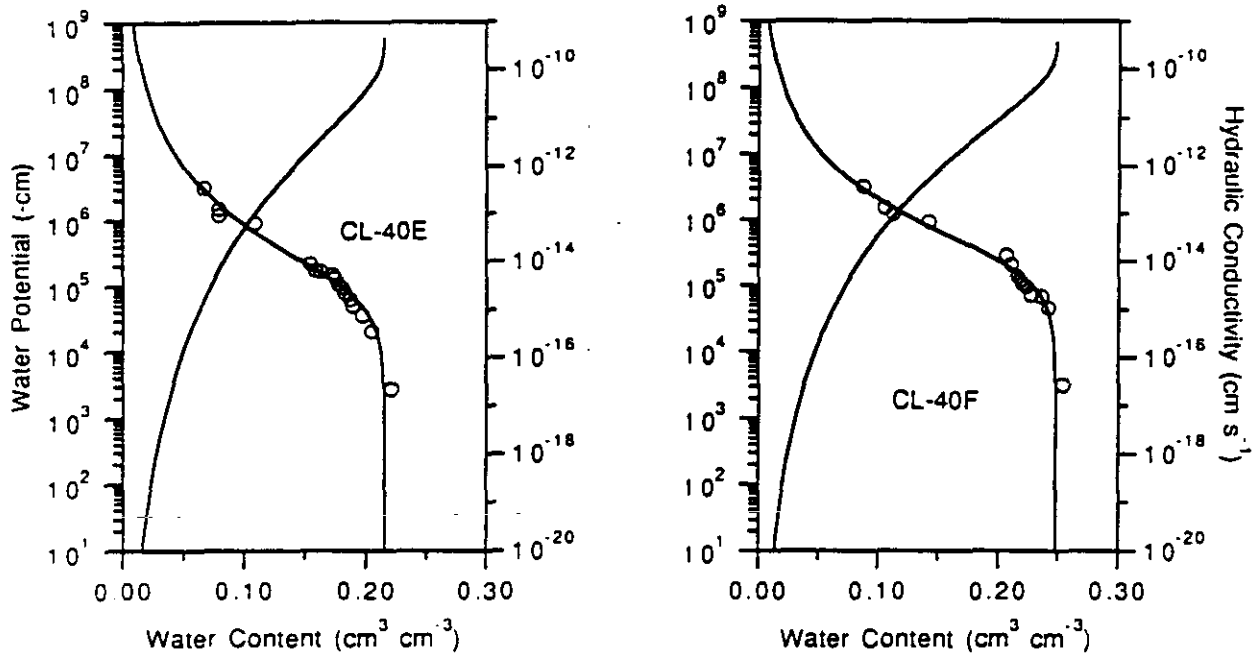

FIGURE A.13. Water Retention and Hydraulic Conductivity Data and Curves for Concrete Samples CL-40E and CL-40F

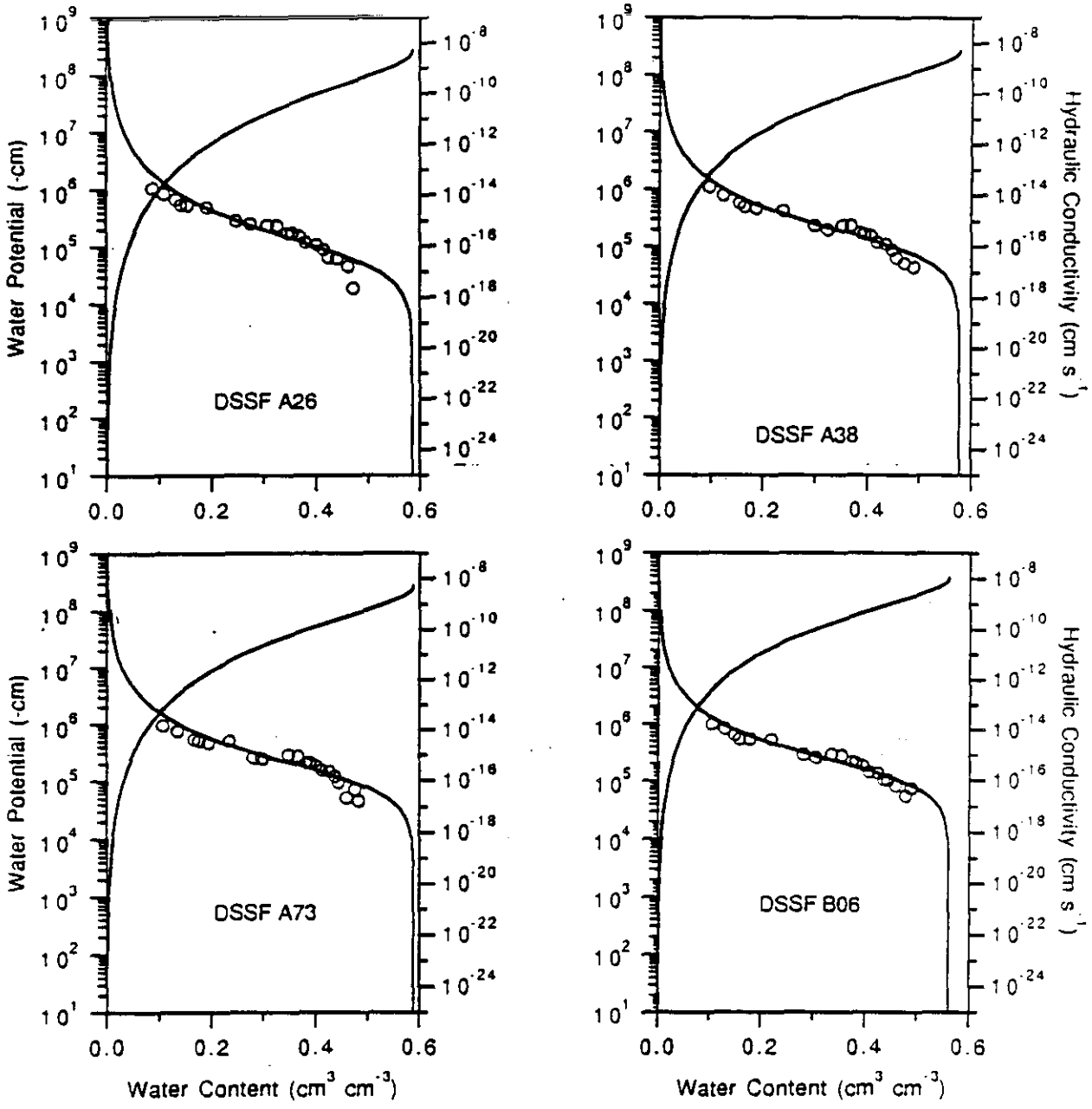

FIGURE A.14. Water Retention and Hydraulic Conductivity Data and Curves for DSSF Grout Samples A26, A38, A73, and B06

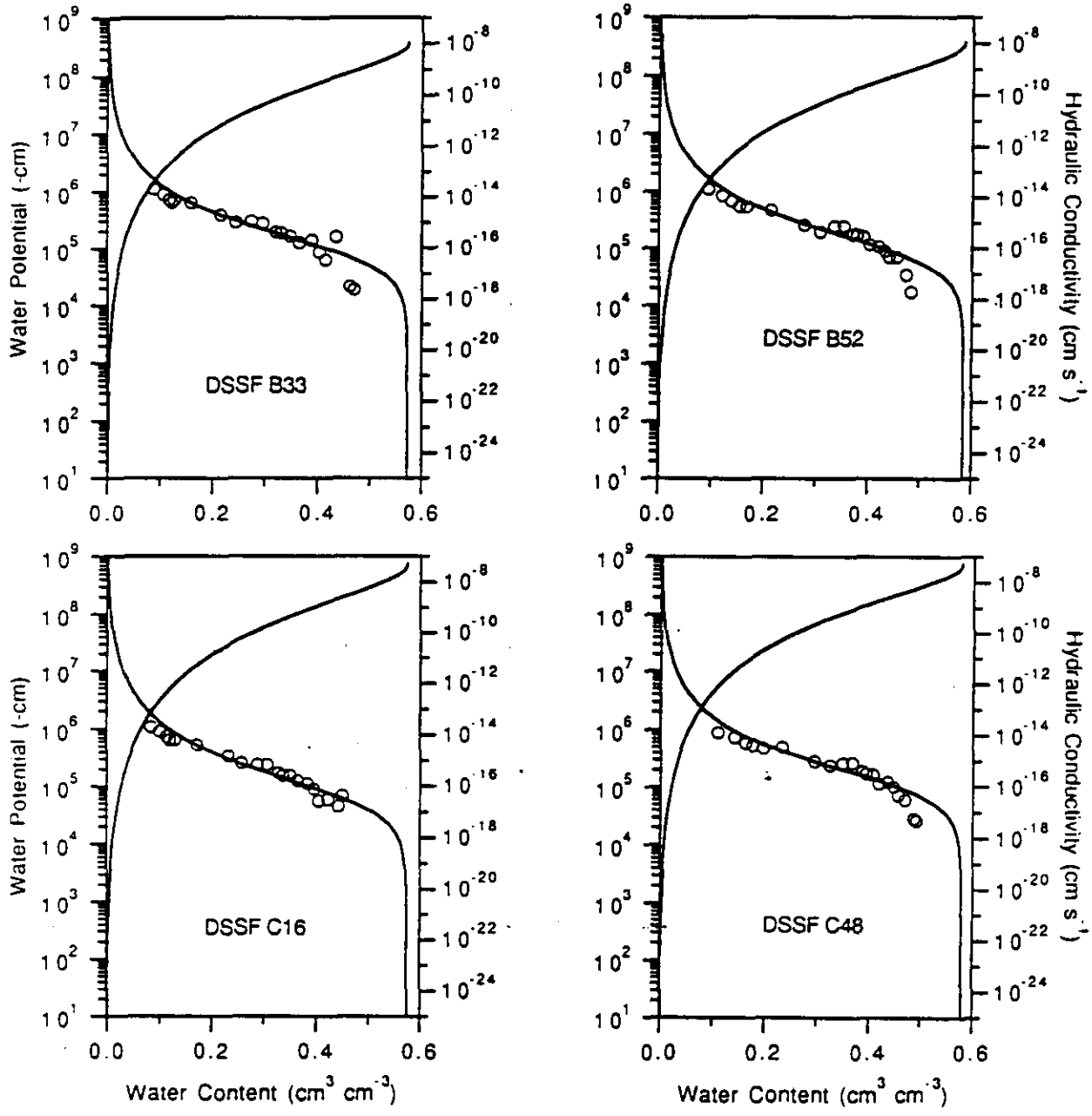

FIGURE A.15. Water Retention and Hydraulic Conductivity Data and Curves for DSSF Grout Samples B33, B52, C16, and C48

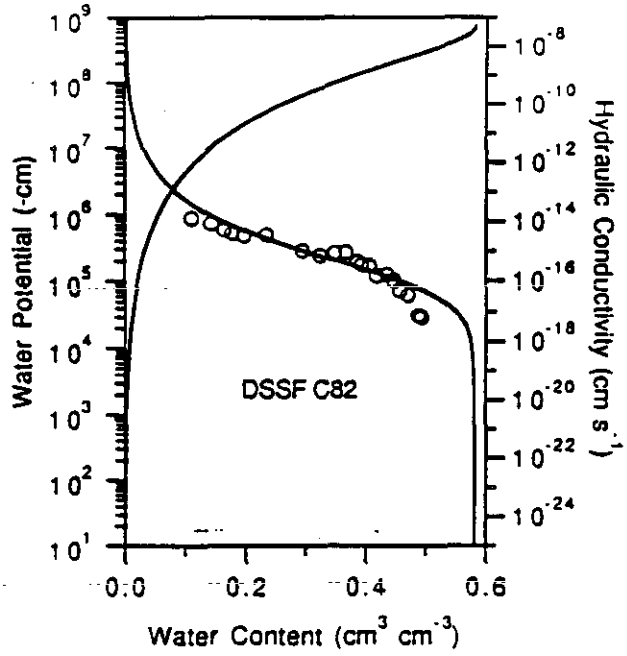

FIGURE A.16. Water Retention and Hydraulic Conductivity Data and Curves for DSSF Grout Sample C82

DISTRIBUTION

No. of Copies

OFFSITE

12 DOE/Office of Scientific and Technical Information

C. Frank, EM-50
DOE Office of Technology Development
Trevion-II
12800 Middlebrook Rd. Germantown, MD 20874

4 DOE Office of Waste Operations
Trevion-II
12800 Middlebrook Rd. Germantown, MD 20874
ATTN: J. A. Coleman, EM-35
M. W. Frei, EM-34
H. Harmon, EM-32
J. E. Lytle, EM-30

J. C. Haugen
DOE Chicago Operations Office 9800 South Cass Avenue Argonne, IL 60439

F. Bazan
Lawrence Livermore National Laboratory
University of California
P.O. Box 808
Livermore, CA 94550

5 Westinghouse Savannah River Company
Savannah River Site
Aiken, SC 29808-0001
ATTN: C. A. Langton
R. M. Wallace
E. Wilhite
E. Stevens
M. Hay

No. of Copies

M. Fuhrmann
Brookhaven National Laboratory
Upton, NY 11973

T. C. Johnson
Nuclear Regulatory Commission MS-623SS
Washington, DC 20555

M. McFadden
DOE Albuquerque Operations Office
P.O. Box 5400
Albuquerque, NM 87115

R. M. Neilson, Jr.
EG&G
P.O. Box 1625
Idaho Falls, ID 83415

3 Oak Ridge National Laboratory
P.O. Box X
Oak Ridge, TN 37831
ATTN: T. M. Gilliam
E. W. McDaniel
R. D. Spence

E. B. Peacock
Wastech, Inc.
P.O. Box 1213
Oak Ridge, TN 37831-1213

D. M. Smith
University of New Mexico
Chemical and Nuclear Engineering Department
Albuquerque, NM 87131

No. of Copies

FOREIGN

A. Atkinson
Atomic Energy Research Establishment
HARWELL
Didcot
Oxfordshire, OX 11 ORA
UNITED KINGDOM

L. P. Buckley
Atomic Energy of Canada Ltd. Chalk River, Ontario KOJ 1JO
CANADA

P. Cote
Environment Canada
Canada Centre for Inland Waters
Burlington, Ontario LTR 4A6
CANADA

R. Dayal
Ontario Hydro
800 Kipling Ave.
Toronto, Ontario M8Z 5S4
CANADA

C. L. Farmer
Atomic Energy Establishment
WINFRITH
Dorchester, Dorset DT2 8DH
UNITED KINGDOM

ONSITE

3 DOE Richland Operations Office

K. W. Bracken
L. A. Huffman
G. L. Sanders

No. of Copies

7 Westinghouse Hanford Company

K. C. Burgard
J. L. Epstein
D. W. Hendrickson
F. M. Mann
J. E. Van Beek
J. A. Voogd
G. F. Williamson

44 Pacific Northwest Laboratory

C. R. Allen
M. P. Bergeron
K. A. Blanchard
C. R. Cole
R. M. Ecker
M. J. Fayer (5)
A. R. Felmy
H. D. Freeman
M. D. Freshley
G. W. Gee
M. J. Graham
P. C. Hays
P. R. Heller
P. M. Irving
C. T. Kincaid
D. K. Kreid
R. J. Lenhard
R. O. Lokken
P. D. Meyer
M. I. McKinley
W. E. Nichols
K. R. Roberson
M. L. Rockhold (5)
W. A. Ross
P. A. Scott
J. R. Serne
R. L. Skaggs
C. S. Sloan
J. H. Westsik, Jr.
G. A. Whyatt
Publishing Coordination
Technical Report Files (5)

This page intentionally left blank.

Appendix K

Status Report on Ionic Diffusion Through Asphalt

This page intentionally left blank.

HGTP-92-0602-02

Draft Letter Report for Westinghouse Hanford Company

STATUS REPORT ON IONIC DIFFUSION THROUGH ASPHALT

P. F. C. Martin
R. J. Serne
V. L. LeGore
C. W. Lindenmeier

November 1992

Prepared for
the U.S. Department of Energy
under Contract DE-AC06-76RLO 1830

Pacific Northwest Laboratory
Richland Washington

LIMITED DISTRIBUTION NOTICE

This document copy, since it is transmitted in advance of patent clearance, is made available in confidence solely for use in performance of work under contracts with the U.S. Department of Energy. This document is not to be published nor its contents otherwise disseminated or used for purposes other than specified above before patent approval for such release or use has been secured, upon request, from Patent Services, Pacific Northwest Laboratory, Richland, Washington 99352.

SUMMARY

Containment structures for grouted wastes produced at the Hanford site incorporate an asphalt/aggregate barrier that surrounds the primary vault of reinforced concrete. The purpose of the asphalt/aggregate barrier is to retard the release of contaminants to the environment, as modeled in performance assessment activities, to acceptably low levels. Tests to determine diffusion rates of ionic contaminants were begun in FY91 and continued in FY92. The continuing experiments were American Nuclear Society (ANS) 16.1 leach tests of asphalt/aggregate composite samples spiked with radionuclides and diffusion analyses of contaminants into asphalt coupons immersed in contaminant spiked solutions. From these tests the diffusion of organic complexed cobalt ($^{60}Co^{2+}$-EDTA), cesium ($^{137}Cs^{+}$), iodide ($^{125}I^{-}$), nitrate (NO_3^-), and pertechnetate ($^{99}TcO_4^-$) were assessed.

Leach tests have yielded effective diffusivities below the baseline value of 1×10^{-10} cm^2/sec used in performance assessment (PA) calculations. Bulk diffusivities for NO_3^- and $^{99}TcO_4^-$, adjusted to a consistent basis for PA calculations, yield diffusivities that are approximately 60% of the PA baseline value for NO_3^- and approximately 25% of the baseline value for $^{99}TcO_4^-$. The other bulk diffusivities are well below the PA baseline value. However, by drying the contaminants onto the aggregate before coating with asphalt it is possible that results are biased low by allowing adsorption on the aggregate to retard release of some contaminants.

Immersion tests on asphalt alone (no aggregate in sample) have yielded diffusion coefficients that are well below the PA calculation baseline. These tests involved determining contaminant concentrations in microtomed slices taken from asphalt "coupons" exposed on one surface to contaminant-spiked solutions to yield a concentration profile. These concentrations were then transformed using the "probit" technique to calculate the diffusivities of the contaminants.

Other activities included the development and fabrication of asphalt/aggregate composite membranes and the manufacture of fourteen half-cell diffusion test assemblies from an improved design. These

half-cells will be used in FY93 to perform further diffusion measurements. The half-cell tests are important because 1) the half-cell membranes are made without incorporated contaminants, 2) the membranes are fabricated using methods representative of those used in construction of the asphalt/aggregate barrier, 3) the membranes incorporate all materials used in the actual barrier, and 4) the half-cells simulate the two diffusion interfaces of the grout disposal system, namely, the vault-asphalt interface and the asphalt-vadose sediment pore water interface.

9413222.1678

INTRODUCTION

At Hanford, the disposal system for grout-solidified tank wastes includes an engineered barrier constructed of an asphalt/aggregate mix measuring approximately one meter thick that surrounds the entire concrete grout containment vault and the vault's leachate collection system. The purpose of this asphalt/aggregate barrier is to greatly impede the diffusion of water-soluble contaminants by interposing a hydrophobic material that breaks contact between dissolved contaminants in the waste form and the surrounding soil and soil pore water. The DSSF grout performance assessment (PA) calculations show that the values chosen for contaminant diffusion through the diffusion barrier are key to determining whether the proposed grout disposal system will minimize long-term risks to acceptable levels.

The values for the diffusion coefficients chosen in PA calculations were gleaned from generic literature. Diffusion of water solutes through asphalt/aggregate are expected to be very small (e.g., D_e values $<10^{-10}$ cm^2/s) such that classical methods to determine diffusion coefficients would require testing activities to span several years. For example, Daiev and Vassilev (1985) found ^{90}Sr diffusion coefficients through pure bitumen to be 1.5 to 3.3 x 10^{-12} cm^2/s in tests that took 6 to 12 years to yield data. The penetration depth of ^{90}Sr was only 0.06 cm and 0.09 cm after 6 and 12 years, respectively.

The purpose of tests conducted in FY91-92 were to determine effective diffusion coefficients for representative contaminants found in DSSF grout through asphalt and the asphalt/aggregate mix used to construct the diffusion barrier. The tests conducted provide Hanford-Site specific data that will verify whether values chosen in the PA calculations are appropriately conservative. That is, our tests experimentally addressed whether the effective diffusion coefficients of contaminants through solid asphalt and asphalt/aggregate mix are less than 1 x 10^{-10} cm^2/s. Because each contaminant could have a distinctly different effective diffusion coefficient, we have studied several important contaminants. The experimental methods being used include the ANS 16.1 leach method, an immersion method and a half-cell method.

METHODS

LEACH TEST METHODS

Selection of radionuclides and ionic species for use in evaluating diffusivity through asphalt were driven by the chemical composition of the waste, a knowledge of which chemical species are most problematic in performance assessment calculations, and also because of practical considerations of experimental detection. Nitrate, $^{99}TcO_4^-$, and $^{129}I^-$ are mobile contaminants within DSSF grout that constitute significant dose and contamination hazards in PA calculations. $^{125}I^-$ was substituted for $^{129}I^-$ because it is a more convenient isotope to use in testing. $^{137}Cs^+$ was chosen to represent other water-soluble contaminants that readily diffuse through both grout and concrete. $^{137}Cs^+$ is also an ideal tracer because it has a long half-life and, as a strong gamma emitter, is easily detectable. Cobalt-60 was used because it forms a strong organic complex with chelators such as EDTA. The behavior of ^{60}Co-EDTA complex should make clear if diffusion is enhanced by organic chelation through increased chelated-contaminant solubility in asphalt.

Table 1 shows the contaminants incorporated into the asphalt/aggregate leach test samples. The samples used in these leach tests consisted of cylinders made from asphalt/aggregate into which the contaminants had been incorporated using the following technique. Contaminants were dried onto the aggregate along with the hydrated lime that is used to enhance the adhesion of asphalt to the aggregate. The contaminant-spiked aggregate was then heated to barrier construction specifications, mixed with molten asphalt, and compacted into cylindrical molds to a void content of less than 4 vol%. Before starting, duplicate samples of asphalt/aggregate (samples 1 through 8 in Table 1) were "cured" in their molds at room temperature or at 90°C for several days. To address precision, triplicate samples 9 through 11 were cured at room temperature.

9413222.1680

TABLE 1. Leach Test Sample Contaminants

Sample	Contaminants
1, 2, 3, 4	NO_3^- and $^{125}I^-$
5, 6, 7, 8	NO_3^- and $^{99}TcO_4^-$
9, 10, 11	$^{137}Cs^+$ and $^{60}Co^{2+}$-EDTA
12, 13, 14	none

Eleven asphalt/aggregate specimens (4.0-cm diameter by 5.1 to 5.7-cm long) are being tested at room temperature. The leach tests employ the ANS 16.1 leaching procedure in which solids of known geometric surface area are immersed in a known quantity of leachate. The samples are periodically immersed in fresh leachant, and the previous leachate is analyzed for concentration of the contaminants. The leachate change is made to ensure that the concentration gradient driving diffusion is as large as practicable. Use of this method also assumes that the asphalt does not react significantly with the leachant, the surface area available for leaching does not change, and that contaminants are not released from the sample by any other time-dependent mechanisms. Meeting these assumptions permits the use of the following equation to calculate a diffusion coefficient (Godbee et al. 1980):

$$D_e = \frac{\pi}{4}\left(\frac{\Sigma a_n}{A_o}\right)^2 \left(\frac{V}{S}\right)^2 \left(\frac{1}{t}\right) \qquad (1)$$

where D_e = bulk diffusivity (cm^2/s)

a_n = amount of contaminant released in the nth water exchange (radionuclide decay corrected to activity at test start)

A_o = initial inventory of contaminant in sample

V = geometric volume of sample (cm^3)

S = geometric surface area of sample (cm^2)

t = total time of leaching (s).

IMMERSION TEST METHODS

The immersion method employed "coupons" of asphalt contained within Teflon® polytetrafluoroethylene (PTFE) molds. A total of 34 samples were prepared and were immersed in one of two 4 M $NaNO_3$ solutions. One solution was spiked with $^{137}Cs^+$, and the other with $^{99}TcO_4^-$. The coupons are approximately 1.3-cm thick x 3.2-cm square. Because asphalt was exposed to the immersion fluid on only one surface, the contaminants could diffuse into the sample in one direction only. Surface PTFE exposed to the immersion solution was removed to approximately half of its 1/8 in. thickness before microtoming asphalt coupons to measure diffusion. PTFE immediately under the exposed surface was assayed for radionuclide activity to ensure that it had served as a barrier to diffusion of contaminants as intended. No net measurable activity was detected below the surface-contaminated slices of the PTFE coupon molds implying that there was no detectable diffusion of contaminants through the PTFE into the asphalt.

Following 263 days of immersion, two coupon samples were removed from each of the immersion baths and rinsed with deionized water. The asphalt coupons were then carefully sectioned using a microtome set to cut a nominal thickness of 20 µm. Any remaining PTFE was pulled from the coupon before the sections were placed into separate tared vials for radionuclide assay or further treatment, such as extraction or dissolution.

Each of the thin sections thus obtained were analyzed for concentration of the contaminant. ^{137}Cs was analyzed by direct gamma counting. Asphalt slices from the same nominal depths of two coupons were composited to increase the activity for improved counting.

Nitrate concentrations were obtained from the microtomed asphalt slices following ^{137}Cs assay by extraction using water vapor, as follows. A small aliquot of deionized water was added to the vials which were then tightly capped and placed in a constant-temperature oven operating at 75°C. After two weeks the vials were cooled and the resulting solutions were analyzed for NO_3^- using Ion Chromatography (IC).

Concentrations of ^{99}Tc were determined by scintillation counting. Microtomed slices from asphalt coupons, immersed in a 200 µCi/L ^{99}Tc 4 M $NaNO_3$ solution, were weighed before being dissolved in aliquots of scintillation cocktail. The scintillation cocktail completely dissolved the asphalt but the solutions were opaque. Aliquots of the resulting opaque solutions were then diluted with more scintillation cocktail to give solutions of equal asphalt concentration so that the reduction in counting efficiency (in this case, light transmission) would be the same for each sample.

The effective diffusion coefficients were determined using probit methods (a mathematical reduction scheme) described in Phillips and Brown (1964), and Brown et al. (1968, 1969). Using the analytical data, the ratios of contaminant concentration, present in each of the asphalt thin sections, over the initial concentration driving diffusion into the coupon, were calculated (C/C_o). These normalized concentration values were then transformed into probits by interpolating corresponding values from a table in Probit Analysis (Finney, 1971). The mathematical manipulations require plotting the probit of normalized concentration, C/C_o, at a given sampling time, versus distance from the interface. A least squares linear regression was performed on the values of probit number versus median distance from the surface. The diffusion coefficient (D) is related to the square of the slope by the following formula:

$$D = \frac{1}{2m^2t}, \ cm^2/s \qquad (2)$$

where m is the slope of the regression line and t is the total time of diffusion (exposure) in seconds.

Use of this mathematical approach assumes that the concentration of the diffusing substance remains constant at the interface (asphalt surface-solution boundary) and that the asphalt specimen's dimensions are semi-infinite (much larger than the distance of penetration of diffusing substances). Data have indicated that both assumptions are valid for these tests.

The technique for these probit tests was based on diffusion from a uniformly contaminated soil sample in contact with an uncontaminated soil sample. After a suitable period, the soil diffusion test produces data distributed in a normal sigmoid curve with its center at the interface between the two soil samples. The test is intended to be semi-infinite in both directions from the interface, consequently, a) on the contaminated sample side, contaminant concentrations increase to the C_o concentration with increasing distance from the interface (depleting contaminant source), b) on the initially uncontaminated side, contaminant concentrations decrease to zero with increasing distance from the interface, and c) contaminant concentration at the interface will equal 50% of the C_o. In our coupon tests diffusion is semi-infinite in only one direction so we must adjust our data analysis scheme as follows.

When applied to the immersion of asphalt coupons immersed in a contaminant-doped fluid, the diffusion conditions are approximated by a constant (non-depleting) contaminant source diffusing into a semi-infinite volume of asphalt. The concentration profile developed with these boundary conditions is one-half the normal sigmoid curve. To apply the probit transformation to the data generated in the asphalt test, the contaminant concentrations are converted to percents (normalized) using C_o' where $C_o' = C_o \times 2$. C_o' represents the initial concentration that would have been needed to develop the concentration profile from a test set up with boundary conditions of the soil diffusion test that produces conditions (b) and (c) above. After conversion or the data from microtomed slices to probits using C_o', the diffusivity is then calculated as described in equation 2.

RESULTS

LEACH TEST RESULTS

Leach tests of radioactively spiked asphalt/aggregate samples have been underway since late April 1991. The latest leachant change-out occurred at an elapsed time of 330 days. Data from leachate analysis for these samples are presented in Table 2.

The data in Table 2 clearly show that different contaminants are released from the asphalt/aggregate samples at different rates, with NO_3^- and $^{99}TcO_4^-$ leaching fastest and ^{137}Cs slowest. Those samples that were cured for several days at 90°C leach at a slower rate than those that were cured at room temperature. It is likely that hot curing produced a better surface film of asphalt around the aggregate, and therefore, produced a sample that released its contaminants more slowly. The incremental leach rates have dropped since the start of the leach test, which may have been the result of an initial release of contaminants through small surface imperfections in the sample. At later intervals the leach rates dropped because contaminant sources near these imperfections had become relatively depleted.

The bulk diffusion coefficients calculated from the laboratory tests assume that the entire volume of the specimen can promote diffusion. However, the PA conceptual model and computer codes assume that diffusion occurs only in the asphalt phase—that is, the aggregate and any air voids cannot support diffusion. To get the same flux of contaminants through the asphalt/aggregate barrier, as measured in the ANS 16.1 leach tests, the leach test-derived values are multiplied by the fractional volume of diffusion-supporting asphalt. Diffusivities are first calculated using a contaminant-concentration driving force defined in the entire asphalt/aggregate mix, this is then adjusted to a driving force based on concentrations that would be found in the asphalt phase. This places the diffusivities on a consistent basis. For this

TABLE 2. Bulk Effective Diffusion Coefficients (cm^2/s) for Contaminants of Asphalt-Coated Aggregate Samples from ANS 16.1 Leach Tests

Contaminant	Cured	D_e (incremental) (224-330 days)	D_e (cumulative) (through 330 days)
$^{125}I^-$ (a)	20°C	$8.1 \pm 5.1 \times 10^{-12}$	$2.8 \pm 1.0 \times 10^{-11}$
	90°C	$3.2 \pm 0.7 \times 10^{-12}$	$1.4 \pm 0.4 \times 10^{-11}$
$^{99}TcO_4^-$	20°C	$3.6 \pm 0.6 \times 10^{-11}$	$1.4 \pm 0.2 \times 10^{-10}$
			$2.3 \pm 0.2 \times 10^{-11}$ (b)
	90°C	$4.9 \pm 0.1 \times 10^{-11}$	$1.2 \pm 0.1 \times 10^{-10}$
			$1.9 \pm 0.2 \times 10^{-11}$ (b)
$^{137}Cs^+$	20°C	$< 3 \times 10^{-14}$	$< 5 \times 10^{-14}$
$^{60}Co^{2+}$-EDTA	20°C	$1.2 \pm 0.3 \times 10^{-11}$	$8.3 \pm 0.9 \times 10^{-12}$
NO_3^- (c)	20°C	$1.5 \pm 0.2 \times 10^{-10}$	$3.5 \pm 0.2 \times 10^{-10}$
			$5.7 \pm 0.2 \times 10^{-11}$ (b)
	90°C	$1.8 \pm 0.1 \times 10^{-10}$	$2.7 \pm 0.1 \times 10^{-10}$
			$4.4 \pm 0.1 \times 10^{-11}$ (b)

(a) I^- incremental period 56-98 days, cumulative period 98 days
(b) values are adjusted by 0.162 (explained in text)
(c) nitrate values are an average of two samples

barrier, the modelers take the test-derived values and multiply by 0.162, the volume fraction of asphalt in the mix[1]. This adjustment means that a reported diffusivity value (Table 2) above 6.17×10^{-10} cm^2/s ($1 \times 10^{-10}/0.162$) would require that PA base conditions be reevaluated. Currently, the highest cumulative diffusion coefficient for NO_3^- is approximately 60% of this value, and the values for $^{99}TcO_4^-$ are approximately 25% of this value.

The effective diffusion coefficient for I^- is approximately ten times ·er than that for TcO_4^-. Past studies have demonstrated little

[1] This has the simultaneous effect of requiring placement of all of the contaminant in the smaller asphalt volume (capable of promoting diffusion) so that contaminant concentrations at the vault/diffusion barrier interface would be 6.25 (1/0.16) times as large as the values in the the bulk homogeneous sample as employed in the leach test.

tendency for either TcO_4^- or I^- to adsorb onto Hanford sediments (in this case, local aggregate). Because adsorption of I^- on the aggregate is unlikely it is unclear what is causing the difference in diffusivities. General literature on iodide does suggest that organic rich sediments can bind iodine strongly. Researchers speculate that iodide (I^-) gets converted to iodine (I_2) in the presence of organic matter. The iodine is then bound strongly. Asphalt, being predominately organic, might be converting iodide to iodine.

The ^{60}Co-EDTA complex and ^{137}Cs are retained quite well compared to $^{99}TcO_4^-$ and NO_3^-. It is concluded that EDTA-complexed contaminants are not mobilized in asphalt to an extent that would cause concern. It is believed that ^{137}Cs retention is most likely a result of adsorption on the aggregate. Cesium release may have been greater if the contaminant had been incorporated in the sample when coating aggregate with asphalt. Despite the fact that the asphalt/aggregate specimens are showing signs of surface changes in the de-ionized water leachant solution there is no indication of an increase in the release of contaminants.

The leachates from these leach tests can be easily monitored for ^{60}Co-EDTA, ^{137}Cs, NO_3^-, and $^{99}TcO_4^-$ with minimal resources on a yearly basis. Therefore, these experiments should be monitored for the duration of the research effort on ionic diffusion through asphalt to observe if the phenomena described above continue.

9413222.1687

IMMERSION TEST RESULTS

The following figures depict data from the immersion of asphalt coupons. In each figure the filled symbols represent values obtained by using a C_o^* based on contaminant concentrations from the first slices microtomed from the asphalt coupons. The empty symbols represent values based on a C_o^* using the contaminant concentrations of the immersion solutions. In addition, a least-squares line was fit to each of the data sets. The data and the line fits are discussed below.

Probit plots for $^{137}Cs^+$ (Figure 1) and NO_3^- (Figure 2) were calculated for asphalt coupons removed from a 100 µCi/L ^{137}Cs-doped 4.0 M $NaNO_3$ immersion bath following 263 days of exposure.

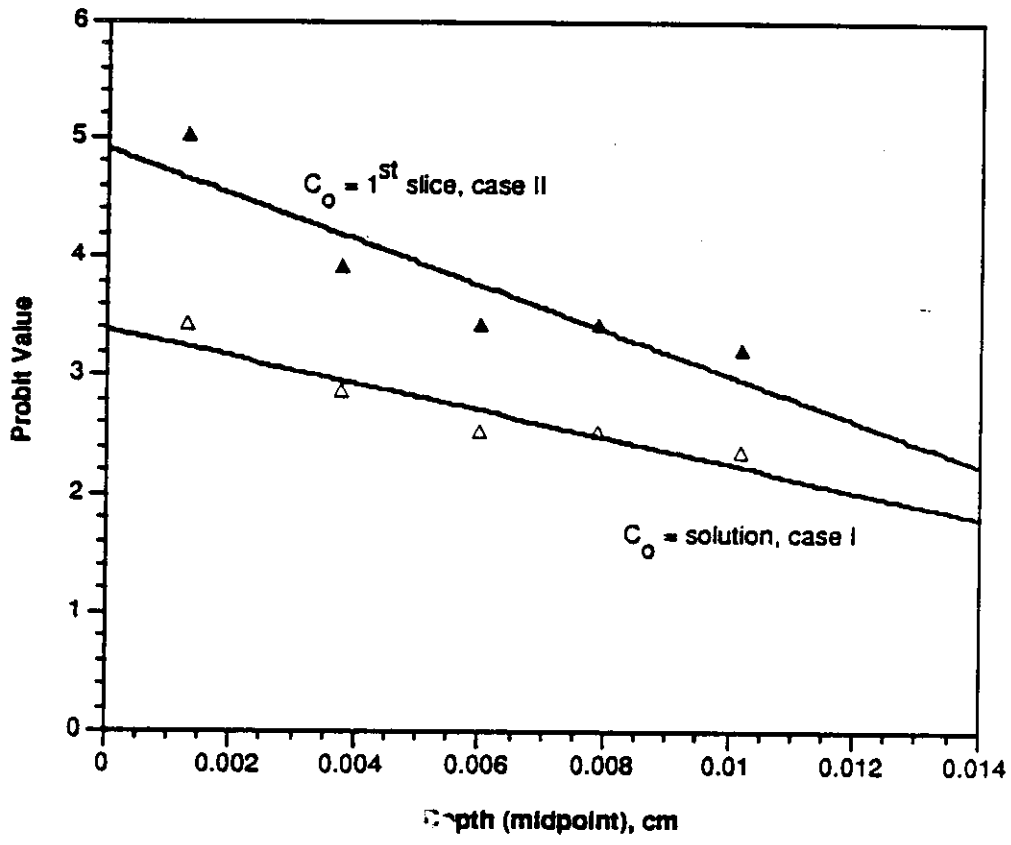

FIGURE 1. ^{137}Cs Probit from Asphalt Coupon Immersion Test

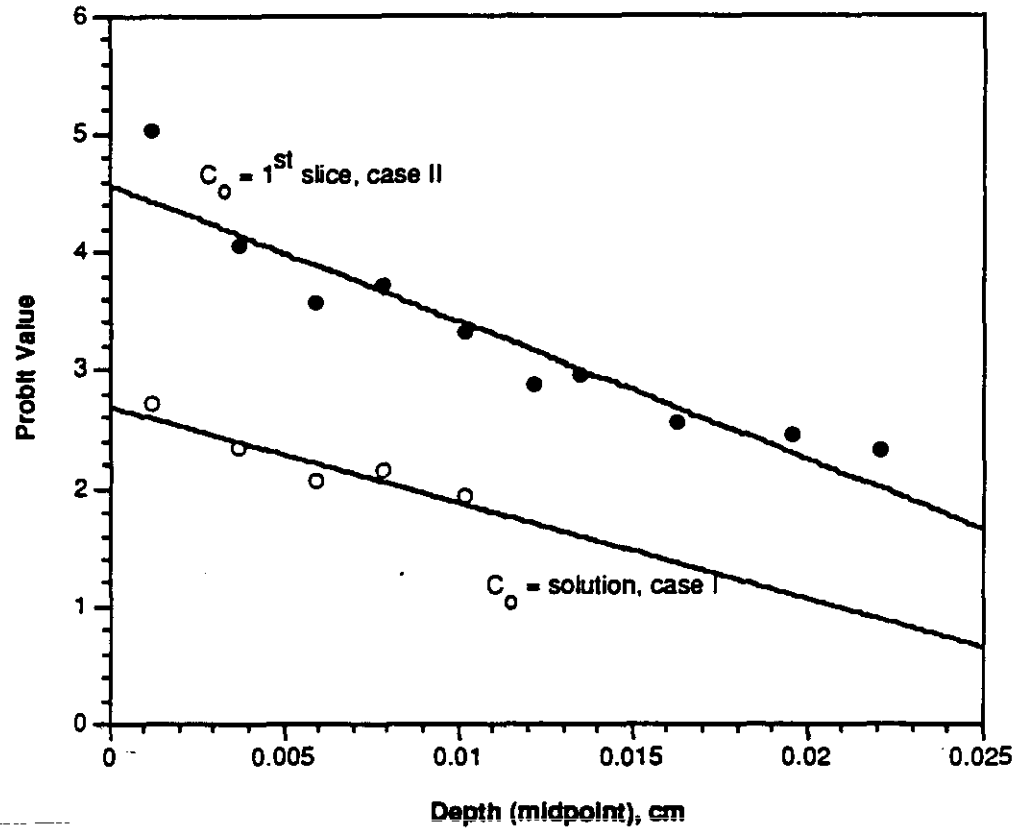

FIGURE 2. NO_3^- Probit from Asphalt Coupon Immersion Test

Technetium probit data (Figure 3) were determined by scintillation counting of dissolved asphalt slices from coupons immersed in a 4 M $NaNO_3$ solution containing 200 µCi/L $^{99}TcO_4^-$. Initially opaque solutions were diluted so that the concentration of asphalt in each vial was identical. In this way reduction of counting efficiency (in this case, light transmission) would be the same for each sample. The intermediate preparatory steps, required to perform these radioassays, resulted in the increased scatter in the probit plot.

Interpretation of the data shown in Figures 1 through 3 requires a knowledge of the solubility of the contaminant in asphalt. Because the solubility data were unavailable when these experiments were begun, the data were evaluated using the following two cases; each making different assumptions about the solubility of the contaminants.

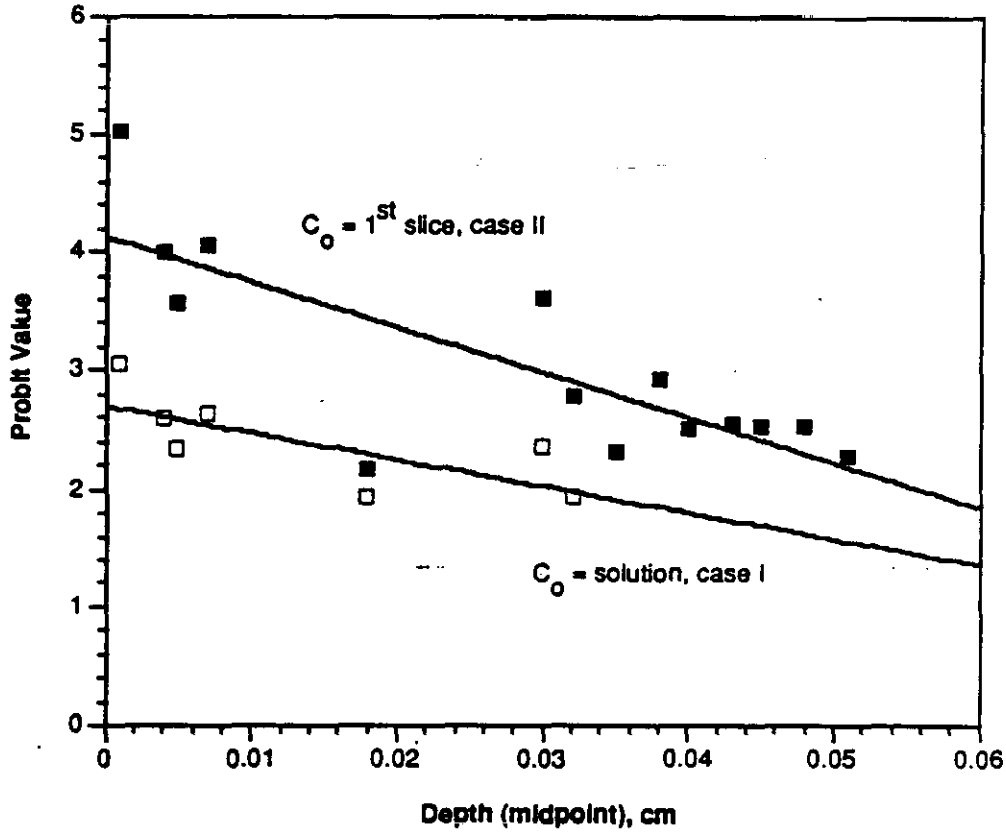

FIGURE 3. $^{99}TcO_4^-$ Probit from Asphalt Coupon Immersion Test

Case I: Initial concentration (C_o') of the contaminant, driving diffusion into the asphalt coupon, equals the concentration of the contaminant in the immersion solution. This case assumes that the contaminant is readily soluble in asphalt, at least at the concentrations present in solutions. (In these experiments this possibility is only likely for radionuclides, not nitrate, because the radionuclides are present in very small quantities). When this case is applied to the immersion test data the resulting normalized concentrations are relatively small because the C_o' chosen is large and the contaminant concentrations in the slices do not approach the C_o' value.

Case II: The solubility and thus the C_o' of the contaminant in the first slice from the asphalt coupon approximately equals the concentration found in that first slice. Alternately, contaminant

solubility in the asphalt has reached equilibrium at the concentration present in the first slice, and it is this concentration, in this layer of asphalt, that is driving diffusion into the bulk of the asphalt sample. This concentration represents a solubility significantly lower than the contaminant concentration in the immersion solution. A linear regression of the data yields a relatively larger slope (more negative). A larger slope yields a smaller effective diffusion coefficient for the contaminant. This is because a steeper slope indicates a relatively rapid decrease in concentration between slices from the coupon, therefore, diffusion of contaminant into the sample is proceeding slowly. Compared to linear regressions of case II probit values, case I probits yield smaller slopes and thereby yield greater diffusivities because contaminant concentrations do not fall off as rapidly. Table 3 shows the diffusivities calculated for cases I and II. These diffusivities are well below the maximum diffusivity of 1×10^{-10} cm^2/s used in current baseline performance assessment calculations.

There are 13 asphalt coupons remaining in the $^{99}TcO_4^-$-doped immersion bath and 6 asphalt coupons remaining in the $^{137}Cs^+$-doped immersion bath. These immersion tests require minimal attention and can be continued through FY95 with a small investment of resources to remove a pair of samples from each of the two baths for microtoming and radioassay. Examination of these samples each fiscal year will improve precision of the contaminant-specific diffusivities because the concentration profiles will develop further into the sample improving the accuracy of the probit transformation.

TABLE 3. Effective Diffusion Coefficients, 263-day Exposure (cm^2/s)

Contaminant	Case I Based on Solution Conc.	Case II Based on Conc. in First Slice
$^{137}Cs^+$	1.7×10^{-12}	6.1×10^{-13}
NO_3^-	4.7×10^{-12}	5.1×10^{-13}
$^{99}TcO_4^-$	4.2×10^{-11}	1.5×10^{-11}

ASPHALT/AGGREGATE "MEMBRANE" DEVELOPMENT

The diffusivities calculated from the ANS 16.1 leach tests may be problematic insofar as the contaminants were incorporated into the sample by drying them onto the aggregate with the lime coating. If this method of contaminant incorporation is responsible for the retention of contaminants, then the diffusivities calculated are too low. This implies that the samples may not reasonably represent the behavior of the actual diffusion barrier. The results may also be problematic because the leach rates have been declining with time. This decrease is perhaps partly attributable to the initial release of contaminants from contaminant sources near defects in the surface of the specimens that have been depleted as the experiment progresses. This implies that an important criterium for assessing the validity of the method has not been met, namely "release of contaminants by other time-dependent mechanism does not occur".

The diffusivities calculated from immersion tests of asphalt-only coupons may be problematic in that they do not incorporate aggregate and because they only simulate one interface present in the waste disposal system. Because the contaminant diffuses only into asphalt and not back out an important component in the behavior of the system may be lacking. This is important because certain contaminants, such as $^{99}TcO_4^-$ and organic-complexed contaminants may actually concentrate in the asphalt and thereby not diffuse as rapidly from the system.

Half-cell diffusion tests do not share these same problematic aspects. Contaminants will not be incorporated into the membrane so artifacts of sample preparation will not be important. In addition the half-cell membranes do incorporate aggregate and are fabricated using techniques that simulate the field construction methods. Most importantly half-cell test assemblies simulate the two diffusion interfaces of the waste disposal system, namely the waste form-asphalt interface and the asphalt-vadose sediment pore water interface.

Half-cell diffusion experiments, conducted in FY91, employed a 0.05 cm thick asphalt-only membrane as a partition between the two half cells. These membranes proved inadequate and failed before definitive

data could be obtained. In FY93, membranes will be composed of asphalt mixed with aggregate compacted to a void content of less than 4 vol%. Because of time constraints, the membrane must be sufficiently thin to allow detection of contaminant diffusion within months. However, the membrane must also be sufficiently thick, and incorporate all materials designed into the barrier, so that the test articles are reasonably representative of the diffusion barrier. The compromise reached for the tests planned for FY93 incorporate aggregate from which the two largest size fractions have been removed. The maximum nominal size aggregate passed a U.S. Standard No. 4 sieve (4.75 mm) and equals 1/2 or less of the nominal membrane thickness of 1.5 to 2.0 cm. Using this size fraction as a maximum resulted in removing 30 wt% of the specified aggregate mix (WHC construction specification B-714-C2, rev. 1).

New weight percents of asphalt and lime were calculated based on the increased surface area resulting from the elimination of the larger aggregate particles. Aggregate was obtained from the construction contractor and separated by sieving into the specified size fractions. These size fractions were further separated into size fractions required by the Asphalt Institute's (1989) Hveem method for laboratory design of pavement mixtures. The Hveem method uses an aggregate surface area calculation to provide a recommended starting point for optimizing asphalt content in a paving mix. Surface area is calculated by summing the weight fraction of all the individual aggregate size ranges multiplied by their associated surface area factors. The method was used to calculate the change in surface area caused by eliminating the larger particle sizes from the half-cell membrane asphalt/aggregate mix. This nominal change was then used to calculate increased vol% asphalt and increased wt% lime by multiplying construction specification asphalt and lime contents by the same nominal change. The asphalt and lime-coated aggregate were heated to the temperatures specified in the construction specification, mixed, and compacted into 4 in. lengths of stainless steel pipe using ASTM (1990) procedures. All compacted samples had less than three percent air voids (diffusion barrier specification stipulates less than four percent air voids).

9413222.1693

Test membranes, developed and fabricated in FY92, include a small band of the stainless steel mold into which the asphalt mix was compacted. This metal ring provides a non-deformable seal between the asphalt-aggregate membrane and the half-cell apparatus. Compacted asphalt/aggregate samples were sectioned into membranes approximately 1.5 to 2.0 cm thick using an abrasive cutting saw with water coolant. The membranes were then ground flat and parallel using a water-cooled surface grinder. In FY93 bubble leak tests will be conducted on the membranes to detect any gross surface-connected porosity. A composite membrane may incorporate surface-connected porosity due to void content and/or aggregate particles that are incompletely coated with asphalt. After leak testing, the aggregate exposed during sawing will be dried and the surfaces of the membranes sealed with a ≤0.05-mm thick coating of asphalt.

The design for the half-cell apparatus was modified to incorporate the membrane with the stainless steel outer ring described above. Rubber (EPDM) O-rings provide the seal between the membrane and the half cells. In addition, an expanded stainless steel support has been added to restrict "cold-flow" sagging of the membrane and permit testing of the membrane at 55°C.

It is anticipated that several months will pass before breakthrough of contaminants can be detected in the "cold" (non-radiotraced) reservoir because contaminants must diffuse through the entire uncontaminated membrane. When buildup of the contaminant has been reliably detected and assayed, the solution in the cold reservoir will be entirely emptied and fresh solution will be added. Buildup of the contaminant must be kept to a minimum because of the assumption of an unchanging concentration-derived driving force in the mathematical model used to calculate the diffusivities (Crank, 1975). Elapsed time for subsequent analyses will be shorter because the membrane will have been "charged" with contaminant. The elapsed time between breakthrough, when the cold solution is replaced, and the time when the contaminant has again built up to a reliably detectable concentration, will yield the data necessary to calculate diffusivities.

CONCLUSIONS

Leach tests of asphalt aggregate samples continue to yield bulk effective diffusivities below the maximum diffusivity (1×10^{-10} cm^2/s) assumed in PA baseline calculations (Table 2). Even though the cumulative diffusivities for NO_3^-, and $^{99}TcO_4^-$ exceed 1×10^{-10} cm^2/s, the PA conceptual model multiplies bulk diffusivities by 0.162 to make the values consistent with a driving force confined to the asphalt phase. Using this factor the diffusivity values for NO_3^- are approximately 60% of the adjusted maximum and $^{99}TcO_4^-$ diffusivity values are approximately 25% of the adjusted maximum.

Other diffusivities calculated from ANS 16.1 leach tests were well below PA baseline values. In addition, it has been observed that the effective diffusion coefficient for I^- is approximately ten times lower than that for TcO_4^-. Past studies have demonstrated little tendency for either TcO_4^- or I^- to adsorb onto Hanford sediments (in this case, local aggregate). Because adsorption on the aggregate is unlikely it is, therefore, unclear what is causing the difference in diffusivities. An observation from technical soils literature that organic rich sediments can convert iodide (I^-) to iodine (I_2) that is then strongly bound to the soil, may be occurring because asphalt is an organic material.

The $^{60}Co^{2+}$-EDTA complex and $^{137}Cs^+$ are retained quite well compared to $^{99}TcO_4^-$ and NO_3^-. It is also concluded that EDTA-complexed contaminants are not mobilized in asphalt to an extent that would cause concern. It is believed that ^{137}Cs retention is most likely a result of adsorption on the aggregate: Cesium release may have been greater if the contaminant had been incorporated into the test sample during aggregate coating with asphalt.

Immersion tests on asphalt-only coupons yielded diffusivities well below PA baseline values. Diffusivities of $^{137}Cs^+$, $^{99}TcO_4^-$, and NO_3^- were calculated using two probit transformation approaches: The first approach used a driving force defined by contaminant concentrations in the immersion solutions (case I), and the second approach used a driving force defined by smaller concentrations found in the top-most slices of asphalt from the coupons (case II).

Half-cell tests employing a composite asphalt/aggregate membrane are necessary to resolve questions about whether the retention of some contaminants in leach tests are artifacts of sample preparation. Results from half-cell tests will also be the most straightforward to interpret because 1) the half-cell membranes are made without incorporated contaminants, 2) the membranes are fabricated using methods representative of those used in construction, 3) the membranes incorporate all materials used in the actual barrier, and most importantly, 4) the half-cells simulate the two diffusion interfaces of the grout disposal system, namely, the vault-asphalt interface and the asphalt-vadose sediment pore water interface.

9413222.1696

REFERENCES

ANS. 1986. Measurement of the Leachability of Solidified Low-Level Radioactive Wastes by a Short Term Test Procedure. ANSI/ANS16.1, American Nuclear Society, La Grange Park, Illinois.

ASTM. 1990. American Society for Testing Materials. 1990 Annual Book of ASTM Standards. Vol. 04.03, Road and Paving Materials; Pavement Management Technologies. Philadelphia, Pennsylvania.
D1559-82, "Standard Test Method for Resistance to Plastic Flow of Bituminous Mixtures Using Marshall Apparatus";
D2041-90, "Standard Test Method for Theoretical Maximum Specific Gravity of Bituminous Paving Mixtures";
D2726-89, "Standard Test Method for Bulk Specific Gravity and Density of Compacted Bituminous Mixtures Using Saturated Surface-Dry Specimens";
D3203-88, "Standard Test Method for Percent Air Voids in Compacted Dense and Open Bituminous Paving Mixtures".

Asphalt Institute. 1989. (Hveem Surface Area). "Chapter 3.2, Aggregate Analysis" and "Chapter 4.3, Asphalt Hot Mix Design Methods". The Asphalt Handbook. MS-4, Asphalt Institute, College Park , Maryland. pp. 100-107, pp. 149-150.

Brown, D. A., J. E. Dunn and B. D. Fuqua. 1969. "Multiple-Ion Diffusion - I. Techniques for Measuring and Calculating Apparent Self-Diffusion Coefficients in Heteroionic Systems," Clay and Clay Minerals. 17:271-277.

Brown, D. A., R. E. Phillips, L. D. Ashlock and B. D. Fuqua. 1968. "Effect of Al^{3+} and H^{+} upon the Simultaneous Diffusion of ^{85}Sr and ^{86}Rb in Kaolinite Clay," Clay and Clay Minerals. 16:137-146.

Crank, J. 1975. The Mathematics of Diffusion - Second Edition, Clarendon Press, Oxford, England.

Daiev, Ch. T., and G. P. Vassilev. 1985. "On the Diffusion of ^{90}Sr From Radioactive Wastes Bitumenized by the Mould Method," J. of Nucl. Mat. 127:132-136.

Finney, D. J. 1971. Probit Analysis, 3rd Edition. Cambridge University Press, Cambridge, England. pp. 283-287.

Godbee, H. W., E. L. Compere, D. S. Joy, A. H. Kibbey, J. G. Moore, C. W. Nestor, Jr., O. U. Anders and R. M. Neilson, Jr. 1980. "Application of Mass Transport Theory to the Leaching of Radionuclides From Waste Solids." Nucl. Chem. Waste Manage. 1:29-35.

Phillips, R. E. and D. A. Brown. 1964. "Ion Diffusion: II. Comparison of Apparent Self and Counter Diffusion Coefficients." Soil Sci. Soc. of Am. Proceed. 28:758-763.

APPENDIX

PROBIT DATA FROM IMMERSION TESTS

9413222.1698

TABLE A1. Probit Data for Diffusivity Calculations

Slice	Mass g	Median Depth, cm	Activity µCi/g	C/C_o x 100 Case I	Probit Case I	C/C_o x 100 Case II	Probit Case II
$^{137}Cs^+$							
1	0.052	0.0013	1.11×10^{-2}	5.55	3.41	50.00	5.00
2	0.049	0.0038	3.05×10^{-3}	1.53	2.84	13.75	3.91
3	0.041	0.0060	1.29×10^{-3}	0.65	2.52	5.83	3.43
4	0.038	0.0079	1.24×10^{-3}	0.62	2.50	5.59	3.41
5	0.057	0.0102	7.93×10^{-4}	0.40	2.35	3.57	3.20
$^{99}TcO_4^-$							
1	0.055	0.0014	9.89×10^{-3}	2.47	3.03	50.00	5.00
2	0.035	0.0036	3.06×10^{-3}	0.77	2.58	15.49	3.98
3	0.035	0.0053	1.45×10^{-3}	0.36	2.31	7.35	3.55
4	0.030	0.0069	3.34×10^{-3}	0.84	2.61	16.91	4.04
5	0.438	0.0184	4.27×10^{-5}	0.01	1.91	0.22	2.15
6	0.020	0.0296	1.59×10^{-3}	0.40	2.35	8.02	3.60
7	0.063	0.0316	2.55×10^{-4}	0.06	1.91	1.29	2.77
8	0.068	0.0349	6.83×10^{-5}	0.02	–	0.35	2.30
9	0.050	0.0377	3.69×10^{-4}	0.09	–	1.87	2.92
10	0.044	0.0401	1.21×10^{-4}	0.03	–	0.61	2.49
11	0.064	0.0427	6.09×10^{-5}	0.02	–	0.31	2.53
12	0.043	0.0453	1.28×10^{-4}	0.03	–	0.65	2.52
13	0.065	0.0480	1.26×10^{-4}	0.03	–	0.64	2.51
14	0.048	0.0508	5.93×10^{-5}	0.01	–	0.30	2.25
NO_3^-			(Conc., g/g)				
1	0.052	0.0013	5.34×10^{-3}	1.08	2.70	50.00	5.00
2	0.049	0.0038	1.81×10^{-3}	0.36	2.31	16.93	4.04
3	0.041	0.0060	7.84×10^{-4}	0.16	2.04	7.34	3.55
4	0.038	0.0079	1.04×10^{-3}	0.21	2.13	9.76	3.70
5	0.057	0.0102	4.69×10^{-4}	0.09	1.91	4.39	3.29
6	0.023	0.0122	1.64×10^{-4}	0.03	–	1.54	2.84
7	0.032	0.0135	2.06×10^{-4}	0.04	–	1.93	2.93
8	0.084	0.0163	7.48×10^{-5}	0.02	–	0.70	2.54
9	0.048	0.0196	5.39×10^{-5}	0.01	–	0.50	2.42
10	0.053	0.0221	3.75×10^{-5}	0.01	–	0.35	2.30

Appendix L

Measurement of Water Vapor Diffusion Through Asphalt Diffusion Barrier Material

9413222.1700

9413222.7101

This page intentionally left blank.

HGTP-92-0606-01

9413222.1702

Appendix L - Hanford Grout Performance Assessment

Measurement of Water Vapor Diffusion Through Asphalt Diffusion Barrier Material

G. A. Whyatt
L. K. Fetrow

February 1992

Prepared for
the U.S. Department of Energy
under Contract DE-AC06-76RLO 1830

Pacific Northwest Laboratory
Richland, Washington 99352

Summary

A solid asphalt/aggregate diffusion barrier currently surrounds the grout disposal vaults. One potential mechanism for long-term release from the grout vaults involves the diffusion of water vapor through the diffusion barrier to the grout. The diffusing water vapor then condenses and drips to the soil carrying contamination with it. The diffusion of the water vapor is driven by a depression in the vapor pressure over the grout caused by the high salt content in the grout waste form.

This report describes the results of experiments intended to quantify the rate at which water vapor diffuses through the solid asphalt/aggregate diffusion barrier. Tests were conducted using lab-prepared samples over a range of air void contents and at two asphalt contents. The asphalt contents were selected as 7.0 wt% and 6.5 wt% on a total mix basis. These correspond to the minimum asphalt content and 0.5 wt% less than the minimum allowed in the construction specification.

In addition, a core sample was taken from the diffusion barrier of vault 105 during construction. Two samples were prepared from this core and were tested in the diffusion apparatus to confirm results obtained on samples prepared in the laboratory.

A reasonable value of diffusivity for the minimum asphalt content (7.0 wt%) and maximum air void content (4.0%) allowed in the construction specification is 2×10^{-5} cm^2/s. Higher asphalt contents and lower void contents result in lower diffusivities. Samples prepared with 6.5 wt% asphalt had diffusivities approximately twice as high at 4% void content. However, diffusivities of 2×10^{-5} cm^2/s are still attainable if the material is compacted to a sufficiently low void content.

The diffusivity value of 2×10^{-5} cm^2/s can be applied in performance assessment calculations to estimate the impact from water vapor diffusing through the intact diffusion barrier. A simple, conservative analysis for drinking-water exposure from a low-volume well indicates that the impact will be approximately 1% of the 4 mrem/yr limit. However, the current PA will consider the impacts of cracking and long-term degradation of the diffusion barrier. Seismic events and biodegradation of the asphalt may eventually open cracks in the diffusion barrier. The amount of water vapor diffusing through these cracks may exceed the amount diffusing through the solid barrier material.

Introduction

Disposal of the low-level fraction of liquid radioactive wastes stored in double-shell tanks on the Hanford Site is scheduled to begin in the 1990s. Disposal will consist of mixing the liquid wastes with cementitious grout-forming solids. The resulting slurry will be pumped into reinforced, 5300 m^3 concrete vaults, where it will harden into a cementitious mass. A diffusion barrier completely surrounds each vault to limit the release of contaminants from the vault to an acceptable level. The current performance assessment two-dimensional modeling effort is focused on modeling two release mechanisms: 1) release by diffusion of contaminants through the grout, concrete vault, and diffusion barrier and 2) advection of water through the grout, resulting from cracks in the diffusion barrier and concrete vault.

The data presented in this report is useful in evaluating a third mechanism termed "water vapor return." The grout contains high concentrations of salts that depress the equilibrium vapor pressure of the pore water within the grout. The soil porosity is at approximately 100% relative humidity since it is in equilibrium with moisture contained in the soil. This provides a driving force for diffusion of water vapor from the soil to the grout. The diffusing water eventually saturates the grout and produces a drip. Since the performance assessment looks at the radiological impacts of disposal over extended time periods, the liquid is assumed to leak from the catch basin through some small flaw in the barrier.

To evaluate the possibility of release through the water vapor diffusion mechanism, laboratory tests have been performed to directly measure the rate of water vapor diffusion through a low-void asphalt pavement barrier material. Results are reported for lab-prepared samples with the minimum asphalt content and with less than the minimum asphalt content at a variety of void contents. The values obtained are then interpreted in terms of the current groundwater and drinking water scenario assumptions. Test results from samples of a core taken during the construction of vault 105 are also presented.

Experimental Design

The experimental apparatus (Figure L.1) consisted of a Cahn model 2000 electrobalance, sealed in a glass housing. For testing lab-prepared samples, the balance was connected through a 2.54-cm (1-in.) diameter, 45.7-cm (18-in.) long flex hose to a diffusion cell consisting of a 10.2-cm (4-in.) diameter pipe with barrier material compacted in it. For testing of core samples, the flex hose length was reduced to 12.7 cm (5 in.) and the core sample was cut to length and sealed into a 15.2-cm (6-in.) diameter pipe.

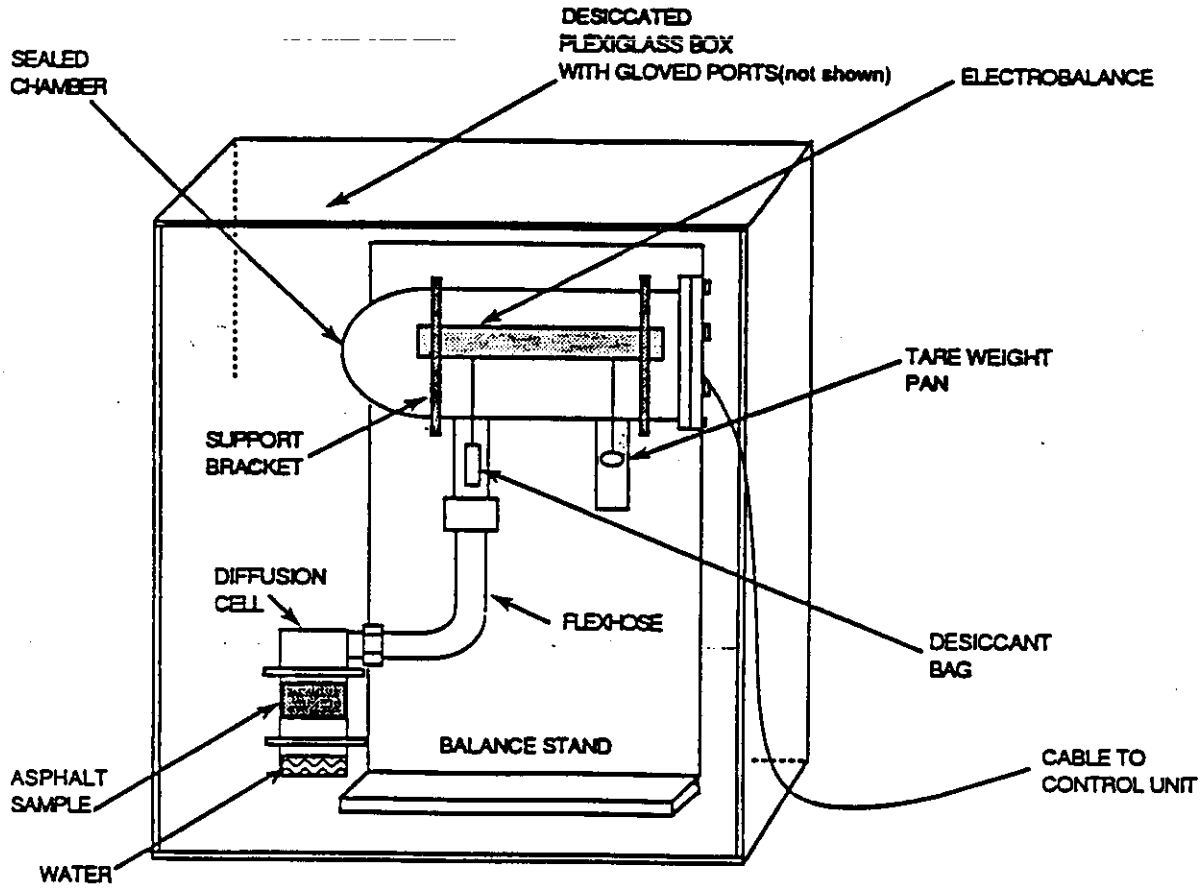

Figure L.1. Schematic of Experimental Configuration

One side of the sample was maintained at 100% relative humidity. The other side of the sample was connected to the flex hose leading to the electrobalance. A nylon bag of desiccant (anhydrous magnesium perchlorate) was suspended from the electrobalance. The weight gain of the desiccant over time was recorded on a strip chart recorder. Measurements were made throughout several weeks to ensure that the rate was at steady-state.

The nominally 15-cm (6-in.) diameter core samples of the diffusion barrier were cut with a diamond saw to a length of 8.3 cm (3.25 in.). The cut for the "wet" side of the sample was performed with water as a lubricant. The "dry" side was cut without lubricant to avoid trapping water in the surface of the sample. The outside diameter of the sample was 14.3 cm (5.625 in.). The core was placed in a sample holder with a 0.38-cm (0.15-in.) gap around the outside of the sample. This gap was filled with AR-6000 asphalt to provide a seal around the edge of the sample. Rubber gaskets with an I.D. of 12.7 cm (5.0 in.) were placed on the top and bottom of the sample to prevent asphalt from leaking or covering the surface of the sample. The bottom of the sample was supported by a stainless steel wire grid, which in turn was supported by a perforated plate. This prevented the sample from sagging or cracking during the test.

The electrobalance was required in order to measure the low rates of water vapor diffusion through the sample. Because the rates were very low, the inleakage to the scale through O-ring seals in the balance enclosure reduced the sensitivity of the device for detecting water vapor diffusion through a sample. To reduce the rates of inleakage, AR-6000 asphalt was used to seal O-ring joints. Ground glass joints were also sealed with asphalt at the top of the joint.

In some cases, the entire apparatus was placed inside a glove box in which humidity was maintained at a reduced level to improve the sensitivity of the measurements. The humidity within the glove box was lower than room air but higher than inside the dry side of the experimental apparatus. The lower humidity in the experimental apparatus was confirmed by disconnecting the diffusion cell and noting the increase in the rate of weight gain when the end of the flexible metal hose was exposed to the air within the glove box. Even with the reduced humidity of the glove box, some inleakage of moisture to the system occurred.

For all lab-prepared samples, a baseline was obtained with a plug in the end of the flexhose instead of a sample. This baseline was then subtracted from the measurement with a sample attached to obtain the amount of weight gain due to diffusion of water vapor through the sample. The baseline was remeasured for each sample. For core samples, the baseline was obtained by measuring the rate with the sample chamber attached prior to adding water to the lower chamber.

The compaction of the lab-prepared samples was performed in the lab using a device equivalent to a Marshall hammer (ASTM D 1559). The repeated blows delivered by a 4.536-Kg (10-lb) weight dropped from a height of 45.7 cm (18 in.) provided compaction of the samples. In ASTM D 1559, the sample is compacted from both sides. In this work the sample was compacted from one side only so that

a seal could be maintained between the sample and the compaction mold. The number of blows determines the degree of compaction of the sample. The more compaction, the lower the air void content and the lower the water vapor diffusivity.

Laboratory samples were prepared using the mix design prepared for construction of the diffusion barrier to surround the grout vaults. The asphalt was AR-6000 obtained from U.S. Oil in Tacoma. The construction specification requires 7.5±0.5 wt% asphalt. The amount of asphalt used in initial tests was 7.0 wt% of the total mix. Therefore, these samples contain the minimum allowable asphalt content. Additional samples were prepared with an asphalt content of 6.5 wt% of total mix. These samples represent material that is too lean in asphalt in order to evaluate the severity of the impact of missing the specification.

The aggregate was obtained from ACME Concrete in Richland and was screened to meet the specification shown in Table L.1. The aggregate was marinated with the lime mixed with water prior to heating and coating with the asphalt. This step is performed on the barrier aggregate to prevent stripping by improving the asphalt-aggregate bond.

The marinated gravel was dried and heated in an oven to 135°C. The asphalt was then heated (but not above 135°C) to allow it to pour easily and the asphalt and aggregate were mixed. After mixing, the mixture was placed back in the oven to bring the temperature back to 135°C. The compaction mold was preheated in the oven with the asphalt mix to 135°C. The Marshall hammer was warmed on a hot plate prior to use to avoid cooling of the asphalt mix during compaction. The thickness of samples varied from 2.5 cm to 7.6 cm (1 to 3 in.).

Low-void samples sealed against the side of the compaction mold. However, some higher void samples did not seal against the side of the mold so that the primary diffusion path was along the interface between the cell wall and the sample rather than through the sample. This led to a high reading even if the sample itself was fairly impermeable to water vapor. To determine if the sample was sealed against the cell wall, one end of the sample was covered with water, and a small helium pressure was applied to the other end of the sample to check for bubbles. If the sample was not sealed against the cell, it was removed from the cell, weighed, and extra asphalt was used to seal the edge of the sample against the cell wall. The sealing process produced a 0.64-cm (0.25-in.) bead of asphalt around the edge of the sample. The area covered by this bead was subtracted from the sample area in calculating the diffusivity for the sample. The weight of asphalt added was taken into account in calculating the density for determination of void content.

The density of pavement samples was measured using ASTM D1188/D 2041. In this procedure the sample is weighed and then cooled and coated with paraffin. The sample is then weighed again in air and then weighed immersed in water. The purpose of the paraffin is to seal the surface of the sample to prevent intrusion of water into the sample during immersion. Using this procedure, the standard

Table L.1. Aggregate Sizing for Laboratory Samples

Specification Screen Size (in.)	Wt% Passing in Specification[a]	Screen Size Used (in.)	Wt% Passing Used in Sample Preparation
5/8 in.	100	5/8 in.	100
1/2 in.	92 - 100	1/2 in.[b]	100
3/8 in.	85 - 95	3/8 in.	90
No. 4	65 - 75	No. 4	70
No. 16	36 - 42	No. 18[c]	39
No. 30	27 - 33	No. 30	30
No. 50	16 - 22	No. 45[c]	19
No. 200[d]	3.5 - 7.5	No. 200[d]	5.5
lime pass No. 200	2.75 - 3.25	lime pass No. 200	3.0

(a) From B-714-C2 specification Rev. 1, section 02147. Values include the weight of lime except as noted for the No. 200 sieve.
(b) Due to the relatively small thickness of the samples being prepared, the 100 passing end of the specification was selected. This prevents a single aggregate particle from spanning half of the sample thickness.
(c) The screen size was selected because it was the closest size that was immediately available. The minor difference is not expected to have any significant impact.
(d) Wt% of aggregate passing. Does not include the lime, which is shown separately below.

deviation is 0.32% void content (determined by ASTM). The procedure used is more accurate and precise than ASTM D 2726/D 2041 that is commonly used for road pavements in which a "saturated surface dry" weight is used to correct for water intrusion during immersion.

Experimental Results

The calculation of diffusivity was performed assuming a one-dimensional steady-state process. The equation for one-dimensional diffusion can be rearranged to solve for diffusivity as a function of measured properties as shown below.

$$D = (m\ dX)/(A\ dC) \tag{1}$$

where D = diffusivity
m = mass rate of water diffusion
dX = thickness of sample
A = area of sample
dC = difference in concentration across sample

Lab Samples, 7.0 wt% Asphalt - The results of experimental water vapor diffusivity measurements using 7.0 wt% asphalt are shown in Table L.2. The footnotes to the table explain the details of each measurement. Some early points are noted as low confidence. The low confidence stems from a possible scale calibration error as well as an increase in confidence in later samples. This is due to the improvement in procedures and equipment used in determining the void content as well as the relatively low level of the baseline for the vapor diffusion measurement. The highest confidence data are plotted in Figure L.2. It is believed that the variability in the data may be greater than suggested by the small scatter about the line. The void content measurements are believed to be within about 0.5% void of the true value.

Lab-Prepared, 6.5 wt% Asphalt - After results in Table L.2 were obtained, additional tests were performed to determine the water vapor diffusivity of samples prepared with asphalt content below the construction specification range. Samples were prepared and tested at 6.5 wt% asphalt (total mix basis). The data are shown below in Table L.3. Figure L.3 shows the data from Tables L.2 and L.3 plotted together. The lower asphalt content appears to increase the diffusion rate of water vapor through the samples. Low diffusion coefficients can still be obtained in the 6.5 wt% asphalt material at low void contents.

Core Samples - Two samples from a core of actual barrier material were tested to confirm results obtained with lab-prepared material. The core was taken from vault 105, east of the leachate sump area with an elevation of 186.8 m (613 ft) at the top of the core. The compaction in this area was performed using a small vibratory steel roller and a small vibratory plate compactor.

Table L.2. Summary of Measurements on 7 wt% Asphalt Samples[a]

Sample	% Air Voids[b]	Thickness (cm)	Wt Gain (mg/d)	Baseline (mg/d)	D_e (cm^2/s)
scoping	1.5[c,d]	2.54	1.6	[e]	$<2.5 \times 10^{-5}$
1	>3.6[d,f]	2.79	5.4	2.3	5.2×10^{-5}
2	>5.8[d,f]	3.18	7.3	3.0	8.4×10^{-5}
3	~0[c,d]	2.47	0.6	0.41	5.0×10^{-6}
4	2.1[c]	2.79	0.62[g]	0.55	$<3.4 \times 10^{-6}$
6	2.4[c]	3.02	0.69[g]	0.59	$<3.7 \times 10^{-6}$
16[h]	5.0[c]	7.14	1.22	0.73	2.1×10^{-5}
24	3.8[c]	5.49	1.32	0.80	1.8×10^{-5}
25	6.1[c]	4.45	1.23	0.63	3.4×10^{-5}[i]

(a) 7.0 wt% on total mix basis.
(b) Construction specification is 4% maximum voids.
(c) Determined using ASTM D 1188/D 2041. Single operator precision σ=0.32, acceptable range of two results on identical samples 0.91.
(d) Value may be affected by scale malfunction.
(e) No baseline obtained, weight gain includes inleakage rate.
(f) Determined using ASTM D 2726/D 2041. Saturated surface dry weight was not recorded, making the reported voids lower than actual. These samples are believed to have greater than four voids. If correctly executed, D 2726/D 2041 has a single operator precision σ=.51, acceptable range=1.44. Multilaboratory precision σ=1.09, acceptable range of results 3.08.
(g) The smallest difference that can be reliably detected between baseline and weight gain with the cell attached is approximately 0.2 mg/d. These samples had rates less than 0.2 mg/d above baseline, so 0.2 mg/d was used to calculate the diffusivity.
(h) This sample used mix obtained from the construction site rather than mix prepared in the laboratory. Compaction was performed in the Laboratory. The asphalt content may be greater than 7.0 wt%.
(i) A significant amount of asphalt was added to the perimeter of the top and bottom edges to seal the sample in the cell. The diffusivity was adjusted upward to account for the reduction in surface area of exposed sample.

The results verify measurements of lab samples that indicated very low diffusion rates of water vapor through the barrier material. Water vapor diffusion rates were not high enough to produce a

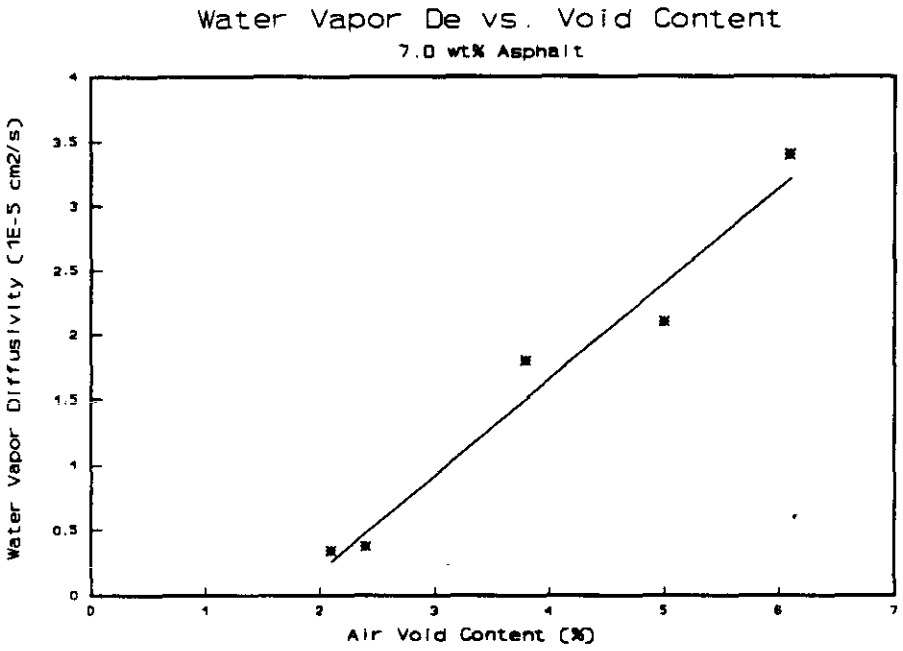

Figure L.2. Plot of Diffusivity as a Function of Void Content. Data points plotted include samples #4, 6, 16, 24, 25. The sample at 5.0 wt% voids was prepared in the laboratory using mix obtained from the construction site. The asphalt content may be greater than 7.0 wt% for this sample.

noticeable change in the baseline water collection rate. However, even without baseline correction, the diffusion rates are low. Although the sensitivity was reduced for the core sample measurements, it is estimated that the diffusivity is less than 2 x 10^{-5} cm^2/s, which is the expected diffusivity for a 7.0 wt% asphalt, 4% void, lab-prepared sample. This is believed to be due to a higher asphalt content[a] and a lower void content.

The reduced sensitivity experienced during core sample tests was the result of a higher baseline rate than in the smaller 10.2-cm (4-in.) diameter lab-prepared samples. It is possible that some water was trapped inside the sample during core drilling and contributed to the higher rate. In any case, the rate dropped very slowly over a long period of time. In testing the cores, the water was not added to the lower

(a) The asphalt content of the core sample was not measured. However, lab samples were prepared at the minimum asphalt content of the construction specification so it is expected that the field-placed material contained more asphalt than lab samples.

Table L.3. Summary of Measurements on 6.5 wt%-Asphalt Samples[a]

Sample	Void Content (%)	Thickness (cm)	Wt. Gain (mg/d)	Baseline (mg/d)	D_e (cm^2/s)
91-9	3.0	2.15	1.07	0.05	3.4×10^{-5}
91-10	6.6	2.24	4.58	–0.0	2.1×10^{-4}
91-12[b]	-	-	-	-	-
91-13	1.7	2.19	0.325	–0.0	1.1×10^{-5}
91-14	3.4	5.25	1.04	0.10	3.0×10^{-5}

(a) 6.5 wt% on total mix basis. Samples 91-1 through 91-8 (not shown) were produced to obtain a compaction curve and do not provide vapor diffusion data.

(b) Sample 91-12 was compacted to 60 blows, which should correspond to a void content of approximately 5%. This sample had open pathways for air movement and was not tested further.

9413222.712

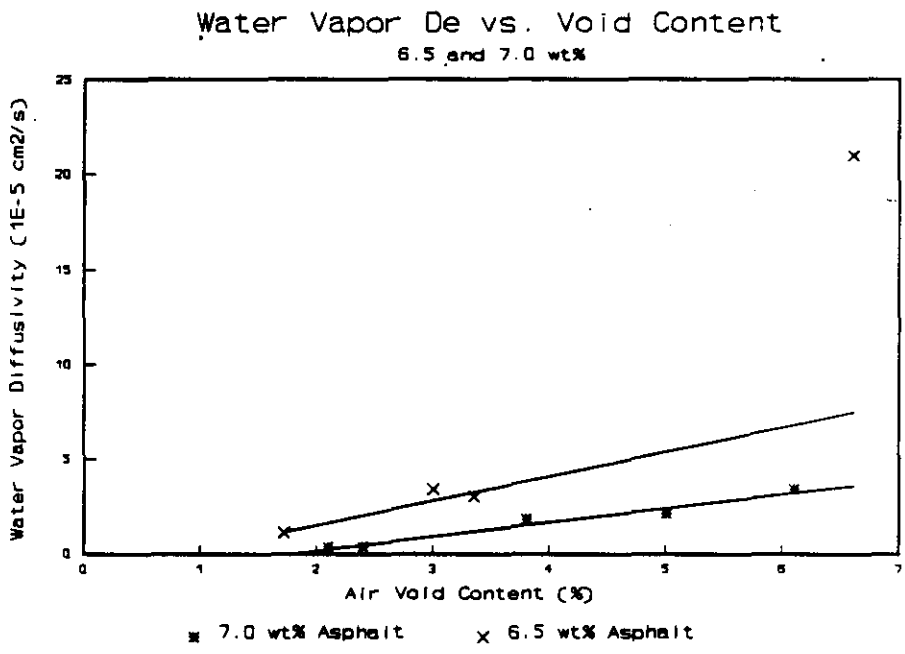

Figure L.3. Comparison of Water Vapor Diffusivity as a Function of Void Content at 6.5 wt% and 7.0 wt% Asphalt (total mix basis). The high 6.5 wt%, 6.6% void sample had a minor leak in the sample itself. The line was plotted excluding this point.

chamber until a reasonable baseline was obtained. After addition of a water source in the lower chamber, the rate of moisture collection continued to fall. There was no apparent response to the rate of water collection at the electrobalance to the presence of the moisture in the source cup. Therefore, if calculated in the normal way these samples would result in a zero diffusivity. To provide some quantification of the results, a range of diffusivity is provided in Table L.4 along with the sample thickness, void content, and baseline prior to water addition to the lower chamber.

This range provides the diffusivity of 0 (zero) resulting from subtraction of the baseline, and a diffusivity value determined by neglecting the baseline and assuming the entire weight gain is due to diffusion through the sample. The upper value provides a conservative bound on the diffusivity for these samples.

The rate of weight gain for each of the two core samples is provided in Figures L.4 and L.5. As can be seen in the figures there is no clear response from the system when moisture is added to the lower chamber. In addition, there was no response from the second core sample test when the water was removed and replaced with desiccant at the end of the test. It takes a very long time to reach a low rate of weight gain in the tests. While testing the first core sample, core sample #2 was stored in a desiccated environment. The fact that the data is better behaved and reaches a lower value for the second sample may indicate the presence of some water within the core resulting from core drilling operations. If this is the case, the water collection rate is controlled by water vapor diffusing out of the sample rather than through the sample from the lower chamber.

Table L.4. Summary of Vault 105 Core Sample Measurements

Sample	Sample Thickness (cm)	Void Content (%)	Rate of wt Gain (mg/d)	Baseline Rate of wt Gain (mg/d)	Diffusivity Range (cm^2/s)[a]
core 1	8.3	0.5	0.91	1.14	$0 - 3.8 \times 10^{-5}$
core 2	8.3	0.3	0.49	1.13[b]	$0 - 2.0 \times 10^{-5}$

(a) In both cases the initial baseline with no water present in the source cup produced results lower than the rate obtained after water addition. The upper limit value is calculated with no correction for the baseline rate of weight gain.

(b) At the end of the test, the water in the source cup was replaced with desiccant. The final baseline was measured at 0.46 mg/d.

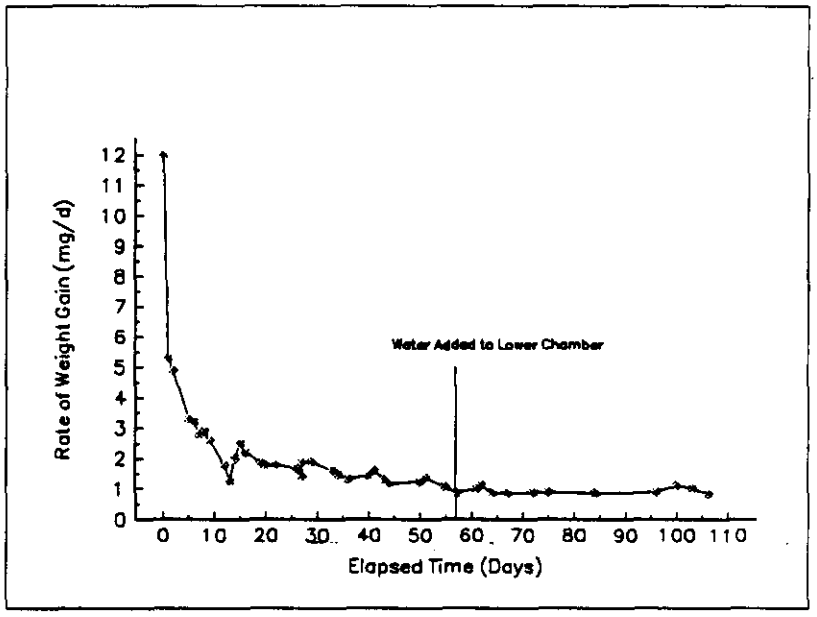

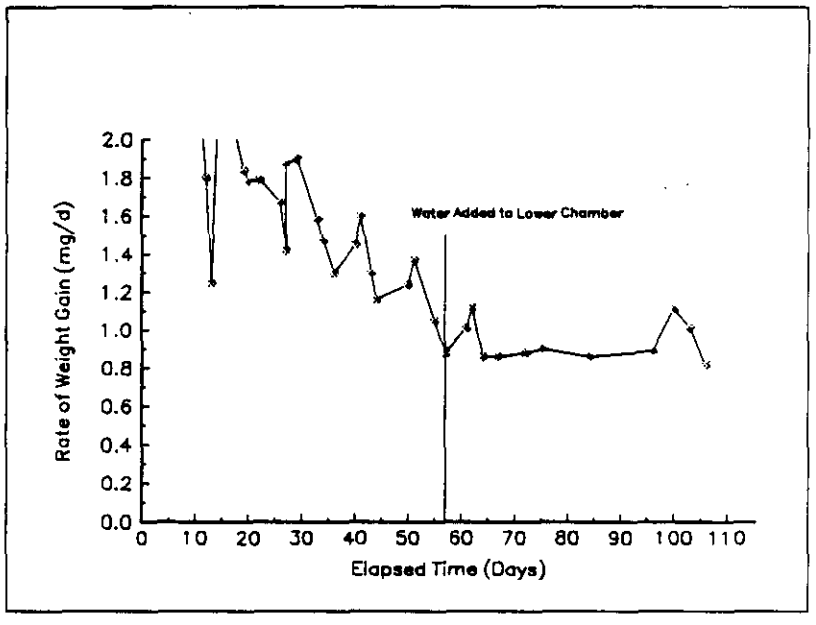

Figure L.4. Rate of Weight Gain of Desiccant for Core #1 vs. Days Connected to the Electrobalance. The lower graph shows an expanded scale to provide more detail in the nearly level region. Water was added to the lower chamber after 57 days.

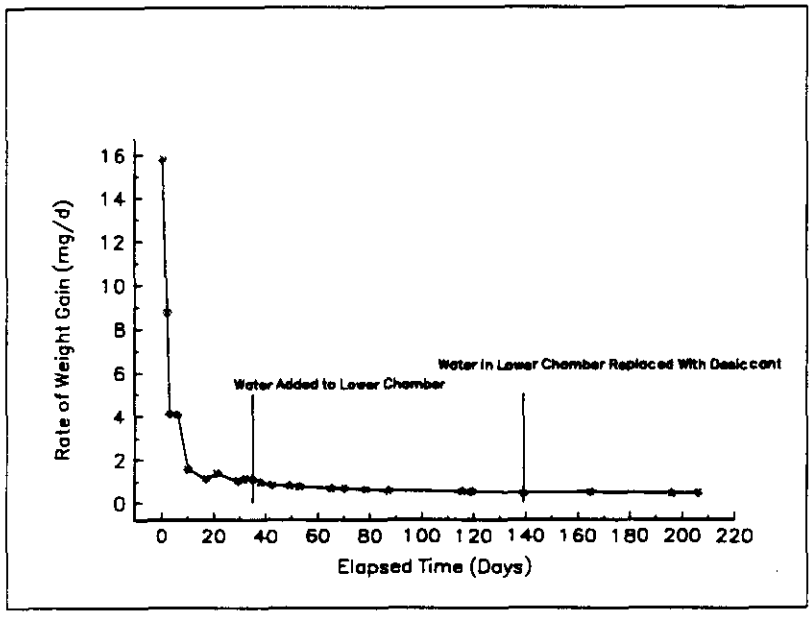

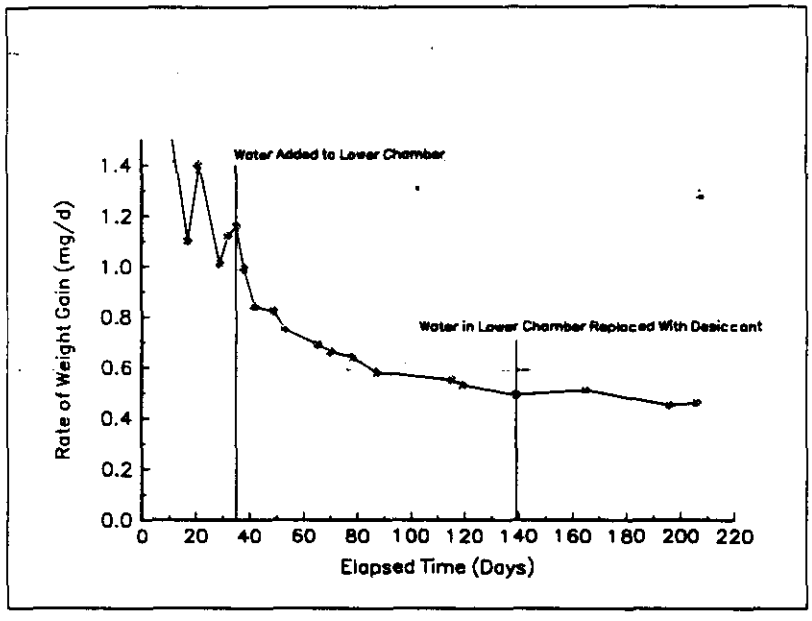

Figure L.5. Rate of Weight Gain of Desiccant for Core #2 vs Days Connected to the Electrobalance. The lower graph shows an expanded scale to provide more detail in the nearly level region. Water was added to the lower chamber after 35 days. At 139 days, the water in the lower chamber was removed and replaced with desiccant.

Interpretation of Results for Performance Assessment

Lab-prepared samples indicate that at the minimum asphalt content (7.0 wt%) and the maximum void content (4.0%) a diffusivity value less than 2×10^{-5} cm^2/s can be expected. The baseline for core sample #1 corresponds to a diffusivity of 3.8×10^{-5} cm^2/s. A 50% change in the baseline would have been detectable in this test. Therefore, the diffusivity for core sample #1 is believed to be less than 2×10^{-5} cm^2/s. Core sample #2 indicated a baseline of 2×10^{-5} cm^2/s with no response to water placement in (or removal from) the source cup. Therefore, a diffusivity of 2×10^{-5} cm^2/s has been selected as a reasonably conservative value for the water vapor diffusivity of intact barrier material.

A required diffusivity of the diffusion barrier was calculated using the following assumptions:

- Consider only ^{99}Tc and ^{129}I dispersed evenly into cold grout and concrete. Grout $R_f = 1.0$ for ^{129}I and $R_f = 5.0$ for ^{99}Tc
- isothermal system at 17°C with 83% relative humidity over grout (after dilution of salts to concrete and cold grout porosity value is 88% relative humidity) and 100% relative humidity outside barrier
- Water vapor diffusion rate is assumed to reach pore volume concentration and is then placed into site recharge to evaluate well concentration. (Ignore transport in vadose and saturated zone other than dilution factor in well.)
- low-volume well dilution factor 0.01 applied to concentration of recharge to the aquifer for uniform 0.1 cm/yr recharge.
- 33 vaults with intact diffusion barrier 91.4-cm (3-ft) thick and area for diffusion of 3×10^7 cm^2
- DOE Order 5400.5 dose conversion factors used to calculate drinking water doses.

Based on these assumptions, a water vapor diffusivity of 2.0×10^{-3} cm^2/s would provide a release approximately equal to the 4 mrem/yr drinking water limit. This maximum allowable value is two orders of magnitude higher than measured values.

Application of a 2×10^{-5} cm^2/s diffusivity in the simple model described above results in a dose of 4.0×10^{-2} mrem/yr or about 1% of the limit. Therefore, the diffusion of water vapor through an intact diffusion barrier is not expected to be of concern. The calculated impact is directly proportional to the diffusivity value.

The major contributors to the difference in impact estimated here and in the January 1991 draft PA are changes in the assumptions for the well intercept and resulting dilution, ^{99}Tc sorption, inventory, and apportionment.

Water vapor diffusion through cracks still has the potential to be a major contributor to release. A conservative calculation indicates a 91.4-cm (3-ft) thick barrier with a 5.0-cm crack running the circumference of the vault could contribute up to 21% of the low-volume well drinking water limit. The result is

directly proportional to crack area so this could represent a number of smaller through-wall cracks. This value was calculated using the following assumptions:

- Only ^{99}Tc and ^{129}I considered in dose calculation.
- Grout R_f=1.0 for ^{129}I and R_f=5.0 for ^{99}Tc.
- Cracks are completely open and straight.
- Contamination is uniform in grout, cold grout, and concrete porosity.
- Transport of water to outside of crack and transport of contaminant to inside of crack are rapid so that release is controlled by diffusion in the air phase.
- Pseudo-steady state value, no time associated with the dose.
- No interaction with other release mechanisms considered.
- Dose calculated using DOE Order 5400.5 dose conversion factors.

This calculation will be refined in the performance assessment to account for the diffusive resistance of the grout, the effects of the vadose zone, and other factors.

Appendix M

Exposure Scenarios and Sources for Parameters

9413222.718

This page intentionally left blank.

Appendix M

Scenario Descriptions

K. Rhoads and S. F. Snyder, Pacific Northwest Laboratory

Following the disposal of grouted waste, individuals or populations may be exposed to radioactive or hazardous materials contained in the grout via a number of pathways. Mechanisms for release of these materials from the Grout Disposal Facility include intrusion into the burial site, direct soil contamination by upward diffusion of radionuclides from the grout, disruption of the disposal facility by natural events, leaching of materials to groundwater, and subsequent transport of groundwater to the Columbia River. The intruder, upward diffusion, and groundwater pathways would be expected to affect a relatively small number of individuals, whereas exposure via the river may impact a much larger population. Eight scenarios for human exposure to radioactive materials from the Grout Disposal Facility were evaluated for this performance assessment. Individual doses were evaluated for two intruder scenarios—one for an individual who drills a well through the disposal facility and another for a resident who inhabits the site after drilling is complete. Three individual scenarios involving use of contaminated groundwater were also considered for drinking water only, irrigation of a home garden, or irrigation of a family farm. The dose to an individual was calculated for two special cases involving upward diffusion from the buried grout in the absence of recharge from precipitation, and for disruption of the disposal site by a catastrophic flood. Collective dose was estimated for a large population using contaminated water from the Columbia River, and for a smaller population using groundwater from a community well. A summary of the exposure routes considered in each scenario is shown in Exhibit M.1.

Each scenario is described in detail in the following sections, and assumptions and parameter values specific to each scenario are provided. The intent of these dose calculations was to model a typical individual, therefore the parameters were selected to generate a "best estimate" dose, rather than a maximum dose. Because only a very small number of individuals exhibit behavior that maximizes their exposure to a particular pathway, the assumption of maximum exposure to all pathways simultaneously results in a situation that is frequently unrealistic (for example, consumption of all food types at the maximum rate implies a total food consumption substantially higher than an individual's annual intake). Therefore, an estimate of the more likely "typical" dose was generated by selecting parameter values indicative of average behavior. When published data were available to justify a typical parameter value, that value was used. However, a number of parameters are required for which there is no published, typical value (i.e., hours spent outdoors), in which case a reasonable but conservative estimate was chosen.

Exhibit M.1. Summary of Exposure Scenarios

	Driller	Post-Driller	Drinking Water	Flood, Upward Diffusion, Irrigated Farm and Garden	River
External exposure from:					
surface soils while:					
outdoors	X	X		X	X
indoors		X		X	X
buried materials while:					
outdoors	X	X			
indoors		X			
surface water					X
immersion in surface water					X
Inhalation of:					
resuspended soil while:					
outdoors	X	X		X	X
indoors		X		X	
Ingestion of:					
soil while outdoors	X	X		X	X
drinking water from:					
groundwater			X	X	
surface water					X
contaminated food types:					
leafy vegs, other vegs, fruit		X		X	X
animal products				X[a]	X
aquatic foods					X
crops irrigated with:					
contaminated groundwater				X	
contaminated surface water					X
animal products fed with crops irrigated with:					
contaminated groundwater				X	
contaminated surface water					X

(a) These pathways were considered for the irrigated farm scenario, but not for the irrigated garden scenario.

M.1 Drilling Scenario

The drilling scenario considered a situation in which an individual would drill through the grout, exhume a portion of the buried material, and subsequently leave the site. This scenario results in the shortest exposure time of the scenarios evaluated, and the activities are assumed to be completed in approximately 1 week. Monuments, barriers, and markers may reduce the probability that such an intrusion could occur, but such measures would not entirely preclude it.

Drilling, either for water or mineral exploration, would transport buried grout to the ground surface. The driller was assumed to remove a cylindrical volume of grout and bring it to the surface in a powder or slurry form, depending on the drilling method used. All drilling debris was then assumed to be uniformly incorporated into the upper soil horizon. Pathways for radiation dose to the driller include external exposure, inhalation of resuspended material, and inadvertent ingestion of contaminated soil.

9413222.1722

M.1.1 Scenario Description

The driller was assumed to drill a 30-cm bore through the entire 9.1-m depth of the grout, removing a total grout volume of 0.64 m^3. As the driller removes material through the borehole to the surface, it would be distributed about the circumference of the borehole and subsequently covered over with more recently exhumed materials.

External exposure doses were assumed to occur over a period of 1 week, during which the driller would be exposed to external radiation from the exhumed grout for 40 hours. This takes into consideration the time required to complete well drilling, breakdown of the drilling equipment, and site grading. The drilling debris was assumed to be uniformly dispersed and graded over a 10- x 10-m area in the vicinity of the well to a depth of 15 cm.

Resuspension of the freshly bored grout by wind or mechanical disturbance introduces a mechanism for inhalation exposure. The driller was assumed to be exposed to the resuspended material for one hour, after which the grout tailings would be covered with more recently exhumed, uncontaminated soil.

Inadvertent ingestion of the exhumed grout tailings was also assumed to occur. The mechanisms for this pathway include ingestion of resuspended dust and soiled-hand-to-mouth contact during the workday.

M.1.2 Scenario Parameters

Pathways considered in the drilling scenario dose calculations include inhalation, external exposure, and ingestion. The scenario-specific parameters used to calculate these doses are tabulated in Exhibit M.2.

Exhibit M.2. Parameter Specific to the Drilling Scenario

Drilling Scenario Parameter (units)	Best Estimate	Basis
Manual redistribution: deep soil/ surface soil dilution factor (m)	6.4E-3	Calculated. Exhumed tailings uniformly distributed over a 100 m^2 area.
Area over which drilling tailings were spread (m^2)	100	Scenario assumption
Hours of exposure to resuspended tailings (h)	1	Scenario assumption
Hours of exposure to ground contamination (h) (external dose)	40	Scenario assumption
Mass loading (g/m^3)	1E-4	U.S. EPA (1992). Data for Kennewick, Washington
Soil ingestion rate (mg/d)	100	U.S. EPA (1989)

M.2 Post-Drilling Home Garden Scenario

The post-drilling home garden scenario was used to estimate the dose for a resident on land that contains soil contaminated by grout tailings which were transported to the surface as a result of drilling through the burial site. Such a situation would occur subsequent to the drilling scenario, where grout tailings brought to the surface during well drilling could be graded into the local soil. This material would present a source of potential radiation exposure to people living on or near the site of original disturbance long after the initial contaminating event. A resident at the site was assumed to be exposed via external exposure, inhalation of resuspended soil, ingestion of crops grown in soil containing the excavated radioactive materials, and incidental soil ingestion. The resident's water supply was assumed to be free from contamination.

M.2.1 Scenario Description

A resident was assumed to occupy a home on the land in which the upper soil layer is uniformly contaminated with grout tailings. The volume of tailings distributed through the upper soil layer is equivalent to that removed in the drilling scenario, or 0.64 m^3. The land area about which the contamination is spread was assumed to be 2500 m^2. A larger area was considered for this scenario than in the driller scenario because of additional spreading of contaminated soil during home construction. The outdoor soil, essentially the area of the garden, was assumed to be uniformly contaminated to a depth of 15 cm over the 2500 m^2 area. The resident in this scenario is exposed via external exposure, inhalation, and ingestion pathways.

External doses in this scenario are a result of exposure to penetrating radiation from radionuclides in the contaminated soil and buried waste. No external exposure doses were calculated for resuspended materials. See section M.1.1 for additional general details regarding external exposure calculations.

Inhalation doses result from the intake of resuspended soil. These doses were calculated by assuming full-time exposure to contamination dispersed in the outdoor air. This 24 h/d exposure to the outdoor air concentration conservatively estimates the indoor-plus-outdoor inhalation dose, because the outdoor air contains a greater mass loading of contaminated soil than indoor air. Indoor soil contamination results from the translocation of outdoor soil to the home interior by foot traffic and blowing dust. The assumption that the indoor-air radionuclide concentration is equivalent to that of the outdoor air overestimates the dose contribution from indoor air.

Ingestion doses in the post-drilling scenario result from consumption of crops grown in contaminated soil as well as inadvertent soil ingestion. The irrigation water source used to support crop growth was assumed to be free of contamination. A crop holdup time was not considered because the long half-life of the radionuclides involved results in negligible radiological decay for any reasonable holdup time between harvest and consumption. Inadvertent soil ingestion results from ingestion of blowing dust, ingestion of soil remaining on food crops, and hand-to-mouth contact.

The major food types assumed to come from the home garden include leafy vegetables (i.e., lettuce, spinach, cabbage), other vegetables (e.g., root crops, tomatoes, broccoli, cucumbers), and fruit (i.e., orchard crops). Cereals (e.g., wheat, oats) are not considered in this home garden scenario because space limitations preclude growing this type of crop in the contaminated area. The fraction of the total diet supplied by the individual's garden was assumed to be 0.25 for leafy and other vegetables and 0.20 for fruit (U.S. EPA 1989).

M.2.2 Scenario Parameters

The post-drilling scenario dose calculations considered external exposure, inhalation, and ingestion of food crops and soil. The scenario-specific parameters used to calculate these doses are tabulated in Exhibit M.3.

M.3 Drinking Water Scenario

The drinking water scenario was limited to exposure via direct consumption of contaminated groundwater. An individual was assumed to obtain drinking water from an aquifer containing leachate from the grout vaults. The leachate was assumed to travel through the unsaturated zone to the aquifer. No water treatment or hold-up between pumping and consumption of the water was considered.

Exhibit M.3. Parameters Specific to the Post-drilling Scenario

Post-drilling/Home Garden Scenario Parameters (units)	Best Estimate	Basis
Hours of exposure to ground contamination (h) (external dose)	4383	Scenario assumption
Hours of inhalation exposure per year (h)	8766	Scenario assumption
Mass loading factor (g/m^3)	1E-04	U.S. EPA 1992. Data for Kennewick, Washington
Soil ingestion rate (mg/d)	100	U.S. EPA 1989.
Fraction of roots in the upper soil	1	Scenario assumption
Manual redistribution: deep soil/surface soil dilution factor (m)	2.6E-4	Calculated. Exhumed tailings distributed over a 2500 m^2 area.
Area contaminated by grout (m^2)	2500	Scenario assumption
Crop growing time (d)		Scenario assumptions
Leafy vegetables	90	
Other vegetables	90	
Fruit	90	
Above-ground biomass (kg_{wet}/y)		Napier et al. 1988
Leafy vegetables	2.0	
Other vegetables	2.0	
Fruit	3.0	
Fraction of diet produced locally		U.S. EPA (1989)
Leafy and other vegetables	0.25	
Fruit	0.20	
Consumption rate (kg_{wet}/y)		Multiple of local diet fraction values and consumption rates from the western region reported in Yang and Nelson (1986)
Leafy vegetables	4.1	
Other vegetables	13.9	
Fruit	7	

This scenario was used to demonstrate that the performance objective for groundwater protection would not be exceeded by leachate from the Grout Disposal Facility for a water intake rate of 2 L/d (730 L/yr), consistent with proposed regulations (56 FR 33050, U.S. DOE 1990).

M.4 Irrigated Farm Scenario

The second of the scenarios that considered agricultural pathways is the irrigated farm scenario. In this scenario, contaminated groundwater would be used to irrigate crops, and as a drinking water source for people and livestock. The farmhouse was assumed to be located at a sufficient distance downgradient from the grout disposal site that external penetrating radiation directly from the buried vaults was not considered. Doses to an individual on the farm result from external exposure, inhalation, and ingestion of food crops, animal products, and contaminated groundwater.

Prior to its establishment as a federal reservation, farms existed on what is now the Hanford Site. Currently, the region surrounding Hanford supports extensive agricultural activity, including production of fruit, wheat, vegetable crops, and meat and milk livestock. Therefore, a scenario that considers this type of irrigated farming is credible after institutional control of the site ends.

M.4.1 Scenario Description

The 20,000-m^2 farm was assumed to be located 100 m hydraulically downgradient from the grout disposal site where groundwater would be contaminated by radioactive materials in leachate from the vaults. The groundwater would then be used as a source of domestic water, livestock drinking water, and irrigation water at a rate of 45 m^3 per day. External doses to an individual on this farm result from exposure to surface soil contaminated by irrigation water.

Inhalation doses result from the intake of contaminated soil resuspended by wind or mechanical disturbance, such as plowing. An individual was assumed to inhale air containing radionuclide concentrations equivalent to those in outdoor air for 8766 h/yr to determine the inhalation dose. The assumption that radionuclide concentrations in indoor and outdoor air were identical provides a conservative inhalation dose estimate, because outdoor air activity concentrations will always be equal to or greater than that of indoor air (see section M.2.1, post-drilling/home garden scenario).

Both the surface soil external exposure calculation and inhalation dose calculation required estimates of the soil radionuclide concentration. The level of soil activity is related to the rate and duration of irrigation water application, which varies with the type of crop. To avoid apportioning farmer occupancy times in the various types of fields, the surface soil activity concentrations used for external dose calculations were calculated separately, using a single irrigation rate and growing season length.

Total ingestion doses combined the doses from the ingestion of food crops, animal products, groundwater, and inadvertent soil ingestion. Inadvertent soil ingestion results from ingestion of blowing dust, ingestion of soil remaining on food crops, and hand-to-mouth contact. All water consumed originates from the groundwater source and the consumption rate is a population average rather than the 2 L/d rate used for the drinking-water scenario. Only a portion of the terrestrial food crops, and animal products, were assumed to originate from the family farm (see Exhibit M.4). The balance of

the diet was assumed to be grown in an uncontaminated location. All grains consumed by the farmer and livestock were assumed to be grown elsewhere on uncontaminated land and irrigated with uncontaminated water.

Radionuclides in the food crops result from irrigating the crops with contaminated groundwater and growing crops in soil contaminated by the irrigation water. For all food categories, holdup time was not considered because the long half-life of the radionuclides involved results in negligible radiological decay for any reasonable holdup time between harvest and consumption.

Radionuclides in animal products are a result of livestock consuming contaminated feed and water. "Meat livestock" (i.e. beef cattle) and dairy cows were assumed to consume fresh forage from the same field. Meat livestock were assumed to consume uncontaminated grain as a stored feed, whereas milk cows consumed stored hay that had been irrigated with the contaminated groundwater. Poultry were assumed to consume feed that was grown on an uncontaminated site. The only radionuclide intake for poultry and eggs results from water consumption.

In this scenario, the quantity of irrigation water required to support production of terrestrial foods and animal products is sufficiently great that the volume of the contaminated plume from the disposal site must be diluted by uncontaminated water from the aquifer. The groundwater concentrations predicted by the transport model were therefore reduced to account for dilution of the contaminated plume (see section 3.4.5).

M.4.2 Scenario Parameters

The irrigated farm scenario dose calculations considered external exposure, inhalation, and ingestion pathways. The parameters used to calculate these doses for the irrigated farm scenario are tabulated in Exhibit M.4.

M.5 Irrigated Garden Scenario

This scenario is similar to the irrigated farm, except that it omits the animal food consumption pathways, permitting use of a lower irrigation rate than the farm scenario. In this case, dilution of the contaminated groundwater plume by uncontaminated water from the aquifer was not assumed because of the lower water volume required for irrigation (see section 3.4.5). All other pathways and parameters in this scenario were identical to those discussed in section M.4 and listed in Exhibit M.4. This scenario was considered because it was not possible to determine in advance of completion of the groundwater modeling whether the increased radionuclide concentrations in groundwater would offset the lower consumption rate of contaminated foods and result in a higher dose to the maximally exposed individual compared with the irrigated farm scenario.

Exhibit M.4 Parameters Specific to the Irrigated Farm Scenario

Irrigated Farm Scenario Parameter (units)	Best Estimate	Basis
Inhalation dose exposure time (h)	8766	Scenario assumption
Hours of exposure to ground contamination (h)	4383	Scenario assumption
Mass loading (g/m^3)	1E-4	U.S. EPA (1992). Data for Kennewick, Washington
Soil ingestion rate (mg/d)	100	U.S. EPA (1989)
Fraction of roots in the upper soil, upper 15 cm	1.0	Scenario assumption
Irrigation water application rate (in./y)	32.4	Scenario assumption
Duration of irrigation (mo/y)	6.5	Typical availability for the Kennewick Irrigation District, Kennewick, Washington. (April 1 through October 15).
Human water consumption rate (L/y)	655	Roseberry and Burmaster (1992)
Local diet fraction		U.S. EPA (1989)
Leafy and other vegetables	0.25	
Fruit	0.20	
Milk	0.46	
Meat, poultry, and eggs	0.44	
Crop growing time (d)		Scenario assumption
Leafy vegetables	90	
Other vegetables	90	
Fruit	90	
Stored feed - milk	90	
Fresh forage - meat, milk	45	
Above-ground biomass (kg_{wet}/m^2)		Napier et al (1988)
Leafy vegetables	2.0	
Other vegetables	2.0	
Fruit	3.0	
Stored feed - milk	1.0	
Fresh forage - meat	1.0	
- milk	1.5	

Exhibit M.4. (contd)

Irrigated Farm Scenario Parameter (units)	Best Estimate	Basis
Consumption rate (kg_{wet}/y)		Multiple of local diet fraction values and consumption rates from the western region reported in Yang and Nelson (1986).
Leafy vegetables	4.1	
Other vegetables	13.9	
Fruit	7.0	
Meat	22	
Poultry	4.6	
Milk	50.8	
Eggs	10.6	
Animal diet fraction		Scenario assumption
Stored feed - milk	0.25	
Fresh forage - meat,milk	0.75	
Livestock water intake rate (L/d)		Napier et al. (1988)
Meat livestock	50	
Dairy cows	60	
Poultry and laying hens	0.3	

M.6 Special Cases

Two special cases involving direct contamination of surface soil were evaluated in addition to the groundwater scenarios. These cases involved contamination of the upper soil surface either by upward diffusion of radionuclides from the grout vaults in the absence of recharge from precipitation, or by disruption of the disposal facility by a catastrophic flood. The upward diffusion scenario was similar to the intruder post-drilling garden scenario (see section M.2), except that both surface and deep soil layers were considered to be contaminated at similar levels. Otherwise, the same pathways and parameters were used for both cases. Soil concentrations for the upward diffusion scenario were estimated using the subsurface transport model for times up to 660,000 years after disposal.

Pathways considered in the flood scenario were similar to the farm scenario, except that irrigation water and drinking water were assumed to be uncontaminated (see Exhibit M.4). The soil concentrations in the flood scenario were based on dispersion of the entire grout inventory in three different volumes, corresponding to 1) the volume used for the 200 Area plateau (78 km^2 x 4 m deep) in the HDWEIS (U.S. DOE 1987), 2) the Hanford Site (1,450 km^2 x 10 m deep), or 3) the Pasco Basin (4,850 m^2 x 10 m deep). The flood scenario is evaluated at 50,000 years after disposal, because this is the approximate predicted time for recurrence of glacial flooding of sufficient severity to disturb the disposal site (see section 2.1.5).

M.7 Columbia River Scenario

The Columbia River scenario was used to estimate dose to the population in the downstream Columbia River region from exposure to contamination in the river. The contamination is the result of groundwater flow into the surface water system. The Columbia River is presently used for drinking water, irrigation, and recreation by a limited number of people living downstream of Hanford, and for the purposes of this analysis, these uses are assumed to increase in the future. Population doses in the river scenario result from external exposure, inhalation of resuspended soil, and ingestion pathways. Doses to individuals were not considered because they would be substantially lower than those in the groundwater scenarios. Radionuclide concentrations in river water are lower than in groundwater as a result of dilution by uncontaminated river water originating upstream from Hanford.

River contamination was assumed to result from contaminated-groundwater recharge to the Columbia River. The groundwater contamination occurs by transport of radioactive leachate from the disposal site through the vadose zone to the aquifer system. The rate at which radionuclides subsequently enter the river depends on the rate at which they enter the groundwater, the extent of radioactive decay, chemical characteristics, the flow rate of the aquifer, and distance to the river.

This scenario is similar to the irrigated farm scenario except that surface water, rather than groundwater, would be used for irrigation and human and animal consumption. Additional pathways were included to evaluate the dose from recreational uses of the Columbia River including swimming, boating, fishing, other shoreline activities, and consumption of fish caught in the river. Dose to the regional population was calculated in this scenario because of the potential for exposure of a larger number of people than in the groundwater scenarios.

At present, this scenario is very conservative for a number of reasons, and would be expected to provide an upper bound to potential exposure of downriver populations in the future. Irrigation water for the majority of the Columbia Basin is obtained from reservoirs located upstream of the Hanford Site, and which are uncontaminated by groundwater coming from beneath the site. Production of all food consumed by the downriver population with contaminated water would require a very large increase in crop production below the site, and a substantial investment in new irrigation projects in this area. The Columbia River is also diluted by a large inflow of water from tributaries immediately below the Tri-Cities area and along its entire course to the Pacific Ocean, resulting in significantly lower radionuclide concentrations than those assumed for this analysis. The availability of alternate sources of drinking and irrigation water from uncontaminated tributaries and groundwater aquifers would further reduce the potential exposure levels for this population.

M.7.1 Scenario Description

The population dose estimates for this scenario result from regional use of the Columbia River as a drinking water supply and irrigation water source. In addition, the river provides a source of recreation. A total of 5 million people were assumed to reside along the river from the Hanford Reach to

the mouth. This represents a significant population increase over present conditions and is a conservative scenario assumption. This same population was used for a previous prospective population dose estimate (U.S. DOE 1989).

External doses result from exposure to irrigated land and from recreational exposure to contamination in the river water. In this scenario, the application rate of Columbia River water used for irrigation is lower than that used in the other scenarios because of differences in climate for the region being considered. The population for this scenario is distributed along the river from the arid climate of the Hanford Reach to the wetter coastal areas. The "average" irrigation rate for this scenario was determined from the precipitation and irrigation rates in Benton County by assuming that the same total quantity of water from precipitation plus irrigation would be required to support crop production all along the river. Because of the higher evapotranspiration rate in the Benton County region, this method probably overestimates the actual irrigation rates required for crop production in the more humid coastal areas, but it does provide a reasonable (and somewhat conservative) approximation.

In this scenario, internal doses may result from inhalation of resuspended soil. An individual was assumed to be outdoors 8766 h/yr for inhalation dose calculations. The indoor air radionuclide concentration was assumed to be equivalent to the outdoor air concentration. This provides a conservative inhalation dose estimate, because outdoor air concentrations will always be greater than or equal to that of indoor air.

Ingestion of food products contaminated by irrigation with river water provides another route for internal radiation exposures. The downriver population was assumed to subsist on its own agricultural products, which include the generalized categories of leafy vegetables, other vegetables, fruits, and cereals. The Columbia River was assumed to provide drinking water for both people and livestock, and all food for human consumption and animal feed crops were assumed to be irrigated with Columbia River water. Livestock consume both fresh feed (pasture grass) and stored feed. Stored feed consists of dry alfalfa hay for milk cows, and cereal grains for beef cattle and chickens (meat and egg layers). Inadvertent soil ingestion was also considered in this scenario.

M.7.2 Scenario Parameters

Columbia River scenario dose calculations consider external exposure, inhalation, and ingestion pathways. The parameters used to calculate these doses for the Columbia River scenario are tabulated in Exhibit M.5.

M.8 Community Well Scenario

This scenario uses the dose calculated for the individual garden scenario (section M.5) to estimate the potential collective dose via a community well. Based on a contaminated plume volume of 25 m^3/d at 100 m from the disposal site, and an individual per capita consumption rate of 0.31 m^3/d

Exhibit M.5. Dose and Exposure Parameters Specific to the Columbia River Scenario

River Scenario Parameter (units)	Best Estimate	Basis
Population size	5.0E+06	Scenario assumption
Inhalation dose exposure time (h)	8766	Scenario assumption
Hours of exposure to ground contamination (h)	4383	Scenario assumption
Hours of recreation time (h)		Scenario assumption
Swimming	10	
Boating	0	
Shoreline	17	
Soil ingestion rate (mg/d)	100	U.S. EPA (1989)
Irrigation water application rate	25.0	USDA (1974). Calculated as average of Benton County average irrigation-plus-precipitation rates minus annual precipitation for counties adjacent to the Columbia River.
Duration of irrigation for surface soil external exposure and inhalation doses (mo/y)	6.5	Typical availability for the Kennewick Irrigation District, Kennewick, Washington. (April 1 through October 15).
Water consumption rate (L/y)	655	Roseberry and Burmaster (1992)
Regional diet fraction		Scenario assumption
All food types	1.0	
Consumption rate (kg_{wet}/y)		Consumption rates from the western region reported in Yang and Nelson (1986).
Leafy vegetables	16.5	
Other vegetables	55.0	
Fruit	35.0	
Cereal	74.0	
Meat	50.0	
Poultry	10.5	
Milk	115.0	
Eggs	24.1	
Fish	0.003	
Crop growing time (d)		Scenario assumption
Leafy vegetables	90	
Other vegetables	90	
Fruit	90	
Cereal	90	
Stored feed - milk	90	
Fresh forage	45	

Exhibit M.5. (contd)

River Scenario Parameter (units)	Best Estimate	Basis
Above-ground biomass (kg_{wet}/m^2)		Napier et al. (1988)
Leafy vegetables	2.0	
Other vegetables	2.0	
Fruit	3.0	
Cereal	0.8	
Stored feed - meat	0.8	
- milk	1.0	
Fresh forage - meat	1.0	
- milk	1.5	
Animal diet fraction		Scenario assumption
Stored feed - meat,milk	0.25	
Fresh forage - meat,milk	0.75	
Livestock water intake rate (L/d)		Napier et al. (1988)
Meat livestock	50	
Dairy cows	60	
Poultry and laying hens	0.3	
Feed intake rate (kg_{wet}/d)		Napier et al. (1988)
Meat livestock	68	
Dairy cows	55	
Poultry and laying hens	0.12	

for domestic use and limited gardening, the maximum number of individuals that could be supported by a community well without additional dilution is approximately 80. The collective dose from this scenario is therefore estimated as 80 times the individual dose for the garden scenario.

M.9 References

56 FR 33050ff. 1991. U.S. Environmental Protection Agency, "National Primary Drinking Water Regulations; Radionuclides." Notice of Proposed Rulemaking, 40 CFR Parts 141 and 142. *Federal Register.*

Napier, B. A., R. A. Peloquin, D. L. Strenge, J. V. Ramsdell. 1988. *GENII - The Hanford Environmental Radiation Dosimetry Software System.* PNL-6584, Vols. 1, 2, and 3. Pacific Northwest Laboratory, Richland, Washington.

Roseberry, A. M., and D. E. Burmaster. 1992. "Lognormal Distributions for Water Intake by Children and Adults." *Risk Analysis*, 12(1): 99-104.

U.S. Department of Agriculture (USDA). 1974. *1974 Census of Agriculture, Washington State and County Data.* Volume I, Part 47, Washington, D.C.

U.S. Department of Energy (DOE). 1990. *Radioactive Waste Management.* Order RL 5820.2A, DOE Richland Field Office, Richland, Washington.

U.S. DOE. 1989. *Draft Environmental Impact Statement, Decommissioning of Eight Surplus Production Reactors at the Hanford Site, Richland, Washington.* DOE/EIS-0119D, DOE, Washington, D.C.

U.S. DOE. 1987. *Final Environmental Impact Statement: Disposal of Hanford Defense High-Level, Transuranic and Tank Wastes.* DOE/EIS-0113, Vol. 1-5, U.S. Department of Energy, Washington, D.C.

U.S. Environmental Protection Agency (EPA). 1992. National Air Data Branch, Aerometric Information Retrieval System. Total Suspended Particulate information for Kennewick, Washington (1985-88).

U.S. EPA. 1989. *Exposure Factors Handbook.* EPA/600/8-89/043, Washington, D.C.

Yang, Y-Y, C. B. Nelson. 1986. "An Estimation of Daily Food Usage Factors for Assessing Radionuclide Intakes in the U.S. Population." *Health Physics*, 50:245-257.

9413222.1735

This page intentionally left blank.

Appendix N

Sensitivity Analysis for Dose and Exposure Assessment Parameters

9413222.1736

This page intentionally left blank.

Appendix N

Sensitivity Analysis for Dose and Exposure Assessment Parameters

S. F. Snyder and K. Rhoads, Pacific Northwest Laboratory

9413222.1738

A sensitivity analysis was performed for the dose and exposure assessment parameters used in the intruder (drilling and post-drilling), irrigated farm, irrigated garden, and Columbia River scenarios that were evaluated using the GENII computer code. The sensitivity analysis results reflect both the degree of uncertainty in each parameter value and that parameter's importance in determining the overall dose estimate for a particular scenario. In general, variations in values of the more sensitive parameters will produce significant changes in the dose estimate, whereas variations in parameters of low sensitivity will not significantly alter the calculated dose estimate. The analysis is intended to show the relative contribution of variations in scenario parameters to uncertainties in the resulting dose estimate.

N.1 Sensitivity Analysis Methods

The GENII-S computer code, described in Appendix I, Section I.3, was used to perform the sensitivity analyses. The code uses the basic exposure and dosimetry algorithms in the GENII software package, with an added feature that allows the user to define probability distribution functions (PDF) for a number of variable parameters. Possible choices for PDFs in the GENII-S code include fixed, uniform, loguniform, normal, lognormal, triangular, and empirical. A fixed PDF is specified by a single value for a parameter; the uniform and loguniform PDFs require minimum and maximum values; upper and lower 99.9% confidence limits define a normal or lognormal distribution; and the triangular distribution requires the definition of a minimum, maximum, and central value. The empirical distribution function allows the user to supply a set of raw data for a given parameter. The PDF for a particular parameter reflects the degree of uncertainty concerning its true value, which may result either from inadequate knowledge, or inherent stochastic variability in the parameter's value, or both.

In performing the sensitivity analysis for each scenario, a specified number of dose calculations were performed using a randomly selected set of values for the variable parameters in each run. In this analysis, a Latin Hypercube sampling technique was used to select a set of parameter values for each of 100 iterations based on the previously defined distributions. When inadequate empirical data was available to define a PDF, a uniform distribution over a range was assumed. Although attempts were made to

define the PDFs for each parameter as realistically as possible, many ranges were defined by default as ±50% of the value used in the deterministic (single point) dose calculations.

Output from the sensitivity analysis consisted of a series of partial rank correlation coefficients (PRCC) between the variable input parameters and the resulting dose estimates for each set of calculations. The relative sensitivity of each parameter was indicated by the absolute value of its partial rank correlation coefficient. The value of the PRCC may range from -1 to 1, where a PRCC of 1 indicates a perfect positive correlation between two variables, and a PRCC = -1 indicates a perfect negative (or inverse) correlation. The correlation coefficient was calculated based on the rank of each parameter's value rather than on the value itself, because the rank transformations are generally more revealing when nonlinear relationships are involved in a model. A stepwise ranking of each sensitive parameter was then performed to evaluate its relative contribution to the total uncertainty in the dose estimate. For the purposes of this analysis, a parameter was considered sensitive if the absolute value of its partial rank correlation coefficient was greater than 0.50.

The sensitivity analyses were performed for a subset of radionuclides in the grout inventory because the number of parameters that could be varied within each scenario was limited. The driller and post-driller scenario sensitivity analyses included the influence of the grout radionuclide inventory for each of four post-disposal times. The irrigated farm and Columbia River scenario sensitivity analyses were conducted for each significant radionuclide using unit concentrations in ground- or surface water. This approach was used to make the sensitivity analysis for dosimetry parameters independent of the sensitivity analysis for groundwater transport parameters, which was performed separately.

N.2 Intruder Scenarios

The sensitivity analyses for the drilling and post-drilling scenarios will be discussed together because of their similarities (see Appendix M, Exhibit M.1, Section M.0). The parameters that were varied for the sensitivity analysis are indicated in Table N.1. All other parameters were assigned fixed values identical to those used for the deterministic scenario DF evaluations (see Appendix M, Exhibits M.2 and M.3).

In this analysis, it was necessary to define a pre-existing correlation for two of the parameters, the "manual redistribution factor" and the "contaminated area." The "manual redistribution factor" parameter relates the volume of grout exhumed during drilling to the area over which it becomes distributed (see Equation 1). The manual redistribution factor is, therefore, strongly correlated to the "contaminated area" parameter. The definition of a high, but not perfect, correlation between these parameters was desired because of uncertainties in the volume of grout exhumed and the depth of surface soil into which the grout is distributed. The defined correlation coefficient was assumed to be -0.75.

Table N.1. Parameter Values Used for Sensitivity Analysis of the Drilling and Post-drilling Scenarios

Parameter (units)	Scenario	Range of Values minimum	central[a]	maximum	PDF[b]
Annual soil exposure time (h)	Drilling	24	40	60	U
	Post-Drilling	1000	4383	4383	U
Annual inhalation exposure time (h)	Drilling	0.5	1	10	U
	Post-Drilling	1000	8766	8766	U
Manual redistribution factor (m^{-1})[c]	Drilling	3.2E-3	6.4E-3	1.3E-2	U
	Post-Drilling	1.3E-4	2.6E-4	6.4E-4	U
Contaminated area (m^2)[c]	Drilling	50	100	200	U
	Post-Drilling	1000	2500	5000	U
Daily soil ingestion rate (mg)	Both	50	100	150	T
Mass loading (g/m^3)	Both	1E-5	1E-4	1E-3	U
Fraction of roots in upper soil layer	Post-Drilling	0.75	1	1	U
Above-ground biomass (wet kg/m^2)	Post-Drilling				U
leafy vegetables		1	2	3	
other vegetables		1	2	3	
fruit		1.5	3	4	
Growing time (d)	Post-Drilling				U
leafy vegetables		30	90	90	
other vegetables		30	90	90	
fruit		60	90	90	
Consumption rate (dry kg/y)	Post-Drilling				U
leafy vegetables		2.1	4.1	6.2	
other vegetables		7.0	13.9	20.9	
fruit		3.5	7.0	10.5	
Soil-to-plant concentration ratio scaling factor	Post-Drilling	0.1	1	10	LU
Animal transfer factor scaling factor	Post-Drilling	0.1	1	10	LU

(a) The central value indicated for the range is the deterministic value used for the scenario DF evaluation. Minimum and maximum values indicate the ranges defined for the specified PDFs.

(b) The probability distribution function (PDF) chosen for each parameter range is indicated (U=uniform, T=triangular, LU=loguniform).

(c) Within each scenario, these parameters are defined to be correlated with a correlation coefficient of -0.75.

$$M = \frac{V}{A} \tag{1}$$

where M = manual redistribution factor

V = activity concentration of grout exhumed (Ci/m^3)

A = contaminated area activity concentration (Ci/m^2)

The specific radionuclides evaluated for the drilling and post-drilling scenarios differ because of the different exposure pathways involved in each scenario. Only those radionuclides that contributed greater than 1 mrem EDE based on the deterministic analysis were included in the sensitivity analyses. The radionuclides included in the drilling scenario sensitivity analyses were strontium-90, tin-126, cesium-137, and americium-241. The radionuclides included in the post-drilling scenario were strontium-90, plutonium-239, technetium-99, americium-241, tin-126, neptunium-237, and cesium-137.

Initial sensitivity analysis results (not shown) indicated that time of intrusion was the most sensitive parameter for the drilling and post-drilling scenarios. Because of the high sensitivity of this variable, a second set of sensitivity analyses was run for both the drilling and post-drilling scenarios at each of the 4 post-disposal times evaluated in the deterministic analysis (100, 300, 500, and 1000 years). Elimination of the dominant sensitivity variable by this procedure permitted better discrimination among the sensitivities of the remaining parameters.

N.2.1 Drilling Scenario Sensitivity Analysis Results

The sensitivity analysis results for the drilling scenario are presented in Table N.2. The partial rank correlation coefficients (PRCC) represent the degree to which the ranked value of the associated parameter was correlated with the magnitude of the dose estimate. In addition, a stepwise ranking of the PRCC for each parameter was used to determine its relative contribution to the total uncertainty in the dose estimate. These values are listed under the "Fractional Contribution to Dose Uncertainty" heading in the table and are perhaps more meaningful than the PRCC value itself. The totals listed in this column indicate the fraction of the total uncertainty in the dose that is attributable to the listed parameters. The remaining uncertainty is due to the aggregate of small contributions from relatively insensitive parameters not included in the table.

For reasons described previously, a correlation was defined between the manual redistribution factor and the size of the contaminated area in this portion of the sensitivity analysis (correlation coefficient = -0.75). The PRCC for the manual redistribution factor was consistently higher than that of the

Table N.2. Results of Sensitivity Analysis for the Intruder Drilling Scenario

	PRCC	Fractional Contribution to Dose Uncertainty
100-year Post-disposal		
Cesium-137 concentration in grout	0.94	0.40
Manual redistribution factor/ contaminated area	0.88	0.35
Soil exposure time	0.86	0.17
Total		0.92
300-year Post-disposal		
Cesium-137 concentration in grout	0.91	0.28
Manual redistribution factor/ contaminated area	0.89	0.36
Soil exposure time	0.87	0.22
Tin-126 concentration in grout	0.53	0.03
Total		0.89
500-year Post-disposal		
Tin-126 concentration in grout	0.96	0.40
Manual redistribution factor/ contaminated area	0.93	0.37
Soil exposure time	0.92	0.18
Total		0.95
1,000-year Post-disposal		
Tin-126 concentration in grout	0.97	0.44
Manual redistribution factor/ contaminated area	0.94	0.33
Soil exposure time	0.93	0.19
Total		0.96

contaminated area parameter, and the contaminated area did not meet the criteria for a sensitive parameter at any time period evaluated. For completeness, the sensitivity of both parameters should *qualitatively* be considered together because of their relatively strong correlation. However, the PRCC and contribution to dose uncertainty reported in the tables apply only to the manual redistribution factor.

The drilling scenario sensitivity analysis indicates that the grout radionuclide concentrations generally control uncertainty in the total dose estimate. At 100 and 300 years post-disposal, Cs-137 was the dominant radionuclide, whereas longer-lived Sn-126 became important at the later times. This corresponded to the results for the deterministic analysis, where Cs-137 and Sn-126 were the major contributors to dose

at the early and late post-disposal times, respectively. Other parameters related to the external exposure pathways (soil exposure time, manual redistribution factor, and contaminated area) contributed substantially to the total dose uncertainty as well. It would be expected that the grout radionuclide concentrations should be somewhat less subject to uncertainty than the other parameters related to future events, which are more difficult to predict prospectively. For the drilling scenario, parameters related to the internal exposure pathways (soil ingestion and inhalation) were of low sensitivity relative to the external exposure pathway parameters, which were responsible for more than 89% of the uncertainty in the total dose estimate.

N.2.2 Post-drilling Scenario Sensitivity Analysis Results

The sensitivity analysis results for the post-drilling scenario are shown in Table N.3. As with the drilling scenario, the PRCC and relative contribution to the total dose uncertainty are shown for each sensitive parameter at four post-disposal times.

The results for the post-drilling scenario are similar to those from the drilling scenario, with radionuclide concentrations and parameters related to the external exposure pathways dominating total uncertainty in the final dose. The controlling radionuclide concentrations are the same as for the drilling scenario—Cs-137 at early post-disposal times and Sn-126 at later times. Parameters related to the internal exposure pathways also make minor contributions to the dose uncertainty in this scenario. The ingestion pathway appears to contribute 2-3% to the total uncertainty at early post-disposal times via the soil-to-plant concentration ratio parameter, which determines plant uptake of radionuclides. At the later times, inhalation parameters (exposure time and mass loading of resuspended soil in air) represent a comparable fraction of the total uncertainty. Again, the external exposure pathways are responsible for greater than 85% of the total uncertainty in the dose estimate for this scenario.

N.3 Irrigated Farm and Columbia River Scenarios

The irrigated farm and Columbia River scenarios will be discussed together because of their similarities (refer to Exhibit M.1 in Appendix M for a scenario comparison). In both scenarios, exposure occurs in a family farm environment via the use of radionuclide contaminated groundwater (irrigated farm) or surface water (the Columbia River) for irrigation and domestic purposes. The family farm scenario evaluates dose to an individual, whereas the river scenario considered collective dose to the entire downriver population. Because collective dose in the river scenario is directly correlated with the number of people exposed to radioactive materials in the river, parameters related to the magnitude of the population were not evaluated in the sensitivity analysis. The variable parameters included in the sensitivity analysis, and the assumed distributions of their associated values, are indicated in Table N.4.

Table N.3. Results of Sensitivity Analysis for the Intruder Post-drilling Scenario

	PRCC	Fractional Contribution to Dose Uncertainty
100-year Post-disposal		
Soil exposure time	0.91	0.29
Cesium-137 concentration	0.89	0.26
Manual redistribution factor/ contaminated area	0.86	0.36
Soil-to-plant CR	0.58	0.03
Total		0.95
300-year Post-disposal		
Soil exposure time	0.90	0.27
Manual redistribution factor/ contaminated area	0.87	0.48
Cesium-137 concentration	0.83	0.14
Soil-to-plant CR	0.51	0.02
Total		0.91
500-year Post-disposal		
Manual redistribution factor/ contaminated area	0.84	0.49
Tin-126 concentration	0.82	0.16
Soil exposure time	0.77	0.13
Mass loading	0.67	0.07
Inhalation exposure time	0.61	0.04
Total		0.89
1,000-year Post-disposal		
Tin-126 concentration	0.88	0.25
Manual redistribution factor/ contaminated area	0.87	0.43
Soil exposure time	0.86	0.17
Mass loading	0.57	0.03
Total		0.88

Table N.4. Parameter Values Used for Sensitivity Analysis of the Irrigated farm and Columbia River Scenarios

Parameter (units)	Scenario	Range of Values minimum	central[a]	maximum	PDF[b]
Annual soil exposure time (h)	Both	1000	4383	4383	U
Annual inhalation exposure time (h)	Both	1000	8766	8766	U
Daily soil ingestion rate (mg)	Both	50	100	150	T
Mass loading (g/m^3)	Both	1E-5	1E-4	1E-3	U
Irrigation application rate (in/y)[c]	Farm	16.2	32.4	48.6	U
	River	0	25	32.4	T
Irrigation application duration (mo/y)[c]	Farm	1.5	5[d]	6.5	T
	River	0	6.5	6.5	U
Fraction of roots in upper soil layer	Farm	0.75	1	1	U
Above-ground biomass (wet kg/m^2)	Farm				U
leafy vegetables		1.0	2.0	3.0	
other vegetables		1.0	2.0	3.0	
fruit		1.5	3.0	4.5	
Growing time (days)					U
leafy vegetables	Both	30	90	90	
other vegetables	Both	30	90	90	
fruit	Both	60	90	90	
fresh feed	Farm	45		60	
Consumption rate (kg/y)					U
leafy vegetables	Farm	2.1	4.1	6.2	
	River	8.2	17	24.7	
other vegetables	Farm	7.0	13.9	20.9	
	River	27.5	55	82.5	
fruit	Farm	3.5	7	10.5	
	River	17.5	35	52.5	
beef	Farm	11.0	22	33.0	
	River	25.0	50	75.0	
poultry	Farm	2.3	4.6	6.9	
	River	5.2	10.5	15.7	
milk	Farm	25.4	50.8	76.4	
	River	57.5	115	172.5	

Table N.4. (contd)

Parameter (units)	Scenario	Range of Values minimum	central[a]	maximum	PDF[b]
eggs	Farm	5.3	10.6	15.9	
	River	12.0	24.1	36.1	
fish	River	3E-4	3E-3	3E-2	
drinking water (l/y)	Both	295.0	655	1455	

(a) The central value indicated for the range is that used in the GENII scenario DF evaluation. Minimum and maximum values indicate the ranges defined for the specified PDFs.

(b) The probability distribution function (PDF) chosen for each parameter range is indicated (U=uniform, T=triangular, LU=loguniform).

(c) Within each scenario, the irrigation application duration and rates are correlated with a correlation coefficient of +0.75 for each terrestrial food (leafy vegetables, other vegetables, and fruit), animal feed crop (fresh forage for milk and beef, and stored feed for milk), and the external exposure calculations.

(d) This value used as the central point of the triangular distribution. The deterministic dose estimate evaluation used 6.5 mo/y as the irrigation duration. The skewed triangular distribution was assumed to best represent the arid region in which the Hanford Site is located.

The farm and river scenarios were evaluated for each radionuclide separately, assuming a unit concentration in ground- or surface water. Only radionuclides that were major contributors to dose in the deterministic calculations were considered for the sensitivity analysis, specifically selenium-79, tin-126 technetium-99, cesium-135, iodine-129, and neptunium-237. In addition, several parameters that were found to be of low sensitivity for the irrigated farm scenario were not evaluated in the sensitivity analysis for the Columbia River scenario. These parameters included the fraction of roots in the upper soil layer, the above-ground biomass for food types, and the growing time for fresh forage for beef and milk. Because of the similarity in exposure pathways for the two scenarios, they were assumed to be relatively unimportant in the river scenario based on the results of the irrigated farm analysis.

Table N.5. Results of Sensitivity Analysis for the Irrigated Farm Scenario

	PRCC	Fractional Contribution to Dose Uncertainty
I-129		
Drinking water consumption	0.96	0.72
Milk consumption rate	0.82	0.11
Milk fresh for. irr. rate	0.64	0.01
Beef fresh for. irr. rate	0.60	0.03
Beef consumption rate	0.55	0.02
Total		0.89
Tc-99		
Drinking water consumption	0.90	0.41
Milk consumption rate	0.84	0.24
Milk fresh for. irr. rate	0.67	0.09
Beef consumption rate	0.64	0.06
Beef fresh for. irr. rate	0.63	0.06
Total		0.86
Np-237		
Drinking water consumption	1.0	1.0
Cs-135		
Drinking water consumption	0.91	0.43
Beef fresh for. irr. rate	0.81	0.15
Beef consumption rate	0.79	0.15
Milk consumption rate	0.60	0.04
Total		0.79
Sn-126		
Beef consumption rate	0.90	0.32
Beef fresh for. irr. rate	0.89	0.30
Drinking water consumption	0.66	0.06
Total		0.68
Se-79		
Drinking water consumption	0.94	0.58
Beef fresh for. irr. rate	0.79	0.11
Beef consumption rate	0.77	0.11
Total		0.80

Table N.6. Results of Sensitivity Analysis for the Columbia River Scenario

	PRCC	Fractional Contribution to Dose Uncertainty
I-129		
Milk fresh for. irr. time	-0.67	0.20
Beef fresh for. irr. time	-0.56	0.17
Total		0.37
Tc-99		
Milk fresh for. irr. time	-0.62	0.07
Milk fresh for. irr. rate	0.55	0.15
Beef fresh for. irr. time	-0.54	0.14
Milk consumption rate	0.52	0.14
Total		0.50
Np-237		
Drinking water consumption	0.88	0.67
Leafy veg irr. time	-0.59	0.09
Total		0.76
Cs-135		
Beef fresh for. irr. time	-0.75	0.40
Milk fresh for. irr. time	-0.54	0.06
Total		0.46
Sn-126		
Beef fresh for. irr. time	-0.88	0.61
Beef consumption rate	0.57	0.07
Total		0.68
Se-79		
Drinking water consumption	1.0	1.0

9413222.1748

N.3.1 Irrigated Farm and River Scenario Sensitivity Analysis Results

In contrast to the intruder scenarios, the sensitivity analyses for the irrigated farm and river scenarios were dominated by parameters related to the ingestion exposure pathways (Tables N.5 and N.6). Drinking water ingestion was the only sensitive parameter for Np-237 in the farm scenario, and it controlled the uncertainty in total dose for all other radionuclides except Sn-126. Parameters related to the animal product ingestion pathways (especially beef and milk production) were most significant for Sn-126, and

also contributed substantially to the uncertainty for other radionuclides (except Np-237) in the irrigated farm scenario. The combined contributions to uncertainty for these pathways represented 68 to 100% of the total uncertainty in the dose estimate.

For the Columbia River scenario, uncertainties in the dose estimate were much less sensitive to the drinking water consumption parameter, with the exception of Np-237 and Se-79. For these nuclides, drinking water consumption was the controlling pathway and accounted for 67-100% of the total uncertainty. The leafy vegetable ingestion pathway also contributed a significant fraction of the total for Np-237. For the remaining radionuclides, the dose was most sensitive to the animal product consumption pathways, however in these cases the sensitive parameters represented a smaller fraction of the total uncertainty (less than 70%) than was the case for the farm scenario.

N.4 Irrigated Home Garden

The irrigated home garden scenario considered the consumption and irrigation of crops with contaminated groundwater. The parameters used in the uncertainty analysis for the irrigated home garden scenario are identical to those used in the irrigated farm scenario (see Table N.4), except for the following:

- No animal products were consumed.
- The minimum fruit growing time was 30 days rather than 60 days. The shorter growing time was used to reflect the growth of berries, rather than assuming primarily tree fruit harvests.

The sensitivity analysis was conducted separately on each radionuclide, assuming a unit concentration in groundwater. Only radionuclides that were major contributors to dose were considered for the sensitivity analysis, specifically selenium-79, tin-126, technetium-99, cesium-135, iodine-129, neptunium-237, and uranium-234.

Drinking-water ingestion was the most sensitive parameter of the home garden scenario for all radionuclides, responsible for more than 74% of the uncertainty in the final dose estimate (Table N.7). For uranium-234, the inhalation pathway parameters are also marginally sensitive.

Table N.7. Results of Sensitivity Analysis for the Irrigated Home Garden Scenario

	PRCC	Fractional Contribution to Dose Uncertainty
I-129		
Drinking-water consumption	1.0	1.0
Tc-99		
Drinking-water consumption	0.96	0.92
Other vegetable consumption	0.73	0.03
Total		0.95
Np-237		
Drinking-water consumption	1.0	1.0
Cs-135		
Drinking-water consumption	1.0	1.0
Sn-126		
Drinking-water consumption	0.96	0.74
Soil exposure time	0.92	0.20
Home irrigation rate	0.86	0.05
Total		0.99
Se-79		
Drinking-water consumption	1.0	1.0
U-234		
Drinking-water consumption	0.99	0.99
Mass loading	0.55	0.005
Inhalation exposure time	0.51	0.0025
Total		0.9975

9413222.1750

This page intentionally left blank.

Appendix O

A Conceptual (Qualitative) Description of the Best Estimate Case

9413222.1752

This page intentionally left blank.

Appendix O

A Conceptual (Qualitative) Description of the Best Estimate Case

C. T. Kincaid, Pacific Northwest Laboratory

9413222.1754

O.1 Abstract

This is a conceptual description of the best estimate case or perhaps a suite of best estimate cases. This qualitative discussion of how we see contaminants leaving the waste disposal system includes a brief description of the physical setting and general conceptual model, and a brief discussion of exposure pathways to justify the attention given to the subsurface pathway. The majority of the appendix is devoted to a description of the elements or components in this highly engineered disposal system, and to our conceptual model of the occurrence of fluid flow and contaminant transport over the short- and long-term as the engineered system degrades and allows contaminants to release from grout. A brief listing of the initial and boundary conditions complete the qualitative presentation of the best estimate case.

The purpose of this qualitative description is to provide a basis for the development of model parameter values for simulations of the best-estimate case(s) that correspond to the expected performance of the system. Toward that end this appendix describes the role of individual elements in the engineered system. The function each component plays in long-term containment and release is outlined in our discussion of fluid flow and contaminant transport. This conceptual model strongly influences how model parameters for simulating the flow of water and the transport of contamination will be determined.

The major elements of the engineered system described in the appendix are as follows: permanent isolation (Hanford) barrier; RCRA cover; backfill soil; gravel; asphalt barrier; RCRA flow grid, catch basin, and sump; thermal insulation board; steel-reinforced concrete vault; and grout. Future performance of the engineered system is cast in four blocks of time; 0 - 100, 100 - 10^3, 10^3 - 10^4, and 10^4 - 10^5 years. Because of the relatively high uncertainty associated with future material properties and the timing and magnitude of degradation, we have chosen to describe the long-term character of the engineered system and the waste it contains in these progressively longer time periods. While arbitrarily assigned, these time periods are the result of increasing uncertainty with increasing time regarding when a given degradation process (e.g., rebar corrosion and seismic stresses) will yield significant degradation to the structural integrity of the system (e.g., through-wall cracking of the concrete vault or asphalt barrier) which leads to a breach in the engineered containment barriers.

This appendix is a record of the consensus achieved regarding the conceptual model for simulating releases and consequences from the disposal of grouted wastes in the proposed engineered system. The next step of selecting and testing submodels and estimating model parameters was not undertaken. Simulations of one or more best estimate cases were not undertaken either. However, this conceptualization provides a valuable basis for understanding the relevance of those conceptualizations and simulations completed and presented in this performance assessment.

O.2 Description of the Physical Setting and General Conceptual Model

The grout waste management area covers approximately 9×10^4 m^2 and the base of vault structures will be 60 to 70-m above the water table of the unconfined aquifer. The 33 vaults containing grouted waste will be paired and placed in rows as shown in Figure O.1. The location of this and other grout program facilities with respect to other Hanford facilities is described in Chapter 2 of the PA.

The PA analysis of the 33 vaults is derived by developing the source term for the saturated zone groundwater model from analysis of an idealized two-dimensional vertical cross section (see Figure O.2) which captures the symmetric half (see Figure O.3) of a pair of vaults located in the vadose zone, i.e., a single vault is analyzed because each pair of vaults shares a single RCRA cover. Two primary assumptions of the conceptual model regarding the substitution of the two-dimensional cross section for the fully three-dimensional field setting are (1) the design and performance of each vault is similar with respect to its engineered systems and its underlying geohydrology, and (2) the flow of water and transport of contamination are predominantly in the vertical direction through the vadose zone and into the unconfined aquifer underlying these vaults. These assumptions are based on our knowledge of the disposal facility and the natural environment in which it has been placed.

Thus, contamination from the 33 vaults moves downward by convection and diffusion to the water table. While the vadose zone that underlies the grout treatment facility is relatively deep, it is assumed the geologic structure or layering is not sufficiently pronounced to result in extensive lateral spreading of contaminants (see Figure O.2). Unlike the 200 West Area which is underlain by the caliche layer, the 200 East Area lacks dominant layering (Lindberg et al. 1992, Appendix C; Fayer and Rockhold 1993, Appendix J) that could result in extensive lateral spreading of contaminants introduced into the subsurface. Therefore, vertical movement of water and contamination is expected to dominate over any lateral spreading.

Conversion of the results from the analysis of a single vault to the field of 33 vaults and the total inventory is achieved by linear scaleup of contaminant flux. Analysis of flow and transport within the vadose zone results in calculation of a fractional release from the unit inventory for the two-dimensional slice of the problem. This fractional release is then applied to the inventory for the entire vault field. This total contaminant flux is then spread evenly over the waste management area as leachate or contaminated recharge to the unconfined aquifer. This calculation does assume that all vaults fail simultaneously.

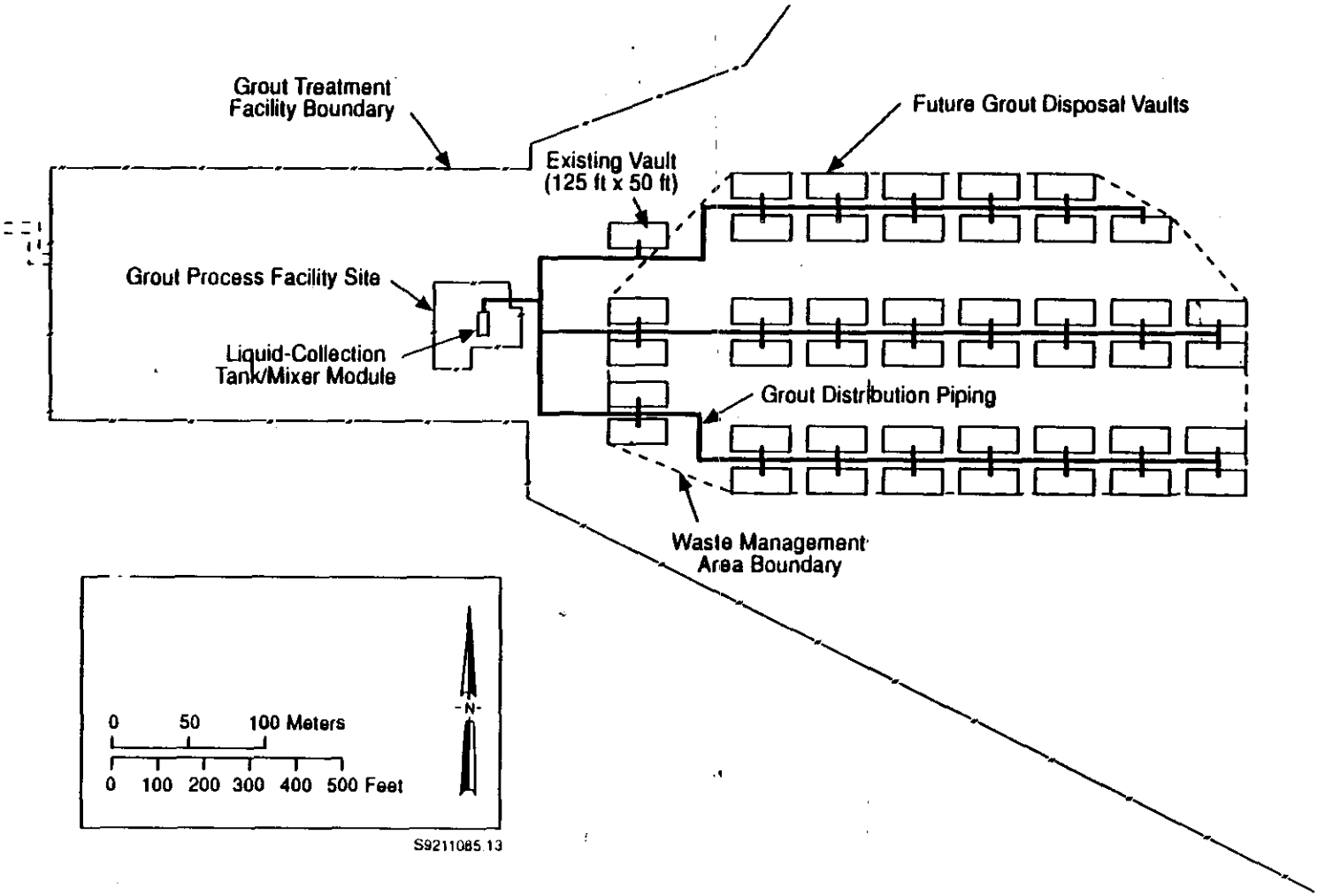

Figure O.1. Areal View of the Grout Treatment Facility Showing the Location of All Vaults

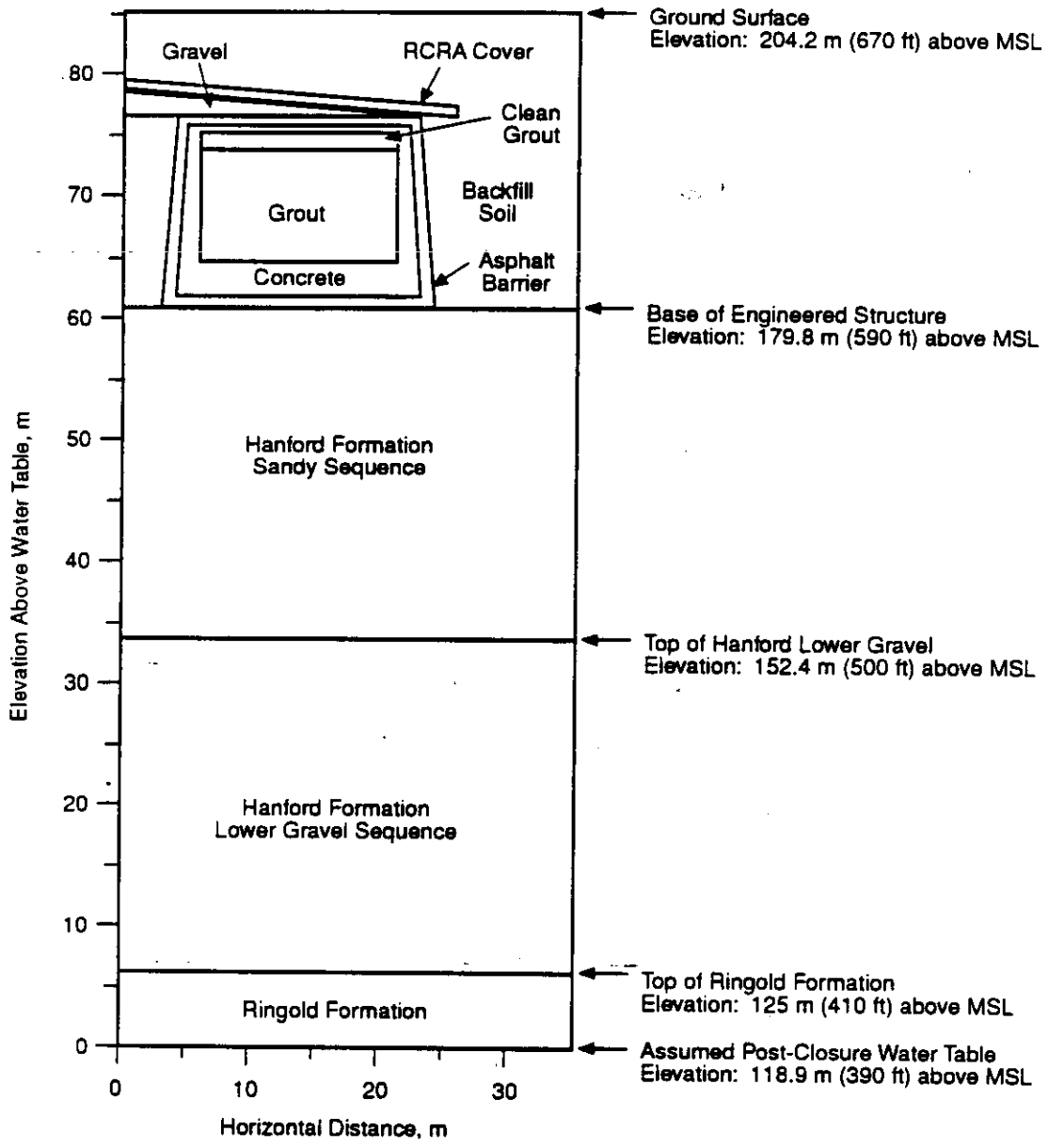

Figure O.2. Two Dimensional Cross Section Showing a Single Vault and the Geologic Cross Section

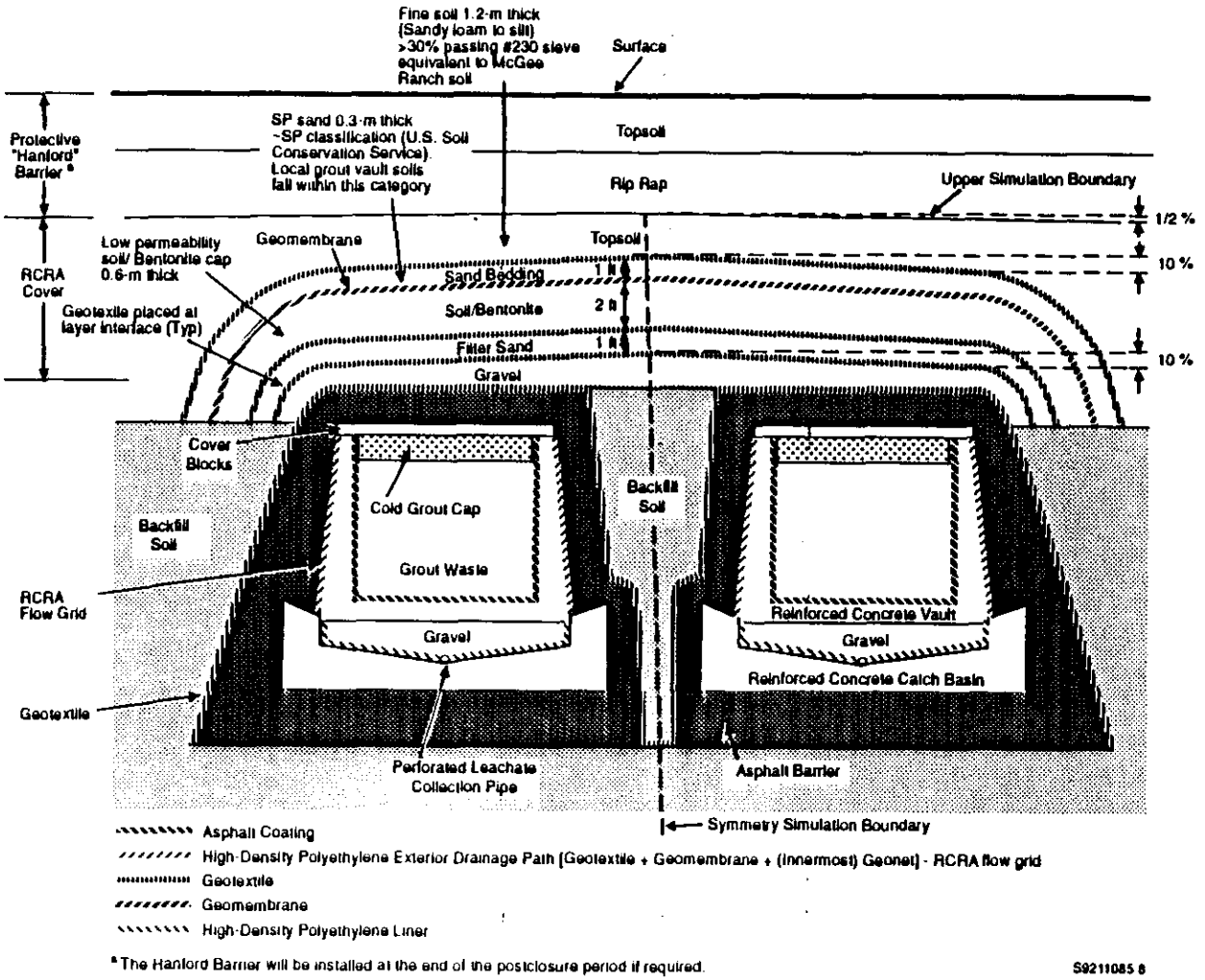

Figure O... Two Dimensional Cross Section Showing the General Conceptual Design of a Vault Pair that Shares a RCRA Cover

While unlikely in an absolute sense, this is justified in light of the time frames of interest, (e.g., thousands to tens of thousands of years), because failure of vaults and releases of contamination could occur over a relatively short period of time, (e.g., several hundred years).

Contamination arriving at the water table is assumed to enter the aquifer underlying the waste management area as a uniform flux (see Figure O.4). In general, two-dimensional simulation of the vadose zone results in a distribution of point concentrations entering the aquifer. Use of a uniform flux is a necessary simplification resulting from the scale-up process which involves the fractional release (an integrated flux) from the base of the two-dimensional cross-section and the land surface area associated with all of the vaults. This is based on an assumption that lateral spreading or dispersion of contamination in the vadose zone is no greater than the surface area of the waste management area. This incorporates a degree of lateral spreading or dispersion in the estimate of contaminant concentration leaving the unsaturated zone. This assumption also implies that the development of preferential flow and transport paths from individual vaults to the water table is improbable. Clastic dikes have been identified within the grout disposal facility; however, they are not believed to be continuous to the water table. If

9413272.1759

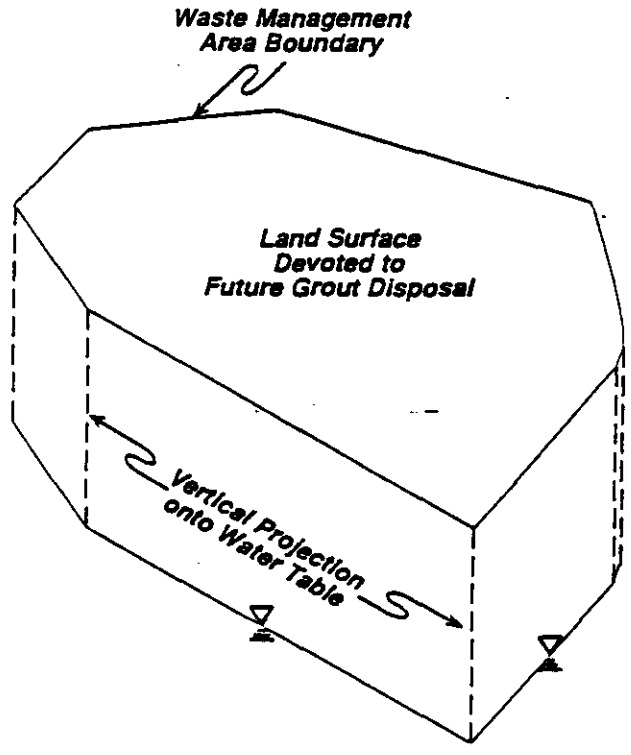

Figure O.4. Three Dimensional Schematic Showing the Vertical Projection of the Grout Vaults Onto the Water Table of the Unconfined Aquifer

they are found to extend to the aquifer, they could represent a preferential flow path. If present, preferential pathways for individual vaults would result in different estimates of flux (e.g., earlier) and point concentrations (e.g., higher) leaving the unsaturated zone and entering the aquifer; however, the effect on overall release from all vaults is assumed to be small.

O.3 Description of the Exposure Pathways

Exposure pathways provide a route for the radioactive waste to come into contact with the biosphere and human beings. It is important to briefly describe scenarios which identify some of these exposure pathways that involve groundwater because our simulations of the unsaturated zone and unconfined aquifer provide input necessary for these scenarios. We are analyzing the potential health threat posed by contaminated groundwater. Several scenarios are examined which are based on the use or consumption of contaminated water; e.g., groundwater as a water source for drinking water, for irrigating a garden, for irrigating a family farm, and water from the Columbia River downstream of the site for both a domestic water supply and a source of irrigation water. An intruder scenario is also included which addresses the threat to human health posed by exhuming the radioactive waste. Greater details on these scenarios can be found in the text of the PA in Chapter 1 and Section 3.3.4.4. Knowing how model simulations are to be used will be a factor in determining the output requirements of analyses. Note that exposure pathways are fixed and not varied throughout the analysis.

O.3.1 Drinking Water Scenario

Only the drinking water exposure pathway is considered in the drinking water scenario. For this scenario the limits established for drinking water have been applied to water pumped from a downgradient well. The performance objective adopted by the grout program for this scenario is a maximum allowable dose received from drinking 2L/d of water. This objective is based on a proposed EPA regulation which allows a 4 mrem/yr effective dose equivalent to the individual who consumes 2L/d of drinking water. Doses for this scenario will be based on a water consumption rate of 2 L/d and the ingestion dose factors recommended by DOE (U.S. DOE 1988b).

O.3.2 Irrigated Garden and Irrigated Farm Scenarios

For the irrigated garden and farm scenarios, all pathways of exposure are considered. A performance goal of 25 mrem/yr effective dose equivalent for all radionuclides to the maximally exposed individual will be used. This is consistent with DOE Order 5820.2A (U.S. DOE 1988a), proposed EPA regulations (proposed 40 CFR 191, see 58 FR 7924; also see Gruhlke, Galpin and Holcomb 1989), and existing NRC regulation (10 CFR 61).

O.3.3 River Scenario

The river scenario is also an all-pathways exposure scenario which evaluates dose to the collective downriver population. Contaminants transported to the river by groundwater are assumed to be mixed in the total river volume, and the water is used for domestic, agricultural, and recreational purposes by the downstream population. Results of the river scenario are anticipated to indicate very low doses to the public because of the large flow of the Columbia River and the low flux of contaminated groundwater. If results of the irrigated farm scenario easily satisfy the all-pathways dose limit of 25 mrem/yr, an integrated population dose should be calculated for the river scenario.

O.3.4 Intruder Scenarios

For these scenarios, an intruder is assumed to drill a well directly into the grout, thus bringing contaminated material to the surface. An individual is then assumed to establish a residence at the site and to use the area for limited agricultural purposes. The performance goal is a maximum dose for continuous exposure to the resident of 100 mrem/yr. The performance goal for dose to the driller is a maximum total dose, including committed dose received over 50 years following a one-time exposure, of 500 mrem. The disposal system incorporates passive controls designed to warn and deter inadvertent intruders for at least 500 years after disposal. Thus, intruder doses will be calculated for 100, 300, 500, and 1,000 years, but compared to the intruder scenario performance goals 500 years after disposal.

O.4 Description of Elements in the Conceptual Model of the Engineered System

Elements of the original engineered system and its surrounding environment were described in Chapter 2 of the PA. Schematic drawings of the two-dimensional structure are shown in Figures O.3 and O.5. The role of individual elements of the engineered system in the current design is described below. Then the long-term containment/release function of each component for this best estimate case is outlined. Our conceptual model is the description of how the system is envisioned to function and degrade in the long term. The conceptual model provides the rationale for choosing model parameters to approximate the flow of water and transport of contamination.

While material science provides insight into the expected long-term changes in material properties, long-term forecasts of how an engineered structure containing a waste form will perform are highly uncertain. This is largely because materials will be used in the engineered system for which only a short record of performance exists; e.g., the Portland cement being used to construct the primary containment structure has only been in use for approximately a century, the asphalt being used to construct a combined convection-diffusion barrier is a separated fraction from a natural petroleum with a short performance history, and the high-density polyethylene (HDPE) material used in the RCRA drainage net and liners has only a 35 year performance record. While the performance of materials such as Portland cement and

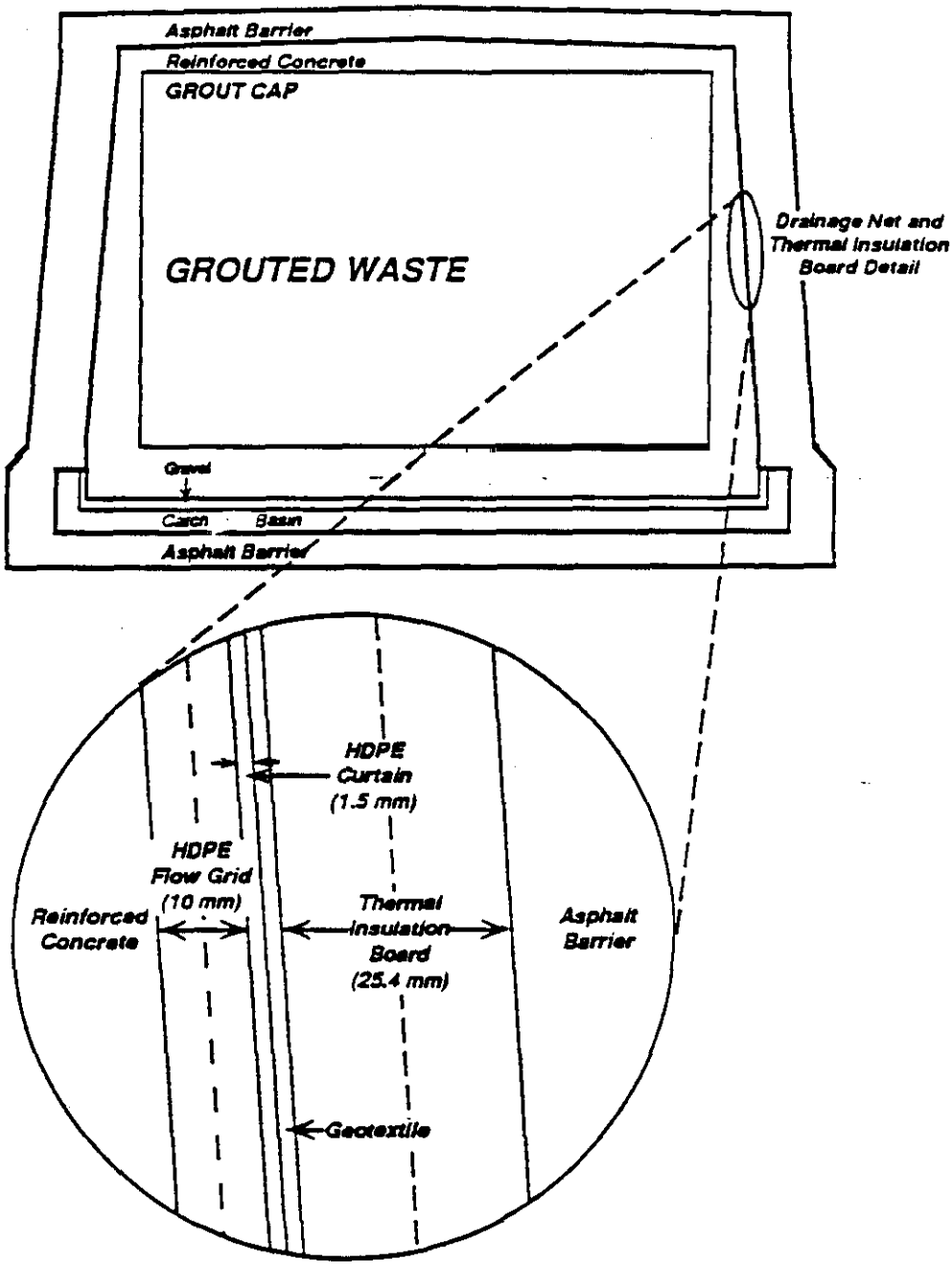

Figure O.5. A Schematic Drawing (two-dimensional vertical cross section) Showing Different Elements of the Engineered Disposal System, and an Exploded View of the Drainage Net and Thermal Insulation Barrier

asphalt pavement is well documented for structures that are above ground (e.g., bridges, building, highways), little information exists about the performance of these materials below ground. Uncertainty in forecasts are also a result of the rather near-term focus of the structural design (i.e., a design or service life of less than 100 years). As a result materials selection and engineering design are not directly related to long-term performance. For these reasons, we have chosen to describe the long-term character of the engineered system and the waste it contains in progressively longer time periods, i.e., 0 - 100, 100 - 10^3, 10^3 - 10^4, and 10^4 - 10^5 years. While arbitrarily assigned, these time periods arise because of the increasing uncertainty with increasing time regarding when a given degradation process (e.g., rebar corrosion and seismic stresses) will yield significant degradation of the structural integrity of the system (e.g., through-wall cracking of the concrete) that in turn leads to a breach in the engineered containment barriers. If peak doses are not predicted within the 10^5 year period, or if longer term secondary peaks are of interest, the simulations should continue indefinitely to be based on the degradation state at the close of the final period.

A brief description of each of the major elements of the engineered system shown in Figures O.3 and 5 follows.

O.4.1 Hanford Unconfined Aquifer

If there is a single case developed for "best estimate" it needs to be an irrigation based scenario. This is the only scenario that will match land-use planning documents and match the irrigated farm and garden all-pathways scenarios. If several cases are developed, they could examine alternate land-use scenarios, e.g., a long-term dormant site or non-irrigated state resulting in long-term 0.1 cm/yr recharge.

O.4.2 Protective (Hanford) Barrier

Located at the soil-atmosphere boundary, this element of the engineered system acts to recycle annual precipitation to the atmosphere by storing it in 1.5 to 2-m of silt-loam soil until evapotranspiration can remove the water during the growing season for both shallow and deep rooted vegetation. The details of this element of the engineered system are not modeled directly in our simulation of the vadose zone. Rather, the results of the research program studying protective barriers have been used to estimate a maximum average annual recharge that could occur through the protective barrier (design objective 0.05 cm/yr). Gee et al. (1992) reported the results obtained on the 200 Area Plateau at the Hanford Site from lysimeters containing silt loam. Lysimeters that were exposed to two times (2X) normal precipitation from 1987 through 1990 produced no drainage regardless of the presence or absence of plants. Unpublished data from continued monitoring of these lysimeters which have since been exposed to three-times (3X) normal precipitation reveal no drainage from vegetated lysimeters but drainage through lysimeters maintained free of vegetation. For the best estimate case a 0.1 cm/yr annual average recharge rate is assumed to apply based on the existing research; this is conservative with respect to both the reported research and the design objective of the isolation barrier program.

It is not uncommon for questions to arise regarding the response of waste disposal systems to a greater recharge rate. Greater recharge could be a consequence of a variety of future events, e.g., climate change arising from changes in greenhouse gases or the onset of the next ice age, unforeseen degradation of the protective barrier system, or future agricultural land use resulting in irrigation on the Hanford Site and directly over the waste disposal units. Note that the design life of the protective barrier system is 1,000 years; however, features such as the gravel admix included in the upper soil layer to prevent excessive wind erosion should enable the barrier to function indefinitely. Historically, the possible effects of greater recharge have been examined by analyzing system response to a uniformly applied 5-cm/yr recharge rate (U.S. DOE 1987, Appendices O, P, and Q). In this PA we will examine the potential impacts of greater recharge by simulating the effects of an increase of 5-cm/yr of recharge uniformly superimposed on present-day recharge for the entire Hanford Site. This will be an envelop or sensitivity case (i.e., not the best estimate case) which quantifies the potential impact of higher recharge.

O.4.3 RCRA Cover

This cover is located between the base of the protective barrier and upper surface of the asphalt barrier. Its purpose is to limit the rate of recharge moving vertically and directly contacting the asphalt barrier and the engineered structures containing waste. The design requirement for saturated hydraulic conductivity, K_{sat}, of the RCRA cover is less than or equal to 1×10^{-7} cm/s (3 cm/yr). It is composed of a mixture of two natural materials; fine soil and clay. The mixture and its field placement will be tested to assure compliance with the K_{sat} requirement. The RCRA cover has a design or service life of 30 years. However, it is composed of natural materials, and, in the vadose setting at the Hanford Site, it may retain its unsaturated hydraulic properties and function as designed indefinitely. That function will limit direct infiltration contacting the waste disposal system to a maximum of 3 cm/yr. In the nominal case of continuous 0.1 cm/yr recharge, virtually all of the recharge moves through the RCRA cover. However, in the high recharge case (≈5 cm/yr), the RCRA cover limits direct recharge to 3 cm/yr and redirects the additional infiltration to the right side of the modeled cross section (see Figure O.2).

O.4.4 Backfill Soil

Construction of the waste disposal system occurs in an excavation. The vault and its surrounding engineered system is entirely buried when completed. Excavated soil is stored and later used to backfill around and above the engineered structure. Soils from the excavations for the first five vaults were sampled and characterized for use in these simulations.

O.4.5 Gravel

Gravel appears twice in the des[illegible] A wedge of gravel is placed immediately above the asphalt barrier, and a layer of gravel is placed in the catch basin. Specifications call for the gravel to be washed and sieved before placement to remove fines and large rock. Thus, it is uniform and clean, and as a result its hydraulic characteristics in an unsaturated environment are distinctly different than those of a common gravel or soil. While such a gravel has a relatively high saturated hydraulic conductivity because of its

open porosity, it acts as a barrier to water flow in the unsaturated zone because of its relatively low unsaturated conductivity and its relatively high (near zero) air entry potential. Thus, given any alternative drainage route requiring lower saturations, water in the surrounding media will move around the gravel (Jury et al. 1991, pp. 110-112). Methods for placing the gravel and overlying material will ensure the integrity of this layer Gravels with substantial open porosity have existed in the Hanford formation sediments for thousands of years. Therefore the hydraulic properties of the gravel layer are assumed not to degrade over time.

The saturated and unsaturated properties of gravel were central to the use of gravel in the waste disposal system design. Its saturated hydraulic properties were the dominant consideration in its selection for the use as a filler for the catch basin. If a leak occurs in the walls or floor of the steel-reinforced concrete vault during the first 30 years, it is important to route the contaminated solution to a sump and remove it from the system. A leak implies a liquid release from the grout through the concrete vault in sufficient quantity to cause saturated conditions in the RCRA flow grid (a required RCRA drainage network described in subsequent paragraphs) resulting in drainage to the catch basin. The saturated hydraulics of the uniform and clean gravel in the catch basin cause the contaminated water to flow to the drain and sump for removal.

The unsaturated hydraulic properties of gravel were a consideration in the decision to place a wedge shaped layer of gravel above the asphalt barrier. The gravel wedge will be overlain by unsaturated filter sand. Pressure of the water phase in the overlying unsaturated sand must approach the air entry potential of the gravel medium before water will move into the gravel. The air entry potential of the uniform and clean gravel is high (i.e., very near atmospheric pressure or zero), and water in overlying or adjacent sand deposits must come nearly to full saturation before such a pressure is reached or exceeded. Because filter sand is composed of fine soils (low air entry potential) and these same fines are absent from the gravel (high air entry potential), water infiltrating through the RCRA cover will be routed to the right side of the waste disposal system (see the modeled cross section in Figure O.3) in the filter sand rather than allowed to drain through the gravel wedge.

O.4.6 Asphalt Barrier

An asphalt barrier[a] at least 1-m thick completely surrounds the vault, catch basin, and sump.[b] Asphalt has three attributes that impact disposal system performance; water does not wet asphalt, wetting is retarded by an asphalt coating, and asphalt has a low diffusion coefficient. The asphalt barrier contains more asphalt and has lower air void space than standard asphalt pavement used in highway and road construction. Thus, its wettability and diffusion properties combined with the asphalt and air content specifications provide a material that should minimize the convection of liquid water and control the diffusion of contaminants.

The asphalt barrier has been analyzed for degradation. However, the common experience of most people, that of watching streets, roads, and highway systems made of asphalt pavement degrade, does not apply directly to the asphalt barrier used in this waste disposal system. The dominant processes leading to the degradation of the much lower quality and thinner asphalt pavements are direct exposure to daily and seasonal cycles of heat and cold, freeze and thaw, sunlight, and traffic loads. Contrast this with the thick and high quality asphalt barrier of the waste disposal system which is buried and not exposed to sunlight, climatic cycles, or traffic loads.

Processes anticipated to cause asphalt barrier degradation are summarized as follows (see Appendix Q):

Process or Mechanism	Associated Degradation
• oxidation of asphalt	• Oxidation will initiate at the surfaces of the asphalt barrier. The bulk of the asphalt in the barrier will oxidize over time. This mechanism will contribute to the brittleness of the barrier.

(a) The design specification for the asphalt barrier calls for an asphalt content of 7.5 ± 0.5% by weight of the total asphalt mixture. Aggregate pretreated with as anti-stripping additive will therefore comprise 92.5 ± 0.5% by weight of the total. Placement specifications call for compaction to a minimum 96% of maximum density, and to less than 4% by volume of air void (Kaiser Engineers Hanford Company 1989).

(b) There is 0.46-m (18 inches) of asphalt barrier overlying 0.46-m of asphalt-coated gravel which form the base of the first four vaults (218-E-16-102 through 105). The remainder of the vault structure is enclosed by 1-m of asphalt barrier. Each of the remaining 29 vaults will be constructed with a complete 1-m asphalt barrier surrounding the entire structure.

• volatilization of asphalt	• Volatilization will probably happen early in the life of asphalt and will result in increased brittleness. The impact of volatilization on the flow or creep properties of asphalt will depend largely on the thermal environment the barrier experiences after placement, i.e., grout cure and radiolytic heating.
• age hardening of asphalt	• Age hardening and polycondensation reactions affect the bulk properties of asphalt and will result in an increase in brittleness. This phenomena could have a significant impact on crack formation in the asphalt barrier. The rates tend to slow with time but at some point can inhibit the crack healing processes because of decreasing ability of the asphalt to flow or creep.
• flow and creep of asphalt	• Based on the above processes that increase brittleness, one subjective estimate is that the barrier will tend to flow and creep for up to 100 years. However, flow and creep behavior is expected to constantly decrease and not occur after 100 years.
• thermal board disintegration	• Cracks (5-mm; horizontal and vertical) in the wall-roof joint area; caused by slumping of the asphalt barrier wall in response to thermal board disappearance.
• short-term seismic stresses	• No cracks; because the probability of significant seismic loading is low in the near term and the asphalt is relatively ductile.
• long-term seismic stresses	• Cracks will be extended or initiated in the hardened or embrittled asphalt and this will accelerate hardening of the overall cross section of asphalt. Asphalt hardening should be a surface phenomena.
• thermal stress	• No cracks; because thermal stresses are highest in the first 300 years and the asphalt should be relatively ductile, reducing the probability of thermal cracking; (thermal events are summarized in the section on thermal insulation board).
• construction joint weakness	• No cracks; because the surface preparations and the healing nature of fresh asphalt are expected to make this weakness insignificant; this expectation of cold joint strength was partially confirmed in tensile testing

• biodegradation	• Biodegradation of exposed surfaces has been confirmed with a measured value for AR-6000 asphalt of 1.17×10^{-4} cm/yr (Luey and Li 1993) after 310 days in contact with wet (70% saturation) soil; it is postulated that the increased surface area exposed by cracks could accelerate the biodegradation and result in increased effective size of cracks; a rate of 1×10^{-4} cm/yr is a best estimate of actual long-term biodegradation in relatively dry soils. Biodegradation is a surface phenomena and it is anticipated that the rate of biodegradation will decrease over time. We also do not anticipate the barrier "disappearing;" instead we expect the asphalt to exist beyond 100,000 years.

The asphalt barrier will be buried in a dark and humid soil environment where biodegradation of exposed asphalt surfaces by microorganisms can occur. In addition, the asphalt may loose its elasticity with time as some components responsible for the elastic and ductile character of the asphalt volatilize and escape the asphalt concrete during the initial 300 year period associated with grout cure and radioactive decay. The resulting embrittlement of the asphalt, when combined with the magnitude of potential seismic events over very long time periods (e.g., 10^3 - 10^5 years), results in an increasing potential for the asphalt barrier to develop through-wall cracks forming a grid pattern on all asphalt surfaces (i.e., top, sides, and base).

O.4.7 RCRA Flow Grid, Catch Basin, and Sump

A RCRA requirement for double containment is satisfied by these elements of the disposal system design. The flow grid or drainage net (see Figure O.5) is composed of high-density polyethylene (HDPE) strands bonded or cast to form a mesh a minimum of 5-mm thick. Two sheets of flow grid (total minimum thickness of 1-cm) are placed on the outer surface of the reinforce-concrete vault. This is followed by a 60 mil (1.5 mm) HDPE curtain and a layer of geotextile. The flow grid is designed to direct any flow of liquids that might escape from the grout through the steel-reinforced concrete vault to the catch basin which underlies the vault. The basin is filled with uniform, clean gravel described above. Flow from the basin drains to the sump which will be pumped to remove any drainage from the vault during the first 30 years of vault service. The real function of this component of the engineered system is to contain and capture liquids until the grout has set and free liquid is removed; a period of time measured in months.

This RCRA system is designed to have a service life of 30 years because of the regulatory requirements under RCRA. It is assumed that it will function as a preferred path for any leachate from the waste disposal system for a much longer period of time. HDPE material should be chemically inert in the grout vault environment, even in the presence of radiation. Radiation exposure causes crosslinking of polymer chains which results in reductions in break strength and break elongation. These effects occur in the Mrad (10^6 rad) range, and become most pronounced at doses of 16 to 37 Mrad. However, location of the

flow grid and curtain outside the concrete wall reduces the dose to about 14 rad. This dose will not have any effect on the HDPE material. Although HDPE materials have only been in existence for about 35 years, plastics experts (e.g., N.R. Gordon, a plastics expert with PNL) believe that properties of HDPE should change very little, even for thousands of years. The only significant physical modification envisioned is some reduction of the flow net thickness (originally 1-cm) because of the viscoelastic (creep) response to external pressures. As is noted in the following description of reinforced concrete, forces originating in the corrosion of steel reinforcement may impact the flow path material but not the overall conclusion that a vertical flow path will exist along the walls of the vault for thousands of years.

The catch basin is composed of reinforced concrete and it is assumed it will degrade as the reinforced-concrete vault is forecast to degrade. Relative movement between the drainage basin and sump pit should be minimal due to the robust structural interface connecting the two structures, e.g., the interface is constructed of reinforced concrete and its thickness reaches 4.572-m (15-ft) (see Figure O.6). A 26 inch outside diameter riser made of carbon steel connects the sump to the land surface. This riser protrudes through the asphalt barrier above the sump. Initially, the sump is filled with gravel to provide volume stability. During closure of the facility, the riser and sump are to be backfilled with a grout slurry. Corrosion of the carbon steel may provide a release pathway if saturated conditions were to exist in the catch basin and sump, and if the asphalt barrier continues to act as an impermeable barrier, (i.e., if the asphalt barrier presents a perfect 'bath tub' situation). It is not envisioned that the basin and sump will function in this way; rather, that liquid under positive pressure (saturated ponding in the catch basin and sump) would drain through the intact or degraded engineered system before significant levels of ponding could occur within the structure.

O.4.8 Thermal Insulation Board

In addition to the 1-cm (minimum thickness) flow net, there is a 2.54-cm (1-in) minimum thickness layer of relatively porous thermal insulation board. This material is placed between the flow-net/HDPE curtain/geotextile and the asphalt barrier as illustrated in Figure O.5. It insulates both the steel-reinforced concrete and the HDPE materials from the thermal shock of the asphalt barrier material when it is placed during construction.[a] An estimate for the disintegration of this wood-based material is based on knowledge of wood disintegration in the anticipated environment (asphalt coated, low moisture, low air availability). The best estimate is that a slow disintegration will occur. The disintegration of this material is

---

(a) Specifications (Kaiser Engineers Hanford Company 1989) for the asphalt barrier call for the mix temperature to not exceed 171°C (340°F) at the batch plant, to be not less than 126.5°C (260°F) at the rear of the laydown machine during placement, and to be not less than 88°C (190°F, average lift mix temperature) before roller compaction is completed. Data collected during placement of the asphalt barriers around vaults 218-E-16-102 through 105 demonstrated that placement temperature was between 143.5 and 149°C (290 and 300°F). Design specifications for the grout formulation call for grout cure to occur at or below 90°C. Estimates of grout temperature resulting from the decay of radionuclides indicate a broad temperature plateau of approximately 55°C (131°F) for a 35 to 50 year period followed by a gradual decline to ambient temperatures after 200 to 300 years.

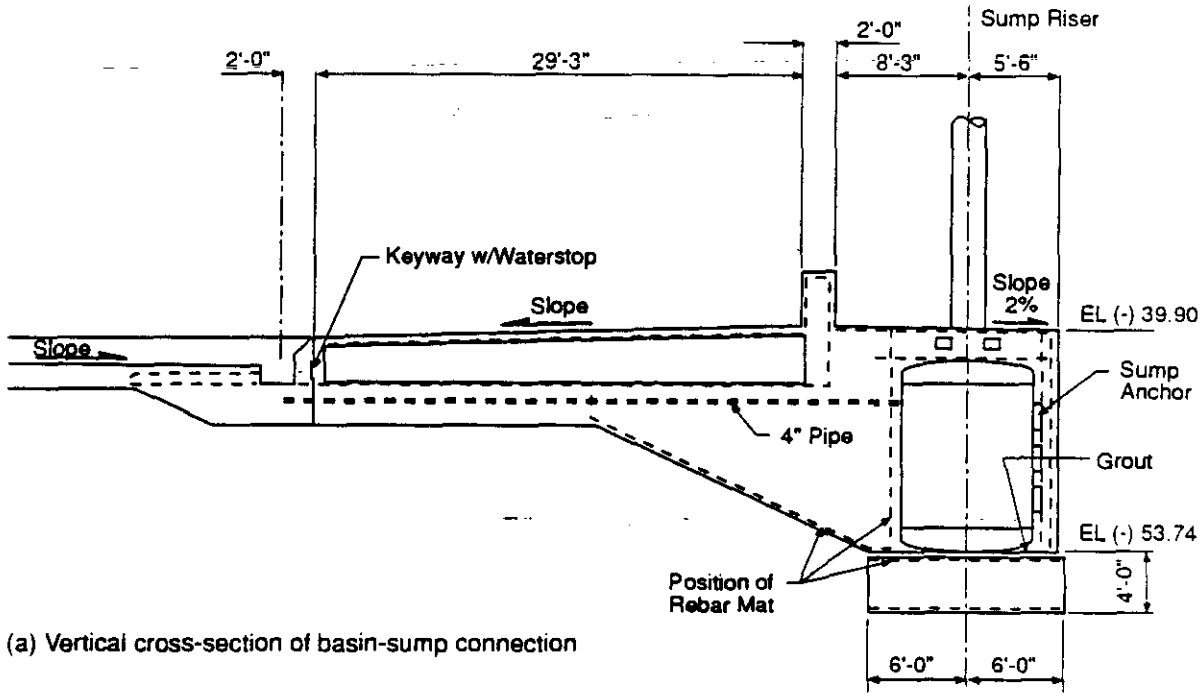

(a) Vertical cross-section of basin-sump connection

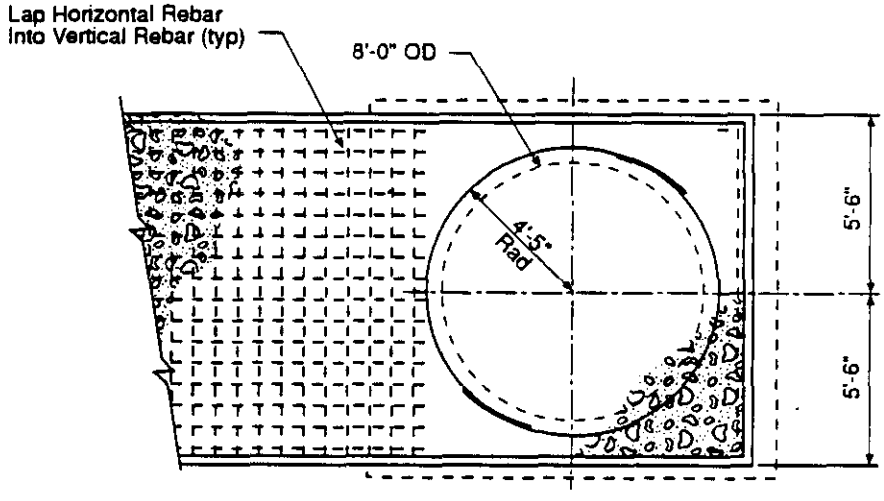

(b) Plan view of basin-sump connection

S9211085.50

Figure O.6. Schematic Drawing Showing the Reinforced-Concrete Structure Connecting the Sump to the Catch Basin

forecast to occur in the 100 to 1,000 year time period. Disintegration of this material will lead to either the formation of a void between the flow net and asphalt barrier wall, or to the gradual and continual compression of the thermal board in response to external loads. In either case, it is anticipated that slumping of the ductile asphalt barrier wall into the space previously occupied by high-integrity thermal insulation board will be sufficient to induce cracks in the vicinity of wall-roof joints of the asphalt barrier.

O.4.9 Steel-Reinforced Concrete Vault

The vault, catch basin, and sump enclosure are all constructed of steel-reinforced concrete. For the grout vault geological environment no near-surface faults nor soil liquefaction potentials have been identified and the potential for seismic stresses to affect the buried structure are low. This was demonstrated by a 0.35g three-dimensional seismic evaluation of a symmetric quarter of the vault in its final configuration, i.e., filled with grout, (B. V. Winkel, 1992, private communication[a]).

The processes anticipated to cause reinforced-concrete material degradation are summarized as follows (see Appendix Q):

Process or Mechanism	Associated Degradation
• short-term seismic stress	• A three-dimensional symmetric quarter of the vault was analyzed for a 0.35 g acceleration event and it demonstrated negligible impact on the design structure.
• long-term seismic stress	• Extension of partial cracks and creation of through cracks in the aged and rebar corroded reinforced-concrete structures.
• short-term rebar corrosion	• Short term rebar corrosion is unlikely because of 1) cathodic protection, 2) high pH level, 3) low permeability of concrete, 4) relatively low chlorides, and 5) presence of asphalt liner separating grout from concrete vault.
• long-term rebar corrosion	• Loss of integrity of reinforcing steel and the associated susceptibility to seismic load failure, and localized cracking of the concrete surface adjacent to rebar and the associated change in hydraulic characteristics of concrete surfaces.
• overburden loads	• Cracks in unreinforced roof plank joints.

(a) Winkel, B. V. 1992. "Grout Vault Asphalt Barrier Seismic Adequacy, Preliminary Report." Memo from B. V. Winkel to R. K. Sanan, BVW-23420-92-001, April 21, 1992.

• corrosion of water stops	• Cracks at construction joints in walls and floors.
• short-term drying shrinkage	• Relatively tight cracks limited to the surface caused by the different drying rates of exterior and interior concrete.
• short-term thermal stress	• Tight cracks on the surface of the concrete are produced by relatively high thermal stress levels resulting from high thermal gradients caused by heat of hydration during grout cure and cesium decay.
• chemical reactions	• While some long-term chemical degradation is likely, the consequences should be minimal because chemical degradation reaction products will tend to bond to the concrete and fill cracks, and relatively few pore volumes of potentially chemically degrading waters are anticipated to flow through the structure. Some resealing is expected in seismically-induced crack openings.

The above listed mechanisms and processes will take their toll over the extended life of the waste disposal system (i.e., 10^5 years); however, the reinforced-concrete structure is assumed to exhibit relatively high integrity for 1,000 years. This level of assumed integrity is a result of the initial integrity and volumetric stability of the structure, the fact that it is buried and thus isolated from the environmental extremes, and the alkaline character of the wastes. A principal mechanism leading to the degradation of the integrity of the reinforced-concrete vault is the corrosion of the reinforcing steel and waterstops caused by the advection and diffusion of waste constituents to the steel surfaces. While unable to quantify the long-term performance of the asphalt liner inside the vault, one should recognize its presence and the role it will play in impeding the migration of contaminants to the steel.

Two classes of cracks are apparent in the preceding description of processes and associated degradation; surface cracks and through-wall cracks. Cracks are anticipated to occur on all concrete surfaces in response to rebar corrosion. Degradation of these surfaces could result in the creation of preferential flow paths from a saturated flow perspective, and in the creation of capillary breaks or barriers to flow from the unsaturated flow perspective. However, the interior portion of the concrete wall (i.e., concrete between the interior and exterior rebar mesh) should retain its original high integrity and low hydraulic conductivity. Releases will not occur solely because of surface cracks. On the other hand, once through-wall cracks appear, they may represent conduits for the release of contaminated liquid from the grout through the reinforced-concrete vault.

With the exception of the joints between roof-plank sections the structure is assumed to function as designed for 100 years. During the 100 to 1,000 year period additional degradation of the roof-plank joints is assumed to be accompanied by degradation of construction joints and the onset of concrete surface degradation resulting from rebar corrosion. In addition to greater degradation of joints and concrete

surfaces, through-wall cracks induced by rebar corrosion and seismic events are forecast to appear during the 10^3 to 10^4 year time period. During the final time period (10^4 to 10^5 years) which represents the indefinite future for the PA analysis, cracks existing after 10^4 years become wider (e.g., 2-mm) and through-wall cracks caused by rebar corrosion and seismic events become more closely spaced (e.g., 0.5-m square grid).

O.4.10 Grout

A considerable and continuing effort exists regarding the formulation of grout and the measurement of its original properties. Standard methods have been used to determine the leachability of a variety of grout formulations and the unsaturated hydraulic properties of a single sample. However, the long-term hydraulic, transport, and attenuation properties of the grout are an area of considerable uncertainty. During the curing process for grout, a cementitious material with a high porosity (55 to 60 % by volume), a very fine pore structure, and continuously connected pore space is formed. While grout cures and excess liquid is removed in a matter of months, the actual curing process continues indefinitely, and, in general, the hydration products of the cement and fly ash continue to be formed, (i.e., hydrated calcium silicate and calcium hydroxide). During hydration, the hydrated cement gel material incorporates pore water and forms precipitates on the surfaces of existing solids that border the pores. Thus, the pore structure will become finer with time as the curing process continues to form hydration products (Dames and Moore 1989).

Care is taken in formulating grout to minimize the potential for formation of expansive minerals that could cause extreme internal stresses and cracking. The formulation efforts attempt to minimize the depletion of OH and the formation of gypsum ($CaSO_4 * 2H_2O$) within the grout. Infiltrating water may import sulfate into the concrete and grout materials; however, sulfate concentrations in water (Dames and Moore 1989) contacting Hanford soils are below concentrations associated with the formation of significant amounts of expansive minerals.

Grout is designed to exhibit relatively good volume stability indefinitely; however, it is not designed to develop the compressive strength and other structural properties of concrete. Consequently, the grout could degrade as the reinforced-concrete vault degrades and external (e.g., seismic) loads are transferred to the grout monolith. Because it will not have sufficient structural strength to bear these loads, it is anticipated that the grout monolith will experience cracking, fracturing, or a generalized breakup in response to vault degradation, (i.e., the timing of grout degradation may correspond to the timing of steel-reinforced concrete vault degradation). The severity of such a degradation process (i.e., timing and magnitude) and the uniformity of associated cracks are unknown and have not been forecast from first principles. However, the grout monolith could experience stresses at points where the vault experiences through-wall cracks because of the inability of the vault structure to bear loads at these locations. It is possible that localized crushing would occur at locations directly opposite corroding rebar and that crushing would be limited to the grout surface. These weakened regions on the grout monolith could then be impacted by seismic loadings, and extensive cracks could form. Thus, as a first approximation, one could assume the grout monolith cracks along planes defined by construction joint cracks in the

reinforced-concrete vault. This would imply 3 cracks in the walls creating 3 horizontal cracks, 1 crack in the floor creating a vertical crack in the center of the cross-section, and 2 cracks crossing the longitudinal axis of the vault (see Figure O.9). Thus, the vertical cross section would include 8 blocks, while the entire monolith would include 24 blocks.

Because of the composition of Hanford soils, natural infiltration percolating into the vault and grout waste form through fine cracks is anticipated to carry with it dissolved carbon dixoide (CO_2). The pH of the infiltrating water will be nearly neutral, but upon reaching either the concrete or grout, the high pH pore fluids will cause the CO_2 to react with CaOH and precipitate calcium carbonate ($CaCO_3$) abruptly in pores or cracks which conduct the infiltrating waters. This mineral precipitation could cause plugging of cracks at high pH interfaces, or a more general filling of cracks along crack surfaces.

Infiltrating water from the surrounding soil environment is expected to be imported in limited quantities. Thus, infiltrating water is expected to affect only a small portion of the grout monolith. Typically, impacts are anticipated at the outer surface of the grout where infiltrating waters bearing dissolved CO_2 first contact the grout as a result of convection and diffusion processes, and in the cracks of the monolith where waters may preferentially flow and diffuse. These impacts will likely be limited to the vicinity of breaks in the concrete and asphalt barrier which provide the pathway for the infiltrating water and chemicals to convect and diffuse to the grout surfaces and cracks. Note that portions of the grout monolith characterized by the discharge of pore water to the surrounding engineered system should not be associated with the precipitation of calcium carbonate, but should be associated with the formation of hydration products. If grout pore water reaches the vadose sediments with its high pH intact, calcium carbonate could precipitate in the sediments.

The overall long-term conceptual model is one of a fractured grout monolith; its matrix made up of blocks of unfractured grout, and its fractures or cracks partially or completely plugged with calcium carbonate or hydration products (hydrated calcium silicate and calcium hydroxide). The continuing formation of hydrated calcium silicate and calcium hydroxide during long-term grout cure should result in a finer pore structure with time in blocks of unfractured grout. Thus, the unsaturated hydraulic performance of the unfractured grout would be conservatively modeled using the original (i.e., freshly cured) unsaturated hydraulic properties measured for grout. The true hydraulic performance of the fractures will depend on the pore structure associated with the fracture openings. A number of alternatives exist, e.g.,

- cracks are open and represent a discontinuity in the unsaturated material,
- cracks are plugged at points where infiltrating waters contact them, (e.g., at the pH front), and open elsewhere,
- cracks are filled throughout their volume w[illegible] calcium carbonate as a result of complete contact with infiltrating water,

- cracks are filled with hydrated calcium silicate and calcium hydroxide formed during long-term cure of the adjacent unfractured grout block, or

- cracks are filled with a combination of calcium carbonate at exterior surfaces, and hydrated calcium silicate and calcium hydroxide on interior surfaces.

Based on our knowledge of the chemistry of grout, and, in particular, the long-term character of its curing process, it is assumed that minerals do form in cracked grout. These minerals are deposited in cracks, and can be envisioned as either fine grained deposits of calcium carbonate along crack surfaces where waters of different pH would contact one another, or as fine grained deposits of hydrated calcium silicate and calcium hydroxide formed on grout surfaces that border cracks. As a result, the crack surfaces will likely be coated, if not filled, with fine mineral deposits.

O.5 Description of Changes in the Conceptual Model with Time

On the basis of the level of uncertainty in future material properties and in the timing and magnitude of degradation of engineered materials, we have chosen to describe the long-term character of the engineered system and the waste it contains in four (4) progressively longer time periods, i.e., 0 - 100, 100 - 10^3, 10^3 - 10^4, and 10^4 - 10^5 years. The identification of distinct time periods for the simulation of degraded materials is also justified on the basis of existing modeling capabilities. State-of-the-art codes generally consider constant material (e.g., hydraulic, transport) properties and time varying boundary conditions. Such codes can be applied in a step mode; properties are held constant for each time interval and careful attention is given to ensure a stable and mass conserving simulation following changes to material properties. The paragraphs that follow are based on the previously described degradation of individual elements in the engineered system. They present the way it is envisioned that elements of the system will work as a whole, and how that will change with time.

O.5.1 Conceptual Model of the 0 - 100 Year Period

During the first 100 years the grouted waste and surrounding engineered system is assumed to function as designed. For example, if a grout vault leaks in its first 30 years of operation, it is assumed the leaked fluid will be routed by the flow grid or drainage net to the gravel-lined catch basin, by the 4-inch drain to the sump, and then be removed by pumping for further treatment and disposal. It is assumed that any significant degradation of the waste disposal system during the first 100 year period of institutional control would be detected by surveillance or monitoring programs and corrected.

Degradation during this period is anticipated to be limited to surface biodegradation of the asphalt barrier at the soil-asphalt interface, and cracking at roof plank joints (see Figure O.7). The rate of biodegradation is assumed to be approximately twice the rate described previously for AR-6000 asphalt, (i.e.,

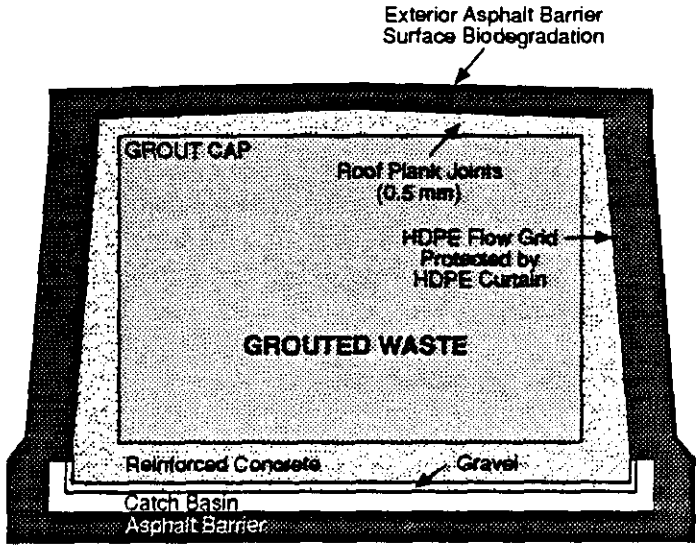

(a) End view cross-section of vault.

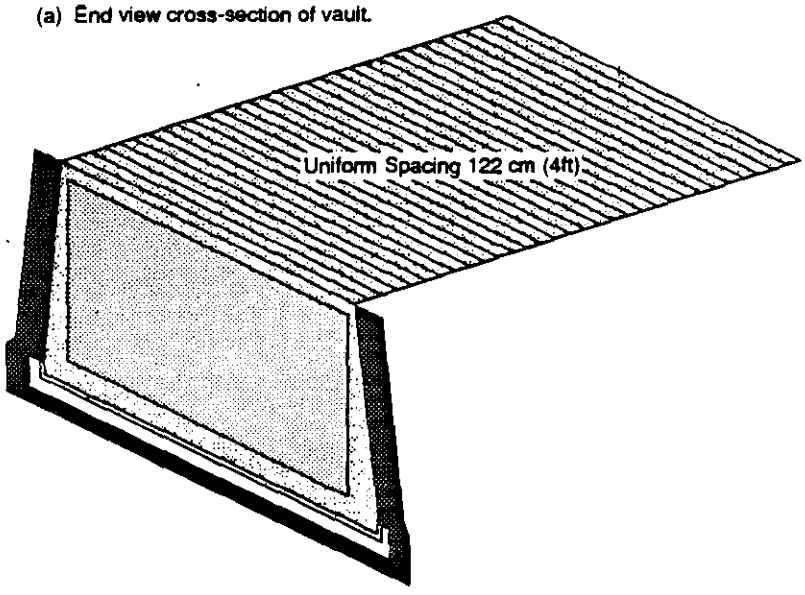

(b) Schematic of roof plank joint orientation and distribution

S9211085.52

Figure O.7. Schematic Drawing Showing the Degradation During the 0 - 100 Year Period, and an Exploded View of Roof-Plank Joint Orientation and Distribution

$2 \times 1 \times 10^{-4}$ cm/yr = 2×10^{-4} cm/yr). Roof plank joints run the width of the vault and are composed of unreinforced grout covered by a thin layer of concrete. They are assumed to be cracked by overburden loading.

Despite this minor cracking of an interior component of the engineered system, the overall system retains its high integrity and does not allow the convection of waste to the soil environment because the original 1-m thick asphalt barrier has not cracked. Isolated from the surrounding soil environment by the hydrophobic asphalt barrier, the fully saturated grout undergoes a temperature pulse (90°C) during cure and experiences heat generation and temperature buildup (55°C) by radioactive (cesium) decay. The interior of the vault has an asphalt coating which should eliminate or make negligible any leakage during this initial 100 year period. The grouted waste is assumed to function as an intact monolith during this period even if thermal and shrinkage cracks develop.

O.5.2 Conceptual Model of the 100 - 10^3 Year Period

It is anticipated that degradation after 100 years will have a minor but recognizable effect on the integrity of the engineered system by the end of the 100 to 1,000 year period. Note that the size and spacing of cracks described below are end-state descriptions, and should not necessarily be associated with the beginning of the time period.

The asphalt barrier is degraded in two ways during this time period; 1) horizontal and vertical cracks (5-mm) caused by the disintegration of the thermal insulation board and slumping of the asphalt barrier walls (see Figure O.8) appear in the upper corners, and 2) biodegradation takes place on the interior and exterior surfaces of the asphalt barrier, and on the crack surfaces of the asphalt barrier. Cracks in the asphalt barrier are assumed to biodegrade on both sides of the crack, (i.e., the original crack is bordered by biodegraded asphalt). These cracks in the upper corners are the first through-wall cracks in the asphalt barrier and they represent an avenue for water to enter and contaminants to leave the reinforced-concrete vault.

The appearance of through-wall cracks in the asphalt barrier, and the presence of the HDPE drainage net, geotextile, and thermal insulation board create a potential for biodegradation on the interior surface of the asphalt barrier. Infiltrating water could enter the engineered system and find its way to the interior surface, thus providing the necessary environment, (i.e., nutrients and microorganisms), for biodegradation to occur on both the interior and exterior surfaces of the asphalt barrier. Thus, interior and exterior surface biodegradation of the asphalt barrier is anticipated to begin during this time period.

The reinforced-concrete vault is assumed to experience three types of degradation during this time period; 1) increased cracking at roof-plank joints, 2) through-wall cracks at construction joints caused by corrosion of steel water stops, and 3) surface cracks on all concrete surfaces caused by rebar corrosion (see Figure O.8). The roof-plank joint cracks increase to 1-mm width. Construction joints are assumed to corrode and become 0.5-mm wide. There are a maximum of five (5) construction joints spaced vertically in each vault wall. These joints (steel water stops) are placed in the structure at the end of a concrete pour

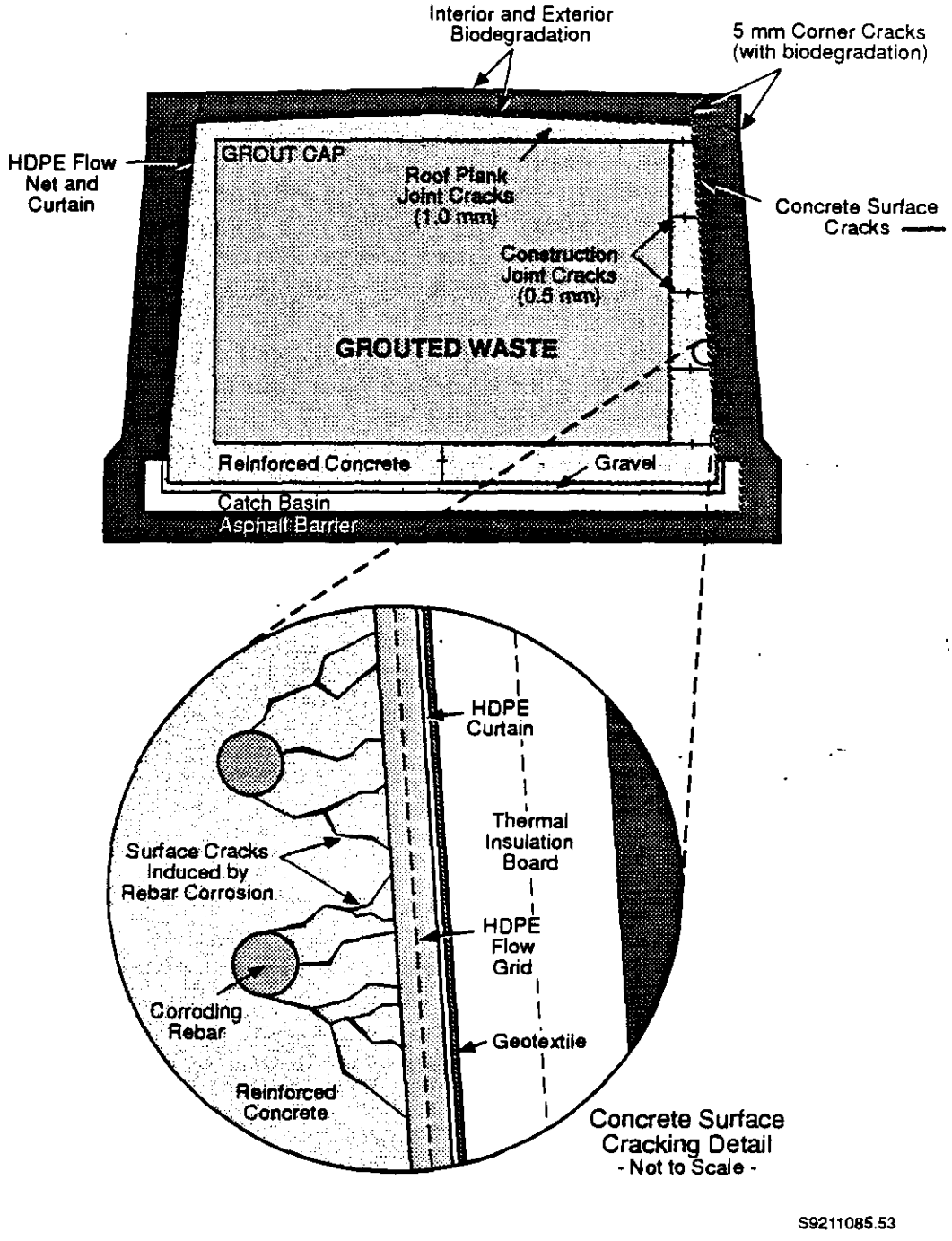

Figure O.8. Schematic Drawing Showing the Degradation During the 100 -10^3 Year Period, and an Exploded View of Cracking on Concrete Surfaces

to ensure a good seal between one pour and the next. The contractor has the option to construct continuous walls that have no joints. The floor of the vault and the catch basin contain approximately 190 and 130 linear feet of construction joints respectively (see Figure 0.9). Surface cracking of reinforced-concrete is a result of the onset of rebar corrosion. This cracking does not result in through-wall cracks during this time interval; however, degradation of the surface does alter its hydraulic properties. For example, the porosity must increase when the concrete is cracked, the water retention relationships must also be different for intact and cracked concrete, and the saturated hydraulic conductivity must increase. These changes may cause the cracked concrete surface to be less conductive than the intact concrete in an unsaturated setting while being more conductive in a saturated setting. In addition, if saturated conditions result, the orientation of the surface dictates the flow direction because a preferential flow path is created. Wall surfaces become vertical flow paths, and floor surfaces become horizontal flow paths.

Following our conceptual model of the grout waste form and its degradation, seismic events and the transfer of external loads from the concrete vault structure to the grout monolith would cause fracturing of the grout monolith. Based on the spacing of corroded construction joints and the corresponding creation of 0.5-mm through-wall cracks at their locations in the concrete vault, when the grout monolith is exposed to seismic loads it is assumed the monolith will break into eight (8) blocks in the two-dimensional cross-section analyzed. It is further assumed that grout and concrete vault cracks would match up horizontally and vertically (i.e., align with the construction joints in the concrete vault).

During this period of time the grout, reinforced-concrete vault, gravel- catch basin, and asphalt barrier should come into hydraulic equilibrium with one another because of the cracks that have developed in the reinforced concrete structures and the hydraulic communication they allow. This equilibrium will depend both on the continuity of mass relationship and the constitutive equations adopted for the hydraulic characteristics of each engineered and natural component. Assuming grout is initially fully saturated, any liquid available for drainage from the grouted waste will drain through the corroded joints, along preferential flow paths associated with the drainage net and cracked concrete surfaces, into the gravel and catch basin, and finally into the unmaintained sump.

The current conceptualization of the disposal system focuses on liquid movement. However, a two-phase study of the vault and barriers is ongoing, and the presence of two (¼ inch o.d.) stainless steel gas vents (see Figure 0.10) connecting the gravel in the catch basin to the backfill soil plays an important role in any model including a gas phase. For the current study, i.e., this performance assessment, the gas vents are neglected as a pathway for liquids to migrate to the surrounding soil. Similarly, the steel riser extending from the sump, through the asphalt above the sump, and to the land surface is neglected as a long-term release pathway. It is believed that liquids under positive pressure (i.e., ponding in the catch basin) would drain through the degraded concrete structure and asphalt barrier before they would flood the catch basin and sump causing the gas vents and sump risers to release contaminated liquids.

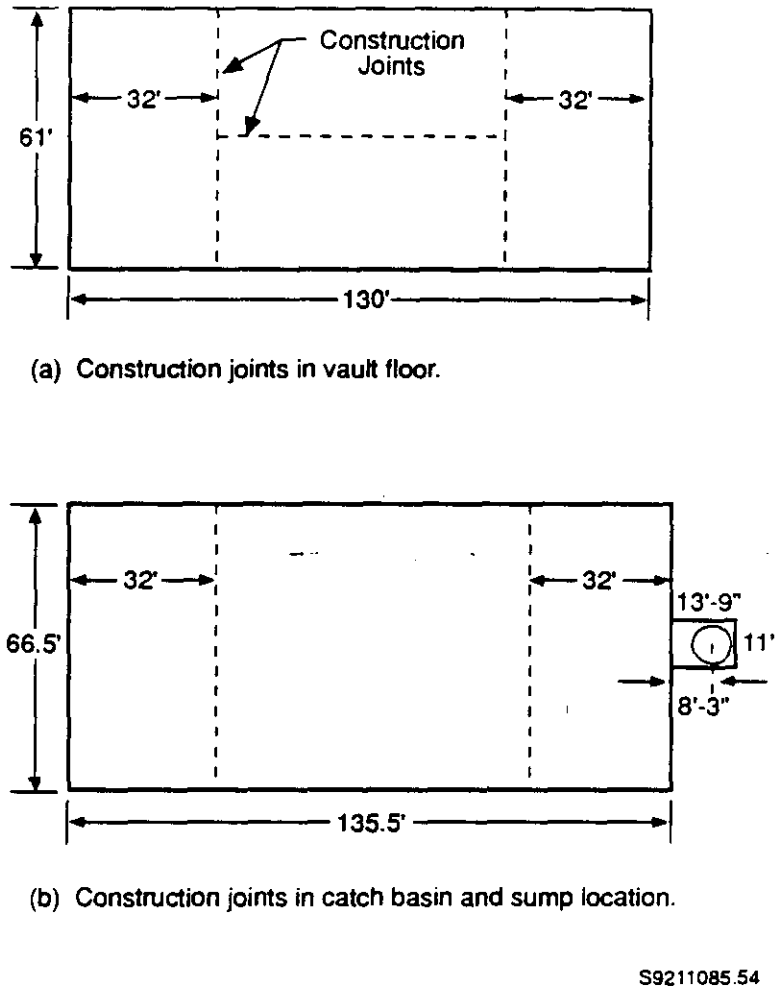

Figure O.9. Schematic Drawing Showing the Position of Construction Joints in the Vault Floor and the Catch Basin

O.5.3 Conceptual Model of the 10^3 - 10^4 Year Period

It is anticipated that degradation during this time period will involve continued biodegradation of the asphalt barrier (interior, exterior, and crack surfaces), a gradual increase in the size of existing concrete cracks, and the creation of patterned through-wall cracks in the reinforced-concrete as a result of rebar corrosion and seismic events (see Figure O.11). Again, note that the size and spacing of cracks described below are end-state descriptions, and should not necessarily be associated with the beginning of the time period.

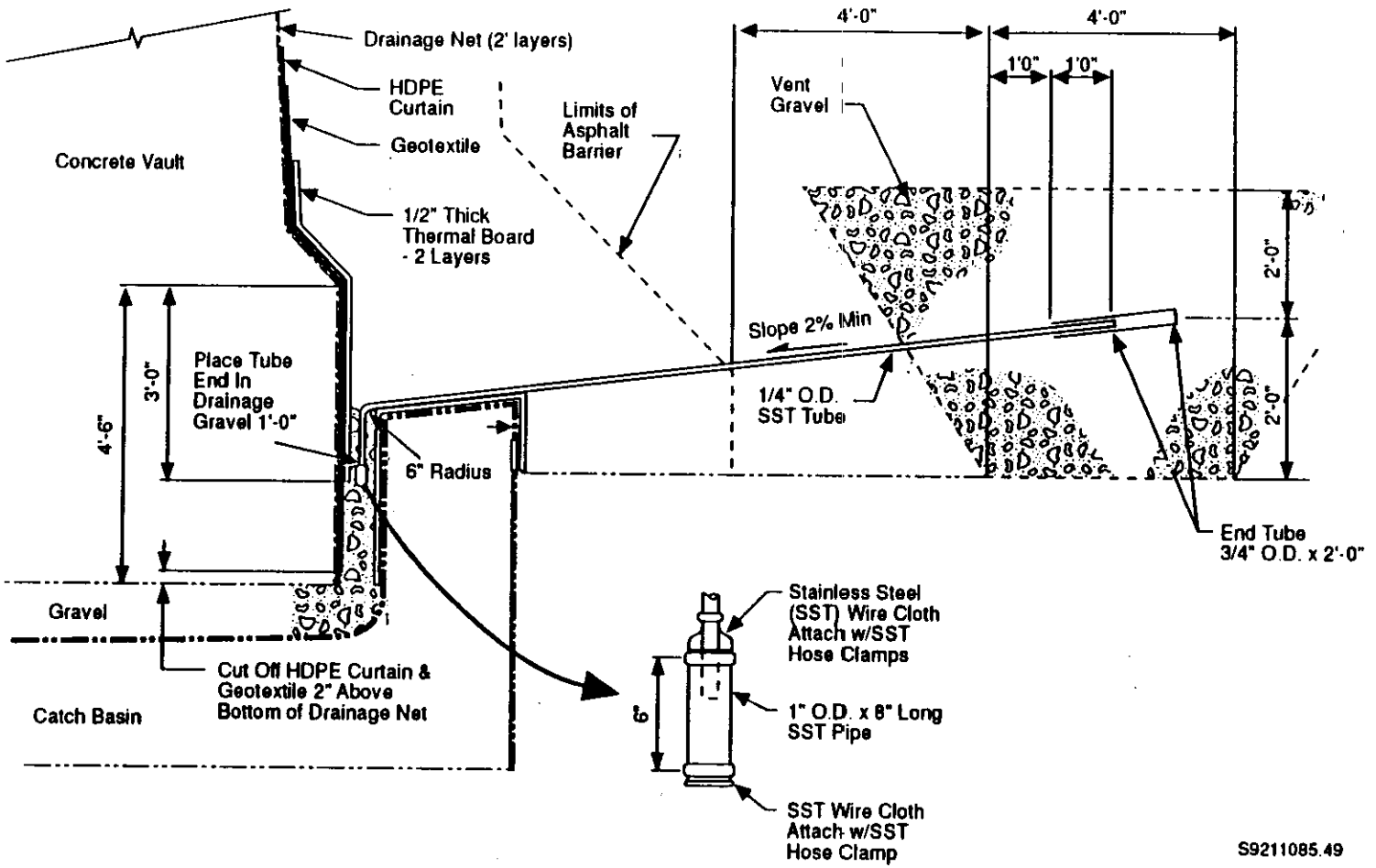

Figure O.10. Schematic Drawing Showing the 1/4 Inch Gas Vents (0.25 inch O.D. and 0.18 inch I.D.) Placed in the Gravel Layer Between the Vault and Catch Basin

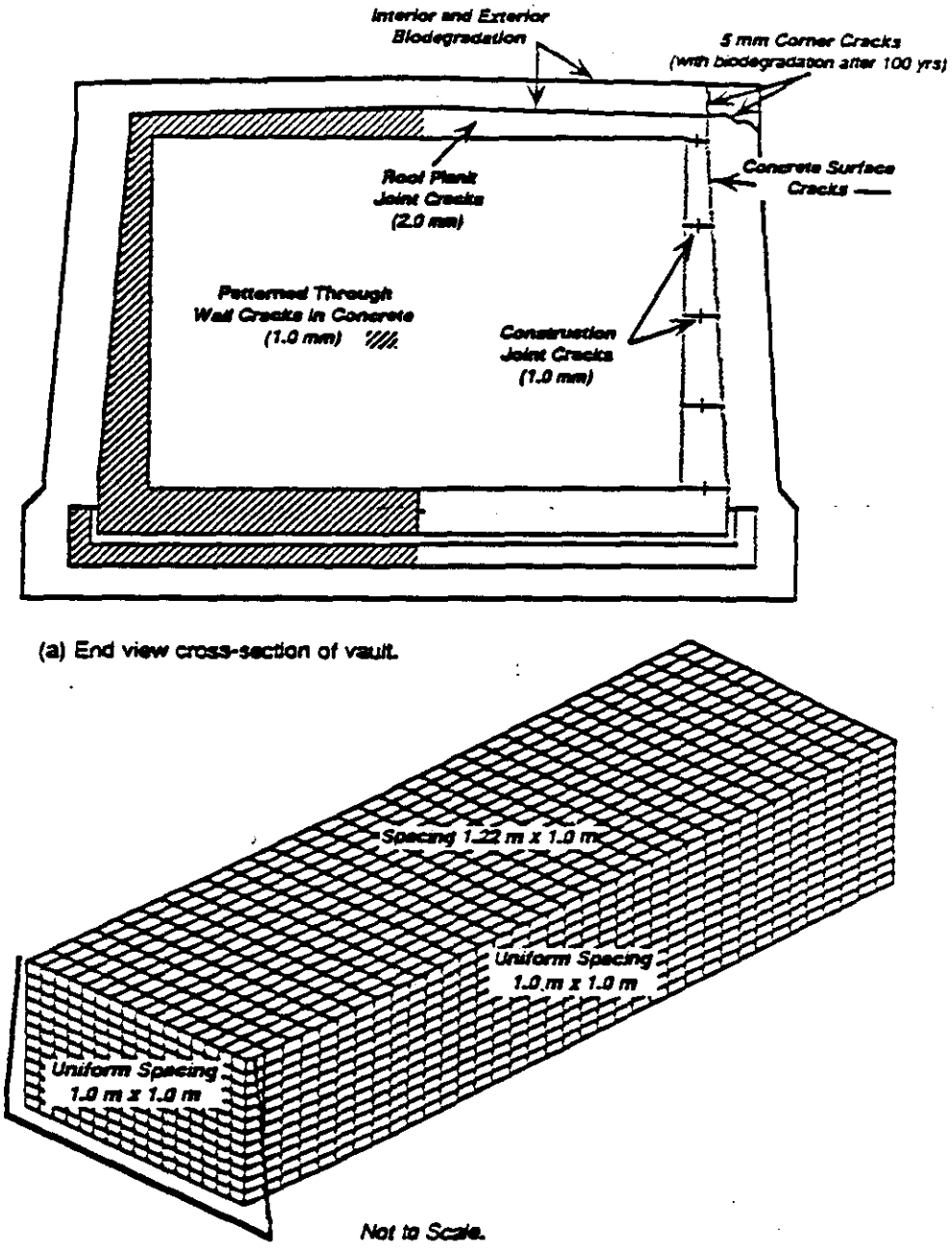

Figure O.11. Schematic Drawing Showing the Degradation During the 10^3 -10^4 Year Period, and an Exploded View of Patterned Through-Wall Cracks in Reinforced Concrete

During this time period, the asphalt barrier continues to biodegrade. No new through-wall cracks develop. Biodegradation occurs on the interior and exterior surfaces of the barrier, and on crack surfaces associated with the horizontal and vertical cracks (5-mm) located in the upper corners of the barrier. These cracks and their neighboring biodegraded asphalt barrier (e.g., barrier aggregate) still represent the only through-wall openings in the asphalt barrier.

The reinforced-concrete vault is assumed to experience four types of degradation during this time period; 1) increased cracking at roof-plank joints, 2) increases in the size of through-wall cracks at construction joints caused by continuing steel water-stop corrosion, 3) increased cracking on all concrete surfaces because of rebar corrosion, and 4) creation of through-wall cracks resulting from rebar corrosion and seismic events. The roof-plank joint cracks increase to 2-mm width. The previously described wall and floor construction joints are assumed to further corrode and become 1-mm wide. Greater cracking of reinforced-concrete surfaces is a result of continued rebar corrosion. This corrosion and surface cracking has now weakened the structure to an extent that through-wall cracks develop (1-mm on 1-m grid) during this time interval. Continued degradation of concrete surfaces alters hydraulic properties even more. Creation of the more prevalent through-wall cracks associated with rebar corrosion and seismic stresses causes additional flow of fluid from the vault to the catch basin region. As in the previous time period, this flow follows the preferential flow paths, i.e., through-wall cracks in the concrete, drainage net, gravel-catch basin, and sump.

Following our conceptual model of grout degradation, seismic events and the transfer of external loads from the concrete vault structure to the grout monolith would cause additional fracturing of the grout monolith. Based on the through-wall crack spacing of the concrete vault, it is assumed the grout monolith will break into 1-m cubes. It is assumed that grout and concrete vault cracks will matchup horizontally and vertically.

During this period of time the grout, reinforced-concrete vault, gravel-catch basin, and asphalt barrier should continue to come into hydraulic equilibrium under the conditions of the additional cracks that have developed in the reinforced concrete structures and the hydraulic communication they allow. The only through-wall cracks in the asphalt barrier are still located at the upper corners. While some contamination will discharge from the upper corner of the disposal system, the movement of contaminant is largely within the engineered structure. Any liquid available for drainage from the grouted waste will drain through corroded joints and rebar corrosion cracks, along preferential flow paths associated with the drainage net and cracked concrete surfaces, into the gravel and catch basin, and finally into the unmaintained sump. As in the preceding time period, drainage from the catch basin and sump is assumed to be directed downward through the degraded structure and driven by any existing positive pressure caused by a buildup of liquid leached from the overlying structure. Thus, the presence of the gas vents and the sump riser is again neglected.

O.5.4 Conceptual Model of the 10^4 - 10^5 Year Period

It is anticipated that degradation during this time period will involve continuing interior and exterior surface biodegradation of the asphalt barrier, continued surface biodegradation in the 5-mm upper corner cracks, gradual increases in the size of existing surface cracks in concrete structures, an increase in the size and density of patterned through-wall cracks in the reinforced-concrete, an increase in the size and density of patterned cracks in the grout, and, finally, the appearance of patterned through-wall cracks in the asphalt barrier (see Figure O.12). The size and spacing of cracks described below are end-state descriptions, and should not necessarily be associated with the beginning of the time period.

The asphalt barrier is now degraded in two ways; 1) biodegradation of interior and exterior surfaces of the asphalt barrier and of all crack surfaces, and 2) patterned cracking on all asphalt barrier surfaces (top, bottom, and sides). The final state of patterned (1-mm on 1-m grid) through-wall cracks in the asphalt barrier is the result of embrittlement and recurring stresses related to seismic events. The patterned cracking also provides more surfaces for biodegradation. The two-surface biodegradation previously applied to cracks in the upper corners of the barrier is now also applied to the patterned through-wall cracks (see Figures 0.12 and 0.13). These patterned through-wall cracks and their biodegradation represent a significant flow path between the grouted waste and soil. The density of 1-m cracks is so great (see Figure 0.12b) that it is highly improbable that all cracks would appear at the beginning of this time period. A more reasonable approach is to assume that cracks develop over some period of time. As an example, Figure O.13b shows the timing of the appearance of horizontal cracks in the walls of the asphalt barrier predicted by a linear model. In this particular model we assume the upper-corner cracks appear after 100 years, that thirteen (13) additional cracks appear in the ≈15-m high wall, and that they appear linearly with respect to time over the 100 - 10^5 year period. Suggested locations for cracks shown in the schematic columns superimposed on Figure O.13b are based on the assumptions that a crack will appear near the bottom early in the time period, and that the progression of crack generation follows a simple doubling pattern that further divides existing segments of the wall.

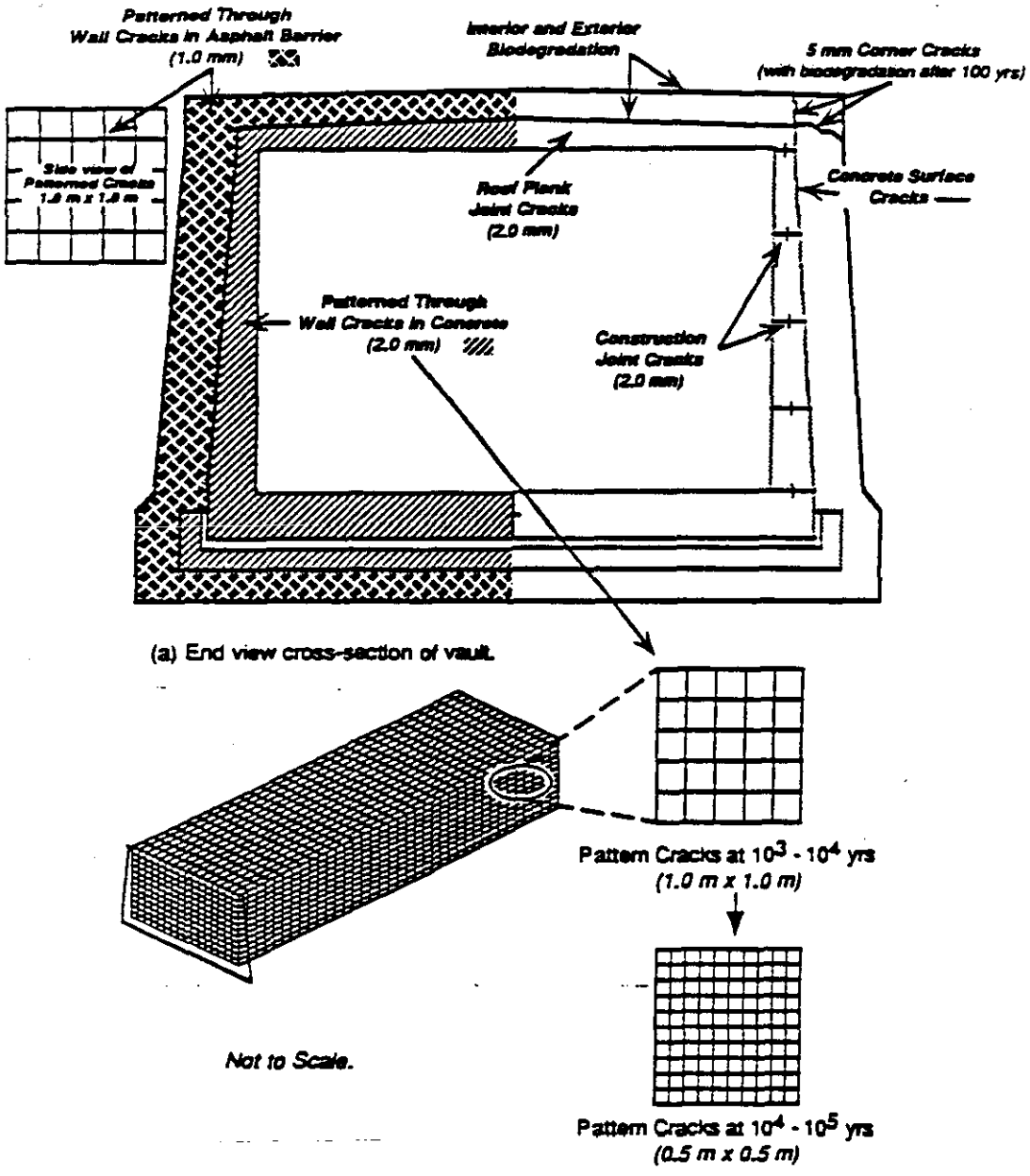

(b) Schematic of changes in patterned cracks in reinforced concrete.

Figure O.12. Schematic Drawing Showing the Degradation During the 10^4 -10^5 Year Period, and an Exploded View of Patterned Through-Wall Cracks in the Reinforced Concrete Vault and Asphalt Barrier

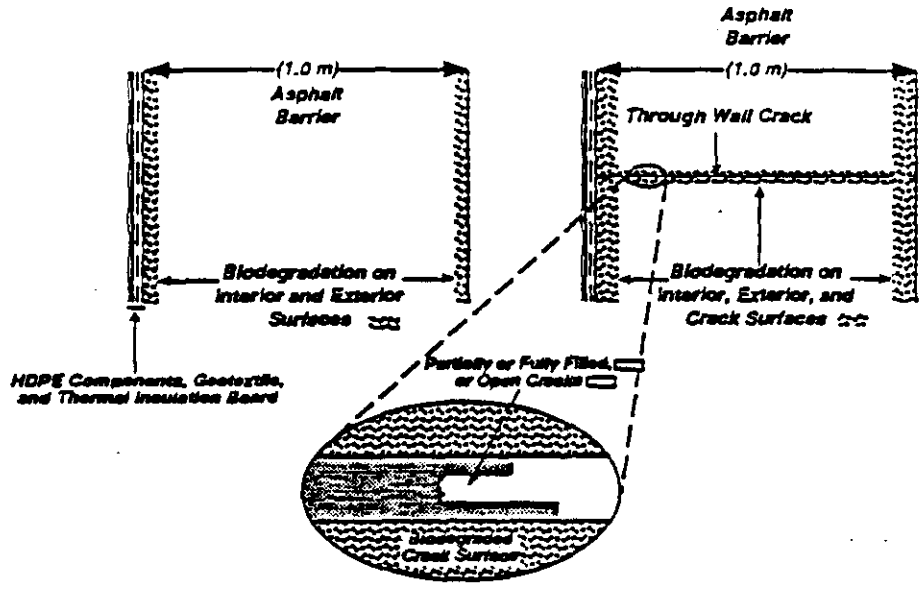

(a) Schematic showing sequence of biodegradation surfaces and of crack biodegradation and filling.

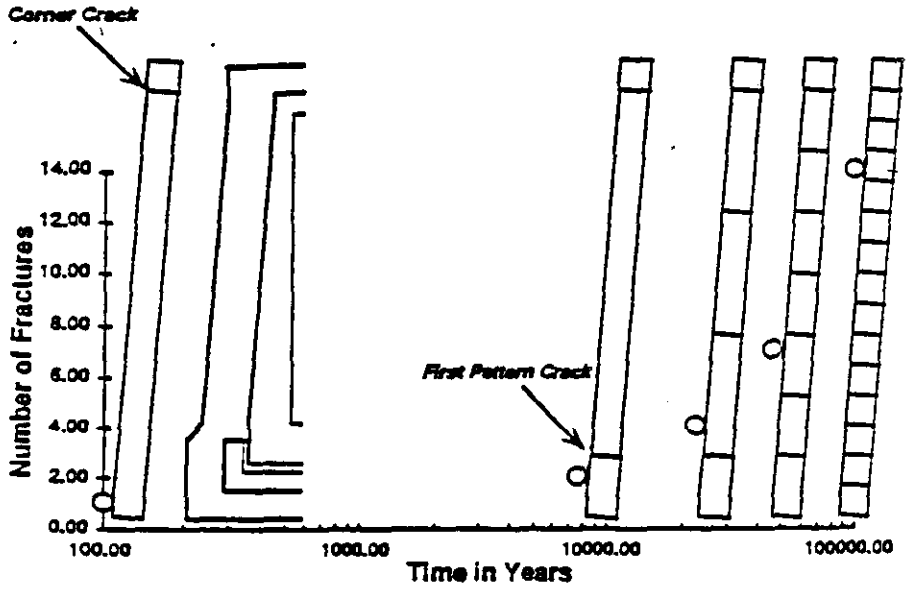

(b) End view of the sequence of horizontal cracks predicted with a linear pattern crack model.

Figure O.13. Schematic Drawings Showing a Cross-Sectional View of Biodegradation for an Intact and Cracked Asphalt Barrier, and a Semi-Log Plot of Crack Occurrence and Distribution as a Function of Time for Horizontal Wall Cracks from a Linear Cracking Model

The reinforced-concrete vault is assumed to experience four types of degradation during this time period; 1) maintenance of established cracks at roof-plank joints, 2) increased size of through-wall cracks at construction joints, 3) increased cracking on all concrete surfaces because of rebar corrosion, and 4) increased size and density of through-wall cracks resulting from rebar corrosion and seismic events. The roof-plank joint cracks remain at 2-mm width. The previously described wall and floor construction joints are assumed to further corrode and become 2-mm wide. Greater cracking of reinforced-concrete surfaces is a result of continued rebar corrosion. This corrosion and cracking has now further weakened the structure to the extent that additional through-wall cracks develop (2-mm cracks on 0.5-m grid) during this time interval.

Continued cracking of concrete surfaces alters hydraulic properties even more. Creation of the more prevalent through-wall cracks associated with rebar corrosion and seismic stresses causes additional flow of fluid from the vault to the catch basin region. As in the previous time period, this flow follows the preferential flow paths, i.e., through-wall cracks in the concrete, drainage net, gravel-catch basin, and sump. The release continues because of the drainage made possible by through-wall cracks in the asphalt barrier.

Seismic events and the transfer of external loads from the concrete vault structure to the grout monolith cause additional fracturing of the grout monolith. Based on the through-wall crack spacing of the concrete vault, it is assumed the grout monolith will break into 0.5-m cubes. It is again assumed that grout and concrete vault cracks matchup horizontally and vertically.

During this period of time the grout, reinforced-concrete vault, gravel-catch basin, and asphalt barrier will come into hydraulic equilibrium under the conditions of the additional cracks that have developed in the grout, reinforced concrete structures and the asphalt barrier. This implies a hydraulic equilibrium with the surrounding and underlying soil environment because of the hydraulic communication that cracks in the asphalt barrier allow. While some contaminant may still discharge from the upper corners, the dominant flow of water and transport of contaminant will be downward through the cracked and more conductive asphalt barrier. This conceptualization is based on the presence of the drainage net and cracked concrete surfaces. Under the unsaturated conditions anticipated, the hydraulic properties of these elements of the degraded engineered system should cause the greatest portion of the release to occur downward through the fractured concrete and cracked asphalt concrete underlying the vault. Lateral movement of water and waste across the fractured concrete surfaces and drainage net should be minimal provided unsaturated hydraulics govern the flow of water in the engineered system.

Consideration of the two stainless steel gas vents in the gravel layer separating the vault from catch basin, and of the carbon steel riser above the sump will no longer be necessary. It is assumed that discharge through the cracked asphalt barrier will dominate release from the engineered disposal system.

O.6 Initial Conditions

Initial conditions for the flow of water are outlined below for the various elements of the engineered disposal system, including the backfill soil, as shown in Figure O.2. Initial conditions for the transport of contaminant are concentration of zero (c=0) in all materials expect the grout which is assigned unit concentration (c=1).

Backfill soil: initially assigned moisture content of 19%vol (10%wt) found to correspond with optimal compaction of backfill during placement around the present facility.

RCRA cover: initially assigned moisture content and related pressure shall be consistent with construction practice (considering optimal compaction and any constraints in placing high clay content materials).

Gravel: initially in equilibrium with the pressure in the backfill soil which surrounds gravel (this initial condition is assigned to both gravel deposits; the gravel wedge and gravel drain).

Asphalt barrier: initially dry (devoid of any water), contains maximum 4%vol voids, minimum 16.2%vol asphalt, and 79.8%vol aggregate. The assumption that the asphalt is initially dry is because the asphalt barrier is created and laid at high temperature. Thus, water is driven off prior to placement and compaction of the barrier.

HDPE drainage net: initially dry.

Steel-reinforced concrete: initially fully saturated and allowed to drain to reach an equilibrium with the HDPE drainage net.

Grout: initially fully saturated and allowed to drain to reach an equilibrium with the surrounding reinforce concrete vault.

Hanford formation: initially assigned moisture content consistent with the infiltration rate being simulated; 0.1 cm/yr for most cases.

Ringold formation: initially assigned moisture content consistent with the infiltration rate being simulated; 0.1 cm/yr for most cases.

O.7 Boundary Conditions

Boundary conditions for flow and transport simulations are outlined below for the upper, vertical, and lower boundaries.

O.7.1 Upper Boundary Underlying the Protective Barrier

Flow analysis: assign a uniform recharge of

- 0.1-cm/yr (expected short- and long-term boundary value)
- 5-cm/yr (unexpected greater recharge boundary value)

Transport analysis: create a zero convective and diffusive release boundary. Because the velocity is already assigned a downward directed value, one need not assign a Dirichlet or fixed concentration boundary condition to ensure a zero convective component to the release. Thus, one is able to assign a homogeneous Neumann boundary condition, (i.e., a fixed concentration gradient of zero). This will ensure zero convective and diffusive release at the upper boundary, but will allow the surface materials to be contaminated by upward diffusion if the diffusive process can overcome the convective process.

O.7.2 Vertical Symmetry Boundaries

Flow analysis: zero velocity normal to symmetry boundaries, ($v_n = 0$)

- left; symmetry with the adjacent vault under the same RCRA cover
- right; symmetry with the adjacent column of vault pairs

Transport analysis: zero concentration gradient normal to symmetry boundaries, ($\partial c/\partial n = 0$).

- left; symmetry with the adjacent vault under the same RCRA cover
- right; symmetry with the adjacent column of vault pairs

O.7.3 Lower Boundary at the Water Table

Flow analysis: the water table forms the bottom boundary of the domain

- pressure head (p) or matric potential (ψ) equals atmospheric pressure, ($p = 0$); or total head (p_t) equals elevation (z), ($p_t = z$).

Transport analysis: the bottom boundary is the interface between the unsaturated zone and the water table or unconfined aquifer. As such, contamination from the unsaturated zone should be able to enter the aquifer by both convective and diffusive processes, e.g.,

$$q_n = \alpha_{ni} q_i = \alpha_{ni}[v_i c - D_{ij}(\partial c/\partial x_j)]$$

However, some assumption would need to be made defining the relationship between the concentration and concentration gradient at the boundary. If this type of boundary condition is not available, the normal gradient should be assigned a zero value ($\partial c/\partial n = 0$). This will force all curie or mass flux to leave the domain through the convection process and enable one to readily calculate flux as a product of Darcy velocity and contaminant concentration.

O.8 Comments to be Resolved, July 9, 1993

When efforts to complete the best estimate conceptualizations, parameter estimations, and simulations were stopped in April 1993, this statement of the conceptual model was being reviewed by the Steering Committee. While time has permitted resolution of some of the comments received at that time, the following are unresolved comments.

Asphalt barrier: We should have some discussion of the impact of the actual base of vaults 102 through 105 on the overall performance of 33 vaults.

Seismic events: Some delineation should be made with regard to the approximate time scale implied by the use of long and short time periods with regard to seismic events. Perhaps some discussion of relative probabilities of a given seismic event could be used to make the distinction clear.

General description: A general description of the entire engineered system and the functions of the component parts would provide a good introduction to the sections discussing the degradation of the components. While Figure O.2 helps in this regard a summary paragraph of so would help with reader orientation.

Assumed: The word "assumed" is frequently used in the discussion. Where possible the discussion should be modified to indicate that some basis exists for making the particular assumption being discussed. This could be based on analysis or technical judgement or whatever. Failure to state the technical basis for an "assumption" will almost assuredly result in a technical challenge. The rewording of sentences incorporating the word "assumed" should be considered to make the presentation stronger.

Time line: A figure showing the time line of engineered structure degradation would be useful in keeping a reader on track and present the opportunity to present a comparison of the times that we are discussing in the PA, with historic events.

Temperature dependence of properties: In establishing the properties to be used in the analysis for the various components of the system, will influence of temperature on the effective diffusivity be

considered. Information published in 1981 suggest that elevated temperature (25°C compared to 90°C) can change the effective diffusivities of various constituents in a given waste form by three orders of magnitude.[a]

A Thought Question: Given the discussion regarding the detection of leaks during the first 100 years and regarding the effectiveness of the asphalt liner, what should be our response be if we detect any fluid in the sump during the first 30 years? Would this indicate that the system had failed and that recovery was in order? What would be the effect of "early vault failure" on the dose to the public?

Seismic event analysis: The way the seismic events are discussed do not appear to be quite correct. As I understand the approach, the probability of a seismic event of a given magnitude increases with time. As such for a particular structure with a life time of 30 years, there is a probability X of experiencing a seismic event of magnitude M. As the life of the structure is increased, the probability of experiencing a seismic event of a given magnitude M increases (becomes greater than X). Summarily, for a given probability of occurrence X the magnitude of the event that the longer lived structure will sustain will increases (becomes greater than M). But, the absolute timing of the event is largely unknown. As such it is difficult to say with any assurance that a seismic event of a given magnitude will occur in any given time period.

Design basis events: One possible strategy that could be used to develop a basis for degradation and degraded system response would be to develop a series of "design basis events" that the engineered disposal system would be subjected to at on a predetermined schedule. The disposal system in its degraded state could be subjected to seismic events to help quantify the integrity of the system over the long term. Such a series of design basis events could be shown to be conservative based on statistical analysis of the historic and archaeological record.

Simplify the writing to assure readability: I (R. Karnesky) found (the description of the best estimate conceptual model) to be reasonably complete and to have a good fundamental basis (when taken together with the earlier information presented to the Steering Committee). Realizing that the prediction of the degradation of engineered barriers and engineered systems is highly uncertain, I felt that it was a credible job. The writing, while clear was, in my opinion unnecessarily complex and needs to be simplified in the final document to assure readability.

Study of pore-volumes of infiltration contacting waste: The amount of contact between grouted waste and infiltrating water could be further explored and quantified through simulations by labeling the infiltrating water, (not the waste in the grout), and tracing the infiltration front.

(a) Barnes, M. W., et al. 1981. "Stability of I and Sr Radiophases in Cement Matrices." *Scientific Basis for Waste Management* Vol. 6, pp. 147-154.

Hydraulics and contaminant release: Prior to simulating "degraded" grout, some comparative modeling should be performed to determine the implications for contaminant release from different conceptualizations of fractured grout and from assumed hydraulics characteristics of mineral deposits in cracks.

Backfill soil geochemistry: It would be useful if a discussion regarding the types of rocks and minerals found in the back-fill soil and/or the gravel was included to provide a basis and justification for the assumed formation of calcium carbonate as infiltration contacts the cementitious vault and waste.

Unconfined aquifer: A description of the aquifer initial and boundary conditions should be provided; any changes in climate over time that would lead to changes in water table elevation should be described or the possibility discussed.

Volume stability: Note the solid nature of the waste and engineered structure result in negligible potential for loss of volume and settlement.

Figures of I.C. and B.C.: Prepare and include graphic depictions of initial and boundary conditions for both the unsaturated zone and the unconfined aquifer.

Parameter assignments: Alternate approaches need to be presented for arriving at the most likely case(s); approaches to modeling the features in the conceptual model; approaches to making parameter assignments consistent with conceptual model and all field and laboratory data.

Degradation of grout: The document needs a consistent logic for grout degradation: consistent with mechanisms identified for concrete and asphalt, and consistent with the knowledge of grout from other DOE sites, e.g., Savannah River.

Corrosion of reinforcing steel: The vault contains cross tie stirrups (No. 5, 5/8 inch diameter rebar) and it is not clear that corrosion of these stirrups has been considered in crack development estimates.

Natural analogues: Stronger comparisons need to be made between analogues such as Portland and ancient cements, and the AR-6000 asphalt and natural asphalt.

During the initial 100 to 300 years when temperature cycles occur, (e.g., (1) asphalt pour, compaction and cooling, (2) 90°C grout cure period, and (3) 55°C cesium decay period could cracking of the asphalt occur during cooling?

Gravel: There is a need to study several aspects of the integrity of the gravel wedge. How large a depression or soil infiltration zone can the gravel tolerate before downward drainage would result?

Hydraulic and transport properties: There is a need to measure and use hydraulic and transport properties of intact and degraded components of the system, (i.e., asphalt barrier, steel-reinforced concrete, grout, gravel, etc).

Degradation: There is need to quantify the degradation possible at key points, (e.g., construction joints, roof-plank joints, HDPE flow net, gravel).

O.9 References

58 FR 7924. 1992. U.S. Environmental Protection Agency. "Environmental Radiation Protection Standards for the Management and Disposal of Spent Nuclear Fuel, High-Level and Transuranic Radioactive Wastes." Proposed Amendment to 40 CFR 191. *Federal Register.*

10 CFR Part 61. U.S. Nuclear Regulatory Commission. "Licensing Requirements for Land Disposal of Radioactive Waste." *U.S. Code of Federal Regulations.*

Dames and Moore. 1989. "Report of Geotechnical Investigation, Proposed Hanford Waste Vitrification Plant; Hanford, Washington." Prepared for Kaiser Engineers Hanford Company, November 15, 1989. Dames and Moore, Richland, Washington.

Fayer, M. J., and M. R. Rockhold. 1993. *Physical and Hydraulic Properties of Sediments and Engineered Materials Associated with Grouted Double-Shell Tank Waste Disposal at Hanford.* PNL-xxxx, Pacific Northwest Laboratory, Richland, Washington.

Gee, G. W., M. J. Fayer, M. L. Rockhold, and M. D. Campbell. 1992. "Variations in Recharge at the Hanford Site." *Northwest Science* 66(4):237-250.

Gruhlke J. M., F. L. Galpin, and W. F. Holcomb. 1989. "Overview of EPA's Environmental Standards for the Land Disposal of LLW and NARM Waste--1989." In *Eleventh Annual Department of Energy Low-Level Waste Management Conference*, Vol. 1, RU24-RU32. CONF-890854. Idaho National Engineering Laboratory, Idaho Falls, Idaho.

Jury, W. A., W. R. Gardner, and W. H. Gardner. 1991. *Soil Physics (fifth edition).* John Wiley & Sons, New York.

Kaiser Engineers Hanford Company. 1989. "Construction Specifications for the Diffusion Break (for grouted waste disposal facilities, grout vault pair 218-E-16)." Specification #B-714-C2, Rev 1, Section 02147, pages 02147-1 - 02147-10.

Lindberg, J. W., J. V. Borghese, B. N. Bjornstad, and M. P. Connelly. 1992. *Geology and Aquifer Characteristics of the Grout Treatment Facility*. WHC-SD-EN-TI-071, Rev. 0, Westinghouse Hanford Company, Richland, Washington.

Luey, J., and S. W. Li. 1993. *Determination of the Biodegradation Rate of Asphalt for the Hanford Grout Vaults*. PNL-8599, Pacific Northwest Laboratory, Richland, Washington.

U.S. Department of Energy (DOE). 1987. *Final Environmental Impact Statement: Disposal of Hanford Defense High Level, Transuranic and Tank Wastes, Hanford Site, Richland, Washington*. Volume 1 and Volume 3, Appendices O, P and Q. DOE/EIS-0113, Vol 1-5, U.S. Department of Energy, Washington, D.C.

U.S. DOE. 1988a. "Radioactive Waste Management." DOE Order 5820.2A.

U.S. DOE. 1988b. *Internal Dose Conversion Factors for Calculation of Dose to the Public*. DOE/EH-0071. U.S. Department of Energy, Washington, D.C.

U.S. DOE. 1990. "Radioactive Waste Management." Richland Operations Supplement to DOE Order 5820.2A.

This page intentionally left blank.

Appendix P

Additional Details of Data, Analysis, and Results

9413222.1796

This page intentionally left blank.

Appendix P

Additional Details of Data, Analysis, and Results

The arrangement of this appendix follows the organization of Chapters 3 and 4 of the performance assessment. The section headings in this appendix identify the corresponding text material from the performance assessment chapters. This appendix is intended to complement the information in the performance assessment and is not written as a "standalone" document. Additional detail is provided only for select sections of the performance assessment; thus, if additional information was available to support Sections 4.1 and 4.3, but not Section 4.2, only Sections 4.1 and 4.3 would be represented here.

P.1 Section 3.2.5, Flow and Transport Models

The stated purpose of the companion text in the performance assessment was to define terminology, but to do so without relying on or providing detailed equations. In this section a similar presentation is presented; however, equations are employed to more clearly illustrate the relationships between predicted quantities and model parameters. Most material will follow the sequence of topics that appeared in Section 3.2.5 of the performance assessment. However, material is appended to the section on water flow on the following special topics: 1) methods for calculating equivalent saturated hydraulic conductivity and 2) a composite hydraulic model for unsaturated flow in cracked or fractured media. Material on the special transport topic of methods for calculating equivalent diffusion coefficients follows the Section 3.2.5.2 on contaminant transport.

P.1.1 Section 3.2.5.1, Water Flow

Brief descriptions of the equations governing water flow in saturated and unsaturated porous media are followed by a similarly brief presentation of equations governing water vapor diffusion.

Saturated Water Flow. Water flowing through a porous media is governed by the empirical relationship known as Darcy's law and the equation describing the conservation of water mass (Freeze and Cherry 1979). Written in a one-dimensional form, Darcy's law is:

$$Q = -K \frac{dh}{dl} A \qquad \textbf{(P.1)}$$

where Q = flow rate (L^3/T)

K = hydraulic conductivity (L/T)

dh/dl = hydraulic gradient (L/L)

h = hydraulic head (L)

l = length or longitudinal spatial coordinate (L)

A = cross sectional area (L^2).

In Equation P.1, the flow rate is proportional to the hydraulic conductivity multiplied by the hydraulic gradient (change in hydraulic head, h, in the direction of flow, l) and the cross sectional area. The proportionality constant for this empirical relationship is contained within the hydraulic conductivity. The average linear velocity of water (v) is the flow rate divided by the cross sectional area of the water. This cross section is the total cross section (A) multiplied by the effective porosity in the case of ground-water flow or by water content in the case of unsaturated flow. In equation form, the average linear velocity is as follows:

$$v = Q/(An_e) \text{ for saturated media} \tag{P.2}$$

or

$$v = Q/(A\theta) \text{ for unsaturated media} \tag{P.3}$$

where v = average linear velocity, or pore-water velocity (L/T)

n_e = effective porosity of a saturated porous medium (-)

θ = volumetric moisture content in an unsaturated medium (-)

and Q and A are as defined above.

Water movement through saturated porous media is governed by the combination of Darcy's law and the conservation of water mass. The latter is quantified through a simple control volume approach where the water mass entering and leaving is equated to the change in water mass within the control volume. Darcy's law is used to relate hydraulic gradient to the rate at which water enters and leaves the

control volume. Changes in the ability of a porous medium to store water are also related to the hydraulic head. The resulting basic equation used to describe transient water flow in a saturated porous media is expressed as follows (Freeze and Cherry 1979):

$$\frac{\partial}{\partial x}\left(K_x\frac{\partial h}{\partial x}\right) + \frac{\partial}{\partial y}\left(K_y\frac{\partial h}{\partial y}\right) + \frac{\partial}{\partial z}\left(K_z\frac{\partial h}{\partial z}\right) = S_s\frac{\partial h}{\partial t} \qquad \textbf{(P.4)}$$

where K_x, K_y and K_z are saturated hydraulic conductivities in the x, y and z directions (L/T), h is hydraulic head (L), and S_s is specific storage (L^{-1}).

Solution of this equation and its associated initial and boundary conditions provides the spatial distribution of hydraulic head, h(x,y,z,t), at points in space and moments in time. Simulations based on the above, or similar forms of the groundwater flow equation, also depend on a knowledge of the spatial distributions of basic geohydrologic parameters of hydraulic conductivity and specific storage, and the fundamental geometry of the flow system such as the thickness and areal extent of the flow system or aquifer.

Definitions of Potential and Pressure Head. Water movement within the unsaturated zone is governed by the total water potential, ψ_t, which is the combination of the soil water potential, ψ_w, and the gravitational potential, ψ_z, i.e.,

$$\psi_t = \psi_w + \psi_z \qquad \textbf{(P.5)}$$

Water potential is formally defined (Hanks and Ashcroft 1980, pg 20-28) as the amount of work that a unit quantity of water in an equilibrium soil-water system is capable of doing when it moves to a pool of water in the reference state at the same temperature. The reference state commonly chosen is pure free water at a specific elevation and temperature.

The soil water potential, ψ_w, is more easily understood if it is broken down into component potentials; pressure, solute, and matric potentials, e.g.,

$$\psi_w = \psi_p + \psi_s + \psi_m \qquad \textbf{(P.6)}$$

All of the potentials are defined with regard to a unit quantity of water. However, three methods of specifying the unit quantity exist; mass, volume, and weight. If the quantity of water is expressed as a weight, the units of potential in the SI system are centimeters (cm) of water. If the quantity of water is expressed as a volume, the units of potential are dynes/cm^2 (the same units as pressure).

Weight is one of the most convenient methods of specifying the unit of water potential. Gravitational potential, ψ_z, is then the difference in elevation of the point in question and a reference point.

The matric potential, ψ_m, is related to the adsorptive forces of the soil matrix (hence the term "matric"). If the quantity of water is expressed as a weight, matric potential is the vertical distance between that point in the soil and the water surface of a manometer filled with water and connected to the soil point in question via a ceramic cup. In an unsaturated soil the water surface of the manometer will always be below the point in the soil, and the matric potential is a negative quantity. In a saturated soil (e.g., at and below the water table) the matric potential is generally assigned a value of zero.

The pressure potential, ψ_p, applies to saturated soils. Where water is expressed as a weight, pressure potential is the vertical distance from the point in question in the soil to the water surface of a piezometer connected to the point. Pressure potential is zero at and above the level of the water in the piezometer. Below this level, pressure potential is always positive and it increases with increasing depth below this water level.

Solute potential, ψ_s, arises because of soluble materials, such as salts, in the soil solution and the presence of a semipermeable membrane in the system (Hanks and Ashcroft 1980, pg 50-51). A semipermeable membrane is a material that allows water to flow but does not permit salts to pass through it. In soils alone, the solute potential is relatively unimportant in liquid water flow because there are no semipermeable membranes. However, cell walls in plant roots do represent non-perfect membranes, and air-water interfaces are near perfect membranes. In soil physics one is often interested in the salt concentration that produces a given solute potential. An approximate relationship is given by

$$\psi_s = - RTC_s \qquad \text{(P.7)}$$

where R is the universal gas constant (82 bars cm^3/mol K), T is absolute temperature (K), and C_s is solute concentration (mol/cm^3). However, an exact value of C_s is difficult to estimate because it is the summation of all species including the dissociation into ionic species in the soil water.

In general, one is concerned only with liquid water flow in the soil, and the solute component is assumed to be essentially zero. For liquid water flow in the absence of a solute potential component, the total potential is,

$$\psi_t = \psi_p + \psi_m + \psi_z \tag{P.8}$$

This combination of potentials appears often in analyses of soil water, and therefore, it has been given the name hydraulic potential, ψ_h, (i.e., $\psi_t = \psi_h$ when $\psi_s = 0$).

Often, in unified models of liquid water flow in porous media, (i.e., those that address water flow in both unsaturated and saturated domains), the general term used to describe the dependent variable is not soil water potential, ψ_w, but "pressure head, h." This terminology evolved from the modeling of saturated ground water systems which predates the simulation of unsaturated domains, and the use of length (cm) units to quantity both pressure head in the saturated system and potential in the unsaturated system. Within the numerical model the dependent variable, pressure, is negative in the unsaturated domain, zero at the water table of the unconfined aquifer, and positive in the saturated domain beneath the water table.

Unsaturated Water Flow. In the saturated zone all pores are filled with water, in the unsaturated zone they are not. A positive water pressure exists in the saturated zone while a negative pressure exists in the unsaturated zone. Darcy's law and the conservation of water mass still govern the movement of water; however, Darcy's law must be modified to account for capillary forces which affect both the driving force (pressure) and the hydraulic conductivity in the unsaturated zone. These modifications to Darcy's law were first recognized by Buckingham in 1907 (Jury et al. 1991) and were incorporated into the governing equation for transient water flow in the unsaturated zone by Richards (1931). Hence, the classical equation used to describe transient unsaturated water flow is known as Richards' equation, i.e.,

$$\frac{\partial}{\partial x}\left[K_x(\psi)\frac{\partial \psi}{\partial x}\right] + \frac{\partial}{\partial y}\left[K_y(\psi)\frac{\partial \psi}{\partial y}\right] + \frac{\partial}{\partial z}\left[K_z(\psi)\left(\frac{\partial \psi}{\partial z} + 1\right)\right] = C(\psi)\frac{\partial \psi}{\partial t} \tag{P.9}$$

where $K_x(\psi)$, $K_y(\psi)$, $K_z(\psi)$ = unsaturated hydraulic conductivities (L/T) in the x, y and z directions which are a function of pressure head or tension (L/T)

ψ = pressure head or tension (L) which is dependent on the degree of saturation, S, or moisture content, θ

C = specific capacitance (L^{-1}) and is defined as $d\theta/d\psi$

S = saturation is θ/n, where θ is the moisture content (dimensionless) and n is the porosity of the media (dimensionless).

The solution of Richards' equation with associated initial and boundary conditions defines the pressure head, $\psi(x,y,z,t)$, in an unsaturated domain at points in space and moments in time. Pressure head is

converted to total hydraulic head, h(x,y,z,t), by adding the elevation head (z = vertical distance from an arbitrarily assigned elevation datum) to the pressure head, i.e., $h = \psi + z$. It is the gradient of total head that determines the movement of water in the unsaturated zone. In addition to a knowledge of initial and boundary conditions, and the geometric constraints of the system (e.g., the thickness and areal extent of soil layers), simulation of the unsaturated zone requires a knowledge of soil characteristic relationships for each soil strata or layer modeled. These relationships define moisture content as a function of pressure head, and unsaturated hydraulic conductivity or relative permeability as a function of pressure head, i.e.,

$$\theta = \theta(\psi) \tag{P.10}$$

$$K = K(\psi), \text{ or } K = K_{sat}K_r(\psi) \tag{P.11}$$

where $K(\psi)$ = unsaturated hydraulic conductivity (L/T)

K_{sat} = saturated hydraulic conductivity (L/T)

$K_r(\psi)$ = relative hydraulic conductivity, K/K_{sat} (-).

Classical examples of characteristic curves illustrating the influence of soil texture on water retention and unsaturated hydraulic conductivity are shown in Figures P.1 and P.2.

Use of the characteristic curves in numerical models generally requires that the data be described by analytical models. This technique promotes efficiency in numerical solutions because values can be determined exactly, thus avoiding interpolation between data points in a table and assuring continuous derivatives necessary for evaluating the specific capacitance. A number of methods have been developed to describe characteristic curves. The relationship selected for use in this performance assessment is a closed-form analytical model for representing the water retention characteristics and unsaturated hydraulic conductivity function, published by van Genuchten (1978).

From the van Genuchten method, the moisture content (θ) as a function of pressure head (ψ) is given by:

$$\theta = (\theta_s - \theta_r)\left[\frac{1}{1 + (\alpha\psi)^n}\right]^m + \theta_r \tag{P.12}$$

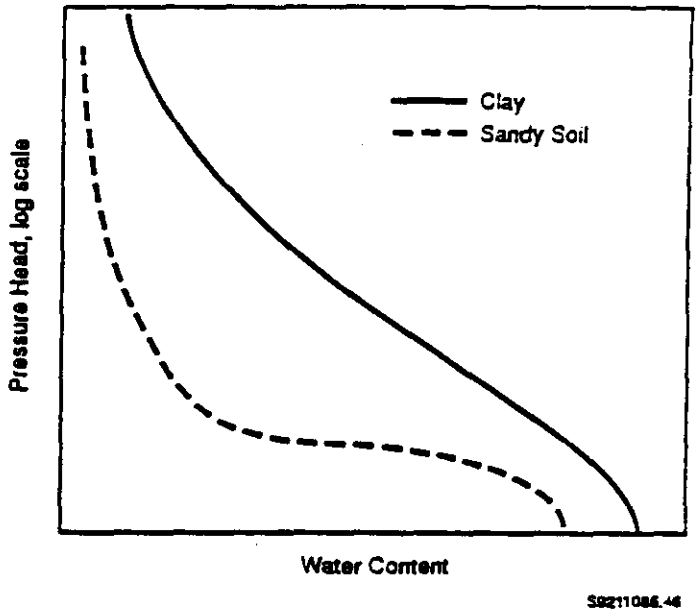

Figure P.1. Example of Water Retention Characteristics Showing the Effect of Soils with Different Textures (Hillel 1982, p. 76)

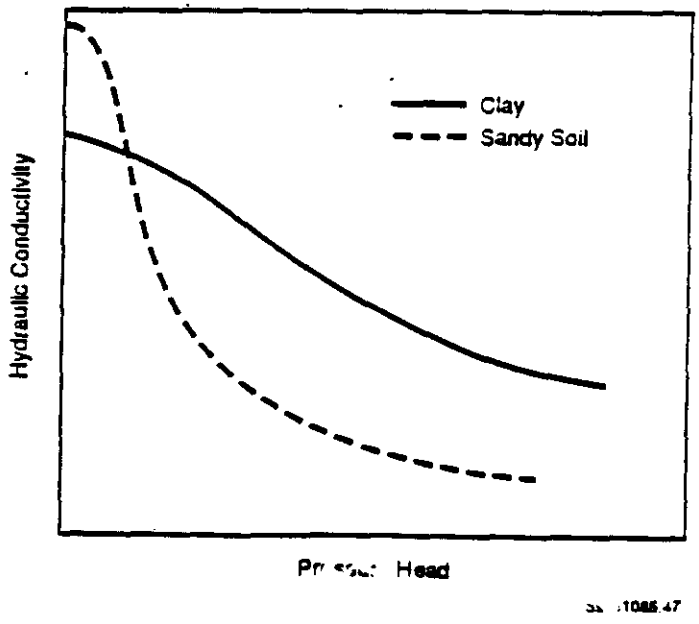

Figure P.2. Example of Unsaturated Hydraulic Conductivity Showing Its Dependency on Pressure in Soils of Different Textures (log-log scale) (Hillel 1982, p. 113)

where $m = (1 - 1/n)$

θ = the volumetric moisture content

θ_s = saturated volumetric water content (dimensionless)

θ_r = residual volumetric water content (dimensionless)

α = fitting parameter (L^{-1}), approximately equal to the air entry pressure

n = fitting parameter (dimensionless)

ψ = the pressure head or capillary pressure head.

The saturated and residual moisture contents, and fitted parameters α and n, are parameters for which specific values are provided from measured data for each of the specific materials or soils involved in the problem set (see Appendix J).

From this relationship, the hydraulic conductivity can be expressed in terms of a pressure relationship as a function of the moisture content. One method developed by Mualem (1976) was used in the performance assessment to estimate unsaturated hydraulic conductivity from the water-retention data. Mualem's model is based on the relationship between the pore size distribution and water retention characteristics and is expressed by the following equation:

$$K_r(S_e) = S_e^n \left[\int_0^{S_e} \frac{dS_e}{h} \Big/ \int_0^1 \frac{dS_e}{h} \right]^2 \qquad \textbf{(P.13)}$$

where K_r = relative hydraulic conductivity (dimensionless)

S_e = effective saturation (dimensionless).

Based on the best fit of this model to 45 soils, Mualem (1976) indicated that the exponent n should be 0.5.

Van Genuchten (1978) used the water retention function given in Equation P.8 and solved Equation P.9 analytically. This solution is given in the following expression:

$$K_r = \frac{K}{K_s} = \frac{\{1 - (\alpha\psi)^{n-1}[(1 + (\alpha\psi)^n]^{-m}\}^2}{[1 + (\alpha\psi)^n]^{m/2}} \qquad \text{(P.14)}$$

where $m = (1 - 1/n)$

K_r = the relative hydraulic conductivity (dimensionless)

ψ = the capillary pressure head in centimeters of water

K_s = the saturated hydraulic conductivity in cm/s

and α, n are the fitted parameters. This equation can be used to develop the relationship of pressure head to unsaturated hydraulic conductivity as depicted in Figure P.2. Parameters specific to the materials included in this performance assessment and based on available data are presented in Appendix J.

Water Vapor Flow. Water vapor diffusion (or return) will not lead to significant releases of radionuclides while the asphalt barrier remains intact. However, the source of water becomes more significant if the asphalt barrier degrades and cracks over time. The relative importance of water vapor diffusion is increased if advection through the grout is limited (e.g., by the capillary break provided by the gravel layer currently planned to be placed over the grout vaults). The rate of water vapor diffusion or return to the grout or concrete surface can be calculated using the following expression of the diffusion equation:

$$m = -D_v \frac{dC}{dx} A \qquad \text{(P.15)}$$

where m = mass rate of water diffusion to the grout or vault surface (M/T)

A = effective diffusional cross sectional area of the vault (L^2)

D_v = vapor diffusivity (L^2/T)

dC/dx = gradient of the vapor concentration (M/L^3)

x = thickness of the barrier material (L)

and the change in concentration is calculated using a knowledge of the depression in vapor pressure and the ideal gas assumption.

9413222.1806

Equivalent Saturated Hydraulic Conductivity. Of the five parameters in the van Genuchten-Mualem model which define unsaturated soil hydraulic characteristics (θ_s, θ_r, α, n, and K_{sat}), only the saturated hydraulic conductivity, K_{sat}, can be defined in an equivalent sense based on available literature. This equivalence can be done rigorously only for saturated applications to fluid flow in porous media. The application in this performance assessment is to unsaturated fluid flow. Therefore, the unsaturated hydraulic conductivities produced by the van Genuchten-Mualem model using the equivalent K_{sat} were assumed to be appropriately scaled by the relative permeability function. There are actually two classical equivalent models defined in the literature (Harr 1962, pg. 27)--one for flow parallel to the strata having different values of saturated hydraulic conductivity, and another for flow perpendicular to the strata.

Assuming fluid flow parallels the stratification (e.g., flow is horizontal in a horizontal crack and in the media surrounding the crack, or flow is vertical in a vertical crack and in the media surrounding the crack), the cumulative discharge from the different strata must be duplicated by an equivalent hydraulic conductivity, K_{sat}^{eq}. Flow in each strata is driven by the same hydraulic gradient and it also applies to the equivalent porous media. Thus, as shown by Harr (1962, pg. 27) the equivalent saturated hydraulic conductivity in the direction of flow will be:

$$K_{sat}^{eq} = \sum_{m=1}^{n} \left[K_{sat}^{m} \cdot d_m \right] / d_{total} \qquad \textbf{(P.16)}$$

where K_{sat}^{eq} = equivalent saturated hydraulic conductivity (L/T)

K_{sat}^{m} = saturated hydraulic conductivity of the mth strata or layer (L/T)

d_m = thickness of the mth strata or layer (L)

d_{total} = total thickness of the computational cell (L)

n = number of strata or layers in the computational cell.

The equivalent saturated hydraulic conductivity that applies to a computational cell for a porous media equivalent to a partially biodegraded asphalt is based on the theory of equivalent properties for flow perpendicular to the direction of stratification (Harr 1962, pg. 27). Assuming water flow is unidirectional and perpendicular to the stratification (e.g., flow is horizontal through a series of vertically aligned strata, or vertical through a series of horizontal strata), the flow defined by Darcy's equation through each of the different strata must be equal. However, Darcian flow through each will be driven by a different hydraulic gradient. This same Darcian flow can be duplicated by an equivalent saturated hydraulic conductivity, K_{sat}^{eq}, which uses the overall or cumulative hydraulic gradient across all the strata. As shown by Harr (1962, pg. 27), the equivalent saturated hydraulic conductivity will be:

$$K_{sat}^{eq} = d_{total}\left\{\sum_{m=1}^{n}\left[d_m/K_{sat}\right]\right\}^{-1} \tag{P.17}$$

where the definition of variables are unchanged from the preceding equation.

Composite Hydraulic Model for Cracks. An alternate conceptual model for incorporating the hydraulic influence of through-wall cracks consists of a composite model in which the crack properties (assumed to be those of backfill soil) are combined with concrete matrix properties to form the composite material's (both cracks and matrix) properties. The composite model (Klavetter and Peters 1986) was selected because it is based on the assumption that pressure head is the same in both the matrix and fracture. For a given pressure head, the saturations for the fractures (S_f) and for the matrix (S_m) are calculated using the van Genuchten moisture retention curves with backfill soil parameters for S_f and concrete parameters for S_m. The composite material saturation (S_c) is calculated by the following equation:

$$S_c = \left[S_f \cdot ECF + S_m \cdot (1 - ECF) \cdot 0.2258\right]/n_e \tag{P.18}$$

where ECF = effective crack fraction (dimensionless)

0.2258 = porosity of concrete matrix (dimensionless)

n_e = effective porosity of composite material [ECF + (1 - ECF) (0.2258)] (dimensionless).

The relative permeability ($k_{r,c}$) of the composite material is given by the following equation:

$$k_{r,c}(S_c) = \left[K_f \cdot ECF \cdot k_{r,f}(S_f) + K_m \cdot (1 - ECF) \cdot k_{r,m}(S_m)\right]/K_{sat} \tag{P.19}$$

where ECF = effective crack fraction (dimensionless)

K_f = fracture saturated conductivity = 3×10^{-2} cm/s

$k_{r,f}$ = relative permeability of crack = relative permeability of backfill soil as a function of S_f (Mualem model is used) (dimensionless)

K_m = matrix saturated conductivity = 3.75×10^{-10} cm/s

$k_{r,m}$ = relative permeability of matrix (concrete properties) as a function of S_m (dimensionless)

K_{sat} = composite material saturated conductivity $[K_f(ECF) + K_m(1 - ECF)]$ (L/T).

P.1.2 Section 3.2.5.2, Contaminant Transport

Terms are defined and equations presented for transport phenomena in porous media as modeled in this performance assessment. Additional details are provided for the topics of diffusion and sorption which appear in the body of the report. In addition, concepts used to determine equivalent diffusion coefficients for diffusion parallel and perpendicular to sediment stratification are given.

Diffusion. Diffusion may be driven by a combination of different forces which may or may not act in a particular situation. In pressure diffusion, the presence of a significant pressure gradient may cause some separation of a mixture. In forced diffusion, separation of a mixture may result if there is an external force acting unequally on different components of a mixture. An example of such a system would be an ionic solution with differently charged ions under the influence of an electrical field. Thermal diffusion occurs in systems in which there is a strong thermal gradient present. However, in the vast majority of applications the most important type of diffusion is that which occurs in response to a concentration gradient. A more complete discussion of diffusion effects is provided by Bird, Stewart, and Lightfoot (1960, pg. 567). In this performance assessment, only ordinary diffusion which is driven by a concentration gradient is considered. The mass of a diffusing contaminant through a given cross sectional area per unit time is proportional to the negative of the concentration gradient. This relationship, Fick's first law, can be written as (Freeze and Cherry 1979, page 103):

$$F = -D\frac{dC}{dl} A \qquad \textbf{(P.20)}$$

where F = mass flux per unit time (M/T)

D = diffusion coefficient in the conducting fluid (L^2/T)

C = solute concentration (M/L^3)

dC/dl = concentration gradient (M/L^4), a negative quantity in the direction of diffusion.

The transport of contaminants from the vault and through the engineered system and natural environment has been modeled using the advection-diffusion equation. Sorption was also considered, but it will be added to the equation later. If the transport were purely diffusive, Fick's first law would be

combined with the equation of continuity for diffusive flux. The differential equation known as Fick's second law is obtained, which relates the concentration of the diffusing substance in space and time (Freeze and Cherry 1979, page 104), i.e.,

$$\frac{\partial C}{\partial t} = D^{*} \cdot \frac{\partial^2 C}{\partial x^2} \tag{P.21}$$

where D^{*} is the apparent diffusion coefficient for mobile chemical species in the porous media. Apparent diffusion coefficients for ions in porous media are smaller than in water because ions in the fluid follow longer, more tortuous paths as a result of the solid matrix. The apparent coefficient value, D^{*}, is related to the diffusion coefficient in water

$$D^{*} = \omega D \tag{P.22}$$

where ω is always less than one and accounts for the tortuosity of the pores. Laboratory values of ω range from 0.5 to 0.01 (Freeze and Cherry 1979, page 104).

The governing equation for advective and diffusive transport can be derived using the control volume concept and accounting for both advective and diffusive flux. The resulting equation of continuity, combined with Fick's first law and the Buckingham modified Darcy's law, yields the following governing equation:

$$D^{*}\left(\frac{\partial^2 C}{\partial x^2} + \frac{\partial^2 C}{\partial y^2} + \frac{\partial^2 C}{\partial z^2}\right) - v_x\frac{\partial C}{\partial x} - v_y\frac{\partial C}{\partial y} - v_z\frac{\partial C}{\partial z} = \frac{\partial C}{\partial t} \tag{P.23}$$

where v_i = average linear velocity (L/T) in the ith direction, ($i=1,2,3 \Rightarrow x,y,z$)

D^{*} = apparent diffusion coefficient (L^2/T)

C = solute concentration in the aqueous phase (M/L^3).

This form of the equation is written for non-reactive, dilute, dissolved constituents in homogeneous, isotropic flow systems under both steady-state and unsteady flow field conditions. Solution to Equation P.23 provides the distribution of solute concentrations at points in space and moments in time. This

solution requires knowledge of the average linear velocity along the flow path and the apparent diffusion coefficient. If the tortuosity correction is neglected, the diffusion coefficient must be known.

Water content is known to affect diffusion, and hence the effective diffusion coefficient, in unsaturated soils (Kemper and van Schaik 1966). The molecular diffusion coefficient for all species in pore water was assumed to be 2.5×10^{-5} cm^2/s. In this analysis, the effective diffusion coefficients for the RCRA cover, backfill soil, and underlying natural sediments of the unsaturated profile were modified according to the empirical relationship published by Kemper and van Schaik (1966). The effective diffusion coefficient as a function of the volumetric moisture content is as follows:

$$D_e(\theta) = D_{ab}\ (a)\ (e^{b\theta}) \qquad \textbf{(P.24)}$$

where D_e = effective diffusion coefficient of an ionic species in a particular soil

D_{ab} = effective diffusion coefficient of the same species in water.

Data collected by Olsen, Kemper and van Schaik (1965) and Porter et al. (1960) for soils using sodium chloride as the diffusing species fit the equation with "b = 10" and "a" being a function of soil surface area. The soils used in these studies ranged from sandy loam to clay soils, with the value for "a" ranging from 0.005 to 0.001, respectively (Olsen and Kemper 1968).

To be consistent with the measured data, values of "a" and "b" were selected as 0.005 and 10, respectively, for this performance assessment. These coefficients were measured for several Hanford soils using $NaNO_3$ in a half-cell diffusion experiment. The coefficients determined in the experiments gave comparable estimates of the effective diffusion coefficients in the soil at expected water contents.

Equivalent Diffusion Coefficients. As in the case of hydraulic properties, there are two classical equivalent diffusion coefficient models that have been defined in the literature (Crank 1975) and are applicable to this study--one for diffusion parallel to a suite of strata having different diffusion coefficient values, and another for diffusion orthogonal to the strata.

The equivalent diffusion coefficient that applies to a computational cell for a porous media equivalent to a partially biodegraded asphalt is based on the theory of equivalent properties of laminates under steady-state conditions (Crank 1975, pg. 267). Assuming diffusive transport is unidirectional and orthogonal to the stratification (e.g., diffusion is horizontal through a series of vertically aligned strata, or vertical through a series of horizontal strata), the transport by diffusion through each of the different strata must be equal. However, diffusive transport through each will be driven by a different concentration

gradient. This same diffusive transport can be duplicated by an equivalent diffusion coefficient, D_{eq}, which uses the overall or cumulative concentration gradient across all the strata. As shown by Crank (1975, pg. 267), the equivalent diffusion coefficient will be:

$$D_{eq} = d_{total}\left\{\sum_{m=1}^{n}\left[d_m/D_m\right]\right\}^{-1} \qquad \textbf{(P.25)}$$

where D_{eq} = equivalent diffusion coefficient (L^2/T)

D_m = diffusion coefficient of mth strata or layer (L^2/T)

d_m = thickness of the mth strata or layer (L)

d_{total} = total thickness of the computational cell (L)

n = number of strata or layers in the computational cell.

Equivalent diffusion coefficients for computational cells containing a crack are based on a similar concept. Assuming diffusive transport is unidirectional and parallel to the stratification (e.g., diffusion is horizontal in a horizontal crack and in the surrounding media, or vertical in a vertical crack and in the surrounding media), the cumulative transport by diffusion from the different strata must be duplicated by an equivalent diffusion coefficient, D_{eq}. The same concentration gradient applies to the individual strata and the equivalent media. Thus, as shown by Crank (1975, pg. 273), the equivalent diffusion coefficient in the direction of flow will be:

$$D_{eq} = \sum_{m=1}^{n}\left[D_m \cdot d_m\right]/d_{total} \qquad \textbf{(P.26)}$$

where the definition of variables is unchanged from the preceding equation. As in the preceding case, and to be consistent with the hydraulic properties assigned to cracks in the engineered structure, the diffusion coefficient of the backfill soil is assigned to the crack.

Dispersion. No additional information for equation development included because the dispersion process was not explicitly modeled.

Sorption. The transport of some contaminants from the grout waste through the barrier system into the vadose zone and into the underlying groundwater system will also be affected by the geochemical interaction of the contaminants with surrounding solids and liquids. The net effect of geochemical interactions is quantified by the linear sorption isotherm model and ultimately by an empirical parameter referred to as the distribution coefficient (R_d). The distribution coefficient is a term used to represent all contaminant sorption or retardation processes such as chemical precipitation/dissolution, adsorption/desorption, filtration of colloids, cation-anion exchange, and exchange of stable isotopes with a radionuclide. R_d is determined in the laboratory on soil samples or estimated from groundwater concentrations. This coefficient is the ratio of the amount of sorbed species per gram of solid to the amount of the species remaining in solution per milliliter. The relationship between the R_d for porous media and the retardation factor which appears in the transport equation is commonly expressed in the following manner (Freeze and Cherry 1979):

$$R = 1 + (\rho_b/\theta)R_d \qquad \textbf{(P.27)}$$

where R = retardation factor (dimensionless)

ρ_b = bulk density of the material (M/L^3)

θ = volumetric water content of the material (dimensionless)

R_d = distribution coefficient (L^3/M).

For most applications, the retardation factor, R, is assumed to be constant and all associated reaction mechanisms are assumed to be reversible. These assumptions are based on a more global assumption that the chemical environment along the flow path remains constant for a given type of porous media or material.

Use of the linear sorption isotherm model in the transport equation results in an expression whereby the diffusion and the advection terms are divided by the retardation factor as follows:

$$D_i^*\left(\frac{\partial^2 C_i}{\partial x^2} + \frac{\partial^2 C_i}{\partial y^2} + \frac{\partial^2 C_i}{\partial z^2}\right) - v_x\frac{\partial C_i}{\partial x} - v_y\frac{\partial C_i}{\partial y} - v_z\frac{\partial C_i}{\partial z} = R_i\frac{\partial C_i}{\partial t} \qquad \textbf{(P.28)}$$

or as it is more commonly written,

$$\frac{D_i^*}{R_i}\left(\frac{\partial^2 C_i}{\partial x^2} + \frac{\partial^2 C_i}{\partial y^2} + \frac{\partial^2 C_i}{\partial z^2}\right) - \frac{v_x}{R_i}\frac{\partial C_i}{\partial x} - \frac{v_y}{R_i}\frac{\partial C_i}{\partial y} - \frac{v_z}{R_i}\frac{\partial C_i}{\partial z} = \frac{\partial C_i}{\partial t} \qquad \text{(P.29)}$$

where D_i^* = apparent or effective diffusion coefficient for i^{th} species (L^2/T)

C_i = concentration of ith species (M/L^3)

R_i = retardation factor for i^{th} species.

Note that a retardation factor of 2 will reduce the diffusion coefficient and average linear velocities by half; a factor of 10 will reduce them by an order of magnitude.

The distribution coefficient is affected by both the surface chemistry properties of sediment minerals as well as the solution chemistry of the pore fluids. Vadose zone sediments do not exhibit much variation beyond pH or cation exchange capacity (Ames and Serne 1991), which are functions of mineral surface properties. Pore fluid chemistry (e.g., pH, Eh, and dissolved solids) in porous materials is controlled by mineral-fluid reactions and is generally dominated by the minerals present, particularly for systems with high solid-to-liquid ratios. Also, both vadose zone and groundwater pathways are inhomogeneous, which can cause some variation in sorption properties with distance. For these reasons, as well as the lack of site-specific geochemical data, it is generally accepted that a constant retardation factor model based on a range of empirically determined values is satisfactory for performance assessment calculations if sufficient conservatism is included (Ames and Serne 1991).

Decay. No additional information or equation development included because material in body of document was sufficient.

P.2 Section 3.3.1, Radionuclides and Chemical Inventories

P.2.1 Daughter Product Ingrowth

In the simulation of transport within the vadose zone, each transport group is modeled using a unit concentration and neglecting radioactive decay. The inventory and radioactive decay for each radionuclide is then applied to the results to calculate groundwater and well concentrations. In cases where short-lived daughter products are produced and can be expected to be in secular equilibrium with the parent, the daughter is assumed to be present for the purpose of calculating the dose. However, for

species with long-lived daughter products, the calculational approach does not allow for ingrowth of long-lived daughter products during the transport simulation. These daughter products may have transport properties in the vadose zone that are different from the parent such that the transport of the daughter may be accelerated or retarded compared to the parent radionuclide.

One radionuclide for which the ingrowth of daughters needs to be considered is neptunium-237. The dose impact of the daughter products can be bounded by an assumption that the daughters exist in secular equilibrium with the parent radionuclide. Under this assumption, the doses from daughter products are approximately as large as those from neptunium-237, resulting in approximately a factor of two increase in the drinking-water dose at longer time frames (>200,000 years). Because of the potential significance of the daughters in this case, the issue has been examined in greater detail.

Neptunium-237 decays as follows:

neptunium-237 ($t_{1/2}$ = 2.2E6 yr) decays by alpha to

protactinium-233 ($t_{1/2}$ = 27 day) decays by beta to

uranium-233 ($t_{1/2}$ = 1.62E5 yr) decays by alpha to

thorium-229 ($t_{1/2}$ = 7340 yrs) which then decays through eight short half-life decays, eventually reaching bismuth-209 which is stable.

The additional dose impact is primarily attributed to the activity of thorium-229 and its short half-life daughters. The question for the performance assessment is whether the thorium-229 will grow into equilibrium as the neptunium-237 decays during transport from the grout to the groundwater. Any uranium-233 or thorium-229 either initially in the grout or produced in the grout due to radioactive decay will be held effectively within the grout due to the sorption (model R_d = 2625 versus 125 for neptunium-237). After release from the grout, uranium-233 generated from neptunium-237 decay would be transported more rapidly than the neptunium-237 in the soil column (model R_d = 0 versus R_d = 3.0 for neptunium-237). This would be a beneficial effect since the daughter would be transported out of the vadose zone and appear in the well primarily as uranium-233, which has a much lower dose impact than thorium-229. If the uranium-233 undergoes decay to thorium-229 in the soil column, the thorium-229 will be strongly sorbed to the soil (R_d = 21 versus 3 for neptunium-237) and much of it will decay prior to reaching the well.

A very conservative treatment would be to assume that the neptunium-237 and its daughter products transport at the same rate in the soil column and that the thorium-229 begins ingrowth at the point of release from the grout. This neglects the beneficial effect of more rapid transport of uranium-233 and the strong sorption of thorium-229 in the soil. The half-lives of the radionuclides can be used to simulate the decay and ingrowth of daughters over time. The travel time of neptunium-237 in the vadose zone is approximately 30,000 years. Figure P.3 shows the ingrowth of uranium-233 and thorium-229 over a

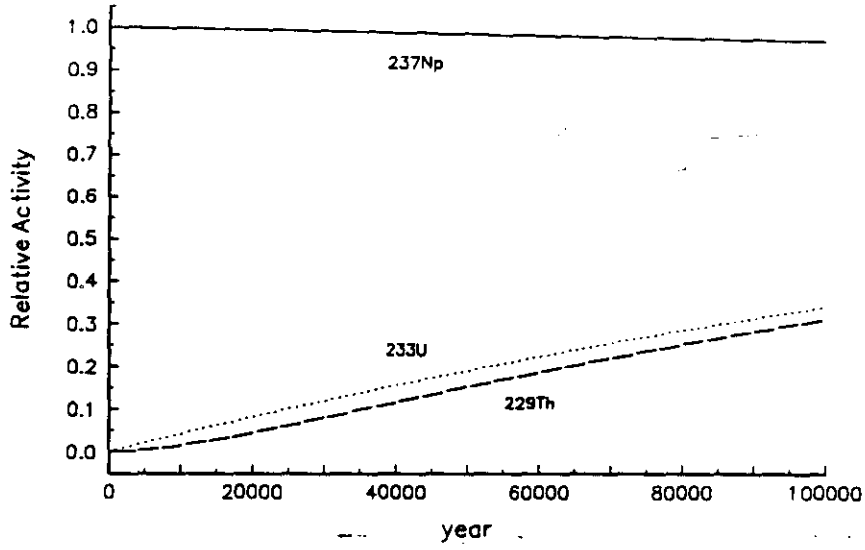

Figure P.3. Ingrowth of Neptunium-237 Daughter Products as a Function of Time

100,000-year period. At secular equilibrium, the activities of thorium-229 and neptunium-237 would be equal and the resulting doses would be about double, with the majority of the increase being due to the thorium-229 and daughters. After 30,000 years the thorium-229 is about 8% of the parent activity and at 100,000 years it is 31%. Under these conditions, the drinking-water dose at long times would be increased by approximately 8%. Even assuming a 100,000-year travel time, the dose would only be increased approximately 31%. Thus, even without the beneficial effects resulting from greater mobility as uranium-233 and lesser mobility as thorium-229, the increases in dose are not large.

Based on this analysis, it was concluded that the ingrowth of neptunium-237 would not have a significant influence on the dose at the well. Therefore, doses calculated for neptunium-237 in groundwater-related scenarios do not include the long-lived daughter products. Note that formation of long-lived daughter products is considered in analysis of the intruder and flood scenarios where the inventory is decayed within the grout and is then disturbed and distributed for the dose calculation.

P.3 Section 3.3.3.1, Initial Release Model For Grout

P.3.1 Diffusion in Grout

P.3.1.1 Review of Available Data on Release of Iodine-129 and Technetium-99 from Grout

Technetium-99 and iodine-129 are the most important radionuclides relative to the performance objectives for groundwater-related scenarios. This section reviews the data available on the release of iodine and technetium from grout waste forms. The basis for neptunium sorption is provided in Section P.2.2.1. The various wastes for which grouts have been tested for release of technetium and iodine are shown in Table P.1. The current formulation for Tank 106-AN waste (currently the first tank planned for grouting) is also included for comparison. The form of the tracers used in the leach tests is shown as well.

All leach data presented here used groundwater as the leachant. Data has also been collected using deionized water. Results obtained when using deionized water are often different than results obtained when using groundwater. Sometimes release is retarded and other times it is accelerated, but the results are within a factor of 10 of the groundwater leachant results.

The data for technetium and iodine release from phosphate/sulfate waste (PSW) grout are fairly comprehensive. Experiments have been conducted with two different specimen sizes and two different waste form loadings, and the leaching has been done using two different test configurations. Table P.2

Table P.1. Dry Blend Formulations and Tracers Used in Technetium and Iodine Leach Tests

	PSW (70% phosphate, 30% sulfate)	CRW	T-106-AN (actual waste)	DSSF	Current 106-AN Formulation
Dry Blend Constituents (wt%)					
Portland cement type I/II	41	42	5	6	21
Class F fly ash	40	40	47.5	47	68
Attapulgite clay	11	--	--	--	11
Indian Red pottery clay	8	8	--	--	--
Calcium hydroxide	--	10	--	--	--
Ground blast furnace slag	--	--	47.5	47	--
Mix Ratio (g dry blend/ L waste)	840	840	1080	1080	1007
Tracer Form	^{125}I as NaI, (I^-) ^{99}Tc as NH_4TcO_4, (TcO_4^-)	^{125}I as NaI, (I^-) ^{99}Tc as NH_4TcO_4, (TcO_4^-)	Unknown, Actual waste	^{125}I as NaI, (I^-) ^{99}Tc as NH_4TcO_4, (TcO_4^-)	

Table P.2. Summary of 223-Day Leach Test Results for Iodine and Technetium in PSW Grout (Serne et al. 1989a)

Tracer Isotope	Tracer Concentration (mCi/L)	Sample Size	Test Configuration: ANS 16.1 De (cm^2/s)	Test Configuration: Static De (cm^2/s)
^{125}I	0.05	small	$6.1 \pm 5.7 \times 10^{-11}$	$5.3 \pm 0.6 \times 10^{-9}$
^{125}I	0.05	large	1.3×10^{-11}	--
^{125}I	0.5	small	$1.2 \pm 0.3 \times 10^{-10}$	$3.43 \pm 2.30 \times 10^{-9}$
^{125}I	0.5	large	1.3×10^{-11}	--
^{99}Tc	0.08	small	$1.4 \pm 0.9 \times 10^{-11}$	$3.0 \pm 0.9 \times 10^{-11}$
^{99}Tc	0.08	large	2.3×10^{-11}	--
^{99}Tc	0.20	small	$2.8 \pm 2.6 \times 10^{-11}$	$3.9 \pm 0.4 \times 10^{-11}$
^{99}Tc	0.20	large	6.8×10^{-11}	--

9413222.1818

provides a summary of results. Note that the effective diffusivities provided here are based on the concentration in the bulk grout rather than in the pore fluid. As can be seen in Table P.2, different effective diffusivities for I^- are obtained in the two different leach test configurations. The diffusivities obtained in static leach tests are approximately 30 to 100 times greater than those obtained in the ANS 16.1 leach test. This difference probably is not due to formation of carbonate on the sample because other species do not have significantly different behavior between the two types of tests (for example, see ^{99}Tc results in Table P.2) . It is possible that the release of I^- is affected by the higher leachant pH in the static test. The results for TcO_4^- indicate that the effective diffusivity is 2 to 5 times greater in a larger sample. The reason for this difference is not known.

The leach results for technetium and iodine in cladding removal waste (CRW) grouts are shown in Table P.3. For this waste, tests have been run with a constant waste loading (0.5 mCi/L I^- and 0.036 mCi/L TcO_4^-) and a single sample size, but the leaching has been conducted in several different configurations. In addition to the data shown in Table P.3, data on release from crushed grout has also been obtained. The leach tests were conducted for periods of 200 to 425 days with two to four replicates. As with PSW results, I^- leaches faster than the TcO_4^-. Flow-through tests produced the most rapid release, while ANS 16.1 tests produced the slowest release. The possibility of advection within the grout and the possible difference in boundary conditions compared to a static leach test introduces some uncertainty in the meaning of results for the flow-through tests. Linear pore velocities in the flow-through tests ranged from 1.7×10^{-3} cm/h to 2 cm/h, while the calculated effective diffusivities varied by about a factor of 5.

Table P.4 summarizes information available on grout produced using actual waste from Tank 106-AN. The tests were conducted over a period of only 46 days and only a small number of specimens were tested. In addition, the analysis for iodine-129 and technetium-99 in the waste prior to grouting and in leachates presented a major challenge. Iodine-129 was present as a very minor component

Table P.3. Summary of Leach Test Results for Iodine and Technetium in CRW Grout (Serne and Wood 1990)

Test Configuration	Effective Diffusivity (cm^2/s)	
	$^{125}I^-$	$^{99}TcO_4^-$
ANS 16.1	0.6 to 1.1 x 10^{-9}	1.8 to 3.4 x 10^{-12}
Static	1.6 to 1.9 x 10^{-9}	1.7 to 1.8 x 10^{-11}
Flow-Through	2.5 to 3.4 x 10^{-8}	0.3 to 1.2 x 10^{-10}
Flow-Through, Packed in Soil	0.8 to 4.1 x 10^{-8}	0.6 to 3.3 x 10^{-10}

Table P.4. Summary of Leach Results for Tank 106-AN Grout Leach Results: Test Duration 46 Days (Serne et al. 1989b)

Isotope	Diffusivity Obtained in Leach Test Configuration	
	ANS 16.1 (cm^2/s)	Static (cm^2/s)
^{129}I	3.1 x 10^{-8}	4.5 to 7.3 x 10^{-8}
$^{99}TcO_4^-$	3.6 x 10^{-8}	4.3 to 6.4 x 10^{-8}

(activity seven orders of magnitude lower than cesium-137, five orders of magnitude lower than strontium-90). The technetium data are also suspect. Original inventory was rather low and reproducibility of measured values in replicate samples was not good. In general, the data reported in Table P.4 are likely biased towards higher-than-actual effective diffusivities because of the analytical difficulties. The approach taken was to assume that analytical results in leachates that were below detection limits were in fact legitimate values.

ORNL also performed leach tests with deionized water and simulated Tank 106-AN grouts. They found technetium to leach about 350 times slower than the leach rate determined at Hanford (Tallent et al. 1988).

Data for double-shell slurry feed (DSSF) grouts produced using the dry blend shown in Table P.1 are quite extensive. A summary of the data is provided in Table P.5. Technetium leaching over a 154-day period was studied using specimens of five different sizes and five different waste loadings. Iodine leaching was studied over a 91-day period using one specimen size with three different iodine waste loadings. Both the ANS 16.1 and static leach test configurations were used for each isotope. As in testing with other wastes, I^- leaches much faster than TcO_4^- in the DSSF tests. Unlike testing with other wastes, diffusivities obtained in static tests are not markedly higher than they are in the ANS 16.1 tests. The leach rate does not appear to be a function of waste loading in the grout for I^-.

Table P.5. DSSF Grout: Leach Data for I^- (91-day tests) and TcO_4^- (154-day tests) Using Static and ANS 16.1 Test Configurations (Serne et al. 1992)

Isotope	Concentration (mCi/L)	Diffusivity Obtained in Leach Test Configuration: ANS 16.1 (cm^2/s)	Static (cm^2/s)
I^-	0.5	3.4×10^{-8}	$3.7 \pm 0.3 \times 10^{-8}$
I^-	5.0	4.2×10^{-8}	$8.9 \pm 3.8 \times 10^{-8}$
I^-	50.0	3.4×10^{-8}	$4.8 \pm 0.6 \times 10^{-8}$
TcO_4^-	0.1	1.8×10^{-10}	6.3×10^{-10}
TcO_4^-	0.3	3.2×10^{-10}	7.7×10^{-11}
TcO_4^-	1.0	7.0×10^{-10}	1.4×10^{-9}
TcO_4^-	3.0	6.7×10^{-10}	1.0×10^{-9}
TcO_4^-	10.0	3.0×10^{-9}	6.1×10^{-10}
Data at various sample sizes:			
TcO_4^-	0.3	$4.0 \pm 3.1 \times 10^{-9}$	--

On the other hand, TcO_4^- leach data suggest some dependence upon technetium inventory. The larger the TcO_4^- inventory, the larger the calculated effective diffusivity. The separate tests for technetium release as a function of specimen size showed no effects that could be attributed to specimen size, but the results are not consistent with separate inventory tests on small samples conducted at the same TcO_4^- loading (0.3 mCi/L). The technetium leach rate from the various sizes of specimens is about a factor of 10 higher than the technetium inventory samples that had the same inventory. Based on this information, it is concluded that any given grout mixing/curing campaign can add about one order-of-magnitude variation in leach results for minor contaminants. Additional detail is provided in Serne et al. (1992).

Based on the leach data collected on various grouts, an estimate of the expected effective diffusivities for iodine and technetium was made as shown in Table P.6. Some conservatism exists in these numbers because the calculated effective diffusivity is observed to decrease with the duration of the leach test. However, experimental work (Lokken 1992) has indicated that the diffusion coefficient for nitrate in grout cured at high temperature over long time periods increases to values approaching 1×10^{-6} cm^2/s. Because of this, the diffusion coefficients have been degraded prior to their application in the model to provide a diffusivity for iodine of 1×10^{-6} cm^2/s. Finally, in the numerical model, the concentration driving force for diffusion is defined in pore volume of the grout rather than the total grout volume. Therefore, the diffusivities are adjusted for use with the pore solution driving force prior to application in the compliance case models. A summary of the diffusivities selected and used is provided in Table P.6.

Table P.6. Selection of Effective Diffusion Coefficients for Compliance Case Models

Contaminant	Selected Effective Diffusivity (cm^2/s)[a]	Degraded Diffusivity Assuming High-Temperature Curing (cm^2/s)[a]	Compliance Case Diffusivity (cm^2/s)[b]
I^-	5.0×10^{-8}	1.0×10^{-6}	5.8×10^{-7}
TcO_4^-	1.0×10^{-8}	2.1×10^{-7}	1.2×10^{-7} [c]

(a) Concentration driving force based on grout volume.
(b) Concentration driving force based on grout pore volume.
(c) Implemented in model as a diffusivity of 5.8×10^{-7} cm^2/s and a distribution coefficient of 2 ml/g.

9413222.1821

P.3.2 Sorption in Grout

P.3.2.1 Review of Available Data on Neptunium Leaching from Cement and Cement Leachate/Sediment Adsorption

At this time, there is not any Hanford grout-specific data for neptunium release or adsorption from leachate onto Hanford sediments. Values used in the performance assessment were chosen to be conservative estimates based on general literature. Because of the importance of neptunium-237 in the long-term performance assessment calculations, the data that is available for neptunium is discussed here to provide some insight into the conservative nature of the assumptions regarding the mobility of neptunium-237.

At present, neptunium has not been spiked into any of the simulated Hanford grout samples that have been leach tested. The neptunium activity in actual Hanford grouts (phosphate-sulfate and Tank 106-AN) and their leachates have also not been measured although it is appropriate to state that neptunium activities in leachates had to be low because rather detailed nuclide analyses did not detect any neptunium activity in actual grout leachates. Tank 106-AN leachates were treated with wet chemical techniques to specifically concentrate and separate various actinides for alpha counting, but only plutonium-239 and -240, americium-241, and curium-244 were found in some of the samples at very low concentrations (Serne et al. 1989).

There have been four neptunium-Hanford sediment adsorption studies documented. In the first, Bensen (1961) examined the adsorption on minerals of radionuclides in Hanford reactor effluent cooling water. One of the radionuclides studied was neptunium-237, which was adsorbed on 25 different common sulfide, silicate and carbonate minerals, crushed to particle size 0.05 to 0.25 mm, in equilibrium tests

with trace amounts in Columbia River water at 80°C. According to Bensen, neptunium was adsorbed poorly or not at all by the minerals tested. The test conditions are not directly relevant to Hanford grout leachate but the data do suggest that neptunium may be mobile. Routson et al. (1975, 1976) determined neptunium Rd values for a Washington sand. The properties of this soil are given in Table P.7. The neptunium Rd values are given in Table P.8. Pre-equilibrations of the soils with nonradioactive solutions prior to contact with the traced solution containing neptunium-237 were carried out. Calcium nitrate and sodium nitrate salts were used as calcium and sodium ion sources. Cation exchange of NpO_2^+ cannot be the principal adsorption mechanism because Na^+ concentration essentially does not affect the neptunium Rd values from no sodium competition to 3.0M Na^+ competition. Calcium has some effect on the neptunium Rd, but much less than there would be if neptunium adsorption were due to ion exchange.

Sheppard et al. (1976) determined neptunium distribution coefficients on two Washington soils. The distilled water-trace neptunium-237 solutions and soils were equilibrated over long periods of time to obtain a rate of change per month in the distribution coefficient values. The 50-day values are given in Table P.9. A positive value for the monthly change in the distribution means an increase in the size of the

Table P.7. Properties of Hanford Soil (Routson et al. 1976)

Soil	$CaCO_3$, mg/g	Silt, wt%	Clay, wt%	CEC, meq/100 g	pH
Washington Soil (Burbank sandy loam)	0.8	10.1	0.5	4.9	7.0

Table P.8. Neptunium Rd (ml/g) as a Function of Soil and Solution (Routson et al. 1976)

	Calcium		Sodium	
Soil	0.002 M	0.2 M	0.015 M	3.00 M
Washington	2.37	0.36	3.9	3.2

Table P.9. Neptunium 50-Day Distribution Values Computed from Sheppard et al. (1976)

Soil Identity	Neptunium Distribution, ml/g	Monthly Change in Distribution, %
Burbank loamy sand	15.4	+48
Ritzville silt loam	[illegible]2	+28

distribution value. The distribution was determined in the same way that a Rd value is determined, but does not have the connotation that equilibrium has been attained.

The neptunium Rd value of about 3.9 ml/g was given by Routson et al. (1975, 1976) for the Burbank sandy loam without sodium in the solution. Sheppard et al. (1976), apparently for the same conditions, gives a neptunium 50-day distribution coefficient value of 15.4 ml/g for Burbank sandy loam and states that this value is increasing at the rate of +48%/month. At 100 days, the distribution coefficient was approximately 50 ml/g on the Burbank sandy loam. The differences between the neptunium Rd of Sheppard and Routson are disconcerting given the fact that Sheppard's soil sample was obtained from Routson. However, Sheppard showed that his Burbank sample contained 21.2% silt and 2.8% clay with a pH of 8.1 and a cation-exchange capacity of 5.94 meq/100 g compared to Routson's Burbank soil sample (see Table P.9). Sheppard's Burbank sample must have contained calcite ($CaCO_3$) to attain a pH of 8.1. There is no evidence in Sheppard et al. (1976) that his soil samples were pre-equilibrated in any way with the nonradioactive solution before the neptunium tracer was added, or that a blank solution without the soil was run with the soil equilibrations for reference and to observe container adsorption. In addition, Sheppard reported that his neptunium-237(V) in the aqueous phase equilibrating with Ritzville soil could be partially filtered on Whatman number 50 filter paper. Routson, on the other hand, reported that upon filtering previously centrifuged samples of solution containing neptunium and in contact with Burbank or South Carolina subsoil through 0.01 and 0.45 µm filters, no evidence of colloidal neptunium-237 was found. This is further evidence that Sheppard's high neptunium distribution values require further elucidation in light of Routson's results.

Serne et al. (1993) measured neptunium adsorption onto a sediment from Hanford's 200 West Area. The sediment's physical/chemical characteristics are shown in Table P.10. Several adsorption tests were performed using three distinct solutions. Two solutions represented leachates from solid wastes that included typical cardboard, paper, rubber, cloth, etc. The two leachates contained significant concentrations, 250 to 500 mg/L dissolved organic carbon. One of the leachates had a pH of 12, resulting from equilibration with crushed cement. Aside from the enriched organic content and lower sodium, nitrate, and other salts present in Hanford grout leachate, this solid waste leachate in contact with cement is quite similar to DSSF grout leachate. The third solution used in adsorption tests was an uncontaminated Hanford groundwater. Distribution coefficients for these three solutions traced with NpO_2^+ ions over a period from 5 to 44 days of contact are shown in Table P.11.

The data in Table P.11 show that NpO_2^+ is not soluble in a high pH environment in the presence of Hanford sediment. (Most of the neptunium precipitated out of blank test tubes as well as tubes containing sediment.) These data lead us to conclude that neptunium will likely remain strongly bound within the grouts and will leach at very slow rates as does the other actinides studied (uranium, americium, plutonium; see Serne et al. 1989 and Serne and Wood 1990). Any neptunium that does leach into the highly alkaline grout leachate should react with Hanford sediment and adsorb. The competition of the high concentrations of sodium and potassium (up to 600 mg/L and 60 mg/L, respectively) should not lower the Rd value significantly based on the Routson et al. (1976) work on the effects of calcium and

Table P.10. Characteristics of the 200 West Area Hanford Sediment

Sand, %	Silt, %	Clay, %	$CaCO_3$, %	TOC, %	CEC, meg/100 g	pH	Mineralogy of < 2 mm, %
87	7	6	2.00	0.2	5.2 ± 2.0	7.9	Plagioclase 26
							Quartz 43
							Mica/Illite 7
							Kaolinite 7
							Smectite 3

Table P.11. Neptunium Rd Values (ml/g) for Various Solutions Contacting Hanford Sediment (values shown as ± indicate one standard deviation based on three samples)

Solution	5 days	44 days	Average
Wood/paper leachate	6 ± 2	20 ± 7	13 ± 7
All waste/cement leachate	200 ± 70	> 3,000	> 1,600
Groundwater	14 ± 3	29 ± 4	22 ± 9

sodium competition (see Table P.8) and the Staunton, Clay and Rees (1990) work showing that sodium does not reduce neptunium adsorption even at very high concentrations (0.1 M).

An Rd value as large as 100 ml/g seems justified for highly alkaline solutions contacting Hanford sediments. For more neutral pH and dilute waters such as groundwater, a range of 10 to 20 ml/g would be defensible based on Sheppard et al. (1976) and Serne et al. (1993). A conservative value of 3 ml/g was used in the performance assessment calculations for neptunium adsorption onto Hanford sediments.

Meyer, Arnold and Case (1985) show that NpO_2^+ adsorption onto minerals in the presence of carbonate is reduced to values of one-half to one-third those when carbonate is not present. Bidoglio, DePlano and Chatt (1983) suggest that NpO_2^+ complexes with carbonate/bicarbonate are relatively weak. In the Hanford grout environment, carbonate is effectively removed in reactions with the $Ca(OH)_2$ that forms during cement hydration. Thus, we might expect neptunium adsorption to be high in the very near field surrounding the grout vault.

Bondietti (1982) found that neptunium(V), [NpO_2^+], adsorption under slightly alkaline pH conditions (pH = 8) onto shale was greater than uranium(VI) and plutonium(IV), Rd = 70 ml/g, whereas under slightly acidic conditions, pH = 5.8, neptunium adsorption was much lower than uranium(VI) and plutonium(IV) at Rd = 5 ml/g. Girvin et al. (1991) also found the neptunium(V) adsorption dramatically increased on amorphous iron oxyhydroxides as pH was raised above a value of six.

Allard et al. (1982) found that neptunium adsorption, as well as most metals that hydrolyze, increased dramatically when the neutral species $NpOOH^{o}$ [for neptunium(V)] and $Np(OH)_4^{o}$ [for neptunium(IV)] predominates in solution.

One study of neptunium adsorption directly onto Portland cement, 70-year-old weathered concrete, sulfate resistant cement, high alumina cement, silica cement, fly ash and blast furnace slag was found. In all cases the solution was simulated pore waters based on the chemical composition of waters in equilibrium for 4 months with crushed material. The pore waters all had pH values between 12.4 and 13.4 and were predominately at potassium, sodium rich hydroxide solution. Crushed cements between 0.090 and 0.125 mm (very fine sand-sized) were contacted with simulated pore waters that had been traced with 1.9×10^{-7}M neptunium(V). Adsorption ratios were measured after 0.25, 1, 6, 42 and 90 days. The tests were performed in controlled atmosphere chambers free of CO_2. The solid-to-solution ratio was 0.02-g cement/ml of solution. After one day of contact the neptunium adsorption reached a steady-state value of 1,000 to 6,000 ml/g with an average for the different cements of about 2,000 ml/g. Details are found in Höglund et al. (1985).

The latter article suggests that neptunium solidified in cement is not readily available to leaching even if it was placed in the cement in its most soluble neptunium(V) form. It is not clear whether the neptunium is actually adsorbed by cement hydration products, precipitates as insoluble phases or co-precipitates with hydration phases. We next review articles where neptunium is mixed with solidifying agents and leached by traditional leach tests.

Only one investigation was found where the leaching of neptunium from cement waste forms was discussed. The article, Ewart et al. (1992), discusses the leaching of neptunium(IV) from concrete under reducing conditions expected in a deep-geologic repository. At an Eh value of -400mv, the equilibrium neptunium solution concentration at pH values ranging from 9.8 to 13.0 was 8×10^{-9}M. The data suggest that $Np(OH)_4$ solid is controlling the release of neptunium and that anionic complexes such as $Np(OH)_5^-$ cannot be very stable. Rai and Ryan (1985) agree that $Np(OH)_5^-$ must not be a strong complex. Unfortunately, the work with neptunium(IV) solids and reduced solutions may not be relevant to Hanford grout solidification and subsurface disposal in vadose zone sediments. Oxidizing conditions that will allow NpO_2^+, [Np(V)], to predominate are expected. Neptunium(V) is much more soluble and may leach more rapidly from grout. For example, Keiling and Marx (1991) took leachate from a Portland cement-saturated salt water test and added $NpO_2(OH)$ solid in excess. At equilibrium (pH = 12.3), the neptunium solution concentration was between 2 and 9×10^{-4}M, almost 5 orders of magnitude larger than the Ewart et al. results on neptunium(IV) dissolving out of concrete. Similar redox sensitive results for neptunium release from glass and subsequent migration of leached neptunium through glauconite sand were found by Bidoglio, Avogadro and DePlano (1985). The leach rate of neptunium from glass under oxidizing conditions was ten times greater than under reducing conditions.

In summary, a distribution coefficient of 10 to 20 ml/g is expected in the vadose zone soils. However, because of the limited data available a value of 3 ml/g has been selected to assure the analysis is conservative. In the grout, the distribution coefficient is likely in the range of 1,000 to 6,000 ml/g based

on the work by Höglund et al. (1985). However, because the data is not directly applicable to double-shell tank waste grout, a conservative value of 125 ml/g has been selected within the grout. Although similar sorption may occur within the concrete as well, no sorption has been assumed in the concrete regions of the problem.

P.4 Section 3.6.5.3, Sensitivity Cases

This text discusses Cases 2.3C and 2.3D in Table 3.46. Differences between the central sensitivity case and Case 2.3C and 2.3D are listed below. Because of these differences, it is not appropriate to compare the results of these two cases to those of the central sensitivity case.

- The asphalt and concrete do not have discrete cracks as are present in the central sensitivity case.
- The grout diffusivity in Cases 2.3C and 2.3D (5.78×10^{-7} cm^2/s) has been adjusted to account for the concentration driving force being in the pore solution, which reduces the magnitude applied in the central sensitivity case (1.0×10^{-6} cm^2/s) by a factor of 0.5781 (the volume fraction pore solution of grout).
- The saturated hydraulic conductivity of the barrier is 3×10^{-5} cm/s (rather than 1×10^{-20} cm/s) in the asphalt barrier, simulating a 1-mm crack every meter.
- The asphalt barrier is given backfill soil water retention properties.
- The asphalt barrier is assigned a diffusivity of 4.2×10^{-9} cm^2/s compared to 1×10^{-10} cm^2/s in the central sensitivity case.
- In addition, the simulations were run only for 25,000 years to reduce the computation time required.

P.5 Section 4.1.1, Vadose Zone Results

In the performance assessment, results were presented for the moisture content and Darcy velocities for the central sensitivity case at 10,000 years. A number of plots are provided here with additional data for the central sensitivity case at other times. A contour plot of the moisture content in the system at 100 years is shown in Figure P.4. The corresponding vertical and horizontal Darcy velocities at 100 years are provided in Figures P.5a and P.5b. Figure P.6 shows the moisture content contours at 1,000 years and Figure P.7 provides details of the moisture content in the upper region of the system. The corresponding horizontal and vertical Darcy velocities at 1,000 years are provided in Figures P.8a and P.8b. Figures P.9, P.10a, and P.10b correspond to Figures 4.1, 4.2A, and 4.2B, respectively, shown in Chapter 4 and are

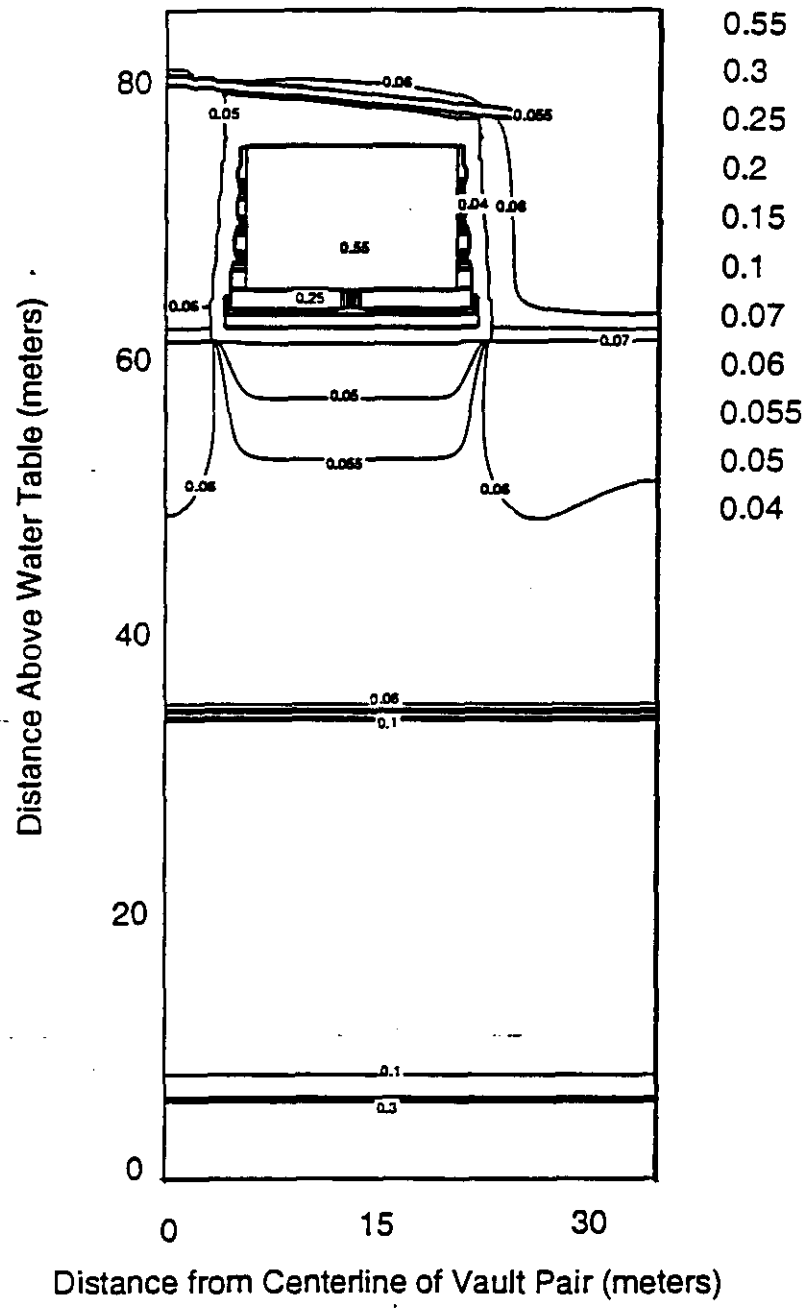

Figure P.4. Central Compliance Case (Case 1.0): Moisture Content Contours for the Vadose Zone at 100 Years. Values at the right indicate the volume fraction moisture at which contours are drawn.

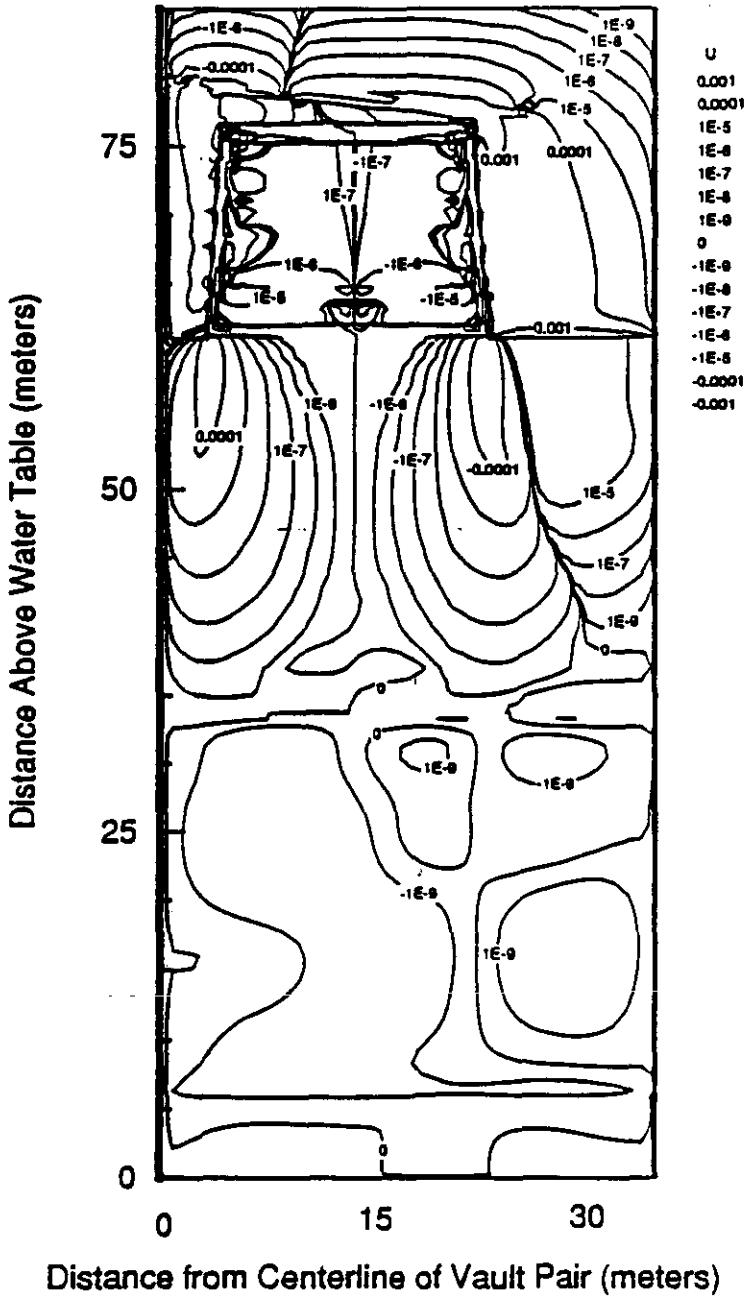

Figure P.5a. Central Compliance Case (Case 1.0): Contour Plots of the Horizontal Darcy Velocities at 100 Years

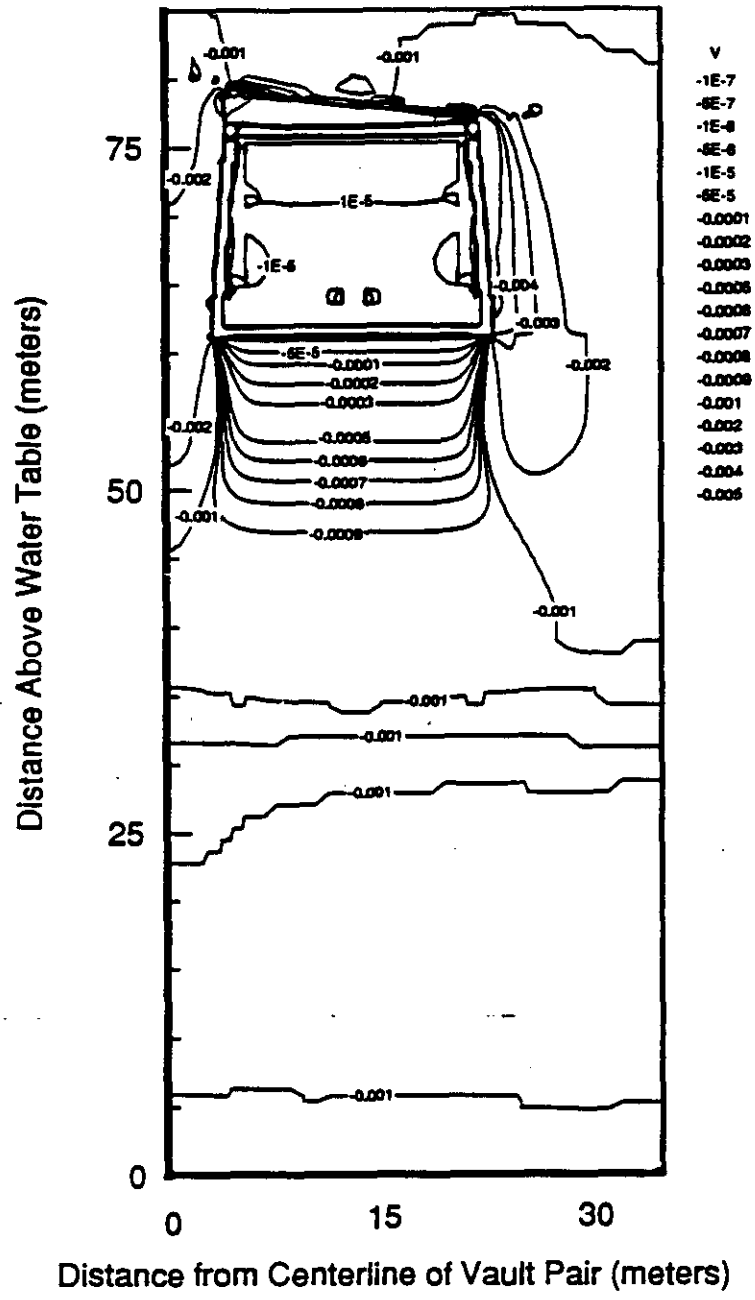

Figure P.5b. Central Compliance Case (Case 1.0): Contour Plots of the Vertical Darcy Velocities at 100 Years

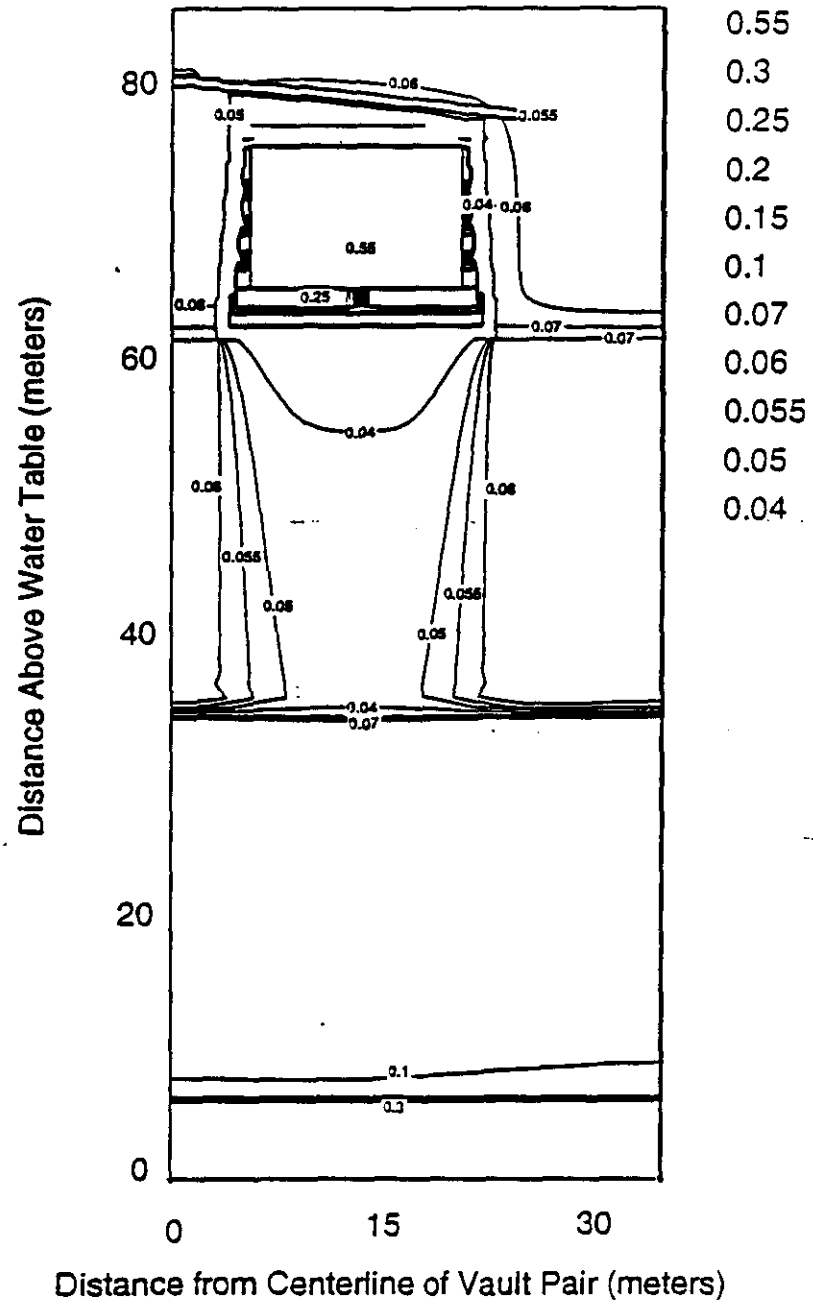

Figure 1.6. Central Compliance Case (Case 1.0): Moisture Content Contours for the Vadose Zone at 1,000 Years. Values at the right indicate the volume fraction moisture at which contours are drawn.

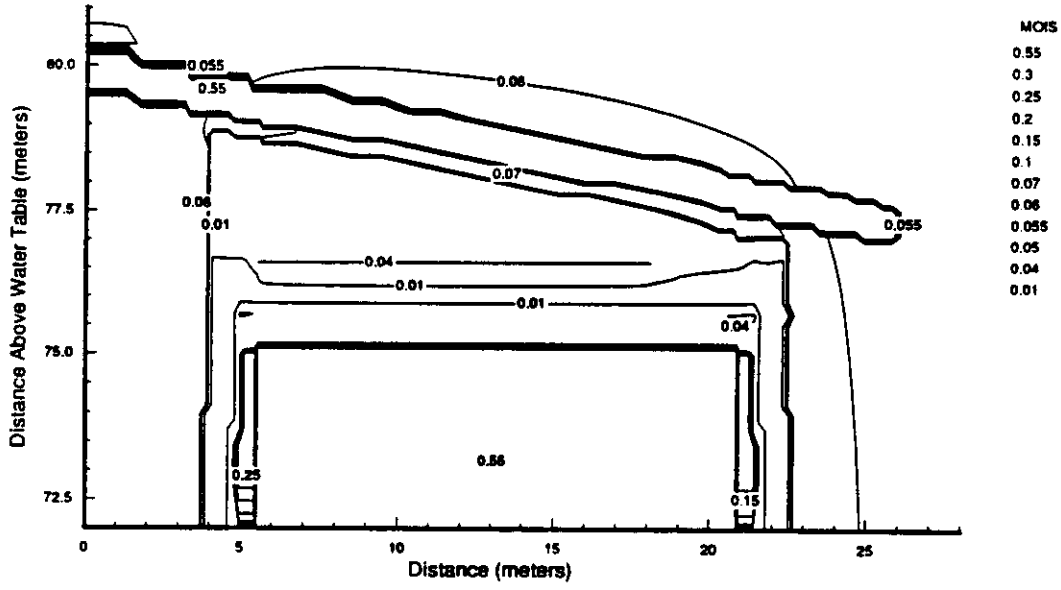

Figure P.7. Central Compliance Case (Case 1.0): Details of the Moisture Content Contours in Upper Vault and Surrounding Vadose Zone Region at 1,000 Years. Values at the right indicate the volume fraction moisture at which contours are drawn.

provided here for ease of comparison only. Figure P.11 provides additional details of the upper region of the system in the central compliance case. Figure P.12 provides the moisture content contours for the central compliance case at 50,000 years. Figures P.13a and P.13b provide the corresponding Darcy velocities at 50,000 years.

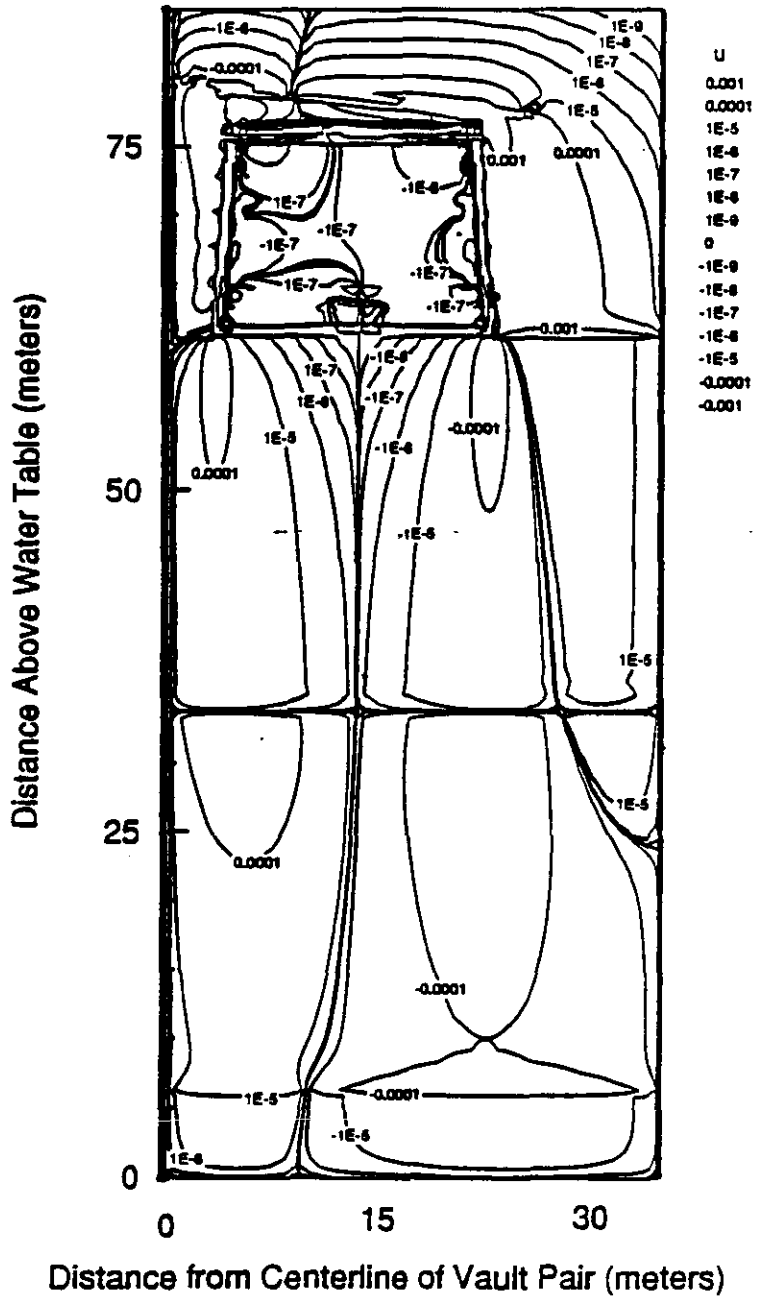

Figure P.8a. Central Compliance Case (Case 1.0): Contour Plots of the Horizontal Darcy Velocities at 1,000 Years

9413222.1832

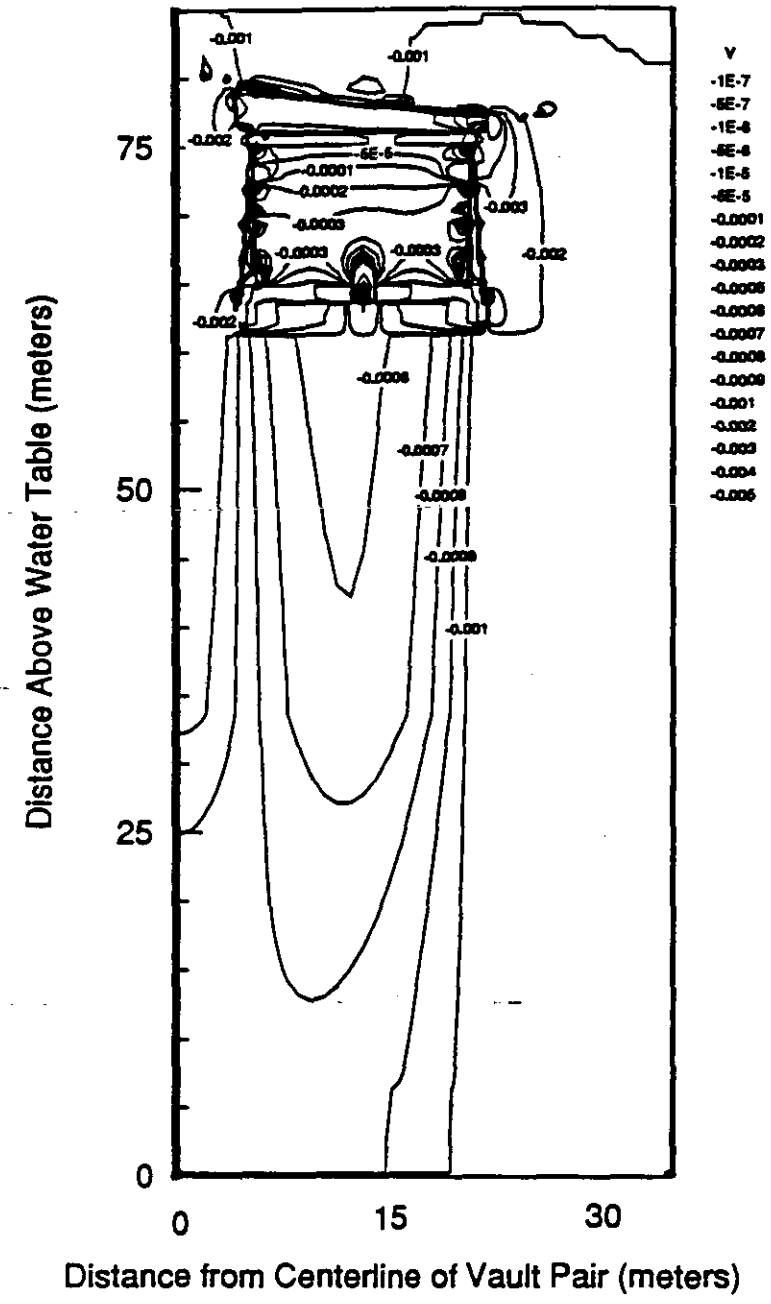

Figure P.8b. Central Compliance Case (Case 1.0): Contour Plots of the Vertical (right) Darcy Velocities at 1,000 Years

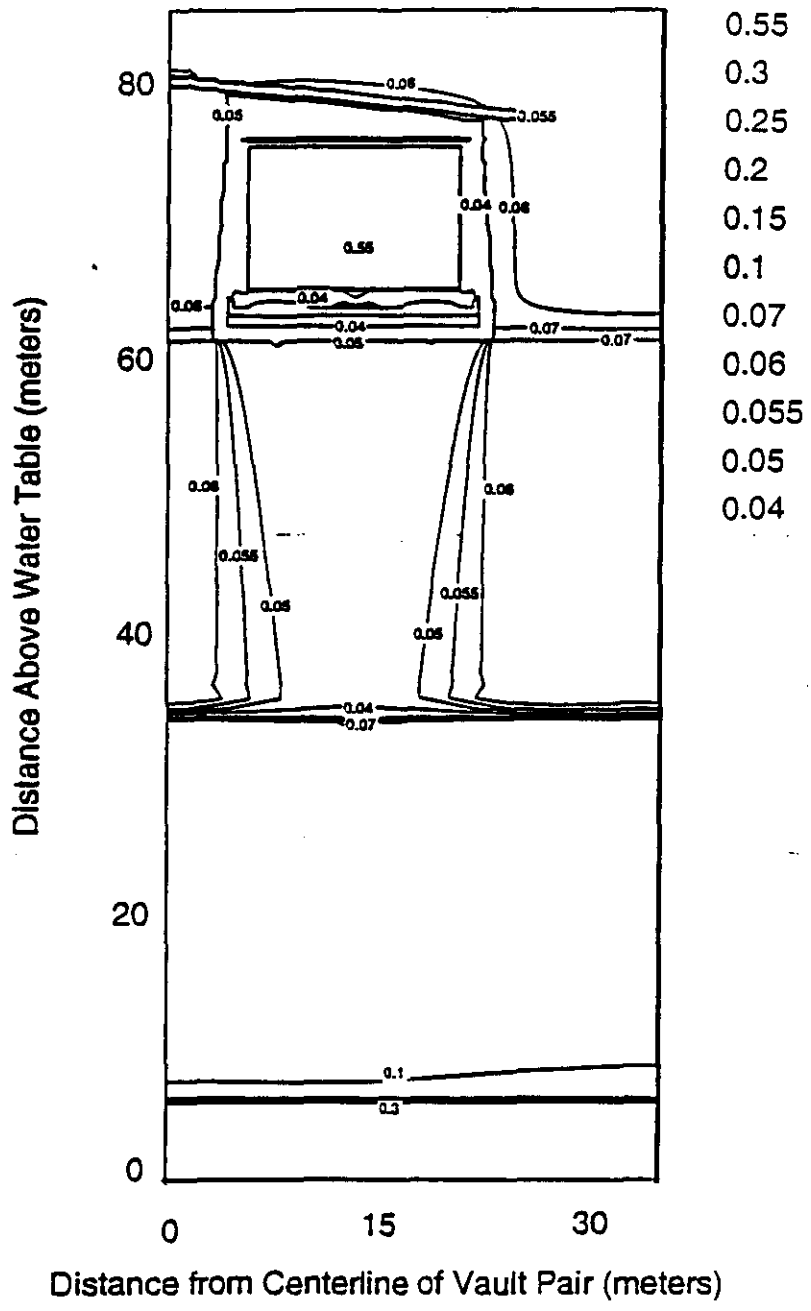

Figure P.9. Central Compliance Case (Case 1.0): Moisture Content Contours for the Vadose Zone at 100 Years. Values at the right indicate the volume fraction moisture at which contours are drawn.

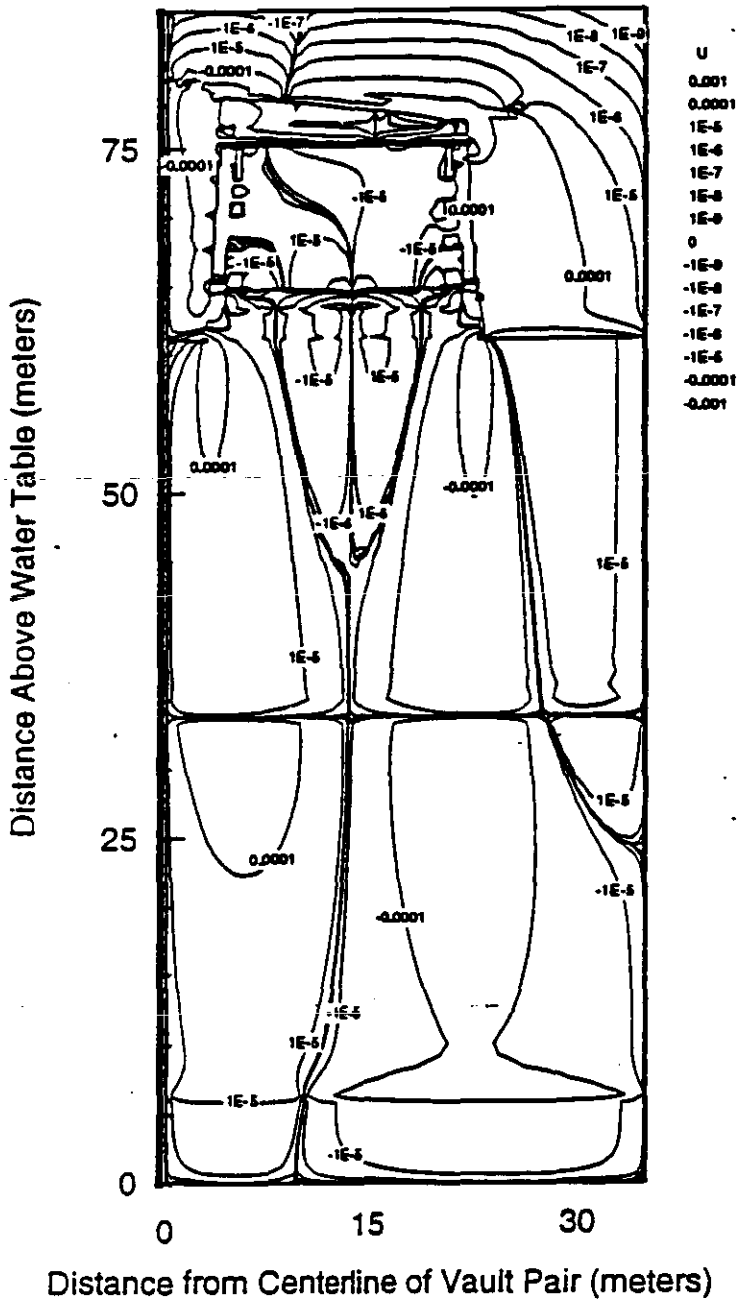

Figure P.10a. Central Compliance Case (Case 1.0): Contour Plots of the Horizontal Darcy Velocities at 10,000 Years. Same as Figure 4.2A in main document.

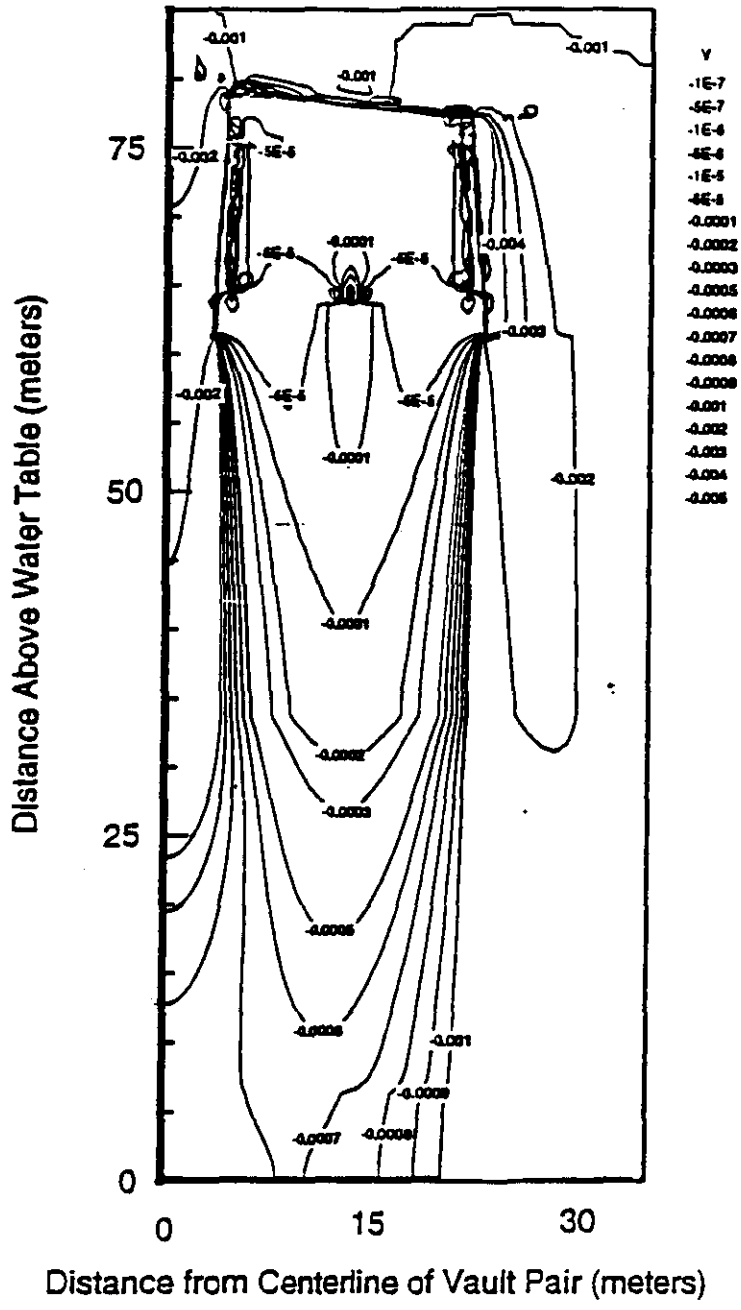

Figure P.10b. Central Compliance Case (Case 1.0): Contour Plots of the Vertical (right) Darcy Velocities at 10,000 Years. Same as Figure 4.2B in main document.

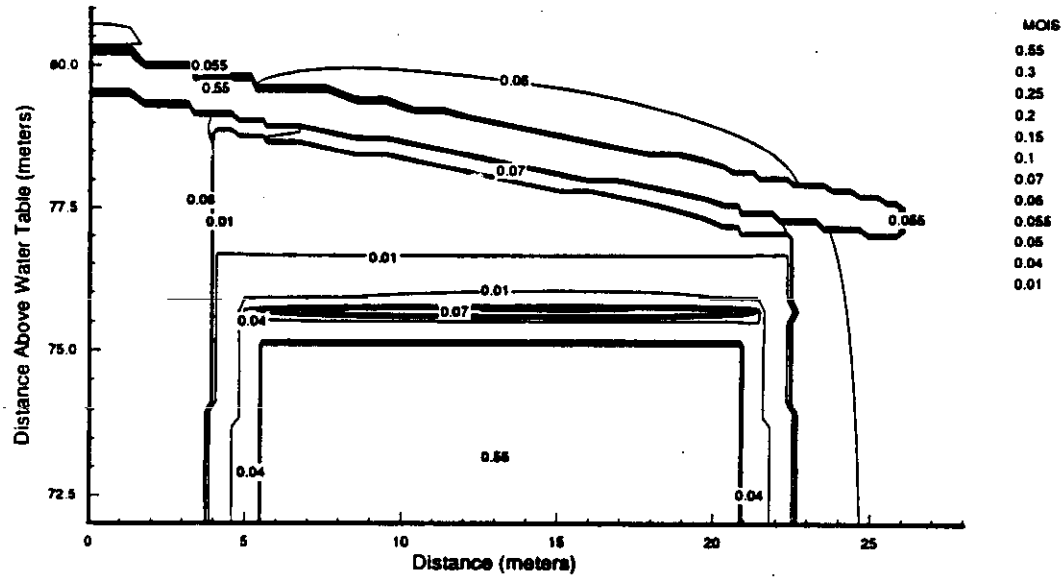

Figure P.11. Central Compliance Case (Case 1.0): Details of the Moisture Content Contours in Upper Vault and Surrounding Vadose Zone Region at 10,000 Years. Values at the right indicate the volume fraction moisture at which contours are drawn.

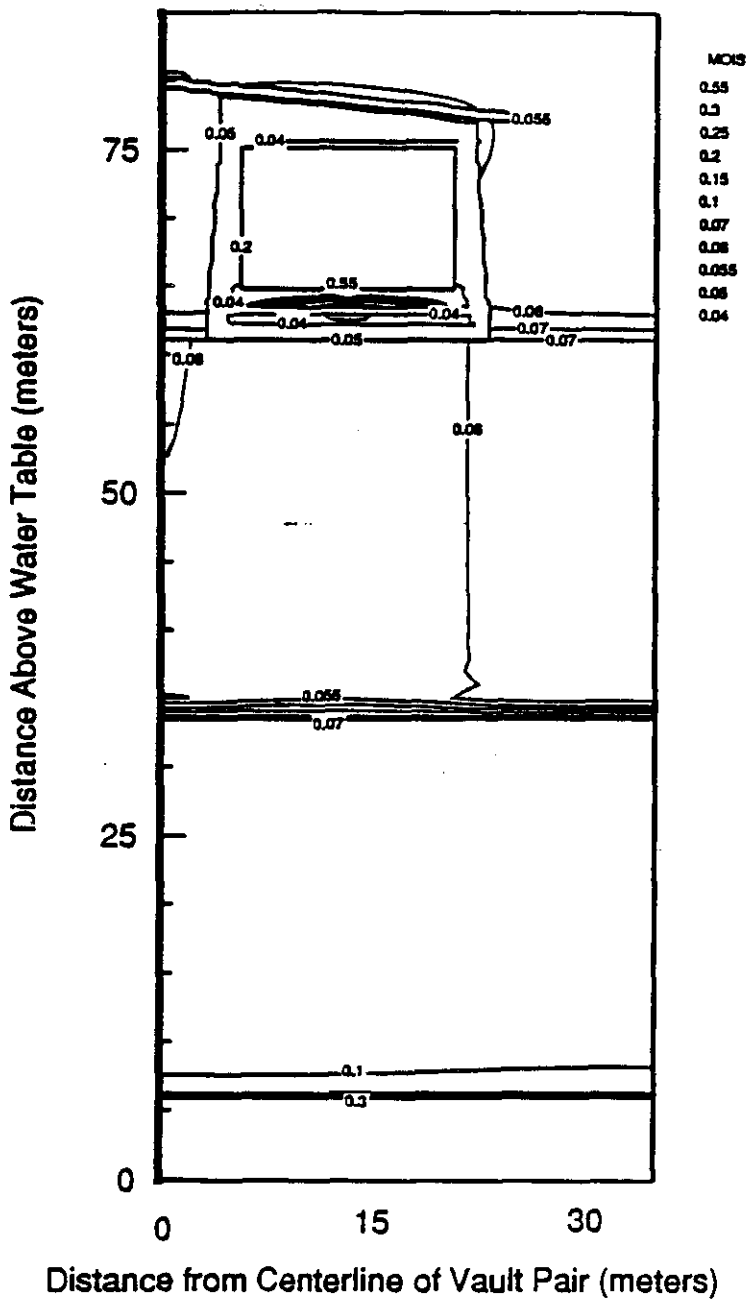

F''ure P.12. Central Compliance Case (Case 1.0): Details of the Moisture Content Contours in Upper Vault and Surrounding Vadose Zone Region at 50,000 Years. Values at the right indicate the volume fraction moisture at which contours are drawn.

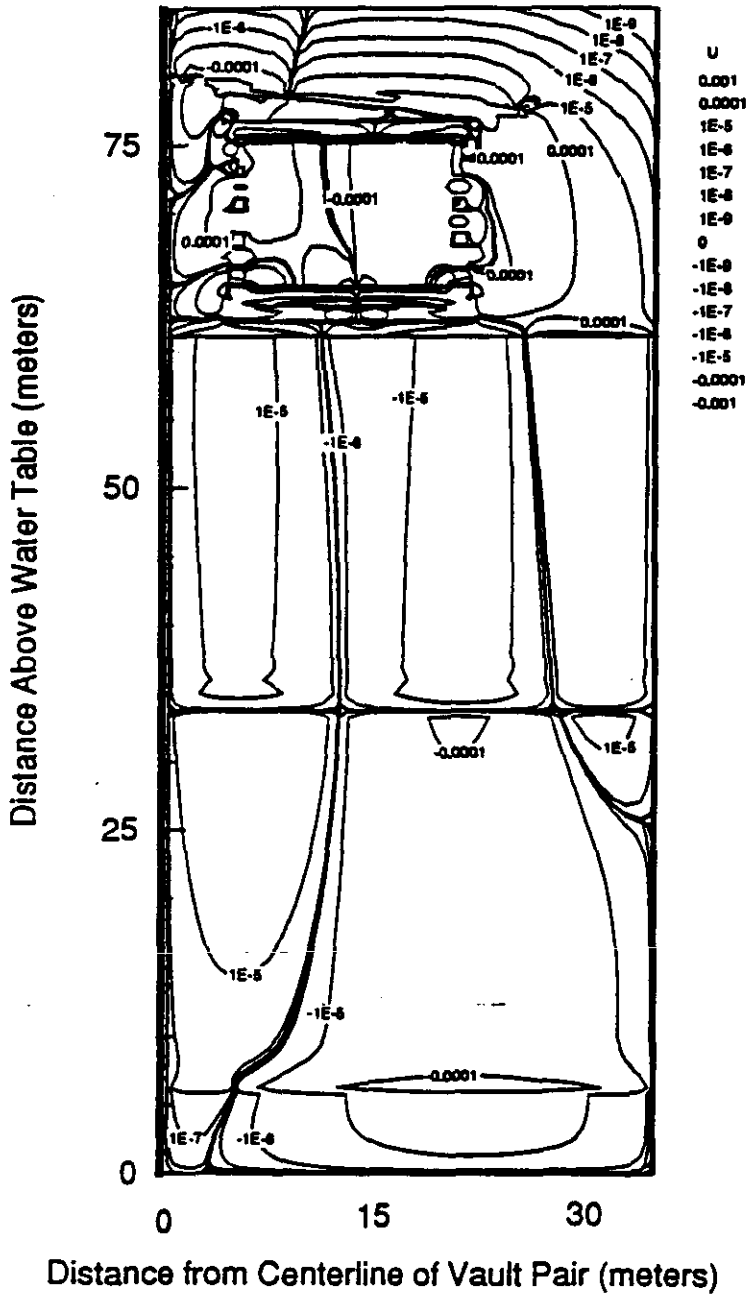

Figure P.13a. Central Compliance Case (Case 1.0): Contour Plots of the Horizontal Darcy Velocities at 50,000 Years

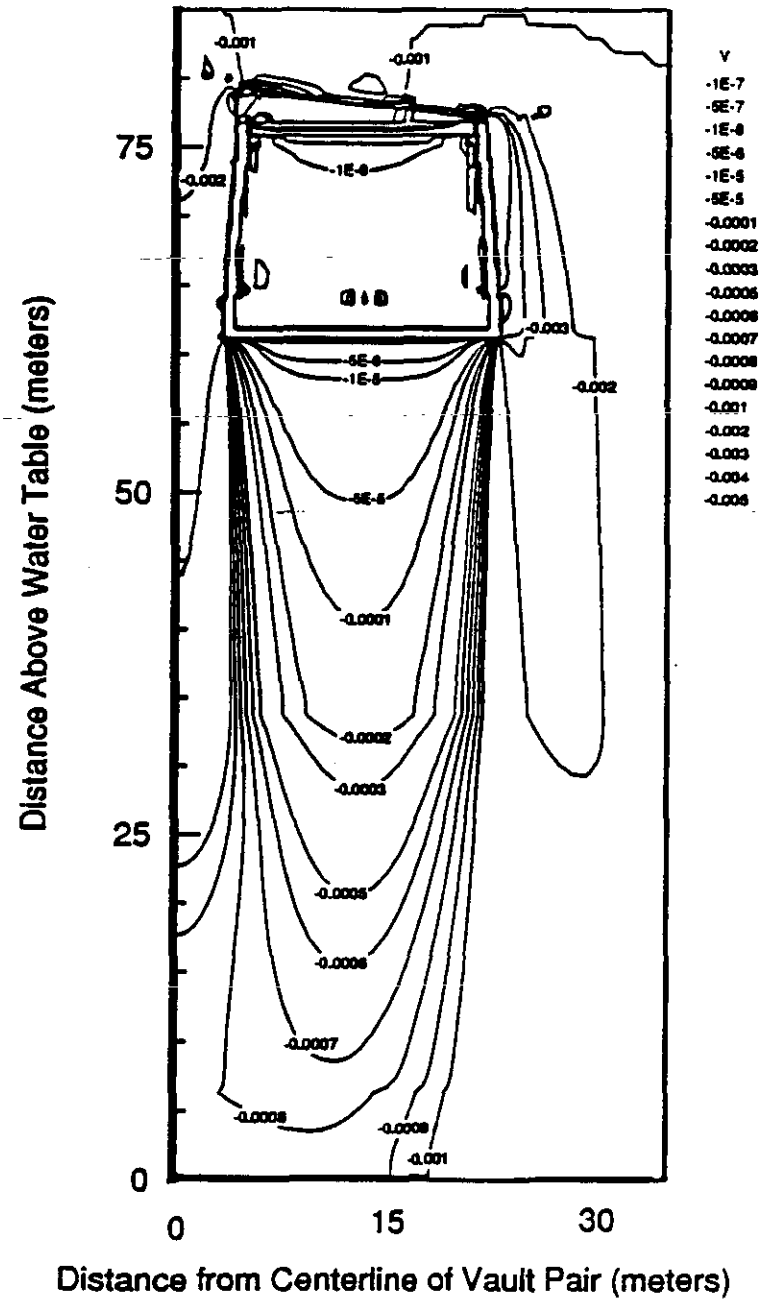

Figure P.13b. Central Compliance Case (Case 1.0): Contour Plots of the Vertical (right) Darcy Velocities at 50,000 Years

P.5.1 Section 4.1.1.2, Release to Groundwater

A plot of the fractional release per year by transport group was provided in Chapter 4 (Figure 4.6). The same information is provided in Figure P.14 except that it is plotted as the cumulative percent of mass released to the aquifer. At a value of 100 all of the mass has been released. The actual values exceed the value of 100 due to a positive mass balance error. This error is discussed in Section P.6.

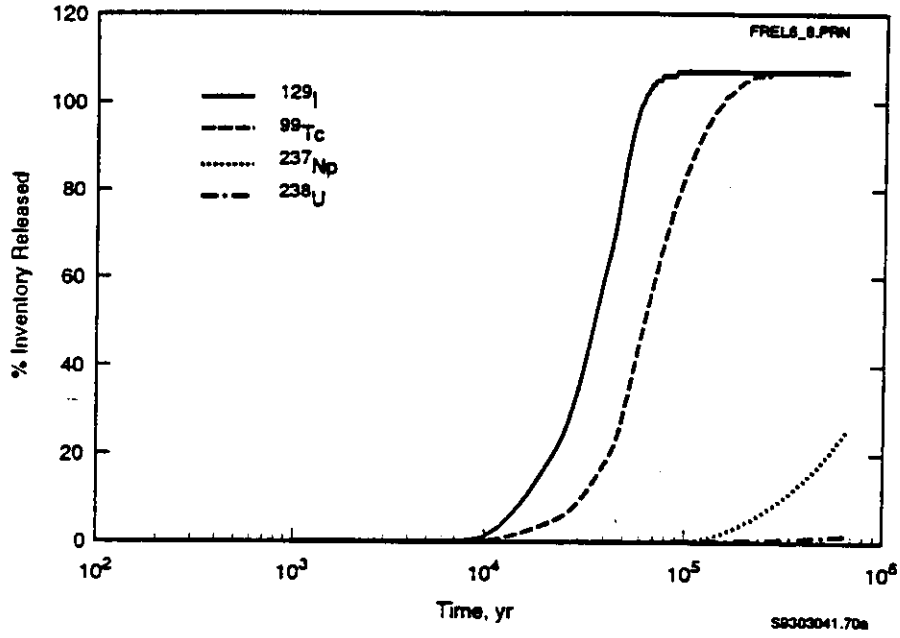

Figure P.14. Cumulative Percent of Mass Released to the Aquifer. Iodine-129 corresponds to transport grouping 1A, technetium-99 corresponds to grouping 2A, neptunium-237 corresponds to grouping 3C, and uranium-238 corresponds to group 4A. Figure does not include radioactive decay.

Similar information is contained for transport group 1A (iodine-129) in Figure P.15. However, this figure is plotted on a linear-linear scale and provides the fraction released from a region of the engineered system rather than release to the water table, and information on the amount of material leaving the region by diffusive or advective mechanisms. The region is defined by a rectangle that passes along the boundary between the top of the asphalt barrier and the gravel and then down from the top outside corners of the asphalt barrier. Rather than following the slope of the wall, the region drops straight down through the sloping asphalt barrier wall and passes between the asphalt barrier and side of the catch basin. The bottom of the flux region is placed between the asphalt barrier and the soil.

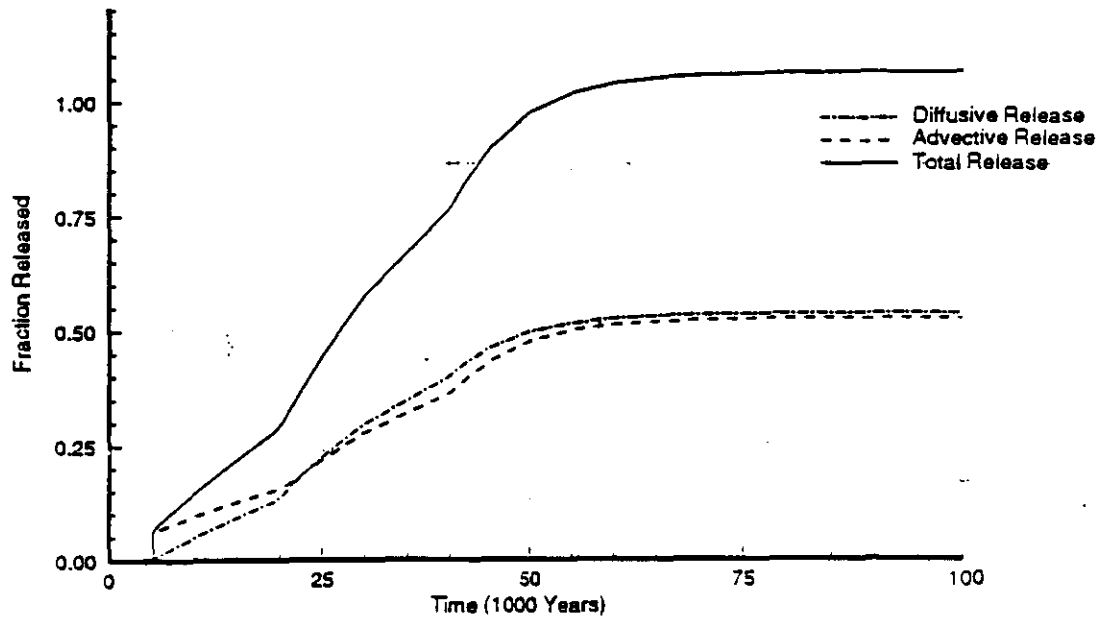

Figure P.15. Case 1.0 (central compliance case): Fractional Release of Group 1A (iodine-129) from Region of Engineered System by Diffusive and Advective Mechanisms

A similar plot is provided in Figure P.16, only it is drawn for transport group 2A (technetium-99). As can be seen in the plots, the release from this region is very nearly split evenly between diffusive and advective mechanisms.

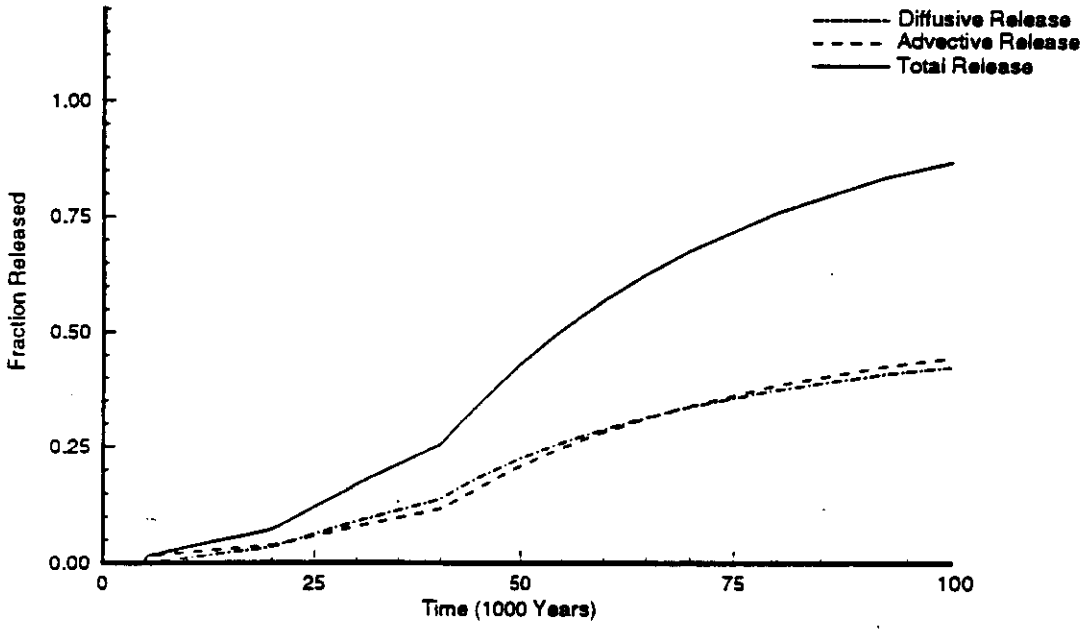

Figure P.16. Case 1.0 (central compliance case): Fractional Release of Group 2A (technetium-99) from Region of Engineered System by Diffusive and Advective Mechanisms

Fractional release by diffusion and advection from the region of the engineered system is provided for compliance cases: Case 1.1 (delayed cracking), Figures P.17 and P.18; Case 1.2 (no HDPE flow path), Figures P.19 and P.20; and Case 1.3 (composite model), Figures P.21 and P.22.

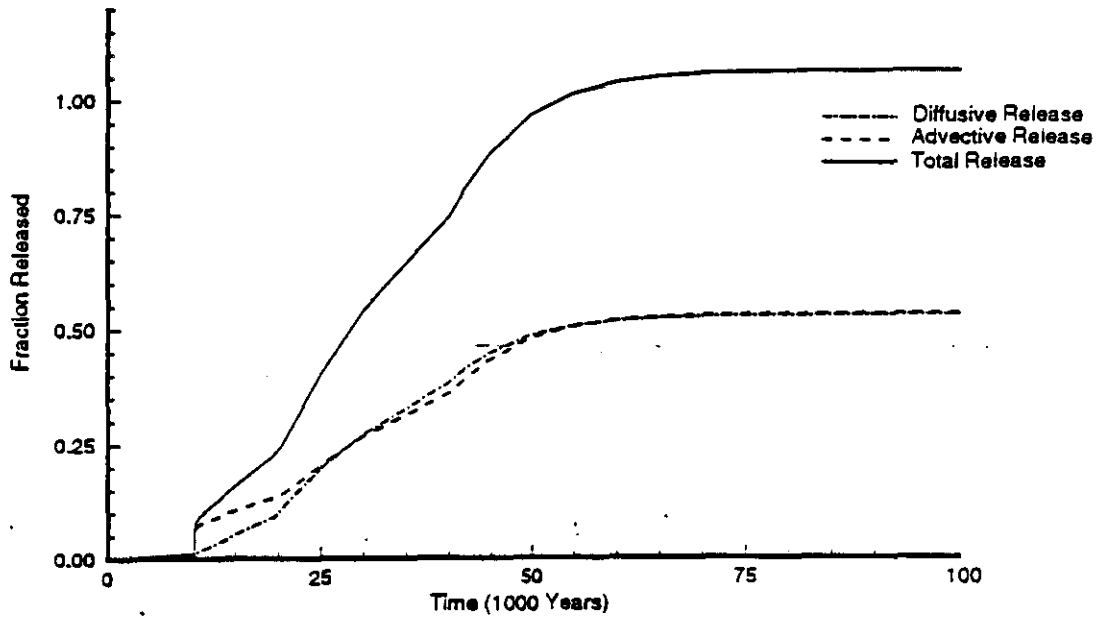

Figure P.17. Case 1.1 (delayed cracking): Fractional Release of Group 1A (iodine-129) from Region of Engineered System by Diffusive and Advective Mechanisms

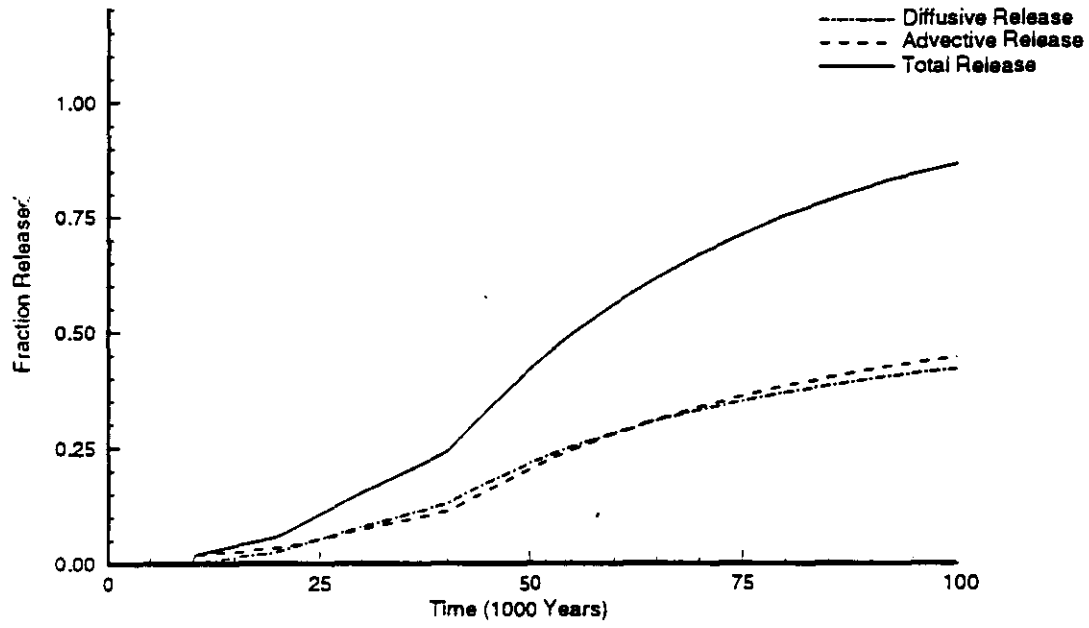

Figure P.18. Case 1.1 (delayed cracking): Fractional Release of Group 2A (technetium-99) from Region of Engineered System by Diffusive and Advective Mechanisms

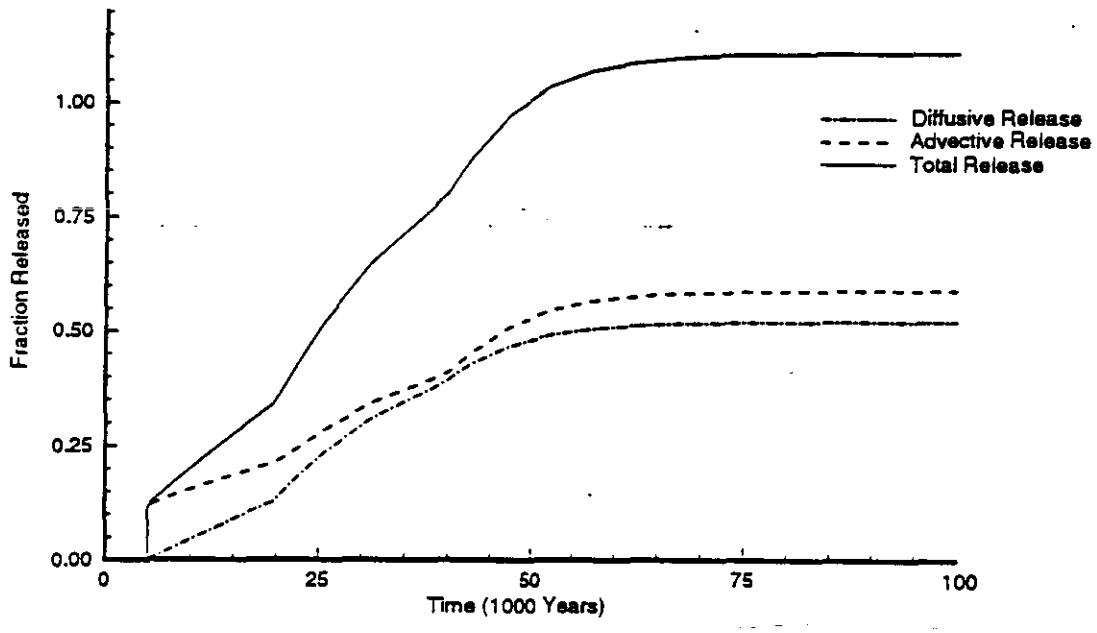

Figure P.19. Case 1.2 (no HDPE flow path): Fractional Release of Group 1A (iodine-129) from Region of Engineered System by Diffusive and Advective Mechanisms

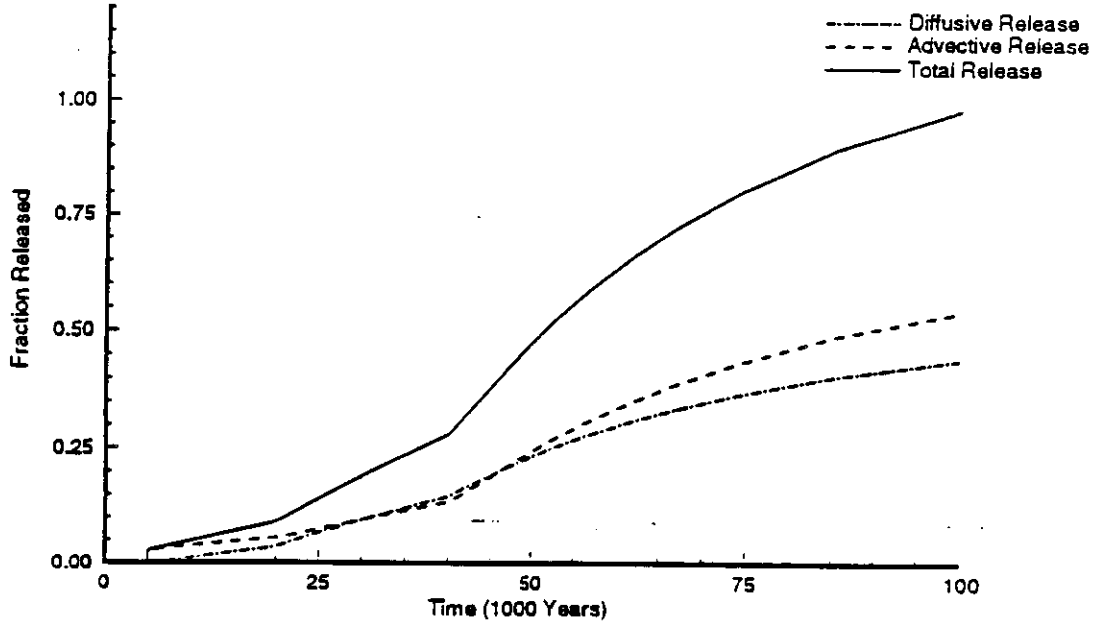

Figure P.20. Case 1.2 (no HDPE flow path): Fractional Release of Group 2A (technetium-99) from Region of Engineered System by Diffusive and Advective Mechanisms

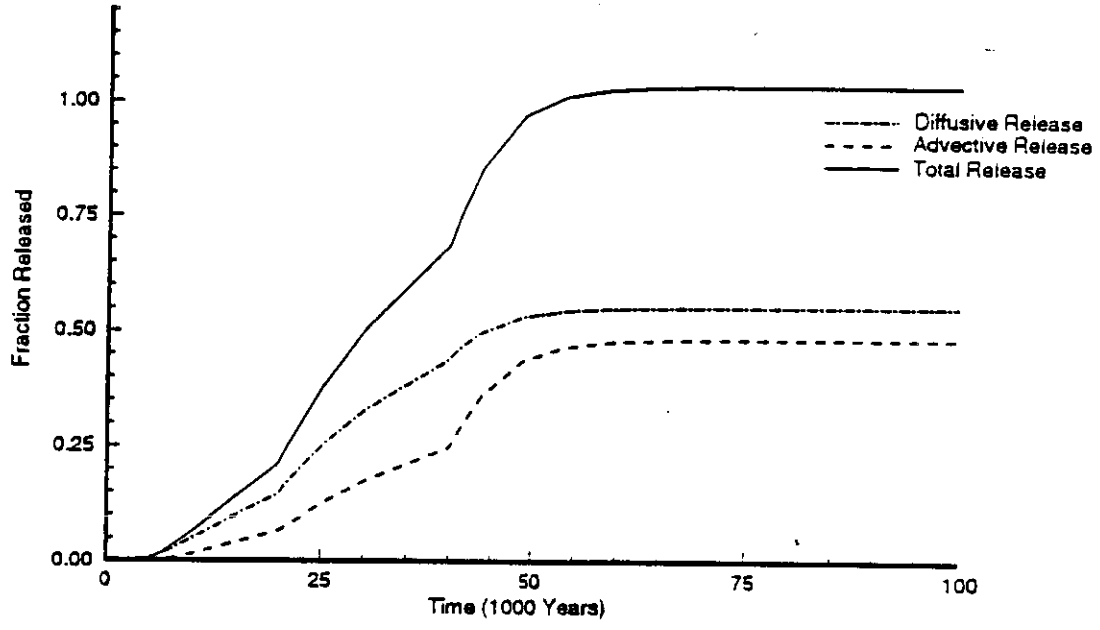

Figure P.21. Case 1.3 (composite model): Fractional Release of Group 1A (iodine-129) from Region of Engineered System by Diffusive and Advective Mechanisms

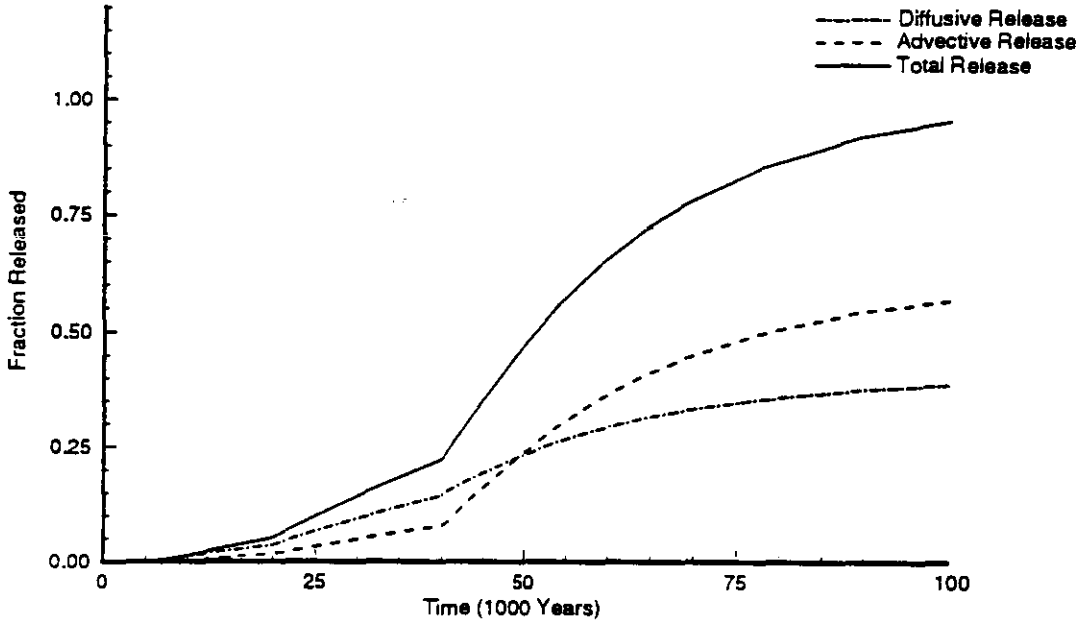

Figure P.22. Case 1.3 (composite model): Fractional Release of Group 2A (technetium-99) from Region of Engineered System by Diffusive and Advective Mechanisms

P.6 Section 4.1.2, Dose Results for Groundwater Pathway

P.6.1 Mass Balance Information for Compliance Cases

Water was added to computational cells within the compliance case simulations to simulate water vapor diffusion. As the result of a default feature of the code (which was unknown at the time), the water was added at the concentration of the cells rather than as clean water. This resulted in a mass balance error which is always positive and is most severe when water vapor diffusion rates and concentrations in the affected nodes are the highest. The mass balance is computed for the problem as a whole, as well as for a region containing much of the engineered system. The boundary for the mass balance within the engineered system is a rectangular area, the top of which follows the boundary between the asphalt barrier and the gravel. The bottom of the rectangle is between the asphalt barrier and the underlying soil. The sides are vertical and are in line with the backfill soil/asphalt barrier interface at the top corners of the asphalt barrier. Because the vault wall surface and asphalt barrier slope outwards, the sides of the rectangular area pass from the outside of the asphalt barrier at the top corner, to the catch basin/asphalt barrier interface near the lower corners. This region is referred to as the "engineered system" even though it excludes some areas of the asphalt barrier. All of the vapor diffusion sources are included within this region.

The mass balance over time for the central compliance case is illustrated in Figure P.23 for the entire problem as well as for the engineered system. The normalized total mass (NTM) which is plotted is defined as:

$$NTM = \frac{(X_{system} + X_{flux})}{(X_{system\ initial})} \tag{P.30}$$

where X_{system} = total mass within boundary at time of interest

X_{flux} = integral of flux across the boundary over time

$X_{system\ initial}$ = initial mass within boundary.

The mass balance error results for Cases 1.1 (delayed cracking), 1.2 (no HDPE flow path), and 1.3 (composite model) are shown in Figures P.24, P.25, and P.26, respectively. The mass balance errors in Figures P.23, P.24, and P.25 indicate similar mass balance errors in that the errors occur in the engineered system, always increase with time, and are of similar magnitude. However, Figure P.26, which shows the mass balance obtained using the composite model for concrete cracking, indicates a different mass balance problem. The error within the engineered system appears to be similar to that in other compliance cases and is probably due to the same water vapor diffusion source problem. The mass balance in the remainder of the problem, however, shows a negative error which is larger than the error caused by the water vapor diffusion. In addition, the direction of the error is apparently not constant. The cause of the mass balance problem is not known. Because the engineered system contains all of the concrete and mass balance for the engineered system is not different in this case, the difference in mass balance is not attributed to the composite model being used for concrete water retention properties.

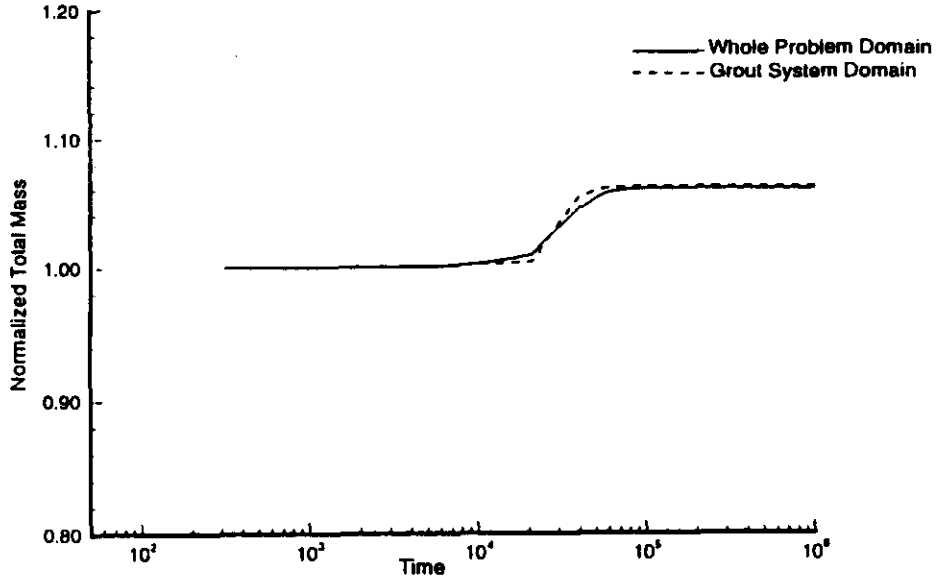

Figure P.23. Case 1.0 (central compliance case): Mass Balance as a Function of Time. Separate mass balances are tracked for the engineered system region (described above) and for the entire problem domain.

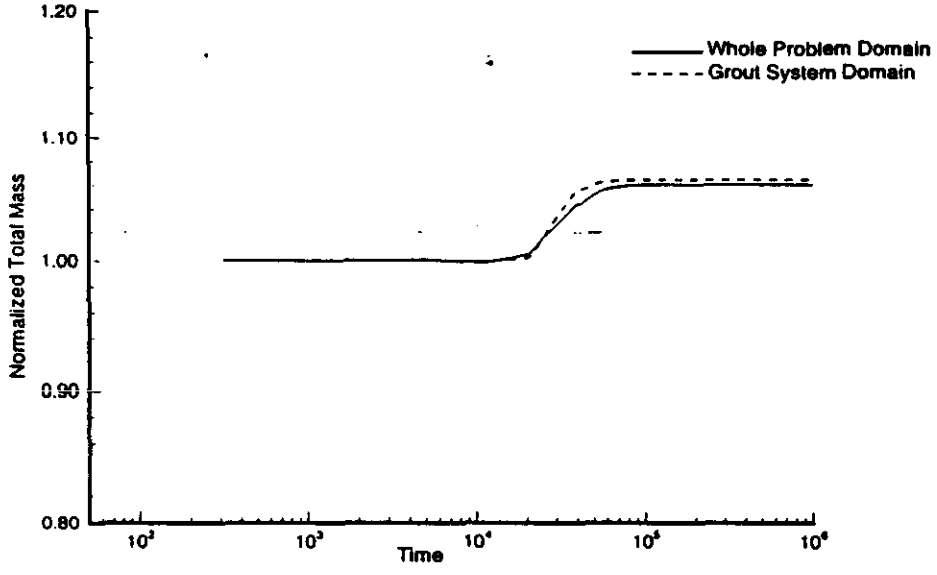

Figure P.24. Case 1.1 (delayed cracking): Mass Balance as a Function of Time. Separate mass balances are tracked for the engineered system region (described above) and for the entire problem domain.

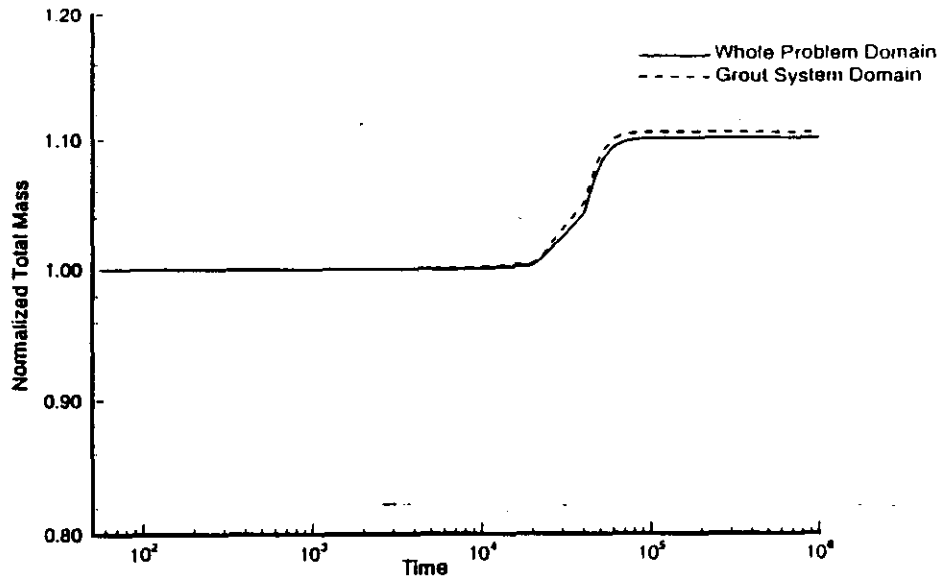

Figure P.25. Case 1.2 (no HDPE flow path): Mass Balance as a Function of Time. Separate mass balances are tracked for the engineered system region (described above) and for the entire problem domain.

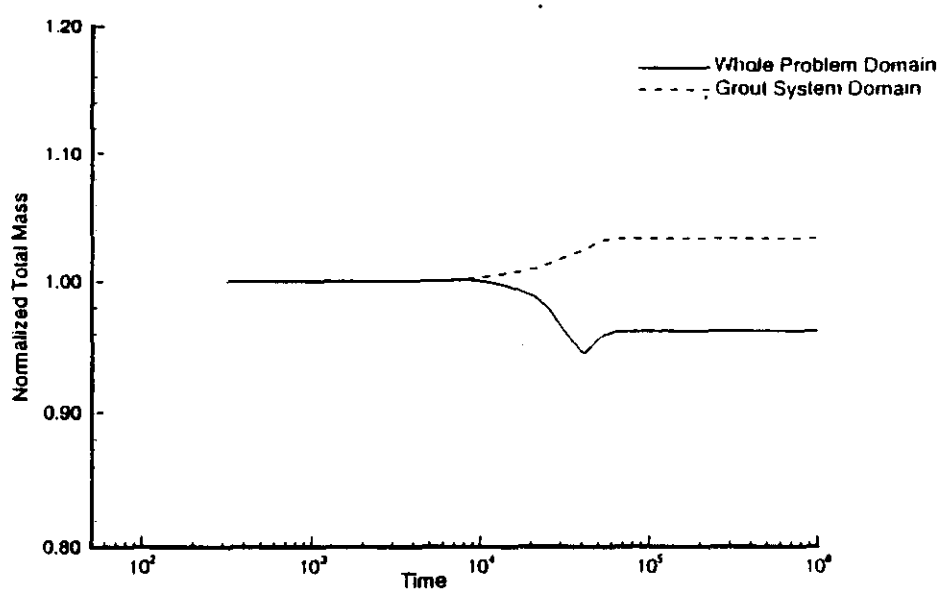

Figure P.26. Case 1.3 (composite model): Mass Balance as a Function of Time. Separate mass balances are tracked for the engineered system region (described above) and for the entire problem domain.

P.7 Section 4.1.4.4, Analysis of High Recharge

As described in Chapter 4, Case 1.4 analyzed a recharge rate of 5 cm/yr using a staged degradation model similar to that in the compliance cases. The moisture content contours resulting from a recharge rate of 5 cm/yr are shown in Figure P.27. The mass balance errors experienced in this case were greater than those experienced in cases with 0.1-cm/yr recharge. Figure P.28 shows a plot of the mass balance error for transport grout 1A (containing iodine-129) over time. The mass balance error is fairly small until 5,000 years and then increases rapidly. Separate mass balances are shown for the engineered system and the entire problem domain. As can be seen in Figure P.28, the source of the mass balance error is not within the engineered system. For comparison, see Figure P.23, which shows the mass balance error over time for the central compliance case. The mass balance error in the high recharge case appears to be due to a different phenomenon. The magnitude of the error is much greater than in the central compliance case, and the error appears to occur in the vadose zone rather than the engineered system. In addition, the error both increases and decreases at different times while the central compliance case error only increases.

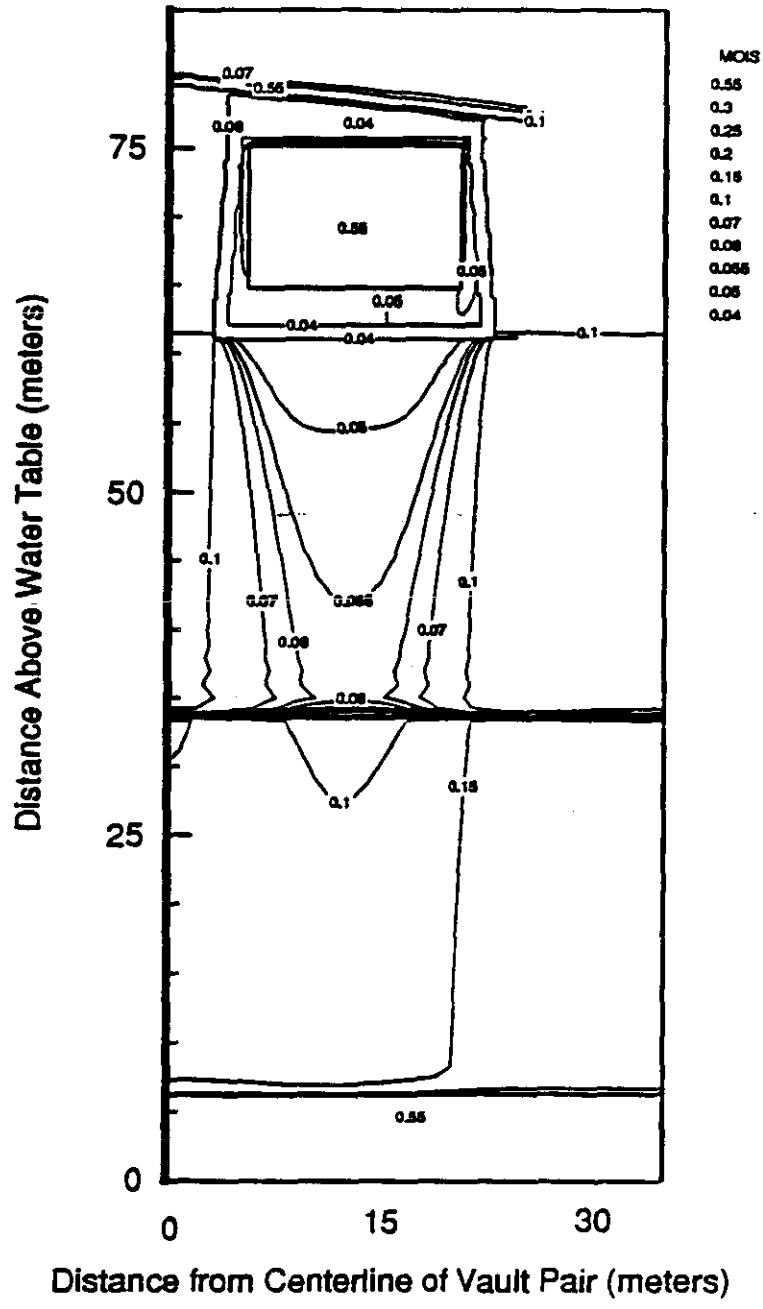

Figure P.27. Case 1.4 (high recharge): Moisture Content Contours Within Vadose Zone at 10,000 Years for 5.0 cm/yr Recharge

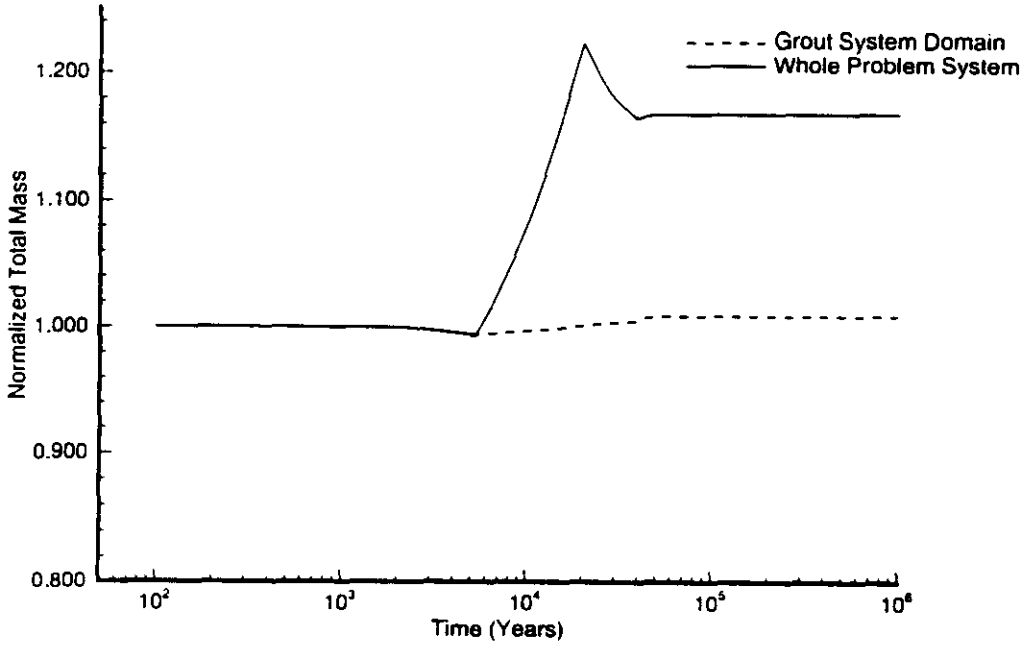

Figure P.28. Mass Balance Error Over Time for Iodine-129 in Case 1.4

Figures P.29 and P.30 illustrate the amount of advective and diffusive transport from the engineered system in Case 1.4. As can be seen in the figures, the amount of transport occurring by advection is higher in this case as was the case with the 0.1-cm/yr recharge rate (see Figures P.15 and P.16).

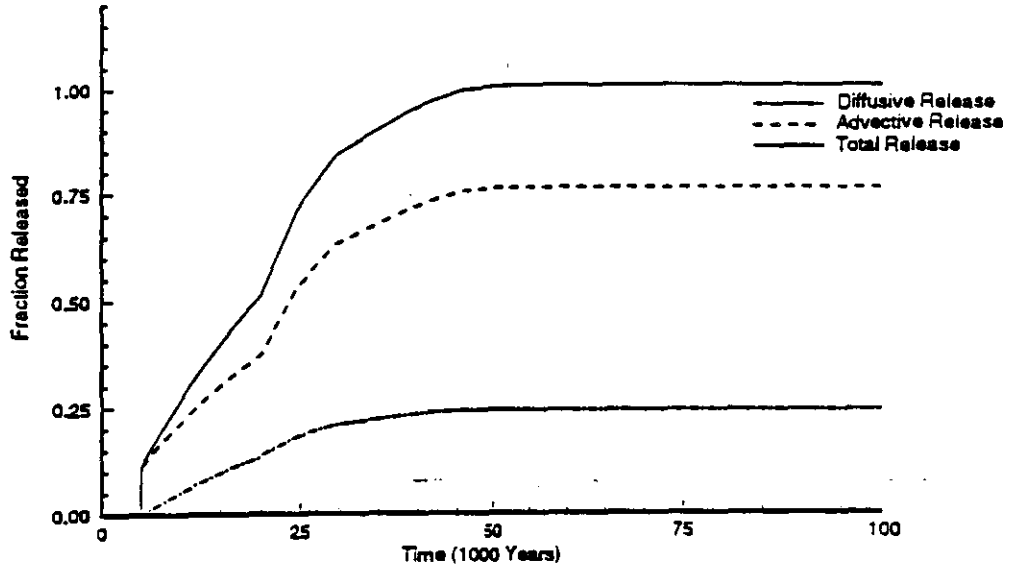

Figure P.29. Release of Transport Group 1A (iodine-129) from the Engineered System by Advective and Diffusive Mechanisms

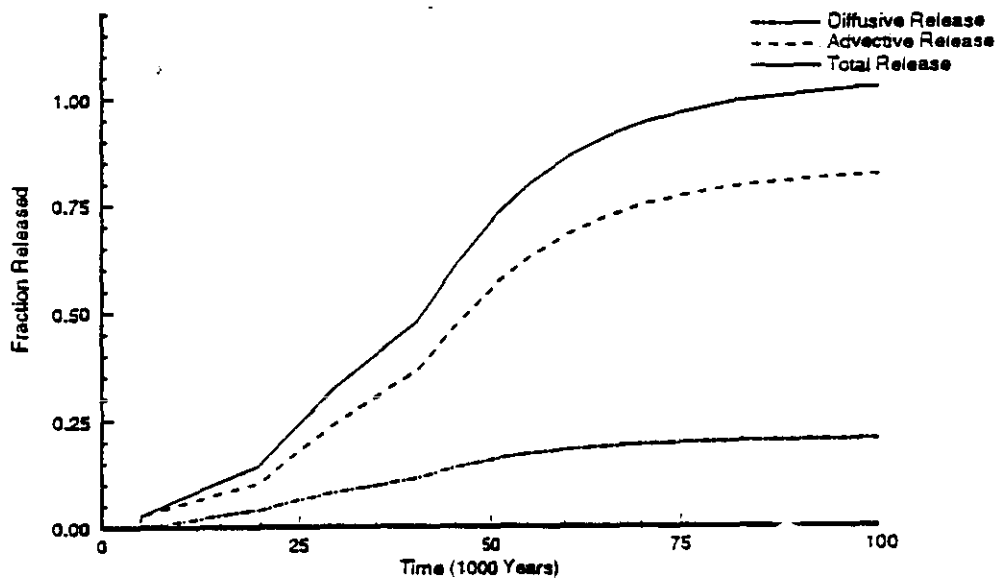

Figure P.30. Release of Transport Group 2A (technetium-99) from the Engineered System by Advective and Diffusive Mechanisms

P.8 Section 4.2.1.1, Central Sensitivity Case

P.8.1 Mass Balance Information

Figure P.31 shows the mass balance error experienced in Case 2.0 (central sensitivity case).

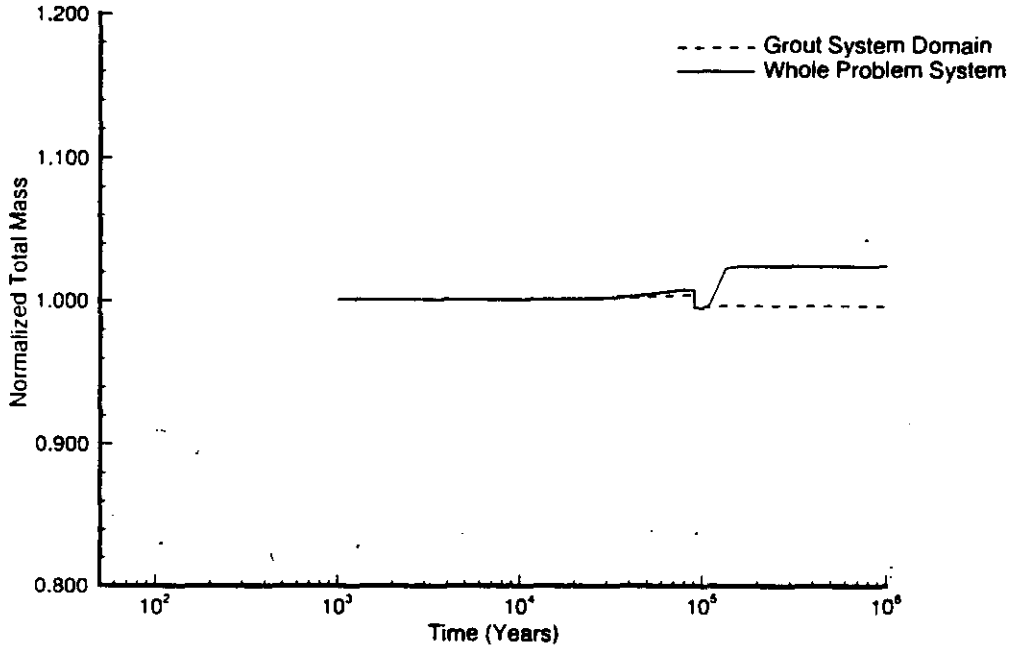

Figure P.31. Mass Balance Error for Case 2.0 (central sensitivity case). The central sensitivity case does not include a water source within the problem.

P.8.2 Water Flux in Cracks

In an attempt to increase understanding of the behavior of the central sensitivity case, the amount of water passing through the cracks in the barrier was monitored during the simulation. In the central sensitivity case, all cracks are modeled as 10-cm cracks filled with backfill soil. The flowrates into cracks (+) and out of cracks (-) are shown below for the 90,000-year period in which the barrier is intact. The flows are constant with time.

Crack Location	L/yr/Vault
Upper right vertical	+ 8.0
Upper left vertical	+ 5.9
Upper right horizontal	+16.0
Upper left horizontal	+ 6.0
Lower right horizontal	-18.0
Lower left horizontal	-18.1

9413222.1856

P.9 Section 4.2.1.3, Sensitivity Cases for Engineered System

P.9.1 Grout

As noted in Chapter 4, the comparison between Cases 2.2D and 2.0 indicated that a two order-of-magnitude increase in diffusion coefficient produced a small counter intuitive increase in release. This was attributed to diffusion into the concrete where hydraulic conductivities are smaller than in the grout.

During this calculation, a boundary was drawn around the grout and cold grout along the inner boundary of the concrete on the top, bottom, and left side of the grout. On the right side of the problem, the boundary is located one node into the grout rather than at the grout/concrete interface. The flux out of this rectangular area from advection and diffusion was monitored over time in both Cases 2.2D and 2.0. The transport out of the region is 15% greater at 16,000 years for transport group 1A (iodine-129) with the higher diffusion coefficient. After 26,000 years, the integrated release from the grout is approximately equal. At this time in the central sensitivity case analysis, advection accounted for 31% of the cumulative contaminant transport across this boundary. In the case with a lower grout diffusion coefficient, advection accounted for 64% of the transport from the grout region. This information is consistent with the hypothesis that the higher diffusivity increased release by reducing the transport into the concrete where hydraulic conductivities (as well as diffusion coefficients) are lower. In the case of neptunium-237, the reduction in diffusion coefficient results in a small decrease in release. This is because the release is controlled by sorption in the grout while sorption is not modeled in the concrete. Therefore, for neptunium-237, transport into the concrete results in greater mobility rather than less.

P.9.2 RCRA Cover and Recharge Rate

Case 2.5B examined the impact of a recharge rate of 5 cm/yr. As outlined in Chapter 4, this produced approximately a factor of 10 increase in peak dose prior to barrier degradation and caused the arrival of contamination to occur much earlier. The flow into and out of the cracks was measured as it was in the central sensitivity case. The flow through cracks is provided below.

Crack Location	Flow: L/yr/Vault
Upper right vertical	+ 17.1
Upper left vertical	+ 15.0
Upper right horizontal	+292.8
Upper left horizontal	+ 68.1
Lower right horizontal	-207.0
Lower left horizontal	-186.0

As can be seen, the flows are roughly an order-of-magnitude greater than in the central sensitivity case. Thus, the higher recharge is increasing the flow through the cracks in the barrier. This is believed to be the key mechanism causing the higher level of releases. The high recharge also produces higher advection velocities in the soil, which dramatically shortens the arrival time.

The mass balance information in this case is shown in Figure P.32. As can be seen, the higher recharge increases the mass balance error relative to the central sensitivity case (compare Figure P.31). The reason for this is not known.

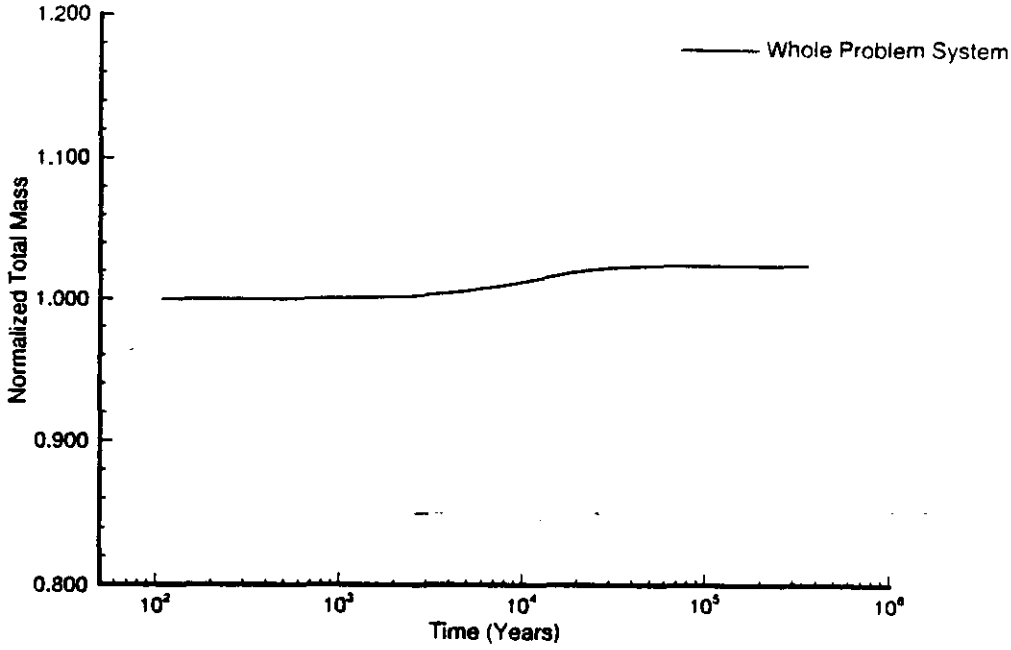

Figure P.32. Mass Balance Information for Case 2.5B, 5-cm/yr Recharge Sensitivity Case

P.9.3 Water Vapor Return

As noted in Chapter 4, the mass balance error was increased when a water source representing the diffusion of water vapor was added to the problem (Case 2.6A). Figure P.33 shows the mass balance error for Case 2.6A over time from 1,000 to 90,000 years. This figure can be compared to the mass balance results from the central sensitivity case shown previously in Figure P.31, which does not include a water source simulating water vapor return. Upon investigation, the increased mass balance error was determined to be due to a default in the code that caused the water source, being introduced to simulate water vapor diffusion, to enter the problem at the concentration currently present in the cell into which it was introduced. Because of this, the effect is most pronounced when the water vapor diffusion rates and concentrations in the cracks are highest. In addition, the problem always results in the addition of mass to the system and in this sense it is conservative. The source of the mass balance problem was not determined until after the compliance case simulations had been executed. Therefore, all compliance case simulations are also subject to this error. Mass balance errors for compliance cases was discussed in Section P.6.

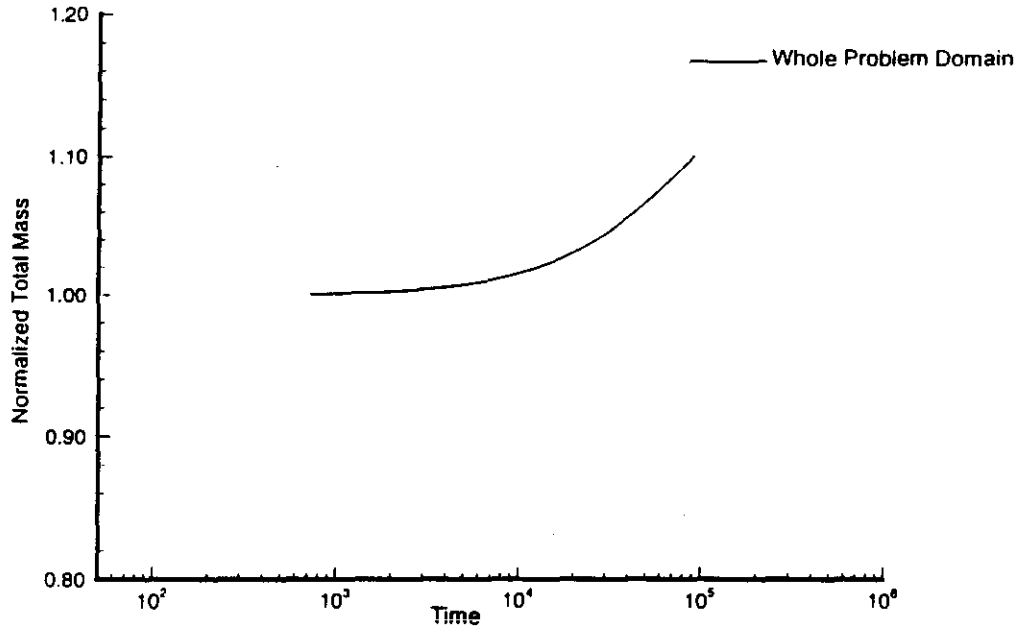

Figure P.33. Mass Balance Error for Case 2.6A from 1,000 to 90,000 Years. Case 2.6A includes a water source in the upper cracks to represent water vapor diffusion.

P.10 Section 4.2.2, Sensitivity of the Unconfined Aquifer Analysis to Irrigated Agriculture

Four cases involving different recharge rates have been analyzed--a natural recharge, a 5-cm/yr increment over natural recharge, and two cases associated with irrigated agriculture. The first represents a post-Hanford aquifer with natural recharge. In this analysis the Grout Disposal Facility received 0.1-cm/yr infiltration through the barrier system. The other cases apply additional annual infiltration amounts of 5, 10.2, and 25.4 cm/yr. The 5-cm/yr case is the high recharge case which appears in the performance assessment. Cases involving 10.2- and 25.4-cm/yr are based on present trends in irrigated agriculture in Benton and Franklin counties. A rate of 10.2 cm/yr is the average recharge rate for a diverse pattern of crops. A rate of 25.4 cm/yr is associated with potatoes. When the Hanford Site becomes available for agriculture, the initial crop probably would be potatoes, which would do well in virgin soils. Crop diversification would take place after only a few years. Irrigated agriculture will probably occur as soon as the public is allowed unrestricted access.

The results of the analysis are summarized in Table P.12. Two blocks of information are presented. The first four rows report the analysis for a high pumping rate of 45 m^3/d, the last four rows report that for a low pumping rate. Several related aspects of these analyses become clear. Greater recharge causes the aquifer thickness to increase. The flow field also shifts from easterly under the 0.1-cm/yr case, to

Table P.12. Summary of Well Intercept Factors for Infiltration and Pumping Rate Combinations

Case (cm/yr)	Aquifer Thickness (m)	Well Intercept (m)	Plume Width (m)	Average Gradient at Facility (dimensionless)	Groundwater or Well Discharge (m^3/d)	Recharge from Facility (m^3/d)	Well Intercept Factor
High Pumping Rate (irrigated farm scenario)							
0.1	21.1	144	255	4.76×10^{-4}	45	0.245	0.00308
5	25.1	160	416	3.9×10^{-4}	45	12.25	0.105
10.2	28.7	170	479	3.2×10^{-4}	45	25.0	0.197
25.4	36.9	32	479	5.28×10^{-4}	45	62.2	0.0924
Low Pumping Rate							
0.1	21.3	--	256	4.18×10^{-4}	24.6	0.245	0.010
5	25.2	--	416	3.1×10^{-4}	29.7	12.25	0.415
10.2	28.7	--	479	3.2×10^{-4}	35.3	25.0	0.708
25.4	36.9	--	479	5.28×10^{-4}	465.4	62.2	0.13366

northeasterly for the 5-cm/yr case, to northward for the 10.2-cm/yr case, and finally to the northwest for the 25.2-cm/yr case. This rotation of the flow field is a result of water which mounds on the plateau region of the site as it finds a way around Gable Mountain and to the Columbia River. As groundwater deepens in response to recharge, it simply finds it easier to move through the gap between Gable Mountain and Gable Butte and to the river, than to move directly east to the river. The plume width estimate is a direct result of the flow field rotation. As the field rotates from an easterly flow to a northerly flow, the longer axis of the site becomes perpendicular to the flow field. Clearly, the highest recharge case has a different response than the others. The depth of aquifer in this case implies that groundwater flow is occurring in the Hanford formation gravel sequence. This explains the greatly reduced well intercept width and the increased groundwater discharge.

Both analyses, negligible and 45-m^3/d pumping rates, produce the highest well intercept factor for the case involving a diverse pattern of crops similar to those of Benton and Franklin counties. The lowest factors and greatest reduction in concentrations are a result of the lowest recharge, 0.1 cm/yr, which is associated with the permanent isolation barrier. This low recharge rate was employed in the majority of performance assessment cases.

P.11 References

Allard, B., U. Olofsson, B. Torstenfelt, H. Kipatsi and K. Andersson. 1982. "Sorption of Actinides in Well-Defined Oxidation States on Geologic Media." *Scientific Basis for Nuclear Waste Management V*. Materials Research Society Vol. 11, Pittsburg, Pennsylvania, p. 775-782.

Ames, L. L., and R. J. Serne. 1991. *Compilation of Data to Estimate Groundwater Migration Potential for Constituents in Active Liquid Discharges at the Hanford Site*. PNL-7660, Pacific Northwest Laboratory, Richland, Washington.

Benson, D. W. 1961. *Mineral Adsorption of Radionuclides in Reactor Effluent*. HW-69225, Hanford Works (General Electric), Richland, Washington.

Bidoglio, G., A. Avogadro, and A. DePlano. 1985. "Influence of Redox Environments on the Geochemical Behavior of Radionuclides." *Scientific Basis for Nuclear Waste Management IX*. Materials Research Society Vol. 50, Pittsburg, Pennsylvania, p. 709-716.

Bird, R. B., W. E. Stewart, and E. N. Lightfoot. 1960. *Transport Phenomena*. John Wiley & Sons, Inc., New York.

Bondietti, E. A. 1982. "Mobile Species of Pu, Am, Cm, Np and Tc in the Environment." *Environmental Migration of Long-Lived Radionuclides*. IAEA-SM-257/42, p. 81-96, International Atomic Energy, Vienna, Austria.

Crank, J. 1975. *The Mathematics of Diffusion*. Oxford University Press, London.

Ewart, F. T., J. L. Smith-Briggs, H. P. Thomason, and S. J. Williams. 1992. "The Solubility of Actinides in a Cementitious Near-Field Environment." *Waste Management* 12:241-252.

Freeze, R. A., and J. A. Cherry. 1979. *Groundwater*. Prentice-Hall, Englewood Cliffs, New Jersey.

Girvin, D. C., L. L. Ames, A. P. Schwab, and J. E. McGarrah. 1991. "Neptunium Adsorption on Synthetic Amorphous Iron Oxyhydroxide." *J. of Colloid Interface Sci.* 141:67-78.

Harr, M. E. 1962. *Groundwater and Seepage*. McGraw-Hill Book Company, New York.

Hillel, D. 1982. *Introduction to Soil Physics*. Academic Press. New York.

Höglund, S., L. Eliasson, B. Allard, K. Andersson, and B. Torstenfelt. 1985. "Sorption of Some Fission Products and Actinides in Concrete Systems." *Scientific Basis for Nuclear Waste Management IX*. Materials Research Society. Vol. 50, Pittsburg, Pennsylvania, p. 683-690.

Jury, W. A., W. R. Gardner, and W. H. Gardner. 1991. *Soil Physics*. John Wiley & Sons, New York.

Keiling, Ch., and G. Marx. 1991. "Investigations into the Influence of Organic Complexing Agents on the Leaching Behavior and Mobility of Radionuclides Solidified in ILW Forms." *Radiochimica Acta*. 52/53:287-290.

Kemper, W. D., and J. C. van Schaik. 1966. "Diffusion of Salts in Clay-Water Systems." *Soil Sc. Soc. Am. Proc.* 30:534-540.

Klavetter, E. A., and R. R. Peters. 1986. *Estimation of Hydrologic Properties of An Unsaturated, Fractured Rock Mass*. SAND84-2642, Sandia National Laboratories, Albuquerque, New Mexico.

Meyer, R. E., W. D. Arnold, and F. I. Case. 1985. *Valence Effects on the Sorption of Nuclides on Rocks and Minerals II*. NUREG/CR-4114, ORNL-6137, Oak Ridge National Laboratory, Oak Ridge, Tennessee.

Mualem, Y. 1976. "A New Model for Predicting the Hydraulic Conductivity of Unsaturated Porous Media." *Water Resour. Res.* 12(3):513-522.

Olsen, S. R., and W. D. Kemper. 1968. *Advances in Agronomy* 20:91-151.

Porter, L. K., W. D. Kemper, R. D. Jackson, and B. C. Stewart. 1960. "Chloride Diffusion in Soils as Influenced by Moisture Content." *Soil Sc. Soc. Am. Proc.* 24:460-463.

Rai, Dhanpat, and J. L. Ryan. 1985. "Neptunium (IV) Hydrous Oxide Solubility Under Reducing and Carbonate Conditions." *Inorg. Chem.* 24:247-251.

Richards, L. A. 1931. "Capillary Conduction of Liquids in Porous Mediums." *Physics* 1:318-313.

Routson, R. C., G. Jansen, and A. V. Robinson. 1975. *Sorption of ^{99}Tc, ^{237}Np, and ^{241}Am on Two Subsoils From Differing Weathering Intensity Areas*. BNWL-1889, Pacific Northwest Laboratory, Richland, Washington.

Routson, R. C., G. Jansen, and A. V. Robinson. 1976. "Sorption of ^{99}Tc, ^{237}Np, and ^{241}Am on Two Subsoils from Differing Weathering Intensity Areas." *Health Phys.* 33:311-317.

Serne, R. J., W. J. Martin, V. L. LeGore, C. W. Lindenmeier, S. B. McLaurine, P.F.C. Martin and R. O. Lokken. 1989a. *Leach Tests on Grouts Made with Actual and T[illegible] Metal-Spiked Synthetic Phosphate/Sulfate Waste*. PNL-7121, Pacific Northwest Laboratory, Richland, Washington.

Serne, R. J., W. J. Martin, R. O. Lokken, V. L. LeGore, C. W. Lindenmeier, and P. C. Martin. 1989b. *Leach and EP Toxicity Tests on Grouted Waste from Tank 106-AN*. PNL-6960, Pacific Northwest Laboratory, Richland, Washington.

Serne, R. J., and M. I. Wood. 1990. *Hanford Waste-Form Release and Sediment Interaction-A Status Report with Rationale and Recommendations for Additional Studies*. PNL-7297, Pacific Northwest Laboratory, Richland, Washington.

Serne, R. J., and M. I. Wood. 1990. *Hanford Waste-Form Release and Sediment Interaction*. PNL-7297, Pacific Northwest Laboratory, Richland, Washington.

Serne, R. J., R. O. Lokken, and L. J. Criscenti. 1992. "Characterization of Grouted Low-Level Waste to Support Performance Assessment." *Waste Management* 12:271-287.

Serne, R. J., C. W. Lindenmeier, J. L. Conca, V. L. LeGore, K. J. Cantrell, J. A. Campbell, J. E. Amonette, and M. I. Wood. 1993. *Solid Waste Leach Characteristics and Contaminant-Sediment Interactions*. PNL-draft, Pacific Northwest Laboratory, Richland, Washington.

Sheppard, J. C., J. A. Kittrick, and T. L. Hardt. 1976. *Determination of Distribution Ratios and Diffusion Coefficients of Neptunium, Americium, and Curium in Soil-Aquatic Environments*. RLO-2221-T-12-2 (WSU 76/13-33), Washington State University, Pullman, Washington.

Staunton, S., P. G. Clay, and L. V. C. Rees. 1990. "Diffusion of Neptunium (V) in Clays." *Radiochimica Acta*. 49:147-153.

Tallent, O. K., E. W. McDaniel, G. D. Del Cul, K. E. Dodson, and D. R. Trotter. 1988. "Immobilization of Technetium and Nitrate in Cement-Based Materials." *Mat. Res. Soc. Symp. Proc.* 12:23-32.

van Genuchten, M. Th. 1978. *Calculating the Unsaturated Hydraulic Conductivity with a New, Closed-Form Analytical Model*. Research Report 78-WR-08, Water Resources Program, Department of Civil Engineering, Princeton University, Princeton, New Jersey.

Appendix Q

Best Estimate Crack Predictions for the Grout Vault Engineered Barriers

9413222.1864

9413272.1066

This page intentionally left blank.

Appendix Q

Best Estimate Crack Predictions for the Grout Vault Engineered Barriers

B. V. Winkel, Westinghouse Hanford Company

9413222.1866

Q.1 Introduction

Precise crack predictions in asphalt and concrete are difficult even in controlled laboratory conditions. For the grout vault application, significant uncertainties exist in the stress magnitudes, even for the near-term loadings (settlement, thermal, shrinkage, soil/grout pressures, stress redistributions caused by asphalt creep). These load/stress uncertainties increase with time, particularly with regard to seismic events. Uncertainties in material property changes caused by aging and chemical reactions also increase with time.

Because the cracking estimates are used in flow/transport computer models, it was necessary to establish quantitative predictions. However, because of the uncertainties, it was not reasonable to attempt to numerically derive the quantitative crack estimates. A more reasonable approach was to base the estimates on judgment influenced by the limited available data. Because the uncertainties increase with time, the long-term crack estimates involve greater conjecture and larger spans of time were considered for the longer-term predictions provided in Section Q.3.

Although significant uncertainties exist in quantitative crack predictions, note that, in general, the grout vault design is relatively benign regarding crack potential. During normal loading, the general stress pattern is compressive (i.e. the loading imposed by the soil is inward on all outside surfaces of the vault). Because no structurally significant voids are inside the vault, there cannot be structural collapse or significant displacements and associated opening of cracks in the vault components. The buried, desert sand environment is also a significant factor in minimizing cracking. That is, a buried structure does not experience the freeze/thaw, wet/dry, or hot/cold cycling which is experienced by a surface structure. The aging effects of air/oxygen, sunlight, and drying shrinkage are also reduced.

Therefore, cracking should be minimal and cracks would tend to remain closed. The one potential exception to this statement is with the asphalt walls. Between the asphalt and concrete walls is one inch of thermal insulation board, which may compress and/or disintegrate with time. Should this occur, the voided space may result in a downward flow or "slumping" of the asphalt walls and the asphalt wall could separate from the asphalt roof.

Q.2 Procedures for Establishing Crack Estimates

Given the uncertainties in the crack predictions, the ideal procedure is to perform a probabilistic evaluation. However, a quantitative probabilistic analysis is not feasible because there is insufficient data on the uncertainty distributions for the significant parameters. Another alternative for dealing with significant uncertainties is to base the crack predictions on highly pessimistic assumptions for all parameters involved. However, the resulting combination of worst case assumptions could produce an extremely conservative estimate with little meaning. The grout vault performance assessment analysts' consensus was that the most meaningful approach would be to establish a "best estimate" for each of the potential cracking mechanisms.

The first step in the crack prediction effort was to review the existing literature relative to potential crack mechanisms in concrete and asphalt. For concrete, a relatively comprehensive list of crack mechanisms is available in ACI 224.1R (ACI 1984). Based on ACI 224.1R and other literature on concrete and asphalt cracking, it was decided to develop a grout vault "relative significance" number for each of the potential cracking mechanisms. A significance factor for each mechanism was found by multiplying a relative "probability of occurrence" times a "consequence factor" using a scale of 1 to 5. The resulting "significance factor" product potentially ranges from 1 to 25. This effort is summarized in Attachment 1. The results are shown in Table Q.1. The significance factors were used in the crack predictions provided in Section Q.3 below.

The development of the significance factors for concrete cracking, summarized in Attachment 1, was patterned after a Failure Modes and Effects Analysis (FMEA) tool used for evaluating potential failures in military and aerospace hardware. [Refer to DOD (1980).] An FMEA uses relative probability of occurrence and failure consequences to focus on design improvements which will increase reliability in service. It is a relatively simple, qualitative alternative to a full-fledged probabilistic evaluation. The results given in Table Q.1 provide information to identify the more important crack mechanisms for the grout vault application.

In addition to the ACI 224.1R committee report, several other documents about concrete cracking and durability were reviewed. [Refer to Clifton (1989), Walton (1990), Hookham (1991).] The grout vault stress reports were also reviewed (KEH 1991, Winkel 1992). These documents also influenced the cracking estimates described in the next section.

The asphalt cracking predictions were influenced by the following efforts: 1) asphalt pavement literature review, 2) review of grout vault asphalt design documentation, and 3) discussions with asphalt aging experts. The contribution of the asphalt paving experience to the grout vault is limited because the grout vault application significantly departs from a typical pavement design (i.e., loading, thickness, environment, mix design, and design life).

Table Q.1. Relative Significance of Potential Cracking Mechanisms (Listed in order of significance, highest first)

Component	Cracking Mechanism	Significance Factor
Concrete Vault	Long-Term Seismic Loading	16
	Long-Term Rebar Corrosion	16
	Roof Cracking Between Roof Planks	16
	Wall/Floor Construction Joints	15
	Short-Term Drying Shrinkage	9
	Short-Term Thermal Stress	8
	Chemical Degradation Mechanisms	8
	Fresh Concrete Settlement in Floor	6
	Externally Applied Loads	4
	Long-Term Drying Shrinkage	3
	Short-Term Rebar Corrosion	3
	Poor Construction Practices	3
	Design Detailing Errors	3
	Short-Term Seismic Loading	3
	Fresh Concrete Plastic Shrinkage	2
	Weathering	2
Asphalt Barrier	Thermal Board Disintegration	15
	Long-Term Seismic Stresses	8
	Thermal Stresses	6
	Construction Joint Cracks	5
	Shrinkage Cracking	4
	Crack Enlargement from Biodegradation	4
	Fatigue Cracking	3
	Short-Term Seismic Stresses	3

Concerning design documentation, a significant material property testing effort was conducted for the grout vault asphalt mix design (Vallerga 1992). The Vallerga report recommended using a 1% tensile strain criteria to avoid cracking. As indicated in Section Q.1, under normal loading the general stress state is compressive. This means that if the 1% strain criteria is exceeded, it would be local in nature and not project through the wall, for the short term. The one possible exception to this statement is the wall/roof intersection region discussed in Section Q.1.

For the long term, cracking can be influenced by asphalt aging/hardening. If the asphalt becomes embrittled, surface cracks may extend through the wall thickness during a seismic event. Based on consulting with asphalt aging experts, the consensus was that for the thick, relatively impermeable grout vault asphalt walls, the aging, and associated cracking, should be a surface phenomena.

Q.3 Best Estimate Crack Predictions

From Table Q.1, the more significant contributors to concrete cracking for the grout vault are 1) seismic-induced cracking, 2) rebar corrosion, 3) roof cracking between roof planks, and 4) built-in cracks at construction joints. To simplify the concrete cracking predictions, it was assumed that the concrete cracking would be dominated by these four mechanisms. This assumption was influenced by the existence of an asphalt liner on the inside surface of the concrete walls. The sealing effect of this liner should compensate for the minor cracking mechanisms.

Using the procedures discussed in Section Q.2, the best estimate crack predictions given in Table Q.2 were obtained. The rationale for these predictions is summarized in the remainder of this section. Note that the crack descriptions are divided into time periods of increasing length. For flow modeling purposes, it can be assumed that the described cracking occurs in the middle of the period or, more conservatively, in the beginning of the period.

Q.3.1 0- to 100-Year Time Period

As shown in Table Q.2, limited cracking is predicted for the first 100 years. The only expected significant cracking is between the planks in the roof. The roof planks are 4-ft wide precast panels. Following placement, the joints between planks are grouted and a thin, lightly reinforced cap is placed over the entire roof. As overburden weight is added from the roof asphalt and cover soil, it is likely that through-wall cracks will form at the roof plank joints.

Some minor cracking in the concrete is expected from drying shrinkage and/or thermal stresses in the first 100 years. If any of these cracks should extend through the wall, they should remain sealed because of the presence of the asphalt liner. Rebar corrosion should not be significant in the first 100 years because cathodic protection exists for the rebar, if needed. For the asphalt, some cracking may occur in the upper corners due to wall slumping, but it is not expected to extend through the wall because of the compressive character of the stress and the ductile nature of the asphalt.

Q.3.2 100- to 1,000-Year Time Period

For the 100- to 1,000-year time period, the only through-wall cracks predicted for the asphalt are at the top corners. This position is based primarily on the assumption that the asphalt core remains ductile, preventing permanent through-wall cracks. For the concrete, it is assumed that the metal water stops in the construction joints have lost their ability to seal due to corrosion. Some rebar corrosion is predicted, but it is assumed that there is insufficient corrosion and seismic activity to expect significant through-wall cracking.

Concerning rebar corrosion, many quantitative corrosion predictor models in the literature exist. [Refer to Walton (1990).] All of these models are limited to chloride ion attack because, historically,

Table Q.2. Best Estimate Crack Predictions

Time Period (Years)	Component	Through-Wall Crack Descriptions
0 - 100	Asphalt Barrier Concrete Vault	• Initiation of surface cracks in upper corners caused by asphalt wall "slumping," but no through-wall cracks. • 0.5-mm-wide cracks between each 4-ft (122-cm) roof plank. • Wall and floor cracks, if any, will be sealed by asphalt liner. 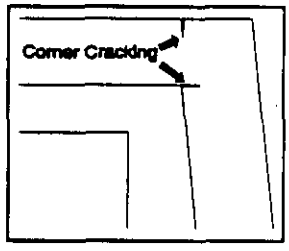
100 - 1,000	Asphalt Barrier	• 5-mm through-wall cracks develop in the wall/roof intersection region, caused by additional wall slumping and seismic activity. • Surface hardening results in some surface cracking, but through-wall cracks exist only in the upper corners. 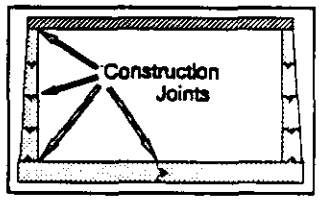
	Concrete Vault	• Asphalt liner and metal waterstops degrade, resulting in all construction joints (5 wall joints and 1 floor joint) effectively acting as 0.5-mm through-wall cracks. • Roof plank joint cracks increase to 1 mm in width due to seismic activity. • Surface cracks develop due to rebar corrosion, but don't extend through the walls, floor, or roof.
1,000 - 10^4	Asphalt Barrier	• Additional hardening, biodegradation, and cracking at the surface, but sufficient soft core prevents crack extension through the wall, except at the upper corners. Upper corner through-wall cracks remain at 5-mm size.
	Concrete Vault	• Construction joint cracks increase in size to 1 mm due to seismic activity. • Roof plank joint cracks increase in size to 2 mm due to seismic activity. • Seismic activity causes 1-mm corrosion-induced surface cracks to extend through the wall at every 10th rebar location [i.e. every 40 in. (~1 m)].
10^4 - 10^5	Asphalt Barrier	• Additional surface degradation (hardening, biodegradation) results in some surface cracks extending through the wall. Assume 1-mm cracks every 1 m. • Upper corner through-wall cracks remain at 5-mm size.
	Concrete Vault	• Construction joint cracks increase in size to 2 mm due to seismic acti[illegible] • Roof plank joint cracks remain at 2 mm. • Corrosion-related cracks increase in size and number to 2 mm every 50 cm.

this has been the source of rebar corrosion (e.g. de-icing salts on bridge decks). The application of these models to the grout vault environment (i.e., chemistry) is questionable. On the positive side, corrosion is less likely for low water cement ratio mix designs and high pH environments, both of which are true for the grout vaults. However, it is difficult to prove that significant rebar corrosion will not eventually occur and it was therefore assumed that corrosion-induced surface cracks develop during the 100- to 1,000-year time period.

Q.3.3 1,000- to 10,000-Year Time Period

Based on the assumption that the asphalt hardening is a surface phenomena, through-wall cracking in the asphalt was assumed to be limited to the upper corners for the 1,000- to 10,000-year time period. This prediction was also influenced by the results of seismic analyses of the grout vault asphalt (Winkel 1992), which indicated relatively low seismic stresses in the asphalt. For the concrete vault, it was assumed that seismic activity results in a widening of the existing cracks as well as through-wall extension of 10% of the corrosion-induced surface cracks.

Q.3.4 10,000- to 100,000-Year Time Period

It was assumed for the 10,000- to 100,000-year time period that biodegradation and surface cracking results in hardening progressing through the thickness of the asphalt barrier. It was further assumed that during seismic events through-wall cracks would occur throughout the asphalt barrier. Cracking of the concrete was assumed to follow the pattern of the previous time period (i.e., widening of existing cracks and the introduction of new cracks).

Q.4 References

ACI. 1984. *Causes, Evaluation, and Repair of Cracks in Concrete Structures.* ACI 224.1R, American Concrete Institute Committee Report, ACI Manual of Concrete Practice, Vol. 3.

Clifton, J. R. and L. I. Knab. 1989. *Service Life of Concrete.* NUREG/CR-5466, NISTIR 89-4086.

DoD. 1980. *Procedures for Performing a Failure Mode, Effects and Criticality Analysis.* MIL-STD-1629A, Department of Defense, November 24, 1980.

Hookham, C. J. 1991. *Structural Aging Assessment Methodology for Concrete Structures in Nuclear Power Plants.* ORNL/NRC/LTR-90/17, March 1991.

KEH. 1991. *Engineering Report, Vault Design, Work Order ER9089.* Kaiser Engineers Hanford, January 1991.

Vallerga, B. A. 1992. *Characterization Study of Asphalt Concrete Barrier Material for Radioactive Waste Vaults*. B. A. Vallerga, Inc., March 1992.

Walton, J. C. 1990. *Models for Estimation of Service Life of Concrete Barriers in Low-Level Radioactive Waste Disposal*. NUREG/CR-5542, September 1990.

Winkel, B. V. 1992. *Grout Vault Asphalt Barrier Seismic Adequacy, Preliminary Report*. Westinghouse Hanford Co., Facility Stress Analysis, April 21, 1992.

9413222.1872

THIS PAGE INTENTIONALLY
LEFT BLANK

Attachment 1

Evaluation of Concrete Cracking Mechanisms

9413222.1873

Summary of Evaluation of Potential Cracking Mechanisms in the Grout Vault Structures

Material	Cracking Mechanism	Probability of Occurrence	Consequence Factor	Significance Factor	Comments
Vault Concrete	Plastic Shrinkage (Fresh Concrete)	1	2	2	Only occurs on hot dry days when improper curing practices are employed. Generally occurs in horizontal slabs, which, for the grout vault, would be the floor of the vault. If such a condition developed in the vault floor, it is highly probable that it would be detected and corrected.
	Fresh Concrete Settlement	3	2	6	Generally occurs immediately above rebar in flat slabs when improper placing procedures are used. Some problems with this mechanism occurred in the initial vaults. Cracks are generally shallow, immediately above the rebar.
	Short-Term Drying Shrinkage (Hardened Concrete)	3	3	9	Generally caused by surface drying faster than the interior, which could occur in the vaults before grout fill. Cracks generally are relatively tight and limited to the surface. Through-wall cracks occur only if full section is in tension (e.g., wall shrinkage restricted by grout).
	Long-Term Drying Shrinkage	1	3	3	In the long term, humid environment of the buried vaults, drying shrinkage should be minimal.
Vault Concrete	Thermal Stress (Short Term)	4	2	8	
	Thermal Stress(Long Term)	1	2	2	Based on conservative thermal stress analysis of grout fill.
	Concrete Chemical Reactions	4	2	8	Some long-term chemical degradation of the concrete is likely. However, it is also likely that the consequences will be minimized because the reaction products are expansive and will tend to seal cracks as they develop. Some seismically-induced crack opening and resealing is expected.
	Weathering	1	2	2	Three types of weathering in ACI 224.1R (freeze/thaw, wet/dry, heating/cooling). As buried structures, the vaults should not experience significant weathering.
	Rebar Corrosion (Short Term)	1	3	3	Short-term rebar corrosion is unlikely because 1) cathodic protection is available, 2) short-term pH is high, 3) low permeability concrete is used, 4) relatively low chlorides with limited free moisture is present, and 5) vault asphalt liner separates grout from the concrete walls.

Summary of Evaluation of Potential Cracking Mechanisms in the Grout Vault Structures (contd)

Material	Cracking Mechanism	Probability of Occurrence	Consequence Factor	Significance Factor	Comments
	Thermal Stress	2	3	6	Asphaltic concrete has a relatively high thermal expansion coefficient, resulting in a higher potential for significant thermal stresses. However, thermal stresses are highest in the first few years following grout fill, when the asphalt should be relatively ductile, reducing the probability of thermal cracking.
	Fatigue Cracking	1	3	3	Fatigue cracking is observed in highway pavements due to the high degree of cyclic loading. Other than some limited cycling due to seismic loading, the vault stresses are not cyclic.
	Seismic Stresses (Short Term)	1	3	3	The short-term seismic mechanism should not be significant because the probability of significant seismic loading is low and in the short term, the asphalt is relatively ductile.
Asphalt Diffusion Barrier	Seismic Stresses (Long Term)	2	4	8	Based on estimates from asphalt aging experts, the vault asphalt hardening should be a surface phenomena. A seismic event could extend or initiate cracks in the hardened surface and accelerate the depth of hardening.
	Construction Joints	1	5	5	Cold pour/construction joints in the asphalt barrier are potential planes of weakness, but the healing nature of the fresh asphalt is expected to make this mechanism insignificant. A high consequence factor was assumed because many cold pour joints are in the asphalt walls.
	Thermal Board Disintegration	3	5	15	Thermal board disintegration could contribute to asphalt wall "slumping" which could produce cracks in the wall/roof joint area. The best estimate disintegration of the thermal board is a minimal, slow process based on wood disintegration in the anticipated environment (asphalt coated, low moisture, low air availability).
Asphalt Diffusion Barrier	Biodegradation-Induced Crack Enlargement	2	2	4	Biodegradation at cracks in highway pavements has been noted in the literature. It is postulated that the increased surface area exposed by cracks could accelerate the biodegradation and increase the effective size of the cracks.

Summary of Evaluation of Potential Cracking Mechanisms in the Grout Vault Structures (contd)

Material	Cracking Mechanism	Probability of Occurrence	Consequence Factor	Significance Factor	Comments
Vault Concrete	Rebar Corrosion (Long Term)	4	4	16	Over a long time period, depassivation of the steel reinforcement is likely due to a gradual lowering of the pH (carbonation and/or leaching). Grout chemistry degradation of the rebar cover concrete also could contribute to an eventual initiation of corrosion.
	Poor Construction Practices	1	3	3	ACI 224.1R lists several poor construction practices which can cause cracking. The grout vault construction is relatively well controlled and should not have significant problems of this type. If construction-related cracking does occur, it is likely to be discovered and corrected.
	Construction Overloads	1	2	2	Concrete is susceptible to cracking during construction because the young concrete has not achieved full strength. However, the carefully controlled grout vault construction should prevent any construction overloads.
	Design Detailing Errors	1	3	3	Since the grout vault design has been subjected to significant review, design/detailing errors are not likely.
Vault Concrete	Externally Applied Loads, Dead Weight/Soil Pressure	2	2	4	Dead weight/soil pressure loadings maximum stress predictions are below the minimum cracking strength.
	Seismic Loading (Short Term)	1	3	3	Short-term probability of a seismic event is low. Consequences are low for nondegraded structure.
	Seismic Loading (Long Term)	4	4	16	Long-term probability of a seismic event is much higher. Long-term consequences are high due to degradation from other mechanisms. This would include both the extension of existing cracks and the introduction of new cracks.
	Roof Cracking Between Precast Planks	4	4	16	Nonreinforced joints between roof planks are filled with field grout followed with a relatively thin layer of concrete topping over the entire roof. Some cracking will likely occur at these locations because of overburden loading.
	Construction Joints	5	3	15	Construction joints are designed into the walls and the floor. Metal water stops seal the joints initially but the long-term sealing ability is questionable.
Asphalt Diffusion Barrier	Shrinkage	2	2	4	Shrinkage may occur from loss of volatiles and/or chemical reactions. The absence of information in the literature on this mechanism leaves the impression that this is not a significant mechanism.